frontiers | Research Topics

Targeted drug discovery in ectopic calcification: Mechanism, prospect, and clinical application

Edited by
Kang Xu, Charareh Pourzand, Jing Xie and Anna Malashicheva

Published in
Frontiers in Pharmacology

ISSN 1664-8714
ISBN 978-2-8325-2421-3
DOI 10.3389/978-2-8325-2421-3

About Frontiers

Frontiers is more than just an open access publisher of scholarly articles: it is a pioneering approach to the world of academia, radically improving the way scholarly research is managed. The grand vision of Frontiers is a world where all people have an equal opportunity to seek, share and generate knowledge. Frontiers provides immediate and permanent online open access to all its publications, but this alone is not enough to realize our grand goals.

Frontiers journal series

The Frontiers journal series is a multi-tier and interdisciplinary set of open-access, online journals, promising a paradigm shift from the current review, selection and dissemination processes in academic publishing. All Frontiers journals are driven by researchers for researchers; therefore, they constitute a service to the scholarly community. At the same time, the *Frontiers journal series* operates on a revolutionary invention, the tiered publishing system, initially addressing specific communities of scholars, and gradually climbing up to broader public understanding, thus serving the interests of the lay society, too.

Dedication to quality

Each Frontiers article is a landmark of the highest quality, thanks to genuinely collaborative interactions between authors and review editors, who include some of the world's best academicians. Research must be certified by peers before entering a stream of knowledge that may eventually reach the public - and shape society; therefore, Frontiers only applies the most rigorous and unbiased reviews. Frontiers revolutionizes research publishing by freely delivering the most outstanding research, evaluated with no bias from both the academic and social point of view. By applying the most advanced information technologies, Frontiers is catapulting scholarly publishing into a new generation.

What are Frontiers Research Topics?

Frontiers Research Topics are very popular trademarks of the *Frontiers journals series*: they are collections of at least ten articles, all centered on a particular subject. With their unique mix of varied contributions from Original Research to Review Articles, Frontiers Research Topics unify the most influential researchers, the latest key findings and historical advances in a hot research area.

Find out more on how to host your own Frontiers Research Topic or contribute to one as an author by contacting the Frontiers editorial office: frontiersin.org/about/contact

Targeted drug discovery in ectopic calcification: Mechanism, prospect, and clinical application

Topic editors

Kang Xu — Hubei University of Chinese Medicine, China
Charareh Pourzand — University of Bath, United Kingdom
Jing Xie — Sichuan University, China
Anna Malashicheva — Institute of Cytology, Russia

Citation

Xu, K., Pourzand, C., Xie, J., Malashicheva, A., eds. (2023). *Targeted drug discovery in ectopic calcification: Mechanism, prospect, and clinical application*. Lausanne: Frontiers Media SA. doi: 10.3389/978-2-8325-2421-3

Table of contents

frontiers | Frontiers in Pharmacology

TYPE Editorial
PUBLISHED 02 May 2023
DOI 10.3389/fphar.2023.1159334

OPEN ACCESS

EDITED BY
Filippo Drago,
University of Catania, Italy

REVIEWED BY
Alexander N. Kapustin,
AstraZeneca, United Kingdom

*CORRESPONDENCE
Kang Xu,
kangxu05@hbtcm.edu.cn

RECEIVED 05 February 2023
ACCEPTED 24 April 2023
PUBLISHED 02 May 2023

CITATION
Xu K, Pourzand C, Xie J and Malashicheva A (2023), Editorial: Targeted drug discovery in ectopic calcification: mechanism, prospect, and clinical application.
Front. Pharmacol. 14:1159334.
doi: 10.3389/fphar.2023.1159334

Editorial: Targeted drug discovery in ectopic calcification: mechanism, prospect, and clinical application

Kang Xu[1]*, Charareh Pourzand[2], Jing Xie[3] and Anna Malashicheva[4]

[1]College of Pharmacy, Hubei University of Chinese Medicine, Wuhan, China, [2]Department of Life Sciences, University of Bath, Bath, United Kingdom, [3]West China Hospital of Stomatology, Sichuan University, Chengdu, China, [4]Institute of Cytology, Saint-Petersburg, Russia

KEYWORDS

ectopic calcification, calcium deposition, therapeutic drugs, soft tissues, targeting

Editorial on the Research Topic
Targeted drug discovery in ectopic calcification: mechanism, prospect, and clinical application

Ectopic calcification is a pathologic deposition of salts or bone growth in soft tissues. It occurs around large joints, such as the hip and elbow, and in various soft tissues, including blood vessels (Persy and D'Haese, 2009), heart valves (Xu et al., 2020), lungs (Bendayan et al., 2000), and kidneys (Priante et al., 2019) Although oxidative stress and inflammation have been identified as the primary determinants of soft tissue calcification, it is initiated and regulated by a series of still poorly understood molecular signaling pathways. Consequently, it is necessary to elucidate the molecular mechanism underlying ectopic calcification and to identify potential drugs to prevent its occurrence and progression.

In this Research Topic, several diseases associated with ectopic calcification, such as aortic valve calcification, pseudoxanthoma elasticum, vascular calcification, keloid fibrosis, renal fibrosis, liver cirrhosis, and Duchenne muscular dystrophy, are discussed. In light of the aforementioned diseases associated with ectopic calcification, their pathogenesis and the search for targeted therapeutic drugs were investigated in depth.

Among these, cardiovascular calcification disease research is a hot Research Topic. Bogdanova et al. provided a summary of the evaluation of aortic valve calcification in *ex vivo*, *in vitro*, and *in vivo* settings. They emphasized the translational studies of calcific aortic valve stenosis with a particular emphasis on human primary cell cultures, which are widely used and appropriate for screening anti-calcification drugs. Murtazalieva et al. evaluated the prognostic significance of valvular inflammation and calcification as measured by ^{18}F-fluorodeoxyglucose (^{18}F-FDG) and ^{18}F-fluoride (^{18}F-NaF) PET/CT in patients with tricuspid (TAV) and bicuspid aortic valves (BAV). In the case of TAV, they viewed 18F-NaF PET/CT as a more accurate and valuable predictor of the hemodynamic progression of calcific AS. Niu et al. demonstrated that BMP type I receptor A (BMPR1A) participates in osteogenic differentiation and is a potential molecular target for preventing vascular calcification. Moreover, Pan et al. reviewed recent research progress on the relationship between various types of sirtuins and vascular calcification and concluded that

once a deeper understanding of the sirtuin family is established, researchers will be able to identify the most effective therapeutic targets and develop clinically applicable drugs for the prevention and treatment of vascular calcification.

Exploring and analyzing the pathogenesis of calcified cardiovascular disease has led to the discovery of numerous useful therapeutic drugs. Statins, immunosuppressants, and anticoagulants were identified by Wen et al. as potential candidates for preventing bioprosthetic heart valve (BHV) calcification. Statins such as rosuvastatin and atorvastatin may significantly reduce calcification of BHV. In addition, anti-thymocyte globulin (ATG), a polyclonal IgG preparation used for immunosuppression induction, uncovered a potential therapeutic strategy for preventing BHV calcification. In addition, the European and American Association Guidelines recommend oral anticoagulation for the first 3 months following surgical implantation of BHV. Huang et al. discovered that andrographolide, a natural terpenoid extracted from the traditional Chinese medicinal plant *Andrographis paniculate*, reduces aortic valve enlargement by inhibiting cell proliferation and osteogenic differentiation through the MAPK-ERK signaling pathway. FLT3 was identified by Wang et al. as a target protein that contributed to calcified aortic valve disease. They demonstrated that Atractylenolide-1, a natural active compound extracted from *Atractylodes macrocephala*, inhibited the phosphorylation of FLT3, thereby blocking the activation of the PI3K/AKT pathway, reducing the production of Hypoxia-inducible factor (HIF)1-α, and subsequently inhibiting the osteogenic differentiation of valve interstitial cells (VICs). In addition, Zhang et al. confirmed that dihydromyricetin (DHM), the most bioactive component of *Ampelopsis grossedentata*, significantly inhibited the osteogenic differentiation of human VICs by inhibiting c-KIT phosphorylation and suppressing IL-6 expression. DHM is an effective pharmacological treatment for preventing the progression of calcified aortic valve disease.

Ectopic myofiber calcification is a pathological characteristic of muscle damage in Duchenne muscular dystrophy (DMD). According to Rumney et al., P2X7 gene overexpression serves as a protective mechanism against dystrophic mineralization. In cultures of dystrophic cells, the use of the P2X7 agonist BzATP decreased the calcifying effects of high phosphate that promoted mineral deposition. Additionally, persistent calcium deposits in the kidneys result in inflammation and cell necrosis, which are associated with severe kidney diseases. Feng et al. developed a predictive drug target method for the diagnosis of renal fibrosis and identified the EGR1 and PLA2G4A genes as the targets for this calcific-associated disease. Chi et al. investigated the diagnostic key targets of tanshinone IIA, which is associated with serum calcium levels, in liver cirrhosis. After bioinformatic analysis, AKR1C3 and TPX2 were identified as the molecular targets involved in the development of liver cirrhosis. Biomechanical regulatory factors also contributed to ectopic calcification, which is quite interesting. Feng et al. provided a summary of the mechano-transduction pathways, such as the TGF-β/Smad signaling pathway, the integrin signaling pathway, and the YAP/TAZ signaling pathway, that are involved in the formation of keloids, which results in excessive collagen disorders and calcinosis. By targeting biomechanical regulatory factors, these findings may facilitate the development of pharmacological interventions for treating ectopic calcification.

In the process of investigating medications for the treatment of ectopic calcification, we will face numerous obstacles. Anti-calcification medications may inhibit bone regeneration or cause osteoporosis. In the recovery period following a bone fracture, elderly patients who must take drugs for the treatment of ectopic calcification diseases face this dilemma. In the subsequent phase of research, it will be crucial to develop drugs that target ectopic calcification without affecting bone mineralization. In addition, for specific cardiac calcifications, such as aortic valve calcification, it is difficult to construct a stable organoid for basic research, such as drug screening or calcification mechanism development, because the cells involved in calcification in valve tissue are difficult to obtain. This lack of a reliable *in vitro* calcification model has severely impeded the progress of anti-ectopic calcification research.

The pathogenesis of ectopic calcification diseases is relatively complicated, involving the activation of multiple molecular signaling pathways and functional genes, the disorder of cellular metabolism, fibrosis of the extracellular matrix, and calcium deposition (Collett and Canfield, 2005; Gonzalo and Villa-Bellosta, 2019). Exploring the underlying mechanisms of ectopic calcification, followed by screening and identifying therapeutic drugs based on associated signal pathways and molecular targets, is an applicable research model for identifying potential drugs for preventing ectopic calcification.

Author contributions

KX wrote the draft, CP, JX, and AM revised, edited the manuscript. All authors were finally approved it.

Acknowledgments

We would like to thank the authors, reviewers, editors and Frontiers Media who contributed to this Research Topic. We also thank the support from the National Natural Science Foundation of China (82204659).

Conflict of interest

The authors declare that the research was conducted in the absence of any commercial or financial relationships that could be construed as a potential conflict of interest.

Publisher's note

References

Bendayan, D., Barziv, Y., and Kramer, M. R. (2000). Pulmonary calcifications: A review. *Respir. Med.* 94, 190–193. doi:10.1053/rmed.1999.0716

Collett, G. D., and Canfield, A. E. (2005). Angiogenesis and pericytes in the initiation of ectopic calcification. *Circulation Res.* 96, 930–938. doi:10.1161/01.RES.0000163634.51301.0d

Gonzalo, S., and Villa-Bellosta, R. (2019). The role of sodium phosphate cotransporters in ectopic calcification. *Endokrynol. Pol.* 70, 496–503. doi:10.5603/EP.a2019.0050

Persy, V., and D'haese, P. (2009). Vascular calcification and bone disease: The calcification paradox. *Trends Mol. Med.* 15, 405–416. doi:10.1016/j.molmed.2009.07.001

Priante, G., Mezzabotta, F., Cristofaro, R., Quaggio, F., Ceol, M., Gianesello, L., et al. (2019). Cell death in ectopic calcification of the kidney. *Cell death Dis.* 10, 466. doi:10.1038/s41419-019-1697-8

Xu, K., Xie, S., Huang, Y., Zhou, T., Liu, M., Zhu, P., et al. (2020). Cell-type transcriptome atlas of human aortic valves reveal cell heterogeneity and endothelial to mesenchymal transition involved in calcific aortic valve disease. *Arteriosclerosis, thrombosis, Vasc. Biol.* 40, 2910–2921. doi:10.1161/ATVBAHA.120.314789

frontiers in Pharmacology

ORIGINAL RESEARCH
published: 04 March 2022
doi: 10.3389/fphar.2022.822143

The Abcc6a Knockout Zebrafish Model as a Novel Tool for Drug Screening for Pseudoxanthoma Elasticum

M. Van Gils[1,2], *A. Willaert*[1,2], *P. J. Coucke*[1,2] *and O. M. Vanakker*[1,2]*

[1]Center for Medical Genetics, Ghent University Hospital, Ghent, Belgium, [2]Department of Biomolecular Medicine, Ghent University, Ghent, Belgium

Pseudoxanthoma elasticum (PXE) is a multisystem ectopic mineralization disorder caused by pathogenic variants in the ABCC6 gene. Though complications of the disease can be treated, PXE itself remains currently intractable. A strategy for rapid and cost-effective discovery of therapeutic drugs would be to perform chemical compound screening using zebrafish, but this approach remains to be validated for PXE. In this paper, we validate a stable CRISPR/Cas9 abcc6a knockout zebrafish model–which has spinal column hypermineralization as its primary phenotypic feature–as a model system for compound screening in ectopic mineralization. We evaluated the anti-mineralization potential of five compounds, which had (anecdotal) positive effects reported in Abcc6 knockout mice and/or PXE patients. Abcc6a knockout zebrafish larvae were treated from 3 to 10 days post-fertilization with vitamin K1, sodium thiosulfate, etidronate, alendronate or magnesium citrate and compared to matching controls. Following alizarin red S staining, alterations in notochord sheath mineralization were semiquantified and found to largely congrue with the originally reported outcomes. Our results demonstrate that the use of this abcc6a knockout zebrafish model is a validated and promising strategy for drug discovery against ectopic mineralization.

Keywords: pseudoxanthoma elasticum, zebrafish, compound screening, alendronate, etidronate, magnesium citrate, sodium thiosulfate, vitamin K1

OPEN ACCESS

Edited by:
Kang Xu,
Hubei University of Chinese Medicine, China

Reviewed by:
Tingwen Zhou,
Huazhong University of Science and Technology, China
Qingjia Chi,
Wuhan University of Technology, China

***Correspondence:**
O. M. Vanakker
olivier.vanakker@ugent.be

Specialty section:
This article was submitted to Experimental Pharmacology and Drug Discovery, a section of the journal Frontiers in Pharmacology

Received: *25 November 2021*
Accepted: *27 January 2022*
Published: *04 March 2022*

Citation:
Van Gils M, Willaert A, Coucke PJ and Vanakker OM (2022) The Abcc6a Knockout Zebrafish Model as a Novel Tool for Drug Screening for Pseudoxanthoma Elasticum. Front. Pharmacol. 13:822143. doi: 10.3389/fphar.2022.822143

1 INTRODUCTION

Pseudoxanthoma elasticum (PXE) is an ectopic calcification disorder caused by biallelic mutations in the ABCC6 (ATP-Binding Cassette, subfamily C member 6)–and in rare cases the ENPP1 (Ectonucleotide Pyrophosphatase/Phosphodiesterase 1)–gene (Nitschke et al., 2012; Nitschke and Rutsch 2012). In PXE aberrant hydroxyapatite crystals are progressively deposited onto elastic fibers, which consequently lose their elastic properties and fragment, leading to a myriad of symptoms. Generally, patients develop skin lesions (papular plaque formation and excessive skin folds in flexural regions), ocular symptoms (peau d'orange, angioid streaks, choroidal neovascularizations, retinal

Abbreviations: Abcc6(a), ATP-binding cassette, sub-family C, member 6(a); Alen, alendronate; ARS, alizarin red S; C, controls; CRISPR, clustered regularly interspaced short palindromic repeats; Dpf, days post-fertilization; ENPP1, ectonucleotide pyrophosphatase/phosphodiesterase 1; Etid, etidronate; MgC, magnesium citrate; PXE, pseudoxanthoma elasticum; STS, sodium thiosulfate; VK, vitamin K; WT, wild type.

haemorrhaging and vision loss) and cardiovascular manifestations (e.g., peripheral artery disease, increased risk of stroke). The phenotypic manifestations of PXE show a high degree of inter- and intrafamilial variability without solid genotype-phenotype correlations, making it difficult for health care professionals to accurately manage patients. Moreover, existing treatment options for PXE are limited and currently focus on slowing down disease progression in patients through lifestyle changes or by treating complications via e.g., cosmetic surgery or intravitreal injection of anti-VEGF antibodies (Vascular Endothelial Growth Factor; Shimada et al., 2021).

As such, there is a pressing need for therapeutic interventions in patient care and in recent years several compounds have been tested for their potential to halt PXE. Some compounds have been described casuistically, such as sodium thiosulfate (STS) (Omarjee et al., 2020). Others, such as vitamin K1 (VK1), have been tested in PXE knockout mice and recently in two PXE zebrafish models with mixed results. In zebrafish models VK1 significantly reduced mineralization (Mackay et al., 2015; Sun et al., 2021) but it did not affect mineralization in murine models (Brampton et al., 2011; Gorgels et al., 2011; Jiang et al., 2011). Similarly, treatment with bisphosphonates showed that etidronate (etid.), but not alendronate (alen.), could slow down ectopic mineralization in Abcc6$^{-/-}$ mice (Li et al., 2015; Pomozi et al., 2017). Finally, there have been two randomized clinical trials in PXE patients evaluating the effect of magnesium and the bisphosphonate etidronate respectively. Increased oral magnesium intake reduced skin elastic fiber calcification, albeit not statistically significant, and had no effect on ophthalmological outcomes (Rose et al., 2019). Oral etidronate therapy did affect progression of vascular mineralization but had no significant effects on eye symptoms (Kranenburg et al., 2018). While drug efficacy needs to be evaluated in patients, such trials are slow and require substantial amounts of resources (compound, time, labor). Moreover, toxicity and long-term effects are a major concern (Pazianas and Abrahamsen 2011; Moore et al., 2015).

Consequently, animal models seem to be a prerequisite for the discovery and testing of drugs that not only halt–but ideally also reverse–excessive calcification in PXE. Unfortunately, while multiple rodent models have been generated for PXE, mouse and rat models are not ideally suited for rapid testing of multiple drugs. Despite being more closely related to humans, ethical and economic drawbacks typically lead to smaller study cohort sizes. Moreover, the phenotypic effects of Abcc6 deficiency in these animals only become apparent after several weeks to months (Gorgels et al., 2005; Li et al., 2014), resulting in elongated exposure periods, high drug consumption and substantial husbandry costs.

Zebrafish models are much better suited for this endeavor. Husbandry is substantially different at lower costs per animal. Their high fecundity, small size and rapid *ex utero* development allow for larger cohorts that require less drug consumption with shorter exposure periods. Furthermore, gene and protein function largely overlaps with humans (Howe et al., 2013) and as zebrafish are maintained on an outbred background, they theoretically should better reflect the genetic diversity of patients than rodent models.

The ABCC6 gene has two orthologues–abcc6a and abcc6b–in zebrafish. While the function of abcc6b remains to be elucidated, abcc6a is a regulator of calcification (Mackay et al., 2015; Van Gils et al., 2018; Sun et al., 2021). We have previously reported on the development and phenotypic characterization of a CRISPR/Cas-9-mediated knockout zebrafish model (dubbed Cmg52) of the abcc6a gene. The Cmg52 allele is a four base-pair deletion (c.180delTCGG) in the second exon of abcc6a and predicted to result in p.R62Cfs*33 (Van Gils et al., 2018). Abcc6a loss-of-function results in progressive hypermineralization of axioskeletal bone structures in homozygous mutants but not in heterozygous animals, though the underlying mechanism remains unclear. In summary, excess mineral growth and fusion of vertebrae leads to a severe phenotype with spinal malformations and shorter stature in adult fish. Moreover, such hypermineralization is already apparent during larval development and semiquatifiable with knockout larvae having significantly more notochord sheath mineralization than their heterozygous and wild type siblings at 9–10 days post-fertilization (dpf) (Van Gils et al., 2018). This phenotype was confirmed to be similar to that of abcc6a missense mutants and recently another abcc6a knockout model (Mackay et al., 2015; Van Gils et al., 2018; Sun et al., 2021). A caveat to the use of zebrafish models for screening is that the expression site of abcc6a - which appears to coincide with osteoblast-like cells and, therefore, skeletal tissue - differs from that of ABCC6 in mammals (Mackay et al., 2015). For this reason we aimed to perform a proof-of-concept study using compounds reported in PXE literature. We hypothesized that, if treatment outcomes with these specific compounds are analogous for the mineralization phenotype of the abcc6a$^{cmg52/cmg52}$ zebrafish and the soft tissue mineralizations of other models, the zebrafish model should be a valid tool in PXE research for drug screening purposes.

2 MATERIALS AND METHODS

2.1 Zebrafish Husbandry and Phenotype

All animals were housed in the Zebrafish Facility of the Ghent Center for Medical Genetics on a 14 h light/10 h dark cycle utilizing semi-closed recirculating systems (ZebTEC, Tecniplast) kept at 27–28°C, pH 7.5 and conductivity ±500 μS. Adult and rearing zebrafish were fed twice a day, once with artemia (1579706, Ocean Nutrition) and once with dry food (GEMMA Micro 75-300, Skretting). Lines were maintained and outbred on an AB background. Animal experiments were approved by the Animal Experimentation Committee of the Ghent University and performed in accordance with the EU Directive 2010/63/EU for animal experiments.

For the compound screening studies, zebrafish allele cmg52 (https://www.zfin.org/ZDB-ALT-200727-1) was used and abcc6a$^{cmg52/+}$ zebrafish (heterozygotes) were in-crossed to obtain abcc6a$^{cmg52/cmg52}$ mutants (knockouts). As previously

reported, in these homozygous abcc6a$^{cmg52/cmg52}$ mutants abcc6a expression is severely diminished by the CRISPR/Cas9 induced c. 180delTCGG allele variant (Van Gils et al., 2018). Consequently, abcc6a$^{cmg52/cmg52}$ larvae more rapidly develop notochord mineralization with occasional vertebral fusion than carrier or wild type siblings. This phenotype can be analyzed as early as 10 days post-fertilization (dpf) by performing alizarin red S calcium deposit staining and semiquantifying notochord mineralizations.

2.2 Compound Screening Setup and Mineral Deposit Staining

Five compounds with previously reported anti-mineralizing activity were selected for a proof-of-concept approach. Treatment dosages were adopted from literature or based on in-house range-finding survivability testing on wild-type (WT) embryos (between 3-7 dpf; **Supplementary Data S1–S3**). Screening was performed using final doses of 80 μM vitamin K1 (95271, Sigma-Aldrich; Mackay et al., 2015), 20 μM sodium thiosulfate (72049, Sigma-Aldrich; toxicity test), 100 μM etidronate (P5248, Sigma-Aldrich; Apschner et al., 2014), 100 μM alendronate (PHR1599, Sigma-Aldrich; toxicity test) and 10 mM magnesium citrate (CDS000001, Sigma-Aldrich; toxicity test). VK1 was dissolved in 1:1 DMSO:ethanol (in accordance with Mackay et al., 2015), the other compounds were water-soluble. Larvae were not fed for the duration of the experiments as feeding introduces a variable influx of phosphate for mineralization and compounds might potentially bind to excess feed (Cotti et al., 2020).

Per experiment cmg52 heterozygotes were in-crossed using established protocols (Westerfield 2000) and resulting offspring was transferred per 100 into 90 mm petri dishes (F11093, M.L.S.) with E3-medium (5 mM NaCl, 0.17mM KCl, 0.33 mM $CaCl_2.2H_2O$, 0.33 mM $MgSO_4.7H_2O$, 5 mM HEPES, pH 7.4) + 0.00001% methylene blue (hence referred to as E3-medium). Medium was refreshed daily and only morphologically normal developing embryos were selected for further experiments at 3 dpf.

At 3 dpf embryos were dechorionated via pronase digestion if necessary and randomized into baskets in equal amounts (N ≤ 20 per basket; 734-0003, VWR) to allow quick swapping and minimal animal handling during the experiments. Baskets were then placed in 6-well plates filled either with 8 ml E3-medium + compound (i.e. treated) or E3-medium + carrier solution (i.e. controls [C]). Solutions were refreshed daily until 10 dpf at which point all larvae were euthanized (25x Tricaine for 10 min at room temperature) and fixated with 4% paraformaldehyde, 0.4 M PO_4-buffer for 1 h at room temperature.

Larvae were then stained for mineral deposition using the Alizarin Red S (ARS) staining technique (Van Gils et al., 2018). Specimens were bleached for 30 min at room temperature with 1%H_2O_2, 1% KOH, 0.5% Triton X-100 and rinsed with distilled water to stop the reaction. Staining was performed overnight at 4°C using 0.05% ARS, 1% KOH, 0.5% Triton X-100 under gentle locomotion. Destaining was performed at room temperature with 30% glycerol and through incremental washing (30%, 50% 70 and 100% glycerol) specimens were stored in glycerol at 4°C. ARS-staining was performed concomitantly for control and compound treated groups of each experiment, sharing solutions and timing to minimize variance.

2.3 Image Analysis

Each group was examined and larvae with apparent spinal mineralization were transferred into Nunc™ glass bottom dishes (150680; Thermo Fischer Scientific) containing 100% glycerol and positioned for lateral view. Of these animals whole-body light microscopy images were taken with a Leica M165 FC microscope under identical conditions (e.g., zoom, aperture, light intensity) per control/compound duo. After imaging, all larvae were then transferred into 96-well plates at designated positions and stored at 4°C for genotyping. Larvae with notochord mineralization in regions other than the tip were considered to have "spinal mineralization".

Images were processed using ImageJ (NIH, Bethesda, MD; Schneider et al., 2012) and spinal mineralization was semiquantified. Images were first converted into 16-bit (i.e., greyscale). tiff files. Excluding the notochord tip, all other segments of the notochord were then delineated and mineralized areas were segmented from the background using threshold analysis. The mineralized areas were then semiquantified per larva.

2.4 Abcc6a Genotyping

Ninety-six-well plates were batch-analyzed per experiment. Per well 100 μL 50 mM NaOH was added and plates were heated to 95°C for 20 min. Following neutralization of pH with 10 μL 1 M Tris-HCl, debris was pelleted and supernatant collected for genotyping.

Abcc6a primer sequences used in TD-PCR and cycle sequencing were: F: 5′-GGTTTGGACTGAGCCATTGT-3'; R: 5′-TCGACCACTTTCACGTTCAC-3'. TD-PCR with 5 μL KAPA2G Robust Hotstart Ready Mix (KK5702, Sigma-Aldrich), 0.1 μL F-primer (30 μM), 0.1 μL R-Primer 30 μM), 2.8 μL ddH2O and 2 μL supernatant was performed (94°C, 4' [94°C, 30"; 58 > 52°C, 30"; 72°C, 1']x6; [94°C, 40"; 52°C, 40"; 72°C, 40"]x25; 72°C, 10′). Amplicons were purified with 1 μL of ExoAP mix (1 μL exonuclease I [M0293S, NEB], 4 μL antarctic phosphatase [M0298L, NEB], 15 μL ddH2O) to 5 μL PCR product and incubating the samples (37°C, 15'; 80°C, 20′).

Cycle sequencing (95°C, 5' [95°C, 10"; 55°C, 5"; 60°C, 4']x25) was then performed using the Big Dye™ Terminator v3.1 kit (4337457, Applied Biosystems). Products were purified via CleanDTR beads (CDTR-0050, GC Biotech) ethanol capturing and sequencing was performed by the Genome Sequencing Unit of the Ghent Center for Medical Genetics. Genotypes were manually checked with FinchTV software (Geospiza).

2.5 Statistical Analysis and Tables

Per experiment image data was stratified according to abcc6a genotype in SPSS26 software (IBM). Shapiro-Wilk normality testing was performed and extreme outliers, if present, were

TABLE 1 | Geno- and phenotypic distribution of the larvae analyzed at 10 dpf. Quantities and distribution of larvae per genotype and phenotype (i.e. presence of mineralized notochord sections other than the tip) are shown for each compound. WT = abcc6a$^{+/+}$ wild types, Htz = abcc6a$^{cmg52/+}$ heterozygotes, KO = abcc6a$^{cmg52/cmg52}$ knockouts.

Cohorts	Spinal mineralization			No Spinal mineralization			Animal Total
	WT	Htz	KO	WT	Htz	KO	
Controls	0	0	15	14	28	3	60
80 μM VK1	0	0	10	11	36	1	58
Controls	0	0	20	28	54	11	113
20 μM STS	0	0	20	33	52	11	116
Controls	4	28	36	31	59	6	164
100 μM Etid	14	22	37	33	56	7	169
Controls	4	28	22	13	18	1	86
100 μM Alen	9	34	22	14	15	0	94
Controls	2	15	22	8	25	0	72
10 mM MgC	1	7	17	14	31	1	71
Controls	12	21	22	3	8	1	67
5 mM MgC	2	5	15	10	33	1	66

excluded. Effect of the compound on mineralization was determined by comparing control and treated groups with two-tailed *T*-tests or Mann-Whitney *U*-tests. Data was considered statistically significant at $p < 0.05$. Following relative normalization of data against the corresponding mean control value, tables (mean ± SD) were generated in Excel (Microsoft).

3 RESULTS

3.1 Vitamin K1 Reduces Spinal Mineralization During Development

One hundred twenty embryos were split into untreated (C: n = 60) and 80 μM VK1-treated (VK1: n = 60) cohorts at 3 dpf. During screening two VK1-treated larvae died, resulting in ARS-staining of 60 controls and 58 VK1-treated animals at 10 dpf. Upon genotyping only abcc6a$^{cmg52/cmg52}$ larvae had developed mineralized segments other than the notochord tip (C: n = 15, VK1: n = 10; **Table 1**) with vitamin K1-treated knockouts showing a significant 42% reduction in mineralization compared to their control counterparts (*t*-Test: $p < 0.05$, **Figures 1A,B**, **Figure 2A**).

3.2 Sodium Thiosulfate Reduces Spinal Mineralization During Development, but Higher Doses Result in Ectopic Mineralization

STS survival testing indicated that embryos and larvae could be treated safely with 35 μM (**Supplementary Data S1**). However, 35 μM STS-treatment completely abolished spinal mineralization while simultaneously causing ventral mineral depositions in a speckled pattern for all treated animals (**Figure 3**). Therefore we reduced the dosage until this pattern disappeared at 20 μM sodium thiosulfate. A total of 120 untreated and 120 20 μM STS-treated embryos were processed in 2 experiments. During treatment, 7 untreated and 4 STS-treated larvae expired (**Table 1**). Following genotyping, only abcc6a knockouts had spinal hypermineralization (C: n = 20; STS: n = 20). On average, spinal mineralization was significantly reduced by at least 55% following sodium thiosulfate treatment (Mann-Whitney *U*-Test: $p < 0.05$ [C: n = 10, STS: n = 8, 55%] and $p < 0.05$ [C: n = 10, STS: n = 12, 57%], **Figures 1C,D**, **Figure 2B**).

3.3 Bisphosphonate treatment Significantly Reduces Spinal Mineralization in abcc6a$^{cmg52/cmg52}$ Larvae

To evaluate the effect of etidronate (etid.) on the spinal mineralization phenotype, 175 embryos were treated with 100 μM etidronate and compared to 175 untreated larvae in two experiments. As 5 untreated and 2 etid.-treated larvae died and genotyping failed for 6 and 4 larvae respectively, 164 untreated and 169 etid.-treated larvae were analyzed (**Table 1**). Spinal mineralization was found for all genotypes, but was only excessive in the knockouts as expected. The number of WT animals with spinal mineralization was too low ($n < 5$ per group) to assess an effect of etidronate on the spinal mineralization. For heterozygotes one experiment had sufficient quantities to perform the analysis, but etidronate treatment had no significant effect (Mann-Whitney *U*-Test: $p > 0.05$ [C: n = 28, Etid: n = 21]). By contrast, mean mineralization in abcc6a knockouts was significantly reduced by approximately 35% following etidronate treatment (*t*-Test: $p < 0.05$ [C: n = 14, Etid: n = 9] and Mann-Whitney *U*-Test: $p < 0.05$ [C: n = 22, Etid: n = 28], **Figures 1E,F**, **Figure 2C**).

Alendronate was tolerated at similar doses as etidronate for the duration of the experiment. We treated 100 larvae with 100 μM alendronate and compared them to 100 controls. Respectively 6 controls and 4 treated animals expired and genotyping failed for 8 and 2 animals resulting in analysis of 86 control and 94 alen.-

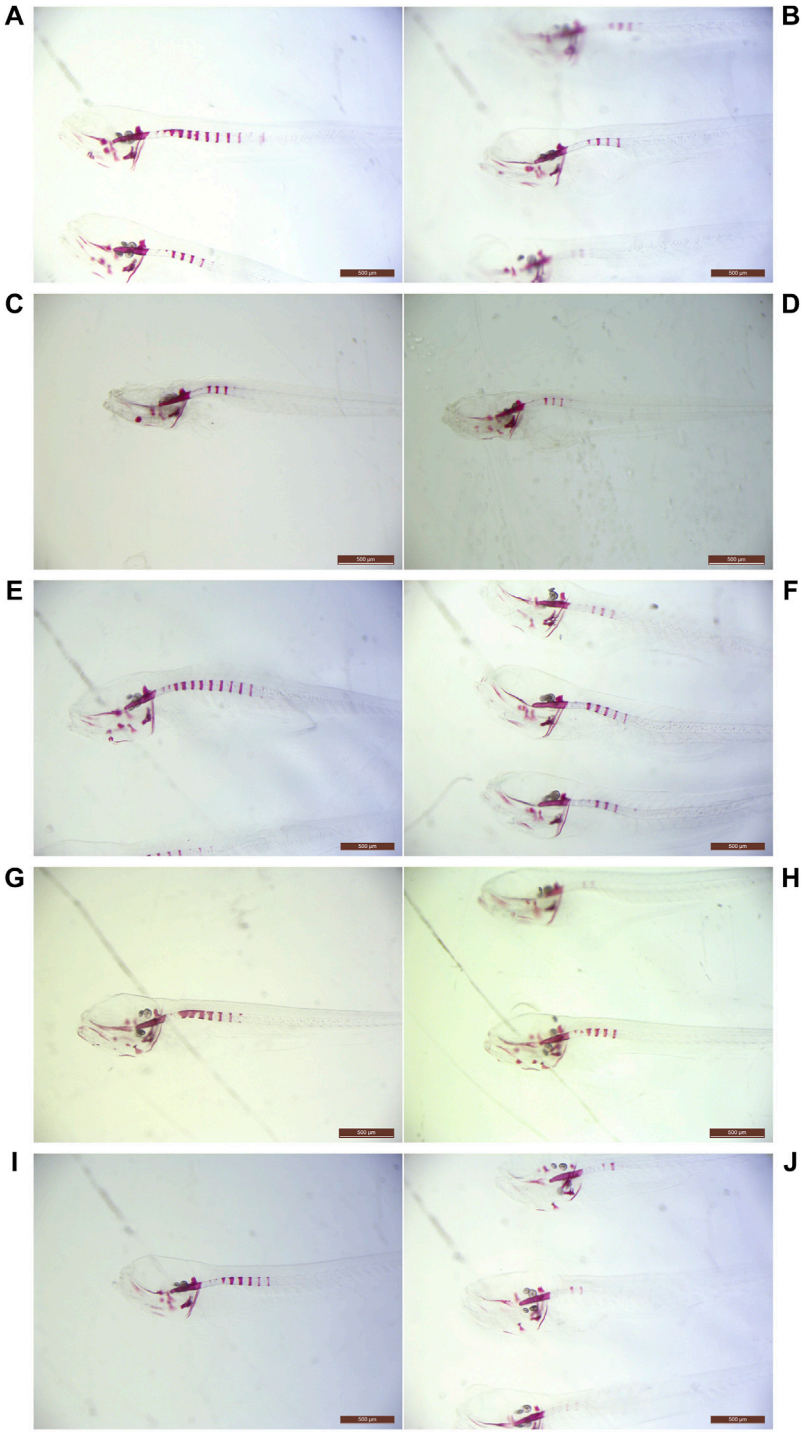

FIGURE 1 | Light microscopy examples of ARS-stained abcc6a$^{cmg52/cmg52}$ specimens. Examples of 10 dpf untreated **(A**,**C**,**E**,**G**,**I)** and treated **(B**,**D**,**F**,**H**,**J)** abcc6a$^{cmg52/cmg52}$ animals. Compounds per set are **(A**,**B)** 80 μM vitamin K1, **(C**,**D)** 20 μM sodium thiosulfate **(E**,**F)** 100 μM etidronate, **(G**,**H)** 100 μM alendronate and **(I**,**J)** 10 mM magnesium citrate.

treated larvae (**Table 1**). Again, mineralization was detected for all genotypes, but without sufficient numbers of WT. In heterozygotes mineralization was not significantly affected by alendronate treatment (Mann-Whitney *U*-Test: $p > 0.05$ [C: $n = 28$, Alen: $n = 34$]). However, treatment significantly reduced spinal hypermineralization by approximately 39% in abcc6a

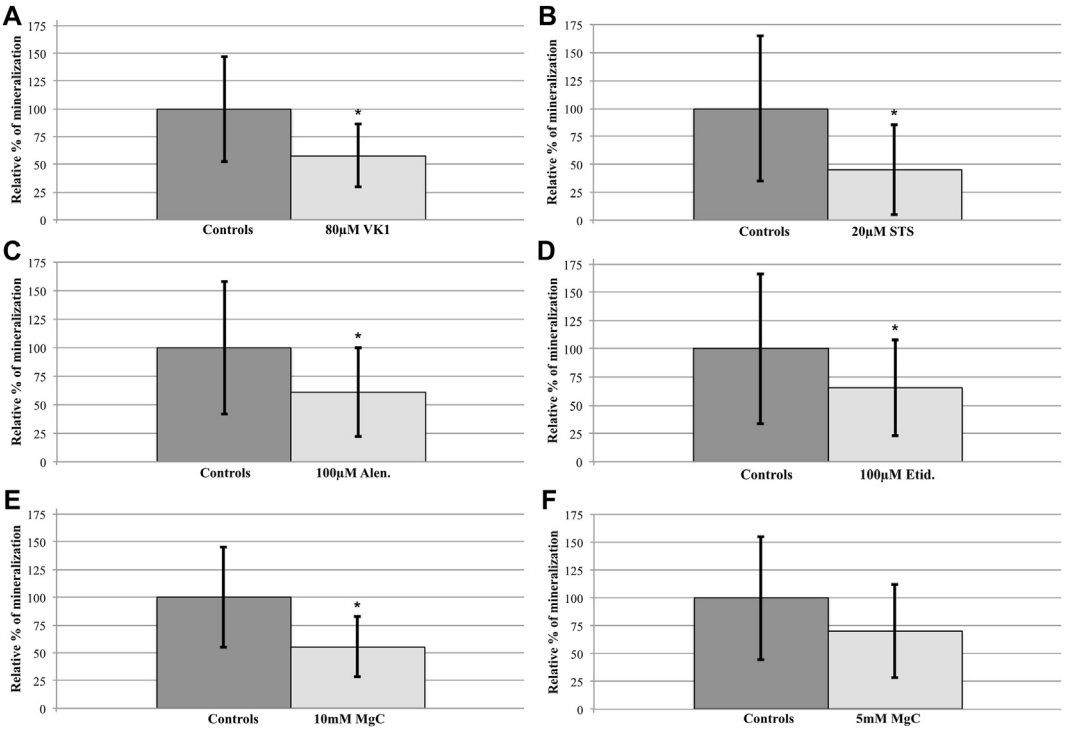

FIGURE 2 | Compound treatment effects on the abcc6a$^{cmg52/cmg52}$ spinal hypermineralization phenotype. After semiquantification and statistical analysis, mean ± SD percentile values of the spinal mineralization were normalized per compound to the respective control values of the untreated abcc6a$^{cmg52/cmg52}$ fish. **(A)** 80 μM VK1 (58 ± 28) versus C (100 ± 48), 42% reduction **(B)** 20 μM STS (45 ± 40) versus C (100 ± 65), 55% reduction **(C)** 100 μM Etid. **(**65 ± 43) versus C (100 ± 67), 35% reduction **(D)** 100 μM Alen. (61 ± 39) versus C (100 ± 58), 39% reduction **(E)** 10 mM MgC (55 ± 27) versus C (100 ± 55), 45% reduction **(F)** 5 mM MgC (70 ± 42) versus C (100 ± 55), 30% reduction. Treatments resulted in significant reductions (*$p < 0.05$), except for 5 mM MgC.

knockouts (Mann-Whitney *U*-Test: $p < 0.05$ [C: $n = 22$, Alen: $n = 22$], **Figures 1G,H**, **Figure 2D**).

3.4 Magnesium citrate Significantly Affects Spinal Mineralization in abcc6a$^{cmg52/cmg52}$ Larvae

Initially, an experiment with 10 mM MgC-treatment doses (C: $n = 80$, MgC: $n = 80$) was performed and 8 untreated and 9 MgC-treated animals perished resulting in comparison of 72 C and 71 MgC larvae (**Table 1**). Treated abcc6a knockouts had a significant decrease in spinal mineralization by 45% (*t*-Test: $p < 0.05$ [C: $n = 22$, MgC: $n = 17$], **Figures 1I,J**, **Figure 2E**). Similar to the bisphosphonate treatments, some WT (C: $n = 2$, MgC: $n = 1$, not analyzed) and heterozygous larvae also had mineralized spinal sections. Magnesium citrate treatment significantly reduced mineralization in heterozygotes by 77% (Mann-Whitney *U*-Test: $p < 0.05$ [C: $n = 15$, MgC: $n = 7$]).

In order to determine a minimal effective dose we performed an additional experiment with 5 mM MgC as a therapeutic dose (C: $n = 80$, MgC: $n = 80$). We analyzed 79 untreated and 67 MgC-treated larvae as respectively 1 and 9 animals perished and sequencing of 4 MgC-treated animals had failed (**Table 1**). Again, spinal mineralization was detected in all genotypes but analysis of WT was not feasible due to the low number of animals. In this setup, 5 mM MgC-treatment did not significantly affect mineralization in heterozygous larvae (18% reduction, Mann-Whitney *U*-Test: $p > 0.05$ [C: $n = 21$, MgC: $n = 5$]). Similarly, spinal mineralization in knockout animals was non-significantly reduced (30%, Mann-Whitney *U*-Test: $p > 0.05$ [C: $n = 22$, MgC: $n = 14$], **Figure 2F**).

4 DISCUSSION

To date the lack of curative treatment options for PXE remains one of the main limitations in patient management. One avenue for (novel) drug discovery is to perform compound screening on animal models with a well-characterized phenotype. Therefore, we evaluated our zebrafish abcc6a knockout line, carrying the Cmg52 allele, as a candidate model. We hypothesized that treatment with compounds implicated in PXE (VK1, STS, bisphosphonates and magnesium) would have a similar effect on the spinal hypermineralization phenotype as what has been reported in PXE murine models and/or patients.

4.1 Vitamin K1

Mackay et al. and Sun et al. reported a significant reduction (rough estimate ±30–45%) in spinal mineralized area when their zebrafish abcc6a$^{-/-}$ models were treated with 80 μM vitamin K1

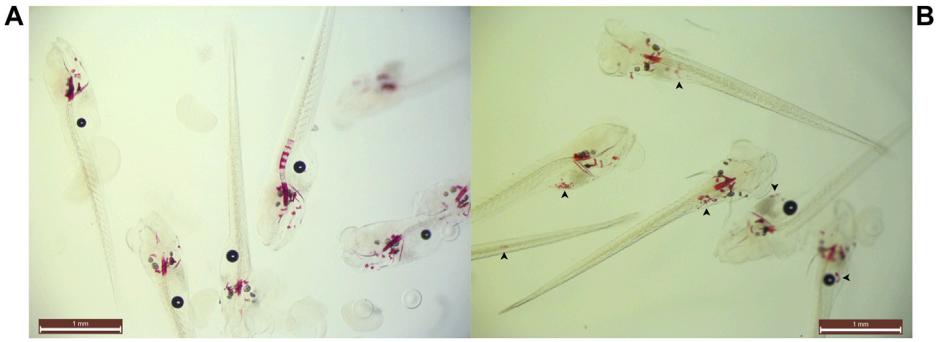

FIGURE 3 | Example of ectopic speckling following 35 μM STS-treatment. Snapshot group images of **(A)** control and **(B)** 35 μM STS-treated larvae at 10 dpf with unknown genotypes. 35μM sodium thiosulfate abolished spinal mineralization and concomitantly ventral mineralized nodules were identified (arrowheads) in all treated animals. Opacity of the specimens prevented identification of the anatomical sites of the nodules.

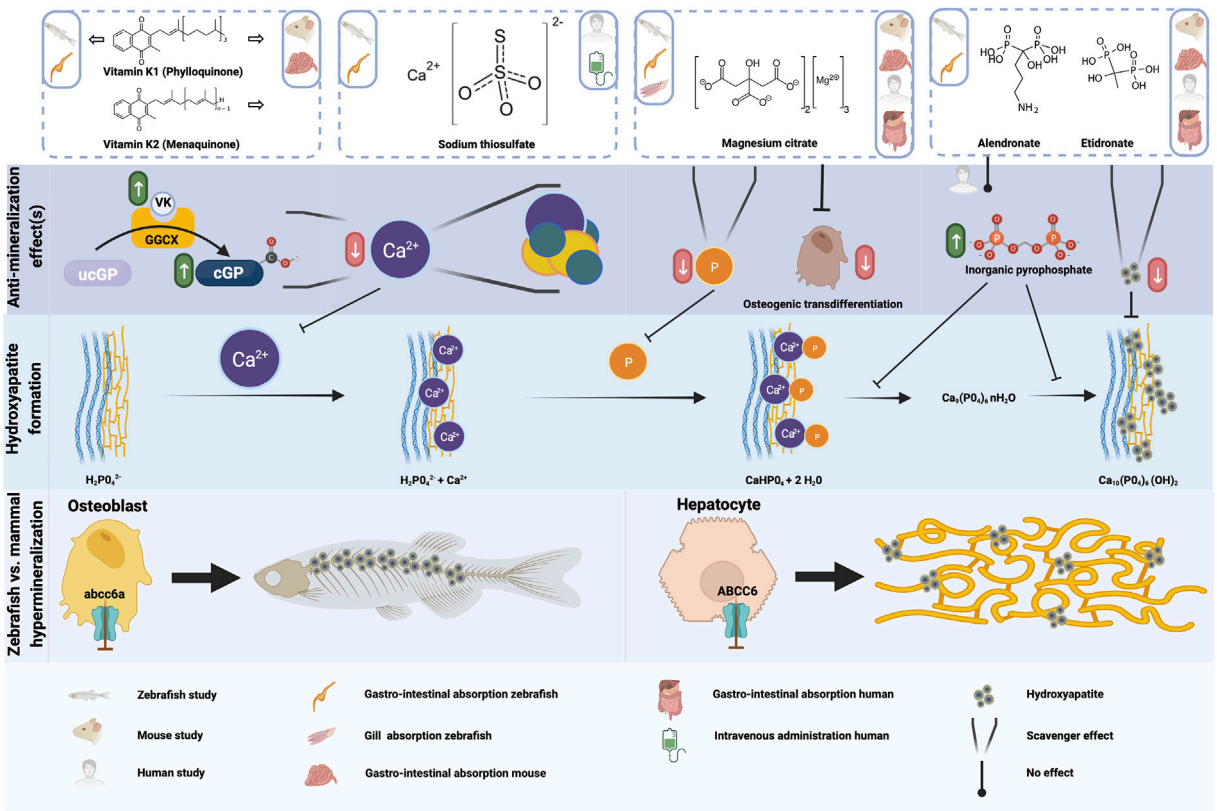

FIGURE 4 | Schematic representation of the anti-mineralization effects of the tested compounds. For the compounds evaluated in the present study, the type of administration or absorption is mentioned in the top row, as well as the type of administration used in any mouse or human studies which were done with this compound. The anti mineralizing effects of the different compounds are shown, as well as where these effect take place in the cascade to form hydroxyapatite crystals. Finally, the differences between the hypermineralization in zebrafish and mammals with respect to abcc6a and ABCC6 deficiency are shown. Figure created with BioRender.com.

(Mackay et al., 2015; Sun et al., 2021). In our setup we found a comparable reduction of 42%, verifying that VK1-treatment has an effect on spinal mineralization, at least in abcc6a$^{-/-}$ zebrafish models. While reduced VK1 serum levels have been reported in PXE patients (Vanakker et al., 2010), beneficial effects of VK1 supplementation against ectopic mineralization could not be demonstrated in rodent models (Brampton et al., 2011; Gorgels et al., 2011; Jiang et al., 2011). This was also the reason behind the lack of human trials for vitamin K supplementation. Expression sites of abcc6a in zebrafish and

ABCC6 in mammals–as well as parts of the affected mineralization sites (Mackay et al., 2015; Sun et al., 2021)–are considerably different which could explain the differential effect of VK1. ABCC6 is predominantly expressed by hepatic (and renal) tissue in mammals with loss-of-function primarily resulting in ectopic calcifications in skin, eye and vascular tissues (Gorgels et al., 2005). By contrast, abcc6a expression coincides with osteoblast-like cells in the craniofacial bones and notochord and, concomitant with VK homeostasis markers, appears to be enriched in the intervertebral disc regions (Fernández et al., 2015; Mackay et al., 2015) (**Figure 4**). Hence, Abcc6a expression is more local at the sites of hypermineralization compared to ABCC6. Though no conclusive data has been established to date, VK might mitigate abcc6a-related dysfunction (e.g. oxidative stress, VK-dependent carboxylation) more readily at the local level in zebrafish compared to the peripheral effects in mammals (Fernández et al., 2015; Nollet et al., 2019). Another consideration herein could be the difference in administration of the compounds. While mouse models were "periodically" subjected to VK supplementation via the chow or via peritoneal injection, zebrafish models were continuously exposed due to immersion into the compound solution. Moreover, zebrafish were treated much earlier during development (i.e. starting in the embryonic stage and pre-mineralization) while only one study investigated the effect of vitamin K treatment in developing mice (Brampton et al., 2011).

While rodent model data appear negative, the existence of a PXE-like disorder with coagulation factor deficiency–caused by GGCX (Gamma-Glutamyl Carboxylase) mutations–where VK-dependent carboxylation is (nearly) abolished suggests an important role for VK in mineralization homeostasis (Vanakker et al., 2010). In addition, warfarin treatment–which blocks vitamin K recycling–exacerbates the aberrant mineralization in both murine and zebrafish PXE models (Li et al., 2013; Mackay et al., 2015). Taken together, there might be a role for VK in mammalian PXE-related mineralization, perhaps as an attenuator of processes via matrix gla protein (MGP) (Theuwissen et al., 2012). Moreover, VK may have a slow impact as beneficial effects have only been reported in a single human cardiovascular disease clinical trial after 3 years of vitamin K supplementation (Vlasschaert et al., 2020). Considering any trial investigating VK in PXE murine models has not lasted longer than a few months, such putative late-onset effects could have been missed.

4.2 Sodium Thiosulfate

Sodium thiosulfate functions as an antioxidant agent and as a chelator capable of dissolving precipitated calcium phosphate-based crystals (**Figure 4**). As such it has been used to treat various ectopic mineralization disorders (e.g. calciphylaxis in chronic kidney disease (Peng et al., 2018), calcinosis cutis (Von Hodenberg et al., 2020; López-Sundh et al., 2021) and one case of severe pseudoxanthoma elasticum (Omarjee et al., 2020)). In this PXE patient, many calcified lesions ameliorated and calcific stenosis of celiac and mesenterial arteries was resolved following treatment (Omarjee et al., 2020). Unfortunately, the therapy requires careful follow-up and lesions quickly reformed after cessation of treatment (Omarjee et al., 2020).

Here we report that 20 μM STS-treatment significantly reduced the spinal mineralization in abcc6a$^{cmg52/cmg52}$ zebrafish by 55%. It appears that dosage should be carefully considered as, despite its tolerability, we discovered a peculiar side effect (i.e. the ventral ectopic spots in wild type, heterozygous and knockout fish) of 35 μM STS-treatment. We are unsure how this spotting pattern occurred as STS-chelated calcium and phosphate particles would normally be excreted into the environment. These ventral sites appear to rudimentary co-locate with the gastrointestinal tract (GIT) but further investigation is required to understand the underlying mechanisms. We see no explanation for this from our experimental set-up; the zebrafish GIT has pH-levels ≥7.5 and calcium thiosulfates would remain highly soluble. Moreover, the medium was refreshed daily, thereby removing excreted particles regularly. To our knowledge, aberrant calcifications due to STS have not been reported in literature. Sodium thiosulfate appears to be generally tolerable though some side effects have been reported with intravenous administration causing nausea, vomiting and metabolic acidosis (Peng et al., 2018; Omarjee et al., 2020) and topical STS-treatment occasionally causing skin irritation (Ma et al., 2019). Thus, sodium thiosulfate might be a promising candidate drug but optimized treatment schedules and diligent patient follow-up appear warranted to minimize side effects and impact on quality of life.

4.3 Bisphosphonates

Bisphosphonates are a group of compounds with structural analogy to inorganic pyrophosphate, an inhibitor of calcification (Kuźnik et al., 2020). Contrary to inorganic pyrophosphate, bisphosphonates are chemically stable and have dual activity. On the one hand these compounds bind calcium phosphate particles thereby preventing growth and sedimentation (**Figure 4**). On the other hand they inhibit bone resorption activity by inducing apoptosis of osteoclasts (Hughes et al., 1995; Rodan and Fleisch 1996). The mechanism by which bisphosphonates exert their anti-osteoclast activity is dependent on their chemical structure. Simple or non-nitrogen-based compounds (e.g. etidronate) form toxic adenosine triphosphate analogs once resorbed from bone by osteoclasts, while nitrogen-containing compounds (e.g. alendronate) inhibit farnesyl diphosphate synthase activity, ultimately suppressing resorption and inducing apoptosis (Rezska and Rodan 2003). Additionally, the nitrogen-based bisphosphonates bind to bone mineral with higher affinity than their simpler counterparts (Kuźnik et al., 2020).

Etidronate and alendronate have been evaluated prior in relation to PXE (and GACI). Intraperitoneal injections of etidronate prior to cardiac injury prevented the dystrophic cardiac calcification phenotype reported in Abcc6$^{-/-}$ mice (Pomozi et al., 2017). Similarly, subcutaneous injection or high doses of etidronate in feed (equivalent to 12x daily dose to treat osteoporosis in humans) halted ectopic mineralization in the muzzle of Abcc6$^{-/-}$ mice (Li et al., 2015, Li et al., 2016). Most importantly, a clinical trial found etidronate therapy halts arterial

calcification in most vascular beds–apart from cardiac arteries–without affecting choroidal neovascularization in PXE (Kranenburg et al., 2018; Bartstra et al., 2020; Risseeuw et al., 2020). In addition, etidronate-coated nanoparticles designed to target elastin resolved mineralization deposits in Enpp1$^{-/-}$ rat aortic cultures (Keuth et al., 2020). Finally, treatment of enpp1$^{-/-}$ zebrafish with 100 μM etidronate significantly reduced spinal hypermineralization during embryonic/larval development (Apschner et al., 2014). In agreement with the literature, treatment of our abcc6a knockout zebrafish, but not wild type or heterozygotes, with 100 μM etidronate during development significantly reduced (35%) spinal hypermineralization, likely by calcification inhibition akin to pyrophosphate. It also confirms that etidronate treatment can be effective in patients with generalized arterial calcification of infancy due to biallelic ABCC6 mutations (Nitschke et al., 2012).

In contrast to earlier reports in mice, we also found alendronate treatment to significantly reduce mineralization (Li et al., 2015; Pomozi et al., 2017). Besides putative species-dependent differences, this can also be explained by the experimental setup. Similar to etidronate, exposure to alendronate occurs much earlier in our model (i.e. prior to notochord mineralization) and was continuous instead of periodic (swimming medium versus dietary intake/injection). Nonetheless, while alendronate is typically administered to patients at much lower dosages than etidronate, our alendronate dose would equate to roughly a 20x higher dosing, which is also much higher than the 12x higher dose applied to mice (Li et al., 2015). This could be due to the higher affinity for bone of nitrogen-based bisphosphonates, suggesting that alendronate is not a feasible therapeutic option for pseudoxanthoma elasticum patients.

4.4 Magnesium Citrate

Magnesium has frequently been implicated as a modulator of cardiovascular disease risk, acting as both a phosphate-binding competitor of calcium - thus delaying calcium phosphate crystal growth - and a suppressor of osteogenic transdifferentiation (Ter Braake et al., 2017) (**Figure 4**). Similarly, dietary magnesium oxide supplementation in Mendelian soft connective tissue mineralopathies inferred beneficial effects. In PXE mouse models a 4–5x increased intake slowed ectopic calcification formation and growth (LaRusso et al., 2009; Gorgels et al., 2010; Kupetsky et al., 2013) while reduced intake exacerbated the phenotype (Jiang and Uitto 2012). Moreover, one study hinted that longer-term dietary magnesium intake might reduce carotid intima-media thickness scores in Abcc6$^{-/-}$ mice, suggesting elevated magnesium intake can ameliorate vascular disease (Kupetsky-Rincon et al., 2012). Additionally, *in utero* development of GACI was prevented if pregnant mice were placed on a high magnesium diet (Kingman et al., 2017). A clinical trial in pseudoxanthoma elasticum patients, however, failed to demonstrate a clear effect of magnesium, though the data interpretation was hampered by clinical variability between patients, confounding effects of parallel treatments (e.g. for the ophthalmological endpoints) and very strict limitations on magnesium dosage (despite it being well tolerated) (Rose et al., 2019). While promising, early and prolonged exposure to high doses (i.e. 10x increase) of dietary magnesium may negatively affect bone mineralization (Ter Braake et al., 2020).

In our experiments we used magnesium citrate. Citrate is suggested to have a regulatory role in bone matrix as it binds to hydroxyapatite crystals and even inhibits transformation of precursor molecules into hydroxyapatite crystals (Hu et al., 2010; Wu et al., 2021). Citrate had not been linked to ectopic mineralization until recently when ANKH (progressive ankylosis protein homolog) was reported to transport both citrate and ATP (Szeri et al., 2020). As ANKH is part of the ectopic mineralization paradigm and appears to be downregulated in PXE fibroblasts (Boraldi et al., 2014; Van Gils et al., 2019) citrate supplementation could potentially benefit pseudoxanthoma elasticum patients. We showed that magnesium citrate has a dosage dependent beneficial effect on the spinal hypermineralization phenotype in the abcc6a$^{cmg52/cmg52}$ larvae, reaffirming the existing literature on magnesium. The extent of the contribution of citrate to the observed anti-mineralization effect remains to be determined, but magnesium and possibly citrate appear to be interesting candidates for therapeutic intervention in pseudoxanthoma elasticum.

In conclusion, our data demonstrate the utility of our CRISPR/Cas9 abcc6a knockout zebrafish model for PXE-specific compound screening studies. While the spinal phenotype certainly differs from the mammalian and patient phenotype, the PXE zebrafish model has several significant benefits. The outbred background paired with high fecundity (i.e. increased sample sizes) would likely enhance the robustness of identified correlations as it better mimics the diversity in genetic background of patients. In addition, the relatively speedy analysis and reduced amounts of compound necessary assert zebrafish as an interesting first line model for discovery of therapeutics or for identification of repurposable drugs already approved for patient care (Brueggeman et al., 2019; Widrick et al., 2019).

DATA AVAILABILITY STATEMENT

The original contributions presented in the study are included in the article/**Supplementary Material**, further inquiries can be directed to the corresponding author.

ETHICS STATEMENT

The animal study was reviewed and approved by Ghent University Animal Experimentation Committee.

AUTHOR CONTRIBUTIONS

Design of the study: MG, OV, AW Experimental work: MG Experimental supervision: PC Data-analysis: MG, OV, AW, PC

First draft writing: MG Manuscript editing and revision of final version: MG, OV, AW, PC Study financing: OV, PC.

FUNDING

MG is supported by a BOF research fellowship from the Ghent University. OV is a Senior Clinical Investigator of the Research Foundation Flanders (FWO), Belgium. This research was also supported by a Methusalem grant (BOF08/01M01108) and a GOA grant (GOA019-21) from the Ghent University.

ACKNOWLEDGMENTS

We would like to thank Hanna De Saffel and Karen Vermeulen for their help as animal caretakers in the Ghent Zebrafish Facility.

SUPPLEMENTARY MATERIAL

The Supplementary Material for this article can be found online at: https://www.frontiersin.org/articles/10.3389/fphar.2022.822143/full#supplementary-material

REFERENCES

Apschner, A., Huitema, L. F., Ponsioen, B., Peterson-Maduro, J., and Schulte-Merker, S. (2014). Zebrafish *Enpp1* Mutants Exhibit Pathological Mineralization, Mimicking Features of Generalized Arterial Calcification of Infancy (GACI) and Pseudoxanthoma Elasticum (PXE). *Dis. Model. Mech.* 7, 811–822. doi:10.1242/dmm.015693

Bartstra, J. W., de Jong, P. A., Kranenburg, G., Wolterink, J. M., Isgum, I., Wijsman, A., et al. (2020). Etidronate Halts Systemic Arterial Calcification in Pseudoxanthoma Elasticum. *Atherosclerosis* 292, 37–41. doi:10.1016/j.atherosclerosis.2019.10.004

Boraldi, F., Annovi, G., Bartolomeo, A., and Quaglino, D. (2014). Fibroblasts from Patients Affected by Pseudoxanthoma Elasticum Exhibit an Altered PPi Metabolism and Are More Responsive to Pro-calcifying Stimuli. *J. Dermatol. Sci.* 74, 72–80. doi:10.1016/j.jdermsci.2013.12.008

Brampton, C., Yamaguchi, Y., Vanakker, O., Van Laer, L., Chen, L. H., Thakore, M., et al. (2011). Vitamin K Does Not Prevent Soft Tissue Mineralization in a Mouse Model of Pseudoxanthoma Elasticum. *Cell Cycle* 10, 1810–1820. doi:10.4161/cc.10.11.15681

Brueggeman, L., Sturgeon, M. L., Martin, R. M., Grossbach, A. J., Nagahama, Y., Zhang, A., et al. (2019). Drug Repositioning in Epilepsy Reveals Novel Antiseizure Candidates. *Ann. Clin. Transl Neurol.* 6, 295–309. doi:10.1002/acn3.703

Cotti, S., Huysseune, A., Koppe, W., Rücklin, M., Marone, F., Wölfel, E. M., et al. (2020). More Bone with Less Minerals? the Effects of Dietary Phosphorus on the post-cranial Skeleton in Zebrafish. *Int. J. Mol. Sci.* 21, 5429. doi:10.3390/ijms21155429

Fernández, I., Vijayakumar, P., Marques, C., Cancela, M. L., Gavaia, P. J., and Laizé, V. (2015). Zebrafish Vitamin K Epoxide Reductases: Expression *In Vivo*, along Extracellular Matrix Mineralization and under Phylloquinone and Warfarin *In Vitro* Exposure. *Fish. Physiol. Biochem.* 41, 745–759. doi:10.1007/s10695-015-0043-z

Gorgels, T. G., Hu, X., Scheffer, G. L., van der Wal, A. C., Toonstra, J., de Jong, P. T., et al. (2005). Disruption of *Abcc6* in the Mouse: Novel Insight in the Pathogenesis of Pseudoxanthoma Elasticum. *Hum. Mol. Genet.* 14, 1763–1773. doi:10.1093/hmg/ddi183

Gorgels, T. G., Waarsing, J. H., de Wolf, A., ten Brink, J. B., Loves, W. J., and Bergen, A. A. (2010). Dietary Magnesium, Not Calcium, Prevents Vascular Calcification in a Mouse Model for Pseudoxanthoma Elasticum. *J. Mol. Med. (Berl)* 88, 467–475. doi:10.1007/s00109-010-0596-3

Gorgels, T. G., Waarsing, J. H., Herfs, M., Versteeg, D., Schoensiegel, F., Sato, T., et al. (2011). Vitamin K Supplementation Increases Vitamin K Tissue Levels but Fails to Counteract Ectopic Calcification in a Mouse Model for Pseudoxanthoma Elasticum. *J. Mol. Med. (Berl)* 89, 1125–1135. doi:10.1007/s00109-011-0782-y

Howe, K., Clark, M. D., Torroja, C. F., Torrance, J., Berthelot, C., Muffato, M., et al. (2013). The Zebrafish Reference Genome Sequence and its Relationship to the Human Genome. *Nature* 496, 498–503. doi:10.1038/nature12111

Hu, Y. Y., Rawal, A., and Schmidt-Rohr, K. (2010). Strongly Bound Citrate Stabilizes the Apatite Nanocrystals in Bone. *Proc. Natl. Acad. Sci. U S A.* 107, 22425–22429. doi:10.1073/pnas.1009219107

Hughes, D. E., Wright, K. R., Uy, H. L., Sasaki, A., Yoneda, T., Roodman, G. D., et al. (1995). Bisphosphonates Promote Apoptosis in Murine Osteoclasts *In Vitro* and *In Vivo*. *J. Bone Miner. Res.* 10, 1478–1487. doi:10.1002/jbmr.5650101008

Jiang, Q., Li, Q., Grand-Pierre, A. E., Schurgers, L. J., and Uitto, J. (2011). Administration of Vitamin K Does Not Counteract the Ectopic Mineralization of Connective Tissues in Abcc6 (-/-) Mice, a Model for Pseudoxanthoma Elasticum. *Cell Cycle* 10, 701–707. doi:10.4161/cc.10.4.14862

Jiang, Q., and Uitto, J. (2012). Restricting Dietary Magnesium Accelerates Ectopic Connective Tissue Mineralization in a Mouse Model of Pseudoxanthoma Elasticum (Abcc6(-/-)). *Exp. Dermatol.* 21, 694–699. doi:10.1111/j.1600-0625.2012.01553.x

Keuth, J., Nitschke, Y., Mulac, D., Riehemann, K., Rutsch, F., and Langer, K. (2020). Reversion of Arterial Calcification by Elastin-Targeted DTPA-HSA Nanoparticles. *Eur. J. Pharm. Biopharm.* 150, 108–119. doi:10.1016/j.ejpb.2020.03.007

Kingman, J., Uitto, J., and Li, Q. (2017). Elevated Dietary Magnesium during Pregnancy and Postnatal Life Prevents Ectopic Mineralization in *Enpp1asj* Mice, a Model for Generalized Arterial Calcification of Infancy. *Oncotarget* 8, 38152–38160. doi:10.18632/oncotarget.16687

Kranenburg, G., de Jong, P. A., Bartstra, J. W., Lagerweij, S. J., Lam, M. G., Ossewaarde-van Norel, J., et al. (2018). Etidronate for Prevention of Ectopic Mineralization in Patients with Pseudoxanthoma Elasticum. *J. Am. Coll. Cardiol.* 71, 1117–1126. doi:10.1016/j.jacc.2017.12.062

Kupetsky, E. A., Rincon, F., and Uitto, J. (2013). Rate of Change of Carotid Intima-media Thickness with Magnesium Administration in Abcc6$^{-/-}$ Mice. *Clin. Transl. Sci.* 6, 485–486. doi:10.1111/cts.12057

Kupetsky-Rincon, E. A., Li, Q., and Uitto, J. (2012). Magnesium Reduces Carotid Intima-media Thickness in a Mouse Model of Pseudoxanthoma Elasticum: A Novel Treatment Biomarker. *Clin. Transl. Sci.* 5, 259–264. doi:10.1111/j.1752-8062.2011.00390.x

Kuźnik, A., Październiok-Holewa, A., Jewula, P., and Kuźnik, N. (2020). Bisphosphonates-much More Than Only Drugs for Bone Diseases. *Eur. J. Pharmacol.* 866, 172773. doi:10.1016/j.ejphar.2019.172773

LaRusso, J., Li, Q., Jiang, Q., and Uitto, J. (2009). Elevated Dietary Magnesium Prevents Connective Tissue Mineralization in a Mouse Model of Pseudoxanthoma Elasticum (*Abcc6(-/-)*). *J. Invest. Dermatol.* 129, 1388–1394. doi:10.1038/jid.2008.391

Li, Q., Guo, H., Chou, D. W., Berndt, A., Sundberg, J. P., and Uitto, J. (2014). Mouse Models for Pseudoxanthoma Elasticum: Genetic and Dietary Modulation of the Ectopic Mineralization Phenotypes. *PLoS ONE* 9, e89268. doi:10.1371/journal.pone.0089268

Li, Q., Guo, H., Chou, D. W., Harrington, D. J., Schurgers, L. J., Terry, S. F., et al. (2013). Warfarin Accelerates Ectopic Mineralization in *Abcc6(-/-)* Mice: Clinical Relevance to Pseudoxanthoma Elasticum. *Am. J. Pathol.* 182, 1139–1150. doi:10.1016/j.ajpath.2012.12.037

Li, Q., Kingman, J., Sundberg, J. P., Levine, M. A., and Uitto, J. (2016). Etidronate Prevents, but Does Not Reverse, Ectopic Mineralization in a Mouse Model of Pseudoxanthoma Elasticum (Abcc6-/-). *Oncotarget* 9, 30721–30730. doi:10.18632/oncotarget.10738

Li, Q., Sundberg, J. P., Levine, M. A., Terry, S. F., and Uitto, J. (2015). The Effects of Bisphosphonates on Ectopic Soft Tissue Mineralization Caused by Mutations in

the *ABCC6* Gene. *Cell Cycle* 14, 1082–1089. doi:10.1080/15384101.2015.1007809

López-Sundh, A. E., Quintana-Sancho, A., Durán-Vian, C., Reguero-DelCura, L., Corrales-Martínez, A. F., Gómez-Fernández, C., et al. (2021). Clinical and Ultrasound Response to Intralesional Sodium Thiosulfate for the Treatment of Calcinosis Cutis in the Setting of Systemic Sclerosis. A Case-Based Review. *Clin. Rheumatol.* 40, 2985–2989. doi:10.1007/s10067-020-05523-4

Ma, J. E., Ernste, F. C., Davis, M. D. P., and Wetter, D. A. (2019). Topical Sodium Thiosulfate for Calcinosis Cutis Associated with Autoimmune Connective Tissue Diseases: The Mayo Clinic Experience, 2012-2017. *Clin. Exp. Dermatol.* 44, e189–92. doi:10.1111/ced.13782

Mackay, E. W., Apschner, A., and Schulte-Merker, S. (2015). Vitamin K Reduces Hypermineralisation in Zebrafish Models of PXE and GACI. *Development* 142, 1095–1101. doi:10.1242/dev.113811

Moore, S. N., Tanner, S. B., and Schoenecker, J. G. (2015). Bisphosphonates: From Softening Water to Treating PXE. *Cell Cycle* 14, 1354–1355. doi:10.1080/15384101.2015.1024585

Nitschke, Y., Baujat, G., Botschen, U., Wittkampf, T., du Moulin, M., Stella, J., et al. (2012). Generalized Arterial Calcification of Infancy and Pseudoxanthoma Elasticum Can Be Caused by Mutations in Either *ENPP1* or *ABCC6*. *Am. J. Hum. Genet.* 90, 25–39. doi:10.1016/j.ajhg.2011.11.020

Nitschke, Y., and Rutsch, F. (2012). Generalized Arterial Calcification of Infancy and Pseudoxanthoma Elasticum: Two Sides of the Same coin. *Front. Genet.* 3, 302. doi:10.3389/fgene.2012.00302

Nollet, L., Van Gils, M., Verschuere, S., and Vanakker, O. (2019). The Role of Vitamin K and its Related Compounds in Mendelian and Acquired Ectopic Mineralization Disorders. *Int. J. Mol. Sci.* 20, 2142. doi:10.3390/ijms20092142

Omarjee, L., Nitschke, Y., Verschuere, S., Bourrat, E., Vignon, M. D., Navasiolava, N., et al. (2020). Severe Early-Onset Manifestations of Pseudoxanthoma Elasticum Resulting from the Cumulative Effects of Several Deleterious Mutations in *ENPP1*, *ABCC6* and *HBB*: Transient Improvement in Ectopic Calcification with Sodium Thiosulfate. *Br. J. Dermatol.* 183, 367–372. doi:10.1111/bjd.18632

Pazianas, M., and Abrahamsen, B. (2011). Safety of Bisphosphonates. *Bone* 49, 103–110. doi:10.1016/j.bone.2011.01.003

Peng, T., Zhuo, L., Wang, Y., Jun, M., Li, G., Wang, L., et al. (2018). Systematic Review of Sodium Thiosulfate in Treating Calciphylaxis in Chronic Kidney Disease Patients. *Nephrology (Carlton)* 23, 669–675. doi:10.1111/nep.13081

Pomozi, V., Brampton, C., van de Wetering, K., Zoll, J., Calio, B., Pham, K., et al. (2017). Pyrophosphate Supplementation Prevents Chronic and Acute Calcification in *ABCC6*-Deficient Mice. *Am. J. Pathol.* 187, 1258–1272. doi:10.1016/j.ajpath.2017.02.009

Reszka, A. A., and Rodan, G. A. (2003). Mechanism of Action of Bisphosphonates. *Curr. Osteoporos. Rep.* 1, 45–52. doi:10.1007/s11914-003-0008-5

Risseeuw, S., van Leeuwen, R., Imhof, S. M., de Jong, P. A., Mali, W. P. T. M., Spiering, W., et al. (2020). The Effect of Etidronate on Choroidal Neovascular Activity in Patients with Pseudoxanthoma Elasticum. *PLoS ONE* 15, e0240970. doi:10.1371/journal.pone.0240970

Rodan, G. A., and Fleisch, H. A. (1996). Bisphosphonates: Mechanisms of Action. *J. Clin. Invest.* 97, 2692–2696. doi:10.1172/JCI118722

Rose, S., On, S. J., Fuchs, W., Chen, C., Phelps, R., Kornreich, D., et al. (2019). Magnesium Supplementation in the Treatment of Pseudoxanthoma Elasticum: A Randomized Trial. *J. Am. Acad. Dermatol.* 81, 263–265. doi:10.1016/j.jaad.2019.02.055

Schneider, C. A., Rasband, W. S., and Eliceiri, K. W. (2012). NIH Image to ImageJ: 25 Years of Image Analysis. *Nat. Methods* 9, 671–675. doi:10.1038/nmeth.2089

Sun, J., She, P., Liu, X., Gao, B., Jin, D., and Zhong, T. P. (2021). Disruption of *Abcc6* Transporter in Zebrafish Causes Ocular Calcification and Cardiac Fibrosis. *Ijms* 22, 278. doi:10.3390/ijms22010278

Szeri, F., Lundkvist, S., Donnelly, S., Engelke, U. F. H., Rhee, K., Williams, C. J., et al. (2020). The Membrane Protein ANKH Is Crucial for Bone Mechanical Performance by Mediating Cellular export of Citrate and ATP. *Plos Genet.* 16, e1008884. doi:10.1371/journal.pgen.1008884

Ter Braake, A. D., Shanahan, C. M., and de Baaij, J. H. F. (2017). Magnesium Counteracts Vascular Calcification: Passive Interference or Active Modulation. *Arterioscler Thromb. Vasc. Biol.* 37, 1431–1445. doi:10.1161/ATVBAHA.117.309182

Ter Braake, A. D., Smit, A. E., Bos, C., van Herwaarden, A. E., Alkema, W., van Essen, H. W., et al. (2020). Magnesium Prevents Vascular Calcification in Klotho Deficiency. *Kidney Int.* 97, 487–501. doi:10.1016/j.kint.2019.09.034

Theuwissen, E., Smit, E., and Vermeer, C. (2012). The Role of Vitamin K in Soft-Tissue Calcification. *Adv. Nutr.* 3, 166–173. doi:10.3945/an.111.001628

Van Gils, M., Nollet, L., Verly, E., Deianova, N., and Vanakker, O. M. (2019). Cellular Signaling in Pseudoxanthoma Elasticum: An Update. *Cell Signal* 55, 119–129. doi:10.1016/j.cellsig.2018.12.009

Van Gils, M., Willaert, A., De Vilder, E. Y. G., Coucke, P. J., and Vanakker, O. M. (2018). Generation and Validation of a Complete Knockout Model of *Abcc6a* in Zebrafish. *J. Invest. Dermatol.* 138, 2333–2342. doi:10.1016/j.jid.2018.06.183

Vanakker, O. M., Martin, L., Schurgers, L. J., Quaglino, D., Costrop, L., Vermeer, C., et al. (2010). Low Serum Vitamin K in PXE Results in Defective Carboxylation of Mineralization Inhibitors Similar to the *GGCX* Mutations in the PXE-like Syndrome. *Lab. Invest.* 90, 895–905. doi:10.1038/labinvest.2010.68

Vlasschaert, C., Goss, C. J., Pilkey, N. G., McKeown, S., and Holden, R. M. (2020). Vitamin K Supplementation for the Prevention of Cardiovascular Disease: Where Is the Evidence? A Systematic Review of Controlled Trials. *Nutrients* 12, 2909. doi:10.3390/nu12102909

Von Hodenberg, C., Neufeld, M., Wohlrab, J., Meyer, D., Ehrchen, J., and Sunderkötter, C. (2020). Topical Sodium Thiosulfate: a Reliable Treatment for Digital Calcinosis Cutis - a Case Series with Six Patients. *J. Dtsch. Dermatol. Ges.* 18, 1181–1183. doi:10.1111/ddg.14191

Westerfield, M. (2000). *The Zebrafish Book. A Guide for the Laboratory Use of Zebrafish (*Danio rerio*)*. 4th ed. Eugene: University of Oregon Press.

Widrick, J. J., Kawahara, G., Alexander, M. S., Beggs, A. H., and Kunkel, L. M. (2019). Discovery of Novel Therapeutics for Muscular Dystrophies Using Zebrafish Phenotypic Screens. *J. Neuromuscul. Dis.* 6, 271–287. doi:10.3233/JND-190389

Wu, X., Dai, H., Yu, S., Zhao, Y., Long, Y., Li, W., et al. (2021). Citrate Regulates Extracellular Matrix Mineralization during Osteoblast Differentiation *In Vitro*. *J. Inorg. Biochem.* 214, 111269. doi:10.1016/j.jinorgbio.2020.111269

Conflict of Interest: The authors declare that the research was conducted in the absence of any commercial or financial relationships that could be construed as a potential conflict of interest.

Publisher's Note: All claims expressed in this article are solely those of the authors and do not necessarily represent those of their affiliated organizations, or those of the publisher, the editors and the reviewers. Any product that may be evaluated in this article, or claim that may be made by its manufacturer, is not guaranteed or endorsed by the publisher.

frontiers | Frontiers in Pharmacology

REVIEW
published: 06 April 2022
doi: 10.3389/fphar.2022.887253

Vascular Calcification: New Insights Into BMP Type I Receptor A

Zhixing Niu[1], Guanyue Su[2], Tiantian Li[2], Hongchi Yu[2], Yang Shen[2], Demao Zhang[1,2] and Xiaoheng Liu[2]**

[1]State Key Laboratory of Oral Diseases, West China Hospital of Stomatology, Sichuan University, Chengdu, China, [2]West China School of Basic Medical Sciences & Forensic Medicine, Sichuan University, Chengdu, China

Vascular calcification (VC) is a complex ectopic calcification process and an important indicator of increased risk for diabetes, atherosclerosis, chronic kidney disease, and other diseases. Therefore, clarifying the pathogenesis of VC is of great clinical significance. Numerous studies have shown that the onset and progression of VC are similar to bone formation. Members of the bone morphogenetic protein (BMP) family of proteins are considered key molecules in the progression of vascular calcification. BMP type I receptor A (BMPR1A) is a key receptor of BMP factors acting on the cell membrane, is widely expressed in various tissues and cells, and is an important "portal" for BMP to enter cells and exert their biological effect. In recent years, many discoveries have been made regarding the occurrence and treatment of ectopic ossification-related diseases involving BMP signaling targets. Studies have confirmed that BMPR1A is involved in osteogenic differentiation and that its high expression in vascular endothelial cells and smooth muscle cells can lead to vascular calcification. This article reviews the role of BMPR1A in vascular calcification and the possible underlying molecular mechanisms to provide clues for the clinical treatment of such diseases.

Keywords: vascular calcification, BMPR1A, VSMCs, ECS, atherosclerosis

OPEN ACCESS

Edited by:
Kang Xu,
Hubei University of Chinese Medicine, China

Reviewed by:
Dangheng Wei,
University of South China, China
Yanfang Zhao,
University of Alabama at Birmingham, United States
Anna Malashicheva,
Institute of Cytology, Russia

****Correspondence:***
Demao Zhang
demao.zhang666@foxmail.com
Xiaoheng Liu
liuxiaohg@scu.edu.cn

Specialty section:
This article was submitted to Experimental Pharmacology and Drug Discovery, a section of the journal Frontiers in Pharmacology

Received: *01 March 2022*
Accepted: *21 March 2022*
Published: *06 April 2022*

Citation:
Niu Z, Su G, Li T, Yu H, Shen Y, Zhang D and Liu X (2022) Vascular Calcification: New Insights Into BMP Type I Receptor A. Front. Pharmacol. 13:887253. doi: 10.3389/fphar.2022.887253

INTRODUCTION

Vascular calcification (VC) is an important indicator of increased risk for diabetes, atherosclerosis, chronic kidney disease (CKD), and other diseases. It is also a key factor for the high morbidity and mortality of cardiovascular and cerebrovascular diseases (Demer and Tintut, 2008; Schenker et al., 2008; Shroff and Shanahan, 2010). VC is characterized by the deposition of mineral calcium as a calcium-phosphate complex in the vascular wall system; its pathogenesis and progression are very similar to those of bone formation (Lee et al., 2020). Both processes involve the activation of bone matrix proteins, calcification-inducing factors, and various signaling pathways in diverse cell types, including vascular smooth muscle cells (VSMCs), macrophages, and endothelial cells (Ecs). At present, our understanding of the pathogenesis of VC includes aging, chronic inflammation, calcium-phosphorus imbalance, oxidative stress, and mitochondrial dysfunction. Recently, the bone-vascular axis theory has provided a new paradigm for the study of VC. It has been found that the ectopic calcification of the vessel wall is often associated with decreased bone density or disturbances in bone metabolism. This phenomenon occurs mostly in postmenopausal women and patients with chronic kidney disease and osteoporosis (Persy and D'haese, 2009; Gu et al., 2020). Based on the theory of bone-vascular axis, many studies have reported the role of BMP ligands in vascular calcification, while BMPR1A, the key receptor of BMPs, has rarely been reported. Studies have confirmed that BMPR1A is necessary for chondrogenesis and osteogenesis, and its

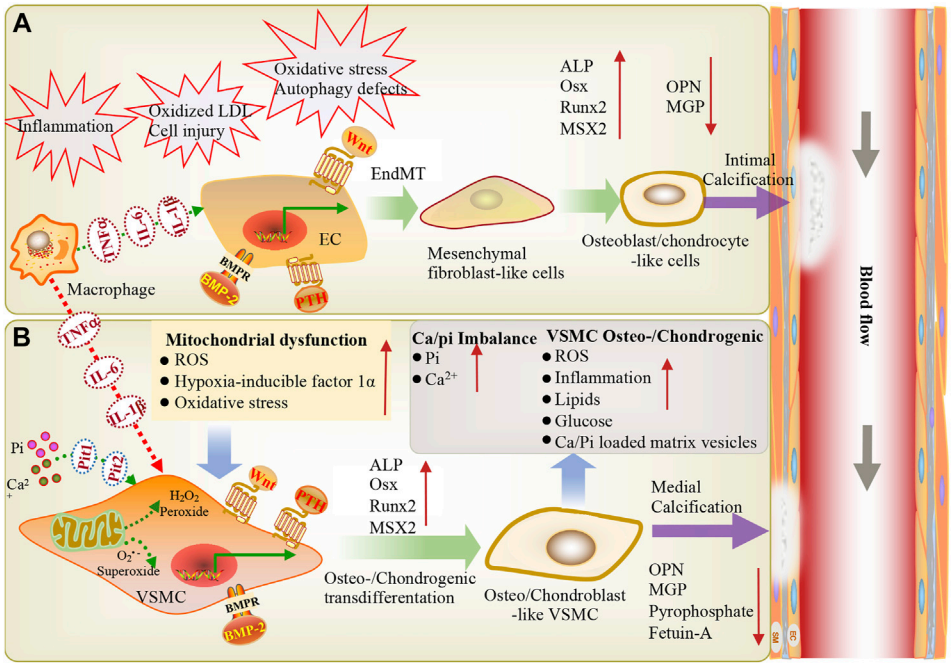

FIGURE 1 | During inflammation, macrophages infiltrate through EC adhesion and migration across endothelial cells, resulting in macrophage activation and the release of inflammatory cytokines (TNF-α, IL-6, IL-1β), further stimulating VSMCs and ECs, eventually leading to vascular calcification. Vascular endothelial cells exposed to shear stress induced by blood flow are more sensitive to shear stress-induced EndMT and BMP-induced osteogenic differentiation, thereby triggering endothelial damage and inducing vascular calcification. **(A)** Endothelial cells can be stimulated via inflammation, oxidative LDL aggregation, cell injury, oxidative stress, and autophagy defects. BMP, PTH and Wnt signaling are involved in endothelial mesenchymal transformation, the differentiation of endothelial cells into mesenchymal fibroblasts, and their further differentiation into osteoblast-like cells. These changes are accompanied by a high expression of osteogenic genes (ALP, Runx2, BMP2, MSX2) and low expression of the calcification inhibitor MGP, leading to intimal calcification. **(B)** Ca^{2+}/P_i imbalance and mitochondrial dysfunction lead to reactive oxygen species production and oxidative stress. BMP, Wnt, and PTH signaling induce the osteogenic/chondrogenic differentiation of vascular smooth muscle cells, ultimately leading to medial calcification. EC: endothelial cells; VSMC: vascular smooth muscle cell; ALP: alkaline phosphatase; Pit1, Pit2: NaPi cotransporters; LDL: low-density lipoprotein; OPN: osteopontin; PTH: parathyroid hormone; Runx2: runt-related transcription factor-2; Msx2: msh homeobox-2; IL1-β: interleukin-1 beta; IL-6: interleukin-6; Osx: osterix; EndMT: endothelial-mesenchymal transition; BMP: Bone morphogenetic protein; ROS: Reactive oxygen species; TNF-α: tumor necrosis alpha; Pi: inorganic phosphate.

overexpression in vascular smooth muscle cells can lead to VC (Mang et al., 2020; Yang et al., 2020). Although BMPR1A has been proposed to be involved in vascular calcification, the specific mechanism remains unclear. In this review, we focus on the role of BMPR1A in vascular calcification and the possible underlying molecular mechanisms to explore its potential therapeutic implications. First, we discussed VC and BMPR1A signaling, followed by its effects on ECs and smooth muscle cells (SMCs), and how an imbalance in BMPR1A signaling leads to VC.

VASCULAR CALCIFICATION

Inducing Factors and Mechanism of Vascular Calcification

VC is a complex process, and numerous *ex vivo* and *in vivo* studies have confirmed that VC is very similar to bone formation in terms of pathogenesis and progression (**Figure 1**) (Neven et al., 2011; Andrews et al., 2018; Durham et al., 2018). In the past few decades, the inducing factors of vascular calcification have been continuously proposed (**Table 1**). The interference of internal and external environments, such as aging, inflammation, diabetes, chronic kidney disease, oxidative stress, and mitochondrial dysfunction, can lead to VC. It has been reported that inflammation-related tumor necrosis factor (TNF-α) and interleukin-1 beta (IL-1β) can induce endothelial-mesenchymal transition (EndMT) by regulating BMPRs. These then induce osteogenic differentiation through the BMPR-JNK signaling axis, promoting vascular calcification (Sanchez-Duffhues et al., 2019). In diabetes, hyperglycemia and an imbalance in mineral ion homeostasis could lead to endothelial cell injury. Calcified vascular cells (CVCs) perceive extracellular damage signaling and induce CVCs to differentiate into osteoblast-like cells by upregulating osteogenic factors and activating Wnt signaling, promoting vascular calcification (Bartoli-Leonard et al., 2018). In chronic kidney disease, calcium and phosphorus imbalance can lead to mitochondrial dysfunction, increase the release of reactive oxygen species, trigger oxidative stress and inflammatory responses, and induce the reverse differentiation of VSMCs into osteoblast-like cells, leading to vascular calcification (Zhu et al., 2020; Phadwal et al., 2021). At the cellular level, when the structure and function of vascular endothelial cells are abnormal, the expression of proinflammatory cytokines TNF-α and IL-1β

TABLE 1 | Inducing factors and the mechanism of vascular calcification.

Inducing factors	Mechanism	References
Calciprotein particles	Phosphate/calcium homeostasis disorders and changes in hormone levels (high FGF23, low vitamin D activity, and high parathyroid hormone)	Kuro, (2021)
Oxyphospholipids and their mediators	Oxyphospholipids in macrophages promote the assembly of inflammatory bodies and the production of cytokines with calcification-promoting properties. Macrophages promote and/or enhance plaque mineralization by generating extracellular vesicles	Chignon et al. (2021)
Platelet	Platelets involved in thrombosis release various bioactive molecules, some of which have calcification-promoting properties. Signal crosstalk between platelets and vascular/valve cells can promote ectopic mineralization	Schurgers et al. (2018)
Aging	Aging causes mitochondrial dysfunction and increased ROS production, activates inflammation, increases oxidative stress, upregulates BMPs and enhances the expression of the osteogenic transcription factor Runx2, which in turn promotes vascular calcification	Kwon et al. (2017)
Inflammation	By releasing proinflammatory cytokines, endothelial cells are induced to transform into mesenchymal cells, and vascular smooth muscle cells are reversely differentiated into osteoblasts, thereby promoting vascular calcification	Sanchez-Duffhues et al. (2019)
Diabetes	Hyperglycemia and an imbalance in mineral ion homeostasis lead to endothelial cell injury. The medial mucosal layer responds by triggering the repair response. CVCs perceive extracellular signals, upregulate osteogenic factors, downregulate sirtuin-1, and activate Wnt signaling, resulting in CVC differentiation into osteogenic cells and promoting vascular calcification	Bartoli-Leonard et al. (2018)
CKD	A decrease in fetal globulin A and pyrophosphate levels, increase in serum phosphate levels (hyperphosphatemia), hyperparathyroidism, and PTH and FGF23 deficiency could lead to calcium and phosphate imbalance and promote vascular calcification	Chen et al. (2020)
Hypertension	Blood pressure fluctuation changes the production of ATP, increases ROS, and disturbs the mitochondrial network in VSMCs, leading to mitochondrial dysfunction and eventually VC.	Bartolak-Suki and Suki, (2020)
Dyslipidemia	Polarization of induced proinflammatory (M1) function in the monocyte/macrophage system leads to an increased release of proinflammatory cytokines (e.g., IL-6, IL-1β, and TNF-α) and the production of reactive oxygen species, which in turn induce the calcification of VSMCs and ECs	Torres-Castro et al. (2016)
High phosphate	High phosphate levels can directly promote VSMC calcification, leading to VSMCs transforming from the contractile to osteochondral phenotype	Bai et al. (2021)
Klotho deficiency	Klotho deficiency leads to the upregulation of BMP2, BMP4, and Runx2 expression and promotes BMP2/VitD3-induced osteogenic transdifferentiation of VSMCs, leading to vascular calcification	Lin and Sun, (2021)

can induce EndMT *via* BMP signaling, thereby inducing osteogenic differentiation and promoting vascular calcification (Sanchez-Duffhues et al., 2019). After being subjected to biological stress or injury, VSMCs can regulate the level of contractile proteins and reconstruct the extracellular matrix (ECM) or differentiate into osteoblast/chondrocyte-like cells to induce vascular calcification (Durham et al., 2018; Pescatore et al., 2019; Lu et al., 2020).

The BMP signaling pathway is vital for osteogenesis, EndMT, and VSMC calcification. Several treatment strategies for vascular calcification related to the BMP signaling pathway have been proposed. For example, BMP antagonists (LDN-193189, which targets the BMP type I receptor; or BMPRIA-Fc, which targets the BMP ligands) inhibit the BMP signaling pathway, which can reduce vascular calcification and improve the survival rate of matrix Gla protein-knockout mice (Malhotra et al., 2015). Furthermore, overexpression of the *MGP* gene inhibits the BMP signaling pathway and reduces BMPR I receptor expression, thereby reducing the formation of vascular calcification in apolipoprotein E-knockout ($ApoE^{-/-}$) mice (Nakagawa et al., 2010; Yao et al., 2010; Ducy et al., 2015; Malhotra et al., 2015). The inhibition of BMP signaling by a high-fat diet reduces intimal calcification in low-density lipoprotein receptor (LDLR)-deficient mice (Derwall et al., 2012). Dorsmorphin homologous 1 inhibits the phosphate-induced differentiation of VSMCs to osteoblast-like cells by inhibiting BMP-2 (Lin et al., 2017). Gla Rich Protein (GRP) interacts with BMP-2 and the BMP-SMAD signaling pathway, inhibiting the BMP-2 signaling pathway and SMAD1/5/8 phosphorylation *via* noggin and dorsmorphin, respectively, to reduce VSMC calcification and bone/cartilage gene expression (Willems et al., 2018).

Intimal and Medial Calcification

Depending on the mechanism of formation and location, VC can be classified as intimal or medial (Yang et al., 2020). Intimal calcification occurs in the inner layer of the blood vessel wall, in a process very similar to endochondral osteogenesis. It mainly occurs during atherosclerosis, which is caused by lipid accumulation, macrophage invasion, smooth muscle cell migration, and the proliferation or transdifferentiation of osteoblast-like cells. Medial calcification (also known as "Monckeberg's medial sclerosis") occurs in the medial layer, and it is commonly observed in aging patients or those with diabetes, CKD, or dyslipidemia. It is also related to mineral metabolism disorders, similar to intramembranous bone formation (Villa-Bellosta and O'Neill, 2018; Chen et al., 2020). In general, the process of these two types of calcification is similar to the transformation of smooth muscle cells into bone and cartilage-like cells through calcium deposition in VSMCs (Lee et al., 2020). Reduced vascular compliance is a common characteristic of both types of calcification. Whether plaque is formed *via* atherosclerosis, calcification, or medial mineralized crystal deposition, the common molecular signaling pathways for

both processes include the regulatory protein BMP2 and the transcription factor Runx2, which drive the bone formation process (Thompson and Towler, 2012; Lee et al., 2020).

THE ROLE OF BMP IN VASCULAR CALCIFICATION

BMP Signaling

BMP signaling is essential for the development of organisms and the stability of the internal environment. It was initially identified by its ability to induce bone and cartilage formation but was later found to be highly expressed during vascular calcification (Cai et al., 2012; Morrell et al., 2016). BMPs are members of the transforming growth factor beta (TGF-β) family of proteins and are expressed in various cells. They bind to receptors *via* ligands to form receptor complexes composed of type I receptors (ALK2, ALK3, and ALK6) and type II receptors (BMPR2, ACVR2A, and ACVR2B) and are widely involved in signal transduction and molecular regulatory processes. BMPs are usually produced by endothelial cells, osteoblasts, and chondrocytes in the bone. However, some studies have found that there are some BMPs in serum samples, indicating that they may circulate in the blood to act at the systemic level (Cheng et al., 2004; Simic et al., 2006). BMP signaling cannot be separated from the interaction between ligands and receptors. Upon the binding of BMP ligands to their respective receptors, type II receptors phosphorylate and activate type I receptors, which in turn phosphorylate intracellular signaling molecules, activating SMAD-dependent and SMAD-independent signaling pathways. The canonical BMP-SMAD-dependent signaling pathway activates R-SMADs (R-SMAD1, R-SMAD5, R-SMAD 8) *via* type I and type II receptors, which then bind to SMAD4 to form a complex that translocates to the nucleus, where it binds to DNA and interacts with transcription factors to regulate transcription of downstream target genes (Miyazono et al., 2005; Sieber et al., 2009; Luo et al., 2010; Cai et al., 2012). BMP-SMAD-independent signaling pathways include the ERK, JNK, and p38 MAPK signaling pathways, whose main roles include regulating apoptosis, epithelial-mesenchymal transition, cell migration, cell proliferation and differentiation, and the extracellular matrix (Yu, et al., 2002). In addition, type I BMP receptors are widely expressed in various cell types, and the affinity of BMPs for type I receptors is higher than that for type II receptors (Lavery et al., 2008). BMP2 was initially found to be an inducer of ectopic bone and can be detected in both the cartilage and bone (Urist, 1965; Nomura and Yamamoto, 2000). BMP2 can stimulate bone formation through the BMP receptor, which preferentially interacts with BMPR1A compared to other receptors (Kai et al., 2009; Mang et al., 2020).

BMPR1A in BMP Signaling

BMPR1A encodes type I TGF-β family receptors in the BMP2 and BMP4 signaling pathways (Mishina et al., 1995). Likewise, BMPR1A is also a serine/threonine kinase transmembrane protein type I receptor expressed in many tissues and plays a critical role in angiogenesis and the regulation of vascular homeostasis (Shi and Massagué, 2003; Lee et al., 2017; Sanchez-de-Diego et al., 2019). BMPR1A is the main type I receptor that transduces BMP signaling in preosteoblasts and has a higher ability to transduce BMP-SMAD signaling than BMPR1B or ACVR1 (Pan et al., 2017). In the absence of BMPR1A, the phosphorylation of Smad decreases while the activation of p38 and Erk increases, changing the balance of the BMP signaling cascade. Studies have shown that BMPR1A deficiency can lead to premature osteoblast differentiation and intramembranous ossification, which is necessary for cartilage formation and osteogenesis (Shi et al., 2017; Mang et al., 2020). Additionally, the inactivation of BMPR1A can lead to the excessive activation of downstream signaling by other BMPI receptors (T. Maruyama et al., 2021). According to a previous study, a lack of BMPR1A will impair the self-renewal, clonal expansion, and osteogenic ability of suture stem cells and plays an important role in inhibiting cell differentiation or promoting asymmetric cell division (T. Maruyama et al., 2021). Another study indicated that increased BMPR1A expression enhances the adipogenic differentiation of mesenchymal stem cells, activating the BMP-pSmad1/5/8 signaling pathway, and contributing to abnormal fat metaplasia and new bone formation in patients with ankylosing spondylitis (Liu et al., 2019). Similarly, BMPR1A is also essential for BMP-induced phosphorylation of Smad1/5/8 in heart valve progenitors (Lockhart et al., 2014). During aortic valve calcification, deletion of BMPR1A or inhibition of its activity can lead to absence of the BMP signaling pathway, resulting in the loss of osteochondrogenic features and blocked calcified nodule formation, thereby preventing aortic valve calcification (Gomez-Stallons et al., 2016). Thus, BMPR1A signaling plays an essential role in restricting preosteoblast proliferation and promoting osteoblast activity.

Role of BMP Signaling in the Bone-Vascular Axis

The bone is not only a site of mineral storage but also the main site for stem cell maintenance and hematopoiesis. It plays a dual role in maintaining the vascular integrity of endothelial progenitor cells and aggravating VC *via* inflammatory cells (Kim et al., 2020). Numerous studies have shown that vascular calcification is highly similar to bone formation. The minerals deposited in the vascular wall are mainly alkaline calcium phosphate in the form of apatite, including hydroxyapatite [Ca_{10} $(PO_4)_6$ (OH) $_2$] crystals, consistent with the composition of bone (Reynolds et al., 2004). Some secreted proteins that connect the bone and blood vessels play important roles in vascular calcification, such as receptor activator for nuclear factor kB (RANK)/RANK ligand (RANKL)/osteoprotegerin (OPG), BMPs, Runx2, osterix (OSX), fetuin-A, and MGP (Pereira and Frazao, 2020). Some studies have also shown that there is an independent negative correlation between bone mineral density and atherosclerosis and that patients with osteoporosis are more prone to aortic and carotid calcification (Hofbauer et al., 2007; Anagnostis et al., 2009; Zhang et al., 2016). In addition, disorders of bone volume and bone turnover in patients with uremia may increase the risk of VC and eventually lead to an extremely high risk of

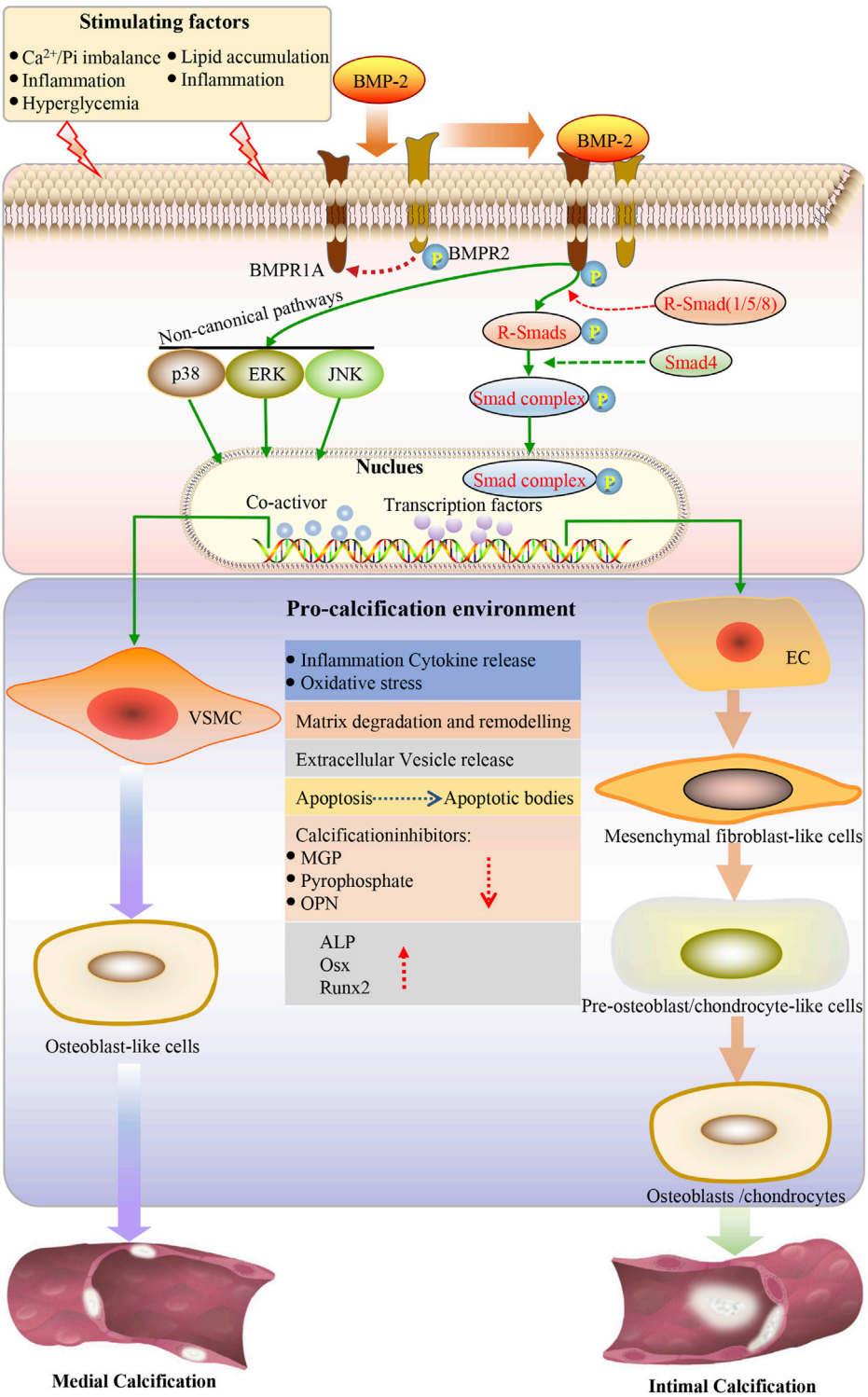

FIGURE 2 | Under the action of stimulating factors, BMP2 binds to the receptor, the type I receptor is phosphorylated by the type II receptor, subsequently activating the classical BMP-SMAD and BMP-noncannonical pathway. SMAD1/5/8 is the effector of the BMP-SMAD pathway. Phosphorylated SMAD1/5/8 forms a heterogeneous complex with SMAD4 and is translocated to the nucleus, where it can regulate the expression of target genes by interacting with other transcription factors. Endothelial cells undergo endothelial mesenchymal transformation and differentiate into mesenchymal fibroblasts, which further differentiate into pre-osteoblasts and osteoblasts in a pro-calcified environment, leading to intimal calcification. VSMCs can be transformed into the bone/cartilage phenotype. Osteogenic/chondroblast-like cells actively promote calcification by reducing the expression of calcification inhibitors, increasing apoptosis, releasing apoptotic bodies and calcified

(*Continued*)

FIGURE 2 | vesicles, remodeling the extracellular matrix, degrading elastin, and releasing proinflammatory cytokines, ultimately increasing oxidative stress. The osteogenic transcription factor induces the expression of Runx2 and osterix in VSMCs. Osterix is upregulated by Runx2 and becomes fully activated. This creates an environment to promote calcification so that vascular calcification can be achieved. EC: endothelial cells; VSMC: vascular smooth muscle cell; ALP: alkaline phosphatase; OPN: osteopontin; Runx2: runt-related transcription factor-2; Osx: osterix; ROS: reactive oxygen species; BMP: bone morphogenetic protein; BMPR1A: BMP type I receptor A; BMPR2: type II receptor; SMAD: homolog of the *drosophila* protein, mothers against decap-entaplegic (MAD) and the *Caenorhabditis elegans* protein SMA; ERK: extracellular signal-regulated kinase; JNK: c-jun N-terminal kinase.

cardiovascular death (Adragao et al., 2009). Some clinical experiments have confirmed that bisphosphonates can inhibit vascular calcification while preventing fracture risk during the treatment of osteoporosis (Kranenburg et al., 2016). Recent studies have shown that BMP-induced miRNAs can regulate the proliferation and migration of VSMCs and induce their phenotypic conversion and that their abnormal regulation can lead to various vascular diseases (Park and Kang, 2020). Therefore, this evidence suggests that crosstalk exists between the bone and the vascular system.

ROLE OF BMPR1A IN VASCULAR CALCIFICATION

Role of BMPR1A in the Osteogenic Differentiation of Endothelial Cells

ECs are an essential component of blood vessels and one of the key factors for maintaining normal cardiovascular function. They are highly active cell monolayers that can rapidly adapt to and respond to endogenous and exogenous signaling. Endothelial dysfunction has been observed in many cardiovascular diseases, including atherosclerosis (Widlansky et al., 2003). Currently, many researchers have studied VC as an outcome of atherosclerosis (Bjorklund et al., 2020). Inflammatory factors (such as TNF-α and IL-1β) and TGF-β family ligands (including BMPs) are jointly involved in the occurrence and development of calcified aortic plaques (Dhore et al., 2001; Gistera and Hansson, 2017). Furthermore, some studies have suggested that ECs can function as a special source of osteogenic progenitors during vascular calcification (Chen et al., 2015; Sanchez-Duffhues et al., 2015; Evrard et al., 2016).

Endothelial cells can undergo a process called EndMT under inflammation, characterized by the loss of endothelial characteristics and the acquisition of fibroblast-like phenotypes, which eventually re-differentiate into osteogenic potential cells under the guidance of various stimuli such as BMPs (**Figure 1A**) (Pavićević et al., 2016; Sanchez-Duffhues et al., 2019). The BMP-Smad signaling pathway plays an important role in EndMT (**Figure 2**). Studies have confirmed that most BMPs promote EndMT through the canonical Smad-dependent pathway and that IL-1β can activate the BMP signaling pathway by upregulating the expression of BMP2 (Shanmugam et al., 2015; Evrard et al., 2016; Hong et al., 2020; Yuan et al., 2021). Under conditions such as hyperglycemia, inflammation, and aging, endothelial cells are stimulated to release extracellular vesicles (EVs) or extracellular matrix protein particles (EMPs), which are enriched in Ca^{2+} and BMP2, and act as nucleation sites for calcification to induce mineralization (Yuan et al., 2021). Previous studies have shown that TNF-α can increase the expression of BMP2 and the release of EMPs in ECs, thus promoting osteogenesis and the calcification of VSMCs (Csiszar et al., 2005; Buendia et al., 2015). It is well known that the BMP2 signaling cascade is initiated by activating BMPR1A (ALK3), BMPR1B (ALK6), and BMPRII (Medici et al., 2010). BMPR1A is widely expressed in endothelial cells, and its overexpression is closely related to the early development of vascular calcification (Vinuesa et al., 2015; Wei et al., 2018). Hong et al. (2020) showed that BMPR1A and BMP type II receptors (BMPR-II, Act-RIIB) could activate IL-1β-induced EndMT, thereby promoting the expression of Runx2 and OSX. Huang et al. (2018) also demonstrated that IL-6 could promote the cell surface translocation of BMPR1A and enhance the BMP-2-induced osteogenic differentiation of mesenchymal cells by amplifying BMP-Smad signaling.

An increasing number of studies indicate that ECs play a significant role in vascular calcification *via* EndMT, the autocrine/paracrine pathway, EC-derived extracellular vesicles, angiogenesis, and mechanotransduction. These findings further confirmed that BMPR1A could induce osteogenic gene expression during vascular endothelial cell mesenchymal transformation and promote calcification plaque production, further promoting vascular calcification.

Role of BMPR1A in the Osteogenic Differentiation of Vascular Smooth Muscle Cells

VSMCs have multiple phenotypes, including osteogenic, contractile, and synthetic, which can be changed from one phenotype to another under certain conditions (Bardeesi et al., 2017). Vascular calcification is an active, complex, and tightly regulated biological process that is mainly related to the transformation of the contractile phenotype of VSMCs to osteoblast-like cells (McCarty and DiNicolantonio, 2014; Evrard et al., 2015). This phenotypic transformation of VSMCs is characterized by the upregulation of osteogenic genes, such as BMP2, Runx2, OSX, ALP, and osteopontin (O'Neill, 2017). VSMCs constitute the majority of the vascular wall, maintaining vascular structure and regulating blood pressure (Waldo et al., 2005). Similar to osteoblasts, VSMCs are derived from mesenchymal precursor cells and express BMP2 (Sun et al., 2017). Apoptosis, the release of extracellular vesicles, the absence of calcification inhibitors (e.g., MGP), senescence-associated DNA damage, and osteo/chondrogenic differentiation are considered the main mechanisms of vascular smooth muscle cells undergoing vascular calcification (Neven et al., 2007; Liu et al., 2013; Schurgers et al., 2013).

VSMCs are the predominant cell type involved in vascular calcification, which can transdifferentiate into the chondrocyte, osteoblast, and osteocyte phenotypes in a calcified environment (**Figure 1B**) (Shroff et al., 2008; Zhu et al., 2011). The BMP-Smad signaling pathway plays an essential role in the transdifferentiation of VSMCs into osteoblasts and chondrocytes (**Figure 2**). Previous studies have reported that BMPR1A and BMPRII are highly expressed in VSMCs and mediate the response of SMCs to BMP2. BMPR1A and BMPRII are the dominant complexes mediating Smad1/5/8 phosphorylation in response to BMP2 (Upton et al., 2008; Goumans et al., 2018). Evidence suggests that the BMP2-Smad1/5/8 signaling pathway is involved in the osteogenic differentiation of VSMCs (Broege et al., 2013; Kee et al., 2014). When VSMCs receive stimulation signaling, phosphorylated Smad1/5/8 can accelerate translocation from the cytoplasm to the nucleus and initiate the osteogenic differentiation of VSMCs, which eventually leads to the increased expression of OSX, Runx2, and alkaline phosphatase (ALP) (Wang et al., 2018; Willems et al., 2018). One study showed that BMP2 accelerated the atherosclerotic intimal calcification in transgenic ApoE$^{-/-}$ mice (Nakagawa et al., 2010). Another study indicated that BMP2 could affect SMC marker (SM22a and SM a-actin) loss and the expression of genes associated with the osteoblast phenotype, such as msh homeobox-2, ALP, and osteopontin (OPN) (Bardeesi et al., 2017). Furthermore, BMP2 plays a vital role in promoting VSMC apoptosis, Reactive oxygen species (ROS) production, and inflammatory responses (Agharazii et al., 2015; Voelkl et al., 2019). The inhibition of BMP2 expression in a CKD mouse model significantly reduced the osteogenic differentiation of VSMCs, thereby reducing BMP2-induced mineralization (Nguyen-Yamamoto et al., 2019). Sun et al. (2017) showed that endogenous BMP2 is involved in the osteogenic differentiation of VSMCs and subsequent calcification under IL-6 induction. BMPR1A, a high-affinity receptor of BMP2, also acts as a bridge to promote vascular calcification and plays a crucial role in the transdifferentiation of VSMCs into osteoblasts or chondrocyte-like cells.

CONCLUSION AND OUTLOOK

Vascular calcification maintains many characteristics of bone formation, including the need to co-activate BMP signaling family members to recruit osteogenic or chondrogenic progenitor cells to promote the development of calcified cardiovascular diseases. Various BMP ligands, receptors, and regulators play environmental, tissue-specific, and time-dependent roles in the recruitment and activation of progenitor cells produced *via* vascular calcification during the development of *in situ* bone. In this review, we focused on discovering how BMPR1A regulates vascular calcification in the BMP-Smad signaling pathway and how damaged vascular endothelial cells and smooth muscle cells lead to VC mediated by BMP signaling. Collectively, BMPs can bind to BMP receptors on VSMCs and endothelial cells, thereby accelerating medial or intimal calcification. BMPR1A, a type I receptor of the BMP-SMAD signaling pathway, can specifically bind to BMP2 and play an important role in activating BMP2-mediated osteogenic differentiation and chondrogenesis.

Although inhibitors targeting BMPI receptors have been developed, the lack of selectivity between their receptors, which can lead to off-target effects and adverse reactions, remains a problem. Therefore, it is essential to develop more specific inhibitors against BMPR1A that may lead to vascular calcification. Using small molecule synthesis, BMPR1A inhibitors that inhibit BMP2-Smad signaling may effectively reduce vascular calcification. Moreover, manipulating BMPR1A expression may be a novel therapeutic strategy to ameliorate the abnormal osteogenic differentiation observed in Vascular calcification. It is worth noting that bone diseases should also be considered in the treatment of vascular calcification based on the bone-vascular calcification theory. In the future, it will be necessary to further investigate the potential mechanism of BMPR1A in Vascular calcification to strengthen the theoretical basis for VC treatment.

AUTHOR CONTRIBUTIONS

DZ and XL designed the scope of the review. ZN wrote the manuscript. GS and TL performed the document searching and prepared the figures. HY and YS guided the planning and critically edited the manuscript. All authors read and approved the final manuscript

FUNDING

This study was supported by the National Natural Science Foundation of China (No. 11802190, 11932014, 31971239, 31870939, 32071312 and 82001062).

ACKNOWLEDGMENTS

The authors thank all investigators and supporters involved in this study.

REFERENCES

Adragao, T., Herberth, J., Monier-Faugere, M. C., Branscum, A. J., Ferreira, A., and Frazao, J. M. (2009). Low Bone Volume-Aa Risk Factor for Coronary Calcifications in Hemodialysis Patients. *Clin. J. Am. Soc. Nephrol.* 4, 450–455. doi:10.2215/CJN.01870408

Agharazii, M., St-Louis, R., Gautier-Bastien, A., Ung, R. V., Mokas, S., Lariviere, R., et al. (2015). Inflammatory Cytokines and Reactive Oxygen Species as Mediators of Chronic Kidney Disease-Related Vascular Calcification. *Am. J. Hypertens.* 28, 746–755. doi:10.1093/ajh/hpu225

Anagnostis, P., Karagiannis, A., Kakafika, A. I., Tziomalos, K., Athyros, V. G., and Mikhailidis, D. P. (2009). Atherosclerosis and Osteoporosis: Age-dependent

Degenerative Processes or Related Entities? *Osteoporos. Int.* 20, 197–207. doi:10.1007/s00198-008-0648-5

Andrews, J., Psaltis, P. J., Bartolo, B. a. D., Nicholls, S. J., and Puri, R. (2018). Coronary Arterial Calcification: A Review of Mechanisms, Promoters and Imaging. *Trends Cardiovasc. Med.* 28, 491–501. doi:10.1016/j.tcm.2018.04.007

Bai, H. Y., Shan, B. S., and Jiang, Y. N. (2021). The Protective Effects of Renin-Angiotensin System Components on Vascular Calcification. *J. Hum. Hypertens.* 35, 410–418. doi:10.1038/s41371-020-0347-z

Bardeesi, A. S. A., Gao, J., Zhang, K., Yu, S., Wei, M., Liu, P., et al. (2017). A Novel Role of Cellular Interactions in Vascular Calcification. *J. Transl Med.* 15, 95. doi:10.1186/s12967-017-1190-z

Bartolak-Suki, E., and Suki, B. (2020). Tuning Mitochondrial Structure and Function to Criticality by Fluctuation-Driven Mechanotransduction. *Sci. Rep.* 10, 407. doi:10.1038/s41598-019-57301-1

Bartoli-Leonard, F., Wilkinson, F. L., Langford-Smith, A. W. W., Alexander, M. Y., and Weston, R. (2018). The Interplay of SIRT1 and Wnt Signaling in Vascular Calcification. *Front. Cardiovasc. Med.* 5, 183. doi:10.3389/fcvm.2018.00183

Bjorklund, G., Svanberg, E., Dadar, M., Card, D. J., Chirumbolo, S., Harrington, D. J., et al. (2020). The Role of Matrix Gla Protein (MGP) in Vascular Calcification. *Curr. Med. Chem.* 27, 1647–1660. doi:10.2174/0929867325666180716104159

Broege, A., Pham, L., Jensen, E. D., Emery, A., Huang, T. H., Stemig, M., et al. (2013). Bone Morphogenetic Proteins Signal via SMAD and Mitogen-Activated Protein (MAP) Kinase Pathways at Distinct Times during Osteoclastogenesis. *J. Biol. Chem.* 288, 37230–37240. doi:10.1074/jbc.M113.496950

Buendia, P., Montes De Oca, A., Madueno, J. A., Merino, A., Martin-Malo, A., Aljama, P., et al. (2015). Endothelial Microparticles Mediate Inflammation-Induced Vascular Calcification. *FASEB J.* 29, 173–181. doi:10.1096/fj.14-249706

Cai, J., Pardali, E., Sánchez-Duffhues, G., and Ten Dijke, P. (2012). BMP Signaling in Vascular Diseases. *FEBS Lett.* 586, 1993–2002. doi:10.1016/j.febslet.2012.04.030

Chen, P. Y., Qin, L., Baeyens, N., Li, G., Afolabi, T., Budatha, M., et al. (2015). Endothelial-to-mesenchymal Transition Drives Atherosclerosis Progression. *J. Clin. Invest.* 125, 4514–4528. doi:10.1172/JCI82719

Chen, Y., Zhao, X., and Wu, H. (2020). Arterial Stiffness: A Focus on Vascular Calcification and its Link to Bone Mineralization. *Arterioscler Thromb. Vasc. Biol.* 40, 1078–1093. doi:10.1161/ATVBAHA.120.313131

Cheng, H., Jiang, W., Phillips, F. M., Haydon, R. C., Peng, Y., Zhou, L., et al. (2004). Osteogenic Activity of the Fourteen Types of Human Bone Morphogenetic Proteins (BMPs). *Urol. Oncol. Semin. Original Invest.* 22, 79–80. doi:10.1016/j.urolonc.2003.12.008

Chignon, A., Bon-Baret, V., Boulanger, M. C., Bosse, Y., and Mathieu, P. (2021). Oxyphospholipids in Cardiovascular Calcification. *Arterioscler Thromb. Vasc. Biol.* 41, 11–19. doi:10.1161/ATVBAHA.120.313790

Csiszar, A., Smith, K. E., Koller, A., Kaley, G., Edwards, J. G., and Ungvari, Z. (2005). Regulation of Bone Morphogenetic Protein-2 Expression in Endothelial Cells: Role of Nuclear Factor-kappaB Activation by Tumor Necrosis Factor-Alpha, H2O2, and High Intravascular Pressure. *Circulation* 111, 2364–2372. doi:10.1161/01.CIR.0000164201.40634.1D

Demer, L. L., and Tintut, Y. (2008). Vascular Calcification: Pathobiology of a Multifaceted Disease. *Circulation* 117, 2938–2948. doi:10.1161/CIRCULATIONAHA.107.743161

Derwall, M., Malhotra, R., Lai, C. S., Beppu, Y., Aikawa, E., Seehra, J. S., et al. (2012). Inhibition of Bone Morphogenetic Protein Signaling Reduces Vascular Calcification and Atherosclerosis. *Arterioscler Thromb. Vasc. Biol.* 32, 613–622. doi:10.1161/ATVBAHA.111.242594

Dhore, C. R., Cleutjens, J. P., Lutgens, E., Cleutjens, K. B., Geusens, P. P., Kitslaar, P. J., et al. (2001). Differential Expression of Bone Matrix Regulatory Proteins in Human Atherosclerotic Plaques. *Arterioscler Thromb. Vasc. Biol.* 21, 1998–2003. doi:10.1161/hq1201.100229

Ducy, P., Mckee, M., Pinero, G. J., Loyer, E., Behringer, R. R., Karsenty, G., et al. (2015). Spontaneous Calcification of Arteries and Cartilage in Mice Lacking Matrix GLA Protein. *Nature* 386, 78–81. doi:10.1038/386078a0

Durham, A. L., Speer, M. Y., Scatena, M., Giachelli, C. M., and Shanahan, C. M. (2018). Role of Smooth Muscle Cells in Vascular Calcification: Implications in Atherosclerosis and Arterial Stiffness. *Cardiovasc. Res.* 114, 590–600. doi:10.1093/cvr/cvy010

Evrard, S., Delanaye, P., Kamel, S., Cristol, J. P., Cavalier, E., and Calcifications, S. S. J. W. G. O. V. (2015). Vascular Calcification: from Pathophysiology to Biomarkers. *Clin. Chim. Acta* 438, 401–414. doi:10.1016/j.cca.2014.08.034

Evrard, S. M., Lecce, L., Michelis, K. C., Nomura-Kitabayashi, A., Pandey, G., Purushothaman, K. R., et al. (2016). Endothelial to Mesenchymal Transition Is Common in Atherosclerotic Lesions and Is Associated with Plaque Instability. *Nat. Commun.* 7, 11853. doi:10.1038/ncomms11853

Gistera, A., and Hansson, G. K. (2017). The Immunology of Atherosclerosis. *Nat. Rev. Nephrol.* 13, 368–380. doi:10.1038/nrneph.2017.51

Gomez-Stallons, M. V., Wirrig-Schwendeman, E. E., Hassel, K. R., Conway, S. J., and Yutzey, K. E. (2016). Bone Morphogenetic Protein Signaling Is Required for Aortic Valve Calcification. *Arterioscler Thromb. Vasc. Biol.* 36, 1398–1405. doi:10.1161/ATVBAHA.116.307526

Goumans, M. J., Zwijsen, A., Ten Dijke, P., and Bailly, S. (2018). Bone Morphogenetic Proteins in Vascular Homeostasis and Disease. *Cold Spring Harb Perspect. Biol.* 10. doi:10.1101/cshperspect.a031989

Gu, W., Wang, Z., Sun, Z., Bao, Z., Zhang, L., Geng, Y., et al. (2020). Role of NFATc1 in the Bone-Vascular Axis Calcification Paradox. *J. Cardiovasc. Pharmacol.* 75, 200–207. doi:10.1097/FJC.0000000000000788

Hofbauer, L. C., Brueck, C. C., Shanahan, C. M., Schoppet, M., and Dobnig, H. (2007). Vascular Calcification and Osteoporosis-Ffrom Clinical Observation towards Molecular Understanding. *Osteoporos. Int.* 18, 251–259. doi:10.1007/s00198-006-0282-z

Hong, O. K., Lee, S. S., Yoo, S. J., Lee, M. K., Kim, M. K., Baek, K. H., et al. (2020). Gemigliptin Inhibits Interleukin-1beta-Induced Endothelial-Mesenchymal Transition via Canonical-Bone Morphogenetic Protein Pathway. *Endocrinol. Metab. (Seoul)* 35, 384–395. doi:10.3803/EnM.2020.35.2.384

Huang, R. L., Sun, Y., Ho, C. K., Liu, K., Tang, Q. Q., Xie, Y., et al. (2018). IL-6 Potentiates BMP-2-Induced Osteogenesis and Adipogenesis via Two Different BMPR1A-Mediated Pathways. *Cell Death Dis* 9, 144. doi:10.1038/s41419-017-0126-0

Kai, H., Seher, A., Schmitz, W., Mueller, T. D., and Nickel, J. (2009). Receptor Oligomerization and beyond: a Case Study in Bone Morphogenetic Proteins. *BMC Biol.* 7, 59. doi:10.1186/1741-7007-7-59

Kee, H. J., Cho, S. N., Kim, G. R., Choi, S. Y., Ryu, Y., Kim, I. K., et al. (2014). Gallic Acid Inhibits Vascular Calcification through the Blockade of BMP2-Smad1/5/8 Signaling Pathway. *Vascul Pharmacol.* 63, 71–78. doi:10.1016/j.vph.2014.08.005

Kim, J. M., Lee, W. S., and Kim, J. (2020). Therapeutic Strategy for Atherosclerosis Based on Bone-Vascular axis Hypothesis. *Pharmacol. Ther.* 206, 107436. doi:10.1016/j.pharmthera.2019.107436

Kranenburg, G., Bartstra, J. W., Weijmans, M., Jong, P. D., Mali, W. P., Verhaar, H. J., et al. (2016). Bisphosphonates for Cardiovascular Risk Reduction: A Systematic Review and Meta-Analysis. *Atherosclerosis* 252, 106–115. doi:10.1016/j.atherosclerosis.2016.06.039

Kuro, O. M. (2021). Klotho and Calciprotein Particles as Therapeutic Targets against Accelerated Ageing. *Clin. Sci. (Lond)* 135, 1915–1927. doi:10.1042/CS20201453

Kwon, D. H., Kim, Y. K., and Kook, H. (2017). New Aspects of Vascular Calcification: Histone Deacetylases and beyond. *J. Korean Med. Sci.* 32, 1738–1748. doi:10.3346/jkms.2017.32.11.1738

Lavery, K., Swain, P., Falb, D., and Alaoui-Ismaili, M. H. (2008). BMP-2/4 and BMP-6/7 Differentially Utilize Cell Surface Receptors to Induce Osteoblastic Differentiation of Human Bone Marrow-Derived Mesenchymal Stem Cells. *J. Biol. Chem.* 283, 20948–20958. doi:10.1074/jbc.M800850200

Lee, H. W., Chong, D. C., Ola, R., Dunworth, W. P., Meadows, S., Ka, J., et al. (2017). Alk2/ACVR1 and Alk3/BMPR1A Provide Essential Function for Bone Morphogenetic Protein-Induced Retinal Angiogenesis. *Arterioscler Thromb. Vasc. Biol.* 37, 657–663. doi:10.1161/ATVBAHA.116.308422

Lee, S. J., Lee, I.-K., and Jeon, J.-H. (2020). Vascular Calcification—New Insights into its Mechanism. *Int. J. Mol. Sci.* 21, 2685. doi:10.3390/ijms21082685

Lin, T., Wang, X. L., Zettervall, S. L., Cai, Y., and Guzman, R. J. (2017). Dorsomorphin Homologue 1, a Highly Selective Small-Molecule Bone Morphogenetic Protein Inhibitor, Suppresses Medial Artery Calcification. *J. Vasc. Surg.* 66, 586–593. doi:10.1016/j.jvs.2016.03.462

Lin, Y., and Sun, Z. (2021). Klotho Deficiency-Induced Arterial Calcification Involves Osteoblastic Transition of VSMCs and Activation of BMP Signaling. *J. Cel Physiol* 237, 720–729. doi:10.1002/jcp.30541

Liu, Y., Drozdov, I., Shroff, R., Beltran, L. E., and Shanahan, C. M. (2013). Prelamin A Accelerates Vascular Calcification via Activation of the DNA Damage Response and Senescence-Associated Secretory Phenotype in Vascular Smooth Muscle Cells. *Circ. Res.* 112, e99–109. doi:10.1161/CIRCRESAHA.111.300543

Liu, Z., Wang, P., Cen, S., Gao, L., and Shen, H. (2019). Increased BMPR1A Expression Enhances the Adipogenic Differentiation of Mesenchymal Stem Cells in Patients with Ankylosing Spondylitis. *Stem Cell Int.* 2019, 1–13. doi:10.1155/2019/4143167

Lockhart, M. M., Boukens, B. J., Phelps, A. L., Brown, C. L., Toomer, K. A., Burns, T. A., et al. (2014). Alk3 Mediated Bmp Signaling Controls the Contribution of Epicardially Derived Cells to the Tissues of the Atrioventricular junction. *Dev. Biol.* 396, 8–18. doi:10.1016/j.ydbio.2014.09.031

Lu, C. L., Liao, M. T., Hou, Y. C., Fang, Y. W., and Ng, Y. Y. (2020). Sirtuin-1 and its Relevance in Vascular Calcification. *Int. J. Mol. Sci.* 21, 1593. doi:10.3390/ijms21051593

Luo, J., Tang, M., Huang, J., He, B.-C., Gao, J.-L., Chen, L., et al. (2010). TGFβ/BMP Type I Receptors ALK1 and ALK2 Are Essential for BMP9-Induced Osteogenic Signaling in Mesenchymal Stem Cells. *J. Biol. Chem.* 285, 29588–29598. doi:10.1074/jbc.M110.130518

Malhotra, R., Burke, M. F., Martyn, T., Shakartzi, H. R., Thayer, T. E., O'rourke, C., et al. (2015). Inhibition of Bone Morphogenetic Protein Signal Transduction Prevents the Medial Vascular Calcification Associated with Matrix Gla Protein Deficiency. *PLoS One* 10, e0117098. doi:10.1371/journal.pone.0117098

Mang, T., Kleinschmidtdoerr, K., Ploeger, F., Schoenemann, A., Lindemann, S., and Gigout, A. (2020). BMPR1A Is Necessary for Chondrogenesis and Osteogenesis, whereas BMPR1B Prevents Hypertrophic Differentiation. *J. Cel Sci.* 133, 246934. doi:10.1242/jcs.246934

Maruyama, T., Stevens, R., Boka, A., Dirienzo, L., Chang, C., Yu, H.-M. I., et al. (2021). BMPR1A Maintains Skeletal Stem Cell Properties in Craniofacial Development and Craniosynostosis. *Sci. Transl. Med.* 13, 12. doi:10.1126/scitranslmed.abb4416

Mccarty, M. F., and Dinicolantonio, J. J. (2014). The Molecular Biology and Pathophysiology of Vascular Calcification. *Postgrad. Med.* 126, 54–64. doi:10.3810/pgm.2014.03.2740

Medici, D., Shore, E. M., Lounev, V. Y., Kaplan, F. S., Kalluri, R., and Olsen, B. R. (2010). Conversion of Vascular Endothelial Cells into Multipotent Stem-like Cells. *Nat. Med.* 16, 1400–1406. doi:10.1038/nm.2252

Mishina, Y., Suzuki, A., Ueno, N., and Behringer, R. R. (1995). Bmpr Encodes a Type I Bone Morphogenetic Protein Receptor that Is Essential for Gastrulation during Mouse Embryogenesis. *Genes Dev.* 9, 3027–3037. doi:10.1101/gad.9.24.3027

Miyazono, K., Maeda, S., and Imamura, T. (2005). BMP Receptor Signaling: Transcriptional Targets, Regulation of Signals, and Signaling Cross-Talk. *Cytokine Growth Factor. Rev.* 16, 251–263. doi:10.1016/j.cytogfr.2005.01.009

Morrell, N. W., Bloch, D. B., Ten Dijke, P., Goumans, M. J., Hata, A., Smith, J., et al. (2016). Targeting BMP Signalling in Cardiovascular Disease and Anaemia. *Nat. Rev. Cardiol.* 13, 106–120. doi:10.1038/nrcardio.2015.156

Nakagawa, Y., Ikeda, K., Akakabe, Y., Koide, M., Uraoka, M., Yutaka, K. T., et al. (2010). Paracrine Osteogenic Signals via Bone Morphogenetic Protein-2 Accelerate the Atherosclerotic Intimal Calcification *In Vivo*. *Arterioscler Thromb. Vasc. Biol.* 30, 1908–1915. doi:10.1161/ATVBAHA.110.206185

Neven, E., Dauwe, S., De Broe, M. E., D'haese, P. C., and Persy, V. (2007). Endochondral Bone Formation Is Involved in media Calcification in Rats and in Men. *Kidney Int.* 72, 574–581. doi:10.1038/sj.ki.5002353

Neven, E., De Schutter, T. M., De Broe, M. E., and D'haese, P. C. (2011). Cell Biological and Physicochemical Aspects of Arterial Calcification. *Kidney Int.* 79, 1166–1177. doi:10.1038/ki.2011.59

Nguyen-Yamamoto, L., Tanaka, K. I., St-Arnaud, R., and Goltzman, D. (2019). Vitamin D-Regulated Osteocytic Sclerostin and BMP2 Modulate Uremic Extraskeletal Calcification. *JCI Insight* 4. doi:10.1172/jci.insight.126467

Nomura, S. A., and Takano-Yamamoto, T. (2000). Molecular Events Caused by Mechanical Stress in Bone. *Matrix Biol.* 19, 91–96. doi:10.1016/S0945-053X(00)00050-0

O'neill, W. C. (2017). Understanding the Pathogenesis of Vascular Calcification: Timing Is Everything. *Kidney Int.* 92, 1316–1318. doi:10.1016/j.kint.2017.07.020

Pan, H., Zhang, H., Abraham, P., Komatsu, Y., Lyons, K., Kaartinen, V., et al. (2017). BmpR1A Is a Major Type 1 BMP Receptor for BMP-Smad Signaling during Skull Development. *Dev. Biol.* 429, 260–270. doi:10.1016/j.ydbio.2017.06.020

Park, N., and Kang, H. (2020). BMP-induced MicroRNA-101 Expression Regulates Vascular Smooth Muscle Cell Migration. *Int. J. Mol. Sci.* 21. doi:10.3390/ijms21134764

Pavićević, V. P., Marković, M. S., Milojević, S. Ž., Ristić, M. S., Povrenović, D. S., and Veljković, V. B. (2016). Microwave-assisted Hydrodistillation of Juniper berry Essential Oil: Kinetic Modeling and Chemical Composition. *J. Chem. Technology Biotechnol.* 91, 883–891. doi:10.1002/jctb.4653

Pereira, L., and Frazao, J. M. (2020). The Bone-Vessel axis in Chronic Kidney Disease: An Update on Biochemical Players and its Future Role in Laboratory Medicine. *Clin. Chim. Acta* 508, 221–227. doi:10.1016/j.cca.2020.05.023

Persy, V., and D'haese, P. (2009). Vascular Calcification and Bone Disease: the Calcification Paradox. *Trends Mol. Med.* 15, 405–416. doi:10.1016/j.molmed.2009.07.001

Pescatore, L. A., Gamarra, L. F., and Liberman, M. (2019). Multifaceted Mechanisms of Vascular Calcification in Aging. *Arteriosclerosis, Thromb. Vasc. Biol.* 39, 1307–1316. doi:10.1161/ATVBAHA.118.311576

Phadwal, K., Vrahnas, C., Ganley, I. G., and Macrae, V. E. (2021). Mitochondrial Dysfunction: Cause or Consequence of Vascular Calcification? *Front Cel Dev Biol* 9, 611922. doi:10.3389/fcell.2021.611922

Reynolds, L., Skepper, J. N., and Joannides, A. (2004). Human Vascular Smooth Muscle Cells Undergo Vesicle-Mediated Calcification in Response to Changes in Extracellular Calcium and Phosphate Concentrations: A Potential Mechanism for Accelerated Vascular Calcification in ESRD. *J. Am. Soc. Nephrol.* 15, 2857–2867. doi:10.1097/01.ASN.0000141960.01035.28

Sanchez-De-Diego, C., Valer, J. A., Pimenta-Lopes, C., Rosa, J. L., and Ventura, F. (2019). Interplay between BMPs and Reactive Oxygen Species in Cell Signaling and Pathology. *Biomolecules* 9. doi:10.3390/biom9100534

Sanchez-Duffhues, G., De Vinuesa, A. G., Lindeman, J. H., Mulder-Stapel, A., Deruiter, M. C., Van Munsteren, C., et al. (2015). SLUG Is Expressed in Endothelial Cells Lacking Primary Cilia to Promote Cellular Calcification. *Arterioscler Thromb. Vasc. Biol.* 35, 616–627. doi:10.1161/ATVBAHA.115.305268

Sanchez-Duffhues, G., Garcia De Vinuesa, A., Van De Pol, V., Geerts, M. E., De Vries, M. R., Janson, S. G., et al. (2019). Inflammation Induces Endothelial-To-Mesenchymal Transition and Promotes Vascular Calcification through Downregulation of BMPR2. *J. Pathol.* 247, 333–346. doi:10.1002/path.5193

Schenker, M. P., Dorbala, S., Hong, E. C., Rybicki, F. J., Hachamovitch, R., Kwong, R. Y., et al. (2008). Interrelation of Coronary Calcification, Myocardial Ischemia, and Outcomes in Patients with Intermediate Likelihood of Coronary Artery Disease: a Combined Positron Emission Tomography/computed Tomography Study. *Circulation* 117, 1693–1700. doi:10.1161/CIRCULATIONAHA.107.717512

Schurgers, L. J., Akbulut, A. C., Kaczor, D. M., Halder, M., Koenen, R. R., and Kramann, R. (2018). Initiation and Propagation of Vascular Calcification Is Regulated by a Concert of Platelet- and Smooth Muscle Cell-Derived Extracellular Vesicles. *Front. Cardiovasc. Med.* 5, 36. doi:10.3389/fcvm.2018.00036

Schurgers, L. J., Uitto, J., and Reutelingsperger, C. P. (2013). Vitamin K-dependent Carboxylation of Matrix Gla-Protein: a Crucial Switch to Control Ectopic Mineralization. *Trends Mol. Med.* 19, 217–226. doi:10.1016/j.molmed.2012.12.008

Shanmugam, N. K., Chen, K., and Cherayil, B. J. (2015). Commensal Bacteria-Induced Interleukin 1beta (IL-1beta) Secreted by Macrophages Up-Regulates Hepcidin Expression in Hepatocytes by Activating the Bone Morphogenetic Protein Signaling Pathway. *J. Biol. Chem.* 290, 30637–30647. doi:10.1074/jbc.M115.689190

Shi, C., Zhang, H., Louie, K., Mishina, Y., and Sun, H. (2017). BMP Signaling Mediated by BMPR1A in Osteoclasts Negatively Regulates Osteoblast Mineralization through Suppression of Cx43. *J. Cel Biochem* 118, 605–614. doi:10.1002/jcb.25746

Shi, Y., and Massagué, J. (2003). Mechanisms of TGF-Beta Signaling from Cell Membrane to the Nucleus. *Cell* 113, 685–700. doi:10.1016/s0092-8674(03)00432-x

Shroff, R. C., Mcnair, R., Figg, N., Skepper, J. N., Schurgers, L., Gupta, A., et al. (2008). Dialysis Accelerates Medial Vascular Calcification in Part by Triggering Smooth Muscle Cell Apoptosis. *Circulation* 118, 1748–1757. doi:10.1161/CIRCULATIONAHA.108.783738

Shroff, R. C., and Shanahan, C. M. (2010). The Vascular Biology of Calcification. *Semin. Dial.* 20, 103–109. doi:10.1681/asn.2009060640

Sieber, C., Kopf, J., Hiepen, C., and Knaus, P. (2009). Recent Advances in BMP Receptor Signaling. *Cytokine Growth Factor. Rev.* 20, 343–355. doi:10.1016/j.cytogfr.2009.10.007

Simic, P., Culej, J. B., Orlic, I., Grgurevic, L., Draca, N., Spaventi, R., et al. (2006). Systemically Administered Bone Morphogenetic Protein-6 Restores Bone in Aged Ovariectomized Rats by Increasing Bone Formation and Suppressing Bone Resorption. *J. Biol. Chem.* 281, 25509–25521. doi:10.1074/jbc.M513276200

Sun, M., Chang, Q., Xin, M., Wang, Q., Li, H., and Qian, J. (2017). Endogenous Bone Morphogenetic Protein 2 Plays a Role in Vascular Smooth Muscle Cell Calcification Induced by Interleukin 6 *In Vitro*. *Int. J. Immunopathol Pharmacol.* 30, 227–237. doi:10.1177/0394632016689571

Thompson, B., and Towler, D. A. (2012). Arterial Calcification and Bone Physiology: Role of the Bone-Vascular axis. *Nat. Rev. Endocrinol.* 8, 529. doi:10.1038/nrendo.2012.36

Torres-Castro, I., Arroyo-Camarena, U. D., Martinez-Reyes, C. P., Gomez-Arauz, A. Y., Duenas-Andrade, Y., Hernandez-Ruiz, J., et al. (2016). Human Monocytes and Macrophages Undergo M1-type Inflammatory Polarization in Response to High Levels of Glucose. *Immunol. Lett.* 176, 81–89. doi:10.1016/j.imlet.2016.06.001

Upton, P. D., Long, L., Trembath, R. C., and Morrell, N. W. (2008). Functional Characterization of Bone Morphogenetic Protein Binding Sites and Smad1/5 Activation in Human Vascular Cells. *Mol. Pharmacol.* 73, 539–552. doi:10.1124/mol.107.041673

Urist, M. R. (1965). Bone: Formation by Autoinduction. *Ann. Surg.* 220, 680–686. doi:10.1126/science.150.3698.893

Villa-Bellosta, R., and O'neill, W. C. (2018). Pyrophosphate Deficiency in Vascular Calcification. *Kidney Int.* 93, 1293–1297. doi:10.1016/j.kint.2017.11.035

Vinuesa, A. G. D., Abdelilah-Seyfried, S., Knaus, P., Zwijsen, A., and Bailly, S. (2015). BMP Signaling in Vascular Biology and Dysfunction. *Cytokine Growth Factor Rev.* 27, 65–79. doi:10.1016/j.cytogfr.2015.12.005

Voelkl, J., Lang, F., Eckardt, K. U., Amann, K., Kuro, O. M., Pasch, A., et al. (2019). Signaling Pathways Involved in Vascular Smooth Muscle Cell Calcification during Hyperphosphatemia. *Cell Mol Life Sci* 76, 2077–2091. doi:10.1007/s00018-019-03054-z

Waldo, K. L., Hutson, M. R., Ward, C. C., Zdanowicz, M., Stadt, H. A., Kumiski, D., et al. (2005). Secondary Heart Field Contributes Myocardium and Smooth Muscle to the Arterial Pole of the Developing Heart. *Dev. Biol.* 281, 78–90. doi:10.1016/j.ydbio.2005.02.012

Wang, S., Hu, S., Wang, J., Liu, Y., Zhao, R., Tong, M., et al. (2018). Conditioned Medium from Bone Marrow-Derived Mesenchymal Stem Cells Inhibits Vascular Calcification through Blockade of the BMP2-Smad1/5/8 Signaling Pathway. *Stem Cel Res Ther* 9, 160. doi:10.1186/s13287-018-0894-1

Wei, X., Wu, W., Li, L., Lin, J., Liu, Q., Gan, L., et al. (2018). Bone Morphogenetic Proteins 2/4 Are Upregulated during the Early Development of Vascular Calcification in Chronic Kidney Disease. *Biomed. Res. Int.* 2018, 8371604. doi:10.1155/2018/8371604

Widlansky, M. E., Gokce, N., Keaney, J. F., and Vita, J. A. (2003). The Clinical Implications of Endothelial Dysfunction. *J. Am. Coll. Cardiol.* 42, 1149–1160. doi:10.1016/s0735-1097(03)00994-x

Willems, B. A., Furmanik, M., Caron, M. M. J., Chatrou, M. L. L., Kusters, D. H. M., Welting, T. J. M., et al. (2018). Ucma/GRP Inhibits Phosphate-Induced Vascular Smooth Muscle Cell Calcification via SMAD-dependent BMP Signalling. *Sci. Rep.* 8, 4961. doi:10.1038/s41598-018-23353-y

Yang, P., Troncone, L., Augur, Z. M., Kim, S. S. J., Mcneil, M. E., and Yu, P. B. (2020). The Role of Bone Morphogenetic Protein Signaling in Vascular Calcification. *Bone* 141, 115542. doi:10.1016/j.bone.2020.115542

Yao, Y., Bennett, B. J., Wang, X., Rosenfeld, M. E., Giachelli, C., Lusis, A. J., et al. (2010). Inhibition of Bone Morphogenetic Proteins Protects against Atherosclerosis and Vascular Calcification. *Circ. Res.* 107, 485–494. doi:10.1161/CIRCRESAHA.110.219071

Yu, L., Hebert, M., and Zhang, Y., E. (2002). TGF-beta Receptor-Activated P38 MAP Kinase Mediates Smad-independent TGF-Beta Responses [S]. *EMBO JOURNAL* 21, 3749–3759. doi:10.1093/emboj/cdf366

Yuan, C., Ni, L., Zhang, C., Hu, X., and Wu, X. (2021). Vascular Calcification: New Insights into Endothelial Cells. *Microvasc. Res.* 134, 104105. doi:10.1016/j.mvr.2020.104105

Zhang, K., Gao, J., Jie, C., Xun, L., and Hui, H. (2016). MICS, an Easily Ignored Contributor to Arterial Calcification in CKD Patients. *AJP Ren. Physiol.* 311, 00189–02016. doi:10.1152/ajprenal.00189.2016

Zhu, D., Mackenzie, N. C., Millan, J. L., Farquharson, C., and Macrae, V. E. (2011). The Appearance and Modulation of Osteocyte Marker Expression during Calcification of Vascular Smooth Muscle Cells. *PLoS One* 6, e19595. doi:10.1371/journal.pone.0019595

Zhu, Y., Han, X. Q., Sun, X. J., Yang, R., Ma, W. Q., and Liu, N. F. (2020). Lactate Accelerates Vascular Calcification through NR4A1-Regulated Mitochondrial Fission and BNIP3-Related Mitophagy. *Apoptosis* 25, 321–340. doi:10.1007/s10495-020-01592-7

Conflict of Interest: The authors declare that the research was conducted in the absence of any commercial or financial relationships that could be construed as a potential conflict of interest.

Publisher's Note: All claims expressed in this article are solely those of the authors and do not necessarily represent those of their affiliated organizations or those of the publisher, the editors, and the reviewers. Any product that may be evaluated in this article, or claim that may be made by its manufacturer, is not guaranteed or endorsed by the publisher.

frontiers | Frontiers in Pharmacology

ORIGINAL RESEARCH
published: 25 April 2022
doi: 10.3389/fphar.2022.899775

Atractylenolide-1 Targets FLT3 to Regulate PI3K/AKT/HIF1-α Pathway to Inhibit Osteogenic Differentiation of Human Valve Interstitial Cells

Jie Wang[1], *Penghua Zhang*[1], *Jing Zhang*[1], *Zhaohui Ma*[1], *Xingqin Tian*[2], *Yan Liu*[3], *Guanghui Lv*[1]* *and Linghang Qu*[4]*

[1]Department of Pharmacy, Taihe Hospital, Hubei University of Medicine, Shiyan, China, [2]Department of Combine Traditional Chinese and Western Medicine, Taihe Hospital, Hubei University of Medicine, Shiyan, China, [3]Children's Medical Center, Taihe Hospital, Hubei University of Medicine, Shiyan, China, [4]College of Pharmacy, Hubei University of Chinese Medicine, Wuhan, China

OPEN ACCESS

Edited by:
Jing Xie,
Sichuan University, China

Reviewed by:
Yuming Huang,
Nanjing Medical University, China
Ming Liu,
Huazhong University of Science and Technology, China
Jun Fang,
Shanghai Jiao Tong University, China

***Correspondence:**
Guanghui Lv
lgh0725@taihehospital.com
Linghang Qu
qulinghang@163.com

Specialty section:
This article was submitted to Experimental Pharmacology and Drug Discovery, a section of the journal Frontiers in Pharmacology

Received: 19 March 2022
Accepted: 06 April 2022
Published: 25 April 2022

Citation:
Wang J, Zhang P, Zhang J, Ma Z, Tian X, Liu Y, Lv G and Qu L (2022) Atractylenolide-1 Targets FLT3 to Regulate PI3K/AKT/HIF1-α Pathway to Inhibit Osteogenic Differentiation of Human Valve Interstitial Cells. Front. Pharmacol. 13:899775. doi: 10.3389/fphar.2022.899775

Atractylenolide-1 (AT-1), a natural active ingredient extracted from *Atractylodes macrocephal*a, was reported to have good anti-fibrotic and anti-inflammatory effects. Osteogenic changes induced by the inflammation of valve interstitial cells (VICs) play a role in the development of calcified aortic valve disease (CAVD). This study aimed to investigate the anti-osteogenic effects of AT-1 in human VICs. Human VICs were exposed to osteogenic induction medium (OM) containing AT-1 to analyze cell viability, as well as protein and osteogenic gene expression. Anti-calcification tests were also performed. mRNA transcriptome sequencing was performed to identify differential genes and pathways regulated by AT-1. Western blotting was used to verify the enrichment pathway, protein-protein interaction (PPI) analysis was conducted to identify drug targets. Finally, molecular docking and inhibitors are used to verify the drug targets. Treatment of VICs with 20 μM AT-1 resulted in no significant cytotoxicity. The addition of AT-1 to OM prevented the accumulation of calcified nodules, and decreases in the level of (Alkaline Phosphatase) ALP and RUNX2 gene and protein expression were observed. Atractylenolide-1 can target FLT3 protein and inhibit the phosphorylation of FLT3, thereby blocking PI3K/AKT pathway activation, reducing the production of Hypoxia inducible factor(HIF)1-α, and inhibiting the osteogenic differentiation of VICs. These results suggest AT-1 as a potential drug for treating calcified aortic valve disease.

Keywords: Atractylenolide-1, calcification, PI3K, FLT3, HIF1-α

INTRODUCTION

Calcified aortic valve disease (CAVD) is one of the most common heart valve diseases worldwide (Liu et al., 2020). About 1.6 million CAVD patients are predicted worldwide by 2017. CAVD leads to heart failure, resulting in tens of thousands of deaths each year (Yadgir et al., 2020). The lesion is characterized by fibrosis, as well as thickening and calcification of the aortic valve (Katsi et al., 2021). CAVD refers to chronic degeneration, fibrosis, and calcium deposition of the fibrous support of the heart valve, which can lead to thickening and hardening of the heart valve, thereby inducing heart valve stenosis, heart failure, or death (K. Xu et al., 2020). The factors influencing its incidence are complex, and the incidence increases with age, seriously threatening human health and life. The early symptoms of CAVD are the destruction of the

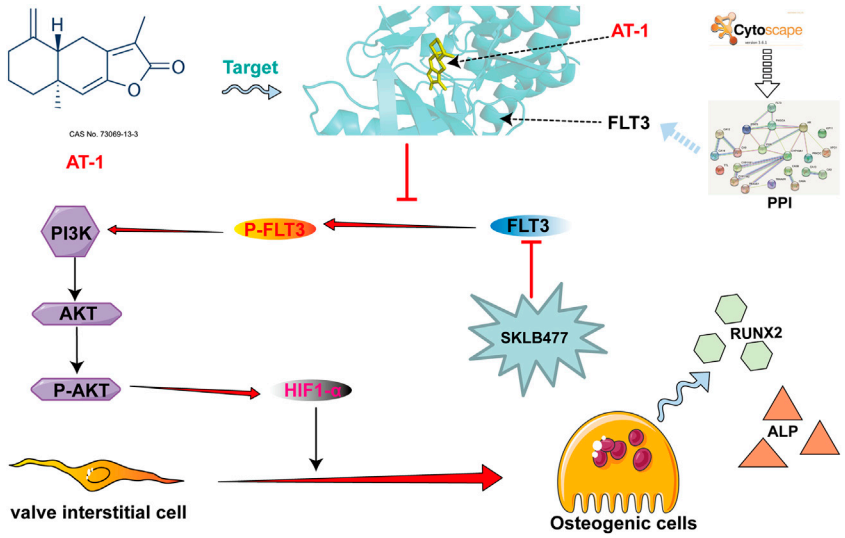

GRAPHICAL ABSTRACT |

endothelial layer on the aortic side of the valve leaflets. Stromal changes occur with age, resulting in thickening of the valve, and then, the leaflets are infiltrated by immune cells (Mohler, 2004). At the same time, angiogenesis is accompanied by the accumulation of cellular debris including lipids ad proteoglycans, which deforms the valve leaflets, calcifies the valve matrix, and stiffens the aortic valve, resulting in aortic valve stenosis and obstruction of the blood flow (Chen & Simmons, 2011). It is estimated that approximately 13% of calcified aortic valves at the time of surgery contain true bone as well as osteoblasts and osteoclasts (Mohler, 2004). The aortic valve consists of three small collagen leaflets, each of which is filled with valve interstitial cells (VICs) (Misfeld & Sievers, 2007). The osteoblastic differentiation of VICs is similar to physiological osteogenesis (Miller et al., 2011). Previous studies showed that inhibiting the osteogenic differentiation of VICs caused by inflammation could be the focus of CAVD treatment (Wang Y. et al., 2021).

Once valve calcification occurs, the lesion is histologically irreversible. The only clinically effective treatment for cardiac valve calcification is valve replacement (Hutcheson et al., 2014). At present, there is no suitable drug for the clinical treatment of CAVD. Therefore, the search for effective drugs for treating CAVD has attracted more and more attention. Traditional Chinese medicine (TCM) has played an important role in the prevention and treatment of heart-related diseases. Previously, the research group conducted anti-calcification screening of a large number of natural active components of Chinese herbal medicines and found some components that may have a therapeutic effect on CAVD, such as nobiletin (K. Xu et al., 2019), andrographolide (AGP) (Wang, et al., 2021a), and cardamonin (Wang, et al., 2021b). Among them, nobiletin and andrographolide have been patented.

Atractylenolide-1 (AT-1) is a natural product extracted from the TCM *Atractylodes macrocephala* or Atractylodes Rhizoma (Qu, et al., 2022a). Many previous studies reported that AT-1 had good anti-inflammatory and anti-fibrotic activity (Du et al., 2022; Guo et al., 2021; Liu, et al., 2021; H.; Xu et al., 2021). Our previous study also showed that AT-1 had a better therapeutic effect on (Dextran sulfate sodium) DSS-induced colitis (Qu, et al., 2022b). However, the therapeutic effect of AT-1 on CAVD has not been reported. Thus, we investigated the inhibitory effect and potential mechanism of AT-1 on the osteogenic differentiation of VICs.

MATERIALS AND METHODS

Cell Culture and Treatments

Human aortic VICs were isolated from patients undergoing Bentall surgery due to acute type I aortic dissection in Tongji Medical College, Huazhong University of Science and Technology. The patients provided written informed consent (**Supplementary Table S1**). The cells were separated according to the method in our previous study (K. Xu et al., 2019). After amplification, fourth or fifth-generation cells were used in all experiments. *In vitro*, osteogenic medium(OM) (Cyagen Biosciences, HUXMA-90021) was used to induce the osteogenic differentiation of the VICs. SKLB4771 was purchased from selleck(#S1099,China).

Cell Viability Testing

VICs were inoculated into 96-well plates, incubated with different concentrations of AT-1 for 48 h, and cell viability was measured using the CCK-8 (GLPBIO,#GK10001) method. VICs were inoculated into 48-well plates, incubated with or without 20 μm AT-1, and photographed under the microscope to record the cell morphology and density at the same time every day (Liu et al., 2020).

Calcification Analysis

VICs were inoculated into 24-well plates and divided into five groups: the control group, OM-stimulated group, OM + AT-1 10 μm group, OM + AT-1 20 μm group, and the OM + AGP group. The OM

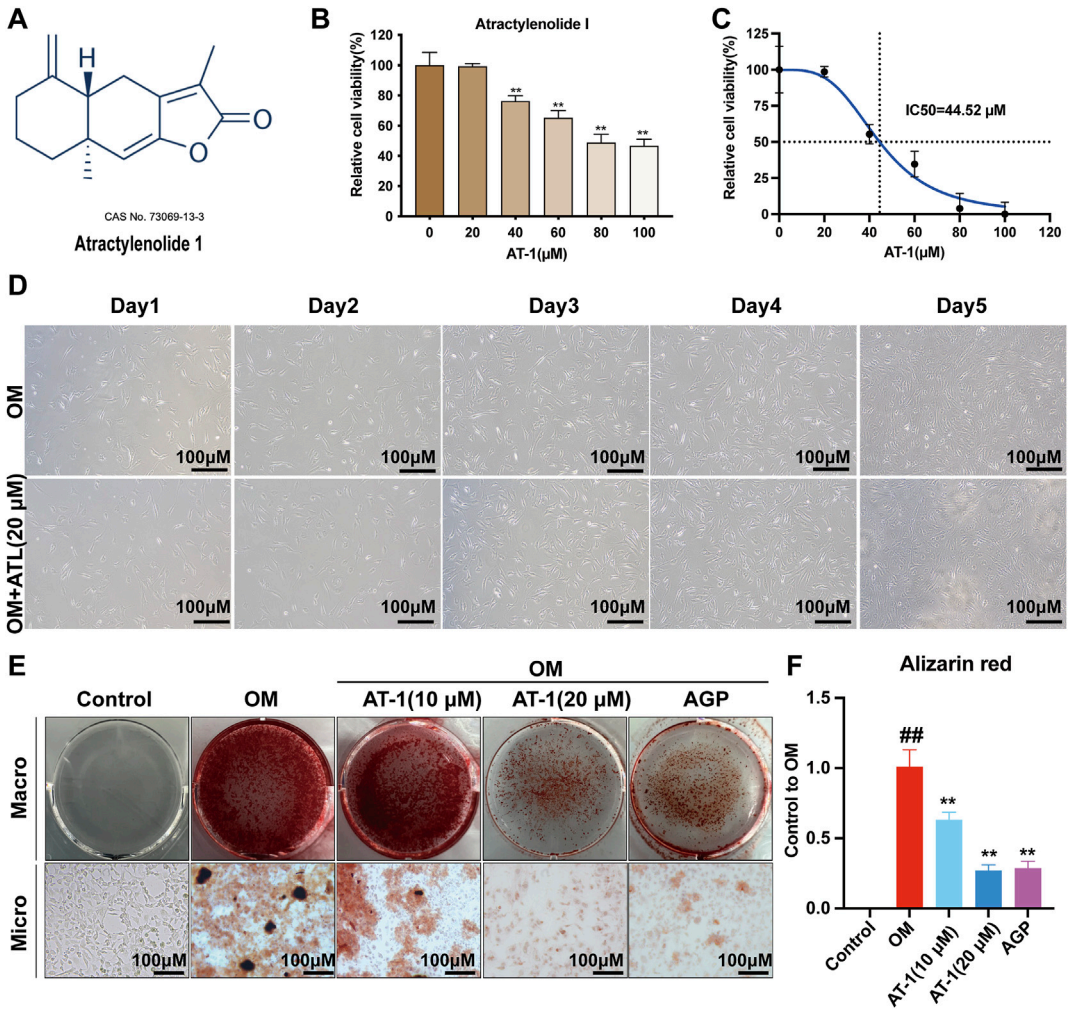

FIGURE 1 | Viability and calcification of VICs treated with AT-1. **(A)** Chemical structure of atractylenolide-1. **(B)** The CCK8 method was used to analyze the effect of treatment with different atractylenolide-1 concentrations on VICs. **(C)** IC50 of atractylenolide-1 in VIC cells. **(D)** Effect of no AT-1 and 20 μM AT-1 on the proliferation of OM-induced VIC cells in 5 days. **(E)** Cells with different treatments (control (normal culture medium), OM (osteogenic medium), OM+10 μM AT-1 (osteoblastic medium plus10 μM AT-1 treatment), OM+20 μM AT-1 (osteoblastic medium plus 20 μM AT-1 treatment), and OM + AGP (osteoblastic medium plus 10 μM andrographolide) were stained with Alizarin Red S. **(F)** Alizarin Red staining statistics. *$p < 0.05$, **$p < 0.01$ indicated a significant difference compared to the control group and #$p < 0.05$, ##$p < 0.01$ indicated a significant difference compared to the OM group, $n = 3$.

medium and therapeutic drugs were changed every three days. After 18 days of continuous culture, the calcified crystals were stained with Alizarin Red. Then, 10% aqueous solution of cetyl-pyridinium chloride solution was added to each well to dissolve the Alizarin Red dye. The amount of Alizarin Red dye was quantified by the absorbance at 550 (Liu et al., 2020).

RT-PCR

VICs were inoculated into 6-well plates, osteogenic differentiation was induced using OM medium, and the cells were treated with different concentrations of AT-1 and positive control drugs. After 48 h, total RNA was isolated from the cells using Trizol reagent.RNA was reverse transcribed into cDNA using a HiScript® II Q RT SuperMix (R223-01) (Vazyme Biotech Co., Ltd., Nanjing, China), and amplified on a PCR instrument, using 2X Universal SYBR Green Fast qPCR Mix (RK21203) (ABclonal Technology, Wuhan, China) for quantification. All primers were as in previous studies and synthesized by Tsingke Biotechnology Co., Ltd. **Supplementary Table S2** shows the primer sequences(Liu et al., 2020). The $2^{-\Delta\Delta CT}$ method was used to analyze the final data (Qu et al., 2021).

Western Blotting

VICs were inoculated into a 6-cm diameter dish and osteogenic differentiation was induced using OM medium. The cells were treated with different concentrations of AT-1 and positive control drugs. Total cellular proteins were collected in RIPA lysate. The protein concentration in the cells was measured using the enhanced BCA protein detection kit. Equal amounts of protein underwent 10% sodium dodecyl sulfate-polyacrylamide gel electrophoresis (SDS-PAGE) and were transferred to a polyvinylidene fluoride (PVDF)

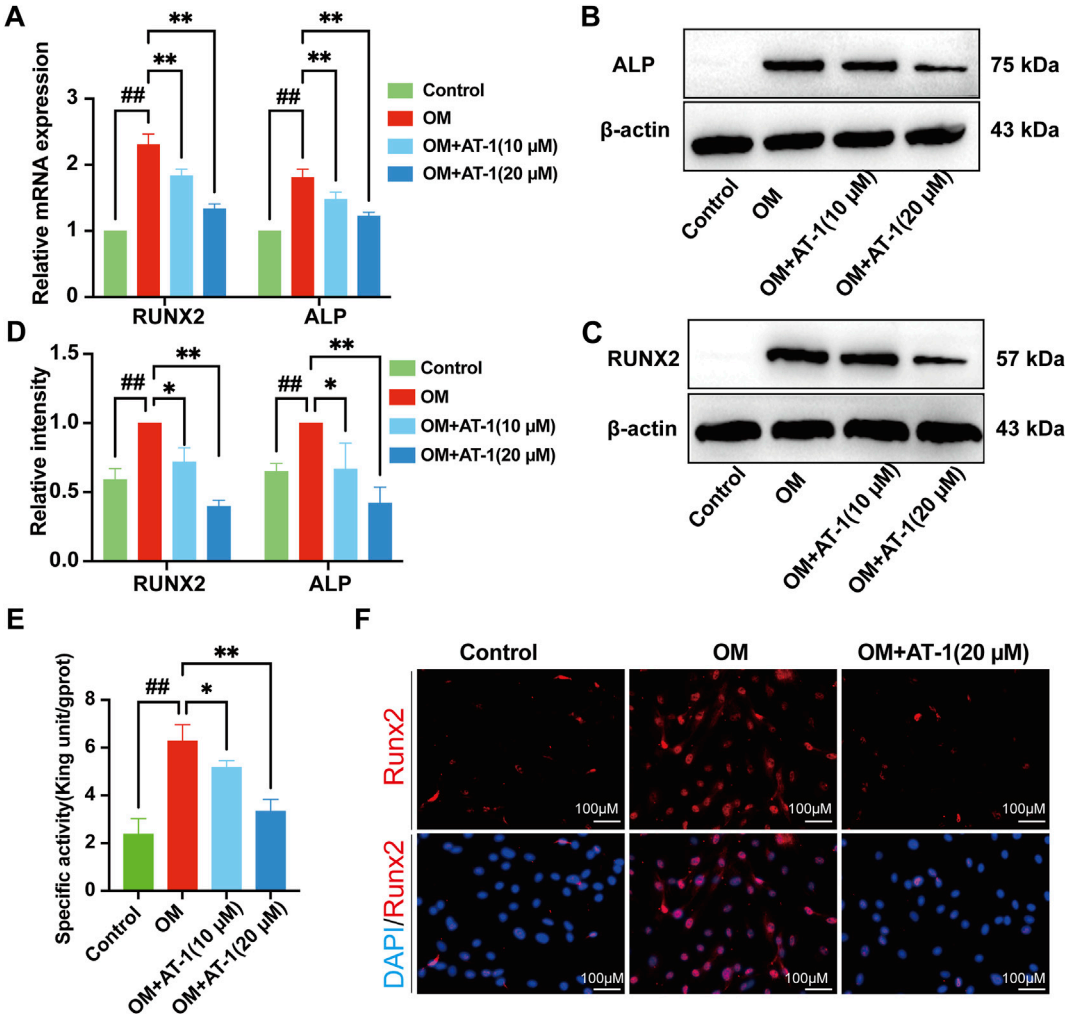

FIGURE 2 | Effect of AT-1 on OM-induced calcific-related gene and protein expression in VICs. **(A)** VICs were stimulated with OM and then treated or not with AT-1 for 48 h. The mRNA RUNX2 and ALP expression levels were analyzed by quantitative real-time polymerase chain reaction (qRT-PCR). **(B, C)** VICs were stimulated with OM and then treated or not with AT-1 and AGP for 48 h and the expression levels of RUNX2 and ALP protein were detected by Western blotting. **(D)** Statistical analysis of Runx2 and ALP protein expression. **(E)** The ALP activity of the VICs was measured using the ALP biochemical kit. **(F)** The expression of RUNX2 in VICs was evaluated at 48 h by immunofluorescence. $^{*}p < 0.05$, $^{**}p < 0.01$ indicated a significant difference compared to the control group and $\#p < 0.05$, $\#\#p < 0.01$ indicated a significant difference compared to the OM group, $n = 3$.

membrane overnight. The membranes were then blocked in 5% skimmed milk powder for one hour and incubated with primary antibodies against β-actin (Solarbio, #K2000558M), RUNX2 (Abcam, ab236639), ALP (Zenbio,#381009), HIF1-α (Abcam, ab179483, FLT3 (Cell Signaling Technology, #3462s), or P-FLT3 (Cell Signaling Technology, #60413) overnight at 4°C. Then, the membranes were washed with Tris-buffered saline with Tween 20 (TBST) at room temperature, followed by incubation with a secondary antibody for one hour. Enhanced chemiluminescence reagents were added, the protein bands were visualized using the Tanon-5200 system. ImageJ software was used to quantify the band density.

Colorimetric Detection of ALP Activity

After the VICs were treated with OM medium and drugs, the culture medium was aspirated, and the cells were washed once with phosphate-buffered saline (PBS). The cells were harvested by scraping them into PBS and collected by centrifugation at 1000 × g at 4°C for 10 min. Homogenization medium was added for mechanical homogenization at 4°C, centrifuged at 10,000 × g for 10 min, and the supernatant was collected. ALP activity was assayed according to the kit manufacturer, and the absorbance at 520 nm was measured with a UV spectrophotometer.

mRNA Profile Detection

Changes in cell mRNA profiles in the different treatment groups were analyzed by RNA-sequencing (RNA-seq). Isolated RNA samples were sent to BGI Co., LTD. in Wuhan for mRNA-seq using BGISEQ-500. Differentially expressed gene (DEG), Kyoto Encyclopedia of Genes and

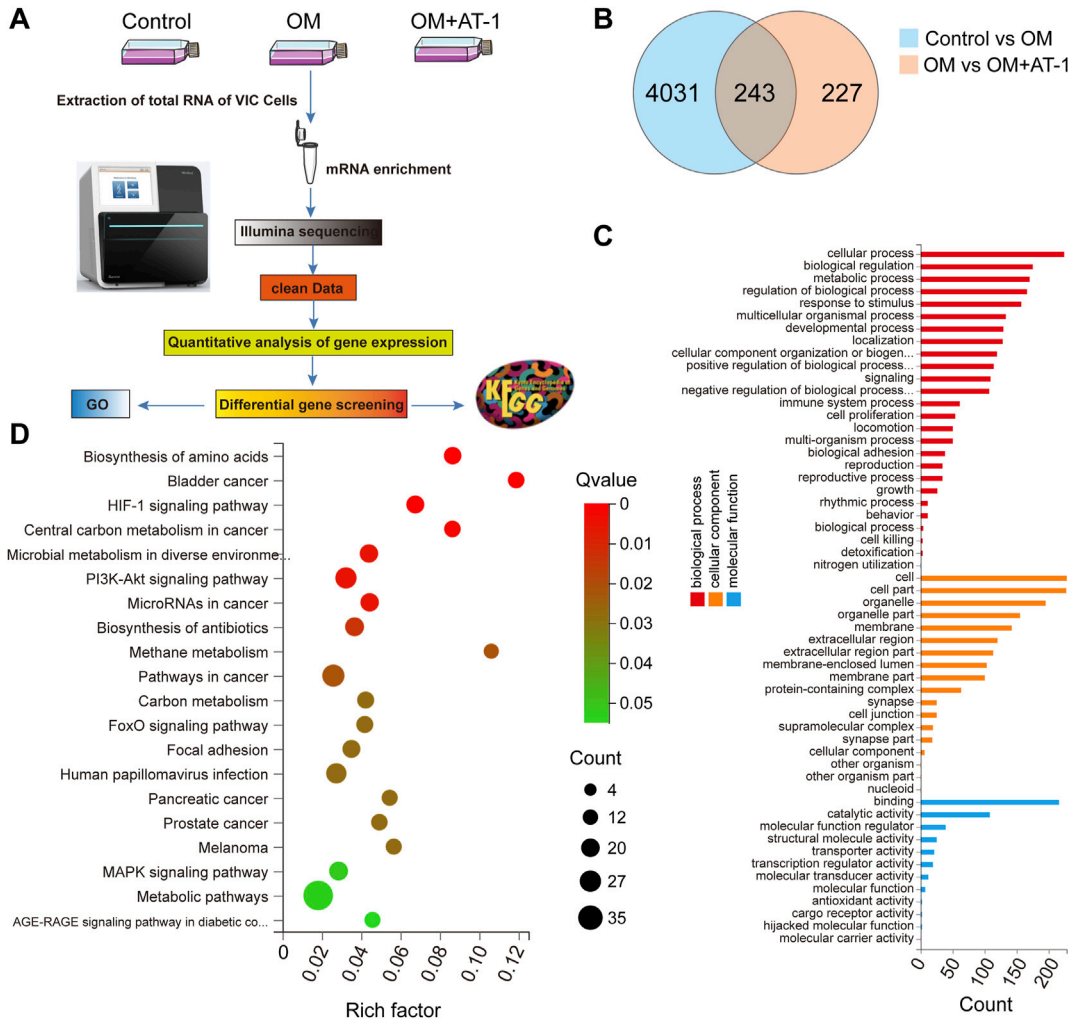

FIGURE 3 | Changes in gene expression under different treatments analyzed by mRNA-seq. **(A)** Schematic diagram of the mRNA transcriptome sequencing process. **(B)** Venn interaction of DEGs of the Control versus the OM group, and the OM group versus the OM + AT-1 group. **(C)** GO enrichment of the commonly detected DEGs, which included molecular function, cellular components, and biological processes. **(D)** KEGG pathway enrichment bubble map, where a larger *p*-value (-log10) indicates a higher degree of enrichment.

Genomes (KEGG), and Gene Ontology (GO) pathway enrichment analyses were performed using the online platform "Dr. Tom 2.0" designed by BGI Tech Co., LTD.

Immunofluorescence

OM stimulated VIC cells were administered with or without AT-1. After 48 h incubation, the medium was discarded and washed three times with PBS. Cells were fixed in 4% paraformaldehyde for 20 min at 25°C. Washed 3 times with PBS. Add 0.1% Triton X-100 and permeabilize for 20 min. Washed 3 times with PBS. Block with goat serum for 20 min. Primary antibody to RUNX2 was added and incubated overnight at 4 degrees. Washed 3 times with PBS. Add secondary antibody and incubate for 1 h. Washed 3 times with PBS. Slides were made and an anti-fluorescence quencher containing DAPI was added. The results were observed under a fluorescence microscope.

Protein-Protein Interaction Network

The String plugin in the Cytoscape software was installedAfter the installation was complete, the proteins that required protein interaction were imported. The cutoff value was set to 0.7. After the protein was imported, a preliminary network diagram was obtained.

Statistical Analysis

Statistical analysis was performed using GraphPad v8.0. Shapiro - Wilk test was applied for Normality tests and variance homogeneity. Data with normal distribution were analyzed by one-way analysis of variance (ANOVA), results are shown as mean ± standard deviation (SD). While those non-normally distributed or with uneven variance

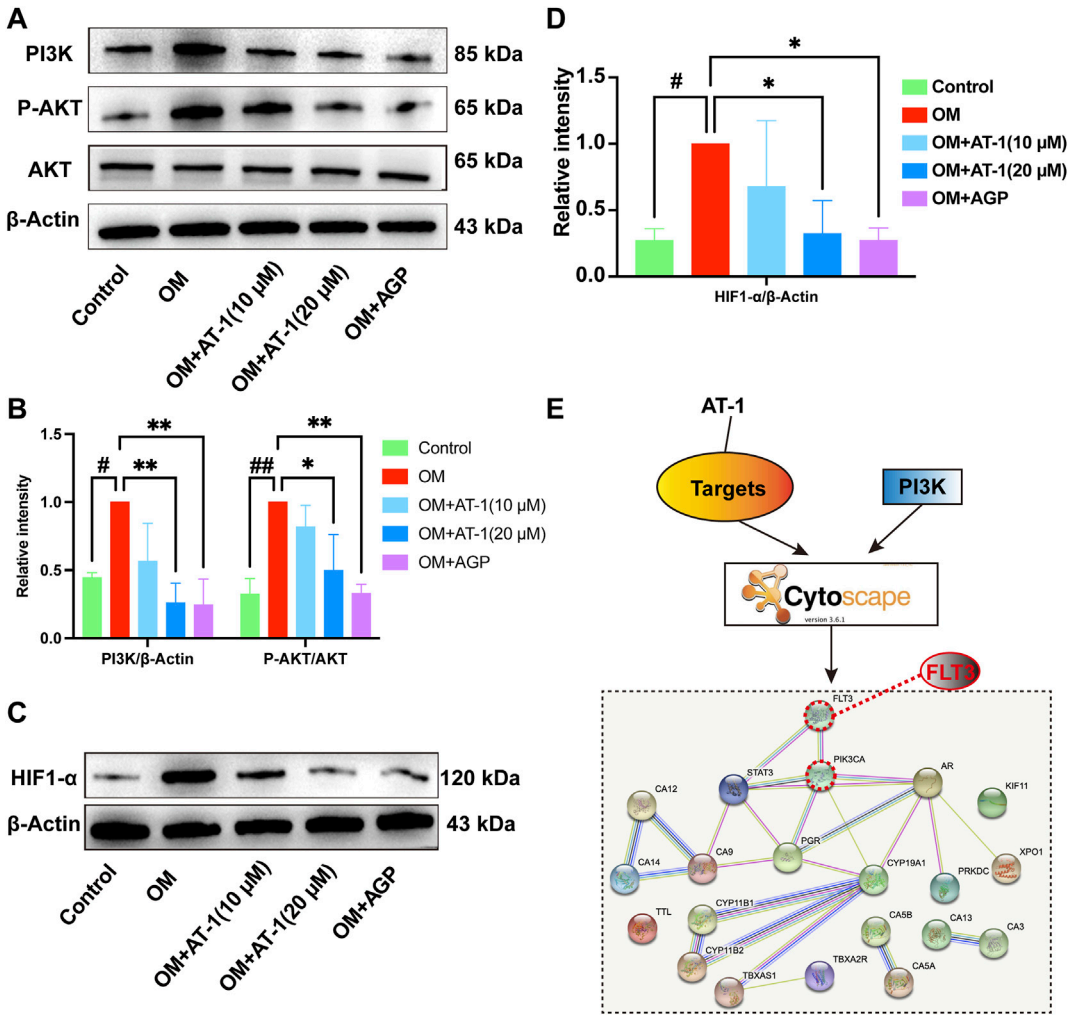

FIGURE 4 | The effect of AT-1 on the PI3K/AKT/HIF1-α pathway and investigations into its upstream targets. **(A)** Effect of different AT-1 and AGP concentrations on the expression of PI3K, AKT, and P-AKT proteins **(B)** Statistical analysis of PI3K/β-actin and P-AKT/AKT. **(C)** Effect of different AT-1 and AGP concentrations on the expression of HIF1-α protein. **(D)** Statistical analysis of HIF1-α/β-actin. **(E)** The predicted AT-1 targets and PI3K pathway proteins were subjected to PPI network association analysis to identify the upstream targets of AT-1 regulating the PI3K pathway. *$p < 0.05$, **$p < 0.01$ indicated a significant difference compared to the control group and #$p < 0.05$, ##$p < 0.01$ indicated a significant difference compared to the OM group, $n = 3$.

were analyzed by Kruskal-Wallis, results are shown as median (quartile). All data except RNA sequencing were analyzed by the above method. A value of $p < 0.05$ was considered statistically significant.

RESULTS

Viability and Calcification of VICs Treated With AT-1

Different concentrations of AT-1 were incubated with VICs for 48 h. The results showed that 0–20 μM AT-1 was not cytotoxic to the VICs (**Figures 1A,B**). Treatment with AT-1 at concentrations of over 40 μM obviously inhibited the proliferation of VICs, with an IC50 of 44.52 μM (**Figure 1C**). We further investigated state of cells treated with 20 μM AT-1 co-incubated with OM-induced VICs for 5 days. The results showed that 20 μM AT-1 did not affect the normal growth and proliferation of OM-induced VICs (**Figure 1D**). VICs were induced in OM medium for 18 days and treated with different concentrations of AT-1. AGP was used as the positive control. The Alizarin Red results showed that 10 and 20 μM AT-1 significantly inhibited the calcification of VICs (**Figures 1E,F**).

Effect of AT-1 on OM-Induced Calcific-Related Gene and Protein Expression in VICs

The expression of the osteogenic differentiation-related genes RUNX2 and ALP was analyzed in VICs cultured in OM with

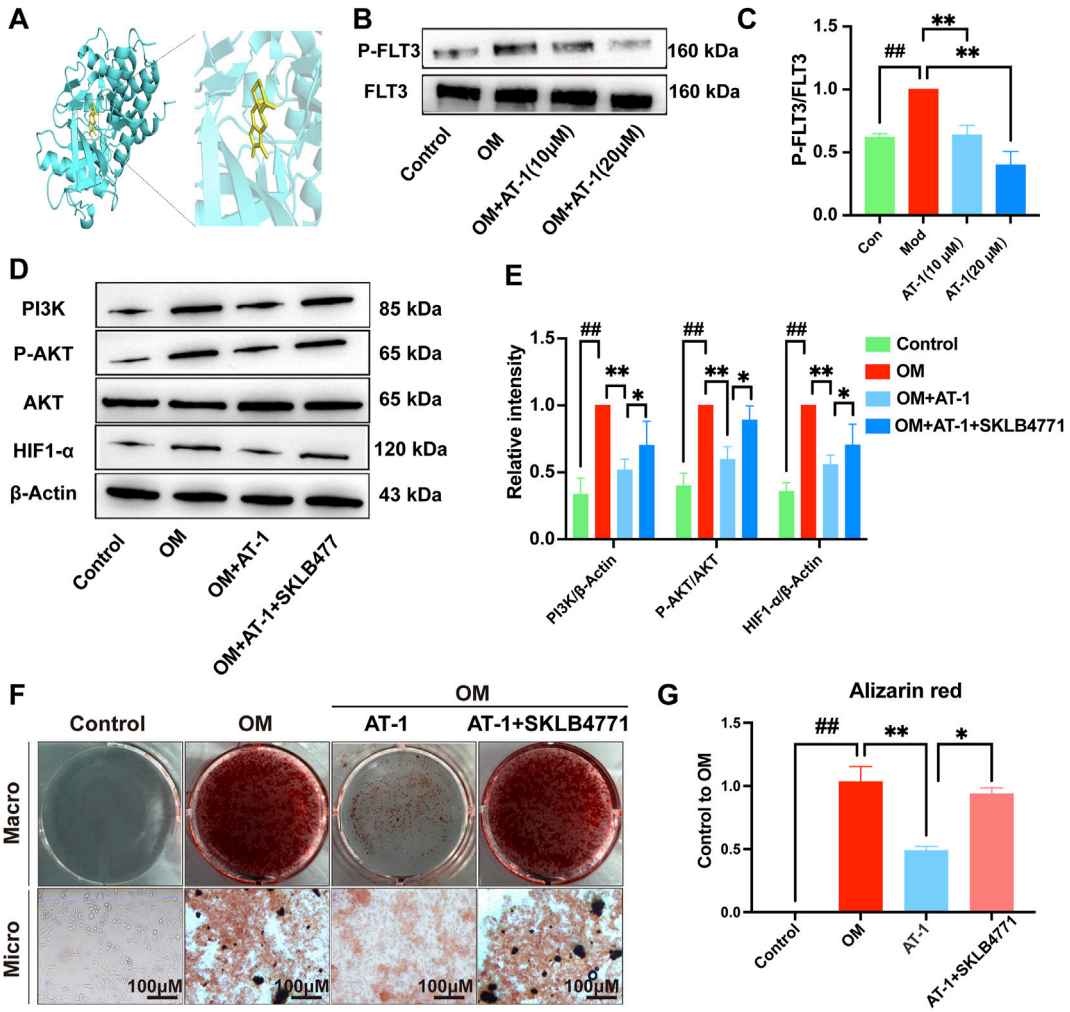

FIGURE 5 | AT-1 inhibits the phosphorylation of FLT3 and the activation of PI3K/AKT/HIF1-α, thereby inhibiting the osteogenic differentiation of VICs. **(A)** Molecular docking technology was used to detect the binding ability of AT-1 to FLT3 protein. **(B)** Effect of different AT-1 concentrations on the level of phosphorylated FLT3 protein in OM-induced VIC cells. **(C)** Statistical analysis of P-FLT3/FLT3. **(D)** Effect of AT-1 treatment with or without FLT3 inhibitor on the regulation of PI3K/AKT/HIF1-α in OM-induced VICs. **(E)** Statistical analysis of PI3K/β-actin, P-AKT/AKT, and HIF1-α/β-actin. **(F)** Cells with different treatments (control, OM, OM+20 μM AT-1, and OM+20 μM AT-1+10 nM SKLB4771) were stained with Alizarin Red S. **(G)** Alizarin Red staining statistics. $^{*}p < 0.05$, $^{**}p < 0.01$ indicated a significant difference compared to the control group and $\#p < 0.05$, $\#\#p < 0.01$ indicated a significant difference compared to the OM group, $n = 3$.

or without AT-1 for 48 h by RT-PCR. OM significantly upregulated ALP and RUNX2 expression ($^{*}p < 0.05$) compared to the control group, whereas ALP and RUNX2 were significantly downregulated in VICs treated with different concentrations of AT-1 in OM medium ($p < 0.05$) (**Figure 2A**).We detected the protein levels of RUNX2 and ALP in VICs stimulated in OM for 48 h by Western blots. AT-1 significantly inhibited increases in the protein expression of RUNX2 and ALP ($p < 0.05$) (**Figures 2B–D**). We used the ALP biochemical kit to measure ALP activity in the cells, which showed that the ALP activity of VICs stimulated by OM increased, and AT-1 inhibited the ALP activity (**Figure 2E**). We also detected the protein expression of RUNX2 in VICs induced by OM medium and treated with 20 μM AT-1 using immunofluorescence. The results showed that 20 μM AT-1 could significantly inhibit the increase in RUNX2 proteins induced by OM medium (**Figure 2F**).

Changes in Gene Expression Under Different Treatments Analyzed by mRNA-Seq

Investigate the mechanism by which AT-1 inhibited the osteogenic differentiation of valve cells, we collected mRNA from the normal group, OM-stimulated group, and the OM-stimulated group plus AT-1 group, and performed mRNA sequencing analysis, then GO enrichment and KEGG enrichment analyses (**Figure 3A**). The Venn diagram showed that there were 243 genes altered by AT-1

(**Figure 3B**). GO enrichment analysis showed that AT-1 mainly affected the biological processes of the cells (**Figure 3C**). KEGG enrichment analysis showed that AT-1 mainly regulated the PI3K-AKT pathway and the HIF1-α pathway (**Figure 3D**).

Effect of AT-1 on the PI3K/AKT/HIF1-α Pathway and Investigation of its Upstream Targets

To verify the mRNA transcriptome sequencing results, we collected proteins from the normal group, OM-stimulated group, OM-stimulated group plus different concentrations of AT-1, and the AGP administration group and performed Western blot analysis. The results showed that AT-1 dose-dependently inhibited the expression of PI3K protein, P-AKT protein, and HIF1-α protein (**Figures 4A–D**). To further clarify how AT-1 regulated the PI3K/AKT/HIF1-α pathway, we predicted the targets of AT-1 through the SwissTarget website, and then imported all the predicted targets and PI3K pathway proteins into Cytoscape software for PPI analysis. The results suggested that AT-1 may regulate the PI3K/AKT pathway by targeting FLT3 (**Figure 4E**).

AT-1 Inhibits the Phosphorylation of FLT3 and Inhibits the Activation of PI3K/AKT/HIF1-α in VICs

To verify the PPI analysis results, we used molecular docking technology to calculate the binding energy between AT-1 and FLT3 protein. The results showed that the binding energy of AT-1 and FLT3 protein was as high as −8.4 kcal/mol, indicating strong binding ability (**Figure 5A**). We compared the expression levels of FLT3 and its phosphorylation in the normal group, OM-stimulated group, and OM-stimulated group plus different doses of AT-1. The results showed that AT-1 dose-dependently inhibited the expression of phosphorylated FLT3 protein (**Figures 5B,C**). To further verify whether AT-1 targeted FLT3 to regulate the PI3K/AKT/HIF1-α pathway, we used the FLT3 inhibitor SKLB477. The addition of SKLB477 prevented the AT-1 inhibition of the PI3K/AKT/HIF1-α pathway (**Figures 5D,E**). The Alizarin Red results showed that the inhibitory effect of AT-1 on the osteogenic differentiation of valve cells was reversed after adding SKLB477 (**Figures 5F,G**).

DISCUSSION

Our results show that AT-1 targeted the FLT3 protein and inhibited the phosphorylation of FLT3, blocking PI3K/AKT pathway activation and reducing the production of HIF1-α, thereby inhibiting the osteogenic differentiation of VICs.

Overactivation or alterations in the PI3K/AKT pathway, which regulates cellular processes including metabolism, proliferation, growth, survival, angiogenesis, and metastasis, are seen in many cancer types. The PI3K/AKT/mTOR pathway is regulated by multiple upstream signaling proteins, which affect many downstream effectors by cooperating with various compensatory signaling pathways (Ersahin, Tuncbag, & Cetin-Atalay, 2015). Many studies have shown that the activation of the PI3K/AKT pathway was involved in promoting the osteogenic differentiation of valve cells and that inhibiting the activation of the PI3K/AKT pathway was an important strategy to prevent valve cell calcification (Zhu et al., 2019). For example, curcumin was shown to inhibit the osteogenic differentiation of valve cells by inhibiting the PI3K/AKT pathway (Zhou et al., 2020). Studies showed that caffeic acid improved calcification in human aortic valve interstitial cells by inhibiting the activation of the AKT/NF-κB/NLRP3 inflammasome pathway (Liu et al., 2020). This study found that AT-1 inhibited PI3K protein and P-AKT protein overexpression in VICs.

HIF1-α is a key transcription factor in response to hypoxia. HIF-1 was shown to be a key regulator of vascular calcification (Patten et al., 2010). HIF-1 α expression was significantly increased in various ischemic organs and tissues such as the retina, nervous system, and myocardium. The protective effect of HIF-1 has also been widely reported in various ischemic models (Yao et al., 2016). Previous studies have also shown that HIF-1 α was regulated by the PI3K/Akt/FRAP and PI3K/Akt/mTOR signaling pathways. HIF-1α and P-Akt protein levels were increased in response to hypoxia in human mesenchymal stem cells. Additionally, peak p-Akt expression occurred earlier than that of HIF-1 α. The PI3K inhibitor LY294002 and the PI3K/mTOR inhibitor NVP-BEZ235 inhibited ischemia-induced p-Akt and HIF-1α activation. The Akt inhibitor wortmannin was also shown to inhibit HIF-1α (Zhong et al., 2000) (Li, Qu, Mao, Xiong, & Mu, 2008). Our study showed that HIF1-α was highly expressed in the osteogenic differentiation process of VICs, and AT-1 significantly inhibited HIF1-α expression.

FLT3 (Fms-like tyrosine kinase, FMS-like tyrosine kinase 3) is a member of the type III receptor tyrosine kinase (RTK III) family (Chougule et al., 2016). In recent years, many large sample studies have reported the important pathological role played by the activation of FLT3 mutation in the occurrence and progression of acute myelocytic leukemia(AML). FLT3 receptor tyrosine kinase is activated in the plasma membrane to transduce RAS/MAPK and PI3K/Akt signaling (Lv et al., 2021). Our study showed that AT-1 could target FLT3 protein and inhibit the phosphorylation of FLT3 protein, thus inhibiting PI3K/Akt/HIF1 pathway activation.

In conclusion, our study found for the first time that AT-1 could inhibit the osteogenic differentiation of VICs, and preliminarily revealed that its mechanism may be related to targeting FLT3 and inhibiting PI3K/Akt/HIF1 pathway activation, providing a new strategy for treating aortic calcification. However, our research still had some limitations. Due to the lack of appropriate animal models and the long time required for the existing animal models, we could not verify the efficacy of AT-1 in the treatment of valve

calcification in the appropriate animal models. Next, we will explore its efficacy and mechanism in animal models.

DATA AVAILABILITY STATEMENT

The datasets presented in this study can be found in online repositories. The names of the repository/repositories and accession number(s) can be found below: https://www.ncbi.nlm.nih.gov/; PRJNA817634.

ETHICS STATEMENT

The animal study was reviewed and approved by the Hubei University of Chinese Medicine Animal Ethics Committee with respect to ethical issues and scientific care.

AUTHOR CONTRIBUTIONS

JW, GL, and LQ conceived, designed, and supervised the experiments. LQ and JW performed the experiment. PZ, JZ, and ZM analyzed the data and prepared figures. LQ wrote the manuscript. XT and YL provided the financial resources. The authors declare that all data were generated in-house, and no paper mill was used. All authors agree to be accountable for all aspects of work ensuring integrity and accuracy.

SUPPLEMENTARY MATERIAL

The Supplementary Material for this article can be found online at: https://www.frontiersin.org/articles/10.3389/fphar.2022.899775/full#supplementary-material

REFERENCES

Chen, J. H., and Simmons, C. A. (2011). Cell-matrix Interactions in the Pathobiology of Calcific Aortic Valve Disease: Critical Roles for Matricellular, Matricrine, and Matrix Mechanics Cues. *Circ. Res.* 108 (12), 1510–1524. doi:10.1161/circresaha.110.234237

Chougule, R. A., Cordero, E., Moharram, S. A., Pietras, K., Rönnstrand, L., and Kazi, J. U. (2016). Expression of GADS Enhances FLT3-Induced Mitogenic Signaling. *Oncotarget* 7 (12), 14112–14124. doi:10.18632/oncotarget.7415

Du, Z., Ma, Z., Lai, S., Ding, Q., Hu, Z., Yang, W., et al. (2022). Atractylenolide I Ameliorates Acetaminophen-Induced Acute Liver Injury *via* the TLR4/MAPKs/NF-Kb Signaling Pathways. *Front. Pharmacol.* 13, 797499. doi:10.3389/fphar.2022.797499

Ersahin, T., Tuncbag, N., and Cetin-Atalay, R. (2015). The PI3K/AKT/mTOR Interactive Pathway. *Mol. Biosyst.* 11 (7), 1946–1954. doi:10.1039/c5mb00101c

Guo, Y., Xiao, Y., Zhu, H., Guo, H., Zhou, Y., Shentu, Y., et al. (2021). Inhibition of Proliferation-Linked Signaling Cascades with Atractylenolide I Reduces Myofibroblastic Phenotype and Renal Fibrosis. *Biochem. Pharmacol.* 183, 114344. doi:10.1016/j.bcp.2020.114344

Hutcheson, J. D., Aikawa, E., and Merryman, W. D. (2014). Potential Drug Targets for Calcific Aortic Valve Disease. *Nat. Rev. Cardiol.* 11 (4), 218–231. doi:10.1038/nrcardio.2014.1

Katsi, V., Magkas, N., Antonopoulos, A., Trantalis, G., Toutouzas, K., and Tousoulis, D. (2021). Aortic Valve: Anatomy and Structure and the Role of Vasculature in the Degenerative Process. *Acta Cardiol.* 76 (4), 335–348. doi:10.1080/00015385.2020.1746053

Li, L., Qu, Y., Mao, M., Xiong, Y., and Mu, D. (2008). The Involvement of Phosphoinositid 3-kinase/Akt Pathway in the Activation of Hypoxia-Inducible Factor-1alpha in the Developing Rat Brain after Hypoxia-Ischemia. *Brain Res.* 1197, 152–158. doi:10.1016/j.brainres.2007.12.059

Liu, M., Li, F., Huang, Y., Zhou, T., Chen, S., Li, G., et al. (2020). Caffeic Acid Phenethyl Ester Ameliorates Calcification by Inhibiting Activation of the AKT/NF-κB/NLRP3 Inflammasome Pathway in Human Aortic Valve Interstitial Cells. *Front. Pharmacol.* 11 (826), 1–9. doi:10.3389/fphar.2020.00826

Liu, M., Wang, R. B., Xing, J. H., and Tang, Y. X. (2021). Atractylenolide Inhibits Apoptosis and Oxidative Stress of HTR-8/SVneo Cells by Activating MAPK/ERK Signalling in Preeclampsia. *Phytomedicine* 93, 153773. doi:10.1016/j.phymed.2021.153773

Lv, K., Ren, J. G., Han, X., Gui, J., Gong, C., and Tong, W. (2021). Depalmitoylation Rewires FLT3-ITD Signaling and Exacerbates Leukemia Progression. *Blood* 138 (22), 2244–2255. doi:10.1182/blood.2021011582

Miller, J. D., Weiss, R. M., and Heistad, D. D. (2011). Calcific Aortic Valve Stenosis: Methods, Models, and Mechanisms. *Circ. Res.* 108 (11), 1392–1412. doi:10.1161/circresaha.110.234138

Misfeld, M., and Sievers, H. H. (2007). Heart Valve Macro- and Microstructure. *Philos. Trans. R. Soc. Lond. B Biol. Sci.* 362 (1484), 1421–1436. doi:10.1098/rstb.2007.2125

Mohler, E. R., 3rd. (2004). Mechanisms of Aortic Valve Calcification. *Am. J. Cardiol.* 94 (11), 1396–1402. doi:10.1016/j.amjcard.2004.08.013

Patten, D. A., Lafleur, V. N., Robitaille, G. A., Chan, D. A., Giaccia, A. J., and Richard, D. E. (2010). Hypoxia-inducible Factor-1 Activation in Nonhypoxic Conditions: the Essential Role of Mitochondrial-Derived Reactive Oxygen Species. *Mol. Biol. Cel* 21 (18), 3247–3257. doi:10.1091/mbc.E10-01-0025

Qu, L., Lin, X., Liu, C., Ke, C., Zhou, Z., Xu, K., et al. (2021). Atractylodin Attenuates Dextran Sulfate Sodium-Induced Colitis by Alleviating Gut Microbiota Dysbiosis and Inhibiting Inflammatory Response through the MAPK Pathway. *Front. Pharmacol.* 12, 665376. doi:10.3389/fphar.2021.665376

Qu, L., Liu, C., Ke, C., Zhan, X., Li, L., Xu, H., et al. (2022a). Atractylodes Lancea Rhizoma Attenuates DSS-Induced Colitis by Regulating Intestinal Flora and Metabolites. *Am. J. Chin. Med.* 50, 525–552. doi:10.1142/s0192415x22500203

Qu, L., Shi, K., Xu, J., Liu, C., Ke, C., Zhan, X., et al. (2022b). Atractylenolide-1 Targets SPHK1 and B4GALT2 to Regulate Intestinal Metabolism and flora Composition to Improve Inflammation in Mice with Colitis. *Phytomedicine* 98, 153945. doi:10.1016/j.phymed.2022.153945

Wang, C., Huang, Y., Liu, X., Li, L., Xu, H., Dong, N., et al. (2021a). Andrographolide Ameliorates Aortic Valve Calcification by Regulation of Lipid Biosynthesis and Glycerolipid Metabolism Targeting MGLL Expression *In Vitro* and *In Vivo*. *Cell Calcium* 100, 102495. doi:10.1016/j.ceca.2021.102495

Wang, C., Xia, Y., Qu, L., Liu, Y., Liu, X., and Xu, K. (2021b). Cardamonin Inhibits Osteogenic Differentiation of Human Valve Interstitial Cells and Ameliorates Aortic Valve Calcification *via* Interfering in the NF-Kb/nlrp3 Inflammasome Pathway. *Food Funct.* 12 (23), 11808–11818. doi:10.1039/d1fo00813g

Wang, Y., Weng, Y., Li, X., Huang, Q., Xiang, Y., Li, X., et al. (2021). Dihydrotanshinone I Inhibits Aortic Valve Interstitial Cell Calcification *via* the SMAD1/5/8/NF-Kb/ERK Pathway. *Biomed. Pharmacother.* 139, 111674. doi:10.1016/j.biopha.2021.111674

Xu, H., Van der Jeught, K., Zhou, Z., Zhang, L., Yu, T., Sun, Y., et al. (2021). Atractylenolide I Enhances Responsiveness to Immune Checkpoint Blockade Therapy by Activating Tumor Antigen Presentation. *J. Clin. Invest.* 131 (10), e146832. doi:10.1172/jci146832

Xu, K., Huang, Y., Zhou, T., Wang, C., Chi, Q., Shi, J., et al. (2019). Nobiletin Exhibits Potent Inhibition on Tumor Necrosis Factor Alpha-Induced Calcification of Human Aortic Valve Interstitial Cells *via* Targeting ABCG2 and AKR1B1. *Phytother Res.* 33 (6), 1717–1725. doi:10.1002/ptr.6360

Xu, K., Xie, S., Huang, Y., Zhou, T., Liu, M., Zhu, P., et al. (2020). Cell-Type Transcriptome Atlas of Human Aortic Valves Reveal Cell Heterogeneity and Endothelial to Mesenchymal Transition Involved in Calcific Aortic Valve Disease. *Arterioscler Thromb. Vasc. Biol.* 40 (12), 2910–2921. doi:10.1161/atvbaha.120.314789

Yadgir, S., Johnson, C. O., Aboyans, V., Adebayo, O. M., Adedoyin, R. A., Afarideh, M., et al. (2020). Global, Regional, and National Burden of Calcific Aortic Valve and Degenerative Mitral Valve Diseases, 1990-2017. *Circulation* 141 (21), 1670–1680. doi:10.1161/circulationaha.119.043391

Yao, H. C., Zhou, M., Zhou, Y. H., Wang, L. H., Zhang, D. Y., Han, Q. F., et al. (2016). Intravenous High Mobility Group Box 1 Upregulates the Expression of HIF-1α in the Myocardium *via* a Protein Kinase B-dependent Pathway in Rats Following Acute Myocardial Ischemia. *Mol. Med. Rep.* 13 (2), 1211–1219. doi:10.3892/mmr.2015.4648

Zhong, H., Chiles, K., Feldser, D., Laughner, E., Hanrahan, C., Georgescu, M. M., et al. (2000). Modulation of Hypoxia-Inducible Factor 1alpha Expression by the Epidermal Growth Factor/phosphatidylinositol 3-kinase/PTEN/AKT/FRAP Pathway in Human Prostate Cancer Cells: Implications for Tumor Angiogenesis and Therapeutics. *Cancer Res.* 60 (6), 1541–1545.

Zhou, T., Wang, Y., Liu, M., Huang, Y., Shi, J., Dong, N., et al. (2020). Curcumin Inhibits Calcification of Human Aortic Valve Interstitial Cells by Interfering NF-Kb, AKT, and ERK Pathways. *Phytother Res.* 34 (8), 2074–2081. doi:10.1002/ptr.6674

Zhu, E., Liu, Z., He, W., Deng, B., Shu, X., He, Z., et al. (2019). CC Chemokine Receptor 2 Functions in Osteoblastic Transformation of Valvular Interstitial Cells. *Life Sci.* 228, 72–84. doi:10.1016/j.lfs.2019.04.050

Conflict of Interest: The authors declare that the research was conducted in the absence of any commercial or financial relationships that could be construed as a potential conflict of interest.

Publisher's Note: All claims expressed in this article are solely those of the authors and do not necessarily represent those of their affiliated organizations, or those of the publisher, the editors and the reviewers. Any product that may be evaluated in this article, or claim that may be made by its manufacturer, is not guaranteed or endorsed by the publisher.

frontiers | Frontiers in Pharmacology

ORIGINAL RESEARCH
published: 29 April 2022
doi: 10.3389/fphar.2022.871748

The Natural Product Andrographolide Ameliorates Calcific Aortic Valve Disease by Regulating the Proliferation of Valve Interstitial Cells *via* the MAPK-ERK Pathway

Yuming Huang[1†], *Ming Liu*[2†], *Chungeng Liu*[2], *Nianguo Dong*[2*] *and Liang Chen*[1*]

[1]Department of Thoracic Surgery, The First Affiliated Hospital of Nanjing Medical University, Nanjing, China, [2]Department of Cardiovascular Surgery, Union Hospital, Tongji Medical College, Huazhong University of Science and Technology, Wuhan, China

OPEN ACCESS

Edited by:
Jing Xie,
Sichuan University, China

Reviewed by:
Yongqiang Sha,
Huaqiao University, China
Jie Li,
University of South Florida, United States

***Correspondence:**
Nianguo Dong
dongnianguo@hotmail.com
Liang Chen
clbright0909@njmu.edu.cn

[†]These authors have contributed equally to this work

Specialty section:
This article was submitted to Experimental Pharmacology and Drug Discovery, a section of the journal Frontiers in Pharmacology

Received: 08 February 2022
Accepted: 28 March 2022
Published: 29 April 2022

Citation:
Huang Y, Liu M, Liu C, Dong N and Chen L (2022) The Natural Product Andrographolide Ameliorates Calcific Aortic Valve Disease by Regulating the Proliferation of Valve Interstitial Cells via the MAPK-ERK Pathway. Front. Pharmacol. 13:871748. doi: 10.3389/fphar.2022.871748

Calcific aortic valve disease (CAVD) is an active pathobiological process that involves fibrosis and calcification of aortic valve leaflets, thereby causing cardiac hemodynamic changes and eventually heart failure. Cell proliferation changes at the initial stage of CAVD are an important target for pharmaceutical intervention. This study aimed to investigate whether andrographolide (AGP) could inhibit the proliferation of valve interstitial cells (VICs) *in vitro* and *in vivo* to delay the process of CAVD. Cell proliferative factors were tested in both healthy and CAVD aortic valve samples. Cell cycle, cell growth, and calcification of VICs were assessed using flow cytometry, CCK8 assay, EdU staining, and Alizarin Red S staining. The expression of cell proliferative factors and osteogenic factors were quantified by qRT-PCR or immunofluorescence staining. The interaction between AGP and ERK (extracellular regulated protein kinases) was detected by molecular docking. In addition, a high-fat diet-fed animal model was used to verify the effect of AGP on CAVD *in vivo*. In conclusion, we found that AGP ameliorates aortic valve incrassation by inhibiting cell proliferation via the MAPK-ERK signaling pathway. Therefore, AGP is a promising drug that prevents the occurrence of CAVD via regulating cell proliferation.

Keywords: CAVD, andrographolide, cell proliferation, valve interstitial cell, MAPK /ERK2 pathway

INTRODUCTION

Calcific aortic valve disease (CAVD) primarily occurs in octogenarians, has high morbidity and mortality rates, and is extremely difficult to treat (Otto and Prendergast, 2014). To date, there is no pharmacological treatment for CAVD and surgery is the only effective cure. Therefore, the effective pharmacological treatment of CAVD remains a research focus (Hutcheson et al., 2014). Based on the histological features, CAVD is divided into two stages: fibrosis and biomineralization. In the initial stage, significant fibrous thickening of the valve interstitium due to a large number of proliferating cells leads to a decrease in leaflet elasticity and an increase in stiffness. Changes in the physical properties of valve leaflets lead to valve dysfunction, resulting in altered cardiac hemodynamics and CAVD-related pathological changes (Mathieu and Boulanger, 2014; Xu et al., 2020).

Andrographolide (AGP) is a natural terpenoid extracted from the traditional Chinese herbal plant *Andrographis paniculata*. AGP has anti-inflammatory, anti-atherosclerotic, and antitumorigenic activities (Yang et al., 2019). Our previous study indicated that AGP could attenuate the ossification

of valve interstitial cells (VICs) by inhibiting the inflammatory response (Huang et al., 2020). In addition, the study by Wang *et al.* reported that AGP could regulate the metabolic function of VICs (Wang et al., 2021a).

In the present study, we evaluated whether AGP could attenuate the abnormal proliferation of VICs during the process of aortic valve calcification. This study is an extension of our previous study, which explored the regulatory function of AGP on the proliferation of VICs and the underlying mechanism thereof. Our research indicated that AGP could inhibit the proliferation of VICs via the MAPK-ERK signaling pathway and ameliorate mice aortic valve incrassation induced by *in vivo* high-fat feeding.

MATERIALS AND METHODS

Cell Culture and Treatments

This study was approved by the Ethics Committee of Wuhan Union Hospital, Tongji Medical College, Huazhong University of Science and Technology in Wuhan, China. Patients provided signed informed consent. Calcific aortic valves samples were obtained from CAVD patients undergoing aortic valve replacement surgery, while control healthy aortic valves were obtained from patients undergoing Bentall surgery. Aortic valves were digested in 2 mg/ml type I collagenase (Sigma-Aldrich, Saint Louis, MO) for 6 h at 37°C, 5% CO_2 after washing with phosphate-buffered saline (PBS). Undigested tissues were removed using the 70 μm nylon cell filters; cells were then seeded in high glucose Dulbecco's modified Eagle's medium (DMEM) supplemented with 10% fetal bovine serum (FBS, Gibco Laboratories, Gaithersburg, MD) for primary cultures. We used the osteogenic medium (OM) to induce the osteogenic differentiation of VICs, and AGP was added to inhibit this process. Every experiment was repeated three times for each aortic valve sample (Xu et al., 2019; Liu et al., 2020; Zhou et al., 2020).

Western Blotting and Immunofluorescence

Western blotting: cell samples were extracted, quantified, and then boiled at 95 °C for min. The protein sample was separated on an 8% sodium dodecyl sulfate-polyacrylamide electrophoresis gel and then transferred on a polyvinylidene fluoride membrane. Finally, primary antibodies were incubated overnight at 4 °C, followed by the corresponding secondary antibodies for protein expression visualization.

Immunofluorescence: Cell samples were seeded on 24-well confocal culture plates at a density of 10,000 cells/well. Samples were washed twice with PBS, fixed in 4% paraformaldehyde for 15 min, and then washed again with PBS. Cells were permeabilized with 0.2% Triton X-100 for 10 min and blocked for 30 min with goat serum albumin (Boster, Wuhan, China). Then, it was incubated with primary antibodies at 4°C overnight, followed by incubating the fluorescent secondary antibody in the dark for 40 min at room temperature. Finally, the samples were washed twice with PBS and incubated with DAPI (Biofroxx GmbH, Einhausen, Germany) for a few minutes to stain the nuclei; then, they were imaged on the Axio Observer Z1 microscope (Zeiss, Oberkochen, Germany). The following antibodies were used: Runx2 (CST: 8486s, 1:1000), ALP (R&D systems: MAB29092, 1:500), CDK1 (Proteintech: 19532-1-AP, 1: 500), KI67 (Proteintech: 27309-1-AP, 1:200), anti-phospho-p38 (Thr180/Tyr182) (CST: 4511, 1:1000), anti-P38 (CST:8690, 1: 1000), anti-phospho-p44/42 mitogen-activated protein kinase (Erk) (Thr202/Tyr204) (CST: 4377, 1:1000), anti-Erk (CST: 4695, 1:1000), and E2F1 (Abcam: ab179445, 1:1000).

RNA Extraction and qPCR Analysis

Total cell RNA was extracted with Trizol reagent (Invitrogen, Carlsbad, CA). The real-time polymerase chain reaction (PCR) was performed on a StepOne Plus thermal cycler (Applied Biosystems, Foster City, CA) using a 2x SYBR Green qPCR Master Mix (High ROX) (Bimake, Houston, TX) following the manufacturer's guide. All the primers were referenced from the previous study (Xu et al., 2019). The final data were analyzed by the $2^{-\frac{\Delta\Delta c}{t}}$ method. The primers used were as follows: CDK1 (F: 5′-TCCTCCAGGGGATTGTGTTTT-3′; R: 5′-GCCAGTTTGATT GTTCCTTTGTC-3′), E2F1 (F: 5′-ACTTT GGTCTCGAGGAGGGT-3′; R: 5′-TGCTATTCCAACGAG GCAGG-3′), and MKI67 (F: 5′-GCCCCTGGAAGATTATGG TGG-3′; R: 5′-GGGTTCTGACTGGTTGTGGTTGT-3′).

FACS for Cell Cycle Cell Viability Assay

VICs (passage 3) were cultured in 60 mm dishes under different treatments. Then, the samples were trypsinized and re-suspended in PBS at $5*10^5$/ml, followed by fixation in 70% precooled ethanol overnight at 4°C, centrifugation, washing, and staining with PI/RNase staining buffer (BD Biosciences) for 30 min at 4°C. Cell counts at different phases of the cell cycle were analyzed by flow cytometry (FCM) as previously described (Huang et al., 2019).

Cell Viability Assay

Cell viability was assessed using the Cell Counting Kit-8 (CCK-8) assay (Bimake.com, Houston, TX, United States) according to the manufacturer's instructions. The cells were seeded at a density of 5,000 cells/well in 24-well plates and cultured for 6 days under different treatments. At the end of each time interval, the cell samples were washed with PBS and incubated with a serum-free medium containing 10% CCK-8 reagent for 4 h at 37°C, 5% CO_2, and 10 μl aliquots were pipetted into a 96-well plate and measured at 450 nm using an enzyme-labeling instrument (Thermo Fisher Scientific).

EdU Assay

Cell proliferation ability was tested by EdU assay (Ribobio bio, Guangzhou, China) according to the manufacturer's instructions. The cells were seeded at a density of 10,000 cells/well in 12-well plates. After different treatments, VICs were cultured in a medium containing Edu for 2 h at 37°C, 5% CO_2. The cell samples were fixed with 4% paraformaldehyde for 15 min then washed with PBS several times, stained with apollo staining solution for 30 min, and observed under the fluorescence microscope.

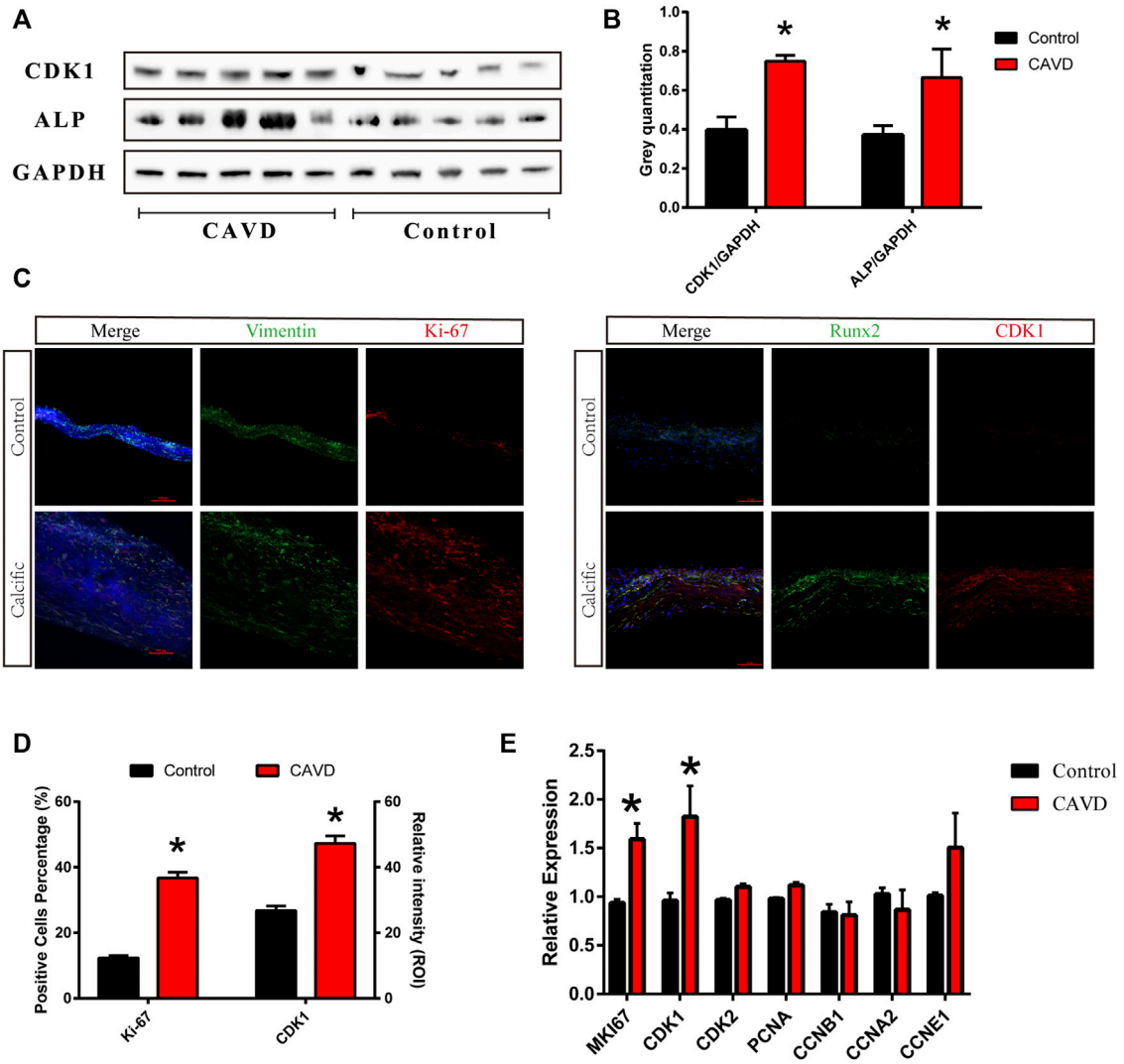

FIGURE 1 | Analysis of the control and CAVD aortic valve samples (n = 5 and 5, respectively). **(A)** Western blotting for CDK1 and ALP proteins on valve tissues. **(B)** Semi-quantitative analysis of protein expression. **(C)** Immunofluorescence staining of CDK1 and Ki-67 on valve tissues. **(D)** Semi-quantitative analysis of fluorescence intensity. **(E)** PCR test for cell proliferation genes on valve tissues. (*) $p < 0.05$ indicates a significant difference.

Molecular Docking

The andrographolide (AGP) compound structure is downloaded from the PubChem database (https://pubchem.ncbi.nlm.nih.gov/). The three-dimensional structure of Erk-2 (PDB ID: 4H3Q) is downloaded from the RCSB Protein Data Bank (www.rcsb.org). Autodock vina 1.1.2 was used for semi-flexible docking. Briefly, the coordinates and box size of the Vina molecule docking were determined, and then the parameter exhaustiveness was set as 20. Except for special instructions, other parameters adopt default values. The best affinity conformation with the lowest docking binding energy is selected as the final docking conformation. Pymol software was used for image construction.

Calcification Analysis

Cells were seeded into 12-well plates cultured in the OM (contained: 10 mM β-glycerophosphate, 100 nM dexamethasone, 50 μg/ml vitamin C, 2% FBS, 100 IU/ml penicillin/streptomycin) with or without AGP for 21 days. The degree of cell calcification was measured by Alizarin Red S stain based on the previous study (Huang et al., 2019,2020).

Animal Model

All animals used in this research were purchased from the Experimental Animal Center of Tongji Medical College, Huazhong University of Science and Technology (Wuhan, China). The $ApoE^{-/-}$ mice were fed a high-fat and high-cholesterol diet (42% fat, 0.25% cholesterol) for 24 weeks to induce aortic valves calcification. To treat CAVD, the disease model mice were treated with AGP at a dose of 10 mg/kg by gavage from 16 to 24 weeks. Then, the heart samples of mice were collected and histologically sectioned to isolate the aortic valves. HE staining was used to evaluate the thickness of the valves. Runx2 expression was analyzed by immunofluorescence staining *in*

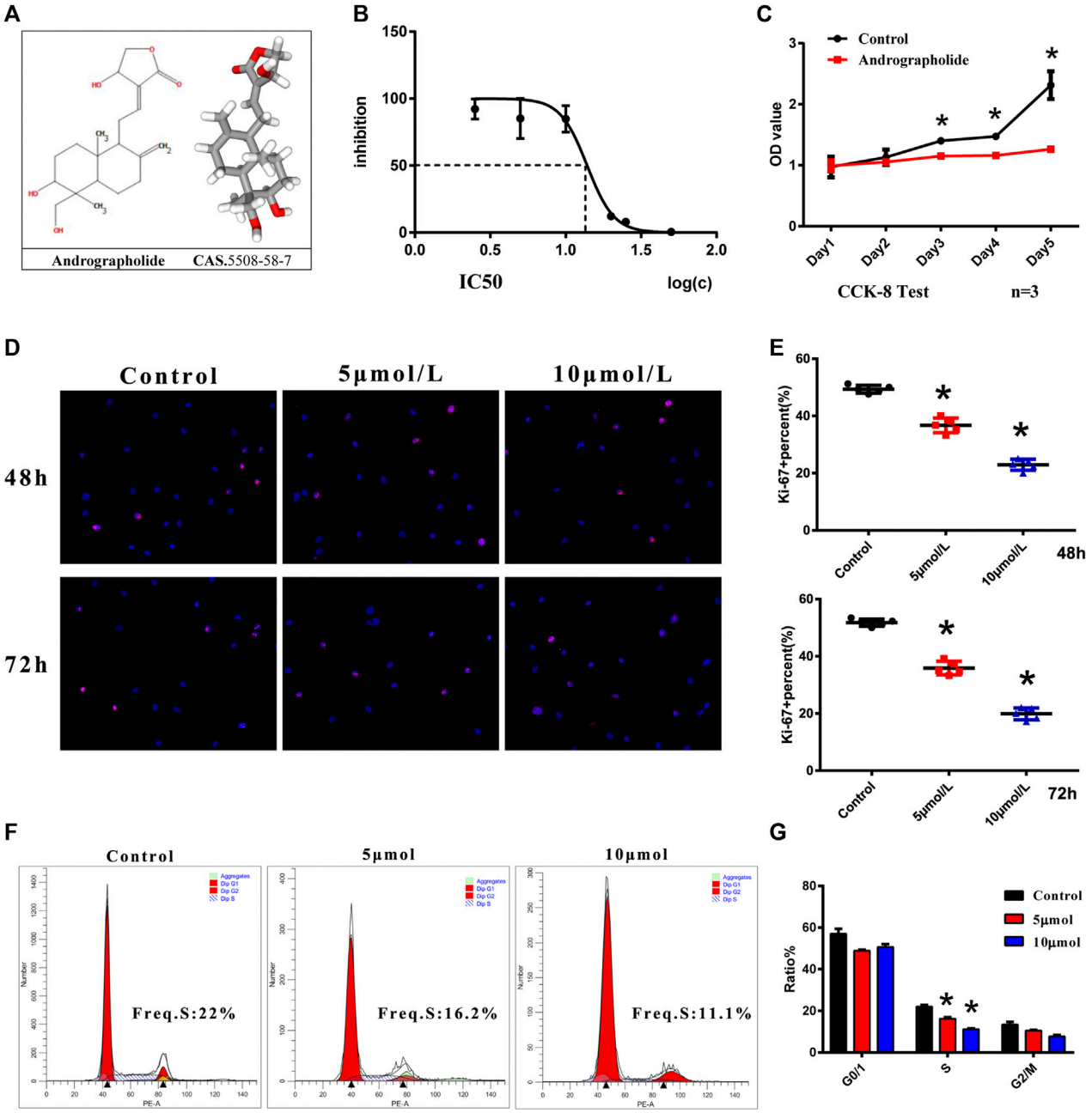

FIGURE 2 | Cell viability and proliferation of VICs with AGP treatment. **(A)** Two- and three-dimensional molecular structure of AGP. **(B)** Cytotoxicity of AGP on VICs. **(C)** Cell proliferation curve after AGP treatment (10 μM) for 5 days compared to the controls ($n = 3$). **(D)** Ki-67 staining of VICs with AGP treatment (red). **(E)** Percentage of Ki-67 positive cells. (*) $p < 0.05$ (vs control) indicates a significant difference. **(F)** Flow cytometry of cell cycle analysis of VICs after AGP treatment (10 μmol/L) for 72 h. **(G)** S, G0/G1, and G2/M phase cells were counted and compared. (*) $p < 0.05$ (vs control) indicates a significant difference ($n = 4$).

vivo. The incrassation and Runx2 intensity were measured in the same way as in our previous study (Wang et al., 2021a).

Statistical Analysis

All experimental data were analyzed and expressed as the mean ± standard deviation (SD). Statistical comparisons were made by the analysis of variance to evaluate differences among different groups. The *p*-value less than 0.05 was considered statistically significant.

RESULTS

Increased Proliferation of VICs in CAVD

We performed western blotting and immunofluorescence staining on aortic valve tissues to detect the proliferation of VICs in aortic valves from the control and CAVD groups. The cell proliferation-related factors, cyclin-dependent kinase 1 (CDK1), and Ki-67 were upregulated in the CAVD group compared to the control group

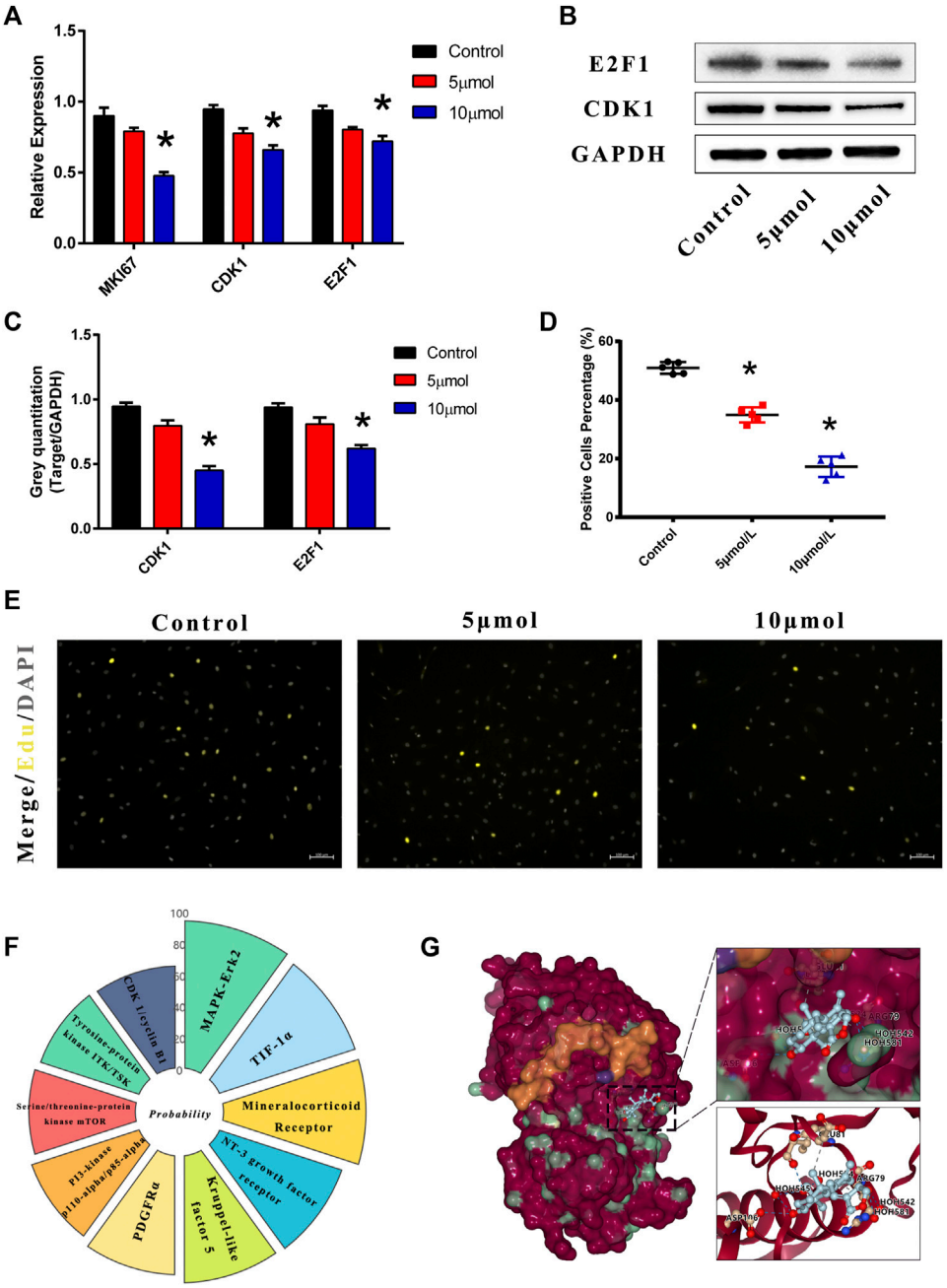

FIGURE 3 | AGP downregulated the cell proliferation genes and protein expression levels. Predicted molecular targets and docking of AGP. **(A)** AGP (5 and 10 μmol/L) inhibited gene expression levels of *CDK1*, *E2F1*, and *MKI67*. **(B)** AGP (5 and 10 μmol/L) inhibited protein expression levels of *CDK1* and *E2F1*. **(C)** Analysis of protein expression levels of CDK1 and E2F1. Data are collected by gray semi-quantification and compared to GAPDH. (*) $p < 0.05$ (vs control) indicates a significant difference. **(D)** Percentage of EdU positive cells. (*) $p < 0.05$ (vs control) indicates significant difference. **(E)** Fluorescence staining of EdU assay in VICs under AGP conditions (yellow). **(F)** Nightingale rose of probabilities in the top 10 targets from the online tool "SwissTargetPrediction." **(G)** ERK protein was selected for further molecular docking analysis. AGP successfully accessed the pocket structure of the protein molecule.

(**Figure 1A,C**). The expressions of ALP and CDK1 proteins were significantly increased in the CAVD group compared to the control group (*$p < 0.05$; **Figure 1B**). The results of immunofluorescence staining were consistent with those of western blotting (*$p < 0.05$; **Figure 1D**). Furthermore, cell proliferation-related genes were tested via real-time PCR; CDK1 and MKI67 genes were significantly upregulated in the CAVD group compared to the control group (*$p < 0.05$; **Figure 1E**). Briefly, the proliferation of VICs was significantly increased due to the pathophysiological changes in CAVD.

AGP Inhibits the Proliferation of VICs *in vitro*

The 2D and 3D structures of AGP are shown in **Figure 2A**. The toxicity of AGP on VICs was assessed by determining the IC50 values, which showed that AGP has significant cytotoxicity at concentrations >10 mM (**Figure 2B**). The results indicated that 10 μM is the suitable AGP concentration for our experiments. In addition, the CCK-8 assay was used to analyze cell proliferation after treatment with AGP for 5 days. The results indicated that the cell viability of the AGP group significantly decreased starting from day 3 when compared with the control group (*$p < 0.05$; **Figure 2C**). Ki-67 staining indicated that cell proliferation was significantly inhibited after treatments with 5 and 10 μmol/L AGP for 48 and 72 h, respectively (*$p < 0.05$; **Figure 2D,E**). Correspondingly, cell cycle analysis showed that the numbers of VICs involved in the S-phase were decreased when cultured in 5 and 10 μM AGP medium for 72 h (*$p < 0.05$; **Figure 2F,G**).

AGP Regulates Osteogenic-Medium-Induced Proliferative Gene/Protein Expression

VICs were treated with AGP for 2 h at doses of 5 and 10 μmol/L. Compared to the control group, expression levels of cell proliferative genes were inhibited by AGP in VICs (**Figure 3A**). AGP significantly downregulated the mRNA levels of MKI67 (*$p < 0.05$), CDK1 (*$p < 0.05$), and E2F1 (*$p < 0.05$). Similar to the gene expression after treatment, AGP inhibited the CDK1 protein synthesis and downregulated E2F1 expression (*$p < 0.05$; **Figure 3B,C**). Based on the immunofluorescence staining of the EdU assay (**Figure 3E**), 5 and 10 μmol/L AGP inhibited cell proliferation activity relative to the control group, consistent with the levels of gene and protein expression (*$p < 0.05$; **Figure 3D**). SwissTarget prediction provided more than 10 potential molecular targets for AGP (**Figure 3F**), and Erk protein was selected for further molecular docking analysis, based on the previous literature on AGP (**Figure 3G**). The results indicated that AGP successfully bound to ERK (extracellular regulated protein kinases) using the residues HOH581, HOH542, HOH524, and HOH545 (red dot), via hydrogen bond interactions and residues ASP106, ARG79, GLU81, and ILE83.

AGP Inhibits the Proliferation of VICs via the MAPK-ERK Pathway

Based on the target analysis above, we focused on the MAPK-ERK signaling pathway. The osteogenesis-specific gene *Runx2* and cell proliferative genes *CDK1* and *MKI67* were tested in VICs under an OM culture with or without AGP for 48 h. The results demonstrated that the OM culture significantly increased the expression of *CDK1, MKI67*, and *Runx2*. However, after the addition of AGP to the OM culture, *CDK1, MKI67,* and *Runx2* were significantly downregulated (* vs control group $p < 0.05$; # vs OM + DMSO group $p < 0.05$; **Figure 4A**). The results of the Ki-67 staining were consistent with the PCR results (**Figure 4C**). AGP significantly inhibited the OM-induced cell proliferative activity (* vs control group $p < 0.05$; # vs OM + DMSO group $p < 0.05$; **Figure 4B**). We detected the protein expression levels of phosphorylated ERK and P38 after OM treatment with or without AGP and found that AGP effectively reversed the OM-induced upregulation of phosphorylated ERK and P38 protein expression (**Figure 4D,G**). After being cultured in OM for 21 days, VICs were tested for calcification using Alizarin Red S staining. OM + DMSO and OM + AGP groups stained positively for Alizarin Red S, showing significant differences compared to the control group (**Figure 4E**). Semi-quantitation of stain intensity indicated an approximately 1-fold decrease in the OM + AGP group compared to the OM + DMSO group (* vs control group $p < 0.05$; # vs OM + DMSO group $p < 0.05$; **Figure 4F**).

AGP Ameliorates Valve Thickening in High-Fat Diet-Fed Mice

We used the high-fat diet-fed animal model to verify the effect of AGP on CAVD *in vivo*. Hematoxylin and eosin (HE) staining and Runx2 immunofluorescence staining were performed on the aortic valve samples of mice (**Figure 5A,B**). The results demonstrated that the aortic valves of high-fat diet-fed mice were significantly thickened, while AGP feeding ameliorated the aortic valve incrassation (* vs control group $p < 0.05$; # vs HF (high-fat diet) group $p < 0.05$; **Figure 5C**). Immunofluorescence staining showed that AGP significantly reduced the *Runx2* expressions induced by high-fat diet-feeding *in vivo* (* vs control group $p < 0.05$; # vs HF group $p < 0.05$; **Figure 5D**).

DISCUSSION

In this study, AGP was used as a negative regulator of CAVD and we found that AGP could delay CAVD progression. Mechanistically, AGP could act as a modulator of the MAPK-ERK signaling pathway to inhibit the cell proliferation activity of VICs and ameliorate the incrassation of aortic valves. Both *in vivo* and *in vitro* experiments supported our conclusions.

In this study, we performed western blotting, immunofluorescence staining, and real-time PCR test on aortic valve tissues. We found that the cell proliferative factors were upregulated due to the pathophysiological changes in CAVD. In the current research, CAVD was divided into two different stages according to the histological features: fibrosis and biomineralization (Mathieu and Boulanger, 2014; Kostyunin et al., 2019). Histological examination revealed significant fibrosis and thickening accompanied by numerous proliferating cells, resulting in decreased elasticity and increased hardness of the valve leaflets (Jenkins et al., 2020). The cell proliferative factors in aortic valves are upregulated by growth factors, such as transforming growth factors, fibroblast growth factors, or epidermal growth factors, which are abnormally increased in CAVD (Wu et al., 2017; Cho et al., 2018). Therefore, drugs that inhibit early valve calcification according to this feature may be effective treatments for CAVD (Wang et al., 2021b). AGP is a natural compound that

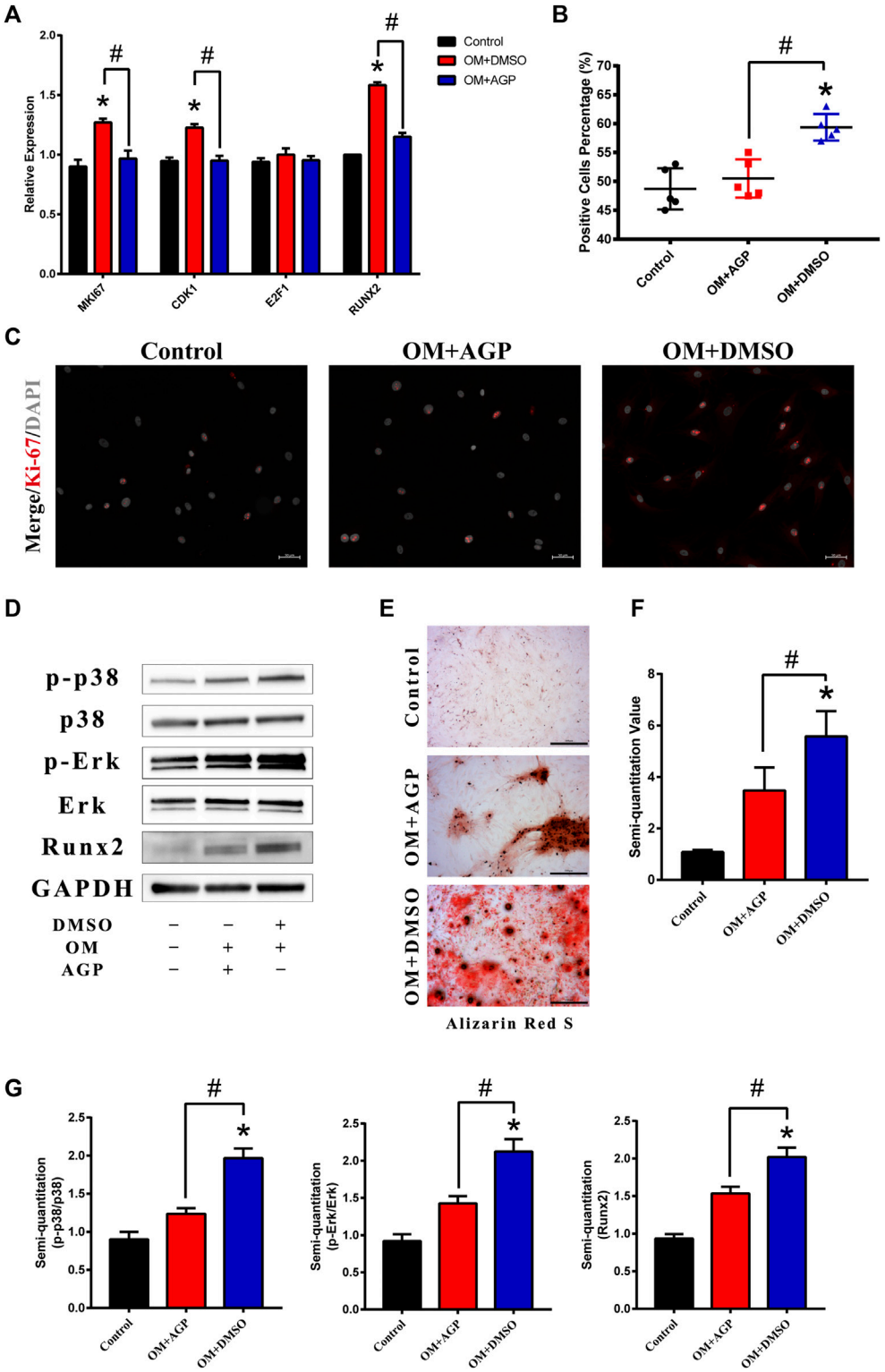

FIGURE 4 | AGP inhibited cell proliferation induced by OM via the MAPK-ERK pathway. **(A)** PCR test for MKI67, CDK1, E2F1, and Runx2 of VICs stimulated by OM with or without AGP for 48 h. **(B)** Percentage of Ki-67 positive cells. (*) $p < 0.05$ (vs control) and (#) $p < 0.05$ (vs OM + DMSO) indicate significant difference. **(C)** Immunofluorescence staining of MKI67 (red). **(D)** Western blotting for Runx2, phosphorylated ERK (p-ERK), total ERK, phosphorylated p38 (p-p38), and total p38 of the cells stimulated by OM with or without AGP for 72 h. **(G)** Statistical analysis of protein expression of Runx2, p38, and ERK according to the gray semi-quantification compared to the GAPDH expression. (*) $p < 0.05$ (vs control) and (#) $p < 0.05$ (vs OM + DMSO) indicate significant difference. **(E,F)** Alizarin Red S staining and semi-quantification of VICs under different cultures: control, OM + DMSO, and OM + AGP (*) $p < 0.05$ (vs control). and (#) $p < 0.05$ (vs OM + DMSO) indicate significant difference ($n = 3$).

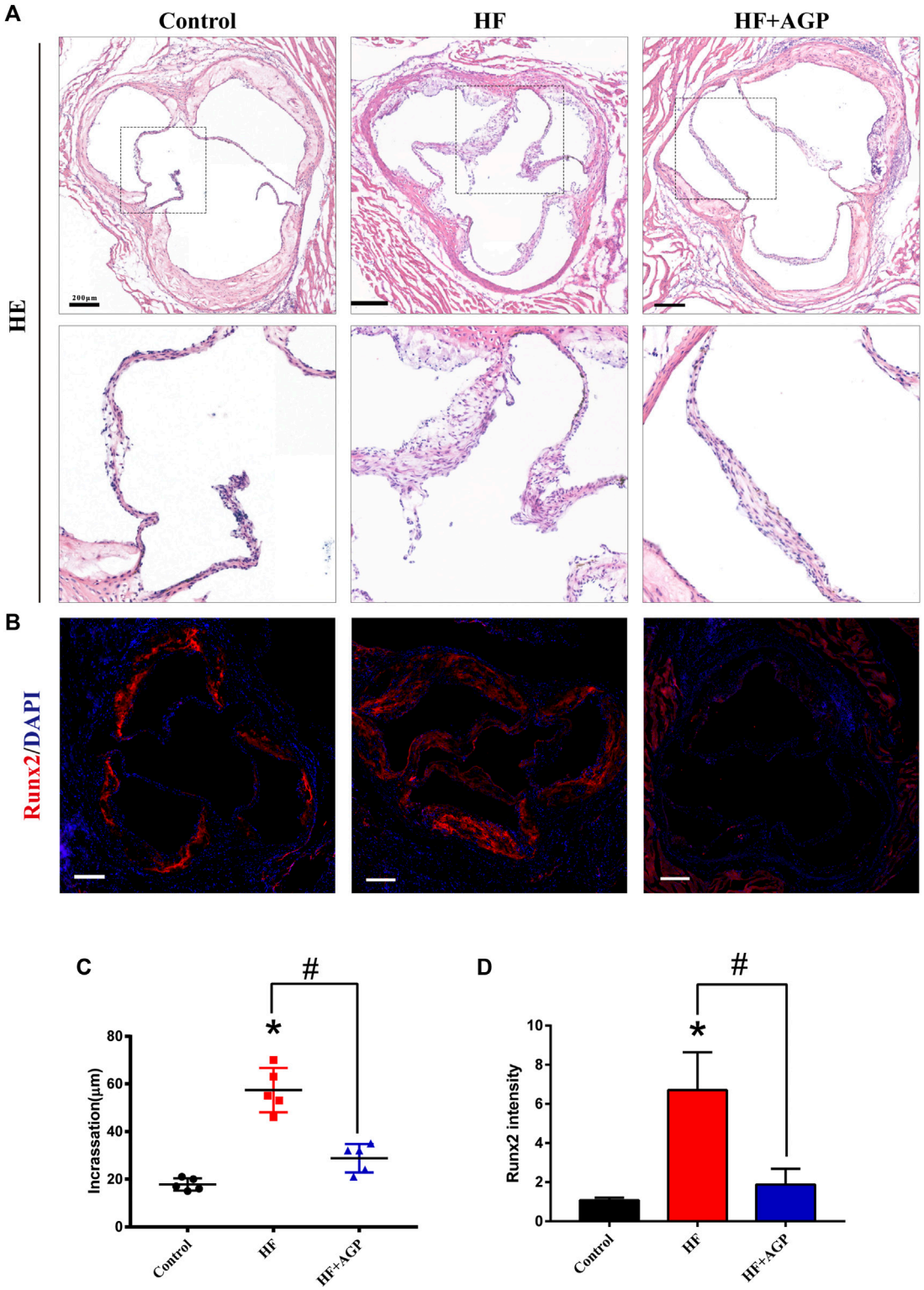

FIGURE 5 | AGP delayed aortic valve disease in high-fat diet-fed (HF) mice. **(A)** Hematoxylin and eosin (HE) staining of HF mice aortic valves with or without AGP treatment (bar = 100 μm). **(B)** Runx2 immunofluorescence staining of HF mice aortic valves with or without AGP treatment (bar = 100 μm). **(C)** Statistical analysis of mice aortic valve calcific incrassation. **(D)** Statistical analysis of mice aortic valve Runx2 fluorescence intensity. (*) $p < 0.05$ (vs control group) and (#) $p < 0.05$ (vs HF group) indicate a significant difference.

we used in our previous study and found that it inhibits the osteogenic transition of VICs (Huang et al., 2020). In this study, we verified that AGP inhibits cell proliferation activity as well. This new finding suggests that AGP may play a role in the early lesions of CAVD, thereby expanding the time window of use of this drug. The osteogenic transition of VICs in CAVD is the most important and widely studied target for the development of pharmacological treatments (Lindman et al., 2016). However, the identification of cell proliferation as a drug target is a breakthrough for drug development. The causal relationship between cell proliferation and osteogenic transition remains controversial (Hulin et al., 2019). Some studies reported that the cell cycle changed during the osteogenic transition, and stimulation of osteogenic induction promoted cell proliferation in the initial stage but cell apoptosis dominated in the terminal stages. In contrast, some studies suggested that cell proliferation occurred when VICs were transformed into osteoblasts in the terminal stages (Rutkovskiy et al., 2017).

In our research, we found that AGP could inhibit cell proliferation via the MAPK-ERK signaling pathway, which may play an important role in cell proliferation and osteogenic transition. In our previous study, we identified AGP as a modulator of NF-κB pathway activation in VICs through transcriptome sequencing analysis. A comprehensive analysis of the relationship between the two signaling pathways suggests that when the MAPK-ERK signaling pathway is inhibited, the NF-KB signaling pathway is also affected (Ott et al., 2014; Zielinska and Katanaev, 2019). We performed target prediction using molecular docking simulations and found ERK2 protein as a promising drug target (Ferreira et al., 2015). However, further research is needed to determine the mechanism underlying the binding of AGP to the ERK protein. We also performed an *in vivo* experiment in mouse disease models to verify our findings. Based on the results of *in vivo* experiments, AGP can effectively delay valve thickening caused by high-fat diet feeding as well as Runx2 factor expression.

Our research had several limitations. Additional research is needed to verify the AGP target of ERK2 protein and the relationship between them. Another limitation was the *in vivo* pharmacokinetics of AGP; some studies suggest that AGP is not readily absorbed. Finally, the specificity and efficacy of AGP for valvular disease need to be determined, which is a major issue in the drug development for valvular disease (Myasoedova et al., 2018).

CONCLUSION

AGP inhibited OM-induced cell proliferation and calcification of VICs primarily via the MAPK-ERK signaling pathway. AGP may be a promising therapeutic supplement to prevent and delay the occurrence and progression of CAVD.

DATA AVAILABILITY STATEMENT

The original contributions presented in the study are included in the article/supplementary materials; further inquiries can be directed to the corresponding authors.

ETHICS STATEMENT

The studies involving human participants were reviewed and approved by the Ethics Committee of Tongji Medical College, Huazhong University of Science and Technology in Wuhan, China. The patients/participants provided their written informed consent to participate in this study. The animal study was reviewed and approved by the Ethics Committee of Tongji Medical College, Huazhong University of Science and Technology in Wuhan, China.

AUTHOR CONTRIBUTIONS

YH: conceptualization, data curation, supervision, writing—original draft. ML: conceptualization and supervision. CL: formal analysis and data curation. ND: data curation and resources. LC: data curation, supervision, and resources.

FUNDING

This work was supported by the National Key R&D Program of China (2016YFA0101100).

ACKNOWLEDGMENTS

We thank LetPub (www.letpub.com) for the linguistic assistance during the preparation of this manuscript.

REFERENCES

Cho, K. I., Sakuma, I., Sohn, I. S., Jo, S. H., and Koh, K. K. (2018). Inflammatory and Metabolic Mechanisms Underlying the Calcific Aortic Valve Disease. *Atherosclerosis* 277, 60–65. doi:10.1016/j.atherosclerosis.2018.08.029

Ferreira, L. G., Dos Santos, R. N., Oliva, G., and Andricopulo, A. D. (2015). Molecular Docking and Structure-Based Drug Design Strategies. *Molecules* 20 (7), 13384–13421. doi:10.3390/molecules200713384

Huang, Y., Xu, K., Zhou, T., Zhu, P., Dong, N., and Shi, J. (2019). Comparison of Rapidly Proliferating, Multipotent Aortic Valve-Derived Stromal Cells and Valve Interstitial Cells in the Human Aortic Valve. *Stem Cell Int* 2019, 7671638. doi:10.1155/2019/7671638

Huang, Y., Zhou, X., Liu, M., Zhou, T., Shi, J., Dong, N., et al. (2020). The Natural Compound Andrographolide Inhibits Human Aortic Valve Interstitial Cell Calcification via the NF-Kappa B/Akt/ERK Pathway. *Biomed. Pharmacother.* 125, 109985. doi:10.1016/j.biopha.2020.109985

Hulin, A., Hortells, L., Gomez-Stallons, M. V., O'donnell, A., Chetal, K., Adam, M., et al. (2019). Maturation of Heart Valve Cell Populations during Postnatal Remodeling. *Development* 146 (12), 173047. doi:10.1242/dev.173047

Hutcheson, J. D., Aikawa, E., and Merryman, W. D. (2014). Potential Drug Targets for Calcific Aortic Valve Disease. *Nat. Rev. Cardiol.* 11 (4), 218–231. doi:10.1038/nrcardio.2014.1

Jenkins, W. S., Simard, L., Clavel, M. A., Foley, T. A., Araoz, P. A., Miller, J. D., et al. (2020). Pathophysiology of Aortic Valve Calcification and Stenosis: Novel Insights from Reconstructed Multiplanar Computed Tomography. *JACC Cardiovasc. Imaging* 13 (10), 2255–2258. doi:10.1016/j.jcmg.2020.04.024

Kostyunin, A. E., Yuzhalin, A. E., Ovcharenko, E. A., and Kutikhin, A. G. (2019). Development of Calcific Aortic Valve Disease: Do We Know Enough for New Clinical Trials? *J. Mol. Cel Cardiol* 132, 189–209. doi:10.1016/j.yjmcc.2019.05.016

Lindman, B. R., Clavel, M. A., Mathieu, P., Iung, B., Lancellotti, P., Otto, C. M., et al. (2016). Calcific Aortic Stenosis. *Nat. Rev. Dis. Primers* 2, 16006. doi:10.1038/nrdp.2016.6

Liu, M., Li, F., Huang, Y., Zhou, T., Chen, S., Li, G., et al. (2020). Caffeic Acid Phenethyl Ester Ameliorates Calcification by Inhibiting Activation of the AKT/NF-κB/NLRP3 Inflammasome Pathway in Human Aortic Valve Interstitial Cells. *Front. Pharmacol.* 11, 826. doi:10.3389/fphar.2020.00826

Mathieu, P., and Boulanger, M. C. (2014). Basic Mechanisms of Calcific Aortic Valve Disease. *Can. J. Cardiol.* 30 (9), 982–993. doi:10.1016/j.cjca.2014.03.029

Myasoedova, V. A., Ravani, A. L., Frigerio, B., Valerio, V., Moschetta, D., Songia, P., et al. (2018). Novel Pharmacological Targets for Calcific Aortic Valve Disease: Prevention and Treatments. *Pharmacol. Res.* 136, 74–82. doi:10.1016/j.phrs.2018.08.020

Ott, C., Jacobs, K., Haucke, E., Navarrete Santos, A., Grune, T., and Simm, A. (2014). Role of Advanced Glycation End Products in Cellular Signaling. *Redox Biol.* 2, 411–429. doi:10.1016/j.redox.2013.12.016

Otto, C. M., and Prendergast, B. (2014). Aortic-valve Stenosis-Ffrom Patients at Risk to Severe Valve Obstruction. *N. Engl. J. Med.* 371 (8), 744–756. doi:10.1056/NEJMra1313875

Rutkovskiy, A., Malashicheva, A., Sullivan, G., Bogdanova, M., Kostareva, A., Stensløkken, K. O., et al. (2017). Valve Interstitial Cells: The Key to Understanding the Pathophysiology of Heart Valve Calcification. *J. Am. Heart Assoc.* 6 (9), 6339. doi:10.1161/JAHA.117.006339

Wang, C., Huang, Y., Liu, X., Li, L., Xu, H., Dong, N., et al. (2021a). Andrographolide Ameliorates Aortic Valve Calcification by Regulation of Lipid Biosynthesis and Glycerolipid Metabolism Targeting MGLL Expression *In Vitro* and *In Vivo*. *Cell calcium* 100, 102495. doi:10.1016/j.ceca.2021.102495

Wang, C., Xia, Y., Qu, L., Liu, Y., Liu, X., and Xu, K. (2021b). Cardamonin Inhibits Osteogenic Differentiation of Human Valve Interstitial Cells and Ameliorates Aortic Valve Calcification via Interfering in the NF-Kb/nlrp3 Inflammasome Pathway. *Food Funct.* 12 (23), 11808–11818. doi:10.1039/d1fo00813g

Wu, B., Wang, Y., Xiao, F., Butcher, J. T., Yutzey, K. E., and Zhou, B. (2017). Developmental Mechanisms of Aortic Valve Malformation and Disease. *Annu. Rev. Physiol.* 79, 21–41. doi:10.1146/annurev-physiol-022516-034001

Xu, K., Huang, Y., Zhou, T., Wang, C., Chi, Q., Shi, J., et al. (2019). Nobiletin Exhibits Potent Inhibition on Tumor Necrosis Factor Alpha-Induced Calcification of Human Aortic Valve Interstitial Cells via Targeting ABCG2 and AKR1B1. *Phytother Res.* 33 (6), 1717–1725. doi:10.1002/ptr.6360

Xu, K., Xie, S., Huang, Y., Zhou, T., Liu, M., Zhu, P., et al. (2020). Cell-Type Transcriptome Atlas of Human Aortic Valves Reveal Cell Heterogeneity and Endothelial to Mesenchymal Transition Involved in Calcific Aortic Valve Disease. *Arterioscler Thromb. Vasc. Biol.* 40 (12), 2910–2921. doi:10.1161/ATVBAHA.120.314789

Yang, M. Y., Yu, Q. L., Huang, Y. S., and Yang, G. (2019). Neuroprotective Effects of Andrographolide Derivative CX-10 in Transient Focal Ischemia in Rat: Involvement of Nrf2/AE and TLR/NF-κB Signaling. *Pharmacol. Res.* 144, 227–234. doi:10.1016/j.phrs.2019.04.023

Zhou, T., Wang, Y., Liu, M., Huang, Y., Shi, J., Dong, N., et al. (2020). Curcumin Inhibits Calcification of Human Aortic Valve Interstitial Cells by Interfering NF-Kb, AKT, and ERK Pathways. *Phytother Res.* 34 (8), 2074–2081. doi:10.1002/ptr.6674

Zielinska, K. A., and Katanaev, V. L. (2019). Information Theory: New Look at Oncogenic Signaling Pathways. *Trends Cell Biology* 29 (11), 862–875. doi:10.1016/j.tcb.2019.08.005

Conflict of Interest: The authors declare that the research was conducted in the absence of any commercial or financial relationships that could be construed as a potential conflict of interest.

Publisher's Note: All claims expressed in this article are solely those of the authors and do not necessarily represent those of their affiliated organizations, or those of the publisher, the editors, and the reviewers. Any product that may be evaluated in this article, or claim that may be made by its manufacturer, is not guaranteed or endorsed by the publisher.

frontiers | Frontiers in Pharmacology

REVIEW
published: 09 May 2022
doi: 10.3389/fphar.2022.906212

Biomechanical Regulatory Factors and Therapeutic Targets in Keloid Fibrosis

Fan Feng[1†], Mingying Liu[2†], Lianhong Pan[1], Jiaqin Wu[1], Chunli Wang[1], Li Yang[1], Wanqian Liu[1], Wei Xu[3]* and Mingxing Lei[1]**

[1]National Innovation and Attracting Talents "111" Base, Key Laboratory of Biorheological Science and Technology, Ministry of Education, College of Bioengineering, Chongqing University, Chongqing, China, [2]School of Comprehensive Health Management, Xihua University, Chengdu, China, [3]Chongqing Clinical Research Center for Dermatology, Chongqing Key Laboratory of Integrative Dermatology Research, Department of Dermatology, Chongqing Hospital of Traditional Chinese Medicine, Chongqing, China

OPEN ACCESS

Edited by:
Jing Xie,
Sichuan University, China

Reviewed by:
Ji Li,
Central South University, China
Weiming Qiu,
General Hospital of Central Theater Command, China

***Correspondence:**
Wanqian Liu
wqliu@cqu.edu.cn
Wei Xu
davidweixucn@gmail.com
Mingxing Lei
mingxing@cqu.edu.cn

[†]These authors have contributed equally to this work

Specialty section:
This article was submitted to Experimental Pharmacology and Drug Discovery, a section of the journal Frontiers in Pharmacology

Received: 28 March 2022
Accepted: 25 April 2022
Published: 09 May 2022

Citation:
Feng F, Liu M, Pan L, Wu J, Wang C, Yang L, Liu W, Xu W and Lei M (2022) Biomechanical Regulatory Factors and Therapeutic Targets in Keloid Fibrosis. Front. Pharmacol. 13:906212. doi: 10.3389/fphar.2022.906212

Keloids are fibroproliferative skin disorder caused by abnormal healing of injured or irritated skin and are characterized by excessive extracellular matrix (ECM) synthesis and deposition, which results in excessive collagen disorders and calcinosis, increasing the remodeling and stiffness of keloid matrix. The pathogenesis of keloid is very complex, and may include changes in cell function, genetics, inflammation, and other factors. In this review, we aim to discuss the role of biomechanical factors in keloid formation. Mechanical stimulation can lead to excessive proliferation of wound fibroblasts, deposition of ECM, secretion of more pro-fibrosis factors, and continuous increase of keloid matrix stiffness. Matrix mechanics resulting from increased matrix stiffness further activates the fibrotic phenotype of keloid fibroblasts, thus forming a loop that continuously invades the surrounding normal tissue. In this process, mechanical force is one of the initial factors of keloid formation, and matrix mechanics leads to further keloid development. Next, we summarized the mechanotransduction pathways involved in the formation of keloids, such as TGF-β/Smad signaling pathway, integrin signaling pathway, YAP/TAZ signaling pathway, and calcium ion pathway. Finally, some potential biomechanics-based therapeutic concepts and strategies are described in detail. Taken together, these findings underscore the importance of biomechanical factors in the formation and progression of keloids and highlight their regulatory value. These findings may help facilitate the development of pharmacological interventions that can ultimately prevent and reduce keloid formation and progression.

Keywords: keloid fibrosis, fibroblast, mechanotransduction, biomechanical factor, matrix force, targeted therapy

Abbreviations: BMP, bone morphogenetic protein; CAV1, Caveolin-1; ECM, excessive extracellular matrix; EMT, epithelial-mesenchymal transition; EGF, epidermal growth factor; ET-1, endothelin-1; FGF-β, fibroblast growth factor β; GDF, growth differentiation factor; HATs, histone acetyl transferases; HCC, hepatocellular carcinoma; HDACs, histone deacetylases; IGF-I, insulin-like growth factor I; IL, interleukin; LOX, lysyl oxidase; MMP, matrix metalloproteinases; MSCs, mesenchymal stem cells; PDGF, platelet-derived growth factor; TAZ, transcroptional coactivator with a PDZ-binding domain; TGF-β, transforming growth factor -β; TIMPs, metalloproteinases; TMEM88, transmembrane protein 88; YAP, Yes-associated protein.

INTRODUCTION

Skin is the largest organ of the human body, covering the entire surface of the human body, with the functions of protection, excretion, body temperature regulation, and others (Hsu et al., 2018a). As the interface between the external environment and internal tissue, skin is easily damaged by infection, disease, trauma, and other factors. When the skin is injured, the healing process can be categorized into hemostasis, inflammation, proliferation, re-epithelialization, and remodeling (Rodrigues et al., 2019). It should be noted that these five processes are only artificially divided. In fact, the healing process after injury is continuous and indivisible. Typically, after the completion of these five processes, the dermal tissue ends up filled with extracellular matrix (ECM) components, but does not overgrow, instead forming a filler tissue that differs from the normal skin structure, which is known as a physiological scar. When the skin healing process is maladjusted, the abovementioned process is further disordered, forming scar hyperplasia, usually accompanied by itching, local discomfort or pain, and other chronic symptoms, which is called a pathological scar. Pathological scarring has been reported in 32–60% of patients after surgery (Mahdavian Delavary et al., 2012).

Pathological scar, mainly including hypertrophic scar and keloid, are skin fibroproliferative disease characterized by an abnormal wound healing process, massive production of ECM mainly composed of collagen disorders and calcinosis, and hyperplasia of dermal tissue (Lee and Jang, 2018). A hypertrophic scar refers to a scar that does not exceed the original injury site. It is generally red or pink, relatively hard and itchy, and often disappears spontaneously after several years. Different from a hypertrophic scar, a keloid has the characteristics of excessive growth beyond the scope of trauma, and is more likely to invade adjacent tissues and cannot be resolved by itself. In other words, a keloid has the characteristics of invasive tumor growth, and therefore, it tends to be considered as a "benign skin tumor" (Limandjaja et al., 2020). Keloids are more likely to relapse after treatment, and are mainly treated via simple surgery, with a high recurrence rate. Therefore, the treatment of keloid is more difficult and requires more attention.

Keloid formation and progression is a complex process, which is believed to be independently or jointly driven by changes in cellular function, genetics, inflammation, and other factors. Of particular interest is the recent evidence that biomechanical factors play a key role in the formation and progression of keloids. Here we begin with an introduction to the various factors involved in the progression of keloid pathology and then describe the recent advances in biomechanical regulation of keloids as accumulated evidence suggests that several mechanotransduction signaling pathways, such as TGF-β/Smad signaling pathway, Integrin signaling pathway, YAP/TAZ signaling pathway, and calcium ion pathway, are involved in the process of keloid fibrosis, and have been proved to play an important role in keloid development. Finally, some potential therapeutic concepts and strategies based on biomechanical factors are described.

KELOID PATHOGENESIS STUDY

A keloid is a skin disorder caused by excessive proliferation of skin fibers. The exact mechanism underlying keloid formation is still not fully understood. Current studies suggest that changes in cell function, genetics, inflammation, and biomechanical factors all play an important role in keloid formation.

Changes in Cellular Function

During the process of keloid formation, the function of many types of cell populations abnormally changes. Fibroblasts are the most abundant cell type in all connective tissues of the body. As far as skin is concerned, fibroblasts mainly form the ECM by constructing different proportions of collagen and elastin to maintain the structural integrity and normal physiological functions of the skin (Plikus et al., 2021; Xue et al., 2022). Fibroblasts, the primary effector cells in keloids, eventually lead to keloid formation by inducing a persistent inflammatory response and excessive ECM deposition (Suarez et al., 2015; Luo et al., 2017). This process is driven by many growth factors, including transforming growth factor -β (TGF-β), platelet-derived growth factor (PDGF), fibroblast growth factor β (FGF-β), and insulin-like growth factor I (IGF-I) (Andrews et al., 2016; Nagar et al., 2021). In keloids, the effects of these growth factors on fibroblasts contribute to the enhanced scar phenotype. Changes in fibroblast phenotypes are believed to be at the core of keloid formation. Studies have shown that the fibroblasts in the center of a keloid are usually in a resting state, whereas those in the periphery are in an abnormal proliferating state. Compared with normal skin fibroblasts, keloid fibroblasts have stronger anti-apoptosis and migration abilities (Wang et al., 2013; Jumper et al., 2017).

Some studies have suggested that keloid formation is associated with metabolic reprogramming of keloid fibroblasts, including the transition from oxidative phosphorylation to aerobic glycolysis. Compared with normal skin, the keloid tissue showed upregulated GLUT-1 expression and enhanced expressions of several glycolytic enzymes, such as HK1, HK2, PFK1, PFK2, PDK1, and PKM2, (Vinaik et al., 2020). Keloid fibroblasts also had higher basic glycolysis and glycolysis capacity and reduced basal oxidative respiration, maximum oxidative respiration, and reserve respiration capacity (Li et al., 2018; Li et al, 2020). GLUT-1-dependent glycolysis and ROS production mediate the proliferation of keloid fibroblasts, and GLUT-1 inhibitor WZB117 can reduce glycolysis and ROS production of keloid fibroblasts (Lu et al., 2021).

Although keloid fibroblasts are still believed to be responsible for keloid formation, recent studies have shifted focus to recognizing the potential role of abnormal epidermal cell populations in scar formation. Basic abnormalities found in keloid keratinocytes with regard to the secretion of wound healing mediators, differentially expressed genes, paracrine action of co-cultured cells, and epithelial-mesenchymal transition (EMT) all support a more active role of keratinocytes in keloid formation (Yan et al., 2015; Hahn et al., 2016; Li and Wu, 2016). In addition, co-culture of abnormal keloid keratinocytes and dermal fibroblasts induces

a pro-fibrotic phenotype and increases the expression of pro-fibrotic factors (Lee et al., 2016).

Genetic Factors

Recent studies have shown that race, genetic susceptibility, age, and gender are patient characteristics that may influence susceptibility to keloids. There are significant differences in scarring among different ethnicities, with worldwide keloid prevalence ranging from 0.09% in the United Kingdom to 16% in Congo, suggesting that individuals with darker skin are more likely to develop it (Kiprono et al., 2015). In addition, keloid has familial genetic characteristics, and family members of keloid patients have a higher disease incidence. For example, the prevalence rate of keloid in the first, second, and third degree relatives of Chinese keloid patients was 7.62, 0.38, and 0.035%, respectively (Lu et al., 2015). In addition, keloid can occur at all ages, but the incidence is highest between the ages of 10 and 30 years (Young et al., 2014).

There is increasing evidence indicating that various different and reversible epigenetic modifications, represented by DNA methylated histone modifications and non-coding RNAs, play key roles in the gene regulation of keloid and downstream fibroblast functions (He et al., 2017; Xu et al., 2019; Lv et al., 2020). Histone modification refers to the processes such as methylation, acetylation, phosphorylation, adenylation, ubiquitination, and ADP ribosylation by related enzymes (Wang et al., 2016a). DNA methylation is involved in keloid formation, and includes processes such as cell proliferation, invasion of myofibroblasts, activation of collagen deposition and disorder (Nyika et al., 2022). Russell et al. found that abnormal DNA methylation and histone acetylation modification of keloid fibroblasts can affect the stability of gene expression, and DNA methylation of HOXA9 and HOXA10 can alter the wound healing ability of keloid fibroblasts (Russell et al., 2010). Liu et al. (2018) further found that SFRP1 promoter methylation promotes keloid formation by promoting Wnt/β-catenin signaling pathway activity and β-catenin and α-SMA mRNA and protein expressions. Functional non-coding RNAs, such as microRNAs (miRNAs) and long non-coding RNAs (lncRNAs), play an important role in the regulation of keloid gene expression (Lv et al., 2020). Wang et al. (2019) found that miR-152-3p expression was significantly upregulated in keloid tissue and keloid fibroblasts compared with normal skin tissue. Further studies showed that miR-152-3p regulates cell proliferation, invasion, and ECM expression by targeting FOXF1 in keloid fibroblasts. Jin et al. (2019) showed that lncRNA HOXA11-AS induced collagen I synthesis *via* Smad5 signal transduction mediated by sponging miR-124-3p to promote keloid formation.

Inflammatory Factors

Studies have shown that inflammatory mediators and inflammatory cells are involved in the entire process of wound healing (Ogawa, 2017; Rodrigues et al., 2019). It is believed that pathological scars are caused by excessive and persistent inflammation, and the intensity of inflammation is positively correlated with the final scar size (Huang et al., 2014). Various inflammatory cells, including (Zhou et al., 2021), mast cells (Bagabir et al., 2012), lymphocytes (Chen et al., 2018), and monocytes (Limandjaja et al., 2019), have been reported to be involved in keloid formation. Among these, macrophages are important cells that initiate an inflammatory response during wound healing and lead to excessive spreading of inflammation. In keloid tissues, macrophages upregulate M2-related genes highly associated with tissue repair and remodeling (Jin et al., 2018). These macrophages further promote the transformation of fibroblasts into myofibroblasts by secreting TGF-β and PDGF, which in turn promotes collagen deposition and scarring (Hesketh et al., 2017). TGF-β is a representative pro-fibrotic cytokine that is most closely related to keloid formation (Berman et al., 2017). In contrast, TGF-β-secreted factors can indirectly contribute to fibrosis through signaling pathways in an inflammatory microenvironment (Hahn et al., 2016). In addition, pro-inflammatory factors such as interleukin (IL)-1α, IL-1β, and IL-8, CKLF-1, and COX-1 are upregulated in the keloid tissue, suggesting that in patients with keloids, pro-inflammatory genes in the skin are sensitive to trauma, which in turn may promote chronic inflammation and lead to excessive keloid growth (Abdou et al., 2014; Lin et al., 2020; Wu et al., 2020).

BIOMECHANICAL FACTORS IN KELOID FORMATION

The abovementioned studies mainly focus on the role of biological factors in keloid formation and have made great progress. They initially revealed the mechanism of occurrence and development of keloids, but the clinical efficacy was not significant after intervention with different targets, indicating that previous studies were incomplete. Recent studies have focused on the role of the external environment, particularly the local mechanical wound environment. Current scientific basis and clinical evidence clearly indicate that biomechanical factors play an important role in keloid formation, contracture, and abnormal keloid development and treatment. Next, we will summarize the research in this area and explore the role of biomechanical factors in keloid formation.

Biomechanical Factors Associated With Skin Wound Healing

Skin injury is a common phenomenon in the human body, and the recovery of anatomical continuity and functional reconstruction of tissue after injury is a complex and dynamic process. Early observations in anatomy and surgery suggest the importance of mechanical tension in wound healing outcomes. For example, Langer lines in the human skin correspond to tension bands that occur naturally in the skin because of the interaction of collagen fibrils and fibroblasts. Conventional assumptions point to the alignment of the underlying ECM, cell orientation and contraction, and muscle involvement in the formation of these invisible lines. Surgical incisions made parallel to these lines reduce tension and heal more easily, with

less scarring than incisions made perpendicular to them (Wong et al., 2011; Yazdani Abyaneh et al., 2014). The mechanical properties of the skin are mainly associated with the composition and tissue of ECM in the dermis (Shook et al., 2018). Collagen, the most abundant protein in ECM, exists in the dermis as fibrin; it provides tensile strength and determines the stiffness and mechanical strength of skin tissues (Nyström and Bruckner-Tuderman, 2019). The skin is also affected by tension, which plays an important role in maintaining homeostasis. There are many sources of skin tension, such as stretching of fore-chest skin caused by breathing and stretching caused by joint movement. Normal mechanical forces on wounds and scars induce tension homeostasis, allowing cells and ECM in tissues to progress normally at different stages of wound healing. The balance of internal and external mechanical forces, represented by ECM, cytoskeleton, intracellular signaling, and applied tensile stress, ensures normal healing of the skin after injury, whereas disruption of this balance may lead to pathological scarring (Harn et al., 2019).

Tension in Keloid Genesis and Development

Research has shown that keloids clearly tend to occur in areas of high stress. Rei Ogawa's map of 1,500 keloid lesions in 483 Japanese patients showed 733 (48.9%) in the anterior thoracic region and 403 (26.9%) in the scapular region, which are the regions usually exposed to continuous or intermittent tension stimulation during daily life activities. Keloid incidence was lower in areas where the skin stretched and contracted less (such as the parietal area or the anterior leg), even in patients with multiple or large keloids (Ogawa et al., 2012). Dohi et al. (2019) also showed that changes in human postural positions (i.e., standing, sitting, and supine) are associated with dynamic changes in local stress/strain distributions, especially in areas prone to keloid formation. In terms of shape, keloids often grow in the direction of skin tension and take on a specific shape, namely, the typical butterfly, crab claw, and dumbbell shape appears on the shoulder, chest, and upper arm, respectively (Ogawa et al., 2003; Jumper et al., 2017). In the fore-chest, for example, keloids often grow horizontally because the pectoralis major muscles contract in a horizontal direction. In addition, elongated vaccine keloids, which are common in the upper arm, are associated with widespread vaccination during childhood: shoulder keloids tend to grow along the long axis because of the tension exerted on the vaccine wound by arm movement. Three-dimensional finite element models based on clinical samples showed that respiratory movements caused stress in the area around the chest keloid, and the stress was concentrated in the area around the bilateral ends of the keloid, resulting in the keloid possibly taking on a crab or butterfly shape (Nagasao et al., 2013). Keloid, as a result of malregulated wound healing, is usually accompanied by inflammation in the early stage, which to some extent promotes excessive proliferation of fibroblasts, increased production of fibroblast products, and high expression of cytokines related to inflammatory reactions in these inflammation-infiltrated areas. Studies have also shown that mechanical force stimulation can continuously activate acute inflammatory pathways, thereby promoting the prolongation of inflammatory period, leading to wound fibrosis, and promoting hyperplasia of fibrous tissue to form keloids (El Ayadi et al., 2020).

In addition, mechanical stimulation is also one of the important factors causing functional changes in keloid cells. Suarez et al. established a new three-dimensional collagen lattice model using photogrammetry and *in vitro* technology to simulate the tension experience of normal skin and keloid tissue *in vivo*. The results showed that three tension-related genes (Hsp27, PAI-2, and integrin α2β1) were up-regulated in keloid fibroblasts under stress, which promoted ECM synthesis and cell proliferation (Suarez et al., 2014). Kiya et al. focused on endothelial cells in keloid dermal microvessels. Dermal microvascular endothelial cells release endothelin-1 (ET-1) in response to continuous uniaxial tensile stress, contributing to fibroblast-to-myofibroblast differentiation, collagen synthesis, and contractile properties via the RhoA/Rho kinase pathway (Kiya et al., 2017). Stretch tension can promote a high expression of integrin αVβ3 in keloid-derived mesenchymal stem cells (MSCs), suggesting that stretch tension may affect MSC secretion (Song et al., 2019). These results suggest that mechanical stimulation can cause functional changes related to wound healing in cells, leading to the development of keloids. Lipid metabolism and their metabolites play an important role in keloid development and are believed to be involved in mechanical transduction (Huang and Ogawa, 2013). Caveolin-1 (CAV-1), as a biofilm marker protein and one of the main scaffold proteins of cell membranes, plays an important role in cell signal transduction, cell adhesion, intracellular cholesterol transport, and lipid metabolism, and is also related to cellular mechanical regulation (Hsu et al., 2018b; Vykoukal et al., 2020). CAV-1 shows low expression in keloid fibroblasts (Zhang et al., 2011). Low expression of CAV-1 decreases cell stiffness, but increases the contractility and migration ability of keloid fibroblasts. In keloid fibroblasts, reduced CAV-1 leads to upregulation of the transcription factor RUNX2, which is a potential regulator of increased ECM production in keloids and is associated with fibrosis (Hsu et al., 2018b).

Matrix Mechanics in keloid Genesis and Development

The influence of matrix mechanics on keloid progression has also attracted the attention of researchers. Stretching and tension of skin may result in overexpression of tension-related proteins in keloids. Keloid formation is also closely related to excessive cell proliferation and ECM deposition (Canady et al., 2013; Xue and Jackson, 2015). Histopathological examination of mature keloid lesions revealed the deposition of connective tissue ECM, particularly collagen I and III with dense fibrous structures. Collagen V and VI were also found to be abundant, especially in the early stages of development. Therefore, up-regulation of collagen VI gene expression can be used as an early biomarker in the process of keloid fibrosis (Andrews et al., 2016). Collagen fibers in keloid tissue are clumped rather than netted, and its fibers are thicker, more parallel, with less cross-linking between fibers (Syed et al., 2011). Another prominent protein found in

keloid ECM is periostin, a stromal cell protein that promotes keloid formation by activating the RhoA pathway to promote TGF-β1 secretion (Zhang et al., 2014; Maeda et al., 2019). These pathological features lead to a large amount of keloid collagen production, pathological cross-linking, and deposition and remodeling of ECM, resulting in matrix stiffness of keloid that is different from that of normal skin. Therefore, matrix stiffness, which is as an important feature and marker of keloid pathology, has received increasing attention in clinical diagnosis of keloids. Changes in ECM content during keloid formation allow tissue stiffness to be characterized by acoustic imaging to observe information about target tissue stiffness. Using shear-wave elastography, researchers have found that the Young's modulus of keloid tissue was around 124.6 KPa, which is much higher than 17.7 KPa of normal skin (Huang et al., 2020; Hang et al., 2021). These advances allow for the noninvasive assessment of progressive tissue stiffness and provide a valuable tool for the clinical understanding of progressive tension and maladaptive wound repair.

Matrix stiffening is not only the pathological result of keloid fibrosis but also an important clue indicating the progression of keloid fibrosis. Although stromal stiffness, an important feature and marker of keloid pathology, has received increasing attention and recognition in the clinical diagnosis of keloid, matrix mechanics has also been shown to facilitate the progression of keloids. Macarak et al. have reported that the higher the stiffness of the basal surface (3, 10, 25 KPa, >1,000 KPa), the higher the expression of the pro-fibrotic gene α-SMA in keloid fibroblasts (Macarak et al., 2021). Kenny et al. (2018) found that increased substrate stiffness specifically stimulated keratinocyte proliferation without affecting adhesion, survival, or terminal differentiation, and was mediated by epidermal growth factor (EGF) signaling. Deng et al. (2021) found that keloid fibroblasts are stiffer than normal fibroblasts when cultured on hydrogels that mimic tissue stiffness. Matrix stiffness contributes to the transformation of normal keloid fibroblasts to a fibrotic phenotype, such as that with higher YAP nuclear expression. In 2010, Kurokawa et al. (2010) constructed three-dimensional images of keloids and hypertrophic scar vessels and found that the number of capillaries in keloids was significantly lower than that in hypertrophic scar, and that the lumen was flatter. This is caused by the pressure of a large number of fibroblasts and collagen in keloids. Excessive proliferation of fibroblasts and a large amount of collagen deposition will also hinder the diffusion of oxygen around, resulting in tissue hypoxia (Lei et al., 2019). Importantly, hypoxia is believed to be a key mechanism underlying keloid formation. Previous studies have shown that keloid fibroblasts proliferate, migrate, invade, and increase collagen synthesis under hypoxic conditions (Zhang et al., 2014; Kang et al., 2020). In addition, hypoxia promotes EMT in keloid fibroblasts and inhibits apoptosis (Kim et al., 2019).

Based on the importance of matrix mechanics in the current process of keloid fibrosis, studies have been conducted to investigate whether targeting keloid matrix mechanics has the potential to treat or even reverse fibrosis. Obviously, the most direct approach toward altering keloid matrix mechanics is to inhibit and slow the increase in keloid stiffness during fibrosis. From this viewpoint, it is possible to reduce the stiffness of keloid matrix by influencing or reducing the factors that promote the stiffening of keloid matrix. As one of the main components of fiber matrix, collagen plays a key role in regulating the mechanical properties of ECM. Therefore, it is possible to reduce the stiffness of ECM and slow down the process of keloid fibrosis by reducing collagen synthesis in ECM or excessive deposition of collagen degraded by collagenase. Transmembrane protein 88 (TMEM88) belongs to the TMEM family and is involved in the regulation of tumorigenesis and fibrogenesis. Zhao et al. (2017a) found that overexpression of TMEM88 inhibited TGF-β1 expression in keloid fibroblasts, thereby decreasing collagen I expression. Tissue inhibitors of matrix metalloproteinases (MMPs) and tissue inhibitors of metalloproteinases (TIMPs) are two important regulators of degradation and remodeling of ECM. Aoki et al. (2014) promoted the degradation of collagen I in keloids by targeting TIMP-1 with small interfering RNA. Lysyl oxidase (LOX) plays an important role in collagen cross-linking, and helps increase tissue stiffness and the resistance of collagen-rich substrates to degradation. Kim (2021) found that keloid dermal fibroblasts showed the highest degree of expression of skin fibrosis markers, such as LOX and four LOX-like family enzymes, at the cell-matrix interface. Epidermal growth factor-mediated LOX expression was significantly reduced, thereby reducing the fibrotic phenotype of keloid fibroblasts and promoting collagen degradation.

In conclusion, current studies suggest that mechanical stimulation can lead to excessive proliferation of fibroblasts at the wound site, ECM deposition, and secretion of more pro-fibrotic factors, thus promoting the continuous increase of ECM stiffness in keloids. At the same time, the matrix mechanics of ECM further promotes the fibrotic phenotype of keloid fibroblasts, thus forming a loop and resulting in continuous invasion of the surrounding normal tissues by keloids. During this process, the mechanical force is one of the initiating factors of keloid formation, and matrix mechanics leads to further keloid development (**Figure 1**).

BIOMECHANICAL FACTORS AND MECHANOTRANSDUCTION PATHWAYS IN KELOIDS

In the pathological process of gradual stiffening of keloid matrix, the cells in keloid sense changes in mechanical properties of the microenvironment and activate mechanical transduction pathways, thus transforming external mechanical stimuli into biochemical signals and ultimately guiding cellular behavior (Mierke, 2022). How matrix mechanics affects and regulates cell fate at a macro to micro scale is still unclear. However, some studies have found that some proteins involved in mechanical transduction pathways play a role in this process. Several mechanically sensitive pathways in keloid development and their effects on keloid progression will be introduced next (**Figure 2**).

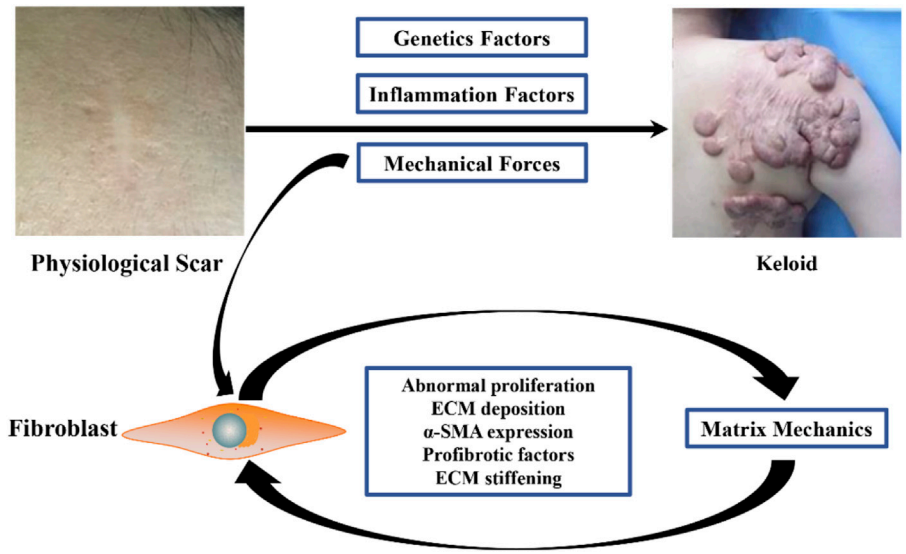

FIGURE 1 | Causes of keloid matrix stiffening during fibrotic progression. Mechanical stimulation can lead to excessive proliferation of wound fibroblasts, deposition of ECM, secretion of more pro-fibrosis factors, and continuous increase of matrix stiffness of keloid ECM. Matrix mechanics resulting from elevated matrix stiffness further activates the fibrotic phenotype of keloid fibroblasts, thus forming a loop that continuously invades surrounding normal tissue.

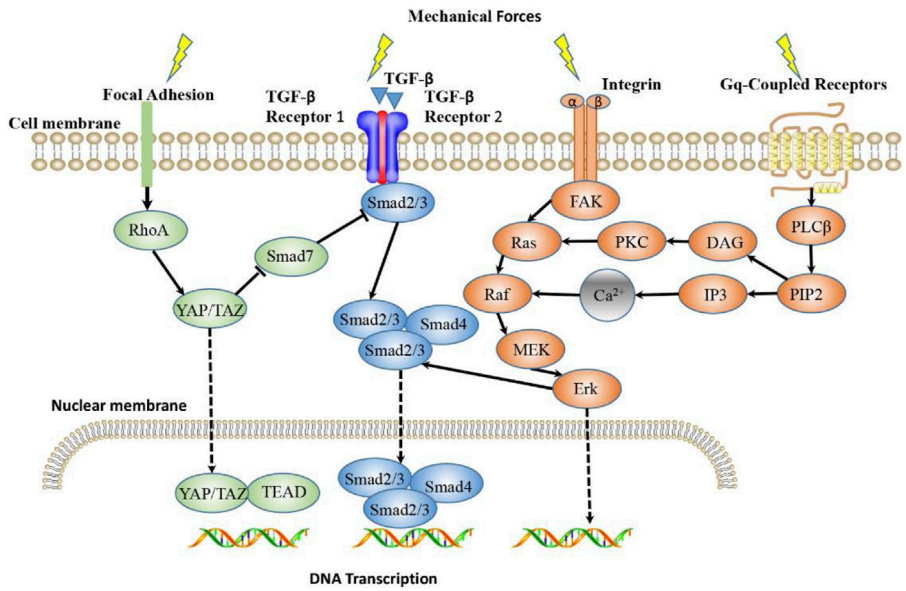

FIGURE 2 | Main Mechanotransduction Signaling Pathways in keloid. TGF-β/Smad, integrin/FAK, YAP/TAZ signaling pathways and Calcium ion signaling are the main mechanotransduction signaling pathways that mediate mechanoresponsiveness. TGF-β senses mechanical forces and signals through Smads, where Smad2/3 binds to Smad4 and enters the nucleus, where they bind DNA and initiate trans-activation of target genes. Integrin signaling induces gene expression through FAK/Erk pathway, and also interferes with TGF-β/Smad signaling pathway. Mechanical stimulation can promote YAP to nuclear transfer and function. The Gq-coupled receptor activated by stretch stimulation can activate PLCβ and produce DAG and IP3. IP3 acts on the intracellular calcium pool to release Ca^{2+}, resulting in the increase of intracellular free calcium ion concentration and the subsequent intracellular reaction of Raf/MEK/Erk pathway.

TGF-β/Smad Signaling Pathway in Keloids

As a classical signaling pathway, the TGF-β signaling pathway has been proved to be an important signaling pathway involved in fibrosis progression during mechanical regulation (Chen et al., 2019). The transforming growth factor superfamily includes TGF-β, bone morphogenetic protein (BMP), and growth differentiation factor (GDF), among which there are three different subtypes of TGF-β in the mammalian genome,

namely TGF-β1, TGF-β2, and TGF-β3. Most of the biological functions of TGF-β superfamily are realized by binding to TGF-β receptor and activating the Smad signaling pathway (Frangogiannis, 2020). TGF-β1 is a stimulant of wound repair and tissue regeneration and a mediator of ECM production. During active wound healing, TGF-β is involved in various processes, including inflammation, angiogenesis, cell proliferation, collagen and matrix production, and wound remodeling (Pakyari et al., 2013). TGF-β is overexpressed in keloid the tissue and regulates the transformation of fibroblasts to myofibroblasts, and TGF-β1 has the highest proportion and the strongest activity. TGF-β1 can stimulate the proliferation and differentiation of keloid fibroblasts, up-regulate the expression of α-SMA and collagen, and promote the synthesis of ECM, thus leading to increased keloid tissue stiffness (Wang et al., 2016b; Zhang et al., 2020). TGF-β level is closely associated with the response of keloids to mechanical forces. Wang et al. (2006) found that keloid-derived fibroblasts exposed to equibiaxial strain produce higher levels of TGF-β1, TGF-β2, and collagen 1α at mRNA and protein levels than those produced by normal skin fibroblasts. Hypoxia induces the transformation of fibroblasts into myofibroblasts by activating TGF-β/Smad3 signaling pathway and increases collagen synthesis in keloid fibroblasts in a hypertrophic keloid microenvironment induced by high matrix stiffness (Zhao et al., 2017b).

Integrin Signaling Pathway in Keloids

Integrin family is a kind of cell adhesion, signal pathway hub and the function of mechanical force signal sensing dimers proteins across the membrane. They are the link of ECM to the actin cytoskeleton in the cell and regulate specific signal transduction cascade reactions. Therefore, the protein is mediated the effect of matrix–cell and the cell–cell interaction, so as to promote the reshaping of the ECM (Bachman et al., 2015). Wound tension is an important factor in activating the integrin signaling pathway, which can directly activate integrin, convert mechanical signals into chemical signals in the cytoplasm, and promote the proliferation and differentiation of fibroblasts and secretion of collagen (Gauthier and Roca-Cusachs, 2018). Keloid fibroblasts showed up-regulated expressions of α1β1 and α2β1 integrins. Integrin α1β1 promoted fibroblast proliferation but inhibited collagen synthesis, whereas α2β1 had the opposite effect (Suarez et al., 2013). Song et al. analyzed integrin expression in keloid-derived mesenchymal stem cells, including α2, α3, α5, αV, α8, α10, α11, β1, and β3, and found that mechanical tension up-regulated the expression of integrin αV and integrin β3, thus up-regulating cell proliferation and collagen synthesis. Moreover, integrin αvβ3 is more sensitive to mechanical tension, and may be a new target for keloid treatment and prevention of keloid recurrence (Song et al., 2019). In addition, integrin also mediated the activation of TGF-β. In the process of TGF-β activation, integrin binds to the pre-domain and releases TGF-β using the stretching force generated by the actin cytoskeleton. At the same time, integrin can be abnormally expressed under the stimulation of TGF-β, promoting physiological and pathological changes in the body (Dong et al., 2017). During keloid formation, increased mechanical forces transmit high pressure through fibroblasts. This pressure is applied on integrins, causing latency-related peptides to unfold and release an active form of TGF-β (Leask, 2013).

YAP/TAZ Signaling Pathway in Keloids

Yes-associated protein (YAP) and transcriptional coactivator with a PDZ-binding domain (TAZ) are among the activated mechanosensory pathways. YAP/TAZ can read a wide range of mechanical cues, such as ECM stiffness and topology, shear stress, and cell shape, and translate these into cell-specific biological effects (Zanconato et al., 2019). This ability to respond to different mechanical signals highlights YAP/TAZ's central role as a general purpose mechanical sensor and effector. Mechanical transduction of YAP/TAZ is mainly controlled by its subcellular localization because YAP/TAZ activation requires its accumulation in the nucleus (Panciera et al., 2017). Gao et al. (2022) study showed that increased nuclear YAP/TAZ staining was observed in keloid tissue fibroblasts compared with that in normal skin. Activation of YAP-TAZ in the nucleus leads to the expression of pro-fibrosis genes, increased α-SMA expression, and excessive matrix deposition (Panciera et al., 2017). YAP/TAZ can be activated by matrix stiffness to further promote the transformation of fibroblasts into myofibroblasts and increase collagen deposition through a positive feedback loop, thereby enhancing the stiffness of the matrix microenvironment and leading to further YAP activation (Liu et al., 2015). Rho/Rho kinase signaling is a key upstream regulator of mechanical and receptor-mediated YAP and TAZ activation and also provides mechanosensory functional connectivity through integrin-based adhesion and tractor-producing actomyosin cytoskeleton. ROCK is a major downstream effector of Rho, driving cell contractility and mediating fibrosis pathology (Johan and Samuel, 2019). Inhibiting ROCK with drugs or inhibitors can alleviate the keloid fibrosis process caused by increased matrix stiffness, thereby disrupting or blocking the cellular response to tissue stiffness (Mun et al., 2014; Kiya et al., 2017).

Calcium Ion Signaling in Keloids

It is believed that many signaling pathways are associated with Ca^{2+} influx, which is associated with a response to mechanical forces. The Gq-coupled receptor activated by stretch stimulation can activate PLCβ and produce DAG and IP3 (Jemal et al., 2014). IP3 acts on the intracellular calcium pool to release Ca^{2+}, resulting in an increase in intracellular free calcium ion concentration and the subsequent intracellular reaction of the Raf/MEK/Erk pathway (Jain et al., 2018). In fibroblasts, uniaxial stretching increases intracellular Ca^{2+} levels (Sakamoto et al., 2010). The Piezo1 channel has been identified as a new mechanically activated cation channel (MAC) reportedly capable of modulating force-mediated cellular biological behavior. In hypertrophic scars, cycling mechanical stretching increased Piezo1 expression and promoted proliferation, migration, and differentiation of human skin fibroblasts and activated Piezo1-mediated influx of calcium (He et al., 2021). Yan et al. (2021) demonstrated phosphoproteome and biological evidence of abnormal calcium homeostasis and induction of abnormal platelet aggregation in keloid fibroblasts. These results suggest that the calcium pathway plays a role in mechanical transduction of keloids. There are also some studies showing that calcium antagonists are effective in treating keloids. Calcium antagonists

reduce ECM production, induce collagenase synthesis, and inhibit IL-6, vascular endothelial growth factor, and fibroblast proliferation (Verhiel et al., 2015). As a calcium channel blocker, verapamil can increase the proteolytic activity of collagenase and regulate collagen metabolism in the ECM. Verapamil treatment increases procollagenase synthesis and decreases fibrous tissue production in keloids (Li and Jin, 2016; Srivastava et al., 2019).

CLINICAL CONTROL OF SKIN TENSION FOR KELOID PREVENTION AND TREATMENT

Biomechanical factors play an important role not only in the occurrence and development of keloids but also in its prevention and treatment. Many targeted biomechanical approaches have been developed for keloid prevention and treatment.

Pharmacological Strategies

Several drugs have been developed to target mechanical transduction signaling pathways. TGF-β has been shown to play an important role in the fibrosis process of keloids, and therefore, multiple therapeutic strategies (including drugs, siRNA, shRNA, and miRNA, among others) have been designed to target TGF-β/Smad signaling to interfere with fibroblast-mediated keloid progression (Zhang et al., 2020; Marty et al., 2021). Ginsenoside Rg3 is a substance extracted from ginseng, a traditional Chinese medicine. Rg3 can inhibit the proliferation of keloid fibroblasts and inhibit the migration of keloid fibroblasts by up-regulating the expression of the anti-fibrosis gene TGF-β3 and down-regulating the expression of the pro-fibrosis gene α-SMA and connective tissue growth factor (Tang et al., 2018). Treatment with integrin αVβ3 inhibitor Cyclo (-RGDfK) resulted in a dramatic decrease of keloid-derived mesenchymal stem cell proliferation, collagen I, and collagen III for 48 h after either static culture or tensile culture (Song et al., 2019). Gao et al. have significantly inhibited the proliferation of keloid fibroblasts, reduced cell migration, induced apoptosis, and down-regulated collagen I production by targeting low endogenous YAP or TAZ knockdown. YAP/TAZ inhibitor verteporfin has shown similar but stronger inhibitory effect on fibroblasts (Gao et al., 2022).

Suture of Intradermal Tension Reduction and Extradermal Tension Reduction Therapy

Surgeons have long known that optimizing incision design is an effective means to reduce wound mechanical tension and prevent postoperative scar hyperplasia. Surgical incisions are usually designed to be parallel to skin Langer's lines, and vertical incision should not be made as far as possible to reduce skin tension. During plastic surgery, Z-plasty, W-plasty, and V-Y plasty are often used to repair scars, so as to disperse the mechanical tension of the incision and reduce the possibility of postoperative scar widening and recurrence (Ogawa, 2019). After keloid excision, degradable subcutaneous or fascial tensioning sutures can be used. Tension is placed on the deep and superficial fascia layers so that the wound edges can join naturally with very little tension, avoiding dermal sutures (Wang et al., 2014; Tsuge et al., 2020). Intralesional injection of Botulinum toxin type A (BoNT-A) is an effective clinical method for preventing and treating keloids. When administered locally, BoNT-A causes temporary paralysis of the wound muscle, thereby reducing disposal tension (Kasyanju Carrero et al., 2019). Skin tensioners can also be used to reduce the postoperative incision tensioning. The skin tensioning device is usually composed of adhesive tape fixing parts on both sides and an adjustable locking part in the middle. The fixing part is worn on both sides of the incision. By adjusting the tension of the incision through the locking part, it can effectively promote wound healing, reduce the occurrence of postoperative incision cracking, reduce mechanical tension of the incision, and avoid excessive keloid development (Chen et al., 2020). In addition to tension therapy, there are many other clinical treatments, including drug therapy (Yang et al., 2021), radiotherapy (Hsieh et al., 2021), cryotherapy (Lee et al., 2020), and stem cell therapy (Bojanic et al., 2021). Although there are many treatment options for keloids, any single treatment can lead to a higher recurrence rate, and multimodal combination therapy is a necessary and effective method at present. For example, after surgical resection, combined therapy with Z-plasty and electron beam irradiation to reduce wound tension can effectively control keloid locally (Wang et al., 2020).

CONCLUSION

Keloids are a fibroproliferative disease caused by excessive growth of fibroblasts and excessive secretion of collagen. Many factors, including changes in cell function, genetic factors, and inflammation factors, play an important role in the occurrence and development of keloids. Biomechanical factors are a basic but relatively unexplored area for understanding keloids. Both macroscopic physical mechanical factors and microscopic matrix mechanical factors at a cellular or molecular level have been proved to have an important impact on the progression of keloid fibrosis and treatment research. Further study on the role of biomechanical factors in the keloid development and modification of mechanical forces or mechanical transduction signals will provide a direction for the development of new therapeutic strategies.

AUTHOR CONTRIBUTIONS

MLE, WX, and WL contributed to conception and design of the study. FF and MLI wrote the first draft of the manuscript and contribute equally to this study. LP, JW, CW, and LY wrote sections of the manuscript. All authors contributed to manuscript revision, read, and approved the submitted version.

FUNDING

This work was supported by National Natural Science Foundation of China (82003384, 11902058); Chongqing Talents: Exceptional Young Talents Project (cstc2021ycjh-bgzxm0197), Fundamental Research Funds for the Central Universities (2020CDJYGSG003), and Scientific Research

Foundation from Chongqing University (02210011044110), and Project for Excellent Talents in Xihua University Grant (Z212031); Natural Science Foundation of Chongqing (cstc2019jcyj-msxmX0741,jxyn2020-6, CQSZYY2020011).

REFERENCES

Abdou, A. G., Maraee, A. H., and Saif, H. F. (2014). Immunohistochemical Evaluation of COX-1 and COX-2 Expression in Keloid and Hypertrophic Scar. *Am. J. Dermatopathol.* 36 (4), 311–317. doi:10.1097/DAD.0b013e3182a27b83

Andrews, J. P., Marttala, J., Macarak, E., Rosenbloom, J., and Uitto, J. (2016). Keloids: The Paradigm of Skin Fibrosis - Pathomechanisms and Treatment. *Matrix Biol.* 51, 37–46. doi:10.1016/j.matbio.2016.01.013

Aoki, M., Miyake, K., Ogawa, R., Dohi, T., Akaishi, S., Hyakusoku, H., et al. (2014). siRNA Knockdown of Tissue Inhibitor of Metalloproteinase-1 in Keloid Fibroblasts Leads to Degradation of Collagen Type I. *J. Investig. Dermatol* 134 (3), 818–826. doi:10.1038/jid.2013.396

Bachman, H., Nicosia, J., Dysart, M., and Barker, T. H. (2015). Utilizing Fibronectin Integrin-Binding Specificity to Control Cellular Responses. *Adv. Wound Care (New Rochelle)* 4 (8), 501–511. doi:10.1089/wound.2014.0621

Bagabir, R., Byers, R. J., Chaudhry, I. H., Müller, W., Paus, R., and Bayat, A. (2012). Site-specific Immunophenotyping of Keloid Disease Demonstrates Immune Upregulation and the Presence of Lymphoid Aggregates. *Br. J. Dermatol* 167 (5), 1053–1066. doi:10.1111/j.1365-2133.2012.11190.x

Berman, B., Maderal, A., and Raphael, B. (2017). Keloids and Hypertrophic Scars: Pathophysiology, Classification, and Treatment. *Dermatol Surg.* 43 Suppl 1 (Suppl. 1), S3s18. doi:10.1097/DSS.0000000000000819

Bojanic, C., To, K., Hatoum, A., Shea, J., Seah, K. T. M., Khan, W., et al. (2021). Mesenchymal Stem Cell Therapy in Hypertrophic and Keloid Scars. *Cell. Tissue Res.* 383 (3), 915–930. doi:10.1007/s00441-020-03361-z

Canady, J., Karrer, S., Fleck, M., and Bosserhoff, A. K. (2013). Fibrosing Connective Tissue Disorders of the Skin: Molecular Similarities and Distinctions. *J. Dermatol Sci.* 70 (3), 151–158. doi:10.1016/j.jdermsci.2013.03.005

Chen, B., Ding, J., Jin, J., Song, N., and Liu, Y. (2020). Continuous Tension Reduction to Prevent Keloid Recurrence after Surgical Excision: Preliminary Experience in Asian Patients. *Dermatol Ther.* 33 (4), e13553. doi:10.1111/dth.13553

Chen, G., Xia, B., Fu, Q., Huang, X., Wang, F., Chen, Z., et al. (2019). Matrix Mechanics as Regulatory Factors and Therapeutic Targets in Hepatic Fibrosis. *Int. J. Biol. Sci.* 15 (12), 2509–2521. doi:10.7150/ijbs.37500

Chen, Z., Zhou, L., Won, T., Gao, Z., Wu, X., and Lu, L. (2018). Characterization of CD_45RO^+ Memory T Lymphocytes in Keloid Disease. *Br. J. Dermatol* 178 (4), 940–950. doi:10.1111/bjd.16173

Deng, Z., Subilia, M., Chin, I. L., Hortin, N., Stevenson, A. W., Wood, F. M., et al. (2021). Keloid Fibroblasts Have Elevated and Dysfunctional Mechanotransduction Signaling that Is Independent of TGF-β. *J. Dermatol Sci.* 104 (1), 11–20. doi:10.1016/j.jdermsci.2021.09.002

Dohi, T., Padmanabhan, J., Akaishi, S., Than, P. A., Terashima, M., Matsumoto, N. N., et al. (2019). The Interplay of Mechanical Stress, Strain, and Stiffness at the Keloid Periphery Correlates with Increased Caveolin-1/ROCK Signaling and Scar Progression. *Plast. Reconstr. Surg.* 144 (1), 58e–67e. doi:10.1097/PRS.0000000000005717

Dong, X., Zhao, B., Iacob, R. E., Zhu, J., Koksal, A. C., Lu, C., et al. (2017). Force Interacts with Macromolecular Structure in Activation of TGF-β. *Nature* 542 (7639), 55–59. doi:10.1038/nature21035

El Ayadi, A., Jay, J. W., and Prasai, A. (2020). Current Approaches Targeting the Wound Healing Phases to Attenuate Fibrosis and Scarring. *Int. J. Mol. Sci.* 21 (3), 105. doi:10.3390/ijms21031105

Frangogiannis, N. (2020). Transforming Growth Factor-β in Tissue Fibrosis. *J. Exp. Med.* 217 (3), e20190103. doi:10.1084/jem.20190103

Gao, N., Lu, L., Ma, X., Liu, Z., Yang, S., and Han, G. (2022). Targeted Inhibition of YAP/TAZ Alters the Biological Behaviours of Keloid Fibroblasts. *Exp. Dermatol* 31 (3), 320–329. doi:10.1111/exd.14466

Gauthier, N. C., and Roca-Cusachs, P. (2018). Mechanosensing at Integrin-Mediated Cell-Matrix Adhesions: from Molecular to Integrated Mechanisms. *Curr. Opin. Cell. Biol.* 50, 20–26. doi:10.1016/j.ceb.2017.12.014

Hahn, J. M., McFarland, K. L., Combs, K. A., and Supp, D. M. (2016). Partial Epithelial-Mesenchymal Transition in Keloid Scars: Regulation of Keloid Keratinocyte Gene Expression by Transforming Growth Factor-β1. *Burns Trauma* 4 (1), 30. doi:10.1186/s41038-016-0055-7

Hang, J., Chen, J., Zhang, W., Yuan, T., Xu, Y., and Zhou, B. (2021). Correlation between Elastic Modulus and Clinical Severity of Pathological Scars: a Cross-Sectional Study. *Sci. Rep.* 11 (1), 23324. doi:10.1038/s41598-021-02730-0

Harn, H. I., Ogawa, R., Hsu, C. K., Hughes, M. W., Tang, M. J., and Chuong, C. M. (2019). The Tension Biology of Wound Healing. *Exp. Dermatol* 28 (4), 464–471. doi:10.1111/exd.13460

He, J., Fang, B., Shan, S., Xie, Y., Wang, C., Zhang, Y., et al. (2021). Mechanical Stretch Promotes Hypertrophic Scar Formation through Mechanically Activated Cation Channel Piezo1. *Cell. Death Dis.* 12 (3), 226. doi:10.1038/s41419-021-03481-6

He, Y., Deng, Z., Alghamdi, M., Lu, L., Fear, M. W., and He, L. (2017). From Genetics to Epigenetics: New Insights into Keloid Scarring. *Cell. Prolif.* 50 (2), 326. doi:10.1111/cpr.12326

Hesketh, M., Sahin, K. B., West, Z. E., and Murray, R. Z. (2017). Macrophage Phenotypes Regulate Scar Formation and Chronic Wound Healing. *Int. J. Mol. Sci.* 18 (7), 545. doi:10.3390/ijms18071545

Hsieh, C. L., Chi, K. Y., Lin, W. Y., and Lee, L. T. (2021). Timing of Adjuvant Radiotherapy after Keloid Excision: A Systematic Review and Meta-Analysis. *Dermatol Surg.* 47 (11), 1438–1443. doi:10.1097/DSS.0000000000003165

Hsu, C. K., Lin, H. H., Harn, H. I., Hughes, M. W., Tang, M. J., and Yang, C. C. (2018a). Mechanical Forces in Skin Disorders. *J. Dermatol Sci.* 90 (3), 232–240. doi:10.1016/j.jdermsci.2018.03.004

Hsu, C. K., Lin, H. H., Harn, H. I., Ogawa, R., Wang, Y. K., Ho, Y. T., et al. (2018b). Caveolin-1 Controls Hyperresponsiveness to Mechanical Stimuli and Fibrogenesis-Associated RUNX2 Activation in Keloid Fibroblasts. *J. Investig. Dermatol* 138 (1), 208–218. doi:10.1016/j.jid.2017.05.041

Huang, C., Akaishi, S., Hyakusoku, H., and Ogawa, R. (2014). Are Keloid and Hypertrophic Scar Different Forms of the Same Disorder? A Fibroproliferative Skin Disorder Hypothesis Based on Keloid Findings. *Int. Wound J.* 11 (5), 517–522. doi:10.1111/j.1742-481X.2012.01118.x

Huang, C., and Ogawa, R. (2013). Roles of Lipid Metabolism in Keloid Development. *Lipids Health Dis.* 12, 60. doi:10.1186/1476-511X-12-60

Huang, S. Y., Xiang, X., Guo, R. Q., Cheng, S., Wang, L. Y., and Qiu, L. (2020). Quantitative Assessment of Treatment Efficacy in Keloids Using High-Frequency Ultrasound and Shear Wave Elastography: a Preliminary Study. *Sci. Rep.* 10 (1), 1375. doi:10.1038/s41598-020-58209-x

Jain, R., Watson, U., Vasudevan, L., and Saini, D. K. (2018). ERK Activation Pathways Downstream of GPCRs. *Int. Rev. Cell. Mol. Biol.* 338, 79–109. doi:10.1016/bs.ircmb.2018.02.003

Jemal, I., Soriano, S., Conte, A. L., Morenilla, C., and Gomis, A. (2014). G Protein-Coupled Receptor Signalling Potentiates the Osmo-Mechanical Activation of TRPC5 Channels. *Pflugers Arch.* 466 (8), 1635–1646. doi:10.1007/s00424-013-1392-z

Jin, J., Zhai, H. F., Jia, Z. H., and Luo, X. H. (2019). Long Non-coding RNA HOXA11-AS Induces Type I Collagen Synthesis to Stimulate Keloid Formation via Sponging miR-124-3p and Activation of Smad5 Signaling. *Am. J. Physiol. Cell. Physiol.* 317 (5), C1001–c1010. doi:10.1152/ajpcell.00319.2018

Jin, Q., Gui, L., Niu, F., Yu, B., Lauda, N., Liu, J., et al. (2018). Macrophages in Keloid Are Potent at Promoting the Differentiation and Function of Regulatory T Cells. *Exp. Cell. Res.* 362 (2), 472–476. doi:10.1016/j.yexcr.2017.12.011

Johan, M. Z., and Samuel, M. S. (2019). Rho-ROCK Signaling Regulates Tumor-Microenvironment Interactions. *Biochem. Soc. Trans.* 47 (1), 101–108. doi:10.1042/BST20180334

Jumper, N., Hodgkinson, T., Paus, R., and Bayat, A. (2017). A Role for Neuregulin-1 in Promoting Keloid Fibroblast Migration via ErbB2-Mediated Signaling. *Acta Derm. Venereol.* 97 (6), 675–684. doi:10.2340/00015555-2587

Kang, Y., Roh, M. R., Rajadurai, S., Rajadurai, A., Kumar, R., Njauw, C. N., et al. (2020). Hypoxia and HIF-1α Regulate Collagen Production in Keloids. *J. Investig. Dermatol* 140 (11), 2157–2165. doi:10.1016/j.jid.2020.01.036

Kasyanju Carrero, L. M., Ma, W. W., Liu, H. F., Yin, X. F., and Zhou, B. R. (2019). Botulinum Toxin Type A for the Treatment and Prevention of Hypertrophic Scars and Keloids: Updated Review. *J. Cosmet. Dermatol* 18 (1), 10–15. doi:10.1111/jocd.12828

Kenny, F. N., Drymoussi, Z., Delaine-Smith, R., Kao, A. P., Laly, A. C., Knight, M. M., et al. (2018). Tissue Stiffening Promotes Keratinocyte Proliferation through Activation of Epidermal Growth Factor Signaling. *J. Cell. Sci.* 131 (10), 780. doi:10.1242/jcs.215780

Kim, H. (2021). Ameliorating Fibrotic Phenotypes of Keloid Dermal Fibroblasts through an Epidermal Growth Factor-Mediated Extracellular Matrix Remodeling. *Int. J. Mol. Sci.* 22 (4), 2198. doi:10.3390/ijms22042198

Kim, J., Kim, B., Kim, S. M., Yang, C. E., Song, S. Y., Lee, W. J., et al. (2019). Hypoxia-Induced Epithelial-To-Mesenchymal Transition Mediates Fibroblast Abnormalities via ERK Activation in Cutaneous Wound Healing. *Int. J. Mol. Sci.* 20 (10). doi:10.3390/ijms20102546

Kiprono, S. K., Chaula, B. M., Masenga, J. E., Muchunu, J. W., Mavura, D. R., and Moehrle, M. (2015). Epidemiology of Keloids in Normally Pigmented Africans and African People with Albinism: Population-Based Cross-Sectional Survey. *Br. J. Dermatol* 173 (3), 852–854. doi:10.1111/bjd.13826

Kiya, K., Kubo, T., Kawai, K., Matsuzaki, S., Maeda, D., Fujiwara, T., et al. (2017). Endothelial Cell-Derived Endothelin-1 Is Involved in Abnormal Scar Formation by Dermal Fibroblasts through RhoA/Rho-Kinase Pathway. *Exp. Dermatol* 26 (8), 705–712. doi:10.1111/exd.13264

Kurokawa, N., Ueda, K., and Tsuji, M. (2010). Study of Microvascular Structure in Keloid and Hypertrophic Scars: Density of Microvessels and the Efficacy of Three-Dimensional Vascular Imaging. *J. Plast. Surg. Hand Surg.* 44 (6), 272–277. doi:10.3109/2000656X.2010.532923

Leask, A. (2013). Integrin β1: A Mechanosignaling Sensor Essential for Connective Tissue Deposition by Fibroblasts. *Adv. Wound Care (New Rochelle)* 2 (4), 160–166. doi:10.1089/wound.2012.0365

Lee, H. J., and Jang, Y. J. (2018). Recent Understandings of Biology, Prophylaxis and Treatment Strategies for Hypertrophic Scars and Keloids. *Int. J. Mol. Sci.* 19 (3), 711. doi:10.3390/ijms19030711

Lee, Y. I., Kim, S. M., Kim, J., Kim, J., Song, S. Y., Lee, W. J., et al. (2020). Tissue-remodelling M2 Macrophages Recruits Matrix Metallo-Proteinase-9 for Cryotherapy-Induced Fibrotic Resolution during Keloid Treatment. *Acta Derm. Venereol.* 100 (17), adv00306. doi:10.2340/00015555-3665

Lee, Y. S., Hsu, T., Chiu, W. C., Sarkozy, H., Kulber, D. A., Choi, A., et al. (2016). Keloid-derived, Plasma/fibrin-Based Skin Equivalents Generate De Novo Dermal and Epidermal Pathology of Keloid Fibrosis in a Mouse Model. *Wound Repair Regen.* 24 (2), 302–316. doi:10.1111/wrr.12397

Lei, R., Li, J., Liu, F., Li, W., Zhang, S., Wang, Y., et al. (2019). HIF-1α Promotes the Keloid Development through the Activation of TGF-β/Smad and TLR4/MyD88/NF-κB Pathways. *Cell. Cycle* 18 (23), 3239–3250. doi:10.1080/15384101.2019.1670508

Li, M., and Wu, L. (2016). Functional Analysis of Keratinocyte and Fibroblast Gene Expression in Skin and Keloid Scar Tissue Based on Deviation Analysis of Dynamic Capabilities. *Exp. Ther. Med.* 12 (6), 3633–3641. doi:10.3892/etm.2016.3817

Li, Q., Qin, Z., Nie, F., Bi, H., Zhao, R., Pan, B., et al. (2018). Metabolic Reprogramming in Keloid Fibroblasts: Aerobic Glycolysis and a Novel Therapeutic Strategy. *Biochem. Biophys. Res. Commun.* 496 (2), 641–647. doi:10.1016/j.bbrc.2018.01.068

Li, Z., and Jin, Z. (2016). Comparative Effect and Safety of Verapamil in Keloid and Hypertrophic Scar Treatment: a Meta-Analysis. *Ther. Clin. Risk Manag.* 12, 1635–1641. doi:10.2147/TCRM.S118748

Limandjaja, G. C., Niessen, F. B., Scheper, R. J., and Gibbs, S. (2020). The Keloid Disorder: Heterogeneity, Histopathology, Mechanisms and Models. *Front. Cell. Dev. Biol.* 8, 360. doi:10.3389/fcell.2020.00360

Limandjaja, G. C., Waaijman, T., Roffel, S., Niessen, F. B., and Gibbs, S. (2019). Monocytes Co-cultured with Reconstructed Keloid and Normal Skin Models Skew towards M2 Macrophage Phenotype. *Arch. Dermatol Res.* 311 (8), 615–627. doi:10.1007/s00403-019-01942-9

Lin, X., Wang, Y., Jiang, Y., Xu, M., Pang, Q., Sun, J., et al. (2020). Sumoylation Enhances the Activity of the TGF-β/SMAD and HIF-1 Signaling Pathways in Keloids. *Life Sci.* 255, 117859. doi:10.1016/j.lfs.2020.117859

Liu, F., Lagares, D., Choi, K. M., Stopfer, L., Marinković, A., Vrbanac, V., et al. (2015). Mechanosignaling through YAP and TAZ Drives Fibroblast Activation and Fibrosis. *Am. J. Physiol. Lung Cell. Mol. Physiol.* 308 (4), L344–L357. doi:10.1152/ajplung.00300.2014

Liu, J., Zhu, H., Wang, H., Li, J., Han, F., Liu, Y., et al. (2018). Methylation of Secreted Frizzled-Related Protein 1 (SFRP1) Promoter Downregulates Wnt/β-Catenin Activity in Keloids. *J. Mol. Histol.* 49 (2), 185–193. doi:10.1007/s10735-018-9758-3

Lu, W. S., Zheng, X. D., Yao, X. H., and Zhang, L. F. (2015). Clinical and Epidemiological Analysis of Keloids in Chinese Patients. *Arch. Dermatol Res.* 307 (2), 109–114. doi:10.1007/s00403-014-1507-1

Lu, Y. Y., Wu, C. H., Hong, C. H., Chang, K. L., and Lee, C. H. (2021). GLUT-1 Enhances Glycolysis, Oxidative Stress, and Fibroblast Proliferation in Keloid. *Life (Basel)* 11 (6), 505. doi:10.3390/life11060505

Luo, L., Li, J., Liu, H., Jian, X., Zou, Q., Zhao, Q., et al. (2017). Adiponectin Is Involved in Connective Tissue Growth Factor-Induced Proliferation, Migration and Overproduction of the Extracellular Matrix in Keloid Fibroblasts. *Int. J. Mol. Sci.* 18 (5), 1044. doi:10.3390/ijms18051044

Lv, W., Ren, Y., Hou, K., Hu, W., Yi, Y., Xiong, M., et al. (2020). Epigenetic Modification Mechanisms Involved in Keloid: Current Status and Prospect. *Clin. Epigenetics* 12 (1), 183. doi:10.1186/s13148-020-00981-8

Macarak, E. J., Wermuth, P. J., Rosenbloom, J., and Uitto, J. (2021). Keloid Disorder: Fibroblast Differentiation and Gene Expression Profile in Fibrotic Skin Diseases. *Exp. Dermatol* 30 (1), 132–145. doi:10.1111/exd.14243

Maeda, D., Kubo, T., Kiya, K., Kawai, K., Matsuzaki, S., Kobayashi, D., et al. (2019). Periostin Is Induced by IL-4/IL-13 in Dermal Fibroblasts and Promotes RhoA/ROCK Pathway-Mediated TGF-β1 Secretion in Abnormal Scar Formation. *J. Plast. Surg. Hand Surg.* 53 (5), 288–294. doi:10.1080/2000656X.2019.1612752

Mahdavian Delavary, B., van der Veer, W. M., Ferreira, J. A., and Niessen, F. B. (2012). Formation of Hypertrophic Scars: Evolution and Susceptibility. *J. Plast. Surg. Hand Surg.* 46 (2), 95–101. doi:10.3109/2000656X.2012.669184

Marty, P., Chatelain, B., Lihoreau, T., Tissot, M., Dirand, Z., Humbert, P., et al. (2021). Halofuginone Regulates Keloid Fibroblast Fibrotic Response to TGF-β Induction. *Biomed. Pharmacother.* 135, 111182. doi:10.1016/j.biopha.2020.111182

Mierke, C. T. (2022). Viscoelasticity, like Forces, Plays a Role in Mechanotransduction. *Front. Cell. Dev. Biol.* 10, 789841. doi:10.3389/fcell.2022.789841

Li, Q. I., Chen, B., and Qin, Z. (2020). Mitochondrial Dysfunction and Morphological Abnormality in Keloid Fibroblasts. *Adv. Wound Care* 9. 539

Mun, J. H., Kim, Y. M., Kim, B. S., Kim, J. H., Kim, M. B., and Ko, H. C. (2014). Simvastatin Inhibits Transforming Growth Factor-β1-Induced Expression of Type I Collagen, CTGF, and α-SMA in Keloid Fibroblasts. *Wound Repair Regen.* 22 (1), 125–133. doi:10.1111/wrr.12136

Nagar, H., Kim, S., Lee, I., Kim, S., Choi, S. J., Piao, S., et al. (2021). Downregulation of CR6-Interacting Factor 1 Suppresses Keloid Fibroblast Growth via the TGF-β/Smad Signaling Pathway. *Sci. Rep.* 11 (1), 500. doi:10.1038/s41598-020-79785-y

Nagasao, T., Aramaki-Hattori, N., Shimizu, Y., Yoshitatsu, S., Takano, N., and Kishi, K. (2013). Transformation of Keloids Is Determined by Stress Occurrence Patterns on Peri-Keloid Regions in Response to Body Movement. *Med. Hypotheses* 81 (1), 136–141. doi:10.1016/j.mehy.2013.04.016

Nyika, D. T., Khumalo, N. P., and Bayat, A. (2022). Genetics and Epigenetics of Keloids. *Adv. Wound Care (New Rochelle)* 11 (4), 192–201. doi:10.1089/wound.2021.0094

Nyström, A., and Bruckner-Tuderman, L. (2019). Matrix Molecules and Skin Biology. *Semin. Cell. Dev. Biol.* 89, 136. doi:10.1016/j.semcdb.2018.07.025

Ogawa, R. (2017). Keloid and Hypertrophic Scars Are the Result of Chronic Inflammation in the Reticular Dermis. *Int. J. Mol. Sci.* 18 (3). 606. doi:10.3390/ijms18030606

Ogawa, R., Mitsuhashi, K., Hyakusoku, H., and Miyashita, T. (2003). Postoperative Electron-Beam Irradiation Therapy for Keloids and Hypertrophic Scars: Retrospective Study of 147 Cases Followed for More Than 18 Months. *Plast. Reconstr. Surg.* 111 (2), 547–555. doi:10.1097/01.PRS.0000040466.55214.35

Ogawa, R., Okai, K., Tokumura, F., Mori, K., Ohmori, Y., Huang, C., et al. (2012). The Relationship between Skin Stretching/contraction and Pathologic Scarring: the Important Role of Mechanical Forces in Keloid Generation. *Wound Repair Regen.* 20 (2), 149–157. doi:10.1111/j.1524-475X.2012.00766.x

Ogawa, R. (2019). Surgery for Scar Revision and Reduction: from Primary Closure to Flap Surgery. *Burns Trauma* 7, 7. doi:10.1186/s41038-019-0144-5

Pakyari, M., Farrokhi, A., Maharlooei, M. K., and Ghahary, A. (2013). Critical Role of Transforming Growth Factor Beta in Different Phases of Wound Healing. *Adv. Wound Care (New Rochelle)* 2 (5), 215–224. doi:10.1089/wound.2012.0406

Panciera, T., Azzolin, L., Cordenonsi, M., and Piccolo, S. (2017). Mechanobiology of YAP and TAZ in Physiology and Disease. *Nat. Rev. Mol. Cell. Biol.* 18 (12), 758–770. doi:10.1038/nrm.2017.87

Plikus, M. V., Wang, X., Sinha, S., Forte, E., Thompson, S. M., Herzog, E. L., et al. (2021). Fibroblasts: Origins, Definitions, and Functions in Health and Disease. *Cell.* 184 (15), 3852–3872. doi:10.1016/j.cell.2021.06.024

Rodrigues, M., Kosaric, N., Bonham, C. A., and Gurtner, G. C. (2019). Wound Healing: A Cellular Perspective. *Physiol. Rev.* 99 (1), 665–706. doi:10.1152/physrev.00067.2017

Russell, S. B., Russell, J. D., Trupin, K. M., Gayden, A. E., Opalenik, S. R., Nanney, L. B., et al. (2010). Epigenetically Altered Wound Healing in Keloid Fibroblasts. *J. Investig. Dermatol* 130 (10), 2489–2496. doi:10.1038/jid.2010.162

Sakamoto, Y., Ishijima, M., Kaneko, H., Kurebayashi, N., Ichikawa, N., Futami, I., et al. (2010). Distinct Mechanosensitive $Ca2^{+}$ Influx Mechanisms in Human Primary Synovial Fibroblasts. *J. Orthop. Res.* 28 (7), 859–864. doi:10.1002/jor.21080

Shook, B. A., Wasko, R. R., Rivera-Gonzalez, G. C., Salazar-Gatzimas, E., López-Giráldez, F., Dash, B. C., et al. (2018). Myofibroblast Proliferation and Heterogeneity Are Supported by Macrophages during Skin Repair. *Science* 362 (6417), 362. doi:10.1126/science.aar2971

Song, H., Liu, T., Wang, W., Pang, H., Zhou, Z., Lv, Y., et al. (2019). Tension Enhances Cell Proliferation and Collagen Synthesis by Upregulating Expressions of Integrin αvβ3 in Human Keloid-Derived Mesenchymal Stem Cells. *Life Sci.* 219, 272–282. doi:10.1016/j.lfs.2018.12.042

Srivastava, S., Kumari, H., and Singh, A. (2019). Comparison of Fractional CO_2 Laser, Verapamil, and Triamcinolone for the Treatment of Keloid. *Adv. Wound Care (New Rochelle)* 8 (1), 7–13. doi:10.1089/wound.2018.0798

Suarez, E., Syed, F., Alonso-Rasgado, T., and Bayat, A. (2015). Identification of Biomarkers Involved in Differential Profiling of Hypertrophic and Keloid Scars versus Normal Skin. *Arch. Dermatol Res.* 307 (2), 115–133. doi:10.1007/s00403-014-1512-4

Suarez, E., Syed, F., Alonso-Rasgado, T., Mandal, P., and Bayat, A. (2013). Up-regulation of Tension-Related Proteins in Keloids: Knockdown of Hsp27, α2β1-integrin, and PAI-2 Shows Convincing Reduction of Extracellular Matrix Production. *Plast. Reconstr. Surg.* 131 (2), 158e–173e. doi:10.1097/PRS.0b013e3182789b2b

Suarez, E., Syed, F., Rasgado, T. A., Walmsley, A., Mandal, P., and Bayat, A. (2014). Skin Equivalent Tensional Force Alters Keloid Fibroblast Behavior and Phenotype. *Wound Repair Regen.* 22 (5), 557–568. doi:10.1111/wrr.12215

Syed, F., Ahmadi, E., Iqbal, S. A., Singh, S., McGrouther, D. A., and Bayat, A. (2011). Fibroblasts from the Growing Margin of Keloid Scars Produce Higher Levels of Collagen I and III Compared with Intralesional and Extralesional Sites: Clinical Implications for Lesional Site-Directed Therapy. *Br. J. Dermatol* 164 (1), 83–96. doi:10.1111/j.1365-2133.2010.10048.x

Tang, M., Bian, W., Cheng, L., Zhang, L., Jin, R., Wang, W., et al. (2018). Ginsenoside Rg3 Inhibits Keloid Fibroblast Proliferation, Angiogenesis and Collagen Synthesis *In Vitro* via the TGF β/Smad and ERK Signaling Pathways. *Int. J. Mol. Med.* 41 (3), 1487–1499. doi:10.3892/ijmm.2018.3362

Tsuge, T., Aoki, M., Akaishi, S., Dohi, T., Yamamoto, H., and Ogawa, R. (2020). Geometric Modeling and a Retrospective Cohort Study on the Usefulness of Fascial Tensile Reductions in Severe Keloid Surgery. *Surgery* 167 (2), 504–509. doi:10.1016/j.surg.2019.07.028

Verhiel, S., Piatkowski de Grzymala, A., and van der Hulst, R. (2015). Mechanism of Action, Efficacy, and Adverse Events of Calcium Antagonists in Hypertrophic Scars and Keloids: A Systematic Review. *Dermatol Surg.* 41 (12), 1343–1350. doi:10.1097/DSS.0000000000000506

Vinaik, R., Barayan, D., Auger, C., Abdullahi, A., and Jeschke, M. G. (2020). Regulation of Glycolysis and the Warburg Effect in Wound Healing. *JCI Insight* 5 (17), 138949. doi:10.1172/jci.insight.138949

Vykoukal, J., Fahrmann, J. F., Gregg, J. R., Tang, Z., Basourakos, S., Irajizad, E., et al. (2020). Caveolin-1-mediated Sphingolipid Oncometabolism Underlies a Metabolic Vulnerability of Prostate Cancer. *Nat. Commun.* 11 (1), 4279. doi:10.1038/s41467-020-17645-z

Wang, L. Z., Ding, J. P., Yang, M. Y., and Chen, B. (2014). Forty-five Cases of Chest Keloids Treated with Subcutaneous Super-tension-reduction Suture Combined with Postoperative Electron-Beam Irradiation. *Dermatol Surg.* 40 (12), 1378–1384. doi:10.1097/DSS.0000000000000163

Wang, R., Bai, Z., Wen, X., Du, H., Zhou, L., Tang, Z., et al. (2019). MiR-152-3p Regulates Cell Proliferation, Invasion and Extracellular Matrix Expression through by Targeting FOXF1 in Keloid Fibroblasts. *Life Sci.* 234, 116779. doi:10.1016/j.lfs.2019.116779

Wang, R., Xin, M., Li, Y., Zhang, P., and Zhang, M. (2016). The Functions of Histone Modification Enzymes in Cancer. *Curr. Protein Pept. Sci.* 17 (5), 438–445. doi:10.2174/1389203717666160122120521

Wang, X., Gao, Z., Wu, X., Zhang, W., Zhou, G., and Liu, W. (2016). Inhibitory Effect of TGF-β Peptide Antagonist on the Fibrotic Phenotype of Human Hypertrophic Scar Fibroblasts. *Pharm. Biol.* 54 (7), 1189–1197. doi:10.3109/13880209.2015.1059862

Wang, X., Liu, Y., Chen, X., Zhang, M., and Xiao, Z. (2013). Impact of MiR-21 on the Expression of FasL in the Presence of TGF-β1. *Aesthet. Surg. J.* 33 (8), 1186–1198. doi:10.1177/1090820X13511969

Wang, Y., Ma, J., Zhang, Z., and Shen, H. (2020). Combined Surgical Excision and Electron External Beam Radiation Improves the Treatment of Keloids: A Descriptive Study. *Dermatol Ther.* 33 (4), e13494. doi:10.1111/dth.13494

Wang, Z., Fong, K. D., Phan, T. T., Lim, I. J., Longaker, M. T., and Yang, G. P. (2006). Increased Transcriptional Response to Mechanical Strain in Keloid Fibroblasts Due to Increased Focal Adhesion Complex Formation. *J. Cell. Physiol.* 206 (2), 510–517. doi:10.1002/jcp.20486

Wong, V. W., Akaishi, S., Longaker, M. T., and Gurtner, G. C. (2011). Pushing Back: Wound Mechanotransduction in Repair and Regeneration. *J. Investig. Dermatol* 131 (11), 2186–2196. doi:10.1038/jid.2011.212

Wu, J., Del Duca, E., Espino, M., Gontzes, A., Cueto, I., Zhang, N., et al. (2020). RNA Sequencing Keloid Transcriptome Associates Keloids with Th2, Th1, Th17/Th22, and JAK3-Skewing. *Front. Immunol.* 11, 597741. doi:10.3389/fimmu.2020.597741

Xu, Z., Guo, B., Chang, P., Hui, Q., Li, W., and Tao, K. (2019). The Differential Expression of miRNAs and a Preliminary Study on the Mechanism of miR-194-3p in Keloids. *Biomed. Res. Int.* 2019, 8214923. doi:10.1155/2019/8214923

Xue, M., and Jackson, C. J. (2015). Extracellular Matrix Reorganization during Wound Healing and its Impact on Abnormal Scarring. *Adv. Wound Care (New Rochelle)* 4 (3), 119–136. doi:10.1089/wound.2013.0485

Xue, M., Zhao, R., March, L., and Jackson, C. (2022). Dermal Fibroblast Heterogeneity and its Contribution to the Skin Repair and Regeneration. *Adv. Wound Care (New Rochelle)* 11 (2), 87–107. doi:10.1089/wound.2020.1287

Yan, L., Cao, R., Wang, L., Liu, Y., Pan, B., Yin, Y., et al. (2015). Epithelial-mesenchymal Transition in Keloid Tissues and TGF-β1-Induced Hair Follicle Outer Root Sheath Keratinocytes. *Wound Repair Regen.* 23 (4), 601–610. doi:10.1111/wrr.12320

Yan, Z., Zhang, W., Xu, P., Zheng, W., Lin, X., Zhou, J., et al. (2021). Phosphoproteome and Biological Evidence Revealed Abnormal Calcium Homeostasis in Keloid Fibroblasts and Induction of Aberrant Platelet Aggregation. *J. Proteome Res.* 20 (5), 2521–2532. doi:10.1021/acs.jproteome.0c00984

Yang, S., Luo, Y. J., and Luo, C. (2021). Network Meta-Analysis of Different Clinical Commonly Used Drugs for the Treatment of Hypertrophic Scar and Keloid. *Front. Med.* 8, 691628. doi:10.3389/fmed.2021.691628

Yazdani Abyaneh, M. A., Griffith, R., Falto-Aizpurua, L., and Nouri, K. (2014). Famous Lines in History: Langer Lines. *JAMA Dermatol* 150 (10), 1087. doi:10.1001/jamadermatol.2014.659

Young, W. G., Worsham, M. J., Joseph, C. L., Divine, G. W., and Jones, L. R. (2014). Incidence of Keloid and Risk Factors Following Head and Neck Surgery. *JAMA. Facial. Plast. Surg.* 16 (5), 379–380. doi:10.1001/jamafacial.2014.113

Zanconato, F., Cordenonsi, M., and Piccolo, S. (2019). YAP and TAZ: a Signalling Hub of the Tumour Microenvironment. *Nat. Rev. Cancer* 19 (8), 454–464. doi:10.1038/s41568-019-0168-y

Zhang, G. Y., Yu, Q., Cheng, T., Liao, T., Nie, C. L., Wang, A. Y., et al. (2011). Role of Caveolin-1 in the Pathogenesis of Tissue Fibrosis by Keloid-Derived Fibroblasts *In Vitro*. *Br. J. Dermatol* 164 (3), 623–627. doi:10.1111/j.1365-2133.2010.10111.x

Zhang, T., Wang, X. F., Wang, Z. C., Lou, D., Fang, Q. Q., Hu, Y. Y., et al. (2020). Current Potential Therapeutic Strategies Targeting the TGF-β/Smad Signaling Pathway to Attenuate Keloid and Hypertrophic Scar Formation. *Biomed. Pharmacother.* 129, 110287. doi:10.1016/j.biopha.2020.110287

Zhang, Z., Nie, F., Kang, C., Chen, B., Qin, Z., Ma, J., et al. (2014). Increased Periostin Expression Affects the Proliferation, Collagen Synthesis, Migration and Invasion of Keloid Fibroblasts under Hypoxic Conditions. *Int. J. Mol. Med.* 34 (1), 253–261. doi:10.3892/ijmm.2014.1760

Zhao, B., Guan, H., Liu, J. Q., Zheng, Z., Zhou, Q., Zhang, J., et al. (2017). Hypoxia Drives the Transition of Human Dermal Fibroblasts to a Myofibroblast-like Phenotype via the TGF-β1/Smad3 Pathway. *Int. J. Mol. Med.* 39 (1), 153–159. doi:10.3892/ijmm.2016.2816

Zhao, H., Lu, F., Cui, S., Zhang, X., Wang, W., Si, E., et al. (2017). TMEM88 Inhibits Extracellular Matrix Expression in Keloid Fibroblasts. *Biomed. Pharmacother.* 95, 1436–1440. doi:10.1016/j.biopha.2017.09.047

Zhou, B., Gao, Z., and Liu, Z. (2021). Important Role of Mechanical Microenvironment on Macrophage Dysfunction during Keloid Pathogenesis. *Exp. Dermatol.* doi:10.1111/exd.14473

Conflict of Interest: The authors declare that the research was conducted in the absence of any commercial or financial relationships that could be construed as a potential conflict of interest.

Publisher's Note: All claims expressed in this article are solely those of the authors and do not necessarily represent those of their affiliated organizations, or those of the publisher, the editors and the reviewers. Any product that may be evaluated in this article, or claim that may be made by its manufacturer, is not guaranteed or endorsed by the publisher.

frontiers | Frontiers in Pharmacology

REVIEW
published: 23 May 2022
doi: 10.3389/fphar.2022.907835

Mammalian Sirtuins and Their Relevance in Vascular Calcification

Xinyue Pan[1†], Caixia Pi[1†], Xianchun Ruan[1,2], Hanhua Zheng[1,2], Demao Zhang[1,2] and Xiaoheng Liu[2*]*

[1]State Key Laboratory of Oral Diseases, West China Hospital of Stomatology, Sichuan University, Chengdu, China, [2]West China School of Basic Medical Sciences and Forensic Medicine, Sichuan University, Chengdu, China

Cardiovascular diseases are a group of diseases with high morbidity and mortality that affect millions of people each year. Vascular calcification (VC) is an active process that involves the mineral deposition of calcium-phosphate complexes. VC is closely related to cardiovascular diseases, such as hypertension, heart failure, and calcific aortic stenosis, and is a type of ectopic calcification that occurs in the vessel walls. The sirtuins (silent mating-type information regulation 2; SIRTs), are a family of histone deacetylases whose function relies on nicotinamide adenine dinucleotide (NAD+). They have non-negligible functions in the regulation of energy metabolism, senescence, apoptosis, and other biological processes. Sirtuins have important effects on bone homeostasis and VC processes that share many similarities with bone formation. Sirtuins have been confirmed to deacetylate a variety of target proteins related to the occurrence and development of VC, thereby affecting the process of VC and providing new possibilities for the prevention and treatment of cardiovascular diseases. To facilitate the understanding of vascular calcification and accelerate the development of cardiovascular drugs, we reviewed and summarized recent research progress on the relationship between different types of sirtuins and VC.

Keywords: cardiovascular disease, vascular calcification, sirtuins, calcium phosphate, histone deacetylase

OPEN ACCESS

Edited by:
Kang Xu,
Hubei University of Chinese Medicine, China

Reviewed by:
Dong Wang,
Qingdao University, China
Arseniy Lobov,
Almazov National Medical Research Centre, Russia

***Correspondence:**
Demao Zhang
demao.zhang666@foxmail.com
Xiaoheng Liu
liuxiaohg@scu.edu.cn

[†]These authors have contributed equally to this work

Specialty section:
This article was submitted to Experimental Pharmacology and Drug Discovery, a section of the journal Frontiers in Pharmacology

Received: *30 March 2022*
Accepted: *09 May 2022*
Published: *23 May 2022*

Citation:
Pan X, Pi C, Ruan X, Zheng H, Zhang D and Liu X (2022) Mammalian Sirtuins and Their Relevance in Vascular Calcification. Front. Pharmacol. 13:907835. doi: 10.3389/fphar.2022.907835

INTRODUCTION

As a type of ectopic calcification, vascular calcification (VC) is the process of mineral deposition, in the form of a calcium-phosphate complexes, in vessel walls. VC is closely related to the occurrence of cardiovascular diseases, such as hypertension, heart failure, and calcific aortic stenosis, which is one of the major causes of human death (Johnson et al., 2006; Cano-Megías et al., 2019). VC is a complex event that is mediated by different types of cells and active processes that are similar to those involves in ossification and bone formation. It is usually not determined by a single factor, but rather, is influenced by multiple factors, including genes, the environment, and blood vessels (Villa-Bellosta et al., 2011). According to the location of mineral deposition, VC can be divided into intimal and medial calcifications. Intimal VC is associated with lipid deposition, inflammation, and necrosis. It often occurs in large arteries, is linked to obstructive arterial disease, and is usually associated with atherosclerosis. The most characteristic feature of medial calcification is the transdifferentiation of vascular smooth muscle cells (VSMCs) into osteoblasts, from a synthetic phenotype to a contractile phenotype. This usually results in reduced blood flow and often occurs in patients with chronic kidney disease (CKD), diabetes, osteoporosis, and hypertension (Wu et al., 2013; Lee et al., 2020a; Singh et al., 2021). VC is a threat to human health, but effective drugs that inhibit or reverse the processes of VC are currently lacking.

Mammalian sirtuins contain seven members: SIRT1-7. They are evolutionarily conserved from bacteria to eukaryotes, with catalytic sites formed by the hydrophobic channel between NAD + binding Rossmann folding domain and Zn2 + binding domain, and most have been confirmed to be protein deacetylases whose function relies on nicotinamide adenine dinucleotide (NAD) (Michan and Sinclair, 2007). According to sequence similarity, mammalian sirtuins are divided into at least four classes: classes I–IV. Class I contains SIRT1-3, SIRT4 belongs to class II, SIRT5 is in class III, and SIRT6 and SIRT7 belong to class IV (Frye, 2000). The sirtuin distribution within cells can differ depending on the protein. The three nuclear proteins are SIRT1, SIRT6, and SIRT7. SIRT3, SIRT4, and SIRT5 are localized in the mitochondria, an organelle in which many important metabolic processes occur. SIRT2 is the only sirtuin that is mainly distributed in the cytoplasm (Michishita et al., 2005). The most studied enzymatic activity of the sirtuin family is deacetylation, represented by SIRT1. However, some of the sirtuin family members have weak deacetylase activity and other enzymatic activities (Michan and Sinclair, 2007). For example, SIRT5 was found to remove succinyl and malonyl from protein lysine residues (Du et al., 2011). Sirtuins have important biological functions and participate in many biological processes, including cell proliferation, apoptosis, DNA repair, and cell metabolism. They are also highly associated with many pathologies, such as neurodegenerative diseases, cardiovascular diseases, and cancer (Carafa et al., 2016).

Among the sirtuin family members, the most abundant one, SIRT1, is widely believed to be closely related to and play a significant protective role in VC (Lu et al., 2020). Moreover, SIRT3 and SIRT6 have been shown to play significant roles in protecting the vasculature against atherosclerosis (Sosnowska et al., 2017). Several signaling pathways connecting sirtuins and VC have been identified (D'Onofrio et al., 2018). However, research on other sirtuin members, especially SIRT5, is lacking. In recent years, the link between sirtuins and VC has been a research focus, and new discoveries have been reported. In this review, we summarize the new research results of SIRT1-7 connected with VC in the past 5 years, with the aim of providing researchers help and inspiration to find effective VC drugs.

VASCULAR CALCIFICATION

Classification of Vascular Calcification

According to the location of mineral deposition, VC can be mainly divided into intimal and medial calcifications. Different types of VC have different characteristics.

In intimal calcification, which is mainly induced by lipid deposition, inflammation, and necrosis, minerals are primarily deposited in the intima of the blood vessels. This often occurs in large arteries, is linked to obstructive arterial disease, and is usually associated with atherosclerosis (Doherty et al., 2003). Intimal calcification occurs over a wide range of patient ages, and with age, the formation of atherosclerotic plaques increases (Abedin et al., 2004). In atherosclerotic lesions, calcification initially appears in the form of microcalcifications (<5 μm) caused by apoptotic or necrotic cells. If this is not controlled, the calcified plaques can gradually progress to large plaques or even rupture, leading to harmful consequences (Roijers et al., 2011). In medial calcification, mineral deposits occur in the medial layer of the vessel wall whose main components are VSMCs and the extracellular matrix full of elastin. Unlike intimal calcification, medial calcification is often associated with CKD, diabetes, hypertension, osteoporosis, and aging (Lanzer et al., 2021). The most important feature of medial calcification is that it is very similar to bone formation processes, because its main cells, VSMCs, lose their original properties and transdifferentiate into osteoblast-like cells through a process regulated by *BMP2*, *MSX2*, *ALP*, and other genes (Iyemere et al., 2006; Shanahan et al., 2011; Leopold, 2015) (**Figure 1A**).

Cell Types Involved in Vascular Calcification

As a complex regulated active process, the occurrence and development of VC involves the participation of various cell types, including vascular wall resident cells, stem cells, and progenitor cells from the circulating blood (Cho et al., 2018).

Endothelial cells (ECs) have phenotypic plasticity and can transform into mesenchymal cells through a process that is commonly referred to as the endothelial-mesenchymal transition (EndMT) (DeRuiter et al., 1997; Arciniegas et al., 2007). EndMT enables ECs to differentiate into stem cells that have the potential to form chondrocytes and osteocytes and is closely related to microvascular mineralization (Medici et al., 2010). Further studies have shown that EndMT is the main mechanism involved in the occurrence and development of atherosclerosis and is also a key factor in atherosclerosis, which has an important relationship with mineral deposition and plaque stability (Boström, 2016; Guihard et al., 2016; Wesseling et al., 2018).

VSMCs are mainly located in the middle layer of blood vessels, secrete extracellular matrix, and regulate blood pressure by regularly contracting and relaxing (Dart and Kingwell, 2001). Similar to ECs, VSMCs can also undergo a phenotypic transition, from a physical contractile phenotype to a pathological synthetic phenotype, when stimulated by some factors such as inflammation and oxidative stress (Frismantiene et al., 2018). The most typical characteristic of the osteo/chondrocyte phenotypic switch is the loss of contractile markers like SM α-actin (SMαA), SM-22α, SM myosin heavy chains SM-1 and SM-2 and the upregulation of mineralization-related markers like Runx2, SP7, osteopontin, osteocalcin, and alkaline phosphatase (ALP) and Sox9 (Schurgers et al., 2018). Phenotypic transformation of VSMCs plays a key role in promoting the progression of VC (Durham et al., 2018; Jaminon et al., 2019). Furthermore, prior studies have suggested that abnormal VSMC proliferation and migration plays an important promoting role in atherosclerosis progression (Doran et al., 2008; Wang et al., 2014) (**Figure 1B**).

Various circulating progenitor cells have been found to be associated with VC, including endothelial progenitor cells (EPCs), mesenchymal stem/progenitor cells, and myeloid cells. In some diseases, such as coronary artery disease and aortic valve stenosis, investigators have found that the proportion of EPCs with an osteogenic phenotype increased (Fadini et al., 2012;

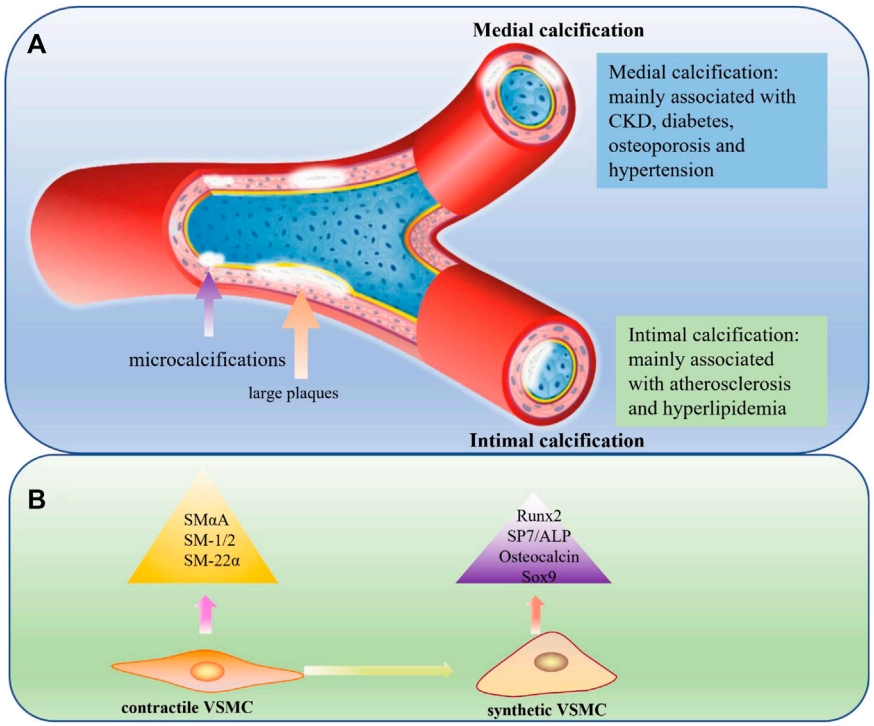

FIGURE 1 | (A) Medial calcification and Intimal calcification. In medial calcification, minerals are mainly deposited in the medial layer of blood vessels and usually associated with CKD, diabetes, osteoporosis and hypertension. In intimal calcification, minerals are primarily deposited in the intimal of the blood vessels and develop from microcalcifications to large plaques, usually associated with atherosclerosis and hyperlipidemia. CKD: chronic kidney disease. **(B)** Comparison of contractile VSMC and synthetic VSMC. VSMCs paly an important role in medial calcification and can undergo a phenotypic transition from a physical contractile phenotype to a pathological synthetic phenotype, lossing contractile markers like SMα-A, SMα-22, SM-1 and SM-2 and expressing mineralization-related markers like Runx2, SP7, ALP, osteopontin and Sox9.

Zhang et al., 2015; Yang et al., 2017a; Al-Hijji et al., 2019). Notably, Liao et al. discovered that bone marrow mesenchymal stem cell transplantation after balloon angioplasty in rats with hyperlipidemia resulted in vascular remodeling and calcification (Liao et al., 2012).

Factors That Cause Vascular Calcification

VC is a highly complex pathological process, and many factors have been found to cause or promote VC. Such discoveries lay the foundation for subsequent drug development. Many factors cause VC, including a variety of cell types, molecules, genes, and environmental factor. For example, extracellular vesicles can be found in calcified aortic media and in atherosclerotic intimal plaques, which suggests a link between the vesicles and VC. Furthermore, calcified extracellular vesicles formed by VSMCs have been found to aggregate with each other to form microcalcification (Hutcheson et al., 2016; Bakhshian Nik et al., 2017). Matrix vesicles belong to extracellular vesicles, and they have been found to play an important role in VC, especially in the early stage (Li et al., 2022a). Duan et al. found that endoplasmic reticulum stress can promote apoptosis, which further accelerated the process of VC and is accompanied by the upregulation of apoptosis markers, such as CHOP and CASP12 (Duan et al., 2009).

Inflammation also plays a role in VC. mRNAs of inflammatory factors, such as Nalp3, ASC, and caspase-1, have been found to be upregulated in calcified VSMCs, while the inhibition of Nalp3 expression by Nalp3KD has been found to block VSMC calcification (Wen et al., 2013). Furthermore, interleukin-6 (IL-6)/soluble interleukin-6 receptor (sIL-6R) complexes, which play a role in the transformation of VSMCs to an osteogenic phenotype, and TNF-α and IL-1β, which participate in the induction of EndMT in human primary aortic ECs, are important inflammatory cytokines that accelerate VC (Kurozumi et al., 2019; Sánchez-Duffhues et al., 2019). In addition, autophagy, apoptosis, osteoporosis, apolipoprotein, and many other factors have been reported to be related to the occurrence and progression of VC (Proudfoot et al., 2000; Sun et al., 2002; Warburton et al., 2007; Dai et al., 2013; Villa-Bellosta and Egido, 2017).

THE ROLES OF SIRTUINS IN VASCULAR CALCIFICATION

The regulatory approach of the sirtuin family is a pattern of epigenetic regulation. Epigenetic regulation is an important regulation mode of eukaryotes. It is the structural adjustment at the chromatin level

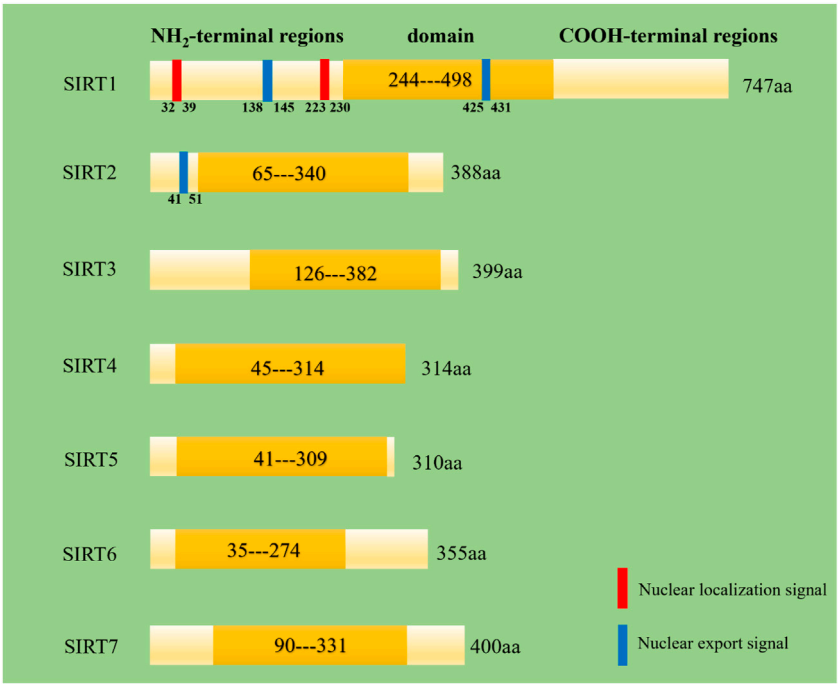

FIGURE 2 | Secondry structures of human SIRT1-7. Domain means a specific combination of secondary structures organized into characteristic three-dimensional structure or fold. These data come from the website http://www.uniprot.org/.

through DNA methylation, histone modification (including methylation, acetylation, phosphorylation, etc.), and small RNA mediation without changing the structure of the DNA sequence, which alters the expression of genes and alters the phenotype of the organism (Goldberg et al., 2007). In the occurrence and development of VC, epigenetic regulation, including histone acetylation, plays an important role (Esteller, 2011). Histone acetylation mainly refers to lysine acetylation catalyzed by lysine acetyltransferase (Weinert et al., 2014). Lysine acetyltransferase includes two types, type A which are located in nucleus and type B which are located in cytoplasm (Li et al., 2020). Lysine acetylation modulates the development of diseases including VC by altering the protein structure or binding affinity with other proteins to alter the function of the corresponding protein (McLendon et al., 2014). For example, the activation of p300, a widely studied lysine acetylase, has been found to upregulate the expression of osteoblast-related genes such as osteocalcin and ALP by increasing the acetylation of histones (H3 and H4) in aortic valvular calcification models (Gu et al., 2019). The opposite process of histone acetylation, histone deacetylation, is catalyzed by lysine deacetylases, which include histone deacetylases (HDACs) and sirtuins (class III HDACs). Although known as histone deacetylases, the sirtuins family can also catalyze non-histone proteins deacetylation, for example, p53 transcription factor, nuclear factor-κB (NFκB), peroxisome proliferator activated receptor (PPAR)and histone acetyltransferase (HAT) p300 (Lu et al., 2020).

Despite belonging to the same protein family, SIRT1-7 have different amino acid compositions and different structural domains, but all of them have a same highly conserved region (**Figure 2**) (Jiao and Gong, 2020). What's more, they have different characteristics in molecular mass, cellular location, enzymatic activity, tissue specificity and biological function (**Table 1**).

Sirtuin 1

SIRT1 is the first discovered and most well-understood sirtuin. The normal expression of SIRT1 is very important for maintaining physiological function, and many diseases are associated with dysregulated SIRT1 expression, such as cancer, neuroinflammation-related diseases, depression, and cardiovascular diseases (Karbasforooshan and Karimi, 2017; Lu et al., 2018; Alves-Fernandes and Jasiulionis, 2019; Jiao and Gong, 2020). SIRT1 contains 747 residues and consists of four regions: N-terminal domain, allosteric site, C-terminal domain, and catalytic core, which is highly conserved (Huhtiniemi et al., 2006; Autiero et al., 2008). The subcellular localization of SIRT1 can vary in different tissues and species. It is mainly expressed in the nucleus, but also can be found in the cytoplasm (Michishita et al., 2005). As a nuclear sirtuin, multiple studies have demonstrated that SIRT1 can deacetylate histones. Alejandro Vaquero et al. found that in humans, SIRT1 could deacetylate histone H1 at lysine 26 and promote facultative heterochromatin formation. They also proved that SIRT1 could catalyze the deacetylation of H3 at lysine 9 and H4 at lysine 16 (Vaquero et al., 2004). Chandrima Das et al. found that human SIRT1 and SIRT2 could deacetylate histone H3 at lysine 56 (Das et al., 2009) (**Figure 3A**).

Studies also found important links between SIRT1, histone deacetylation and VC. Francesca et al. conducted a series of experiments to determine whether SIRT1 can protect against

TABLE 1 | Characteristics of sirtuins including mass, cellular localization, enzymatic activity, tissues and biological functions.

Sirtuins	Mass (Da)[a]	Cellular localization	Enzymatic activity	Tissues[b]	Biological function	References
SIRT1	81,681	Nucleus, cytoplasm	Deacetylase	Low tissue specificity	Regulate oxidative stress and inflammation, aging (life span and health span), calorie restriction/energetics, mitochondrial biogenesis, cellular senescence, endothelial functions, apoptosis/autophagy	(Michishita et al., 2005; Hwang et al., 2013; Singh and Ubaid, 2020; Wang and Chen, 2020)
SIRT2	43,182	Cytoplasm, nucleus	Deacetylase	Enhanced in skeletal muscle, tongue	Neurological function, mitosis regulation, genome integrity, cell differentiation, cell haemostasis, oxidative stress, autophagy	(Michishita et al., 2005; Sayd et al., 2014; Wang et al., 2019b)
SIRT3	43,573	Mitochondria	Deacetylase, Depropionylase	Low tissue specificity	Almost all aspects of mitochondrial metabolism and haemostasis, like urea cycle, TCA cycle, ROS production, apoptosis	(Michishita et al., 2005; Wang et al., 2020; Zhang et al., 2020)
SIRT4	35,188	Mitochondria	Deacetylase, ADP-ribosyltransferase, Lipamidase	Low tissue specificity	Lipid homastasis, Insulin secretion	(Michishita et al., 2005; Haigis et al., 2006; Laurent et al., 2013a; Laurent et al., 2013b; Min et al., 2018)
SIRT5	33,881	Mitochondria	Deacetylase, Desuccinylase, Desmalonylase	Low tissue specificity	Glycolysis, the TCA cycle, fatty acid oxidation, electron transport chain, ketone body formation, nitrogenous waste management	(Michishita et al., 2005; Du et al., 2011; Kumar and Lombard, 2018)
SIRT6	39,119	Nucleus	Deacetylase, Demyristoylase	Low tissue specificity	Heterochromatin stabilization and silencing; stem cell biology; cancer initiation and progression; metabolic homeostasis	(Michishita et al., 2005; Jiang et al., 2013; Tasselli et al., 2017)
SIRT7	44,898	Nucleus	Deacetylase, Desuccinylation	Low tissue specificity	Gene regulation; genome stability; ageing; tumorigenesis	(Michishita et al., 2005; Barber et al., 2012; Li et al., 2016; Blank and Grummt, 2017; Tang et al., 2021)

[a]*These data come from the website https://www.uniprot.org/.*
[b]*This information come from the website https://www.uniprot.org/.*

DNA damage-induced cell senescence and phenotype transformation of VSMCs in diabetes, they found that loss of SIRT1 in diabetes can accelerate DNA damage, which further exacerbated VC, while SIRT1 activation reduced DNA damage partially by deacetylating around H3K27ac mark within the transcription start site, which further promoted the formation of the active MRN repair complex (MRE11 RAD50, NBS1) (Bartoli-Leonard et al., 2021). A study focusing on the relationship between S-adenosine homocysteine hydrolase (SAAH) and atherosclerotic calcification found that adenosine supplementation activated AMP-activated protein kinase, which further induced SIRT1 expression followed by increase of histone H3 deacetylation and thereby inhibited H19 expression in SAHH-deficient VSMCs, which eventually inhibited osteoblastic differentiation of VSMCs (Dai et al., 2022).

Many other studies also confirmed the protective effects of SIRT1 against VC. Notably, lifelong SIRT1 overexpression in mice has been found to relieve large artery stiffening with advancing age (Machin et al., 2020). Certain molecules can affect VC through SIRT1 signaling. The underlying mechanisms can involve against VC by upregulating SIRT1 expression or accelerate the development of VC by downregulating SIRT1 expression. When investigating whether miR-34a could regulate VC, Ileana et al. reported that miR-34a promoted VSMC calcification by downregulating SIRT1 (Badi et al., 2018). Furthermore, HOTAIR overexpression was found to relieve VC caused by phosphate (Pi) overload by regulating the miR-126/Klotho/SIRT1 signaling pathway. Through this pathway, the increased expression of SIRT1 suppressed Wnt/β-catenin signaling and further inhibited VC (Chen et al., 2021a). And Wnt/β-catenin is well verified to play an important role in osteogenesis calcification and alveolar bone remodeling (Wang et al., 2022). Similarly, SIRT1 signaling has been found to be activate during the resveratrol-induced improvement of aortic calcification in ovariectomized rats (Hammad et al., 2021).

Based on these studies, we believe that SIRT1 is an important cardiovascular protective factor with implications in preventing VC.

Sirtuin 2

SIRT2 also has important biological functions and has been found to be associated with many diseases, including cancer, neurological disorders, and cardiovascular diseases (Chen et al., 2020a; Chen et al., 2021b; Taneja et al., 2021). SIRT2 is unique because it is the only sirtuin to be mainly distributed in the cytoplasm and can also be found in the nucleus (Vaquero et al., 2006). SIRT2 consists of a 304-amino acid catalytic core and a 19 residue N-terminal helical extension. The core is mainly composed of two domains: the larger one is a variant of the Rossmann fold23, which exists in many different NAD (H)/NADP (H)-binding enzymes, and the smaller one contains a zinc atom (Finnin et al., 2001). Although mainly located in the cytoplasm, under special circumstances SIRT2 can translocate into the nucleus and deacetylase histones. Studies found that

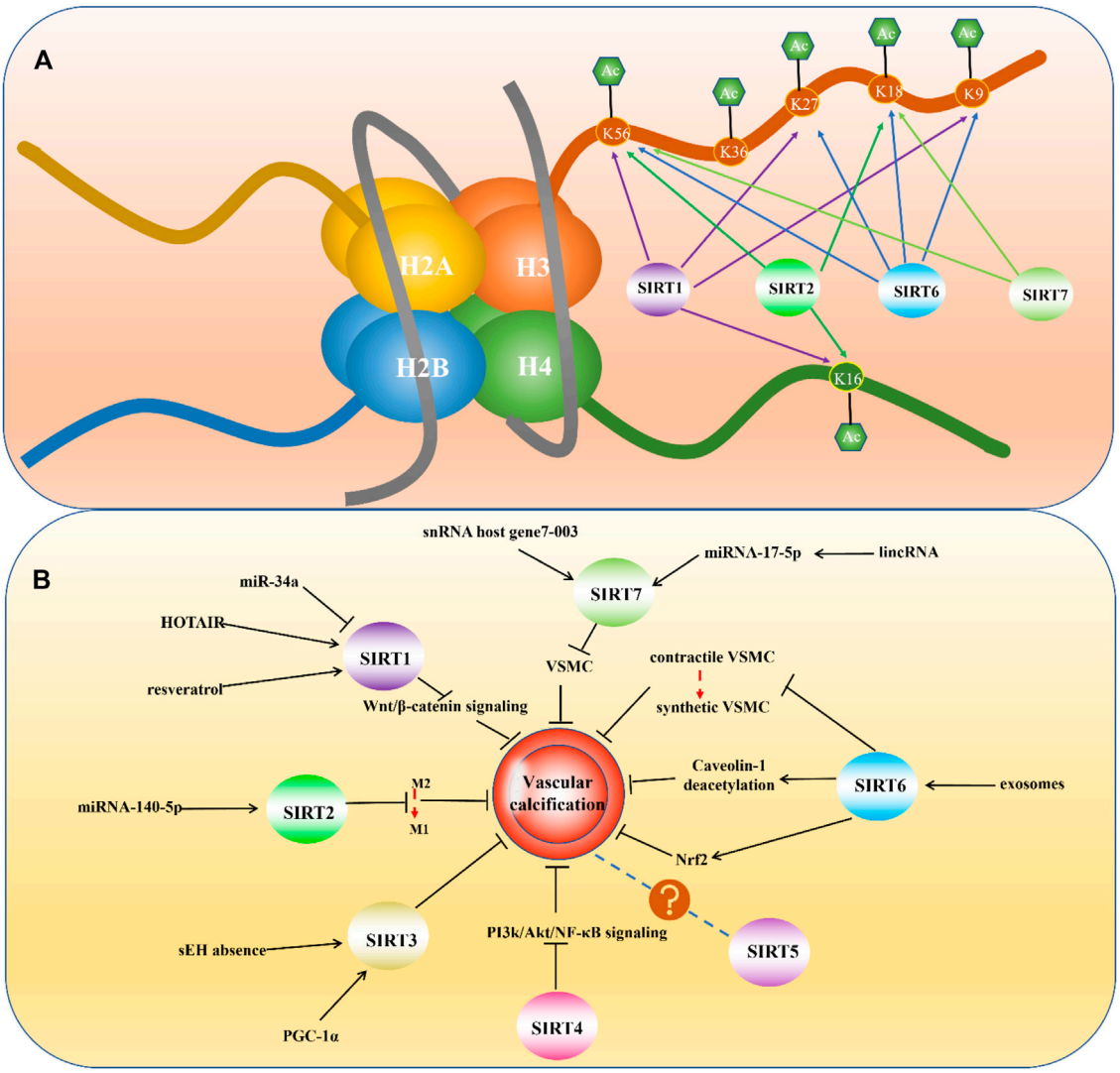

FIGURE 3 | (A) Histone deacetylation sites of mammalian Sirtuins. **(B)** Mammalian Sirtuins and their Relevance in Vascular Calcification.

during infection, SIRT2 could mediate the deacetylation of histone H3K18 (Eskandarian et al., 2013). During mitosis, SIRT2 can also enter the nucleus and deacetylate H4K16 (Vaquero et al., 2006) (**Figure 3A**).

Compared with SIRT1, the influence of SIRT2 on VC has not been thoroughly investigated; however, in recent years, several studies on SIRT2 and atherosclerosis have been reported. Liu et al. studied global gene expression changes caused by SIRT2 knockout in primary human umbilical vein ECs (HUVECs) under oxidative stress. The investigators found that SIRT2 knockout altered the expression of 340 genes that participate in many physiological processes and their functions (Liu et al., 2013). Furthermore, Zhang et al. discovered that SIRT2 overexpression prevented high glucose-induced vascular ECs injury by regulating the p53 and NF-κB signaling pathways (Zhang et al., 2018a). These findings indicate that Sirt2 might be associated with atherosclerosis, considering that ECs are closely related to atherosclerosis. Zhang et al. treated female mice whose LDL receptors were knocked out (LDLr−/−) with different conditions and assessed atherosclerotic plaques in the aortic sinus. This investigation revealed that SIRT2 slowed atherosclerotic plaque progression and stabilized the disease condition in LDLr−/− mice. This effect was achieved by inhibiting the differentiation of macrophages into the M1 phenotype (Zhang et al., 2018b). SIRT2 also functions in the signaling pathway through which other molecules affect atherosclerosis. Notably, microRNA-140-5p, an endogenous small non-coding RNAs, was found to relieve hypertension and oxidative stress in atherosclerosis by functioning on SIRT2 and Nrf2 (Liu et al., 2019).

SIRT2 has been consistently shown to protect against VC, especially atherosclerosis. There remains much to learn regarding SIRT2 and its utility as a target for the development of drugs to prevent and treat VC.

Sirtuin 3

SIRT3 has many important biological functions in endothelial metabolism, angiogenesis, and cardiovascular disease (He et al., 2019). The complete SIRT3 protein is composed of 399 amino acids. There is a mitochondrial targeting sequence composed of 101 amino acids at its N-terminus that is cut off as the protein undergoes activating transformation. SIRT3 contains two domains: the larger one has a Roschmann fold and NAD + binding site, and the smaller one contains a helical complex and a zinc binding group (Jin et al., 2009). Known as mitochondrial sirtuin, human full-length SIRT3 is localized only in the mitochondria, while the short isoform is present in the mitochondria, nucleus, and cytoplasm (Onyango et al., 2002; Scher et al., 2007; Iwahara et al., 2012). Based on existing studies, the effects of SIRT3 on the vasculature are primarily protective (Liu et al., 2021a).

SIRT3 influences both medial calcification, which is closely related to VSMCs, and intimal calcification, which is primarily linked to ECs. Jing et al. used a rat model to explore the correlation between SIRT3 gene expression and EC apoptosis in atherosclerosis. The investigators found that SIRT3 expression was downregulated in the aorta of rats with atherosclerosis and closely related to apoptosis. This finding suggests that SIRT3 has a protective effect on atherosclerosis and may be found to be an important target for preventing atherosclerosis in the future (Jing et al., 2019).

Several recent studies have confirmed the protective role of SIRT3 in VC in patients with CKD. He et al. investigated the role of soluble epoxide hydrolase (sEH) as a potential regulator of VC in CKD. The investigators found that knocking out of sEH slowed the progression of VC linked to CKD through promoting SIRT3 expression (He et al., 2021). Furthermore, Feng et al. discovered the positive function of PGC-1α in CKD-related VC, which involved the restoration of SIRT3 expression and reduction in mitochondrial oxidative stress (Feng et al., 2019).

As SIRT3 research continues, its role in VC will be better understood. Furthermore, SIRT3 may also play an important role in VC prevention and VC treatment.

Sirtuin 4

SIRT4 is important for the regulation of energy metabolism and mitochondrial function. The abnormal expression of SIRT4 is related to diabetes, liver disease, cancer, heart disease, and many other diseases (Betsinger and Cristea, 2019). Similar to SIRT3, SIRT4 is mainly distributed in mitochondria (Michishita et al., 2005). An increasing number of studies on SIRT4 have been conducted in recent years. However, reports related to VC remain relatively lacking, and the role of SIRT4 in VC remains unclear. It is well known that the most relevant enzymatic activity of sirtuins and VC involves deacetylase activity, however, the deacetylase activity of SIRT4 is weak (Li et al., 2018). This observation does not necessarily imply that SIRT4 has no effect on VC.

Several studies have identified a protective role of SIRT4 in atherosclerosis. For example, Tao et al. explored the function of SIRT4 in atherosclerosis progression. They found that in HUVECs, SIRT4 expression was inhibited by oxLDL treatment, while SIRT4 overexpression enhanced oxLDL-induced HUVEC proliferation induced by oxLDL and curbed cell apoptosis. Further analysis showed that SIRT4 overexpression improved the survival rate of HUVEC cells and reduced the expression of inflammatory factors in HUVEC cells that were induced by oxLDL, by inhibiting PI3K/Akt/NF- κ B signaling (Tao et al., 2019). This study changed our previous view and inspired further investigators to continue to explore SIRT4. It cannot deny SIRT4 as a potential target for developing valuable medicines to prevent or treat atherosclerosis, but the feasibility of SIRT4 as a therapeutic target still needs more research to explore.

Sirtuin 5

SIRT5 has many significant regulatory roles in normal physiological and pathological processes, particularly in neoplasia (Kumar and Lombard, 2018). The human *SIRT5* gene encodes two major SIRT5 isoforms, SIRT5iso1, which contains 310 amino acids, and SIRT5iso2, which is composed of 299 amino acids. The main difference between them is in their C-termini (Mahlknecht et al., 2006; Matsushita et al., 2011). SIRT5 is mainly localized in the mitochondria (Michishita et al., 2005). Similar to SIRT4, its deacetylation activity is weak even undetectable. However, it has enzymatic activities other than acetylation, such as lysine demalonylation and desuccinylation activities (Du et al., 2011). However, focusing on the studies about SIRT5 and VC, valuable references can't be found. Even about the connection of SIRT5 to ECs and VSMCs, none related studies have been found. Considering that SIRT5 has almost no deacetylation activity, which is important in vascular biology, it is reasonable to speculate that SIRT5 has little connection with VC. However, with continuous efforts and subsequent in-depth research, it is possible that there will be new discoveries in the future.

Sirtuin 6

SIRT6 has many functions in regulating lifespan, and abnormal SIRT6 expression has been found to be involved in the pathogenesis of many health-threatening diseases, such as steatohepatitis, diabetes, tumors, neurodegenerative diseases, and cardiovascular diseases (Liu et al., 2021b). Consisting of 355 amino acids, SIRT6 is composed of a putative catalytic sirtuin core and two flanking extensions: a N-terminal extension and a C-terminal extension (Pan et al., 2011). SIRT6 is also situated in the nucleus but is different from SIRT1 in its subnuclear localization (Michishita et al., 2005). It is widely accepted that SIRT6 has deacetylase activity and plays a protective role in VC. Located in nucleus, SIRT6 has been found to deacetylate histone H3 at lysine 9 and regulate telomeric chromatin (Michishita et al., 2008). What's more, studies also demonstrated SIRT6 could act on lysine 56 on the global core of histone H3 (Michishita et al., 2009). A chemical biology approach also revealed deacetylation of H3K18 and H3K27 by SIRT6 (Wang et al., 2016) (**Figure 3A**).

Studies have shown that SIRT6 can inhibit VC progression by catalyzing histones. Mandy et al. found that SIRT6 could protect telomeres from damage by deacetylating telomere chromatin at H3K9 and H3K27, thereby preventing VSMCs senescence, which ultimately prevented the occurrence of atherosclerosis (Grootaert et al., 2021).

SIRT6 can affect VC processes, including intimal and medial calcification, by regulating VSMCs, ECs and other cells. In CKD, SIRT6 can inhibit the osteogenic transdifferentiation of VSMCs from a contractile phenotype to a synthetic phenotype, which is the central process in medial calcification, by binding to runt-related transcription factor 2 (Runx2) and causing its deacetylation (Li et al., 2022b). Having known that ECs are important for preventing atherosclerosis, Xu et al. conducted a series of studies that investigated the influence of SIRT6 on ECs, and the results confirmed that SIRT6 played an important role in preventing endothelial dysfunction in mice and the development of atherosclerosis (Xu et al., 2016). A new study showed SIRT6 could act on and deacetylate caveolin-1 in ECs, which activated autophagic degradation of caveolin-1 and inhibited high glucose stimulated LDL transport, which further inhibited the formation of atherosclerosis in diabetes (Zhao et al., 2022). Greiten et al. also confirmed that SIRT6 can prevent oxidative stress, endothelial dysfunction, and vascular dysfunction (Greiten et al., 2021).

The mechanism by which SIRT6 protects endothelial function has also been investigated. Jin et al. studied the role of SIRT6 in minute cholesterol crystals and concluded that SIRT6 could inhibit cholesterol crystal-induced endothelial dysfunction by activating Nrf2 (Jin et al., 2020). EC dysfunction and senescence can be promoted by SIRT6 deficiency, and the mechanism involves the downregulation of forkhead box M1 expression (Lee et al., 2020b). In addition to VSMCs and ECs, the normal expression of SIRT6 in bone marrow-derived cells has functional implications. SIRT6 deficiency in these cells can cause atherosclerosis, in which macrophage scavenger receptor1 plays a central role (Arsiwala et al., 2020). Exosomes are important regulatory structures that have been widely studied in recent years and are involved in the regulation of SIRT6-related signaling pathways. Wang et al. found that exosomes derived from bone marrow mesenchymal stem cells could activate the SIRT6-HMGB1 deacetylation signaling pathway, which restrained high phosphate-induced aortic calcification and protected renal function (Wei et al., 2021).

As an important vascular protective factor, SIRT6 deserves more attention and research, and it is also promising for the development of drugs to prevent or treat VC.

Sirtuin 7

SIRT7 used to be the least studied sirtuin, but some research breakthroughs have confirmed that SIRT7 has important biological functions and is associated with a variety of diseases, including heart disease, fatty liver, and many types of tumors (Li et al., 2019). SIRT7 is also concentrated in the nucleus, but its subnuclear localization differs from that of SIRT1 and SIRT6 (Michishita et al., 2005). As nuclear sirtuin, study found that SIRT7 were capable of deacetylating histone H3 at lysine 18 and played an important role in maintaining oncogenic transformation of cancer cells (Barber et al., 2012). Besides, H3K36 has been found deacetylating substrates of SIRT7 (Wang et al., 2019a)(**Figure 3A**). Except for the deacetylation activity, histone desuccinylation activity was also found in SIRT7. More accurately, SIRT7 could desuccinylate histone H3 at lysine 122 and played a role in chromatin compaction and genome stability (Li et al., 2016).

The link between SIRT7, histone deacetylation and VC is not clear, but certain investigations have found that SIRT7 has a protective effect on the progression of VC, especially in atherosclerosis. Zheng et al. explored the function of SIRT7 in regulating the proliferation and migration of VSMCs using an atherosclerosis cell model and concluded that SIRT7 inhibited VSMCs proliferation and migration, which further promoted atherosclerosis by enhancing Wnt/β-catenin activation, and these findings suggest that SIRT7 inhibits the progression of atherosclerosis (Zheng et al., 2018). Certain small molecules have been found to affect atherosclerosis by modulating SIRT7 expression. Notably, Zheng et al. found that the small nucleolar RNA host gene 7-003 can act on the miR-1306-5p/SIRT7 signaling pathway, thereby inhibiting the proliferation, migration, and invasion of VSMCs. This indirectly proves the significant role of SIRT7 in atherosclerosis (Zheng et al., 2021). Furthermore, Wang et al. concluded that p53-dependent lincRNA-p21 could upregulate SIRT7 expression by acting on microRNA-17-5p to prevent VSMCs proliferation and counteract VSMCs apoptosis in atherosclerosis (Wang et al., 2021). In the future, research on SIRT7 needs to be conducted to improve our understanding of the role of SIRT7 in VC development. Whether SIRT7 can be used as a target for the treatment of VC also needs more research to prove.

DISCUSSION

VC is associated with hypertension, atherosclerosis, and other cardiovascular diseases; however, there are no clinically available measures to treat VC. Therefore, it is necessary to develop drugs that can prevent or reverse the pathological process of VC. Researchers have found that sirtuins play a significant role in maintaining the physiological functions of the vasculature. Sirtuins protect the physiological state of VSMCs and ECs, enabling them to cope with adverse conditions that occur during lipid deposition, oxidative stress, and inflammation, thereby preventing the occurrence of VC. The signaling pathways involved in the molecular link between sirtuins and VC are constantly being elucidated. Based on these findings, some potential drugs have been discovered that modulate the process of VC by changing the expression of sirtuins and regulating related signaling pathways. Liu et al. found that spermidine could inhibit VC in CKD by acting on the SIRT1 signaling pathway, specifically by upregulating the expression of SIRT1 (Liu et al., 2021c). Chen et al. also concluded that Intermedin1-53 could increase the expression of SIRT1 by activating PI3K/Akt, AMPK, and cAMP/PKA signaling, thereby inhibiting the progression of VC related to aging (Chen et al., 2020b). Additionally, Han et al. found that acacetin could resist mitochondrial damage induced by a high-glucose environment, whereas inhibiting the expression of SIRT3 eliminated the protective effect of acacetin. Further analysis showed that acacetin suppressed atherosclerosis aggravated by diabetes may be mediated by activating the Sirt1/Sirt3/AMPK signaling pathway to protect mitochondrial function (Han et al., 2020). Notably, 17b-estradiol was found to inhibit the senescence of ECs and slow down the process of atherosclerosis.

However, the underlying mechanism remained unclear until Xiang et al. determined that 17b-estradiol inhibited H_2O_2-induced senescence in human umbilical vein ECs by upregulating SIRT3 expression and promoting autophagy, which eventually slowed the progression of atherosclerosis (Xiang et al., 2020).

Although all of SIRTs belong to the sirtuin family, but why the effects of knocking them out are not the same? It is possible that the different consequences are related to their different enzymatic activities. The most well-known enzymatic activity of the sirtuin family is deacetylation, but only SIRT1, SIRT2, SIRT3, and SIRT7 have been identified to have a strong deacetylation activity (Jiao and Gong, 2020). However, SIRT4 was found to have ADP-ribosyltransferase and lipamidase activities (Haigis et al., 2006; Min et al., 2018). SIRT5 was found to possess potent desuccinylation and demalonylation activities (Yang et al., 2017b). The demyristoylating activity of SIRT6 was also found (Jiang et al., 2013). Besides, existing research is mostly based on findings from postnatal studies, but are there some seemingly unimportant sirtuins that actually play an important role during the embryonic period? In other words, are the functions of sirtuins temporally specific? With the continuous advancement of research technology and the continuous exploration of more research, the answer will be clearer.

Although it seems that targeting sirtuins might be effective in VC treatment, whether sirtuin therapeutics can only hold back further progress or even take a turn for the worse calcification remains unclear. In general, the sirtuin family is closely related to VC, and the roles played by different sirtuins are constantly being discovered. Based on the current knowledge, except for SIRT5, other sirtuins play a protective role in VC more or less (**Figure 3B**). The development of drugs against VC and cardiovascular diseases based on sirtuin is also very promising. In any case, it is undoubtedly important to further understand the influence of sirtuins on VC and the specific mechanisms through which they function. Only after a deeper understanding of the sirtuin family is established will researchers be able to elucidate the best therapeutic targets and develop clinically applicable drugs for the prevention and treatment of VC.

AUTHOR CONTRIBUTIONS

DZ and XL designed the scope of the review. XP wrote the manuscript. XR and HZ performed the document searching and prepared the figures. CP guided the planning and critically edited the manuscript. All authors read and approved the final manuscript.

FUNDING

This study was supported by the National Natural Science Foundation of China (No. 11932014, 31971239, and 82001062).

ACKNOWLEDGMENTS

The authors thank all investigators and supporters involved in this study.

REFERENCES

Abedin, M., Tintut, Y., and Demer, L. L. (2004). Vascular Calcification: Mechanisms and Clinical Ramifications. *Arterioscler. Thromb. Vasc. Biol.* 24, 1161–1170. doi:10.1161/01.ATV.0000133194.94939.42

Al-Hijji, M., Narula, N., Go, J. L., Khosla, S., Enriquez-Sarano, M., Loeffler, D., et al. (2019). Circulating Osteogenic Progenitor Cells in Mild, Moderate, and Severe Aortic Valve Stenosis. *Mayo Clin. Proc.* 94, 652–659. doi:10.1016/j.mayocp.2019.01.005

Alves-Fernandes, D. K., and Jasiulionis, M. G. (2019). The Role of SIRT1 on DNA Damage Response and Epigenetic Alterations in Cancer. *Int. J. Mol. Sci.* 20. doi:10.3390/ijms20133153

Arciniegas, E., Frid, M. G., Douglas, I. S., and Stenmark, K. R. (2007). Perspectives on Endothelial-To-Mesenchymal Transition: Potential Contribution to Vascular Remodeling in Chronic Pulmonary Hypertension. *Am. J. Physiol. Lung Cell Mol. Physiol.* 293, L1–L8. doi:10.1152/ajplung.00378.2006

Arsiwala, T., Pahla, J., van Tits, L. J., Bisceglie, L., Gaul, D. S., Costantino, S., et al. (2020). Sirt6 Deletion in Bone Marrow-Derived Cells Increases Atherosclerosis - Central Role of Macrophage Scavenger Receptor 1. *J. Mol. Cell Cardiol.* 139, 24–32. doi:10.1016/j.yjmcc.2020.01.002

Autiero, I., Costantini, S., and Colonna, G. (2008). Human Sirt-1: Molecular Modeling and Structure-Function Relationships of an Unordered Protein. *PloS one* 4, e7350. doi:10.1371/journal.pone.0007350

Badi, I., Mancinelli, L., Polizzotto, A., Ferri, D., Zeni, F., Burba, I., et al. (2018). miR-34a Promotes Vascular Smooth Muscle Cell Calcification by Downregulating SIRT1 (Sirtuin 1) and Axl (AXL Receptor Tyrosine Kinase). *Arterioscler. Thromb. Vasc. Biol.* 38, 2079–2090. doi:10.1161/ATVBAHA.118.311298

Bakhshian Nik, A., Hutcheson, J. D., and Aikawa, E. (2017). Extracellular Vesicles as Mediators of Cardiovascular Calcification. *Front. Cardiovasc Med.* 4, 78. doi:10.3389/fcvm.2017.00078

Barber, M. F., Michishita-Kioi, E., Xi, Y., Tasselli, L., Kioi, M., Moqtaderi, Z., et al. (2012). SIRT7 Links H3K18 Deacetylation to Maintenance of Oncogenic Transformation. *Nature* 487, 114–118. doi:10.1038/nature11043

Bartoli-Leonard, F., Wilkinson, F. L., Schiro, A., Serracino Inglott, F., Alexander, M. Y., and Weston, R. (2021). Loss of SIRT1 in Diabetes Accelerates DNA Damage-Induced Vascular Calcification. *Cardiovasc Res.* 117, 836–849. doi:10.1093/cvr/cvaa134

Betsinger, C. N., and Cristea, I. M. (2019). Mitochondrial Function, Metabolic Regulation, and Human Disease Viewed through the Prism of Sirtuin 4 (SIRT4) Functions. *J. Proteome Res.* 18, 1929–1938. doi:10.1021/acs.jproteome.9b00086

Blank, M. F. I., and Grummt, I. (2017). The Seven Faces of SIRT7. *Transcription* 8, 67–74. doi:10.1080/21541264.2016.1276658

Boström, K. I. (2016). Where Do We Stand on Vascular Calcification? *Vasc. Pharmacol.* 84, 8–14.

Cano-Megías, M., Guisado-Vasco, P., Bouarich, H., de Arriba-de la Fuente, G., de Sequera-Ortiz, P., Álvarez-Sanz, C., et al. (2019). Coronary Calcification as a Predictor of Cardiovascular Mortality in Advanced Chronic Kidney Disease: a Prospective Long-Term Follow-Up Study. *BMC Nephrol.* 20, 188.

Carafa, V., Rotili, D., Forgione, M., Cuomo, F., Serretiello, E., Hailu, G. S., et al. (2016). Sirtuin Functions and Modulation: from Chemistry to the Clinic. *Clin. Epigenetics* 8, 61. doi:10.1186/s13148-016-0224-3

Chen, G., Huang, P., and Hu, C. (2020). The Role of SIRT2 in Cancer: A Novel Therapeutic Target. *Int. J. Cancer* 147, 3297–3304. doi:10.1002/ijc.33118

Chen, X., Lu, W., and Wu, D. (2021). Sirtuin 2 (SIRT2): Confusing Roles in the Pathophysiology of Neurological Disorders. *Front. Neurosci.* 15, 614107. doi:10.3389/fnins.2021.614107

Chen, Y., Huang, C., Zhu, S. Y., Zou, H. C., Xu, C. Y., and Chen, Y. X. (2021). Overexpression of HOTAIR Attenuates Pi-Induced Vascular Calcification by Inhibiting Wnt/β-Catenin through Regulating miR-126/Klotho/SIRT1 axis. *Mol. Cell Biochem.* 476, 3551–3561. doi:10.1007/s11010-021-04164-8

Chen, Y., Zhang, L. S., Ren, J. L., Zhang, Y. R., Wu, N., Jia, M. Z., et al. (2020). Intermedin1-53 Attenuates Aging-Associated Vascular Calcification in Rats by Upregulating Sirtuin 1. *Aging (Albany NY)* 12, 5651–5674. doi:10.18632/aging.102934

Cho, H. J., Lee, J. W., Cho, H. J., Lee, C. S., and Kim, H. S. (2018). Identification of Adult Mesodermal Progenitor Cells and Hierarchy in Atherosclerotic Vascular Calcification. *Stem Cells* 36, 1075–1096. doi:10.1002/stem.2814

D'Onofrio, N., Servillo, L., and Balestrieri, M. L. (2018). SIRT1 and SIRT6 Signaling Pathways in Cardiovascular Disease Protection. *Antioxid. Redox Signal* 28, 711–732. doi:10.1089/ars.2017.7178

Dai, X., Liu, S., Cheng, L., Huang, T., Guo, H., Wang, D., et al. (2022). Epigenetic Upregulation of H19 and AMPK Inhibition Concurrently Contribute to S-Adenosylhomocysteine Hydrolase Deficiency-Promoted Atherosclerotic Calcification. *Circ. Res.* 101161circresaha121320251. doi:10.1161/CIRCRESAHA.121.320251

Dai, X. Y., Zhao, M. M., Cai, Y., Guan, Q. C., Zhao, Y., Guan, Y., et al. (2013). Phosphate-induced Autophagy Counteracts Vascular Calcification by Reducing Matrix Vesicle Release. *Kidney Int.* 83, 1042–1051. doi:10.1038/ki.2012.482

Dart, A. M., and Kingwell, B. A. (2001). Pulse Pressure-Aa Review of Mechanisms and Clinical Relevance. *J. Am. Coll. Cardiol.* 37, 975–984. doi:10.1016/s0735-1097(01)01108-1

Das, C., Lucia, M. S., Hansen, K. C., and Tyler, J. K. (2009). CBP/p300-mediated Acetylation of Histone H3 on Lysine 56. *Nature* 459, 113–117. doi:10.1038/nature07861

DeRuiter, M. C., Poelmann, R. E., VanMunsteren, J. C., Mironov, V., Markwald, R. R., and Gittenberger-de Groot, A. C. (1997). Embryonic Endothelial Cells Transdifferentiate into Mesenchymal Cells Expressing Smooth Muscle Actins *In Vivo* and *In Vitro*. *Circ. Res.* 80, 444–451. doi:10.1161/01.res.80.4.444

Doherty, T. M., Asotra, K., Fitzpatrick, L. A., Qiao, J. H., Wilkin, D. J., Detrano, R. C., et al. (2003). Calcification in Atherosclerosis: Bone Biology and Chronic Inflammation at the Arterial Crossroads. *Proc. Natl. Acad. Sci. U. S. A.* 100, 11201–11206. doi:10.1073/pnas.1932554100

Doran, A. C., Meller, N., and McNamara, C. A. (2008). Role of Smooth Muscle Cells in the Initiation and Early Progression of Atherosclerosis. *Arterioscler. Thromb. Vasc. Biol.* 28, 812–819. doi:10.1161/ATVBAHA.107.159327

Du, J., Zhou, Y., Su, X., Yu, J. J., Khan, S., Jiang, H., et al. (2011). Sirt5 Is a NAD-dependent Protein Lysine Demalonylase and Desuccinylase. *Science* 334, 806–809. doi:10.1126/science.1207861

Duan, X., Zhou, Y., Teng, X., Tang, C., and Qi, Y. (2009). Endoplasmic Reticulum Stress-Mediated Apoptosis Is Activated in Vascular Calcification. *Biochem. Biophys. Res. Commun.* 387, 694–699. doi:10.1016/j.bbrc.2009.07.085

Durham, A. L., Speer, M. Y., Scatena, M., Giachelli, C. M., and Shanahan, C. M. (2018). Role of Smooth Muscle Cells in Vascular Calcification: Implications in Atherosclerosis and Arterial Stiffness. *Cardiovasc Res.* 114, 590–600. doi:10.1093/cvr/cvy010

Eskandarian, H. A., Impens, F., Nahori, M. A., Soubigou, G., Coppée, J. Y., Cossart, P., et al. (2013). A Role for SIRT2-dependent Histone H3K18 Deacetylation in Bacterial Infection. *Science* 341, 1238858. doi:10.1126/science.1238858

Esteller, M. (2011). Cancer Epigenetics for the 21st Century: What's Next? *Genes Cancer* 2, 604–606. doi:10.1177/1947601911423096

Fadini, G. P., Albiero, M., Menegazzo, L., Boscaro, E., Agostini, C., de Kreutzenberg, S. V., et al. (2012). Procalcific Phenotypic Drift of Circulating Progenitor Cells in Type 2 Diabetes with Coronary Artery Disease. *Exp. Diabetes Res.* 2012, 921685. doi:10.1155/2012/921685

Feng, H., Wang, J. Y., Yu, B., Cong, X., Zhang, W. G., Li, L., et al. (2019). Peroxisome Proliferator-Activated Receptor-γ Coactivator-1α Inhibits Vascular Calcification through Sirtuin 3-Mediated Reduction of Mitochondrial Oxidative Stress. *Antioxid. Redox Signal* 31, 75–91. doi:10.1089/ars.2018.7620

Finnin, M. S., Donigian, J. R., and Pavletich, N. P. (2001). Structure of the Histone Deacetylase SIRT2. *Nat. Struct. Biol.* 8, 621–625. doi:10.1038/89668

Frismantiene, A., Philippova, M., Erne, P., and Resink, T. J. (2018). Smooth Muscle Cell-Driven Vascular Diseases and Molecular Mechanisms of VSMC Plasticity. *Cell Signal* 52, 48–64. doi:10.1016/j.cellsig.2018.08.019

Frye, R. A. (2000). Phylogenetic Classification of Prokaryotic and Eukaryotic Sir2-like Proteins. *Biochem. Biophys. Res. Commun.* 273, 793–798. doi:10.1006/bbrc.2000.3000

Goldberg, A. D., Allis, C. D., and Bernstein, E. (2007). Epigenetics: a Landscape Takes Shape. *Cell* 128, 635–638. doi:10.1016/j.cell.2007.02.006

Greiten, L. E., Zhang, B., Roos, C. M., Hagler, M., Jahns, F. P., and Miller, J. D. (2021). Sirtuin 6 Protects against Oxidative Stress and Vascular Dysfunction in Mice. *Front. Physiol.* 12, 753501. doi:10.3389/fphys.2021.753501

Grootaert, M. O. J., Finigan, A., Figg, N. L., Uryga, A. K., and Bennett, M. R. (2021). SIRT6 Protects Smooth Muscle Cells from Senescence and Reduces Atherosclerosis. *Circ. Res.* 128, 474–491. doi:10.1161/CIRCRESAHA.120.318353

Gu, J., Lu, Y., Deng, M., Qiu, M., Tian, Y., Ji, Y., et al. (2019). Inhibition of Acetylation of Histones 3 and 4 Attenuates Aortic Valve Calcification. *Exp. Mol. Med.* 51, 79–14. doi:10.1038/s12276-019-0272-9

Guihard, P. J., Yao, J., Blazquez-Medela, A. M., Iruela-Arispe, L., Boström, K. I., and Yao, Y. (2016). Endothelial-Mesenchymal Transition in Vascular Calcification of Ins2Akita/+ Mice. *PloS one* 11, e0167936. doi:10.1371/journal.pone.0167936

Haigis, M. C., Mostoslavsky, R., Haigis, K. M., Fahie, K., Christodoulou, D. C., Murphy, A. J., et al. (2006). SIRT4 Inhibits Glutamate Dehydrogenase and Opposes the Effects of Calorie Restriction in Pancreatic Beta Cells. *Cell* 126, 941–954. doi:10.1016/j.cell.2006.06.057

Hammad, S. K., Eissa, R. G., Shaheen, M. A., and Younis, N. N. (2021). Resveratrol Ameliorates Aortic Calcification in Ovariectomized Rats via SIRT1 Signaling. *Curr. Issues Mol. Biol.* 43, 1057–1071. doi:10.3390/cimb43020075

Han, W. M., Chen, X. C., Li, G. R., and Wang, Y. (2020). Acacetin Protects against High Glucose-Induced Endothelial Cells Injury by Preserving Mitochondrial Function via Activating Sirt1/Sirt3/AMPK Signals. *Front. Pharmacol.* 11, 607796. doi:10.3389/fphar.2020.607796

He, W., Huang, J., Liu, Y., Xie, C., Zhang, K., Zhu, X., et al. (2021). Deletion of Soluble Epoxide Hydrolase Suppressed Chronic Kidney Disease-Related Vascular Calcification by Restoring Sirtuin 3 Expression. *Cell Death Dis.* 12, 992. doi:10.1038/s41419-021-04283-6

He, X., Zeng, H., and Chen, J. X. (2019). Emerging Role of SIRT3 in Endothelial Metabolism, Angiogenesis, and Cardiovascular Disease. *J. Cell Physiol.* 234, 2252–2265. doi:10.1002/jcp.27200

Huhtiniemi, T., Wittekindt, C., Laitinen, T., Leppänen, J., Salminen, A., Poso, A., et al. (2006). Comparative and Pharmacophore Model for Deacetylase SIRT1. *J. Comput. Aided Mol. Des.* 20, 589–599. doi:10.1007/s10822-006-9084-9

Hutcheson, J. D., Goettsch, C., Bertazzo, S., Maldonado, N., Ruiz, J. L., Goh, W., et al. (2016). Genesis and Growth of Extracellular-Vesicle-Derived Microcalcification in Atherosclerotic Plaques. *Nat. Mater* 15, 335–343. doi:10.1038/nmat4519

Hwang, J. W., Yao, H., Caito, S., Sundar, I. K., and Rahman, I. (2013). Redox Regulation of SIRT1 in Inflammation and Cellular Senescence. *Free Radic. Biol. Med.* 61, 95–110. doi:10.1016/j.freeradbiomed.2013.03.015

Iwahara, T., Bonasio, R., Narendra, V., and Reinberg, D. (2012). SIRT3 Functions in the Nucleus in the Control of Stress-Related Gene Expression. *Mol. Cell Biol.* 32, 5022–5034. doi:10.1128/MCB.00822-12

Iyemere, V. P., Proudfoot, D., Weissberg, P. L., and Shanahan, C. M. (2006). Vascular Smooth Muscle Cell Phenotypic Plasticity and the Regulation of Vascular Calcification. *J. Intern Med.* 260, 192–210. doi:10.1111/j.1365-2796.2006.01692.x

Jaminon, A., Reesink, K., Kroon, A., and Schurgers, L. (2019). The Role of Vascular Smooth Muscle Cells in Arterial Remodeling: Focus on Calcification-Related Processes. *Int. J. Mol. Sci.* 20. doi:10.3390/ijms20225694

Jiang, H., Khan, S., Wang, Y., Charron, G., He, B., Sebastian, C., et al. (2013). SIRT6 Regulates TNF-α Secretion through Hydrolysis of Long-Chain Fatty Acyl Lysine. *Nature* 496, 110–113. doi:10.1038/nature12038

Jiao, F., and Gong, Z. (2020). The Beneficial Roles of SIRT1 in Neuroinflammation-Related Diseases. *Oxid. Med. Cell Longev.* 2020, 6782872. doi:10.1155/2020/6782872

Jin, L., Wei, W., Jiang, Y., Peng, H., Cai, J., Mao, C., et al. (2009). Crystal Structures of Human SIRT3 Displaying Substrate-Induced Conformational Changes. *J. Biol. Chem.* 284, 24394–24405. doi:10.1074/jbc.M109.014928

Jin, Z., Xiao, Y., Yao, F., Wang, B., Zheng, Z., Gao, H., et al. (2020). SIRT6 Inhibits Cholesterol Crystal-Induced Vascular Endothelial Dysfunction via Nrf2 Activation. *Exp. Cell Res.* 387, 111744. doi:10.1016/j.yexcr.2019.111744

Jing, S. H., Yu, B., and Qiao, H. (2019). Correlation between Endothelial Cell Apoptosis and SIRT3 Gene Expression in Atherosclerosis Rats. *Eur. Rev. Med. Pharmacol. Sci.* 23, 9033–9040. doi:10.26355/eurrev_201910_19305

Johnson, R. C., Leopold, J. A., and Loscalzo, J. (2006). Vascular Calcification: Pathobiological Mechanisms and Clinical Implications. *Circ. Res.* 99, 1044–1059. doi:10.1161/01.RES.0000249379.55535.21

Karbasforooshan, H., and Karimi, G. (2017). The Role of SIRT1 in Diabetic Cardiomyopathy. *Biomed. Pharmacother.* 90, 386–392. doi:10.1016/j.biopha.2017.03.056

Kumar, S., and Lombard, D. B. (2018). Functions of the Sirtuin Deacylase SIRT5 in Normal Physiology and Pathobiology. *Crit. Rev. Biochem. Mol. Biol.* 53, 311–334. doi:10.1080/10409238.2018.1458071

Kurozumi, A., Nakano, K., Yamagata, K., Okada, Y., Nakayamada, S., and Tanaka, Y. (2019). IL-6 and sIL-6R Induces STAT3-dependent Differentiation of Human VSMCs into Osteoblast-like Cells through JMJD2B-Mediated Histone Demethylation of RUNX2. *Bone* 124, 53–61. doi:10.1016/j.bone.2019.04.006

Lanzer, P., Hannan, F. M., Lanzer, J. D., Janzen, J., Raggi, P., Furniss, D., et al. (2021). Medial Arterial Calcification: JACC State-Of-The-Art Review. *J. Am. Coll. Cardiol.* 78, 1145–1165. doi:10.1016/j.jacc.2021.06.049

Laurent, G., de Boer, V. C., Finley, L. W., Sweeney, M., Lu, H., Schug, T. T., et al. (2013). SIRT4 Represses Peroxisome Proliferator-Activated Receptor α Activity to Suppress Hepatic Fat Oxidation. *Mol. Cell Biol.* 33, 4552–4561. doi:10.1128/MCB.00087-13

Laurent, G., German, N. J., Saha, A. K., de Boer, V. C., Davies, M., Koves, T. R., et al. (2013). SIRT4 Coordinates the Balance between Lipid Synthesis and Catabolism by Repressing Malonyl CoA Decarboxylase. *Mol. Cell* 50, 686–698. doi:10.1016/j.molcel.2013.05.012

Lee, O. H., Woo, Y. M., Moon, S., Lee, J., Park, H., Jang, H., et al. (2020). Sirtuin 6 Deficiency Induces Endothelial Cell Senescence via Downregulation of Forkhead Box M1 Expression. *Aging (Albany NY)* 12, 20946–20967. doi:10.18632/aging.202176

Lee, S. J., Lee, I. K., and Jeon, J. H. (2020). Vascular Calcification-New Insights into its Mechanism. *Int. J. Mol. Sci.* 21. doi:10.3390/ijms21082685

Leopold, J. A. (2015). Vascular Calcification: Mechanisms of Vascular Smooth Muscle Cell Calcification. *Trends Cardiovasc Med.* 25, 267–274. doi:10.1016/j.tcm.2014.10.021

Li, L., Dong, Z., Yang, J., Li, Q., Lei, Q., Mao, J., et al. (2019). Progress in Roles and Mechanisms of Deacetylase SIRT7. *Sheng Wu Gong Cheng Xue Bao* 35, 13–26. doi:10.13345/j.cjb.180139

Li, L., Shi, L., Yang, S., Yan, R., Zhang, D., Yang, J., et al. (2016). SIRT7 Is a Histone Desuccinylase that Functionally Links to Chromatin Compaction and Genome Stability. *Nat. Commun.* 7, 12235. doi:10.1038/ncomms12235

Li, P., Ge, J., and Li, H. (2020). Lysine Acetyltransferases and Lysine Deacetylases as Targets for Cardiovascular Disease. *Nat. Rev. Cardiol.* 17, 96–115. doi:10.1038/s41569-019-0235-9

Li, T., Yu, H., Zhang, D., Feng, T., Miao, M., Li, J., et al. (2022). Matrix Vesicles as a Therapeutic Target for Vascular Calcification. *Front. Cell Dev. Biol.* 10, 25. doi:10.3389/fcell.2022.825622

Li, W., Feng, W., Su, X., Luo, D., Li, Z., Zhou, Y., et al. (2022). SIRT6 Protects Vascular Smooth Muscle Cells from Osteogenic Transdifferentiation via Runx2 in Chronic Kidney Disease. *J. Clin. investigation* 132. doi:10.1172/jci150051

Li, Y., Zhou, Y., Wang, F., Chen, X., Wang, C., Wang, J., et al. (2018). SIRT4 Is the Last Puzzle of Mitochondrial Sirtuins. *Bioorg Med. Chem.* 26, 3861–3865. doi:10.1016/j.bmc.2018.07.031

Liao, J., Chen, X., Li, Y., Ge, Z., Duan, H., Zou, Y., et al. (2012). Transfer of Bone-Marrow-Derived Mesenchymal Stem Cells Influences Vascular Remodeling and Calcification after Balloon Injury in Hyperlipidemic Rats. *J. Biomed. Biotechnol.* 2012, 165296. doi:10.1155/2012/165296

Liu, G., Chen, H., Liu, H., Zhang, W., and Zhou, J. (2021). Emerging Roles of SIRT6 in Human Diseases and its Modulators. *Med. Res. Rev.* 41, 1089–1137. doi:10.1002/med.21753

Liu, J., Wu, X., Wang, X., Zhang, Y., Bu, P., Zhang, Q., et al. (2013). Global Gene Expression Profiling Reveals Functional Importance of Sirt2 in Endothelial Cells under Oxidative Stress. *Int. J. Mol. Sci.* 14, 5633–5649. doi:10.3390/ijms14035633

Liu, Q. Q., Ren, K., Liu, S. H., Li, W. M., Huang, C. J., and Yang, X. H. (2019). MicroRNA-140-5p Aggravates Hypertension and Oxidative Stress of Atherosclerosis via Targeting Nrf2 and Sirt2. *Int. J. Mol. Med.* 43, 839–849. doi:10.3892/ijmm.2018.3996

Liu, X., Chen, A., Liang, Q., Yang, X., Dong, Q., Fu, M., et al. (2021). Spermidine Inhibits Vascular Calcification in Chronic Kidney Disease through Modulation of SIRT1 Signaling Pathway. *Aging Cell* 20, e13377. doi:10.1111/acel.13377

Liu, Y., Shen, X., Pang, M., Sun, Z., Qian, Y., Xue, W., et al. (2021). Role of Histone Deacetylase Sirt3 in the Development and Regression of Atherosclerosis. *Life Sci.* 272, 119178. doi:10.1016/j.lfs.2021.119178

Lu, C. L., Liao, M. T., Hou, Y. C., Fang, Y. W., Zheng, C. M., Liu, W. C., et al. (2020). Sirtuin-1 and its Relevance in Vascular Calcification. *Int. J. Mol. Sci.* 21. doi:10.3390/ijms21051593

Lu, G., Li, J., Zhang, H., Zhao, X., Yan, L. J., and Yang, X. (2018). Role and Possible Mechanisms of Sirt1 in Depression. *Oxid. Med. Cell Longev.* 2018, 8596903. doi:10.1155/2018/8596903

Machin, D. R., Auduong, Y., Gogulamudi, V. R., Liu, Y., Islam, M. T., Lesniewski, L. A., et al. (2020). Lifelong SIRT-1 Overexpression Attenuates Large Artery Stiffening with Advancing Age. *Aging (Albany NY)* 12, 11314–11324. doi:10.18632/aging.103322

Mahlknecht, U., Ho, A. D., Letzel, S., and Voelter-Mahlknecht, S. (2006). Assignment of the NAD-dependent Deacetylase Sirtuin 5 Gene (SIRT5) to Human Chromosome Band 6p23 by *In Situ* Hybridization. *Cytogenet Genome Res.* 112, 208–212. doi:10.1159/000089872

Matsushita, N., Yonashiro, R., Ogata, Y., Sugiura, A., Nagashima, S., Fukuda, T., et al. (2011). Distinct Regulation of Mitochondrial Localization and Stability of Two Human Sirt5 Isoforms. *Genes cells.* 16, 190–202. doi:10.1111/j.1365-2443.2010.01475.x

McLendon, P. M., Ferguson, B. S., Osinska, H., Bhuiyan, M. S., James, J., McKinsey, T. A., et al. (2014). Tubulin Hyperacetylation Is Adaptive in Cardiac Proteotoxicity by Promoting Autophagy. *Proc. Natl. Acad. Sci. U. S. A.* 111, E5178–E5186. doi:10.1073/pnas.1415589111

Medici, D., Shore, E. M., Lounev, V. Y., Kaplan, F. S., Kalluri, R., and Olsen, B. R. (2010). Conversion of Vascular Endothelial Cells into Multipotent Stem-like Cells. *Nat. Med.* 16, 1400–1406. doi:10.1038/nm.2252

Michan, S., and Sinclair, D. (2007). Sirtuins in Mammals: Insights into Their Biological Function. *Biochem. J.* 404, 1–13. doi:10.1042/BJ20070140

Michishita, E., McCord, R. A., Berber, E., Kioi, M., Padilla-Nash, H., Damian, M., et al. (2008). SIRT6 Is a Histone H3 Lysine 9 Deacetylase that Modulates Telomeric Chromatin. *Nature* 452, 492–496. doi:10.1038/nature06736

Michishita, E., McCord, R. A., Boxer, L. D., Barber, M. F., Hong, T., Gozani, O., et al. (2009). Cell Cycle-dependent Deacetylation of Telomeric Histone H3 Lysine K56 by Human SIRT6. *Cell Cycle* 8, 2664–2666. doi:10.4161/cc.8.16.9367

Michishita, E., Park, J. Y., Burneskis, J. M., Barrett, J. C., and Horikawa, I. (2005). Evolutionarily Conserved and Nonconserved Cellular Localizations and Functions of Human SIRT Proteins. *Mol. Biol. Cell* 16, 4623–4635. doi:10.1091/mbc.e05-01-0033

Min, Z., Gao, J., and Yu, Y. (2018). The Roles of Mitochondrial SIRT4 in Cellular Metabolism. *Front. Endocrinol. (Lausanne)* 9, 783. doi:10.3389/fendo.2018.00783

Onyango, P., Celic, I., McCaffery, J. M., Boeke, J. D., and Feinberg, A. P. (2002). SIRT3, a Human SIR2 Homologue, Is an NAD-dependent Deacetylase Localized to Mitochondria. *Proc. Natl. Acad. Sci. U. S. A.* 99, 13653–13658. doi:10.1073/pnas.222538099

Pan, P. W., Feldman, J. L., Devries, M. K., Dong, A., Edwards, A. M., and Denu, J. M. (2011). Structure and Biochemical Functions of SIRT6. *J. Biol. Chem.* 286, 14575–14587. doi:10.1074/jbc.M111.218990

Proudfoot, D., Skepper, J. N., Hegyi, L., Bennett, M. R., Shanahan, C. M., and Weissberg, P. L. (2000). Apoptosis Regulates Human Vascular Calcification *In Vitro*: Evidence for Initiation of Vascular Calcification by Apoptotic Bodies. *Circ. Res.* 87, 1055–1062. doi:10.1161/01.res.87.11.1055

Roijers, R. B., Debernardi, N., Cleutjens, J. P., Schurgers, L. J., Mutsaers, P. H., and van der Vusse, G. J. (2011). Microcalcifications in Early Intimal Lesions of

Atherosclerotic Human Coronary Arteries. *Am. J. Pathol.* 178, 2879–2887. doi:10.1016/j.ajpath.2011.02.004

Sánchez-Duffhues, G., García de Vinuesa, A., van de Pol, V., Geerts, M. E., de Vries, M. R., Janson, S. G., et al. (2019). Inflammation Induces Endothelial-To-Mesenchymal Transition and Promotes Vascular Calcification through Downregulation of BMPR2. *J. pathology* 247, 333–346.

Sayd, S., Junier, M. P., and Chneiweiss, H. (2014). SIRT2, a Multi-Talented Deacetylase. *Med. Sci. Paris.* 30, 532–536. doi:10.1051/medsci/20143005016

Scher, M. B., Vaquero, A., and Reinberg, D. (2007). SirT3 Is a Nuclear NAD+-dependent Histone Deacetylase that Translocates to the Mitochondria upon Cellular Stress. *Genes Dev.* 21, 920–928. doi:10.1101/gad.1527307

Schurgers, L. J., Akbulut, A. C., Kaczor, D. M., Halder, M., Koenen, R. R., and Kramann, R. (2018). Initiation and Propagation of Vascular Calcification Is Regulated by a Concert of Platelet- and Smooth Muscle Cell-Derived Extracellular Vesicles. *Front. Cardiovasc Med.* 5, 36. doi:10.3389/fcvm.2018.00036

Shanahan, C. M., Crouthamel, M. H., Kapustin, A., and Giachelli, C. M. (2011). Arterial Calcification in Chronic Kidney Disease: Key Roles for Calcium and Phosphate. *Circ. Res.* 109, 697–711. doi:10.1161/CIRCRESAHA.110.234914

Singh, A., Tandon, S., and Tandon, C. (2021). An Update on Vascular Calcification and Potential Therapeutics. *Mol. Biol. Rep.* 48, 887–896. doi:10.1007/s11033-020-06086-y

Singh, V., and Ubaid, S. (2020). Role of Silent Information Regulator 1 (SIRT1) in Regulating Oxidative Stress and Inflammation. *Inflammation* 43, 1589–1598. doi:10.1007/s10753-020-01242-9

Sosnowska, B., Mazidi, M., Penson, P., Gluba-Brzózka, A., Rysz, J., and Banach, M. (2017). The Sirtuin Family Members SIRT1, SIRT3 and SIRT6: Their Role in Vascular Biology and Atherogenesis. *Atherosclerosis* 265, 275–282. doi:10.1016/j.atherosclerosis.2017.08.027

Sun, H., Unoki, H., Wang, X., Liang, J., Ichikawa, T., Arai, Y., et al. (2002). Lipoprotein(a) Enhances Advanced Atherosclerosis and Vascular Calcification in WHHL Transgenic Rabbits Expressing Human Apolipoprotein(a). *J. Biol. Chem.* 277, 47486–47492. doi:10.1074/jbc.M205814200

Taneja, A., Ravi, V., Hong, J. Y., Lin, H., and Sundaresan, N. R. (2021). Emerging Roles of Sirtuin 2 in Cardiovascular Diseases. *FASEB J. official Publ. Fed. Am. Soc. Exp. Biol.* 35, e21841. doi:10.1096/fj.202100490r

Tang, M., Tang, H., Tu, B., and Zhu, W. G. (2021). SIRT7: a Sentinel of Genome Stability. *Open Biol.* 11, 210047. doi:10.1098/rsob.210047

Tao, Y., Yu, S., Chao, M., Wang, Y., Xiong, J., and Lai, H. (2019). SIRT4 Suppresses the PI3K/Akt/NF-κB S-ignaling P-athway and A-ttenuates HUVEC I-njury I-nduced by oxLDL. *Mol. Med. Rep.* 19, 4973–4979. doi:10.3892/mmr.2019.10161

Tasselli, L., Zheng, W., and Chua, K. F. (2017). SIRT6: Novel Mechanisms and Links to Aging and Disease. *Trends Endocrinol. Metab.* 28, 168–185. doi:10.1016/j.tem.2016.10.002

Vaquero, A., Scher, M., Lee, D., Erdjument-Bromage, H., Tempst, P., and Reinberg, D. (2004). Human SirT1 Interacts with Histone H1 and Promotes Formation of Facultative Heterochromatin. *Mol. Cell* 16, 93–105. doi:10.1016/j.molcel.2004.08.031

Vaquero, A., Scher, M. B., Lee, D. H., Sutton, A., Cheng, H. L., Alt, F. W., et al. (2006). SirT2 Is a Histone Deacetylase with Preference for Histone H4 Lys 16 during Mitosis. *Genes Dev.* 20, 1256–1261. doi:10.1101/gad.1412706

Villa-Bellosta, R., and Egido, J. (2017). Phosphate, Pyrophosphate, and Vascular Calcification: a Question of Balance. *Eur. Heart J.* 38, 1801–1804. doi:10.1093/eurheartj/ehv605

Villa-Bellosta, R., Millan, A., and Sorribas, V. (2011). Role of Calcium-Phosphate Deposition in Vascular Smooth Muscle Cell Calcification. *Am. J. Physiol. Cell PhysiolCell Physiol.* 300, C210–C220. doi:10.1152/ajpcell.00229.2010

Wang, F., and Chen, H. Z. (2020). Histone Deacetylase SIRT1, Smooth Muscle Cell Function, and Vascular Diseases. *Front. Pharmacol.* 11, 537519. doi:10.3389/fphar.2020.537519

Wang, H., He, F., Liang, B., Jing, Y., Zhang, P., Liu, W., et al. (2021). p53-Dependent LincRNA-P21 Protects against Proliferation and Anti-apoptosis of Vascular Smooth Muscle Cells in Atherosclerosis by Upregulating SIRT7 via MicroRNA-17-5p. *J. Cardiovasc Transl. Res.* 14, 426–440. doi:10.1007/s12265-020-10074-9

Wang, K., Xu, C., Xie, X., Jing, Y., Chen, P. J., Yadav, S., et al. (2022). Axin2+ PDL Cells Directly Contribute to New Alveolar Bone Formation in Response to Orthodontic Tension Force. *J. Dent. Res.*, 220345211062585.

Wang, P., Xu, T. Y., Guan, Y. F., Zhao, Y., Li, Z. Y., Lan, X. H., et al. (2014). Vascular Smooth Muscle Cell Apoptosis Is an Early Trigger for Hypothyroid Atherosclerosis. *Cardiovasc Res.* 102, 448–459. doi:10.1093/cvr/cvu056

Wang, S., Zhang, J., Deng, X., Zhao, Y., and Xu, K. (2020). Advances in Characterization of SIRT3 Deacetylation Targets in Mitochondrial Function. *Biochimie* 179, 1–13. doi:10.1016/j.biochi.2020.08.021

Wang, W. W., Angulo-Ibanez, M., Lyu, J., Kurra, Y., Tong, Z., Wu, B., et al. (2019). A Click Chemistry Approach Reveals the Chromatin-dependent Histone H3K36 Deacylase Nature of SIRT7. *J. Am. Chem. Soc.* 141, 2462–2473. doi:10.1021/jacs.8b12083

Wang, W. W., Zeng, Y., Wu, B., Deiters, A., and Liu, W. R. (2016). A Chemical Biology Approach to Reveal Sirt6-Targeted Histone H3 Sites in Nucleosomes. *ACS Chem. Biol.* 11, 1973–1981. doi:10.1021/acschembio.6b00243

Wang, Y., Yang, J., Hong, T., Chen, X., and Cui, L. (2019). SIRT2: Controversy and Multiple Roles in Disease and Physiology. *Ageing Res. Rev.* 55, 100961. doi:10.1016/j.arr.2019.100961

Warburton, D. E., Nicol, C. W., Gatto, S. N., and Bredin, S. S. (2007). Cardiovascular Disease and Osteoporosis: Balancing Risk Management. *Vasc. Health Risk Manag.* 3, 673–689.

Wei, W., Guo, X., Gu, L., Jia, J., Yang, M., Yuan, W., et al. (2021). Bone Marrow Mesenchymal Stem Cell Exosomes Suppress Phosphate-Induced Aortic Calcification via SIRT6-HMGB1 Deacetylation. *Stem Cell Res. Ther.* 12, 235. doi:10.1186/s13287-021-02307-8

Weinert, B. T., Iesmantavicius, V., Moustafa, T., Schölz, C., Wagner, S. A., Magnes, C., et al. (2014). Acetylation Dynamics and Stoichiometry in *Saccharomyces cerevisiae*. *Mol. Syst. Biol.* 10, 716. doi:10.1002/msb.134766

Wen, C., Yang, X., Yan, Z., Zhao, M., Yue, X., Cheng, X., et al. (2013). Nalp3 Inflammasome Is Activated and Required for Vascular Smooth Muscle Cell Calcification. *Int. J. Cardiol.* 168, 2242–2247. doi:10.1016/j.ijcard.2013.01.211

Wesseling, M., Sakkers, T. R., de Jager, S. C. A., Pasterkamp, G., and Goumans, M. J. (2018). The Morphological and Molecular Mechanisms of Epithelial/endothelial-To-Mesenchymal Transition and its Involvement in Atherosclerosis. *Vasc. Pharmacol.* 106, 1–8. doi:10.1016/j.vph.2018.02.006

Wu, M., Rementer, C., and Giachelli, C. M. (2013). Vascular Calcification: an Update on Mechanisms and Challenges in Treatment. *Calcif. Tissue Int.* 93, 365–373. doi:10.1007/s00223-013-9712-z

Xiang, X., Huang, J., Song, S., Wang, Y., Zeng, Y., Wu, S., et al. (2020). 17β-estradiol Inhibits H2O2-Induced Senescence in HUVEC Cells through Upregulating SIRT3 Expression and Promoting Autophagy. *Biogerontology* 21, 549–557. doi:10.1007/s10522-020-09868-w

Xu, S., Yin, M., Koroleva, M., Mastrangelo, M. A., Zhang, W., Bai, P., et al. (2016). SIRT6 Protects against Endothelial Dysfunction and Atherosclerosis in Mice. *Aging (Albany NY)* 8, 1064–1082. doi:10.18632/aging.100975

Yang, L., Ma, X., He, Y., Yuan, C., Chen, Q., Li, G., et al. (2017). Sirtuin 5: a Review of Structure, Known Inhibitors and Clues for Developing New Inhibitors. *Sci. China Life Sci.* 60, 249–256. doi:10.1007/s11427-016-0060-7

Yang, S. W., Hennessy, R. R., Khosla, S., Lennon, R., Loeffler, D., Sun, T., et al. (2017). Circulating Osteogenic Endothelial Progenitor Cell Counts: New Biomarker for the Severity of Coronary Artery Disease. *Int. J. Cardiol.* 227, 833–839. doi:10.1016/j.ijcard.2016.10.036

Zhang, B., Ma, Y., and Xiang, C. (2018). SIRT2 Decreases Atherosclerotic Plaque Formation in Low-Density Lipoprotein Receptor-Deficient Mice by Modulating Macrophage Polarization. *Biomed. Pharmacother.* 97, 1238–1242. doi:10.1016/j.biopha.2017.11.061

Zhang, H., Wang, L. J., Si, D. L., Wang, C., Yang, J. C., Jiang, P., et al. (2015). Correlation between Osteocalcin-Positive Endothelial Progenitor Cells and Spotty Calcification in Patients with Coronary Artery Disease. *Clin. Exp. Pharmacol. Physiol.* 42, 734–739. doi:10.1111/1440-1681.12366

Zhang, J., Xiang, H., Liu, J., Chen, Y., He, R. R., and Liu, B. (2020). Mitochondrial Sirtuin 3: New Emerging Biological Function and Therapeutic Target. *Theranostics* 10, 8315–8342. doi:10.7150/thno.45922

Zhang, W., Liu, D., Ren, J., Zhou, P., and Han, X. (2018). Overexpression of Sirtuin2 Prevents High Glucose-Induced Vascular Endothelial Cell Injury by Regulating the P53 and NF-Kb Signaling Pathways. *Biotechnol. Lett.* 40, 271–278. doi:10.1007/s10529-017-2487-y

Zhao, Y., Jia, X., Yang, X., Bai, X., Lu, Y., Zhu, L., et al. (2022). Deacetylation of Caveolin-1 by Sirt6 Induces Autophagy and Retards High Glucose-Stimulated LDL Transcytosis and Atherosclerosis Formation. *Metabolism* 131, 155162. doi:10.1016/j.metabol.2022.155162

Zheng, J., Chen, K., Wang, H., Chen, Z., Xi, Y., Yin, H., et al. (2018). SIRT7 Regulates the Vascular Smooth Muscle Cells Proliferation and Migration via Wnt/β-Catenin Signaling Pathway. *Biomed. Res. Int.* 2018, 4769596. doi:10.1155/2018/4769596

Zheng, J., Tan, Q., Chen, H., Chen, K., Wang, H., Chen, Z., et al. (2021). lncRNA-SNHG7-003 Inhibits the Proliferation, Migration and Invasion of Vascular Smooth Muscle Cells by Targeting the miR-1306-5p/SIRT7 Signaling Pathway. *Int. J. Mol. Med.* 47, 741–750.

Conflict of Interest: The authors declare that the research was conducted in the absence of any commercial or financial relationships that could be construed as a potential conflict of interest.

Publisher's Note: All claims expressed in this article are solely those of the authors and do not necessarily represent those of their affiliated organizations, or those of the publisher, the editors and the reviewers. Any product that may be evaluated in this article, or claim that may be made by its manufacturer, is not guaranteed or endorsed by the publisher.

frontiers | Frontiers in Pharmacology

ORIGINAL RESEARCH
published: 24 May 2022
doi: 10.3389/fphar.2022.909975

Prediction of Aortic Stenosis Progression by ^{18}F-FDG and ^{18}F-NaF PET/CT in Different Aortic Valve Phenotypes

Patimat Murtazalieva[1], Darya Ryzhkova[2], Eduard Malev[1], Ekaterina Zhiduleva[1] and Olga Moiseeva[1]*

[1]Non-coronary Heart Disease Department, Almazov National Medical Research Centre, Saint Petersburg, Russia, [2]Department of Nuclear Medicine and Theranostics, Almazov National Medical Research Centre, Saint Petersburg, Russia

Background: Different imaging techniques, such as echocardiography (ECHO) and CT, allow to assess aortic stenosis (AS) severity and could be used to study its progression. But only PET/CT open opportunities to assess activity of valvular inflammation and calcification *in vivo*. The aim of this study was to assess prognostic value of valvular inflammation and calcification measured by ^{18}F-FDG and ^{18}F-NaF PET/CT in patients with tricuspid (TAV) and bicuspid aortic valve (BAV).

Methods: The study included 71 patients aged 40–70 years with mild, moderate and severe asymptomatic calcific AS. Patients were divided into two groups according to valve morphology: with BAV and TAV. All patients underwent standard ECHO, CT calcium scoring PET/CT with ^{18}F-NaF and ^{18}F-FDG. All patients were evaluated during a follow-up visit with evaluation of ECHO parameters. (16.8 ± 4.2 months).

Results: TAV and BAV groups were comparable in AS severity by ECHO (peak aortic jet velocity (Vmax): 2.90 [2.60; 3.50] vs. 2.96 [2.55; 3.31] m/s, $p = 0.83$). TBR max ^{18}F-FDG did not vary in TAV and BAV patients (1.15 [1.06; 1.23] vs. 1.11 [1.03; 1.20], $p = 0.39$). Both groups did not differ in valvular calcification degree (Agatston score 1,058 [440; 1798] vs. 1,128 [533; 2,360], $p = 0.55$) and calcification activity assessed by ^{18}F-NaF uptake level (TBR max 1.50 [1.30; 1.78] vs. 1.48 [1.27; 1.83], $p = 0.97$). ^{18}F-NaF TBR max was associated with AS severity measured by Vmax in men and women with TAV ($r = 0.54$; $p = 0.04$ vs. $r = 0.53$; $p = 0.03$). In BAV group this relationship was true only in female patients ($r = 0.1$; $p = 0.67$ vs. $r = 0.7$; $p = 0.0004$). There was no association between Vmax and TBR max ^{18}F-FDG was revealed in TAV and BAV groups. During follow-up period, the most important positive predictors of AS progression in TAV obtained by multinomial logistic regression analysis were Vmax, and ^{18}F-NaF TBR. Whereas in BAV the highest predictive value showed model included age and Vmax.

Conclusion: ^{18}F-NaF PET/CT may be considered as the valuable predictor for hemodynamic progression of calcific AS in case of TAV. ^{18}F-FDG PET/CT does not play a significant role to predict the AS progression.

Keywords: aortic stenosis, bicuspid aortic valve, calcification, aortic stenosis progression, positron emission tomography, 18 F -sodium fluoride, 18 F -fluorodeoxyglucose

OPEN ACCESS

Edited by:
Kang Xu,
Hubei University of Chinese Medicine, China

Reviewed by:
Chunli Wang,
Chongqing University, China
Mao Chen,
Sichuan University, China

****Correspondence:***
Patimat Murtazalieva
murtazalieva_pm@almazovcentre.ru

Specialty section:
This article was submitted to Experimental Pharmacology and Drug Discovery, a section of the journal Frontiers in Pharmacology

Received: *31 March 2022*
Accepted: *21 April 2022*
Published: *24 May 2022*

Citation:
Murtazalieva P, Ryzhkova D, Malev E, Zhiduleva E and Moiseeva O (2022) Prediction of Aortic Stenosis Progression by ^{18}F-FDG and ^{18}F-NaF PET/CT in Different Aortic Valve Phenotypes. Front. Pharmacol. 13:909975. doi: 10.3389/fphar.2022.909975

INTRODUCTION

Aortic stenosis (AS) represents the most common indication for valve surgery as well as for catheter interventions in valvular heart disease (Iung et al., 2019). Despite many recent advances in AS management, no pharmacotherapy has demonstrated its efficacy to prevent AS progression (Pawade et al., 2021; Vahanian et al., 2022). The incidence of AS has been increasing, that may contribute to significant burden on healthcare system.

The most common etiology of AS is known to be a calcification of the tricuspid aortic valve (TAV) or congenital heart defect - bicuspid aortic valve (BAV). Intraoperatively, BAV is represented in 50% of AS surgical interventions, while TAV is observed in 30–40% (Roberts and Ko, 2005). Other etiological factors, such as chronic rheumatic heart disease, infective endocarditis and single-leaf aortic valve are less common.

The specific factors that may facilitate aortic valve calcification remain underinvestigated whereas the underlying pathogenetic mechanisms have not been well defined, so treatment options to prevent AS progression are lacking. It is known that conventional risk factors for the atherosclerosis such as age, sex, hypertension, elevated serum cholesterol, smoking and diabetes are also associated with aortic valve calcification (Stewart et al., 1997; Eveborn et al., 2014; Martinsson et al., 2014; Yan et al., 2017). Notably, early initiation and progression of AS in those with TAV correlate mainly with cardiometabolic risk factors, whereas in BAV subjects, the genetic predispositions and abnormal valve morphology have an independent contribution to the AS progression (Shen et al., 2020).

Recent histology and molecular biology studies support the hypothesis for the aortic valve calcification as a part of the immuno-inflammatory process associated with endothelial cell damage, accumulation of oxidized low-density lipoproteins and inflammatory signaling pathway activation (Venardos et al., 2014; Zheng et al., 2019). At the next stage, the progression of AS contributes to the transition of valvular interstitial cells to an osteoblast-like phenotype with the subsequent aortic valve calcification (Bogdanova et al., 2018). Although the pathogenesis of AS goes far beyond just hemodynamic valve damage, this mechanism plays a significant role in patients with BAV.

Despite the fact that the pathophysiological mechanisms of calcification are being actively studied, there is still no effective preventive tactics to avoid surgical intervention. Further experimental researches, both *in vitro* and *in vivo*, as well as clinical studies are required for adequate treatment and prophylaxis of valvular calcification. Contemporary diagnostic tools including positron emission tomography (PET) and PET/computed tomography (CT) represent new opportunities to evaluate the inflammation and calcification process in real clinical settings.

Being integrated molecular anatomic imaging modality PET/CT technique could provide detailed information about the specific disease activity *in vivo*. In recent years, PET has utilized two radioactive tracers: ^{18}F-fluorodeoxyglucose (^{18}F-FDG) to estimate the degree of inflammation of the aortic valve in patients with AS and ^{18}F-fluoride (^{18}F-NaF) to assess calcification. ^{18}F-FDG is a glucose analogue which is accumulated in metabolically active cells and represents a sensitive marker of vascular inflammation (Tawakol et al., 2006; Honda et al., 2016). ^{18}F-NaF is a bone tracer that binds to hydroxyapatite, a crucial component of valvular calcification with greater surface area in regions of microscopic calcification. Higher valvular ^{18}F-NaF uptake is independently associated with more rapid disease progression and therefore represents a potential biomarker of AS disease activity (Dweck et al., 2014). ^{18}F-NaF PET/CT can also be considered as diagnostic tool providing assessment of calcification level along with estimation of treatment efficacy. However, there no data about valve inflammation and calcification activity *in vivo* measured by PET/CT using outlined above radiotracers in BAV and TAV patients and their prognostic value.

The aim of this study was to assess prognostic value of valvular inflammation and calcification measured by ^{18}F-FDG and ^{18}F-NaF PET/CT in patients with TAV and BAV.

MATERIALS AND METHODS

Patient Population

Study enrolled 71 patients aged 40–70 years with mild, moderate and severe asymptomatic calcific AS. Patients with rheumatic heart disease, infective endocarditis, severe chronic kidney disease, prior thoracic radiotherapy or aortic valve interventions were not included. Patient enrollment was performed in 2015–2016. The study protocol was approved by the research ethics committee of the Almazov National Medical Research Centre, and all participants provided written informed consent.

As part of the baseline examination, information on conventional cardiovascular risk factors including age, sex, hypertension, diabetes, lipid profile, smoking, family history of cardiovascular diseases was analyzed. Standard echocardiography using the Vivid 7.0 system (GE, United States) was performed to all participants by the same team of sonographers and cardiologists, while all images were analyzed by experienced readers at the same laboratory according to the American Society of Echocardiography Guidelines (Baumgartner et al., 2009). Doppler echocardiographic values of AS severity included peak aortic jet velocity, mean gradient obtained by the Bernoulli formula, and aortic valve area calculated by the continuity equation and indexed to body surface area (iAVA). Left ventricular systolic function was assessed using left ventricular ejection fraction as measured by the biplane Simpson method. Stroke volume was also calculated and indexed to body surface area.

Multimodal Imaging Using Combined ^{18}F-FDG and ^{18}F-NaF PET/CT

PET/CT with ^{18}F-FDG and ^{18}F-NaF was performed in all patients (Discovery 710, GE). The study protocol of ^{18}F-NaF PET/CT included intravenous injection of a 300 MBq ^{18}F-NaF during at least 0,5–1 min. CT scan for attenuation correction was

TABLE 1 | Clinical characteristics of patients.

	TAV			BAV			p
	Men (*n* = 15)	**Women (*n* = 16)**	**p**	**Men (*n* = 19)**	**Women (*n* = 21)**	**P**	
Age, years	63 [57; 65]	64 [62; 67]	0.52	54 [49; 62]	60 [55; 64]	0.33	**0.001***
Body mass index, kg/m^2	28.7 [26.7; 30.6]	31.8 [28.5; 34.2]	0.1	26.7 [25.2; 33.0]	27.2 [25.6; 31.5]	0.7	0.07
Body surface area, m^2	2.08 [1.94; 2.18]	1.84 [1.74; 2.01]	**0.01***	2.14 [2.00; 2.20]	1.82 [1.73; 2.04]	**0.01***	0.91
Systolic BP, mm Hg	140 [130; 150]	148 [128; 160]	0.5	130 [120; 140]	130 [125; 150]	0.7	0.72
Diastolic BP, mm Hg	80 [75; 85]	80 [80; 88]	0.13	80 [75; 85]	80 [70; 85]	0.6	0.37
Hypertension, n (%)	14 (93%)	15 (94%)	0,96	15 (79%)	19 (90%)	0.31	0.26
Coronary atherosclerosis, n (%)	12 (80%)	6 (38%)	**0,017***	1 (5%)	5 (24%)	0.057	**0.0001***
Diabetes mellitus, n (%)	7 (47%)	3 (19%)	0.097	2 (11%)	1 (5%)	0.49	**0.007***
Atrial fibrillation, n (%)	4 (27%)	3 (19%)	0.6	2 (11%)	3 (14%)	0.72	0.26
Total cholesterol, mmol/l	4.45 [3.87; 5.42]	5.65 [5.03; 5.91]	**0.002***	4.88 [4.03; 5.63]	5.54 [4.78; 6.32]	0.15	0.46
HDL-C, mmol/l	1.12 [1.03; 1.33]	1.49 [1.27; 1.66]	**0.002***	1.06 [0.89; 1.41]	1.49 [1.27; 1.66]	**0.02***	0.54
LDL-C, mmol/l	2.64 [1.96; 3.22]	3.67 [3.09–3.87]	**0.004***	2.91 [2.29; 3.62]	3.55 [2.88–3.96]	0.12	0.53
Glucose, mmol/l	6.01 [5.46; 6.46]	5.70 [5.25; 6.36]	0.49	5.66 [5.14; 5.89]	5.43 [5.21; 5.68]	0.33	**0.034**
eGFR, mL/min/1,73m^2	76.0 [67.5; 91.2]	73.9 [61.89; 91.78]	0.56	89.1 [75.8; 93.4]	75.84 [65.89; 81.70]	**0.03**	0.44
ACE inhibitors/ARBs, n (%)	13 (87%)	12 (75%)	0.41	14 (74%)	14 (67%)	0.63	0.31
B-blockers, n (%)	12 (80%)	9 (56%)	0.16	12 (63%)	15 (71%)	0.58	0.98
Warfarin, n (%)	2 (13%)	0	0.13	2 (11%)	1 (5%)	0.49	0.86
DOACs, n (%)				0	2 (10%)	0.17	0.2
Aspirin, n (%)	13 (87%)	9 (56%)	0.06	8 (42%)	8 (38%)	0.8	**0.009**
Statins, n (%)	14 (93%)	11 (69%)	0.08	9 (47%)	9 (43%)	0.77	**0.01**
Echocardiography							
Vmax, m/s	2.8 [2.4; 3.6]	3.0 [2.7; 3.5]	0.5	2.9 [2.6; 3.5]	3.0 [2.5; 3.2]	0.65	0.83
Mean gradient, mm Hg	17.0 [13.2; 29.0]	20.0 [15.5; 27.0]	0.48	22.0 [15.0; 29.0]	22.0 [15.0; 26.0]	0.56	0.92
Index AVA, cm^2/m^2	0.59 [0.50–0.88]	0.73 [0.57–0.85]	0.89	0.77 [0.63–0.96]	0.61 [0.54–0.75]	0.12	0.56
LVEF (%)	64 [59; 73]	68 [64; 73]	0.22	64 [60; 66]	65 [63; 67]	0.42	0.09
Index SV (ml/m^2)	35.4 [31.2; 41.9]	29.0 [25.5; 32.7]	**0.02**	36.9 [27.9; 51.3]	29.7 [23.4; 38.3]	0.06	0.36
AR (moderate, severe), n (%)	1 (7%)	0	0.29	5 (26%)	2 (10%)	0.16	0.06
PET/CT							
Agatston score, AU	1,388 [513; 2,705]	736 [380; 1,153]	**0.003***	2,324 [1,038; 3,020]	933 [404; 1,394]	**0.004***	0.55
Index Agatston score, AU/m^2	676 [222; 1,513]	392 [220; 615]	**0.017***	1,153 [527; 1,361]	480 [236; 664]	**0.17**	0.42
^{18} F-FDG TBR max	1.18 [1.08; 1.42]	1.10 [1.04; 1.16]	**0.014***	1.14 [1.07; 1.24]	1.09 [1.02; 1.16]	0.15	0.39
^{18} F-FDG TBR mean	1.14 [1.03; 1.20]	1.09 [1.01; 1.14]	0.18	1.08 [1.01; 1.16]	1.05 [1.02; 1.11]	0.3	0.49
^{18} F-FDG TBR max/mean	1.54 [1.36; 1.84]	1.39 [1.26; 1.47]	**0.031***	1.40 [1.30; 1.55]	1.34 [1.23; 1.49]	0.31	0.4
^{18} F-NaF TBR max	1.65 [1.45; 1.83]	1.44 [1.18; 1.68]	**0.033***	1.64 [1.38; 1.88]	1.33 [1.18; 1.82]	**0.047***	0.97
^{18} F-NaF TBR mean	1.45 [1.28; 1.65]	1.25 [1.18; 1.41]	**0.031***	1.43 [1.32; 1.72]	1.23 [1.15; 1.50]	**0.004***	0.83
^{18} F-NaF TBR max/mean	2.03 [1.94; 2.53]	1.89 [1.77; 2.08]	**0.033***	2.26 [1.87; 2.67]	1.74 [1.57; 2.64]	**0.059**	0.95

ACE inhibitors, angiotensin-converting-enzyme inhibitors; AR, aortic regurgitation; ARBs, angiotensin receptor blockers; BAV, bicuspid aortic valve; BP, blood pressure; DOACs, direct oral anticoagulants; eGFR - estimated glomerular filtration rate using MDRD formula; HDL-C, high-density lipoprotein cholesterol; iAVA, indexed aortic valve area; LDL-C, low-density lipoprotein cholesterol; LVEF, left ventricular ejection fraction; SV, stroke volume; TAV, tricuspid aortic valve; TBR max, maximal tissue to background ratio; TBR mean, mean tissue to background ratio; TBR max/mean, maximal tissue to mean background ratio; V max, peak aortic jet velocity.
Statistically significant values with p *less than 0.05 are highlighted.*

performed in 90 min after radiotracer injection, during that period the patient was positioned on the bed in the supine position, and the patient's heart was located in the center of the field of view. Immediately after the CT series PET emission scanning was performed in static mode without changing of the patient's position. PET-CT with ^{18}F-FDG required special preprocedural planning. To avoid the physiological ^{18}F-FDG uptake in myocardium the patient should keep to low-carbohydrate diet within 3 days before the PET procedure. The study was performed after 12 h of fasting. The study protocol included intravenous injection of a 300–370 MBq ^{18}F-FDG during at least 0,5–1 min. The CT scan for attenuation correction was performed in 60 min after radiotracer injection, during that period the patient was positioned on the bed in the supine position, and the patient's heart was located in the center of the field of view. Immediately after the CT series PET emission scanning of the same area was performed in static mode without changing the patient's position. PET-CT images were reconstructed on the 128 × 128 matrix in the 300 mm field using the iterative reconstruction algorithm.

Semiquantitative analysis of the PET/CT results was implemented. Image interpretation was performed by two independent experts (experienced in cardiovascular imaging). The circular region of interest (ROI) of 3.52 square millimeters was drawn around areas of maximal radiotracers uptake in the valve (target) and then maximal and mean levels of standardized uptake value (SUV) were estimated within ROI. Blood-pool activity was used as a background with assessment of SUV maximal and mean levels within the same ROI in the left atrium. Maximal, mean and maximal/mean ratios between SUV mean target and SUV mean background (TBR max, TBR mean and TBR max/mean) were calculated. CT calcium scoring was

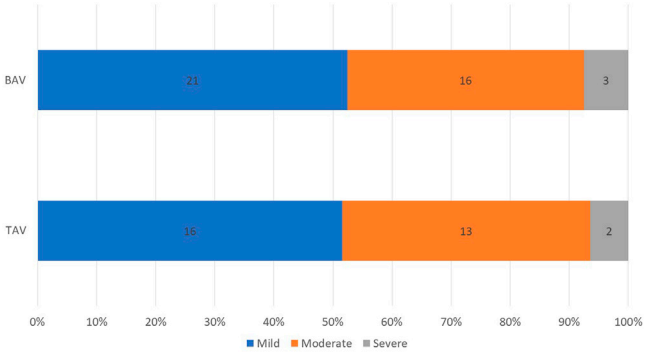

FIGURE 1 | Distribution of AS severity by groups.

performed using dedicated software and expressed as Agatston units.

Follow-Up

During follow-up visit all patients underwent general clinical assessment and echocardiography as the first-line imaging modality in AS. Follow up was performed in 18 ± 6 months after the baseline examination. The analysis of inter-observer reproducibility of peak velocity and mean gradient measurements in patients with AS (based on 20 echocardiographic examinations assessed by 25 different experts) demonstrated better reproducibility of peak aortic velocity (Vmax) compared with mean gradient assessment, suggesting that Vmax should be the preferred indicator to evaluate AS progression (Sacchi et al., 2018). Significant AS progression was defined as deterioration during follow up to the moderate or severe AS in patients with previously mild AS, or identification of severe AS in patients with previously moderate AS, along with increasing of the Vmax more than 0.3 m/s per year or new aortic valve surgery indications.

Statistical Analysis

Continuous variables were tested for normality by the Shapiro-Wilk test. Results were expressed as mean ± SD, median (percentile 25–75), or percentage as appropriate. Differences between groups were evaluated by a 2-way ANOVA; Wilcoxon rank sum test. Spearman's rank correlation coefficient was used to assess the relationship between CT, PET and echocardiographic values. The clinical factors associated with fast AS progression were analyzed using the univariate binary logistic regression analysis. Statistically

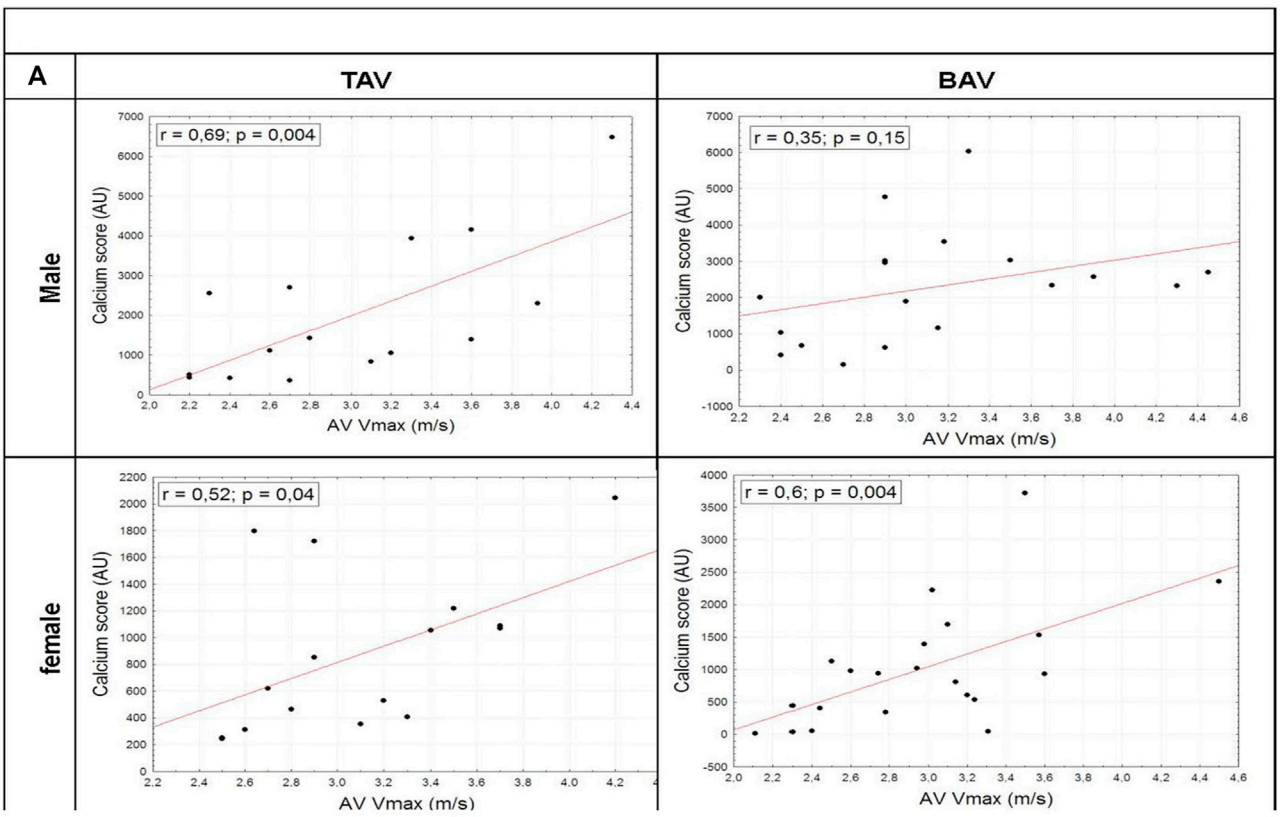

FIGURE 2 | Correlations between Vmax and Agatston score **(A)**, V max and ^{18}F-NaF TBR max, ^{18}F-NaF TBR mean, ^{18}F-NaF TBR max/mean in BAV and TAV groups **(B)**.

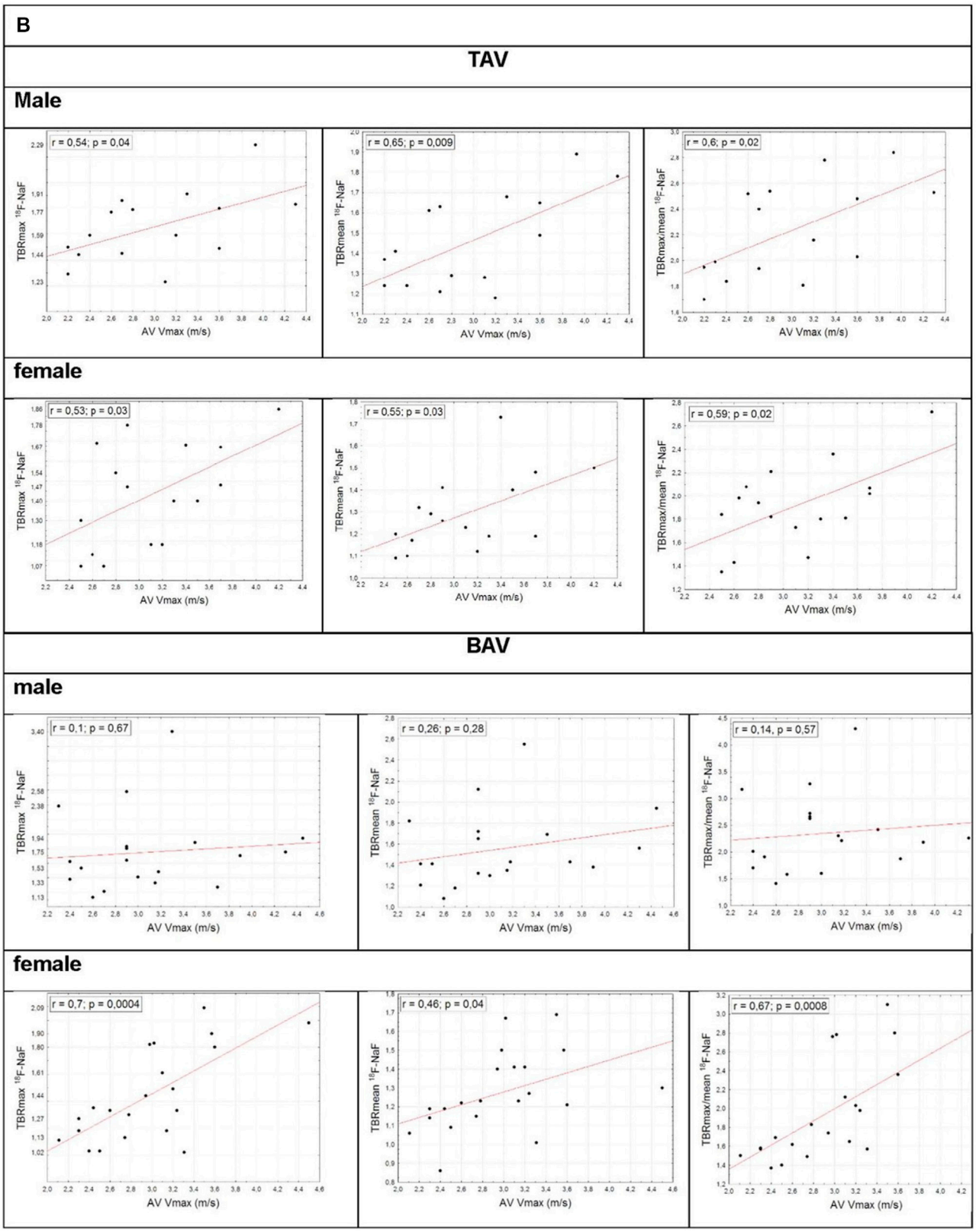

FIGURE 2 | (Continued).

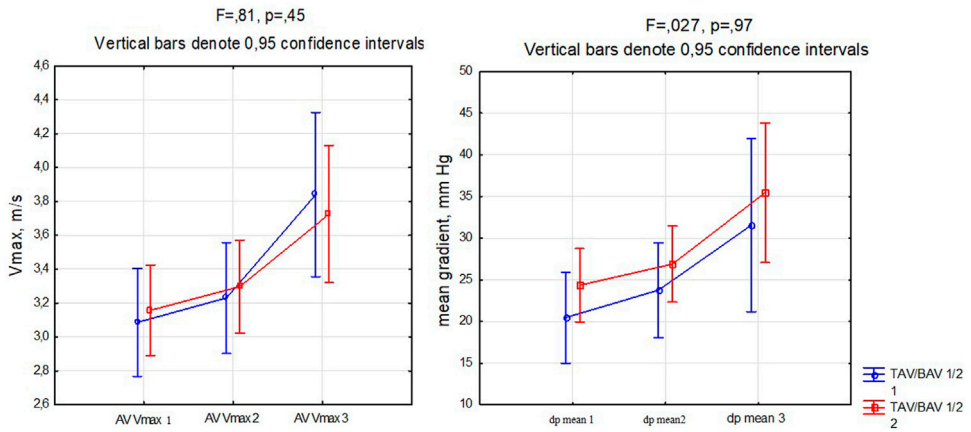

FIGURE 3 | V max and mean gradient dynamics by groups during follow up.

TABLE 2 | Results of univariate binary logistic regression analysis to investigate predictors of AS progression.

	As (*n* = 71)			TAV (*n* = 31)			BAV (*n* = 40)		
	OR	**95% CI**	**p**	**OR**	**95% CI**	**p**	**OR**	**95% CI**	**P**
Age	1.06	0.99–1.14	0.07	1.001	0.88–1.14	0.99	1.08	0.99–1.18	0.09
Male	0.61	0.24–1.58	0.31	0.68	1.66–2.8	0.59	0.55	0.14–2.05	0.37
Smoking	1.3	0.39–4.34	0.67	2.55	0.69–16.55	0.33	0.7	0.12–4.18	0.7
Obesity	1.15	0.43–3.01	0.78	1.47	0.36–6.05	0.59	0.76	0.18–3.1	0.7
Hypertension	1.17	0.26–5.33	0.84	0.93	0.53–16.39	0.96	1.09	0.17–6.85	0.92
TAV	0.57	0.22–1.5	0.26						
Diabetes mellitus	1.91	0.57–6.41	0.3	2	0.43–9.53	0.38	0.92	0.76–11.17	0.95
Coronary atherosclerosis	**2.83**	**1.03–7.73**	**0.043**	2.76	0.58–12.98	0.2	2.2	0.46–10.62	0.33
Cholesterol	0.92	0.68–1.25	0.61	0.93	0.65–1.33	0.7	0.89	0.53–1.51	0.68
LDL-C	0.81	0.55–1.2	0.3	0.88	0.59–1.32	0.54	0.67	0.34–1.32	0.25
HDL-C	0.99	0.24–4.14	0.99	0.52	0.04–6.89	0.62	1.31	0.23–7.53	0.76
CRP	0.99	0.9–1.1	0.91	1.08	0.91–1.28	0.4	0.89	0.67–1.17	0.38
GFR	1.01	0.98–1.05	0.49	1.01	0.97–1.06	0.64	1.02	0.97–1.08	0.51
β-blockers	1.93	0.67–5.56	0.22	1.65	0.36–7.6	0.52	2.29	0.51–10.28	0.28
ACE inhibitors/ARBs	3.13	0.91–10.75	0.07	2.17	0.33–14.06	0.42	3.75	0.69–20.38	0.13
Calcium channel blockers	0.81	0.3–2.22	0.68	0.64	0.15–2.77	0.55	0.9	0.22–3.75	0.89
Statins	**13.5**	**2.84–64.15**	**0.001**			0.99	**9.6**	**1.77–52.17**	**0.009**
Aspirin	**2.96**	**1.09–8.02**	**0.03**	1.25	0.26–5.94	0.78	**4.89**	**1.21–19.71**	**0.02**
Warfarin	2.31	0.36–14.77	0.38			0.99	0.92	0.08–11.17	0.95
Vmax	**8.44**	**2.65–26.89**	**0.000**	**19.81**	**2.4–163.18**	**0.006**	**5.2**	**1.31–20.61**	**0.02**
mean gradient	**1.14**	**1.06–1.23**	**0.000**	**1.24**	**1.06–1.45**	**0.006**	**1.12**	**1.02–1.21**	**0.02**
iAVA	**0.03**	**0.002–0.56**	**0.02**	**0.003**	**0.00–0.62**	**0.03**	0.11	0.004–2.12	0.16
Severity	**3.7**	**1.55–8.82**	**0.003**	**4.35**	**1.09–17.28**	**0.04**	**3.46**	**1.1–10.84**	**0.03**
index SV	0.97	0.92–1.01	0.16	0.97	0.88–1.08	0.6	0.97	0.92–1.03	0.28
IMMLV	1.01	0.99–1.02	0.17	1.02	0.99–1.05	0.21	1.01	0.99–1.02	0.35
EF	0.98	0.91–1.05	0.49	0.94	0.86–1.04	0.24	1.004	0.89–1.13	0.95
Calcium Score	**1.001**	**1–1.001**	**0.014**	**1.002**	**1.001–1.004**	**0.01**	**1**	**1–1.001**	**0.34**
Calcium Score/m2	**1.001**	**1–1.002**	**0.009**	**1.004**	**1.001–1.007**	**0.01**	**1.001**	**1–1.002**	**0.28**
^{18}F-NaF TBR max	**7.06**	**1.55–32.27**	**0.01**	**3652.59**	**14.3–932,992.9**	**0.004**	2.45	0.59–10.16	0.22
^{18}F-NaF TBR mean	**27.47**	**2.96–254.47**	**0.004**	**38,979.76**	**26.38–576,021.09**	**0.01**	6.2	0.67–57.09	0.11
^{18}F-NaF TBR max/mean	**4.88**	**1.66–14.36**	**0.004**	**681.93**	**5.19–89,651.37**	**0.009**	2.48	0.83–7.38	0.1
^{18}F-FDG TBR max	17.72	0.63–497.02	0.09	29.84	0.24–3764.89	0.17	7.48	0.05–1030.57	0.42
^{18}F-FDG TBR mean	6.78	0.12–373.06	0.35	29.76	0.1–8701.57	0.24	0.16	0.00–332	0.64
^{18}F-FDG TBR max/mean	6.1	0.64–58.57	0.12	21.12	0.55–806.95	0.1	1.72	0.08–36.22	0.73

ACE inhibitors, angiotensin-converting-enzyme inhibitors; ARBs, angiotensin receptor blockers; BAV, bicuspid aortic valve; BP, blood pressure; CRP, C-reactive protein, DOACs, direct oral anticoagulants; EF, ejection fraction; eGFR, estimated glomerular filtration rate using MDRD formula; HDL-C, high-density lipoprotein cholesterol; iAVA – indexed aortic valve area; IMMLV, indexed myocardial mass of left ventricle; LDL-C, low-density lipoprotein cholesterol; LVEF, left ventricular ejection fraction; SV, stroke volume; TAV, tricuspid aortic valve; TBR max, maximal tissue to background ratio; TBR mean, mean tissue to background ratio; TBR max/mean, maximal tissue to mean background ratio; V max, peak aortic jet velocity. Statistically significant values with p *less than 0.05 are highlighted.*

TAV

	B	S. E.	Wald	df	Sig.	Exp (B)	Lower	Upper
Vmax	3,529	1,662	4,508	1	,034	34,075	1,312	885,064
18F-NaF TBRmax	9,062	3,677	6,073	1	,014	8621,593	6,390	11632283,00
Constant	-24,705	9,054	7,445	1	,006	,000		

Area	Standard Error	Asymptotic significance	Asymptotic 95% C. I. Lower Bound	Asymptotic 95% C. I. Upper Bound
,942	,040	,000	,863	1,000

Sensitivity 80%

Specificity 87%

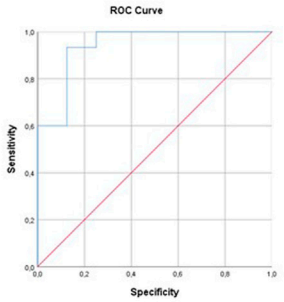

BAV

	B	Standard Error	Wald	df	Sig.	Exp (B)	95% C. I. for EXP(B) Lower	95% C. I. for EXP(B) Upper
Vmax	1,649	,702	5,510	1	,019	5,201	1,313	20,610
Constant	-5,701	2,210	6,655	1	,010	,003		

Area	Standard Error	Asymptotic significance	Asymptotic 95% C. I. Lower Bound	Asymptotic 95% C. I. Upper Bound
,714	,087	,027	,544	,884

Sensitivity 50%

Specificity 73%

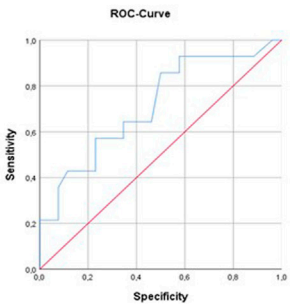

FIGURE 4 | Results of the ROC analysis in all patient and TAV and BAV groups.

significant variables ($p < 0.05$) were included in multivariate logistic regression analysis. Statistical significance was taken at level $p < 0.05$. The predictive value of model was estimated using ROC analysis. The sensitivity and specificity for the resulting model were also calculated. All analyses were carried out using Statistica 12 and IBM SPSS Statistics 26.0.

RESULTS

Clinical Assessment

Patients were divided into two groups according to the valve morphology: BAV and TAV. Aortic valve phenotype was identified by echocardiography and cardiac CT. Patient with TAV were significantly older compared to those with BAVs (**Table 1**). In TAV and BAV groups male:female ratio was 0.9:1. There were no differences found in systolic and diastolic blood pressure and prevalence of hypertension. Unsurprisingly, incidence of coronary atherosclerosis and diabetes mellitus were higher in TAV patients, as well as statin and antiplatelet therapy use and serum glucose level. Nevertheless, there were not significant differences in lipid profile parameters, that may be related to high dyslipidemia prevalence in both groups.

In order to examine whether there was a difference in obtained variables according to age analysis of variance for categorical data and analysis of covariance for quantitative characteristics were performed to compare groups regarding to age. After adjusting for age, serum glucose level in both groups did not differ. When comparing TAV and BAV patients while considering age, results didn't show statistically significant difference for hypertension, coronary atherosclerosis and diabetes mellitus. TAV and BAV patients were matched for the major echocardiography AS severity parameters: Vmax, mean gradient and iAVA. There were no differences revealed by groups in EF, indexed SV and moderate-to-severe AR incidence. Distribution according to the AS severity was comparable in both groups (**Figure 1**).

Males and females in both groups were matched for age, body mass index, systolic and diastolic blood pressure, prevalence of hypertension and diabetes mellitus. Body surface area and creatinine level were predictably higher in men. Glomerular filtration rate was lower in women in BAV group, at the same time both male and female patients did not suffer significant chronic renal disease. In TAV group worse lipid profile in women may be explained by coronary atherosclerosis frequency, and thus intensive statin therapy in men. Both groups were matched in medical therapy. Hemodynamic severity of AS determined by Vmax, mean transvalvular gradient, iAVA was comparable in men and women in TAV and BAV groups. Both groups did not differ in valvular calcification value (Agatston score) and

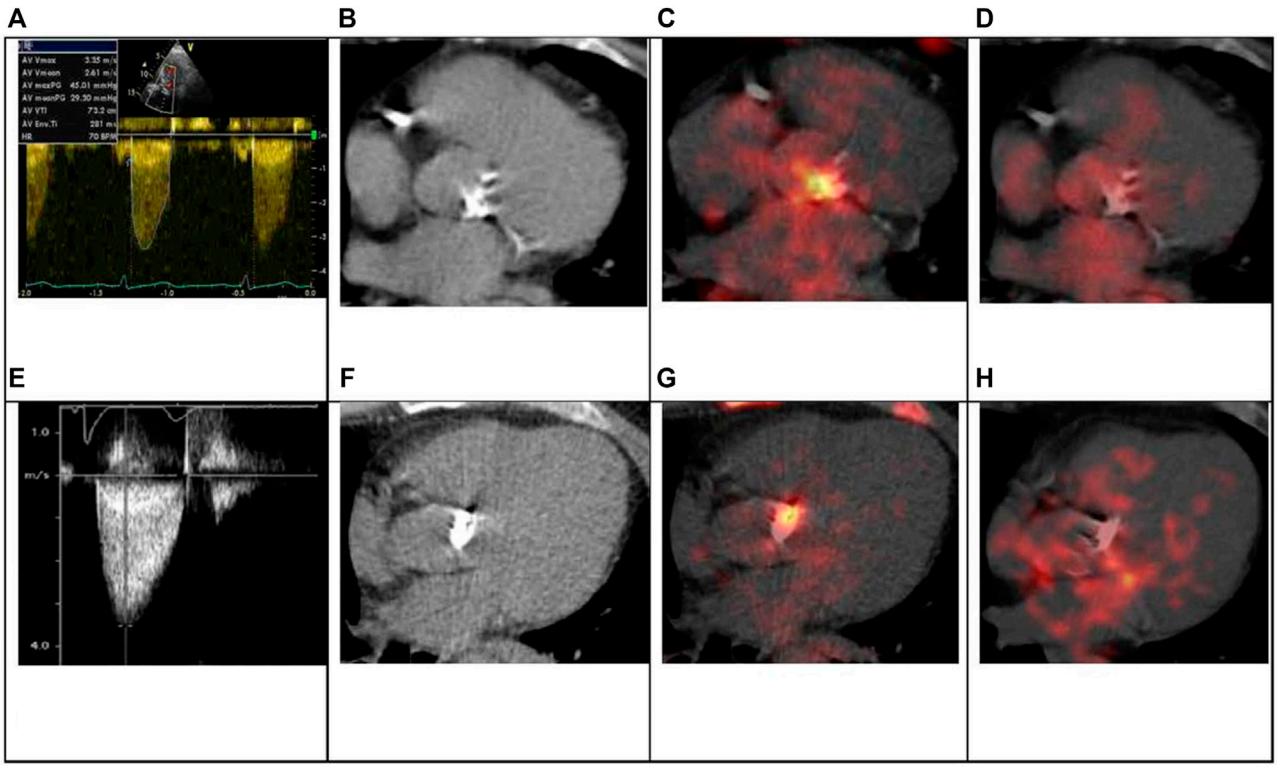

FIGURE 5 | TAV and BAV patient with moderate AS. 64-years old asymptomatic patient with TAV. Echo parameters: Vmax 3.35 m/s, mean gradient 29 mmHg **(A)**. CT revealed and severe aortic valve calcification: Agatston Score 3139 AU **(B)**. ^{18}F-NaF PET/CT demonstrated marked accumulation of the radiotracer: ^{18}F-NaF TBR max 1.91 **(C)**. ^{18}F-FDG valve accumulation was not significant, ^{18}F-FDG TBR max 1.05 **(D)**. 2 years hence symptoms manifested, Vmax increased to 4.2 m/s and aortic valve replacement was performed. 51-years old patient with BAV. Echo parameters: Vmax 3.4 m/s, mean gradient 30 mmHg **(E)**. CT revealed and severe aortic valve calcification: Agatston Score 4769 AU **(F)**. ^{18}F-NaF PET/CT demonstrated significant accumulation of the radiotracer: ^{18}F-NaF TBR max 2.58 **(G)**. ^{18}F-FDG valve uptake was not increased, ^{18}F-FDG TBR max 1.17 **(H)**. There was no clinical or hemodynamic progression registered during 4-years follow up.

disease activity (^{18}F-NaF TBR max, ^{18}F-NaF TBR mean, max/mean TBR). The degree of valvular inflammation estimated by ^{18}F-FDG TBR max, TBR mean and TBR max/mean also did not differ in TAV and BAV patients. Additionally inflammatory tracer activity did not differ in groups despite ACE inhibitors/ARBs or statins treatment. Predictably, in both groups aortic valve Agatston Score was higher in men. Furthermore, PET/CT demonstrated more advanced calcification in male patients. In TAV patients ^{18}F-FDG accumulation was higher in men, that possibly related to greater prevalence of the coronary atherosclerosis and systemic chronic inflammation in this subgroup. Agatston score and ^{18}F-NaF TBR max, ^{18}F-NaF TBR mean, ^{18}F-NaF TBR max/mean values correlated with AS severity estimated by Vmax in men and women with TAV. In BAV group this association was true only in female patients (**Figure 2**).

Follow up

All 71 patients underwent clinical and echocardiographic evaluation during follow-up visits. The mean time interval between the two echocardiograms was 16.8 ± 4.2 months. Doppler transthoracic echocardiography was performed to all patients.

Following the results, the rate of AS progression varied highly between patients. During this time period the mean systolic gradient and Vmax value increased from 22.3 to 25.8 mm Hg and from three to 3.2 m/s respectively, while iAVA parameter was stable (0.73 cm^2/m^2). The annual growth rate of Vmax value was 0.11 ± 0.27 m/s per year.

There was also third follow up visit in 34 patients. Mean time period was 46 months (from 22 to 74 months). It was demonstrated that progression rates measured by Vmax and mean gradient did not differ between groups (**Figure 3**).

Significant AS progression was defined as deterioration during follow up to the moderate or severe AS in patients with previously mild AS, or identification of severe AS in patients with previously moderate AS, along with increasing of the Vmax more than 0.3 m/s per year or new aortic valve surgery indications. Among all participants 29 (41%) patients fulfilled such criteria.

The clinical predictors of AS progression were analyzed using the binary logistic regression. Based on the univariate binary logistic regression analysis data, it was demonstrated that baseline AS severity, V max, mean gradient, iAVA, aortic valve Agatston Score, ^{18}F-NaF TBR, coronary atherosclerosis and use of statins and antiplatelet agents contributed to rapid progression of AS (**Table 2**). Notable, that in BAV patients iAVA was not associated with AS progression that possible related to technical complexity of AVA quantification due to not truly circular left ventricular outflow tract.

The multivariate binary logistic regression analysis of these predictors was performed to evaluate independent predictors of AS progression. In TAV group close correlation between Agatston Score and ^{18}F-NaF TBRmax was observed ($r = 0.78$; $p < 0.001$). Due to multicollinearity of these parameters, we included in the multivariate regression analysis ^{18}F-NaF TBRmax. The most important positive predictors of AS progression in TAV obtained by multivariate logistic regression analysis were Vmax and ^{18}F-NaF TBRmax. Whereas in BAV the highest predictive value showed model included Vmax (**Figure 4**). All presented indicators showed good predictive value. **Figure 5** demonstrates clinical cases of TAV and BAV patient with moderate AS and different progression rates of valvular heart disease.

DISCUSSION

It was demonstrated that baseline AS severity (measured by V max) correlated with high risk of disease progression, that was in accordance with previous studies (Bohbot et al., 2017; Yang et al., 2021). The effect of aortic valve phenotype on the AS progression remains uncertain. Most of the earlier studies that analyzed the factors associated with AS progression did not evaluate the role of valve phenotype. Most commonly, TAV and BAV patients were analyzed together, with a large predominance of TAV patients and/or comorbidities that differed greatly between men and women. The few studies that assessed the impact of valve phenotype on AS progression demonstrated no association between BAV and progression rate (Chan et al., 2010; Nguyen et al., 2015). In our cohort, men and women in both groups were well matched for all clinical data and hemodynamic severity of AS. In TAV and BAV patients progression rates were similar.

Over the last decade it has become possible to evaluate AS pathogenesis *in vivo*. The degree of valve inflammation, measured by ^{18}F-FDG accumulation, is considered to be most crucial at the early stages of the AS, while high ^{18}F-NaF accumulation, representing microcalcification activity, is known to be a strong predictor of AS progression (Dweck et al., 2012; Dweck et al., 2014). Nevertheless, inhibitors of calcification pathway (denosumab and alendronic acid) were found to be ineffective in the context of inhibition of AS progression measured by Vmax, Agatston Score and ^{18}F-NaF. However, this study did not take into account valve phenotype and gender differences in AS calcification (Pawade et al., 2021).

We estimated the role of the main pathological processes—inflammation and calcification in AS progression with consideration to the traditional cardiovascular risk factors in TAV and BAV patients. Our study demonstrated comparable valve calcification degree and microcalcification activity in patients with different aortic valve morphology. Moreover, in TAV and BAV groups the rate of ^{18}F-FDG accumulation did not correlate with AS severity, while ^{18}F-NaF accumulation was associated with both echocardiography parameters of AS severity and aortic valve Agatston index by CT. However, males with BAV did not demonstrate correlation between AS severity, aortic valve calcification degree and disease activity. Multivariate analysis revealed that rapid AS progression in TAV patients was determined by baseline AS severity, and calcification activity by of ^{18}F-NaF PET/CT. While in BAV patients baseline aortic valve calcification did not influence on AS prognosis whereas Vmax value along with age were the main predictors of AS progression. Biological background for this phenomenon is still unclear but might be due to different significance of provocative aortic valve calcification factors in women and men, such as vitamin D receptors and growth factors (Aggarwal et al., 2013). Taking this into consideration, therapy, targeted on inhibition of calcification mechanisms, seems to be more beneficial for patients with TAV.

To date, there are no effective medical therapies to delay AS progression and the only available treatment option for symptomatic severe AS remains surgical or transcatheter aortic valve replacement with a mechanical or bioprosthetic valve. However, these two techniques may be associated with significant complications: the implantation of a mechanical valve increases the risk of thrombosis and requires a life-long anticoagulation therapy. On the other hand, the bioprosthetic valves are prone to structural deterioration, resulting in limited long-term durability that can lead to reoperation in less than 15 years (Zhao et al., 2016). Effective medical treatment is required to reverse the progression of AS and to reduce the need for aortic valve replacement that would contribute to better clinical outcome in such patients. Novel drug therapies should target valve-specific and sex-related signaling pathways to be more effective.

Our results should be interpreted in the context of certain limitations.

The study population is not large enough to exclude the contribution of other risk factors to AS progression. While the study points to several new risk factors, the mechanisms by which they operate are not clear. It is important that groups were not matching by age. Despite we took into account age as a cofactor, its influence cannot be completely ruled out. The progression of AS was presumed to be linear based on follow up echocardiography scans over an average of 18 ± 6 months. However, it is possible that AS progression was not linear and the correlation between AS progression and aortic valve calcification was variable with different intervals.

In conclusion, ^{18}F-NaF PET/CT may be considered as the valuable predictor for hemodynamic progression of calcific AS in case of TAV. ^{18}F-FDG PET/CT does not play a significant role to predict the development of severe aortic stenosis.

DATA AVAILABILITY STATEMENT

The original contributions presented in the study are included in the article/supplementary material, further inquiries can be directed to the corresponding author.

ETHICS STATEMENT

The studies involving human participants were reviewed and approved by the Ethics Committee of the Almazov National Medical Research Centre. The patients/participants provided their written informed consent to participate in this study.

AUTHOR CONTRIBUTIONS

PM, EZ, and EM performed data collection, statistical analysis, and wrote manuscript. DR and PM analyzed PET/CT. DR and OM provided the critical revision of the manuscript. All authors contributed to the article and approved the submitted version.

FUNDING

This study has been supported by the Ministry of Health, grant number AAAA-A20-120092490041-0.

REFERENCES

Aggarwal, S. R., Clavel, M. A., Messika-Zeitoun, D., Cueff, C., Malouf, J., Araoz, P. A., et al. (2013). Sex Differences in Aortic Valve Calcification Measured by Multidetector Computed Tomography in Aortic Stenosis. *Circ. Cardiovasc Imaging* 6, 40–47. doi:10.1161/CIRCIMAGING.112.980052

Baumgartner, H., Hung, J., Bermejo, J., Chambers, J. B., Evangelista, A., Griffin, B. P., et al. (2009). Echocardiographic Assessment of Valve Stenosis: EAE/ASE Recommendations for Clinical Practice. *Eur. J. Echocardiogr.* 10, 1–25. doi:10.1093/ejechocard/jen303

Bogdanova, M., Kostina, A., Zihlavnikova Enayati, K., Zabirnyk, A., Malashicheva, A., Stensløkken, K. O., et al. (2018). Inflammation and Mechanical Stress Stimulate Osteogenic Differentiation of Human Aortic Valve Interstitial Cells. *Front. Physiol.* 9, 1635. doi:10.3389/fphys.2018.01635

Bohbot, Y., Rusinaru, D., Delpierre, Q., Marechaux, S., and Tribouilloy, C. (2017). Risk Stratification of Severe Aortic Stenosis with Preserved Left Ventricular Ejection Fraction Using Peak Aortic Jet Velocity: An Outcome Study. *Circ. Cardiovasc. Imaging* 10, e006760. doi:10.1161/CIRCIMAGING.117.006760

Chan, K. L., Teo, K., Dumesnil, J. G., NiTam, A. J., and Tam, J. (2010). Effect of Lipid Lowering with Rosuvastatin on Progression of Aortic Stenosis: Results of the Aortic Stenosis Progression Observation: Measuring Effects of Rosuvastatin (ASTRONOMER) Trial. *Circulation* 121, 306–314. doi:10.1161/CIRCULATIONAHA.109.900027

Dweck, M. R., Jones, C., Joshi, N. V., Fletcher, A. M., Richardson, H., White, A., et al. (2012). Assessment of Valvular Calcification and Inflammation by Positron Emission Tomography in Patients with Aortic Stenosis. *Circulation* 3125, 76–86. doi:10.1161/CIRCULATIONAHA.111.051052

Dweck, M. R., Jenkins, W. S., Vesey, A. T., Pringle, M. A., Chin, C. W., Malley, T. S., et al. (2014). 18F-sodium Fluoride Uptake is a Marker of Active Calcification and Disease Progression in Patients with Aortic Stenosis. *Circ. Cardiovasc. Imaging* 7 (2), 371–378. doi:10.1161/CIRCIMAGING.113.001508

Eveborn, G. W., Schirmer, H., Lunde, P., Heggelund, G., Hansen, J. B., and Rasmussen, K. (2014). Assessment of Risk Factors for Developing Incident Aortic Stenosis: the Tromsø Study. *Eur. J. Epidemiol.* 29, 567–575. doi:10.1007/s10654-014-9936-x

Honda, A., Tahara, N., Nitta, Y., Tahara, A., Igata, S., Bekki, M., et al. (2016). Vascular Inflammation Evaluated by [18F]-Fluorodeoxyglucose-Positron Emission Tomography/computed Tomography Is Associated with Endothelial Dysfunction. *Arterioscler. Thromb. Vasc. Biol.* 36, 1980–1988. doi:10.1161/ATVBAHA.116.307293

Iung, B., Delgado, V., Rosenhek, R., Price, S., Prendergast, B., Wendler, O., et al. (2019). Contemporary Presentation and Management of Valvular Heart Disease: The EURObservational Research Programme Valvular Heart Disease II Survey. *Circulation* 140, 1156–1169. doi:10.1161/CIRCULATIONAHA.119.041080

Martinsson, A., Östling, G., Persson, M., Sundquist, K., Andersson, C., Melander, O., et al. (2014). Carotid Plaque, Intima-Media Thickness, and Incident Aortic Stenosis: A Prospective Cohort Study. *Arterioscler. Thromb. Vasc. Biol.* 34, 2343–2348. doi:10.1161/ATVBAHA.114.304015

Nguyen, V., Cimadevilla, C., Estellat, C., Codogno, I., Huart, V., Benessiano, J., et al. (2015). Haemodynamic and Anatomic Progression of Aortic Stenosis. *Heart* 101, 943–947. doi:10.1136/heartjnl-2014-307154

Pawade, T. A., Doris, M. K., Bing, R., White, A. C., Forsyth, L., Evans, E., et al. (2021). Effect of Denosumab or Alendronic Acid on the Progression of Aortic Stenosis: A Double-Blind Randomized Controlled Trial. *Circulation* 143, 2418–2427. doi:10.1161/CIRCULATIONAHA.121.053708

Roberts, W. C., and Ko, J. M. (2005). Frequency by Decades of Unicuspid, Bicuspid, and Tricuspid Aortic Valves in Adults Having Isolated Aortic Valve Replacement for Aortic Stenosis, with or without Associated Aortic Regurgitation. *Circulation* 111 (7), 920–925. doi:10.1161/01.CIR.0000155623.48408.C5

Sacchi, S., Dhutia, N. M., Shun-Shin, M. J., Zolgharni, M., Sutaria, N., Francis, D. P., et al. (2018). Doppler Assessment of Aortic Stenosis: A 25-operator Study Demonstrating Why Reading the Peak Velocity is Superior to Velocity Time Integral. *Eur. Heart J. Cardiovasc. Imaging* 19, 1380–1389. doi:10.1093/ehjci/jex218

Shen, M., Tastet, L., Capoulade, R., Arsenault, M., Bédard, É., Clavel, M. A., et al. (2020). Effect of Bicuspid Aortic Valve Phenotype on Progression of Aortic Stenosis. *Eur. Heart J. Cardiovasc. Imaging* 21, 727–734. doi:10.1093/ehjci/jeaa068

Stewart, B. F., Siscovick, D., Lind, B. K., Gardin, J. M., Gottdiener, J. S., Smith, V. E., et al. (1997). Clinical Factors Associated with Calcific Aortic Valve Disease. Cardiovascular Health Study. *J. Am. Coll. Cardiol.* 29, 630–634. doi:10.1016/s0735-1097(96)00563-3

Tawakol, A., Migrino, R. Q., Bashian, G. G., Bedri, S., Vermylen, D., Cury, R. C., et al. (2006). *In Vivo* 18F-fluorodeoxyglucose Positron Emission Tomography Imaging Provides a Noninvasive Measure of Carotid Plaque Inflammation in Patients. *J. Am. Coll. Cardiol.* 48, 1818–1824. doi:10.1016/j.jacc.2006.05.076

Vahanian, A., Beyersdorf, F., Praz, F., Milojevic, M., Baldus, S., Bauersachs, J., et al. (2022). 2021 ESC/EACTS Guidelines for the Management of Valvular Heart Disease. *Eur. Heart J.* 43, 561–632. doi:10.1093/eurheartj/ehab395

Venardos, N., Nadlonek, N. A., Zhan, Q., Weyant, M. J., Reece, T. B., Meng, X., et al. (2014). Aortic Valve Calcification is Mediated by a Differential Response of Aortic Valve Interstitial Cells to Inflammation. *J. Surg. Res.* 190, 1–8. doi:10.1016/j.jss.2014.03.051

Yan, A. T., Koh, M., Chan, K. K., Guo, H., Alter, D. A., Austin, P. C., et al. (2017). Association between Cardiovascular Risk Factors and Aortic Stenosis: The CANHEART Aortic Stenosis Study. *J. Am. Coll. Cardiol.* 69, 1523–1532. doi:10.1016/j.jacc.2017.01.025

Yang, L. T., Boler, A., Medina-Inojosa, J. R., Scott, C. G., Maurer, M. J., Eleid, M. F., et al. (2021). Aortic Stenosis Progression, Cardiac Damage, and Survival: Comparison between Bicuspid and Tricuspid Aortic Valves. *JACC Cardiovasc. Imaging* 14, 1113–1126. doi:10.1016/j.jcmg.2021.01.017

Zhao, D. F., Seco, M., Wu, J. J., Edelman, J. B., Wilson, M. K., Vallely, M. P., et al. (2016). Mechanical versus Bioprosthetic Aortic Valve Replacement in Middle-Aged Adults: A Systematic Review and Meta-Analysis. *Ann. Thorac. Surg.* 102, 315–327. doi:10.1016/j.athoracsur.2015.10.092

Zheng, K. H., Tsimikas, S., Pawade, T., Kroon, J., Jenkins, W. S. A., Doris, M. K., et al. (2019). Lipoprotein(a) and Oxidized Phospholipids Promote Valve Calcification in Patients with Aortic Stenosis. *J. Am. Coll. Cardiol.* 73, 2150–2162. doi:10.1016/j.jacc.2019.01.070

Conflict of Interest: The authors declare that the research was conducted in the absence of any commercial or financial relationships that could be construed as a potential conflict of interest.

Publisher's Note: All claims expressed in this article are solely those of the authors and do not necessarily represent those of their affiliated organizations, or those of the publisher, the editors and the reviewers. Any product that may be evaluated in this article, or claim that may be made by its manufacturer, is not guaranteed or endorsed by the publisher.

frontiers | Frontiers in Pharmacology

REVIEW
published: 02 June 2022
doi: 10.3389/fphar.2022.835825

Models and Techniques to Study Aortic Valve Calcification *in Vitro*, *ex Vivo* and *in Vivo*. An Overview

Maria Bogdanova[1†], *Arsenii Zabirnyk*[1,2*†], *Anna Malashicheva*[3], *Daria Semenova*[3], *John-Peder Escobar Kvitting*[4], *Mari-Liis Kaljusto*[4], *Maria del Mar Perez*[5], *Anna Kostareva*[6,7], *Kåre-Olav Stensløkken*[1], *Gareth J Sullivan*[1,8,9,10,11‡], *Arkady Rutkovskiy*[1,12‡] and *Jarle Vaage*[1,2,13‡]

[1]Department of Molecular Medicine, Institute of Basic Medical Sciences, University of Oslo, Oslo, Norway, [2]Department of Research and Development, Division of Emergencies and Critical Care, Oslo University Hospital, Oslo, Norway, [3]Institute of Cytology, Russian Academy of Sciences, Saint Petersburg, Russia, [4]Department of Cardiothoracic Surgery, Oslo University Hospital, Oslo, Norway, [5]Sanifit Therapeutics, Palma de Mallorca, Spain, [6]Almazov National Medical Research Centre, Saint Petersburg, Russia, [7]Department of Woman and Children Health, Karolinska Institute, Stockholm, Sweden, [8]Norwegian Center for Stem Cell Research, Oslo University Hospital and University of Oslo, Oslo, Norway, [9]Institute of Immunology, Oslo University Hospital, Oslo, Norway, [10]Hybrid Technology Hub - Centre of Excellence, Institute of Basic Medical Sciences, University of Oslo, Oslo, Norway, [11]Department of Pediatric Research, Oslo University Hospital, Oslo, Norway, [12]Department of Pulmonary Diseases, Oslo University Hospital, Oslo, Norway, [13]Institute of Clinical Medicine, University of Oslo, Oslo, Norway

Aortic valve stenosis secondary to aortic valve calcification is the most common valve disease in the Western world. Calcification is a result of pathological proliferation and osteogenic differentiation of resident valve interstitial cells. To develop non-surgical treatments, the molecular and cellular mechanisms of pathological calcification must be revealed. In the current overview, we present methods for evaluation of calcification in different *ex vivo*, *in vitro* and *in vivo* situations including imaging in patients. The latter include echocardiography, scanning with computed tomography and magnetic resonance imaging. Particular emphasis is on translational studies of calcific aortic valve stenosis with a special focus on cell culture using human primary cell cultures. Such models are widely used and suitable for screening of drugs against calcification. Animal models are presented, but there is no animal model that faithfully mimics human calcific aortic valve disease. A model of experimentally induced calcification in whole porcine aortic valve leaflets *ex vivo* is also included. Finally, miscellaneous methods and aspects of aortic valve calcification, such as, for instance, biomarkers are presented.

Keywords: aortic valve, interstitial cells, endothelial cells, calcification, animal models, calcified aortic valve disease, imaging

OPEN ACCESS

Edited by:
Paolo Poggio,
Monzino Cardiology Center (IRCCS), Italy

Reviewed by:
Najma Latif,
The Magdi Yacoub Institute, United Kingdom
Veronika Myasoedova,
Monzino Cardiology Center (IRCCS), Italy

***Correspondence:**
Arsenii Zabirnyk
arsenii.zabirnyk@medisin.uio.no

[†]*These authors have contributed equally to this work and share first authorship*

[‡]*These authors have contributed equally to this work*

Specialty section:
This article was submitted to Experimental Pharmacology and Drug Discovery, a section of the journal Frontiers in Pharmacology

Received: *14 December 2021*
Accepted: *29 April 2022*
Published: *02 June 2022*

Citation:
Bogdanova M, Zabirnyk A, Malashicheva A, Semenova D, Kvitting J-PE, Kaljusto M-L, Perez MdM, Kostareva A, Stensløkken K-O, Sullivan GJ, Rutkovskiy A and Vaage J (2022) Models and Techniques to Study Aortic Valve Calcification in Vitro, ex Vivo and in Vivo. An Overview. Front. Pharmacol. 13:835825. doi: 10.3389/fphar.2022.835825

1 INTRODUCTION

Calcific aortic valve disease (CAVD) is a slowly progressing disorder starting with non-symptomatic thickening and sclerosis of valve leaflets. Severe calcification causes deformation of the valve tissue and ultimately aortic stenosis (AS). It is the most common form of valve disease in the Western world and it will become an increasing health burden with an ageing populations (Stewart et al., 1997; Nkomo et al., 2006; Takkenberg et al., 2008; Osnabrugge et al., 2013).

Calcification of the aortic valve is an active, proliferative process that results from inflammation, fibrosis and bone matrix formation (Rajamannan et al., 2011; Mathieu et al., 2014; Rutkovskiy et al.,

2017), mediated by the signaling pathways common to valvulogenesis and osteogenesis (Dutta and Lincoln, 2018). Currently, the main therapeutic option is open heart surgery and replacement with a valve prosthesis, although endovascular or minimally invasive techniques are being introduced for an increasing number of patients. Considering the costs and risks involved in surgical and endovascular replacement, pharmacological inhibition of CAVD ought to be a priority of research (Bhatia et al., 2016).

The basic mechanisms of aortic valve calcification are still poorly understood. Unraveling the cellular and molecular mechanisms of valve calcification may open up new therapeutic options, which is why researchers are in need of reliable and relevant models (Pawade et al., 2015). The valve interstitial cells (VIC) are believed to play a key role in the calcification process and VIC in culture appear to be the most relevant *in vitro* model for valve calcification (Takkenberg et al., 2008; Mathieu et al., 2014; Rutkovskiy et al., 2017). This is particularly true due to the lack of good animal models–the pathophysiology of aortic stenosis is quite unique to humans (Sider et al., 2011; Gomez Stallons et al., 2016). Experimentally induced calcification in VIC is an accurate and affordable model of *in vitro* aortic valve calcification. It is also suitable for screening potential pharmacological inhibitors. Different techniques or variants of *in vitro* models that are used in investigations leading to inconsistencies across the studies (Goto et al., 2019). This is also true for *ex vivo* and *in vivo* models of the disease, where the methods vary wildly.

Presently available models to study aortic valve calcification are not optimal, however, they are what we have for now. Exact techniques for measuring the amount of calcification as well as exact content of trace elements are important parts of research studies. Good methods for evaluating aortic valve calcification by different imaging techniques have become increasingly important due to catheter-based implantation of valve prostheses. Exact information about the calcification of the valve and valvular annulus are decisive for a successful result. The purpose of this article is to give an overview of methods for investigating cellular and molecular mechanisms of aortic valve calcification as well as techniques to measure the amount of calcium and calcification. Cultures of VIC have been given special attention as they are extensively used to study the cellular and molecular mechanisms of calcification. Furthermore, we present an overview of different *in vitro*, *ex vivo*, and *in vivo* models to study calcification as well as methods to investigate calcification and CAVD in patients.

2 MORPHOLOGY OF THE AORTIC VALVE

Human aortic valve leaflets have three main layers: the *fibrosa* facing the aorta, the *spongiosa* in the middle and the *ventricularis* facing the ventricle. This tri-layer structure is populated with VIC, and the surface is covered with a monolayer of valve endothelial cells (VEC). VICs are able to synthesize and regulate remodeling of extracellular matrix components. VEC function as a barrier, a signaling interface, they produce a number of substances that potentially regulate VIC, and may have an active role in valve calcification (Tao et al., 2012; Rattazzi and Pauletto, 2015). Injury to the valve endothelium might even be the trigger of the whole process. In a healthy valve, VIC are quiescent and have characteristics akin to fibroblasts. Under certain conditions VIC can undergo differentiation to either myofibroblasts or osteoblast-like cells (Rutkovskiy et al., 2017). At the time of surgery, approximately 13% of stenotic valves have inclusions of osteoblasts and osteoclasts along with organized lamellar bone matrix. Around 83% have signs of dystrophic calcification, possibly mediated by myofibroblasts (Mohler et al., 2001). While the exact mechanism is unclear, the myofibroblasts may contract the extracellular matrix, creating cellular aggregates (nodules), where the cells undergo apoptosis. This leads to calcium phosphate precipitation around apoptotic bodies (Chen and Simmons, 2011) and turns micro-calcification into macro-calcification.

3 MEASURING AMOUNTS OF CALCIUM

3.1 In Cell Cultures

3.1.1 Alizarin Red Staining and Quantification of Calcification in Cell Cultures

Alizarin Red (1.2-dihydroxyanthraquinone) staining is the most common method used to assess calcification in cell culture. It stains mineralized matrix, binding to different bivalent ions, mostly calcium. Although it is not the most accurate method to detect calcium content, it is optimal in terms of time consumption, simplicity, and cost (Bowler and Merryman, 2015). Alizarin Red provides a visual picture of calcium distribution in cell culture. It is also possible to quantify the signal by extracting the dye with acetic acid and measuring its concentration spectroscopically. Another common method for identification of calcium deposits is von Kossa staining. The latter dye unlike Alizarin Red reacts with phosphates and carbonates in calcium deposits (Puchtler and Meloan, 1978; Prins et al., 2014). An alternative method for quantifying calcification is cetylpyridinium chloride extraction. This method is less labor intensive, but less sensitive than Alizarin Red (Gregory et al., 2004). Another method to quantify calcium in cell cultures is the colorimetric method. This method needs solubilization of calcium deposits with HCl. The calcium content of HCl supernatants is then determined colorimetrically using commerical kits. This technique can also be used for tissue biopsies (Jono et al., 2000; Poggio et al., 2014; Hortells et al., 2015; Gayrard et al., 2020). In addition to that, many other calcium deposits detection methods have been developed including fluorescent and peptide–based dyes (Lee et al., 2012; Macri-Pellizzeri et al., 2018; Sim et al., 2018).

3.2 *Ex vivo*

3.2.1 Microscopy

Standard light microscopy today has a limited place in the analysis of mineral content. However, some information may be obtained with polarized light microscopy. For instance, ectopic deposits and amorphous masses may be characterized as

containing apatite (Cottignoli et al., 2015a). More detailed information about mineral content can be detected by confocal microscopy collecting Raman spectra. This has been used in a few studies attempting to characterize the mineral content of calcified valves, sometimes in combination with infrared spectra (Mangialardo et al., 2012) or powder X-ray diffraction (Gourgas et al., 2020). Raman spectra can assess the crystallinity of mineral deposits, and peaks in the spectra suggest that the main mineral in calcified valves is carbonated hydroxyapatite (Gourgas et al., 2020). Unfortunately, however, there are severe limitations as to how much qualitative and quantitative information can be obtained regarding mineral content and composition of calcified aortic valves using techniques based on light microscopy.

3.2.2 Electron Microscopy

Both scanning and transmission electron microscopy have been used in several studies to characterize the biomineralization of calcified aortic valves and in particular their morphology (Mangialardo et al., 2012; Danilchenko et al., 2013; Cottignoli et al., 2015a; Cottignoli et al., 2015b; Gourgas et al., 2020). These techniques also show disturbances in the organic parts of the leaflets and the extracellular matrix such as disorganized bundles of collagen fibers. It is also described "the presence of biological niches within the calcified extracellular matrix, small, unfilled cavities inside rock that may be formed through a variety of processes" (Cottignoli et al., 2015b). These techniques also show details of different shapes of the crystalline structure: semispherical, laminar crystals, and spherical particles that make the calcified masses. The masses are described as bioapatite and also form needle or rod like crystals (Cottignoli et al., 2015b). Electron microscopy is the method with the highest resolution, but it is very labor-intensive, making its routine application difficult. However, additional methods are necessary for qualitative studies of calcification and crystals.

3.2.3 Micro-Computed Tomography (Micro-CT)

A novel method to describe the morphology and density of calcification and minerals in explanted aortic valves is micro-CT (Orzechowska et al., 2014). Micro-CT has a resolution of one micron; it is suitable for studying porosity, bone thickness, density, particle size, fiber orientation, etc. The level of x−ray signal attenuation is proportional to the material density and thickness. This could be interpreted as different levels of calcification. Soft tissue presents with very low attenuation calcifications, while bone matrix causes high attenuation, which creates high contrast images. Using micro-CT it is possible to assess the amount of calcified tissue in relation to the total volume of valve leaflet or the whole valve. In a study of explanted aortic valves, micro-CT showed a strong correlation between the amount of calcification and the severity of aortic stenosis (Chitsaz et al., 2012). Another study using micro-CT identified aortic valve deposits as B-type carbonate-containing hydroxyapatite (Orzechowska et al., 2014). In general, however, this technique does not give detailed information on the mineral composition, rather information on material density. Thus, it may give ratios between soft tissue and more calcified (harder) tissue.

3.2.4 Inductively Coupled Plasma Optical Emission Spectrometry and Inductively Coupled Plasma Mass Spectrometry (ICP-OES and ICP-MS)

The information obtained from this technique (chemical analysis) is not comparable to the others, as the approaches described above are able to study the crystal morphology, particle size, etc. However, ICP-OES and ICP-MS are techniques used for elemental analysis concentration (Hanć et al., 2011). There are some drawbacks, such as, it is a destructive technique: you have to digest the samples before analysis.

These techniques are superior for quantifying calcium (see 4.2.2.) and a broad series of trace elements (Heitkemper et al., 1994; Baralkiewicz et al., 2007; Sneddon and Vincent, 2008; Kreitals and Watling, 2014; Paraskova et al., 2015). In particular, these techniques have been quite extensively used for industrial purposes with ramifications for biology and forensic medicine (Carpenter, 1985). In veterinary medicine this technique has been used, to measure 14 trace elements from bovine liver biopsies (Braselton et al., 1997). Recently, there has been a shift towards the utilization of ICP-MS which offers a low detection limit combined with high sample throughput. ICP-MS also offers analysis of at least 25 trace elements in a biological sample. With a few exceptions, the lower detection limit of trace element and minerals is 1 nmol/L or less (Wilschefski and Baxter, 2019).

3.2.5 Miscellaneous, Minerals and Crystals of Calcified Aortic Valves

Among other methods used for characterization of biomineralogy and chemical composition are X-ray microanalysis coupled with energy-dispersive X-ray (Danilchenko et al., 2013) and direct chemical analysis, X-ray diffraction and Fourier transform infrared (Prieto et al., 2011). However, these techniques are usually used as adjunctive methods and in combinations with other techniques. Until quite recently, there was little knowledge regarding the analysis of the exact composition of calcified aortic valves. However, modern techniques have taught us more about the composition, structure, and formation of calcified valves. Mineralogical analyses of calcified valves to gain information about crystallization may be important and possibly an underestimated part of understanding the calcification process.

3.3 Imaging *in vivo*

Reliable imaging of the aortic valve has become increasingly important in recent years in parallel with the increase of catheter-based valve replacements (Bettinger et al., 2017; Francone et al., 2020; Mittal and Marcus, 2021). Usually a multimodality approach is recommended for evaluation of calcification, the characteristics of the valve itself and the aortic root. There are excellent reviews discussing imaging far beyond the scope of this overview (Salemi and Worku, 2017;

Pawade et al., 2019; Francone et al., 2020; Ternacle and Clavel, 2020; Tzolos et al., 2020; Fletcher et al., 2021).

3.3.1 Echocardiography

Echocardiography is the standard clinical basis of all heart valve evaluations. It is safe, not expensive, widely available, and non-invasive. The key assessment criteria of aortic stenosis are combination of aortic valve area, mean gradient across the valve, and peak flow velocity. Details of the method including its limitations are beyond the scope of this review (Chong et al., 2019). Important to note is that echocardiography cannot quantify calcium. However, echocardiography is the standard technique to evaluate valve function, degeneration, leaflet stiffness due to fibrosis, and calcification of the aortic valve with the development of aortic stenosis. Transesophageal echocardiography provides better imaging than transthoracic, in particular to differentiate between tri- and bicuspid aortic valves (Yousry et al., 2012; Yousry et al., 2015).

3.3.2 Computed Tomography (CT)

CT is the method to choose to evaluate and quantify aortic valve calcification as calcium score measured by Agatston score "which accounts for both the density and volume of CT-measured calcium and correlates closely with the weight of calcium in explanted aortic valves" (Kang et al., 2010). Aortic valve calcium score also correlates well with calcific aortic valve disease progression and prognosis (Messika-Zeitoun et al., 2007; Nguyen et al., 2015) and is closely associated with severity of aortic stenosis measure by echocardiography (Cowell et al., 2003; Cueff et al., 2011; Tastet et al., 2017). For exact evaluation of the role of assessment of aortic valve calcification by CT, it is necessary to be aware of a series of pitfalls as described by *Pawade et al.* (Pawade et al., 2019). This is particularly important in younger patients (<51 years) with bicuspid aortic valves where *Shen et al.* found no correlation between mean gradient across the aortic valve and aortic valve calcium density (Shen et al., 2017). Several studies have also shown that women have lower calcification loads than men for the same aortic stenosis severity (Aggarwal et al., 2013; Gourgas et al., 2020). Standard CT cannot detect the early stages with micro-calcification, it can only visualize confluent areas of macro-calcification (Bailey et al., 2016). However, recently contrast-enhanced CT has been shown to be able to assess not only calcium, but also non-calcific (fibrotic) aortic valve composition, allowing assessment of early CAVD (Cartlidge et al., 2021; Grodecki et al., 2021).

3.3.3 Magnetic Resonance Imaging (MRI)

MRI is not routinely used and is far less widespread than CT. It is rather a supplementary imaging technique. However, it has an increasing role in the planning of endovascular aortic valve procedures (Mittal and Marcus, 2021). In the recent consensus document by the European Society of Cardiovascular Radiology, it is explicitly stated that MRI have many potential advantages in such situations (Francone et al., 2020). This includes all necessary measurements of the valve and the aortic root as well as evaluation of ventricular function and the aorta. Furthermore, MRI has some distinct advantages to avoid the use of contrast in cases with severe kidney failure. Unfortunately, it does not provide reliable calcium score.

3.3.4 Positron Emission Tomography (PET)

PET uses radioactive isotopes, which concentrate in regions with high metabolic activity, thus being able to detect changes on the molecular and cellular level before anatomic changes occur. 18F-sodiumfluoride accumulation was found to correlate with calcification in the aortic valve (Dweck et al., 2014) and it is able to detect micro-calcification in the vasculature (Vancheri et al., 2019) and in valves (Hutcheson et al., 2014). 18F-sodiumfluoride binds to hydroxyapatite on calcified nodules and is quantitatively shown to be associated with faster progression of CAVD (Dweck et al., 2014; Jenkins et al., 2015). Furthermore, accumulation of 18F-sodiumfluoride is also associated with bio-prosthetic aortic valve degeneration (Cartlidge et al., 2019). So far PET is primarily a research tool and less used in clinical investigations, partly due to costs and lower availability in clinical practice. However, PET may be helpful to develop our understanding of aortic stenosis, both its molecular background as well as its development, risk stratification, and progression in patients (Pai et al., 2006; Rojulpote et al., 2020). In particular, it may be a powerful tool when it localizes the process in 3D, in combination with CT and/or MRI (Tzolos et al., 2020).

4 COLLECTION OF HUMAN AORTIC VALVES FOR CELL ISOLATION

For studies in cell cultures, cells from human aortic valves are preferred in order to eliminate species differences. Exceptions are relevant when *in vivo* animal experiments are performed or when using transgenic models. Calcified human aortic valves are fairly easy to obtain if the laboratory is situated in the proximity of a cardiac surgery unit. Calcified aortic valves can be harvested from patients with aortic valve stenosis undergoing aortic valve replacement. Cells from a valve can be freshly isolated and usually retain moderate to high degree of viability. The degree of cell viability/quantity/proliferation for each donor is individual. It depends among others on the level of the valve calcification where severe calcified valves result in the inferior cell isolation yield. Of note: patients with rheumatic aortic valve stenosis, a late inflammatory complication of group A *Streptococcal pharyngitis*, represent a totally different disease (Wallby et al., 2013) which is not included or discussed here.

Healthy valves are less readily available. There are several potential sources of non-calcified human aortic valves (Rutkovskiy et al., 2017). The ideal one is from donor hearts that were considered unsuitable for transplantation. Other possibilities include valves from explanted hearts of heart transplant recipients.

For isolation of cells from explanted aortic valves, timing is critical, in particular for the isolation of VEC. By placing the leaflets in saline immediately after excision and keeping at +4 C enhances viability, opening a window of several hours for VEC

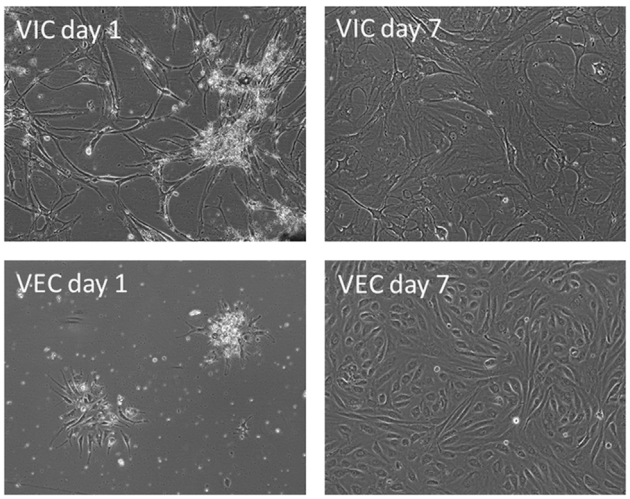

FIGURE 1 | Interstitial (VIC) and endothelial (VEC) cells isolated from human aortic valves shown on first and seventh days after isolation. Phase contrast microscopy.

isolation. VIC are less sensitive to time before isolation, however, we recommend isolation of VIC within the first 24 h. According to our experience with aortic valve cells from autopsy material acceptable viability can be expected for up to 24 h post mortem which is in accordance of what has been reported earlier (Gall et al., 1998). Gender may also be important: valves from men have more advanced calcification at the same age as women, whereas stenotic valves from women have increased levels of fibrosis compared to men (Aggarwal et al., 2013). It is also important to avoid mixing bicuspid (BAV) and tricuspid (TAV) aortic valves since there are differences in the molecular and cellular mechanisms that underlie calcification of BAV and TAV (Kostina et al., 2018).

5 ENDOTHELIAL AND INTERSTITIAL CELLS FROM HUMAN AORTIC VALVES

Handling of cells and cell cultures are presented in more details than other techniques here because it is probably the most widely spread and concise method to study the basic cellular and molecular events of aortic valve calcification. Additionally, cell culture models are also used for initial screening of potential inhibitory drugs (Dutta et al., 2021; Natorska et al., 2021; Parra-Izquierdo et al., 2021; Wang et al., 2021).

5.1 Isolation and Culture

The most widely used and reproducible techniques for isolation of VEC and VIC have been derived from methods that originally employed porcine material (Gould and Butcher, 2010). The quality of plastic on which the cell culture is seeded is crucial for good VIC growth. Normal practice is to use standard cell growth medium containing DMEM supplemented with 10–15% fetal bovine serum (FBS) and antibiotics. The day after isolation, the VICs are usually visible, and they present a fibroblast-like morphology (**Figure 1**). During cultivation, the media is changed twice a week until a confluence of 70–80% is attained (usually within 1 week, see **Figure 1**). At this point the VIC are harvested using trypsin/EDTA and seeded at a high density (we recommend to not exceed ratio of 1:2), which is a crucial factor for survival of VICs isolated from calcified valves. It is recommended to passage VICs after achieving density around 90–95%. VECs are usually isolated by swabbing cells from the surface of the leaflet or via vortexing collagenase–treated leaflets. On the second day in culture, the rosette-like colonies of VECs should form. VECs are grown until a confluence of 70–80% is attained (usually within 1 week, **Figure 1**). VEC then passaged at a ratio of 1:3. Primary cells in culture are known to change particular properties with each passage, thus the number of passages is important to report (Yperman et al., 2004; Goto et al., 2019). An important precaution with regards to the culture of primary VECs and VICs is to ensure they are mycoplasma-free, therefore all cultures should be kept in a quarantine area until a *mycoplasma* test has been conducted.

5.2 Purification and Characterization

Isolated VEC from calcified valves will invariably be contaminated with VICs, which will threaten to outgrow them over time. Therefore, an enrichment step is highly recommended, for instance, magnetic-activated cell sorting 1 week after initial isolation (Gould and Butcher, 2010). Human VEC can be enriched using the surface markers PECAM-1/CD31 (Platelet endothelial cell adhesion molecule-1), providing a discriminatory marker for enrichment. The main steps or the cell isolation procedure are summarized in **Figure 2**. Following enrichment, it is recommended to assess the purity of the respective cell populations using markers that allow the delineation of each cell type. The VEC population may be assessed using flow cytometry against the endothelial marker CD31 (Gould and Butcher, 2010) and/or von Willebrand factor (vWF) (Gould and Butcher, 2010) and VE-cadherin (Farrar and Butcher, 2014) (**Figure 3**). We routinely observe high purity, with 95% of the population being CD31 positive (**Figure 3**). Flow cytometry data are well in line with the immunocytochemistry staining. The cell population should not exhibit alpha-smooth muscle actin expression (αSMA) in immunocytochemistry assessment (**Figure 3**). However, using flow cytometry we observed that approximately 7.5% cells are positive for αSMA. This can suggest either VIC culures are contaminated or the presence of cells bearing both markers, such as VEC undergoing mesenchymal transition (**Figure 4**).

αSMA is common marker used to separate human VIC population from VECs (Gould and Butcher, 2010) and is useful to assess the purity of the VIC population. The expression of αSMA is low in healthy human valves, and relatively high in calcified valves (Olsson et al., 1994). Higher expression of αSMA is associated with myofibroblastic differentiation, which is one of the hallmarks of CAVD. It is suggested that cultured VICs can spontaneously differentiate into myofibroblast-like cells as they increase αSMA expression with time (Pho et al., 2008; Monzack and Masters, 2011; Latif et al., 2015a; Porras et al., 2017). The spontaneous myofibroblast differentiation is believed to be a result of the novel physical

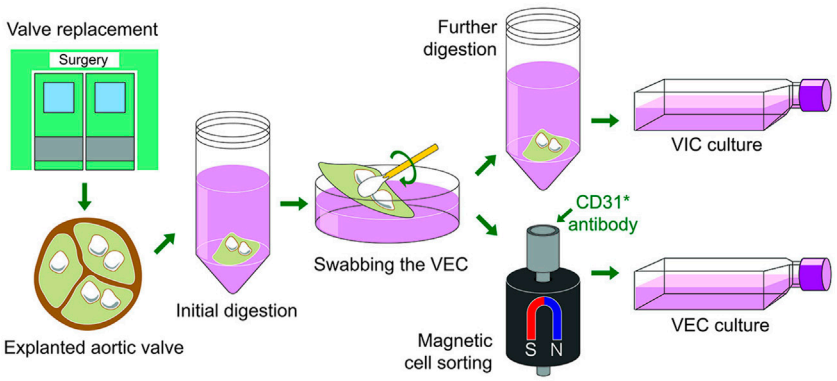

FIGURE 2 | A schematic overview of the main steps of the calcified human aortic valves collection, digestion and valvular interstitial and endothelial cells isolation.

environment, which influences cells via mechanoreceptors. It is well established that rigid substrates promote myofibroblast differentiation in fibroblasts. It may be related to the physical properties of the substrate (culture plastic) as stiffer substrates are known to promote myofibroblast phenotype (Yip et al., 2009). Some authors propose culturing VIC in "fibroblast medium" to potentially reduce expression of myofibroblastic markers such as αSMA, transgelin, and extra domain-A fibronectin (Latif et al., 2015a; Porras et al., 2017). Alternatively, one can try to use cells with low passage numbers to be as close to the original phenotype as possible.

Using flow cytometry, we observed that approximately 90% of VIC from calcified aortic valves were positive for αSMA (**Figure 4**). The presence of αSMA was further verified by immunostaining (**Figure 3**). Possible contamination with VEC in the VIC population was assessed by immunostaining for vWF, CD31, and VE-cadherin (**Figure 3**). This can be further validated using flow cytometry for CD31 (**Figure 4**). There has been efforts to find additional markers that are highly expressed in human VICs, for example, vimentin (Latif et al., 2007; Latif et al., 2015a), prolyl-4-hydroxilase (Taylor et al., 2000; Osman et al., 2006a) and markers of bone-morrow mesenchymal stem cells: fibroblast surface antigen (CD90) (Latif et al., 2007; Latif et al., 2015a) and CD44 (Latif et al., 2007). The relevance of these markers for separation of human VICs from VEC have not been confirmed. We observed expression of vimentin and CD90 in both human VEC and VIC populations and do not recommend the use of these markers for purification of human VIC. It has also been suggested that calponin can be utilized as a VIC marker, especially associated with progression of CAVD (Plazyo et al., 2018; Bogdanova et al., 2019).

5.3 2D or 3D Culture Models of Human Aortic Valve Cells

5.3.1 Interstitial Cells

2D models of culturing VIC and VEC are most common, although 3D cultures are used as well. 3D cultures have been suggested to have some advantages providing a more physiologically relevant model for the cells because VIC are influenced by their microenvironment (Hjortnaes et al., 2015; Ravi et al., 2015; Hjortnaes et al., 2016; van der Valk et al., 2018; Bracco Gartner et al., 2019). This is highlighted by Hjortnaes and co-workers when cell are cultured in 3D hybrid hydrogels composed of hyaluronic acid and gelatin (Hanć et al., 2011). They state the following: "The elastic modulus of 3D hydrogels used in our study (~20kPA) corresponds to the perceived modulus of the fibrosa as measured by micropipette aspiration up to 21 kPA" Furthermore, "We previously showed that the 3D hydrogel platform maintains a quiescent VIC phenotype identified in healthy heart valves, thus providing a platform to study phenotypic changes associated with CAVD" as well as "The 3D approach presented in this work can maintain healthy quiescent VIC population and thus can model the entire cellular process". However, there are several limitations of the 3D model. The hydrogel platform is static and the composition of their hydrogel is different when compared to the *in vivo* extracellular matrix. The 3D cultures are more difficult to subject to mechanical stimulation and the diffusion through the gel should be taken into account when performing chemical stimulations. Although 3D platform may in some ways be attractive, 2D cultures for VIC are still leading in the field due to simplicity and standardization. For general use, the superiority of 3D cultures use can so far be discussed.

5.3.2 Co-Cultures of Valve Endothelial and Interstitial Cell

Recent studies of the molecular and cellular mechanisms of CAVD have emphasized the importance of VEC-VIC interactions. Porcine VIC have reduced expression of the myofibroblastic gene αSMA when co-cultured with VECs (Butcher and Nerem, 2006), implying that VECs are involved in the regulation and maintenance of the VIC phenotype. This is also corroborated by several studies demonstrating that VECs inhibited myofibroblastic or osteogenic differentiation of porcine VIC in co-culture (Kennedy et al., 2009; Richards et al., 2013; Gould et al., 2014), suggesting an important role of VEC-VIC interaction for cellular valve homeostasis. Dysfunction or denudation of VECs, have also been implicated as an initiator of VIC transformation leading to calcification (Leopold, 2012;

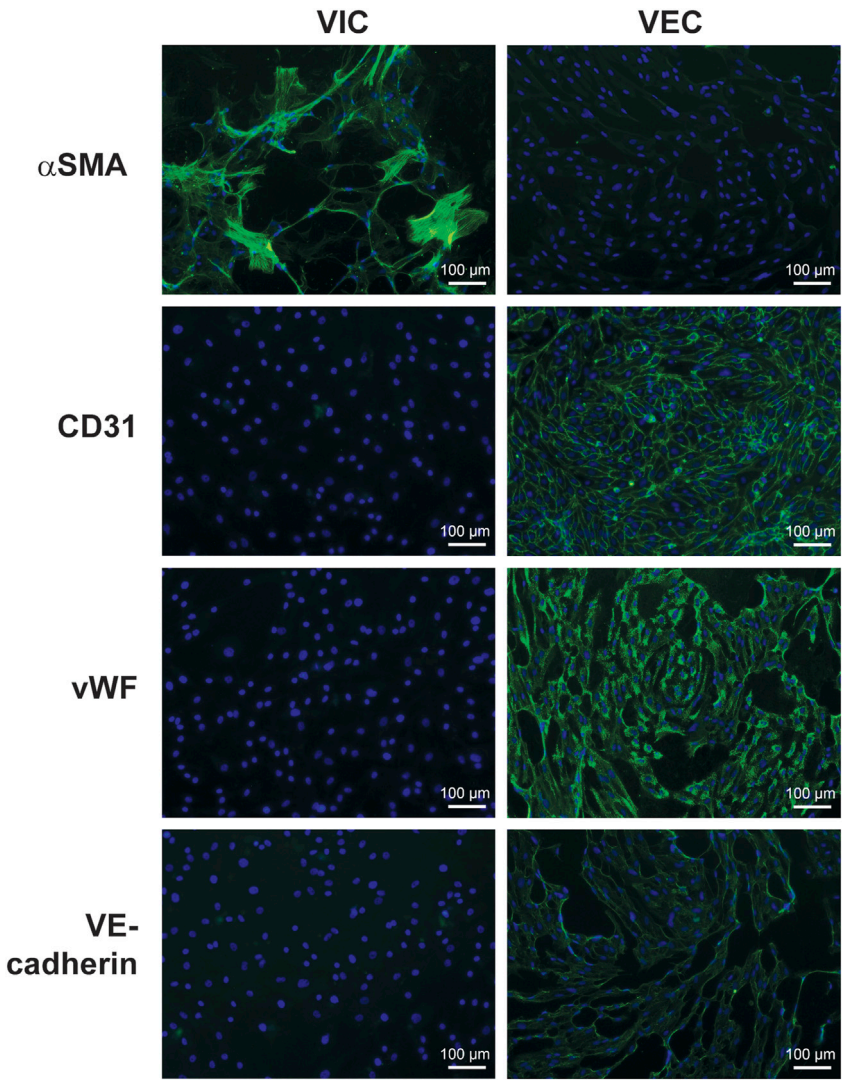

FIGURE 3 | Immunofluorescence staining for fibroblastic and endothelial markers in valve interstitial (VIC) and endothelial cells (VEC). Cells were isolated from human aortic valves with calcification (n = 3) and separated by magnetic-activated cell sorting. The pictures show expression of alpha-smooth muscle actin (αSMA) in VIC and cluster of differentiation 31 (CD31), vascular endothelial cadherin (VE-Cadherin), and von Willebrand factor (vWF) in VEC. The nuclei were stained with Hoechst 3342 (blue).

Gomel et al., 2018; Hulin et al., 2018). It was recently suggested that VEC isolated from different sides of the valve have a different effect on the VIC calcification through cadherin-11 (Johnson and Merryman, 2021).

Static 3D co-cultures of human VEC and VIC are suitable for studies of cell type interactions. We seeded VIC pre-mixed with collagen and when the gels were cast, VEC were seeded on top. The endpoints included gene expression changes, as well as the contraction of collagen gels by the VIC, being a function of their myofibroblast differentiation. More details on this topic are provided in **Section 5.4.3**. We also have positive experience with 2D co-cultures where the VIC are seeded at 90% density and then VEC are seeded directly on top of the VIC in the amount that is sufficient to achieve the same density in the top monolayer.

An interesting version of 3D co-cultures was recently reported by van der Valk et al., where they engineered a 3D-bioprinted model of a human aortic valve (van der Valk et al., 2018). In this study the aortic leaflet tissue was mechanically tested after micro-dissection of different layers. Leaflets were then constructed by bioprinting of 3D hydrogels with encapsulated human VIC. The hydrogels had been tuned to duplicate specific mechanical characteristics of the leaflets. It is too early to conclude how helpful this model is due to limited usage data.

5.4 Osteogenic Differentiation of Valve Interstitial Cells

Osteoblast- and osteoclast-like cells have been identified histologically in human calcified aortic valves (Mohler et al.,

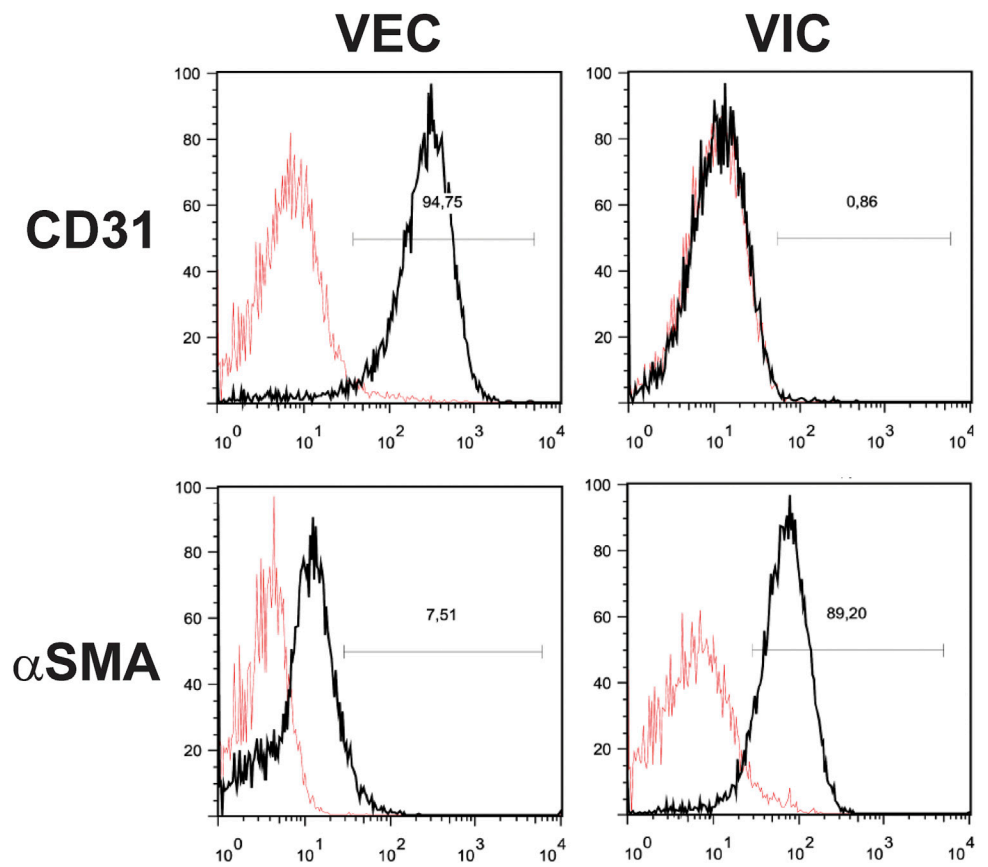

FIGURE 4 | Fluorescence-activated cell sorting (FACS) analysis of valve endothelial (VEC) and interstitial cells (VIC). Cells were isolated from aortic valves with calcification (n = 3). A representative image shows expression of the typical fibroblastic marker protein alpha-smooth muscle actin (αSMA) in VIC, but not in VEC and expression of typical endothelial cell marker CD31 in VEC, but not in VIC.

2001), but not in healthy aortic valves. Many markers that are attributed to osteoblasts have been found in valves of patients with CAVD and the majority of these markers are also expressed by VIC differentiated into osteoblast-like cells *in vitro* (Osman et al., 2007; Galeone et al., 2013; Zhang et al., 2014). The most common formulation of osteogenic medium that triggers calcification and expression of osteogenic markers in human VICs include beta-glycerophosphate, dexamethasone and ascorbic acid, which can be substituted with vitamin D (Osman et al., 2006a; Osman et al., 2006b; Osman et al., 2007; Babu et al., 2008; Galeone et al., 2013). Beta-glycerophosphate is the most potent component of most osteogenic media, as it donates a phosphate group to calcium ions to form calcium phosphate crystals, the main ingredient in mineral bone matrix. Beta-glycerophosphate induces transdifferentiation into osteoblast-like cells, thus increasing osteoblast activity and subsequent calcification (Babu et al., 2008). Dexamethasone stimulates both osteogenic and adipogenic differentiation depending on its concentration. The typical concentration that induces osteogenic differentiation is 0.1 μM, whereas higher concentrations are used to induce adipogenic differentiation (Zhao et al., 2018). Ascorbic acid is an additional cofactor that facilitates osteogenic differentiation by increasing collagen I synthesis (Ishikawa et al., 2004) and secretion (Langenbach and Handschel, 2013). The length of treatment in the majority of studies is 21 days (Osman et al., 2006a; Osman et al., 2006b; Osman et al., 2007; Babu et al., 2008). Basic osteogenic medium can be supplemented with BMP2, which has been demonstrated to be important for valve calcification (Zhang et al., 2014). It has been shown that treatment of human VIC with ATP (Osman et al., 2006a); BMP2 (Bone morphogenetic protein 2), BMP4, BMP7, TGFβ-1 or TGFβ-3 (Osman et al., 2006b) for 21 days can activate expression of alkaline phosphatase (*ALP*), which is a marker of late-stage osteoblastic differentiation. In our hands, the strongest effect was obtained when VICs were stimulated for 21 days with a basic osteogenic medium containing standard cell growth medium (DMEM, 10% FBS) supplemented with 10 mM beta-glycerophosphate, 0.1 μM dexamethasone and 50 μM ascorbic acid. This regimen induced reproducible and robust calcification (Bogdanova et al., 2019).

Another popular formulation of medium that promotes osteogenic differentiation of human VIC (termed "pro-calcifying medium") include DMEM supplemented with 5% FBS, 2 mM NaH_2PO_4 and 50 μg/ml ascorbic acid (Bouchareb et al., 2015; Rogers et al., 2017; Schlotter et al., 2018). Gotto *et al.* (Goto et al., 2019) showed that the calcification potential of

human VIC decreased with passage number in osteogenic medium, but not in pro-calcifying medium. Passage-dependent calcification of VIC cultured in osteogenic medium is regulated by abundance of tissue non-specific alkaline phosphatase (TNAP), an enzyme that hydrolyzes β-glycerophosphate to inorganic phosphate, which can be incorporated into calcium phosphate crystals promoting calcification. TNAP also plays a key role in mineralization by degrading inorganic pyrophosphate (calcification inhibitor) and providing free inorganic phosphate to induce calcification (Hui and Tenenbaum, 1998). Pro-calcifying medium contains inorganic phosphate and therefore does not require TNAP for the calcification process in VIC (Goto et al., 2019). Proteomic analysis of human VICs revealed induced expression of fibrosis- and calcification-related proteins under treatment with both osteogenic and pro-calcifying medium compared to control cells without stimulation, some of these proteins were shared between the two treatment groups (Schlotter et al., 2018). Further studies are required to gain a better understanding of which of the culture media best reflect the natural conditions of aortic valve calcification.

5.4.1 Myofibroblastic Differentiation of Valve Interstitial Cells

Myofibroblasts are defined as fibroblasts that have some properties of smooth muscle cells and are characterized by the presence of stress fibers composed mainly of αSMA, providing the ability to contract the extracellular matrix (Tomasek et al., 2002). The myofibroblast-like cells play an important role in extracellular matrix remodeling in the pathogenesis of aortic valve calcification (Liu et al., 2007). High expression of αSMA is a well described marker of myofibroblasts (Tomasek et al., 2002) which is increased in calcified aortic valves (Olsson et al., 1994). A recent study has proposed that MAPK/ERK as a potential pathway involved in myofibroblast calcification in CAVD (Gonzalez Rodriguez et al., 2021). In addition to αSMA, Calponin and SM22 (Transgelin) are established markers to identify myofibroblast-like cells in human (Latif et al., 2015b; Porras et al., 2017; Kostina et al., 2018).

TGFβ-1 (Transforming growth factor beta 1) is highly expressed in diseased aortic valve leaflets and has been the most extensively studied cytokine in relation to VIC activation and aortic valve calcification (Jian et al., 2003; Walker et al., 2004; Merryman et al., 2007; Hutcheson et al., 2012). As stated above, the majority of animal VICs are positive for αSMA, and its expression varies with the degree of myofibroblastic differentiation. In calcified valves this phenotype is usually widespread, but even then TGFβ-1 added to cultures can further promote it and thereby enhance αSMA expression (Walker et al., 2004; Kennedy et al., 2009; Monzack et al., 2009; Chen et al., 2011; Quinlan and Billiar, 2012). There appears to be species differences with respect to timing of myofibroblastic differentiation in porcine (Cushing et al., 2008) and ovine (Jian et al., 2002; Walker et al., 2004) VIC. After treatment with TGFβ-1 in low-serum medium, αSMA was detected after 24 h in ovine VIC (Gwanmesia et al., 2010), while αSMA was not detected until day 5 in porcine VIC (Gu and Masters, 2010). In our experience VIC isolated from both healthy and calcified human aortic valves have increased expression of αSMA and Calponin, analyzed by flow cytometry, after 4 days of stimulation with a myofibroblastic medium (DMEM, 1% FBS and 5 ng/ml TGFβ-1). Furthermore, stimulated cells from healthy valves are characterized by higher expression of these myofibroblastic markers indicating more prominent myofibroblastic differentiation in comparison with cells from calcified valves. In conclusion, a dynamic increase in αSMA and Calponin expression is a reliable myofibroblastic differentiation marker for human VIC isolated from healthy and calcified aortic valves.

5.4.2 Role of Extracellular Matrix in Myofibroblastic Differentiation

The extracellular matrix plays a key role in the regulation of VIC phenotype and function, including the processes of differentiation (Gwanmesia et al., 2010). Moreover, it is speculated that TGFβ-1 may bind to components of the extracellular matrix and this interaction may be essential for its signaling (Chen and Simmons, 2011; Jenkins, 2008; Wipff and Hinz, 2008). Disruption of the extracellular matrix in valve leaflets in turn alters TGFβ-1 signaling in VIC, leading to remodeling and valve disease (Chen and Simmons, 2011; Jenkins, 2008; Wipff and Hinz, 2008). *In vitro* it has been demonstrated that different coatings on conventional tissue culture plates influence myofibroblastic differentiation in different ways (Chen and Simmons, 2011; Hinton and Yutzey, 2011). Collagen and laminin coatings increase both the calcification process and induction of αSMA in ovine VIC, whereas fibronectin has an opposite effect (Gwanmesia et al., 2010). Laminin, heparin, and fibrin, but not collagen or fibronectin promote nodule formation in porcine VIC (Rodriguez and Masters, 2009). Another factor that influences the differentiation of VIC into myofibroblasts is the rigidity of the matrix (mechanical properties). By varying the concentration of collagen in a 3-dimensional model, very different effects were observed: compliant matrices contribute to osteogenic differentiation and calcification, whereas stiff matrices promote myofibroblastic differentiation and calcification through apoptosis (Yip et al., 2009; Quinlan and Billiar, 2012; Wyss et al., 2012). In addition, the effect of TGFβ-1 on αSMA expression is proportional to the matrix stiffness (Chen et al., 2011). In 2D cultures, stiff substrates such as tissue culture plastic may be sufficient to promote VIC differentiation to myofibroblasts (Kennedy et al., 2009; Benton et al., 2008). A summary of coatings employed for myofibroblastic differentiation of animal VIC and their effect is shown in **Table 1**. Laminin and collagen are the most commonly used coating surfaces for culture of myofibroblasts (Monzack et al., 2009; Rodriguez and Masters, 2009; Yip et al., 2009; Gwanmesia et al., 2010; Chen et al., 2011; Quinlan and Billiar, 2012; Wyss et al., 2012). **Figure 5** shows the comparison of αSMA expression in cells cultured either on laminin or collagen coating after stimulation with myofibroblastic medium.

TABLE 1 | The effect of different coatings on myofibroblastic differentiation of cultured valve interstitial cells from different species.

Coating	Presence in Extracellular matrix of aortic valve	Model	Effect on myofibroblastic differentiation	References
laminin	in the basement membrane	sheep, porcine	↑	(Monzack et al., 2009; Rodriguez and Masters, 2009; Gwanmesia et al., 2010)
heparin	In spongiosa layer	porcine	↑	Rodriguez and Masters, (2009)
fibrin	found in valves of patients with aortic stenosis	porcine	↑	(Benton et al., 2008; Monzack et al., 2009; Rodriguez and Masters, 2009)
collagen	comprises a significant part of fibrosa layer	sheep, porcine	↑ (sheep model) ↑ (porcine model)	(Jian et al., 2002; Rodriguez and Masters, 2009; Gwanmesia et al., 2010)
fibronectin	in fibrosa layer	sheep, porcine	↓	(Benton et al., 2008; Rodriguez and Masters, 2009; Gwanmesia et al., 2010)
plastic	_	porcine	↑	(Benton et al., 2008; Kennedy et al., 2009; Monzack et al., 2009; Rodriguez and Masters, 2009; Gwanmesia et al., 2010)
PEG	_	porcine	↓	Benton et al. (2008)

5.4.3 Myofibroblastic Contractility of Valve Interstitial Cells in 3D Cultures

Actin-myosin cytoskeleton of myofibroblasts is connected with components of extracellular matrix *via* cellular transmembrane receptors, the integrins, allowing cells to contract the surrounding extracellular matrix (Parizi et al., 2000). In order to provide relevant models that reflect the *in vivo* situation in humans with contraction inside the leaflets, VIC isolated from calcified valves can be incorporated into a 3D cell culture system, based on collagen gel (Bond et al., 2007). This allows measuring the contractility of VIC-derived myofibroblasts, which in turn demonstrates their functional attributes (Butcher and Nerem, 2004; Cushing et al., 2008). αSMA expression induced by TGF-β1 stimulation correlates with gel contraction confirming the contractile phenotype of VIC (Hinz et al., 2001). Blocking αSMA polymerization with cytochalasin D attenuates TGF-β1–induced contraction (Walker et al., 2004). These results confirm that VIC contract collagen gel due to their differentiation into myofibroblast-like cells.

The collagen gel constructs, in which the VIC are encapsulated (Cushing et al., 2008), may be created with 2 mg/ml collagen I, 5x DMEM (10% FBS 0.1M NaOH) before VIC are added. After polymerization the gels can be gently detached from the wells (floating model), otherwise the gels are kept attached to the well (stressed model). Whereas the floating model is believed to mimic normal connective tissue, stressed model mimics wound healing situation where cells are under mechanical load transferred from extracellular matrix. To stimulate the human VIC to differentiate into myofibroblasts, the gels containing the cells are treated with DMEM supplemented with 1% FBS and 5 ng/ml TGF-β1. Imaging of floating collagen gels are acquired every 24 h (**Figure 6A**). Collagen gel size is measured and percent contraction is calculated as the change in area from the initial area at time zero. Using this model, we have shown that collagen cell constructs from healthy valves contracted more strongly than if cells were from calcified valves after stimulation with TGF-β1, suggesting higher potential to differentiate into myofibroblasts (Fletcher et al., 2021). A schematic overview of the gel contraction and stressed model formation is shown in **Figure 7**. Although treatment with 10% FBS does not change expression of myofibroblastic marker αSMA in human VIC compared to treatment with 1% FBS, we noticed that treatments with 10% FBS or 1% FBS without TGFβ1 have different effects on gel contractility of human VIC (Bogdanova et al., 2018). A possible explanation is that serum contains factor(s) that can promote myofibroblast contraction (Parizi et al., 2000; Latif et al., 2015a; Porras et al., 2017). Treatment of floating collagen gel constructs with high-serum (10% FBS) leads to significantly greater collagen gel contractility compared to low-serum (1% FBS) and contracted collagen gel at the same level as stimulation by low-serum (1% FBS) together with TGFβ1 (**Figure 6B**). In conclusion, collagen gel contraction is a relevant method to characterize functional attributes of human VIC. However, when results are interpreted, it is important to take into consideration factors discussed above that influences collagen gel contractility.

5.5 Genetic Modification of Valve Endothelial and Interstitial Cells

Both VEC and VIC can be genetically engineered providing tools for unraveling the underlying mechanisms of calcification. We have tested two main gene delivery approaches: 1. Transfection of siRNA using N-TER Nanoparticle delivery system, and 2. Transduction with lentivirus. For the siRNA transfection we assessed the ability of VIC to take up a FITC conjugated siRNA, providing a convenient way to monitor efficiency. Both 10% FBS and serum-free approaches can be used for N-TER Nanoparticle delivery into VIC. Serum free conditions in our hands provided the highest efficiency of transfection with minimal cell death (**Figure 8A**). VEC appeared to be more susceptible than VIC to lentiviral entry, with approximately 77% of cell being transduced as assessed by GFP expression,

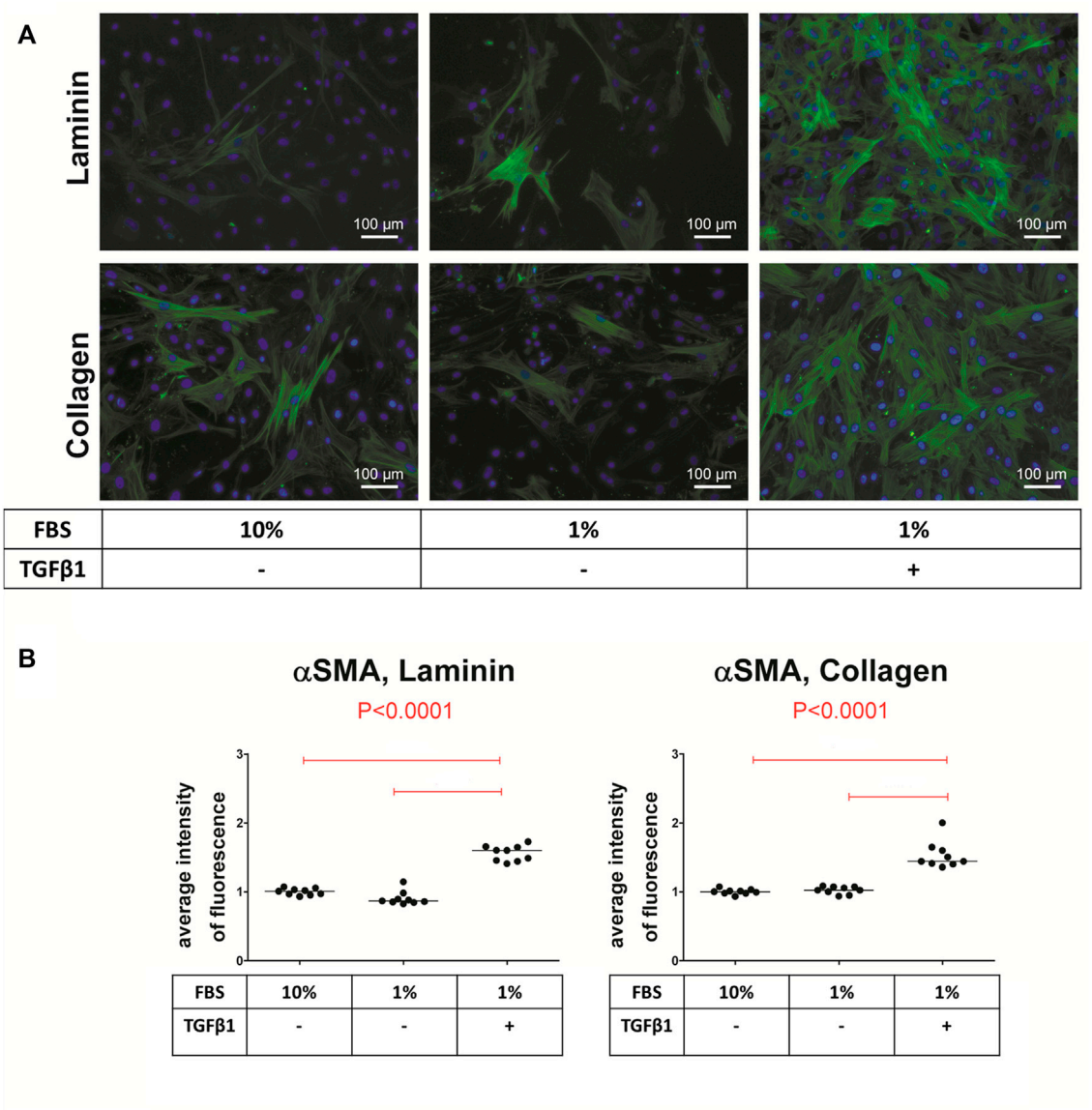

FIGURE 5 | Immunofluorescence staining of valve interstitial cells (VIC) for alpha-smooth muscle actin (αSMA). **(A)** VIC were isolated from aortic valves with calcification (n = 9) and cultured for 14 days on either laminin or collagen, with 10% FBS without TGFβ-1, with 1% FBS without TGFβ-1 or with TGFβ-1. αSMA (green), cell nuclei (Hoechst 3342/blue). **(B)** Quantification of αSMA fluorescence, shown as scatter plot with median. Statistical differences were tested using ANOVA followed by Tukey test. Overall *p*-values from ANOVA analysis are shown in red.

while VIC had a transduction efficiency of 47% in comparison to HEK293 (**Figure 8B**).

6 ANIMAL MODELS

There is generally a lack of animal models that accurately reflect human aortic valve stenosis (Sider et al., 2011). However, animal models are needed to investigate any kind of cardiovascular and soft tissue calcification. In particular to evaluate the effects as well as toxicity of drugs that potentially can inhibit calcification.

6.1 Subcutaneous Implantation of Cusps

One extensively used model to study calcification, is implantation of cusp tissue–or other biological materials - in a subcutaneous pouch of rats or rabbits (Fishbein et al., 1982; Levy et al., 1983; Schoen et al., 1985; Mako and Vesely, 1997). This model has been used to evaluate how different preservation techniques influence calcification in cusps of bio-prosthetic heart valves, but also in other biological materials used for implantation, such as pericardial patches. Calcification develops in about 8 weeks when the material tested is explanted (Kennedy et al., 2009; Richards et al., 2013; Gould et al., 2014; Hulin et al., 2018).

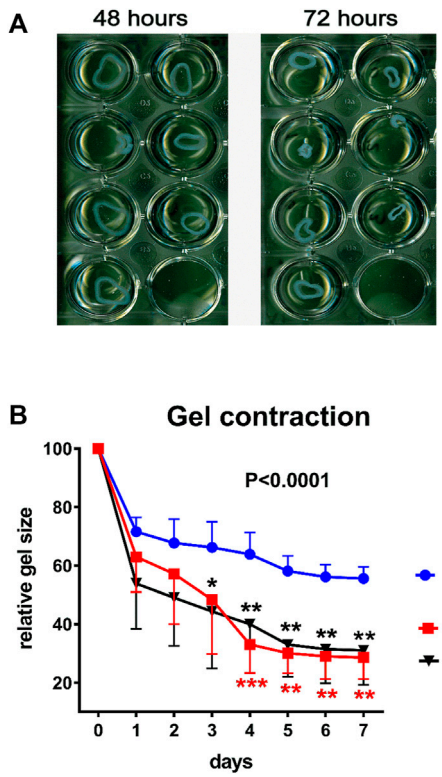

FIGURE 6 | Valve interstitial cells in 3D collagen cultures. Contraction of collagen gel containing cultured interstitial cells from calcified aortic valves (n = 4) and treated with 1% FBS with or without TGF-β1 over a period of 7 days. Panel **(A)** shows how the cultures contract and become smaller. Panel **(B)** shows the collective data of gel contraction of VIC from healthy aortic valves (n = 4) under stimulation with low-serum (1% FBS) with or without TGF-β1 or with high-serum (10% FBS) without TGF-β1. Gel sizes on day 0 were considered as 100%. Data were analyzed by two-way ANOVA with repeated measures. Differences between treatments with 1% FBS with TGF-β1 (shown in red stars) or 10% without TGF-β1 (shown in black stars) compared to 1% FBS without TGFβ1 were determined with Sidak's multiple comparison post-test, *indicates $0.01 < p \leq 0.05$, ** indicates $0.001 < p \leq 0.01$, *** indicates $0.0001 < p \leq 0.001$. Values are expressed as mean ± SD. Overall *p*-value from two-way ANOVA is shown in bold.

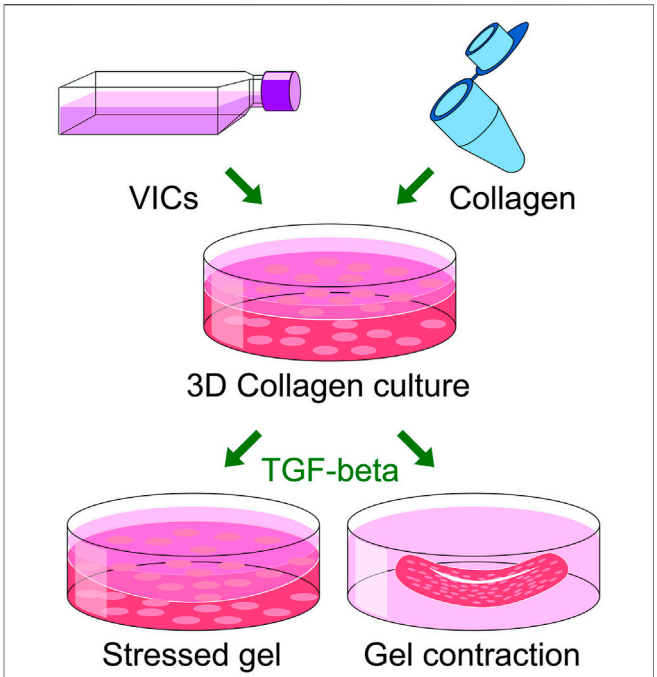

FIGURE 7 | A schematic overview of two 3D cell culture system (stressed gel and gel contraction), based on collagen gel that are being used for measuring the contractility of VIC-derived myofibroblasts.

This model is something between an *in vitro* and *in vivo* model and it is easy to prepare. Although being an un-physiological model, it is suitable for studying inhibition of calcification.

6.2 Aortic Valve Leaflets in Culture

As a more complex model than cell culture, culturing aortic valve leaflets may be a good alternative. In the model hierarchy it brings the investigation one step up from the cell cultures. Unfortunately, this is a model where the use of human tissues is less feasible. Healthy human valves are difficult to obtain, and culturing calcified valves may cause problems of interpretations for analysis of calcification. One possibility is to use parts of explanted calcified valves without macroscopic calcification; another possibility would be to use autopsy material. However, the most common practice is to use porcine aortic valve leaflets, either as parts of leaflets or as whole leaflets in culture medium (Sauren et al., 1983; Xing et al., 2004; Konduri et al., 2005; Balachandran et al., 2006; Chester et al., 2008; El-Hamamsy et al., 2009). Most of these studies have focused on the mechanical, biological or contractile properties of valve leaflet tissue. The best results are achieved with pig leaflets which better reflect the human morphology than mice and rat leaflets (Hinton et al., 2008). Rodent valves are also smaller and provide less material for molecular analysis. Several studies induced calcification in pig aortic leaflets. In one, calcification was induced by cyclic stretch for 2 weeks combined with a high concentration of osteogenic medium (Balachandran et al., 2010). Including mechanical stress may add some similarities to the human situation. In another, *Rathan et al.* induced calcification in porcine aortic leaflets by adding phosphate plus inorganic pyrophosphatase for 8 days (Rathan et al., 2014). Chester et al. (2021) developed another model with whole leaflets where calcification is not induced by osteogenic media, but uses the combination of lipopolysaccharide and inorganic phosphate, to initiate and drive the calcification process by an inflammatory response. One of the advantages is the extensive histological investigation of the calcifying leaflets–both qualitative and quantitative (Chester et al., 2021).

6.2.1 A Novel Model of Calcification *ex vivo* in Whole Valve Leaflets

We have developed a reliable model of cultured whole leaflets from porcine valves (Zabirnyk et al., 2020). Shortly, after animal sacrifice in an authorized abattoir, the hearts are transported on ice to the laboratory where the aortic valve leaflets are dissected free. The whole leaflets are maintained in individual wells of low

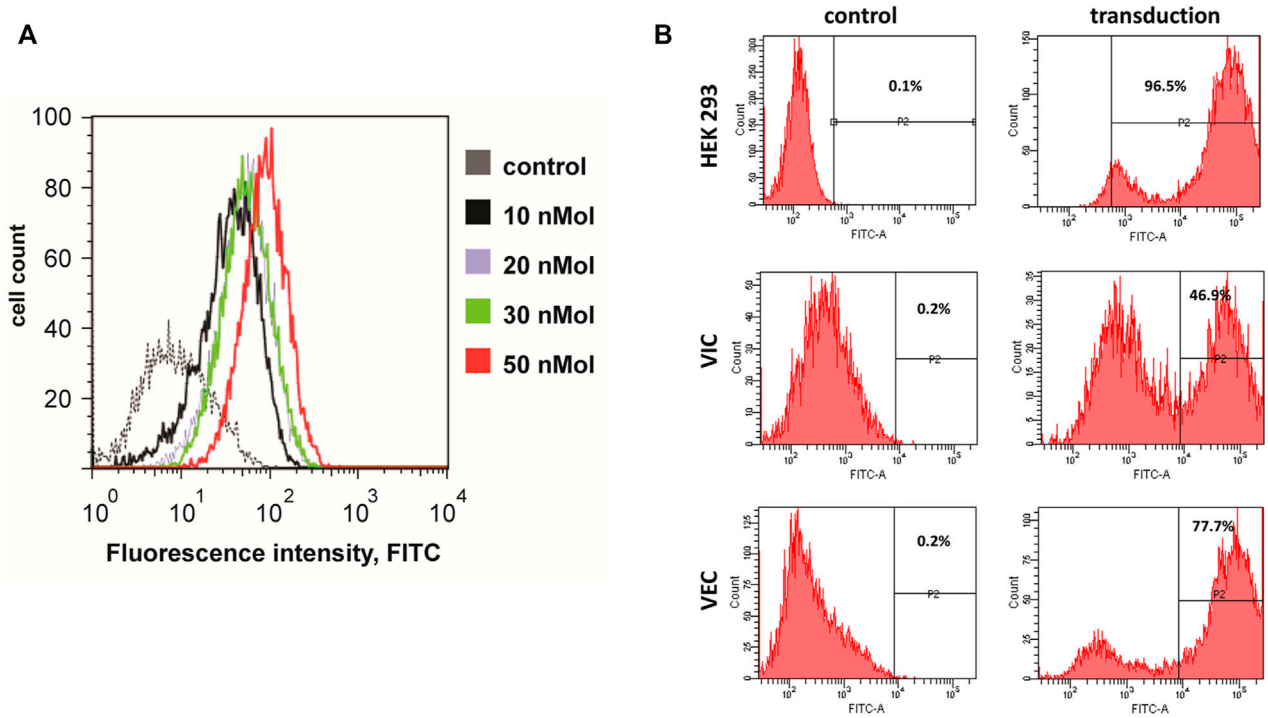

FIGURE 8 | Genetic engineering of valve endothelial (VEC) and interstitial cells (VIC). **(A)** Representative example of fluorescence - activated cell sorting (FACS) analysis of VIC from a calcified aortic valve and transfected with siRNA to mRNA conjugated with fluorescein isothiocyanate (FITC). Transfection kit was used with different concentrations of nanoparticle formulation solution (NFS). Dotted line - negative control (transfected with scrambled siRNA), black line–transfected with 10 nM NFS, blue–20 nM NFS, green -30 nM NFS, red -50 nM NFS (86.5% of cells transfected with siRNA). **(B)** Representative example of fluorescence–activated cell sorting (FACS) analysis of human embryonic kidney cells 293 (HEK293), aortic valve interstitial and endothelial cells from a calcified aortic valve without transduction or transduced with lentiviral construct that encoded green fluorescent protein (GFP).

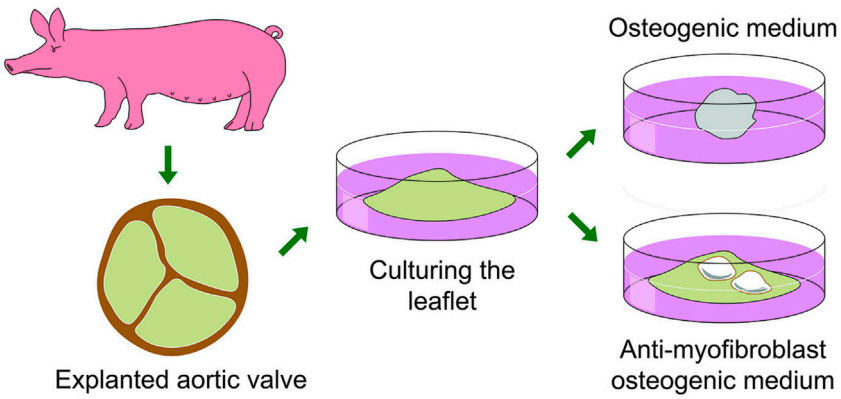

FIGURE 9 | A schematic overview of the whole pig leaflet cultivation and calcification model with the effect of standard osteogenic and anti–myofibroblast media being used.

attachment cell culture plates to avoid cell migration and loss of leaflet integrity. In standard pro-osteogenic media the leaflets shrunk from a leaflet to a ball-like shape due to myofibroblast contraction and with negligible accumulation of calcium deposits. Using anti-myofibroblastic growth medium (low-glucose DMEM, 2% FBS, FGF2 (fibroblast growth factor 2) and insulin), pro-osteogenic stimulation caused strong accumulation of calcium. This formulation prevented leaflets from shrinking, probably by inhibiting myofibroblastic transition of VICs. A schematic overview of the above described culturing pig leaflets in two different growth medias is presented in **Figure 9**.

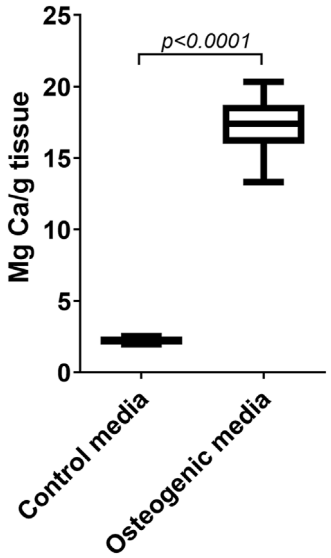

FIGURE 10 | Induced calcification in porcine whole leaflets cultivated *ex vivo*. Calcium accumulation in whole pig leaflets cultivated for 4 weeks in control growth media and in osteogenic media. The amount of calcium was measured by inductively coupled plasma optical emission spectroscopy. The data are shown as box plots and wiskers with 5–95% percentiles.

The validity of the *ex vivo* leaflet models is solely based on the amount of calcium accumulated in the valves. A limitation is that these leaflet models cannot be expected to closely mimic calcification in patients, a process slowly developing over several years. Histological characterization of the leaflets would be valuable. The *in vitro* leaflets cannot obtain the structure of calcified human valves that have ingrowth of vasculature and containing inflammatory cells and bioactive substances derived from the blood stream plus fibrosis. However, what determines the stiffness of a leaflet giving rise to aortic stenosis is fibrosis and the amount of calcification/calcium in the valve.

6.2.2 Measurements of Calcium in Leaflets

After the cultivation for 4 weeks with osteogenic differentiation, the amount of calcium accumulation is assessed. Alizarin Red staining is a good method in cell cultures, but it is not suitable as the multilayer tissue nonspecifically absorbs the dye. One way is to section the leaflet and semi-quantitatively assess the regions stained with Alizarin Red, however this method is rather inaccurate. After comparing several methods of quantifying calcium accumulation, the ICP-OES or ICP-MS appeared to be the most reliable and accurate method in whole leaflet models after tissue digestion. An example of calcium accumulation in the leaflets cultivated in growth and osteogenic media measured by ICP-OES is shown in **Figure 10**.

6.3 Animal Models *in vivo*

As already stated above animal models are a necessary instrument for studying the underlying mechanisms of disease and its treatment. Unfortunately, CAVD is a disease with an unmet need for good animal models despite numerous proposed. The most commonly used animals for modelling CAVD are mice, rat, rabbit and porcine, however, only the latter is able to develop CAVD spontaneously (Sider et al., 2011). Below we have provided an overview of the most commonly used animal models.

6.3.1 Mouse Models

The majority of animal models of CAVD have been developed in mice. This is because of their cost-efficiency, rapid breeding and, most importantly, the availability of genetically modified variants. Regrettably, mouse models have significant limitations. Neither mouse nor rat aortic valve leaflets have the tri-layer structure akin to the human leaflet, only several layers of cells (Hinton et al., 2008). Wild-type mice do not develop aortic valve stenosis, however, a diet-based model has been reported with mild to moderate aortic stenosis (Drolet et al., 2006). A better alternative is transgenic mouse models. Until recently, the most commonly used mouse models contained a single gene mutation which affected lipid metabolism, the low-density lipoprotein receptor ($Ldlr^{-/-}$) and apolipoprotein E deficient mice ($ApoE^{-/-}$). These mice developed significant aortic valve calcification and some signs of CAVD when fed a high cholesterol diet. However, these models do not develop hemodynamically significant aortic valve stenosis (Rajamannan, 2014). To achieve stenosis the complex hypercholesterolemic mouse model with mutations in both Ldlr and ApoB100 (Apolipoprotein B100) ($Ldlr^{-/-}/ApoB^{100/100}$ mice) is necessary. It is efficiency is significantly increased if fed with a high cholesterol Western diet over 12 months (Weiss et al., 2006; Miller et al., 2009; Miller et al., 2010). This model is further developed by addition of a conditional knockout of the microsomal triglyceride transfer protein (*Mttp*) which plays a critical role in production of apolipoprotein B-containing lipoproteins ($Ldlr{-}/{-}/Apob^{100/100}/Mttp^{fl/fl}/Mx1\text{-}Cre^{+/+}$)–the so-called Reversa model. This allows controlled onset of hyperlipidemia during the experimental aortic valve stenosis development (Miller et al., 2009). A recent study reports an improved of $Ldlr^{-/-}/ApoB^{100/100}$ mouse model that develops aortic stenosis earlier – after 6 month with high fat diet treatment - and gives insight into the role of platelet-derived TGF-β1 in CAVD progression (Varshney et al., 2019).

Several non-hyperlipidemic models offer features of CAVD including aortic valve leaflet calcification, but they lack the development of aortic stenosis. They include mice containing mutations in MGP (Matrix Gla protein) (Luo et al., 1997), EGFR (Epidermal growth factor receptor) (Barrick et al., 2009), Klotho (Cheek et al., 2012), RBPJk (Recombination Signal Binding Protein For Immunoglobulin Kappa J Region) (Nus et al., 2011) and IL1RN (Interleukin 1 Receptor Antagonist) (Isoda et al., 2010). Interestingly, despite strong calcification, the combination of high fat diet and vitamin D supplementation does not enhance the aortic stenosis phenotype of the EGFR mouse (Colleville et al., 2019).

Some genetic mouse models resemble human congenital aortic valve defects, which present with increased occurrence of CAVD. Bicuspid aortic valves are reported in mice containing mutations in eNOS (Endothelial nitric oxide synthase) (Lee et al., 2000), Notch1(Notch Receptor 1) (Nigam and Srivastava, 2009), Postn (Periostin) (Tkatchenko et al., 2009). A unicuspid aortic valve with some signs of CAVD was reported in a novel mouse

model heterozygous for a dominant loss-of-function mutation in EGFR (*Egfr* $^{Vel/+}$) (Weiss et al., 2018).

In addition to dietary and genetic mouse models, an *in vivo* valve injury model was developed by insertion of a spring guide wire into the left ventricle via the right common carotid artery under echocardiographic guidance, and scratching the leaflets with the body of the wire (Honda et al., 2014). This model was recently improved to achieve either mild, moderate or severe cusp injury to enable a more reproducible study of different stages of CAVD (Niepmann et al., 2019). It is important to notice that this direct injury models demonstrate typical clinical features of CAVD including inflammation, valve thickening, fibrosis and calcification combined with hemo-dynamically significant aortic stenosis as well as regurgitation (in severe injury). This model together with the *Ldlr*-deficient, *ApoB100*-only mice (*Ldlr* $^{-/-}$/*ApoB*$^{100/100}$) model appears to be the most relevant murine models of CAVD to date.

6.3.2 Rat Models

The rat aortic valve leaflets like the mouse, are not optimal for studies on CAVD because they consist of several cell layers without the tri-layered structure of human aortic valves (Grauss et al., 2003) (see above). A common model of vascular calcification and CAVD in rats is based on intravenous treatment with Warfarin, however, these rats do not develop hemo-dynamically significant aortic stenosis (Price et al., 1998) and warfarin-induced aortic valve calcification differs from the naturally occurring (Venardos et al., 2022). Such rats are phenotypically similar to MGP mutant mice, suggesting similar underlying mechanisms (Tsang et al., 2016). Mirroring the fact that renal failure is also associated with CAVD in humans, several uremic rat models induced by nephrectomy or high-adenine diet develop aortic valve calcification (Shuvy et al., 2008; Roosens et al., 2013a; Roosens et al., 2013b). Furthermore, vitamin D treatment causes vascular and aortic valve calcification in rats, but without aortic stenosis (Roosens et al., 2011). All taken together, rats do not represent an appropriate experimental model of aortic valve calcification with aortic stenosis.

6.3.3 Rabbit Models

Rabbits have both advantages and disadvantages as model for CAVD. They have the tri-layer leaflet composition similar to humans, several similarities in lipoprotein metabolism, and natural mutant and transgenic strains are available. Most frequently a hypercholesterolemic diet is administered to cause CAVD (Guerraty and Mohler Iii, 2007). A 40-weeks treatment with such diet induces early development of aortic stenosis (Cimini et al., 2005). When a hypercholesterolemic diet was coupled with vitamin D-induced hypercalcemia, significant calcium deposition developed in addition to aortic stenosis (Drolet et al., 2003; Guerraty and Mohler Iii, 2007). Another study demonstrated that a hypercholesterolemic and vitamin D2-supplemented diet caused leaflet thickening, calcification, matrix disorganization, and aortic stenosis (Marechaux et al., 2009). This combination appears to provide a better model of CAVD than hypercholesterolemic or vitamin D diets alone (Roosens et al., 2013a). However, a rabbit model using high-cholesterol diet is limited by liver dysfunction and high mortality rates due to cholesterol overload (Hara et al., 2018). In contrast, rabbit genetic models that have alterations in the *Ldlr* and/or apolipoprotein-encoding genes result in hypercholesterolemia even under a cholesterol-free, limited fat diet without cholesterol overload (Sider et al., 2011). Such a model is the Watanabe heritable hyperlipidemic rabbits that develop valve thickening, calcification, aortic stenosis and calcification-related gene activation (Hara et al., 2018). In addition to the hypercholesterolemic models, a hypertensive rabbit model develops increased valve thickness and mild aortic stenosis (Cuniberti et al., 2006).

6.3.4 Pig Models

The pig has tri-layered aortic valve leaflets similar to humans. Unlike mouse, rat and rabbit models, pigs are prone to naturally develop valvular atherosclerotic lesions (Skold et al., 1966). Swine develop valvular lesions and early signs of CAVD when fed with a high-fat/high-cholesterol diet for 5 months (Sider et al., 2014). Aortic valve calcification has been shown to be restricted to the aortic side in early CAVD in a porcine models with hypercholesterolemic diet (Guerraty et al., 2010). The Rapacz-familial hypercholesterolemic swine mutants develop leaflet thickening, increased lipid oxidation and infiltration of macrophages, however, further stimulation is needed to develop more advanced stages of CAVD with aortic stenosis (Porras et al., 2015). Additional swine models with lipid metabolism mutations used in atherosclerosis research may have a potential to be used in CAVD research (Sider et al., 2011). Tsang *et al.* have published a detailed review on the pig as a model for cardiovascular disease including CAVD (Tsang et al., 2016).

6.3.5 Other Animal Models

There are other animal models available, although potentially useful, they are not commonly used. For example, naturally occurring and experimental aortic stenosis has been investigated in dogs (Copeland et al., 1974; Kim et al., 1986; Ahlstrom Ast et al., 2008). Sheep are routinely used as a big animal model to investigate calcification of biological aortic valve prosthesis and homografts *in vivo* (Kheradvar et al., 2017; Theodoridis et al., 2017; Bester et al., 2018). Apparently, calcification occurs very rapidly in sheep compared to humans.

7 MULTIOMNICS

7.1 Proteomics as an Example of Multi-Omnics Approaches

Multi-omnic approaches with proteomics, metabolomics and transcriptomics have recently gained momentum in aortic valve calcification investigations (Schlotter et al., 2018). Here as an example we have listed several approaches to perform proteomics analysis in CAVD research. Several groups have targeted proteome changes in human plasma during the development of calcific aortic valve disease for better understanding the basic mechanisms and to discover biomarkers (Gil-Dones et al., 2012; Satoh et al., 2015; Mourino-Alvarez et al., 2016; Olkowicz et al., 2017; Ljungberg et al., 2018). Additionally, gaining access to the plasma of both

CAVD patients and healthy controls is rather straight-forward. This approach may be useful for the identification of biomarkers of CAVD in the blood of patients. The later aim is especially important because of the current lack of screening for early detection of CAVD. Targeting known problems of the proteome complexity in plasma, Gil–Dones *et al.* (Monzack and Masters, 2011) suggested improved protocols for plasma proteomics analysis in CAVD research.

An *ex vivo* modification of the plasma proteome analysis in patients with calcified aortic valves was reported as a secretome proteomics analysis from the explanted whole human leaflets kept for some time in growth media (Alvarez-Llamas et al., 2013; de la Cuesta et al., 2013). This approach allows one to mimic the secretome entering the circulation from aortic leaflets without interference from other tissues. Another common approach is to perform proteomics on the whole human leaflets explanted during the surgery or autopsy after lysate of the valve leaflets (Martin-Rojas et al., 2015; Weisell et al., 2019). A protein extraction procedure optimization was reported for this approach (Gil-Dones et al., 2010). The use of more advanced proteomics technique such as MALDI-imaging mass spectrometry offers the advantage to investigate the pathophysiological changes taking place in calcified aortic valves while retaining the histopathological context. This allows the simultaneous mapping of hundreds of peptides and proteins present in tissue sections with a lateral resolution of approximately 50–75 microns (Martin-Rojas et al., 2015).

Direct analysis of whole leaflets explanted from humans is most relevant to *in vivo* assessment, however, it has an important drawback as the analysis is performed on all cell types within the valve. Several groups partly overcome this problem by performing macro- (Matsumoto et al., 2012; Suzuki et al., 2016) and microdissection (Schlotter et al., 2018), subdividing the valve into calcified and non–calcified regions.

Another approach is to isolate and propagate *in vitro* VICs and subsequently perform proteomic analysis on human (Yu et al., 2018; Goto et al., 2019), bovine (Renato et al., 2013) or rat (Cui et al., 2017) cell cultures. Some authors have reported clonogenic sub–fractioning of the isolated and cultivated bovine VIC prior to proteomics analysis (Bertacco et al., 2010; Rattazzi et al., 2020). Unfortunately, gene studies in cultured VIC are influenced by the culture process *per se*. At the same time, omics analysis of calcified whole leaflets are "impure" containing material from several cell types in addition to VIC: VEC, vascular cells including smooth muscle cells from vascular ingrowth, as well as macrophages and other inflammatory cells. A combination of the above-mentioned proteomics approaches (whole leaflet, secretome, cell cultures, and plasma proteomics analysis) reveals more data than individual approaches (Martin-Rojas et al., 2017). Microarray and RNA sequencing with transcriptomics, in particular if combined with proteomics, might provide valuable information about signaling of the calcification process.

8 BIOMARKERS OF AORTIC VALVE CALCIFICATION

To identify high-risk asymptomatic patients with aortic stenosis has become a major topic of interest during the last years. However, detailed discussion of risks and indications for surgical intervention is beyond the scope of this article (see review by Lindman et al. (Lindman et al., 2020)). Among a jungle of advanced and sometimes costly imaging modalities which may be predictive of disease progression and mortality in aortic stenosis (Nchimi et al., 2018), a blood sample for measuring circulating biomarkers is a simple, inexpensive, and easily available method to provide information about the stage and possible risks of asymptomatic aortic stenosis. Even if biomarkers represent indirect assessment, they might possibly be helpful to identify progression of CAVD and asymptomatic patients who then would benefit from aortic valve replacement.

Most interest has been focused on natriuretic peptides, in particular brain-natriuretic peptide (BNP) and its pro-hormone N-terminal pro B-type natriuretic peptide (NT-proBNP) as possible biomarkers of aortic stenosis (Weber et al., 2004; Steadman et al., 2010; Clavel et al., 2014; Auensen et al., 2017; Small et al., 2017). The biomarker does not reflect calcification *per se*, but it provides diagnostic and prognostic information about myocardial remodeling as a consequence of aortic stenosis. Marked increased levels of BNP may reflect irreversible injury to the myocardium and has been shown to predict worse outcome in patients after transcatheter aortic valve interventions (O'Neill et al., 2015). The same is the case with cardiac troponins (Köhler et al., 2016). BNP is the only biomarker in the circulation accepted to have prognostic value in the guidelines of the European Society for Cardiology and the European Association for Cardio-Thoracic Surgery (but not for the American Heart Association or the American College of Cardiology).

Recently, a series of other potential biomarkers in the circulation have brokered interest, such as for instance von Willebrand Factor (vWF) due to high shear stress in aortic stenosis (Van Belle et al., 2019). Plasma levels and function of vWF is reduced in parallel with severity of aortic stenosis. The levels are normalized after transcatheter aortic valve intervention, but did not normalize if a paravalvular leakage was present (Van Belle et al., 2016).

Of particular interests for this review are biomarkers that may be directly related to the calcification process. This includes microRNAs (Oury et al., 2016), fetuin-A (Di Minno et al., 2017), osteopontin (Sainger et al., 2013), osteoprogeterin (Ueland et al., 2011), and MGP (Ueland et al., 2010). Notch may have an important role in aortic valve calcification (Kostina et al., 2018) and the Notch ligand Delta-1 is elevated and associated with mortality in patients with symptomatic aortic stenosis (Abraityte et al., 2015). Elmariah *et al.* suggested that a panel of multiple biomarkers including age, NT-proBNP, vWF, and fetuin-A would be valuable for the identification of high-risk patients with aortic stenosis and for timely valve intervention (Elmariah et al., 2018). MacGrogan *et al* also suggested that a set of several genes in blood provided a "gene signature" predicting aortic valve calcification (MacGrogan et al., 2020).

So far neither guidelines of the American Heart Association, the American College of Cardiology, the European Society of Cardiology, nor the European Association for Cardio-Thoracic Surgery include these biomarkers as valuable for evaluation of patients with CAVD. The role of biomarkers as a guide to more aggressive aortic valve replacement in asymptomatic patients has

yet to be investigated. It might well be in the future a profile of several biomarkers may be useful. A full discussion of the field is beyond the scope of this review, however, several concise and recent reviews have been published on this topic (Redfors et al., 2017; Small et al., 2017; Patel and Kumbhani, 2018; Toutouzas et al., 2019; Oury et al., 2020).

9 CALCIUM PHOSPHATE PROTEIN PARTICLES

Circulating calcium phosphate protein particles might be important both for the understanding of the processes leading to calcification and for the development of therapy for both valvular and vascular calcifications. Such particles have not been found in the circulation of healthy individuals, but exist in the circulation of patients with some inflammatory diseases (Smith et al., 2013). The number of particles in the blood can be reduced by sodium thiosulphate which has been suggested to reduce vascular calcification (Cai et al., 2013). Fetuin-A is a key player in the formation of calcium phosphate protein particles. This protein is an endogenous inhibitor of soft tissue calcification by inhibiting formation of calcium phosphate (Heiss et al., 2010). Once a mineral nuclei is formed, fetuin-A binds to the apatite surface and inhibits the formation of larger entities (Price and Lim, 2003). The nanoparticles consisting of calcium phosphate crystals may be a way to clear calcium and inhibit calcification; they are cleared from the circulation in the liver and the spleen, a process which is dependent on scavenger receptors on phagocyte surfaces (Herrmann et al., 2012). The role of calcium phosphate protein particles in soft tissue calcification is uncertain, however, in pro-calcific situations, the particles may have structural transformation into larger particles with a crystalline core and initiate calcification (Jahnen-Dechent et al., 2011). Using nano-analytical electron microscopy techniques, Bertazzo *et al.* found such mineralized particles on the aortic valve even before calcification of the valve (Bertazzo et al., 2013). The presence of these particles might perhaps even initiate CAVD (Bertazzo and Gentleman, 2017). This is in line with findings that crystallinity of hydroxyapatite in 3D cultures with VEC and VIC increase calcium accumulation (Richards et al., 2018). Detailed methods for studying calcium phosphate particles in human serum, on tissues, and in tissues include ultracentrifugation, gel filtration, scanning and transmission electron microscopy, measurements of calcium and phosphate, energy-dispersive X-ray spectroscopy, selected area electron diffraction analyses, and material science technology in general (Price and Lim, 2003; Bertazzo et al., 2013).

10 DISCUSSION

The process of aortic valve calcification is still far from elucidated. In this overview we try to cover presently used methods to study CAVD, from translational studies in cell cultures to patient studies. With the lack of good animal models, translational studies in cell cultures are by far the most frequently used model to clarify the cellular and molecular mechanisms of calcification. Consequently, this is the only model where more detailed techniques were presented. Cells from human aortic valves should be used in order to avoid species differences. Cell models are also suitable for screening of potentially inhibitory drugs. There is an unmet need for good models of aortic valve calcification in animals where the structure of the valve leaflet is similar to the structure of human aortic valve. Moreover, we know too little about the mineral structure of calcified valves including its role. With increasing use of endovascular implantation of aortic valve prostheses, good imaging of the aortic ostium and the valve has become more and more important. Possibly, MRI should be used more extensively. There is also a need for good biomarkers. Unfortunately, although there are suggestions for several biomarkers, it is highly uncertain how they should be used. Biomarkers cannot replace imaging because the structure and degree of stenosis are decisive for clinical decisions.

AUTHOR CONTRIBUTIONS

MB established cell techniques and wrote parts of the manuscript, AZ contributed to cell techniques, established whole valve leaflet model, revised the manuscript and wrote some parts, AM supervised techniques and revised the manuscript, KE contributed to cell techniques, AK supervised and revised the manuscript, J-PEK; MK managed logistics and sampling of aortic valves and revised manuscript, KS supervised work and revised manuscript, MP measured calcium in tissue and revised the manuscript, RS contributed with techniques, GS supervised on cell methodology and revised manuscript, JV initiated and supervised the project, wrote some parts and revised manuscript, AR established cell techniques, co-supervised the project and revised manuscript.

FUNDING

This work has been funded by The South-Eastern Health Authorities by a postdoc scholarship to AR. AZ has been the recipient of a Scientia Fellow scholarship funded by the European Union and the Faculty of Medicine, University of Oslo, and has at present a postdoc scholarship from the Norwegian Health Association. Further funding has been received by the University of Oslo (including PhD scholarship to MB), The Norwegian Health Association, and by Russian Science Foundation (grant # 18-14-00152). GJS was partly supported by the Research Council of Norway through its Center of Excellence funding scheme (project number 262613).

ACKNOWLEDGMENTS

Professor Arnt Fiane, chairman of the Department of Cardiothoracic Surgery, Oslo University Hospital, generously made sampling of heart valves possible. Torunn Flatebø and Kristin Larsen Sand provided technical assistance, Kristin Larsen Sand also helped with the production of **Figure 4**.

REFERENCES

Abraityte, A., Gullestad, L., Askevold, E. T., Nymo, S., Dahl, C. P., Aakhus, S., et al. (2015). The Notch Ligand Delta-like 1 Is Elevated and Associated with Mortality in Patients with Symptomatic Aortic Stenosis. *Int. J. Cardiol.* 180, 18–20. doi:10.1016/j.ijcard.2014.11.111

Aggarwal, S. R., Clavel, M. A., Messika-Zeitoun, D., Cueff, C., Malouf, J., Araoz, P. A., et al. (2013). Sex Differences in Aortic Valve Calcification Measured by Multidetector Computed Tomography in Aortic Stenosis. *Circ. Cardiovasc Imaging* 6 (1), 40–47. doi:10.1161/CIRCIMAGING.112.980052

Ahlstrom Ast, C., Höglund, K., Hult, P., Häggström, J., Kvart, C., and Ask, P. (2008). Assessing Aortic Stenosis Using Sample Entropy of the Phonocardiographic Signal in Dogs. *IEEE Trans. Biomed. Eng.* 55 (8), 2107–2109. doi:10.1109/TBME.2008.923767

Alvarez-Llamas, G., Martín-Rojas, T., de la Cuesta, F., Calvo, E., Gil-Dones, F., Dardé, V. M., et al. (2013). Modification of the Secretion Pattern of Proteases, Inflammatory Mediators, and Extracellular Matrix Proteins by Human Aortic Valve Is Key in Severe Aortic Stenosis. *Mol. Cell Proteomics* 12 (9), 2426–2439. doi:10.1074/mcp.M113.027425

Auensen, A., Hussain, A. I., Falk, R. S., Walle-Hansen, M. M., Bye, J., Pettersen, K. I., et al. (2017). Associations of Brain-Natriuretic Peptide, High-Sensitive Troponin T, and High-Sensitive C-Reactive Protein with Outcomes in Severe Aortic Stenosis. *PLoS One* 12 (6), e0179304. doi:10.1371/journal.pone.0179304

Babu, A. N., Meng, X., Zou, N., Yang, X., Wang, M., Song, Y., et al. (2008). Lipopolysaccharide Stimulation of Human Aortic Valve Interstitial Cells Activates Inflammation and Osteogenesis. *Ann. Thorac. Surg.* 86 (1), 71–76. doi:10.1016/j.athoracsur.2008.03.008

Bailey, G., Meadows, J., and Morrison, A. R. (2016). Imaging Atherosclerotic Plaque Calcification: Translating Biology. *Curr. Atheroscler. Rep.* 18 (8), 51. doi:10.1007/s11883-016-0601-6

Balachandran, K., Konduri, S., Sucosky, P., Jo, H., and Yoganathan, A. P. (2006). An *Ex Vivo* Study of the Biological Properties of Porcine Aortic Valves in Response to Circumferential Cyclic Stretch. *Ann. Biomed. Eng.* 34 (11), 1655–1665. doi:10.1007/s10439-006-9167-8

Balachandran, K., Sucosky, P., Jo, H., and Yoganathan, A. P. (2010). Elevated Cyclic Stretch Induces Aortic Valve Calcification in a Bone Morphogenic Protein-dependent Manner. *Am. J. Pathol.* 177 (1), 49–57. doi:10.2353/ajpath.2010.090631

Baralkiewicz, D., Gramowska, H., Hanć, A., and Krzyzaniak, I. (2007). A Comparison of ICP-OES and ICP-MS in the Determination of Elements in Lake Water. *At. Spectrosc. -Norwalk Connecticut-* 28, 164–170.

Barrick, C. J., Roberts, R. B., Rojas, M., Rajamannan, N. M., Suitt, C. B., O'Brien, K. D., et al. (2009). Reduced EGFR Causes Abnormal Valvular Differentiation Leading to Calcific Aortic Stenosis and Left Ventricular Hypertrophy in C57BL/6J but Not 129S1/SvImJ Mice. *Am. J. Physiol. Heart Circ. Physiol.* 297 (1), H65–H75. doi:10.1152/ajpheart.00866.2008

Benton, J. A., Kern, H. B., and Anseth, K. S. (2008). Substrate Properties Influence Calcification in Valvular Interstitial Cell Culture. *J. Heart Valve Dis.* 17 (6), 689–699.

Bertacco, E., Millioni, R., Arrigoni, G., Faggin, E., Iop, L., Puato, M., et al. (2010). Proteomic Analysis of Clonal Interstitial Aortic Valve Cells Acquiring a Pro-calcific Profile. *J. Proteome Res.* 9 (11), 5913–5921. doi:10.1021/pr100682g

Bertazzo, S., and Gentleman, E. (2017). Aortic Valve Calcification: a Bone of Contention. *Eur. Heart J.* 38 (16), 1189–1193. doi:10.1093/eurheartj/ehw071

Bertazzo, S., Gentleman, E., Cloyd, K. L., Chester, A. H., Yacoub, M. H., and Stevens, M. M. (2013). Nano-analytical Electron Microscopy Reveals Fundamental Insights into Human Cardiovascular Tissue Calcification. *Nat. Mater* 12 (6), 576–583. doi:10.1038/nmat3627

Bester, D., Botes, L., van den Heever, J. J., Kotze, H., Dohmen, P., Pomar, J. L., et al. (2018). Cadaver Donation: Structural Integrity of Pulmonary Homografts Harvested 48 H Post Mortem in the Juvenile Ovine Model. *Cell Tissue Bank.* 19 (4), 743–754. doi:10.1007/s10561-018-9729-7

Bettinger, N., Khalique, O. K., Krepp, J. M., Hamid, N. B., Bae, D. J., Pulerwitz, T. C., et al. (2017). Practical Determination of Aortic Valve Calcium Volume Score on Contrast-Enhanced Computed Tomography Prior to Transcatheter Aortic Valve Replacement and Impact on Paravalvular Regurgitation: Elucidating Optimal Threshold Cutoffs. *J. Cardiovasc Comput. Tomogr.* 11 (4), 302–308. doi:10.1016/j.jcct.2017.04.009

Bhatia, N., Basra, S. S., Skolnick, A. H., and Wenger, N. K. (2016). Aortic Valve Disease in the Older Adult. *J. Geriatr. Cardiol.* 13 (12), 941–944. doi:10.11909/j.issn.1671-5411.2016.12.004

Bogdanova, M., Kostina, A., Zihlavnikova Enayati, K., Zabirnyk, A., Malashicheva, A., Stensløkken, K. O., et al. (2018). Inflammation and Mechanical Stress Stimulate Osteogenic Differentiation of Human Aortic Valve Interstitial Cells. *Front. Physiol.* 9 (1635), 1635. doi:10.3389/fphys.2018.01635

Bogdanova, M., Zabirnyk, A., Malashicheva, A., Enayati, K. Z., Karlsen, T. A., Kaljusto, M. L., et al. (2019). Interstitial Cells in Calcified Aortic Valves Have Reduced Differentiation Potential and Stem Cell-like Properties. *Sci. Rep.* 9 (1), 12934. doi:10.1038/s41598-019-49016-0

Bond, W. S., Roberts, E. L., and Warnock, J. N. (2007). Evaluation of Porcine Aortic Valve Interstitial Cell Activity Using Different Serum Types in Two- and Three-Dimensional Culture. *Tissue Eng.* 13 (2), 343–349. doi:10.1089/ten.2006.0166

Bouchareb, R., Mahmut, A., Nsaibia, M. J., Boulanger, M. C., Dahou, A., Lépine, J. L., et al. (2015). Autotaxin Derived from Lipoprotein(a) and Valve Interstitial Cells Promotes Inflammation and Mineralization of the Aortic Valve. *Circulation* 132 (8), 677–690. doi:10.1161/CIRCULATIONAHA.115.016757

Bowler, M. A., and Merryman, W. D. (2015). *In Vitro* models of Aortic Valve Calcification: Solidifying a System. *Cardiovasc Pathol.* 24 (1), 1–10. doi:10.1016/j.carpath.2014.08.003

Bracco Gartner, T. C. L., Deddens, J. C., Mol, E. A., Magin Ferrer, M., van Laake, L. W., Bouten, C. V. C., et al. (2019). Anti-fibrotic Effects of Cardiac Progenitor Cells in a 3D-Model of Human Cardiac Fibrosis. *Front. Cardiovasc Med.* 6, 52. doi:10.3389/fcvm.2019.00052

Braselton, W. E., Stuart, K. J., Mullaney, T. P., and Herdt, T. H. (1997). Biopsy Mineral Analysis by Inductively Coupled Plasma-Atomic Emission Spectroscopy with Ultrasonic Nebulization. *J. Vet. Diagn Invest* 9 (4), 395–400. doi:10.1177/104063879700900409

Butcher, J. T., and Nerem, R. M. (2004). Porcine Aortic Valve Interstitial Cells in Three-Dimensional Culture: Comparison of Phenotype with Aortic Smooth Muscle Cells. *J. Heart Valve Dis.* 13 (3), 478–485.

Butcher, J. T., and Nerem, R. M. (2006). Valvular Endothelial Cells Regulate the Phenotype of Interstitial Cells in Co-culture: Effects of Steady Shear Stress. *Tissue Eng.* 12 (4), 905–915. doi:10.1089/ten.2006.12.905

Cai, M. M., Smith, E. R., Brumby, C., McMahon, L. P., and Holt, S. G. (2013). Fetuin-A-containing Calciprotein Particle Levels Can Be Reduced by Dialysis, Sodium Thiosulphate and Plasma Exchange. Potential Therapeutic Implications for Calciphylaxis? *Nephrol. Carlt.* 18 (11), 724–727. doi:10.1111/nep.12137

Carpenter, R. C. (1985). The Analysis of Some Evidential Materials by Inductively Coupled Plasma-Optical Emission Spectrometry. *Forensic Sci. Int.* 27 (3), 157–163. doi:10.1016/0379-0738(85)90152-5

Cartlidge, T. R., Bing, R., Kwiecinski, J., Guzzetti, E., Pawade, T. A., Doris, M. K., et al. (2021). Contrast-enhanced Computed Tomography Assessment of Aortic Stenosis. *Heart* 107 (23), 1905–1911. doi:10.1136/heartjnl-2020-318556

Cartlidge, T. R. G., Doris, M. K., Sellers, S. L., Pawade, T. A., White, A. C., Pessotto, R., et al. (2019). Detection and Prediction of Bioprosthetic Aortic Valve Degeneration. *J. Am. Coll. Cardiol.* 73 (10), 1107–1119. doi:10.1016/j.jacc.2018.12.056

Cheek, J. D., Wirrig, E. E., Alfieri, C. M., James, J. F., and Yutzey, K. E. (2012). Differential Activation of Valvulogenic, Chondrogenic, and Osteogenic Pathways in Mouse Models of Myxomatous and Calcific Aortic Valve Disease. *J. Mol. Cell Cardiol.* 52 (3), 689–700. doi:10.1016/j.yjmcc.2011.12.013

Chen, J. H., Chen, W. L., Sider, K. L., Yip, C. Y., and Simmons, C. A. (2011). β-Catenin Mediates Mechanically Regulated, Transforming Growth Factor-B1-Induced Myofibroblast Differentiation of Aortic Valve Interstitial Cells. *Arterioscler. Thromb. Vasc. Biol.* 31 (3), 590–597. doi:10.1161/ATVBAHA.110.220061

Chen, J. H., and Simmons, C. A. (2011). Cell-matrix Interactions in the Pathobiology of Calcific Aortic Valve Disease: Critical Roles for Matricellular, Matricrine, and Matrix Mechanics Cues. *Circ. Res.* 108 (12), 1510–1524. doi:10.1161/CIRCRESAHA.110.234237

Chester, A. H., Kershaw, J. D., Sarathchandra, P., and Yacoub, M. H. (2008). Localisation and Function of Nerves in the Aortic Root. *J. Mol. Cell Cardiol.* 44 (6), 1045–1052. doi:10.1016/j.yjmcc.2008.03.014

Chester, A. H., Sarathchandra, P., McCormack, A., and Yacoub, M. H. (2021). Organ Culture Model of Aortic Valve Calcification. *Front. Cardiovasc Med.* 8, 734692. doi:10.3389/fcvm.2021.734692

Chitsaz, S., Gundiah, N., Blackshear, C., Tegegn, N., Yan, K. S., Azadani, A. N., et al. (2012). Correlation of Calcification on Excised Aortic Valves by Micro-computed Tomography with Severity of Aortic Stenosis. *J. Heart Valve Dis.* 21 (3), 320–327.

Chong, A., Senior, R., and Wahi, S. (2019). Contemporary Imaging of Aortic Stenosis. *Heart Lung Circ.* 28 (9), 1310–1319. doi:10.1016/j.hlc.2019.05.177

Cimini, M., Boughner, D. R., Ronald, J. A., Aldington, L., and Rogers, K. A. (2005). Development of Aortic Valve Sclerosis in a Rabbit Model of Atherosclerosis: an Immunohistochemical and Histological Study. *J. Heart Valve Dis.* 14 (3), 365–375.

Clavel, M. A., Malouf, J., Michelena, H. I., Suri, R. M., Jaffe, A. S., Mahoney, D. W., et al. (2014). B-type Natriuretic Peptide Clinical Activation in Aortic Stenosis: Impact on Long-Term Survival. *J. Am. Coll. Cardiol.* 63 (19), 2016–2025. doi:10.1016/j.jacc.2014.02.581

Colleville, B., Perzo, N., Avinée, G., Dumesnil, A., Ziegler, F., Billoir, P., et al. (2019). Impact of High-Fat Diet and Vitamin D3 Supplementation on Aortic Stenosis Establishment in Waved-2 Epidermal Growth Factor Receptor Mutant Mice. *J. Integr. Med.* 17 (2), 107–114. doi:10.1016/j.joim.2019.01.010

Copeland, J. G., Maron, B. J., Luka, N. L., Ferrans, V. J., and Michaelis, L. L. (1974). Experimental Production of Aortic Valvular Stenosis. Short-Term and Long-Term Studies in Dogs. *J. Thorac. Cardiovasc Surg.* 67 (3), 371–379. doi:10.1016/s0022-5223(19)40509-6

Cottignoli, V., Cavarretta, E., Salvador, L., Valfré, C., and Maras, A. (2015). Morphological and Chemical Study of Pathological Deposits in Human Aortic and Mitral Valve Stenosis: a Biomineralogical Contribution. *Pathol. Res. Int.* 2015, 342984. doi:10.1155/2015/342984

Cottignoli, V., Relucenti, M., Agrosì, G., Cavarretta, E., Familiari, G., Salvador, L., et al. (2015). Biological Niches within Human Calcified Aortic Valves: Towards Understanding of the Pathological Biomineralization Process. *Biomed. Res. Int.* 2015, 542687. doi:10.1155/2015/542687

Cowell, S. J., Newby, D. E., Burton, J., White, A., Northridge, D. B., Boon, N. A., et al. (2003). Aortic Valve Calcification on Computed Tomography Predicts the Severity of Aortic Stenosis. *Clin. Radiol.* 58 (9), 712–716. doi:10.1016/s0009-9260(03)00184-3

Cueff, C., Serfaty, J. M., Cimadevilla, C., Laissy, J. P., Himbert, D., Tubach, F., et al. (2011). Measurement of Aortic Valve Calcification Using Multislice Computed Tomography: Correlation with Haemodynamic Severity of Aortic Stenosis and Clinical Implication for Patients with Low Ejection Fraction. *Heart* 97 (9), 721–726. doi:10.1136/hrt.2010.198853

Cui, L., Rashdan, N. A., Zhu, D., Milne, E. M., Ajuh, P., Milne, G., et al. (2017). End Stage Renal Disease-Induced Hypercalcemia May Promote Aortic Valve Calcification via Annexin VI Enrichment of Valve Interstitial Cell Derived-Matrix Vesicles. *J. Cell Physiol.* 232 (11), 2985–2995. doi:10.1002/jcp.25935

Cuniberti, L. A., Stutzbach, P. G., Guevara, E., Yannarelli, G. G., Laguens, R. P., and Favaloro, R. R. (2006). Development of Mild Aortic Valve Stenosis in a Rabbit Model of Hypertension. *J. Am. Coll. Cardiol.* 47 (11), 2303–2309. doi:10.1016/j.jacc.2005.12.070

Cushing, M. C., Mariner, P. D., Liao, J. T., Sims, E. A., and Anseth, K. S. (2008). Fibroblast Growth Factor Represses Smad-Mediated Myofibroblast Activation in Aortic Valvular Interstitial Cells. *FASEB J.* 22 (6), 1769–1777. doi:10.1096/fj.07-087627

Danilchenko, S., Kuznetsov, V., Stanislavov, A., Kalinkevich, A., Starikov, V., Moskalenko, R., et al. (2013). The Mineral Component of Human Cardiovascular Deposits: Morphological, Structural and Crystal-Chemical Characterization. *Cryst. Res. Technol.* 48. doi:10.1002/crat.201200443

de la Cuesta, F., Alvarez-Llamas, G., Gil-Dones, F., Darde, V. M., Calvo, E., López, J. A., et al. (2013). Secretome of Human Aortic Valves. *Methods Mol. Biol.* 1005, 237–243. doi:10.1007/978-1-62703-386-2_19

Di Minno, A., Zanobini, M., Myasoedova, V. A., Valerio, V., Songia, P., Saccocci, M., et al. (2017). Could Circulating Fetuin A Be a Biomarker of Aortic Valve Stenosis? *Int. J. Cardiol.* 249, 426–430. doi:10.1016/j.ijcard.2017.05.040

Drolet, M. C., Arsenault, M., and Couet, J. (2003). Experimental Aortic Valve Stenosis in Rabbits. *J. Am. Coll. Cardiol.* 41 (7), 1211–1217. doi:10.1016/s0735-1097(03)00090-1

Drolet, M. C., Roussel, E., Deshaies, Y., Couet, J., and Arsenault, M. (2006). A High Fat/high Carbohydrate Diet Induces Aortic Valve Disease in C57BL/6J Mice. *J. Am. Coll. Cardiol.* 47 (4), 850–855. doi:10.1016/j.jacc.2005.09.049

Dutta, P., Kodigepalli, K. M., LaHaye, S., Thompson, J. W., Rains, S., Nagel, C., et al. (2021). KPT-330 Prevents Aortic Valve Calcification via a Novel C/EBPβ Signaling Pathway. *Circ. Res.* 128 (9), 1300–1316. doi:10.1161/CIRCRESAHA.120.318503

Dutta, P., and Lincoln, J. (2018). Calcific Aortic Valve Disease: a Developmental Biology Perspective. *Curr. Cardiol. Rep.* 20 (4), 21. doi:10.1007/s11886-018-0968-9

Dweck, M. R., Jenkins, W. S., Vesey, A. T., Pringle, M. A., Chin, C. W., Malley, T. S., et al. (2014). 18F-sodium Fluoride Uptake Is a Marker of Active Calcification and Disease Progression in Patients with Aortic Stenosis. *Circ. Cardiovasc Imaging* 7 (2), 371–378. doi:10.1161/CIRCIMAGING.113.001508

El-Hamamsy, I., Balachandran, K., Yacoub, M. H., Stevens, L. M., Sarathchandra, P., Taylor, P. M., et al. (2009). Endothelium-dependent Regulation of the Mechanical Properties of Aortic Valve Cusps. *J. Am. Coll. Cardiol.* 53 (16), 1448–1455. doi:10.1016/j.jacc.2008.11.056

Elmariah, S., McCarthy, C., Ibrahim, N., Furman, D., Mukai, R., Magaret, C., et al. (2018). Multiple Biomarker Panel to Screen for Severe Aortic Stenosis: Results from the CASABLANCA Study. *Open Heart* 5 (2), e000916–e. doi:10.1136/openhrt-2018-000916

Farrar, E. J., and Butcher, J. T. (2014). Heterogeneous Susceptibility of Valve Endothelial Cells to Mesenchymal Transformation in Response to TNFα. *Ann. Biomed. Eng.* 42 (1), 149–161. doi:10.1007/s10439-013-0894-3

Fishbein, M. C., Levy, R. J., Ferrans, V. J., Dearden, L. C., Nashef, A., Goodman, A. P., et al. (1982). Calcifications of Cardiac Valve Bioprostheses. Biochemical, Histologic, and Ultrastructural Observations in a Subcutaneous Implantation Model System. *J. Thorac. Cardiovasc Surg.* 83 (4), 602–609. doi:10.1016/s0022-5223(19)37251-4

Fletcher, A. J., Singh, T., Syed, M. B. J., and Dweck, M. R. (2021). Imaging Aortic Valve Calcification: Significance, Approach and Implications. *Clin. Radiol.* 76 (1), 15–26. doi:10.1016/j.crad.2020.04.007

Francone, M., Budde, R. P. J., Bremerich, J., Dacher, J. N., Loewe, C., Wolf, F., et al. (2020). CT and MR Imaging Prior to Transcatheter Aortic Valve Implantation: Standardisation of Scanning Protocols, Measurements and Reporting-A Consensus Document by the European Society of Cardiovascular Radiology (ESCR). *Eur. Radiol.* 30 (5), 2627–2650. doi:10.1007/s00330-019-06357-8

Galeone, A., Brunetti, G., Oranger, A., Greco, G., Di Benedetto, A., Mori, G., et al. (2013). Aortic Valvular Interstitial Cells Apoptosis and Calcification Are Mediated by TNF-Related Apoptosis-Inducing Ligand. *Int. J. Cardiol.* 169 (4), 296–304. doi:10.1016/j.ijcard.2013.09.012

Gall, K. L., Smith, S. E., Willmette, C. A., and O'Brien, M. F. (1998). Allograft Heart Valve Viability and Valve-Processing Variables. *Ann. Thorac. Surg.* 65 (4), 1032–1038. doi:10.1016/s0003-4975(98)00085-x

Gayrard, N., Muyor, K., Notarnicola, C., Duranton, F., Jover, B., and Argilés, À. (2020). Optimisation of Cell and *Ex Vivo* Culture Conditions to Study Vascular Calcification. *PLoS One* 15 (3), e0230201. doi:10.1371/journal.pone.0230201

Gil-Dones, F., Darde, V. M., Alonso-Orgaz, S., Lopez-Almodovar, L. F., Mourino-Alvarez, L., Padial, L. R., et al. (2012). Inside Human Aortic Stenosis: a Proteomic Analysis of Plasma. *J. Proteomics* 75 (5), 1639–1653. doi:10.1016/j.jprot.2011.11.036

Gil-Dones, F., Martin-Rojas, T., Lopez-Almodovar, L. F., de la Cuesta, F., Darde, V. M., Alvarez-Llamas, G., et al. (2010). Valvular Aortic Stenosis: a Proteomic Insight. *Clin. Med. Insights Cardiol.* 4, 1–7. doi:10.4137/cmc.s3884

Gomel, M. A., Lee, R., and Grande-Allen, K. J. (2018). Comparing the Role of Mechanical Forces in Vascular and Valvular Calcification Progression. *Front. Cardiovasc Med.* 5, 197. doi:10.3389/fcvm.2018.00197

Gomez Stallons, M. V., Wirrig-Schwendeman, E. E., Fang, M., Cheek, J. D., Alfieri, C. M., Hinton, R. B., et al. (2016). "Molecular Mechanisms of Heart Valve Development and Disease," in *Etiology and Morphogenesis of Congenital Heart Disease: From Gene Function and Cellular Interaction to Morphology. Tokyo2016*. Editors T. Nakanishi, R. R. Markwald, H. S. Baldwin, B. B. Keller, D. Srivastava, and H. Yamagishi, 145–151. doi:10.1007/978-4-431-54628-3_18

Gonzalez Rodriguez, A., Schroeder, M. E., Grim, J. C., Walker, C. J., Speckl, K. F., Weiss, R. M., et al. (2021). Tumor Necrosis Factor-α Promotes and Exacerbates

Calcification in Heart Valve Myofibroblast Populations. *FASEB J. official Publ. Fed. Am. Soc. Exp. Biol.* 35 (3), e21382. doi:10.1096/fj.202002013rr

Goto, S., Rogers, M. A., Blaser, M. C., Higashi, H., Lee, L. H., Schlotter, F., et al. (2019). Standardization of Human Calcific Aortic Valve Disease *In Vitro* Modeling Reveals Passage-dependent Calcification. *Front. Cardiovasc Med.* 6, 49. doi:10.3389/fcvm.2019.00049

Gould, R. A., and Butcher, J. T. (2010). Isolation of Valvular Endothelial Cells. *J. Vis. Exp.* 46. doi:10.3791/2158

Gould, S. T., Matherly, E. E., Smith, J. N., Heistad, D. D., and Anseth, K. S. (2014). The Role of Valvular Endothelial Cell Paracrine Signaling and Matrix Elasticity on Valvular Interstitial Cell Activation. *Biomaterials* 35 (11), 3596–3606. doi:10.1016/j.biomaterials.2014.01.005

Gourgas, O., Khan, K., Schwertani, A., and Cerruti, M. (2020). Differences in Mineral Composition and Morphology between Men and Women in Aortic Valve Calcification. *Acta Biomater.* 106, 342–350. doi:10.1016/j.actbio.2020.02.030

Grauss, R. W., Hazekamp, M. G., van Vliet, S., Gittenberger-de Groot, A. C., and DeRuiter, M. C. (2003). Decellularization of Rat Aortic Valve Allografts Reduces Leaflet Destruction and Extracellular Matrix Remodeling. *J. Thorac. Cardiovasc Surg.* 126 (6), 2003–2010. doi:10.1016/s0022-5223(03)00956-5

Gregory, C. A., Gunn, W. G., Peister, A., and Prockop, D. J. (2004). An Alizarin Red-Based Assay of Mineralization by Adherent Cells in Culture: Comparison with Cetylpyridinium Chloride Extraction. *Anal. Biochem.* 329 (1), 77–84. doi:10.1016/j.ab.2004.02.002

Grodecki, K., Tamarappoo, B. K., Huczek, Z., Jedrzejczyk, S., Cadet, S., Kwiecinski, J., et al. (2021). Non-calcific Aortic Tissue Quantified from Computed Tomography Angiography Improves Diagnosis and Prognostication of Patients Referred for Transcatheter Aortic Valve Implantation. *Eur. Heart J. Cardiovasc Imaging* 22 (6), 626–635. doi:10.1093/ehjci/jeaa304

Gu, X., and Masters, K. S. (2010). Regulation of Valvular Interstitial Cell Calcification by Adhesive Peptide Sequences. *J. Biomed. Mater Res. A* 93 (4), 1620–1630. doi:10.1002/jbm.a.32660

Guerraty, M., and Mohler Iii, E. R., Iii (2007). Models of Aortic Valve Calcification. *J. Investig. Med.* 55 (6), 278–283. doi:10.2310/6650.2007.00012

Guerraty, M. A., Grant, G. R., Karanian, J. W., Chiesa, O. A., Pritchard, W. F., and Davies, P. F. (2010). Hypercholesterolemia Induces Side-specific Phenotypic Changes and Peroxisome Proliferator-Activated Receptor-Gamma Pathway Activation in Swine Aortic Valve Endothelium. *Arterioscler. Thromb. Vasc. Biol.* 30 (2), 225–231. doi:10.1161/ATVBAHA.109.198549

Gwanmesia, P., Ziegler, H., Eurich, R., Barth, M., Kamiya, H., Karck, M., et al. (2010). Opposite Effects of Transforming Growth Factor-B1 and Vascular Endothelial Growth Factor on the Degeneration of Aortic Valvular Interstitial Cell Are Modified by the Extracellular Matrix Protein Fibronectin: Implications for Heart Valve Engineering. *Tissue Eng. Part A* 16 (12), 3737–3746. doi:10.1089/ten.TEA.2010.0304

Hanć, A., Komorowicz, I., Iskra, M., Majewski, W., and Barałkiewicz, D. (2011). Application of Spectroscopic Techniques: ICP-OES, LA-ICP-MS and Chemometric Methods for Studying the Relationships between Trace Elements in Clinical Samples from Patients with Atherosclerosis Obliterans. *Anal. Bioanal. Chem.* 399 (9), 3221–3231. doi:10.1007/s00216-011-4729-5

Hara, T., Tsukada, N., Okano, M., Ishida, T., Hirata, K. I., and Shiomi, M. (2018). Progression of Calcific Aortic Valve Sclerosis in WHHLMI Rabbits. *Atherosclerosis* 273, 8–14. doi:10.1016/j.atherosclerosis.2018.03.044

Heiss, A., Pipich, V., Jahnen-Dechent, W., and Schwahn, D. (2010). Fetuin-A Is a Mineral Carrier Protein: Small Angle Neutron Scattering Provides New Insight on Fetuin-A Controlled Calcification Inhibition. *Biophys. J.* 99 (12), 3986–3995. doi:10.1016/j.bpj.2010.10.030

Heitkemper, D. T., Kaine, L. A., Jackson, D. S., and Wolnik, K. A. (1994). Practical Applications of Element-specific Detection by Inductively Coupled Plasma Atomic Emission Spectroscopy and Inductively Coupled Plasma Mass Spectrometry to Ion Chromatography of Foods. *J. Chromatogr. A* 671 (1-2), 101–108. doi:10.1016/0021-9673(94)80227-0

Herrmann, M., Schäfer, C., Heiss, A., Gräber, S., Kinkeldey, A., Büscher, A., et al. (2012). Clearance of Fetuin-A-Ccontaining Calciprotein Particles Is Mediated by Scavenger Receptor-A. *Circ. Res.* 111 (5), 575–584. doi:10.1161/CIRCRESAHA.111.261479

Hinton, R. B., Jr., Alfieri, C. M., Witt, S. A., Glascock, B. J., Khoury, P. R., Benson, D. W., et al. (2008). Mouse Heart Valve Structure and Function: Echocardiographic and Morphometric Analyses from the Fetus through the Aged Adult. *Am. J. Physiol. Heart Circ. Physiol.* 294 (6), H2480–H2488. doi:10.1152/ajpheart.91431.2007

Hinton, R. B., and Yutzey, K. E. (2011). Heart Valve Structure and Function in Development and Disease. *Annu. Rev. Physiol.* 73, 29–46. doi:10.1146/annurev-physiol-012110-142145

Hinz, B., Celetta, G., Tomasek, J. J., Gabbiani, G., and Chaponnier, C. (2001). Alpha-smooth Muscle Actin Expression Upregulates Fibroblast Contractile Activity. *Mol. Biol. Cell* 12 (9), 2730–2741. doi:10.1091/mbc.12.9.2730

Hjortnaes, J., Camci-Unal, G., Hutcheson, J. D., Jung, S. M., Schoen, F. J., Kluin, J., et al. (2015). Directing Valvular Interstitial Cell Myofibroblast-like Differentiation in a Hybrid Hydrogel Platform. *Adv. Healthc. Mater* 4 (1), 121–130. doi:10.1002/adhm.201400029

Hjortnaes, J., Goettsch, C., Hutcheson, J. D., Camci-Unal, G., Lax, L., Scherer, K., et al. (2016). Simulation of Early Calcific Aortic Valve Disease in a 3D Platform: A Role for Myofibroblast Differentiation. *J. Mol. Cell Cardiol.* 94, 13–20. doi:10.1016/j.yjmcc.2016.03.004

Honda, S., Miyamoto, T., Watanabe, T., Narumi, T., Kadowaki, S., Honda, Y., et al. (2014). A Novel Mouse Model of Aortic Valve Stenosis Induced by Direct Wire Injury. *Arterioscler. Thromb. Vasc. Biol.* 34 (2), 270–278. doi:10.1161/ATVBAHA.113.302610

Hortells, L., Sosa, C., Millán, Á., and Sorribas, V. (2015). Critical Parameters of the *In Vitro* Method of Vascular Smooth Muscle Cell Calcification. *PLoS One* 10 (11), e0141751. doi:10.1371/journal.pone.0141751

Hui, M., and Tenenbaum, H. C. (1998). New Face of an Old Enzyme: Alkaline Phosphatase May Contribute to Human Tissue Aging by Inducing Tissue Hardening and Calcification. *Anat. Rec.* 253 (3), 91–94. doi:10.1002/(SICI)1097-0185(199806)253:3<91:AID-AR5>3.0.CO;2-H

Hulin, A., Hego, A., Lancellotti, P., and Oury, C. (2018). Advances in Pathophysiology of Calcific Aortic Valve Disease Propose Novel Molecular Therapeutic Targets. *Front. Cardiovasc Med.* 5, 21. doi:10.3389/fcvm.2018.00021

Hutcheson, J. D., Maldonado, N., and Aikawa, E. (2014). Small Entities with Large Impact: Microcalcifications and Atherosclerotic Plaque Vulnerability. *Curr. Opin. Lipidol.* 25 (5), 327–332. doi:10.1097/MOL.0000000000000105

Hutcheson, J. D., Ryzhova, L. M., Setola, V., and Merryman, W. D. (2012). 5-HT(2B) Antagonism Arrests Non-canonical TGF-B1-Induced Valvular Myofibroblast Differentiation. *J. Mol. Cell Cardiol.* 53 (5), 707–714. doi:10.1016/j.yjmcc.2012.08.012

Ishikawa, S., Iwasaki, K., Komaki, M., and Ishikawa, I. (2004). Role of Ascorbic Acid in Periodontal Ligament Cell Differentiation. *J. Periodontol.* 75 (5), 709–716. doi:10.1902/jop.2004.75.5.709

Isoda, K., Matsuki, T., Kondo, H., Iwakura, Y., and Ohsuzu, F. (2010). Deficiency of Interleukin-1 Receptor Antagonist Induces Aortic Valve Disease in BALB/c Mice. *Arterioscler. Thromb. Vasc. Biol.* 30 (4), 708–715. doi:10.1161/ATVBAHA.109.201749

Jahnen-Dechent, W., Heiss, A., Schäfer, C., and Ketteler, M. (2011). Fetuin-A Regulation of Calcified Matrix Metabolism. *Circ. Res.* 108 (12), 1494–1509. doi:10.1161/CIRCRESAHA.110.234260

Jenkins, G. (2008). The Role of Proteases in Transforming Growth Factor-Beta Activation. *Int. J. Biochem. Cell Biol.* 40 (6-7), 1068–1078. doi:10.1016/j.biocel.2007.11.026

Jenkins, W. S., Vesey, A. T., Shah, A. S., Pawade, T. A., Chin, C. W., White, A. C., et al. (2015). Valvular (18)F-Fluoride and (18)F-Fluorodeoxyglucose Uptake Predict Disease Progression and Clinical Outcome in Patients with Aortic Stenosis. *J. Am. Coll. Cardiol.* 66 (10), 1200–1201. doi:10.1016/j.jacc.2015.06.1325

Jian, B., Narula, N., Li, Q. Y., Mohler, E. R., 3rd, and Levy, R. J. (2003). Progression of Aortic Valve Stenosis: TGF-Beta1 Is Present in Calcified Aortic Valve Cusps and Promotes Aortic Valve Interstitial Cell Calcification via Apoptosis. *Ann. Thorac. Surg.* 75 (2), 457–465. doi:10.1016/s0003-4975(02)04312-6

Jian, B., Xu, J., Connolly, J., Savani, R. C., Narula, N., Liang, B., et al. (2002). Serotonin Mechanisms in Heart Valve Disease I: Serotonin-Induced Up-Regulation of Transforming Growth Factor-Beta1 via G-Protein Signal Transduction in Aortic Valve Interstitial Cells. *Am. J. Pathol.* 161 (6), 2111–2121. doi:10.1016/s0002-9440(10)64489-6

Johnson, C. L., and Merryman, W. D. (2021). Side-specific Valvular Endothelial-Interstitial Cell Mechano-Communication via Cadherin-11. *J. Biomech.* 119, 110253. doi:10.1016/j.jbiomech.2021.110253

Jono, S., Peinado, C., and Giachelli, C. M. (2000). Phosphorylation of Osteopontin Is Required for Inhibition of Vascular Smooth Muscle Cell Calcification. *J. Biol. Chem.* 275 (26), 20197–20203. doi:10.1074/jbc.M909174199

Kang, D. H., Park, S. J., Rim, J. H., Yun, S. C., Kim, D. H., Song, J. M., et al. (2010). Early Surgery versus Conventional Treatment in Asymptomatic Very Severe Aortic Stenosis. *Circulation* 121 (13), 1502–1509. doi:10.1161/CIRCULATIONAHA.109.909903

Kennedy, J. A., Hua, X., Mishra, K., Murphy, G. A., Rosenkranz, A. C., and Horowitz, J. D. (2009). Inhibition of Calcifying Nodule Formation in Cultured Porcine Aortic Valve Cells by Nitric Oxide Donors. *Eur. J. Pharmacol.* 602 (1), 28–35. doi:10.1016/j.ejphar.2008.11.029

Kheradvar, A., Zareian, R., Kawauchi, S., Goodwin, R. L., and Rugonyi, S. (2017). Animal Models for Heart Valve Research and Development. *Drug Discov. Today Dis. Models* 24, 55–62. doi:10.1016/j.ddmod.2018.04.001

Kim, K. M., Chang, S. H., Trump, B. F., and Spurgeon, H. (1986). Calcification in Aging Canine Aortic Valve. *Scan Electron Microsc.* (Pt 3), 1151–1156.

Köhler, W. M., Freitag-Wolf, S., Lambers, M., Lutz, M., Niemann, P. M., Petzina, R., et al. (2016). Preprocedural but Not Periprocedural High-Sensitive Troponin T Levels Predict Outcome in Patients Undergoing Transcatheter Aortic Valve Implantation. *Cardiovasc Ther.* 34 (6), 385–396. doi:10.1111/1755-5922.12208

Konduri, S., Xing, Y., Warnock, J. N., He, Z., and Yoganathan, A. P. (2005). Normal Physiological Conditions Maintain the Biological Characteristics of Porcine Aortic Heart Valves: an *Ex Vivo* Organ Culture Study. *Ann. Biomed. Eng.* 33 (9), 1158–1166. doi:10.1007/s10439-005-5506-4

Kostina, A., Shishkova, A., Ignatieva, E., Irtyuga, O., Bogdanova, M., Levchuk, K., et al. (2018). Different Notch Signaling in Cells from Calcified Bicuspid and Tricuspid Aortic Valves. *J. Mol. Cell Cardiol.* 114, 211–219. doi:10.1016/j.yjmcc.2017.11.009

Kreitals, N. M., and Watling, R. J. (2014). Multi-element Analysis Using Inductively Coupled Plasma Mass Spectrometry and Inductively Coupled Plasma Atomic Emission Spectroscopy for Provenancing of Animals at the Continental Scale. *Forensic Sci. Int.* 244, 116–121. doi:10.1016/j.forsciint.2014.08.016

Langenbach, F., and Handschel, J. (2013). Effects of Dexamethasone, Ascorbic Acid and β-glycerophosphate on the Osteogenic Differentiation of Stem Cells *In Vitro*. *Stem Cell Res. Ther.* 4 (5), 117. doi:10.1186/scrt328

Latif, N., Quillon, A., Sarathchandra, P., McCormack, A., Lozanoski, A., Yacoub, M. H., et al. (2015). Modulation of Human Valve Interstitial Cell Phenotype and Function Using a Fibroblast Growth Factor 2 Formulation. *PLoS One* 10 (6), e0127844. doi:10.1371/journal.pone.0127844

Latif, N., Sarathchandra, P., Chester, A. H., and Yacoub, M. H. (2015). Expression of Smooth Muscle Cell Markers and Co-activators in Calcified Aortic Valves. *Eur. Heart J.* 36 (21), 1335–1345. doi:10.1093/eurheartj/eht547

Latif, N., Sarathchandra, P., Thomas, P. S., Antoniw, J., Batten, P., Chester, A. H., et al. (2007). Characterization of Structural and Signaling Molecules by Human Valve Interstitial Cells and Comparison to Human Mesenchymal Stem Cells. *J. Heart Valve Dis.* 16 (1), 56–66.

Lee, J. S., Morrisett, J. D., and Tung, C. H. (2012). Detection of Hydroxyapatite in Calcified Cardiovascular Tissues. *Atherosclerosis* 224 (2), 340–347. doi:10.1016/j.atherosclerosis.2012.07.023

Lee, T. C., Zhao, Y. D., Courtman, D. W., and Stewart, D. J. (2000). Abnormal Aortic Valve Development in Mice Lacking Endothelial Nitric Oxide Synthase. *Circulation* 101 (20), 2345–2348. doi:10.1161/01.cir.101.20.2345

Leopold, J. A. (2012). Cellular Mechanisms of Aortic Valve Calcification. *Circ. Cardiovasc Interv.* 5 (4), 605–614. doi:10.1161/CIRCINTERVENTIONS.112.971028

Levy, R. J., Schoen, F. J., Levy, J. T., Nelson, A. C., Howard, S. L., and Oshry, L. J. (1983). Biologic Determinants of Dystrophic Calcification and Osteocalcin Deposition in Glutaraldehyde-Preserved Porcine Aortic Valve Leaflets Implanted Subcutaneously in Rats. *Am. J. Pathol.* 113 (2), 143–155.

Lindman, B. R., Dweck, M. R., Lancellotti, P., Généreux, P., Piérard, L. A., O'Gara, P. T., et al. (2020). Management of Asymptomatic Severe Aortic Stenosis: Evolving Concepts in Timing of Valve Replacement. *JACC Cardiovasc Imaging* 13 (2 Pt 1), 481–493. doi:10.1016/j.jcmg.2019.01.036

Liu, A. C., Joag, V. R., and Gotlieb, A. I. (2007). The Emerging Role of Valve Interstitial Cell Phenotypes in Regulating Heart Valve Pathobiology. *Am. J. Pathol.* 171 (5), 1407–1418. doi:10.2353/ajpath.2007.070251

Ljungberg, J., Janiec, M., Bergdahl, I. A., Holmgren, A., Hultdin, J., Johansson, B., et al. (2018). Proteomic Biomarkers for Incident Aortic Stenosis Requiring Valvular Replacement. *Circulation* 138 (6), 590–599. doi:10.1161/CIRCULATIONAHA.117.030414

Luo, G., Ducy, P., McKee, M. D., Pinero, G. J., Loyer, E., Behringer, R. R., et al. (1997). Spontaneous Calcification of Arteries and Cartilage in Mice Lacking Matrix GLA Protein. *Nature* 386 (6620), 78–81. doi:10.1038/386078a0

MacGrogan, D., Martínez-Poveda, B., Desvignes, J. P., Fernandez-Friera, L., Gomez, M. J., Gil Vilariño, E., et al. (2020). Identification of a Peripheral Blood Gene Signature Predicting Aortic Valve Calcification. *Physiol. Genomics* 52 (12), 563–574. doi:10.1152/physiolgenomics.00034.2020

Macri-Pellizzeri, L., De Melo, N., Ahmed, I., Grant, D., Scammell, B., and Sottile, V. (2018). Live Quantitative Monitoring of Mineral Deposition in Stem Cells Using Tetracycline Hydrochloride. *Tissue Eng. Part C Methods* 24 (3), 171–178. doi:10.1089/ten.TEC.2017.0400

Mako, W. J., and Vesely, I. (1997). *In Vivo* and *In Vitro* Models of Calcification in Porcine Aortic Valve Cusps. *J. Heart Valve Dis.* 6 (3), 316–323.

Mangialardo, S., Cottignoli, V., Cavarretta, E., Salvador, L., Postorino, P., and Maras, A. (2012). Pathological Biominerals: Raman and Infrared Studies of Bioapatite Deposits in Human Heart Valves. *Appl. Spectrosc.* 66 (10), 1121–1127. doi:10.1366/12-06606

Marechaux, S., Corseaux, D., Vincentelli, A., Richardson, M., Ung, A., Susen, S., et al. (2009). Identification of Tissue Factor in Experimental Aortic Valve Sclerosis. *Cardiovasc Pathol.* 18 (2), 67–76. doi:10.1016/j.carpath.2007.12.014

Martin-Rojas, T., Mourino-Alvarez, L., Alonso-Orgaz, S., Rosello-Lleti, E., Calvo, E., Lopez-Almodovar, L. F., et al. (2015). iTRAQ Proteomic Analysis of Extracellular Matrix Remodeling in Aortic Valve Disease. *Sci. Rep.* 5, 17290. doi:10.1038/srep17290

Martin-Rojas, T., Mourino-Alvarez, L., Gil-Dones, F., de la Cuesta, F., Rosello-Lleti, E., Laborde, C. M., et al. (2017). A Clinical Perspective on the Utility of Alpha 1 Antichymotrypsin for the Early Diagnosis of Calcific Aortic Stenosis. *Clin. Proteomics* 14, 12. doi:10.1186/s12014-017-9147-z

Mathieu, P., Boulanger, M. C., and Bouchareb, R. (2014). Molecular Biology of Calcific Aortic Valve Disease: towards New Pharmacological Therapies. *Expert Rev. Cardiovasc Ther.* 12 (7), 851–862. doi:10.1586/14779072.2014.923756

Matsumoto, K., Satoh, K., Maniwa, T., Araki, A., Maruyama, R., and Oda, T. (2012). Noticeable Decreased Expression of Tenascin-X in Calcific Aortic Valves. *Connect. Tissue Res.* 53 (6), 460–468. doi:10.3109/03008207.2012.702818

Merryman, W. D., Lukoff, H. D., Long, R. A., Engelmayr, G. C., Jr., Hopkins, R. A., and Sacks, M. S. (2007). Synergistic Effects of Cyclic Tension and Transforming Growth Factor-Beta1 on the Aortic Valve Myofibroblast. *Cardiovasc Pathol.* 16 (5), 268–276. doi:10.1016/j.carpath.2007.03.006

Messika-Zeitoun, D., Bielak, L. F., Peyser, P. A., Sheedy, P. F., Turner, S. T., Nkomo, V. T., et al. (2007). Aortic Valve Calcification: Determinants and Progression in the Population. *Arterioscler. Thromb. Vasc. Biol.* 27 (3), 642–648. doi:10.1161/01.ATV.0000255952.47980.c2

Miller, J. D., Weiss, R. M., Serrano, K. M., Brooks, R. M., 2nd, Berry, C. J., Zimmerman, K., et al. (2009). Lowering Plasma Cholesterol Levels Halts Progression of Aortic Valve Disease in Mice. *Circulation* 119 (20), 2693–2701. doi:10.1161/CIRCULATIONAHA.108.834614

Miller, J. D., Weiss, R. M., Serrano, K. M., Castaneda, L. E., Brooks, R. M., Zimmerman, K., et al. (2010). Evidence for Active Regulation of Pro-osteogenic Signaling in Advanced Aortic Valve Disease. *Arterioscler. Thromb. Vasc. Biol.* 30 (12), 2482–2486. doi:10.1161/ATVBAHA.110.211029

Mittal, T. K., and Marcus, N. (2021). Imaging Diagnosis of Aortic Stenosis. *Clin. Radiol.* 76 (1), 3–14. doi:10.1016/j.crad.2020.04.008

Mohler, E. R., 3rd, Gannon, F., Reynolds, C., Zimmerman, R., Keane, M. G., and Kaplan, F. S. (2001). Bone Formation and Inflammation in Cardiac Valves. *Circulation* 103 (11), 1522–1528. doi:10.1161/01.cir.103.11.1522

Monzack, E. L., Gu, X., and Masters, K. S. (2009). Efficacy of Simvastatin Treatment of Valvular Interstitial Cells Varies with the Extracellular Environment. *Arterioscler. Thromb. Vasc. Biol.* 29 (2), 246–253. doi:10.1161/ATVBAHA.108.179218

Monzack, E. L., and Masters, K. S. (2011). Can Valvular Interstitial Cells Become True Osteoblasts? A Side-By-Side Comparison. *J. Heart Valve Dis.* 20 (4), 449–463.

Mourino-Alvarez, L., Baldan-Martin, M., Gonzalez-Calero, L., Martinez-Laborde, C., Sastre-Oliva, T., Moreno-Luna, R., et al. (2016). Patients with Calcific Aortic Stenosis Exhibit Systemic Molecular Evidence of Ischemia, Enhanced Coagulation, Oxidative Stress and Impaired Cholesterol Transport. *Int. J. Cardiol.* 225, 99–106. doi:10.1016/j.ijcard.2016.09.089

Natorska, J., Kopytek, M., and Undas, A. (2021). Aortic Valvular Stenosis: Novel Therapeutic Strategies. *Eur. J. Clin. Invest* 51 (7), e13527. doi:10.1111/eci.13527

Nchimi, A., Dibato, J. E., Davin, L., Schoysman, L., Oury, C., and Lancellotti, P. (2018). Predicting Disease Progression and Mortality in Aortic Stenosis: A Systematic Review of Imaging Biomarkers and Meta-Analysis. *Front. Cardiovasc Med.* 5, 112. doi:10.3389/fcvm.2018.00112

Nguyen, V., Cimadevilla, C., Estellat, C., Codogno, I., Huart, V., Benessiano, J., et al. (2015). Haemodynamic and Anatomic Progression of Aortic Stenosis. *Heart* 101 (12), 943–947. doi:10.1136/heartjnl-2014-307154

Niepmann, S. T., Steffen, E., Zietzer, A., Adam, M., Nordsiek, J., Gyamfi-Poku, I., et al. (2019). Graded Murine Wire-Induced Aortic Valve Stenosis Model Mimics Human Functional and Morphological Disease Phenotype. *Clin. Res. Cardiol.* 108 (8), 847–856. doi:10.1007/s00392-019-01413-1

Nigam, V., and Srivastava, D. (2009). Notch1 Represses Osteogenic Pathways in Aortic Valve Cells. *J. Mol. Cell Cardiol.* 47 (6), 828–834. doi:10.1016/j.yjmcc.2009.08.008

Nkomo, V. T., Gardin, J. M., Skelton, T. N., Gottdiener, J. S., Scott, C. G., and Enriquez-Sarano, M. (2006). Burden of Valvular Heart Diseases: a Population-Based Study. *Lancet* 368 (9540), 1005–1011. doi:10.1016/S0140-6736(06)69208-8

Nus, M., MacGrogan, D., Martínez-Poveda, B., Benito, Y., Casanova, J. C., Fernández-Avilés, F., et al. (2011). Diet-induced Aortic Valve Disease in Mice Haploinsufficient for the Notch Pathway Effector RBPJK/CSL. *Arterioscler. Thromb. Vasc. Biol.* 31 (7), 1580–1588. doi:10.1161/ATVBAHA.111.227561

O'Neill, B. P., Guerrero, M., Thourani, V. H., Kodali, S., Heldman, A., Williams, M., et al. (2015). Prognostic Value of Serial B-type Natriuretic Peptide Measurement in Transcatheter Aortic Valve Replacement (From the PARTNER Trial). *Am. J. Cardiol.* 115 (9), 1265–1272. doi:10.1016/j.amjcard.2015.01.561

Olkowicz, M., Debski, J., Jablonska, P., Dadlez, M., and Smolenski, R. T. (2017). Application of a New Procedure for Liquid Chromatography/mass Spectrometry Profiling of Plasma Amino Acid-Related Metabolites and Untargeted Shotgun Proteomics to Identify Mechanisms and Biomarkers of Calcific Aortic Stenosis. *J. Chromatogr. A* 1517, 66–78. doi:10.1016/j.chroma.2017.08.024

Olsson, M., Rosenqvist, M., and Nilsson, J. (1994). Expression of HLA-DR Antigen and Smooth Muscle Cell Differentiation Markers by Valvular Fibroblasts in Degenerative Aortic Stenosis. *J. Am. Coll. Cardiol.* 24 (7), 1664–1671. doi:10.1016/0735-1097(94)90172-4

Orzechowska, S., Wróbel, A., Goncerz, G., Podolec, P., and Rokita, E. (2014). Physicochemical and Micro-tomographic Characterization of Inorganic Deposits Associated with Aortic Stenosis. *J. Heart Valve Dis.* 23 (1), 40–47.

Osman, L., Chester, A. H., Amrani, M., Yacoub, M. H., and Smolenski, R. T. (2006). A Novel Role of Extracellular Nucleotides in Valve Calcification: a Potential Target for Atorvastatin. *Circulation* 114 (1 Suppl. l), I566–I572. doi:10.1161/CIRCULATIONAHA.105.001214

Osman, L., Chester, A. H., Sarathchandra, P., Latif, N., Meng, W., Taylor, P. M., et al. (2007). A Novel Role of the Sympatho-Adrenergic System in Regulating Valve Calcification. *Circulation* 116 (11 Suppl. l), I282–I287. doi:10.1161/CIRCULATIONAHA.106.681072

Osman, L., Yacoub, M. H., Latif, N., Amrani, M., and Chester, A. H. (2006). Role of Human Valve Interstitial Cells in Valve Calcification and Their Response to Atorvastatin. *Circulation* 114 (1 Suppl. l), I547–I552. doi:10.1161/CIRCULATIONAHA.105.001115

Osnabrugge, R. L., Mylotte, D., Head, S. J., Van Mieghem, N. M., Nkomo, V. T., LeReun, C. M., et al. (2013). Aortic Stenosis in the Elderly: Disease Prevalence and Number of Candidates for Transcatheter Aortic Valve Replacement: a Meta-Analysis and Modeling Study. *J. Am. Coll. Cardiol.* 62 (11), 1002–1012. doi:10.1016/j.jacc.2013.05.015

Oury, C., Côté, N., and Clavel, M. A. (2020). Biomarkers Associated with Aortic Stenosis and Structural Bioprosthesis Dysfunction. *Cardiol. Clin.* 38 (1), 47–54. doi:10.1016/j.ccl.2019.09.005

Oury, C., Servais, L., Bouznad, N., Hego, A., Nchimi, A., and Lancellotti, P. (2016). MicroRNAs in Valvular Heart Diseases: Potential Role as Markers and Actors of Valvular and Cardiac Remodeling. *Int. J. Mol. Sci.* 17 (7). doi:10.3390/ijms17071120

Pai, R. G., Kapoor, N., Bansal, R. C., and Varadarajan, P. (2006). Malignant Natural History of Asymptomatic Severe Aortic Stenosis: Benefit of Aortic Valve Replacement. *Ann. Thorac. Surg.* 82 (6), 2116–2122. doi:10.1016/j.athoracsur.2006.07.043

Paraskova, J. V., Jørgensen, C., Reitzel, K., Pettersson, J., Rydin, E., and Sjöberg, P. J. (2015). Speciation of Inositol Phosphates in Lake Sediments by Ion-Exchange Chromatography Coupled with Mass Spectrometry, Inductively Coupled Plasma Atomic Emission Spectroscopy, and 31P NMR Spectroscopy. *Anal. Chem.* 87 (5), 2672–2677. doi:10.1021/ac5033484

Parizi, M., Howard, E. W., and Tomasek, J. J. (2000). Regulation of LPA-Promoted Myofibroblast Contraction: Role of Rho, Myosin Light Chain Kinase, and Myosin Light Chain Phosphatase. *Exp. Cell Res.* 254 (2), 210–220. doi:10.1006/excr.1999.4754

Parra-Izquierdo, I., Sánchez-Bayuela, T., Castaños-Mollor, I., López, J., Gómez, C., San Román, J. A., et al. (2021). Clinically Used JAK Inhibitor Blunts dsRNA-Induced Inflammation and Calcification in Aortic Valve Interstitial Cells. *FEBS J.* 288 (22), 6528–6542. doi:10.1111/febs.16026

Patel, N., and Kumbhani, D. J. (2018). Clinical Implications of Serum Biomarkers of Cardiac Stress in Aortic Stenosis. *Curr. Heart Fail Rep.* 15 (5), 281–286. doi:10.1007/s11897-018-0403-y

Pawade, T., Sheth, T., Guzzetti, E., Dweck, M. R., and Clavel, M. A. (2019). Why and How to Measure Aortic Valve Calcification in Patients with Aortic Stenosis. *JACC Cardiovasc Imaging* 12 (9), 1835–1848. doi:10.1016/j.jcmg.2019.01.045

Pawade, T. A., Newby, D. E., and Dweck, M. R. (2015). Calcification in Aortic Stenosis: The Skeleton Key. *J. Am. Coll. Cardiol.* 66 (5), 561–577. doi:10.1016/j.jacc.2015.05.066

Pho, M., Lee, W., Watt, D. R., Laschinger, C., Simmons, C. A., and McCulloch, C. A. (2008). Cofilin Is a Marker of Myofibroblast Differentiation in Cells from Porcine Aortic Cardiac Valves. *Am. J. Physiol. Heart Circ. Physiol.* 294 (4), H1767–H1778. doi:10.1152/ajpheart.01305.2007

Plazyo, O., Liu, R., Moazzem Hossain, M., and Jin, J. P. (2018). Deletion of Calponin 2 Attenuates the Development of Calcific Aortic Valve Disease in ApoE-/- Mice. *J. Mol. Cell Cardiol.* 121, 233–241. doi:10.1016/j.yjmcc.2018.07.249

Poggio, P., Branchetti, E., Grau, J. B., Lai, E. K., Gorman, R. C., Gorman, J. H., 3rd, et al. (2014). Osteopontin-CD44v6 Interaction Mediates Calcium Deposition via Phospho-Akt in Valve Interstitial Cells from Patients with Noncalcified Aortic Valve Sclerosis. *Arterioscler. Thromb. Vasc. Biol.* 34 (9), 2086–2094. doi:10.1161/ATVBAHA.113.303017

Porras, A. M., Shanmuganayagam, D., Meudt, J. J., Krueger, C. G., Hacker, T. A., Rahko, P. S., et al. (2015). Development of Aortic Valve Disease in Familial Hypercholesterolemic Swine: Implications for Elucidating Disease Etiology. *J. Am. Heart Assoc.* 4 (10), e002254. doi:10.1161/JAHA.115.002254

Porras, A. M., van Engeland, N. C., Marchbanks, E., McCormack, A., Bouten, C. V., Yacoub, M. H., et al. (2017). Robust Generation of Quiescent Porcine Valvular Interstitial Cell Cultures. *J. Am. Heart Assoc.* 6 (3). doi:10.1161/JAHA.116.005041

Price, P. A., Faus, S. A., and Williamson, M. K. (1998). Warfarin Causes Rapid Calcification of the Elastic Lamellae in Rat Arteries and Heart Valves. *Arterioscler. Thromb. Vasc. Biol.* 18 (9), 1400–1407. doi:10.1161/01.atv.18.9.1400

Price, P. A., and Lim, J. E. (2003). The Inhibition of Calcium Phosphate Precipitation by Fetuin Is Accompanied by the Formation of a Fetuin-Mineral Complex. *J. Biol. Chem.* 278 (24), 22144–22152. doi:10.1074/jbc.M300744200

Prieto, R. M., Gomila, I., Söhnel, O., Costa-Bauza, A., Bonnin, O., and Grases, F. (2011). Study on the Structure and Composition of Aortic Valve Calcific Deposits. Etiological Aspects. *Jbpc* 02, 19–25. doi:10.4236/jbpc.2011.21003

Prins, H. J., Braat, A. K., Gawlitta, D., Dhert, W. J., Egan, D. A., Tijssen-Slump, E., et al. (2014). *In Vitro* induction of Alkaline Phosphatase Levels Predicts *In Vivo* Bone Forming Capacity of Human Bone Marrow Stromal Cells. *Stem Cell Res.* 12 (2), 428–440. doi:10.1016/j.scr.2013.12.001

Puchtler, H., and Meloan, S. N. (1978). Demonstration of phosphates in calcium deposits: a modification of von Kossa's reaction. *Histochemistry* 56 (3-4), 177–185. doi:10.1007/BF00495978

Quinlan, A. M., and Billiar, K. L. (2012). Investigating the Role of Substrate Stiffness in the Persistence of Valvular Interstitial Cell Activation. *J. Biomed. Mater Res. A* 100 (9), 2474–2482. doi:10.1002/jbm.a.34162

Rajamannan, N. M., Evans, F. J., Aikawa, E., Grande-Allen, K. J., Demer, L. L., Heistad, D. D., et al. (2011). Calcific Aortic Valve Disease: Not Simply a Degenerative Process: A Review and Agenda for Research from the National Heart and Lung and Blood Institute Aortic Stenosis Working Group. Executive Summary: Calcific Aortic Valve Disease-2011 Update. *Circulation* 124 (16), 1783–1791. doi:10.1161/CIRCULATIONAHA.110.006767

Rajamannan, N. M. (2014). *Molecular Biology of Valvular Heart Disease2014*. Springer London, 1–150. doi:10.1007/978-1-4471-6350-3

Rathan, S., Yoganathan, A. P., and O'Neill, C. W. (2014). The Role of Inorganic Pyrophosphate in Aortic Valve Calcification. *J. Heart Valve Dis.* 23 (4), 387–394.

Rattazzi, M., Donato, M., Bertacco, E., Millioni, R., Franchin, C., Mortarino, C., et al. (2020). l-Arginine Prevents Inflammatory and Pro-calcific Differentiation of Interstitial Aortic Valve Cells. *Atherosclerosis* 298, 27–35. doi:10.1016/j.atherosclerosis.2020.02.024

Rattazzi, M., and Pauletto, P. (2015). Valvular Endothelial Cells: Guardians or Destroyers of Aortic Valve Integrity? *Atherosclerosis* 242 (2), 396–398. doi:10.1016/j.atherosclerosis.2015.07.034

Ravi, M., Paramesh, V., Kaviya, S. R., Anuradha, E., and Solomon, F. D. (2015). 3D Cell Culture Systems: Advantages and Applications. *J. Cell Physiol.* 230 (1), 16–26. doi:10.1002/jcp.24683

Redfors, B., Furer, A., Lindman, B. R., Burkhoff, D., Marquis-Gravel, G., Francese, D. P., et al. (2017). Biomarkers in Aortic Stenosis: A Systematic Review. *Struct. Heart* 1 (1-2), 18–30. doi:10.1080/24748706.2017.1329959

Renato, M., Bertacco, E., Franchin, C., Arrigoni, G., and Rattazzi, M. (2013). Proteomic Analysis of Interstitial Aortic Valve Cells Acquiring a Pro-calcific Profile. *Methods Mol. Biol.* 1005, 95–107. doi:10.1007/978-1-62703-386-2_8

Richards, J., El-Hamamsy, I., Chen, S., Sarang, Z., Sarathchandra, P., Yacoub, M. H., et al. (2013). Side-specific Endothelial-dependent Regulation of Aortic Valve Calcification: Interplay of Hemodynamics and Nitric Oxide Signaling. *Am. J. Pathol.* 182 (5), 1922–1931. doi:10.1016/j.ajpath.2013.01.037

Richards, J. M., Kunitake, J. A. M. R., Hunt, H. B., Wnorowski, A. N., Lin, D. W., Boskey, A. L., et al. (2018). Crystallinity of Hydroxyapatite Drives Myofibroblastic Activation and Calcification in Aortic Valves. *Acta Biomater.* 71, 24–36. doi:10.1016/j.actbio.2018.02.024

Rodriguez, K. J., and Masters, K. S. (2009). Regulation of Valvular Interstitial Cell Calcification by Components of the Extracellular Matrix. *J. Biomed. Mater Res. A* 90 (4), 1043–1053. doi:10.1002/jbm.a.32187

Rogers, M. A., Maldonado, N., Hutcheson, J. D., Goettsch, C., Goto, S., Yamada, I., et al. (2017). Dynamin-Related Protein 1 Inhibition Attenuates Cardiovascular Calcification in the Presence of Oxidative Stress. *Circ. Res.* 121 (3), 220–233. doi:10.1161/CIRCRESAHA.116.310293

Rojulpote, C., Borja, A. J., Zhang, V., Aly, M., Koa, B., Seraj, S. M., et al. (2020). Role of 18F-NaF-PET in Assessing Aortic Valve Calcification with Age. *Am. J. Nucl. Med. Mol. Imaging* 10 (1), 47–56.

Roosens, B., Bala, G., Droogmans, S., Van Camp, G., Breyne, J., and Cosyns, B. (2013). Animal Models of Organic Heart Valve Disease. *Int. J. Cardiol.* 165 (3), 398–409. doi:10.1016/j.ijcard.2012.03.065

Roosens, B., Bala, G., Gillis, K., Remory, I., Droogmans, S., Somja, J., et al. (2013). Echocardiographic Integrated Backscatter for Detecting Progression and Regression of Aortic Valve Calcifications in Rats. *Cardiovasc Ultrasound* 11, 4. doi:10.1186/1476-7120-11-4

Roosens, B., Droogmans, S., Hostens, J., Somja, J., Delvenne, E., Hernot, S., et al. (2011). Integrated Backscatter for the *In Vivo* Quantification of Supraphysiological Vitamin D(3)-induced Cardiovascular Calcifications in Rats. *Cardiovasc Toxicol.* 11 (3), 244–252. doi:10.1007/s12012-011-9118-y

Rutkovskiy, A., Malashicheva, A., Sullivan, G., Bogdanova, M., Kostareva, A., Stensløkken, K. O., et al. (2017). Valve Interstitial Cells: The Key to Understanding the Pathophysiology of Heart Valve Calcification. *J. Am. Heart Assoc.* 6 (9). doi:10.1161/JAHA.117.006339

Sainger, R., Grau, J. B., Branchetti, E., Poggio, P., Lai, E., Koka, E., et al. (2013). Comparison of Transesophageal Echocardiographic Analysis and Circulating Biomarker Expression Profile in Calcific Aortic Valve Disease. *J. Heart Valve Dis.* 22 (2), 156–165.

Salemi, A., and Worku, B. M. (2017). Standard Imaging Techniques in Transcatheter Aortic Valve Replacement. *J. Thorac. Dis.* 9 (Suppl. 4), S289–s98. doi:10.21037/jtd.2017.03.114

Satoh, K., Yamada, K., Maniwa, T., Oda, T., and Matsumoto, K. (2015). Monitoring of Serial Presurgical and Postsurgical Changes in the Serum Proteome in a Series of Patients with Calcific Aortic Stenosis. *Dis. Markers* 2015, 694120. doi:10.1155/2015/694120

Sauren, A. A., van Hout, M. C., van Steenhoven, A. A., Veldpaus, F. E., and Janssen, J. D. (1983). The Mechanical Properties of Porcine Aortic Valve Tissues. *J. Biomech.* 16 (5), 327–337. doi:10.1016/0021-9290(83)90016-7

Schlotter, F., Halu, A., Goto, S., Blaser, M. C., Body, S. C., Lee, L. H., et al. (2018). Spatiotemporal Multi-Omics Mapping Generates a Molecular Atlas of the Aortic Valve and Reveals Networks Driving Disease. *Circulation* 138 (4), 377–393. doi:10.1161/CIRCULATIONAHA.117.032291

Schoen, F. J., Levy, R. J., Nelson, A. C., Bernhard, W. F., Nashef, A., and Hawley, M. (1985). Onset and Progression of Experimental Bioprosthetic Heart Valve Calcification. *Lab. Invest* 52 (5), 523–532.

Shen, M., Tastet, L., Capoulade, R., Larose, É., Bédard, É., Arsenault, M., et al. (2017). Effect of Age and Aortic Valve Anatomy on Calcification and Haemodynamic Severity of Aortic Stenosis. *Heart* 103 (1), 32–39. doi:10.1136/heartjnl-2016-309665

Shuvy, M., Abedat, S., Beeri, R., Danenberg, H. D., Planer, D., Ben-Dov, I. Z., et al. (2008). Uraemic Hyperparathyroidism Causes a Reversible Inflammatory Process of Aortic Valve Calcification in Rats. *Cardiovasc Res.* 79 (3), 492–499. doi:10.1093/cvr/cvn088

Sider, K. L., Blaser, M. C., and Simmons, C. A. (2011). Animal Models of Calcific Aortic Valve Disease. *Int. J. Inflam.* 2011, 364310. doi:10.4061/2011/364310

Sider, K. L., Zhu, C., Kwong, A. V., Mirzaei, Z., de Langé, C. F., and Simmons, C. A. (2014). Evaluation of a Porcine Model of Early Aortic Valve Sclerosis. *Cardiovasc Pathol.* 23 (5), 289–297. doi:10.1016/j.carpath.2014.05.004

Sim, A. M., Rashdan, N. A., Cui, L., Moss, A. J., Nudelman, F., Dweck, M. R., et al. (2018). A Novel Fluorescein-Bisphosphonate Based Diagnostic Tool for the Detection of Hydroxyapatite in Both Cell and Tissue Models. *Sci. Rep.* 8 (1), 17360. doi:10.1038/s41598-018-35454-9

Skold, B. H., Getty, R., and Ramsey, F. K. (1966). Spontaneous Atherosclerosis in the Arterial System of Aging Swine. *Am. J. Vet. Res.* 27 (116), 257–273.

Small, A., Kiss, D., Giri, J., Anwaruddin, S., Siddiqi, H., Guerraty, M., et al. (2017). Biomarkers of Calcific Aortic Valve Disease. *Arterioscler. Thromb. Vasc. Biol.* 37 (4), 623–632. doi:10.1161/ATVBAHA.116.308615

Smith, E. R., Cai, M. M., McMahon, L. P., Pedagogos, E., Toussaint, N. D., Brumby, C., et al. (2013). Serum Fetuin-A Concentration and Fetuin-A-Containing Calciprotein Particles in Patients with Chronic Inflammatory Disease and Renal Failure. *Nephrol. Carlt.* 18 (3), 215–221. doi:10.1111/nep.12021

Sneddon, J., and Vincent, M. D. (2008). ICP-OES and ICP-MS for the Determination of Metals: Application to Oysters. *Anal. Lett.* 41 (8), 1291–1303. doi:10.1080/00032710802013991

Steadman, C. D., Ray, S., Ng, L. L., and McCann, G. P. (2010). Natriuretic Peptides in Common Valvular Heart Disease. *J. Am. Coll. Cardiol.* 55 (19), 2034–2048. doi:10.1016/j.jacc.2010.02.021

Stewart, B. F., Siscovick, D., Lind, B. K., Gardin, J. M., Gottdiener, J. S., Smith, V. E., et al. (1997). Clinical Factors Associated with Calcific Aortic Valve Disease. Cardiovascular Health Study. *J. Am. Coll. Cardiol.* 29 (3), 630–634. doi:10.1016/s0735-1097(96)00563-3

Suzuki, H., Chikada, M., Yokoyama, M. K., Kurokawa, M. S., Ando, T., Furukawa, H., et al. (2016). Aberrant Glycosylation of Lumican in Aortic Valve Stenosis Revealed by Proteomic Analysis. *Int. Heart J.* 57 (1), 104–111. doi:10.1536/ihj.15-252

Takkenberg, J. J., Rajamannan, N. M., Rosenhek, R., Kumar, A. S., Carapetis, J. R., and Yacoub, M. H. (2008). The Need for a Global Perspective on Heart Valve Disease Epidemiology. The SHVD Working Group on Epidemiology of Heart Valve Disease Founding Statement. *J. Heart Valve Dis.* 17 (1), 135–139.

Tao, G., Kotick, J. D., and Lincoln, J. (2012). Heart Valve Development, Maintenance, and Disease: the Role of Endothelial Cells. *Curr. Top. Dev. Biol.* 100, 203–232. doi:10.1016/B978-0-12-387786-4.00006-3

Tastet, L., Enriquez-Sarano, M., Capoulade, R., Malouf, J., Araoz, P. A., Shen, M., et al. (2017). Impact of Aortic Valve Calcification and Sex on Hemodynamic Progression and Clinical Outcomes in AS. *J. Am. Coll. Cardiol.* 69 (16), 2096–2098. doi:10.1016/j.jacc.2017.02.037

Taylor, P. M., Allen, S. P., and Yacoub, M. H. (2000). Phenotypic and Functional Characterization of Interstitial Cells from Human Heart Valves, Pericardium and Skin. *J. Heart Valve Dis.* 9 (1), 150–158.

Ternacle, J., and Clavel, M. A. (2020). Assessment of Aortic Stenosis Severity: A Multimodality Approach. *Cardiol. Clin.* 38 (1), 13–22. doi:10.1016/j.ccl.2019.09.004

Theodoridis, K., Tudorache, I., Cebotari, S., Calistru, A., Meyer, T., Sarikouch, S., et al. (2017). * Six-Year-Old Sheep as a Clinically Relevant Large Animal Model for Aortic Valve Replacement Using Tissue-Engineered Grafts Based on Decellularized Allogenic Matrix. *Tissue Eng. Part C Methods* 23 (12), 953–963. doi:10.1089/ten.tec.2017.0163

Tkatchenko, T. V., Moreno-Rodriguez, R. A., Conway, S. J., Molkentin, J. D., Markwald, R. R., and Tkatchenko, A. V. (2009). Lack of Periostin Leads to Suppression of Notch1 Signaling and Calcific Aortic Valve Disease. *Physiol. Genomics* 39 (3), 160–168. doi:10.1152/physiolgenomics.00078.2009

Tomasek, J. J., Gabbiani, G., Hinz, B., Chaponnier, C., and Brown, R. A. (2002). Myofibroblasts and Mechano-Regulation of Connective Tissue Remodelling. *Nat. Rev. Mol. Cell Biol.* 3 (5), 349–363. doi:10.1038/nrm809

Toutouzas, K., Stathogiannis, K., Latsios, G., Synetos, A., Drakopoulou, M., Penesopoulou, V., et al. (2019). Biomarkers in Aortic Valve Stenosis and Their Clinical Significance in Transcatheter Aortic Valve Implantation. *Curr. Med. Chem.* 26 (1), 864–827. doi:10.2174/0929867324666170727110241

Tsang, H. G., Rashdan, N. A., Whitelaw, C. B., Corcoran, B. M., Summers, K. M., and MacRae, V. E. (2016). Large Animal Models of Cardiovascular Disease. *Cell Biochem. Funct.* 34 (3), 113–132. doi:10.1002/cbf.3173

Tzolos, E., Andrews, J. P., and Dweck, M. R. (2020). Aortic Valve Stenosis-Multimodality Assessment with PET/CT and PET/MRI. *Br. J. Radiol.* 93 (1113), 20190688. doi:10.1259/bjr.20190688

Ueland, T., Aukrust, P., Dahl, C. P., Husebye, T., Solberg, O. G., Tønnessen, T., et al. (2011). Osteoprotegerin Levels Predict Mortality in Patients with Symptomatic Aortic Stenosis. *J. Intern Med.* 270 (5), 452–460. doi:10.1111/j.1365-2796.2011.02393.x

Ueland, T., Gullestad, L., Dahl, C. P., Aukrust, P., Aakhus, S., Solberg, O. G., et al. (2010). Undercarboxylated Matrix Gla Protein Is Associated with Indices of Heart Failure and Mortality in Symptomatic Aortic Stenosis. *J. Intern Med.* 268 (5), 483–492. doi:10.1111/j.1365-2796.2010.02264.x

Van Belle, E., Rauch, A., Vincent, F., Robin, E., Kibler, M., Labreuche, J., et al. (2016). Von Willebrand Factor Multimers during Transcatheter Aortic-Valve Replacement. *N. Engl. J. Med.* 375 (4), 335–344. doi:10.1056/NEJMoa1505643

Van Belle, E., Vincent, F., Rauch, A., Casari, C., Jeanpierre, E., Loobuyck, V., et al. (2019). von Willebrand Factor and Management of Heart Valve Disease: JACC Review Topic of the Week. *J. Am. Coll. Cardiol.* 73 (9), 1078–1088. doi:10.1016/j.jacc.2018.12.045

van der Valk, D. C., van der Ven, C. F. T., Blaser, M. C., Grolman, J. M., Wu, P. J., Fenton, O. S., et al. (2018). Engineering a 3D-Bioprinted Model of Human Heart Valve Disease Using Nanoindentation-Based Biomechanics. *Nanomater. (Basel)* 8 (5). doi:10.3390/nano8050296

Vancheri, F., Longo, G., Vancheri, S., Danial, J. S. H., and Henein, M. Y. (2019). Coronary Artery Microcalcification: Imaging and Clinical Implications. *Diagn. (Basel)* 9 (4). doi:10.3390/diagnostics9040125

Varshney, R., Murphy, B., Woolington, S., Ghafoory, S., Chen, S., Robison, T., et al. (2019). Inactivation of Platelet-Derived TGF-B1 Attenuates Aortic Stenosis Progression in a Robust Murine Model. *Blood Adv.* 3 (5), 777–788. doi:10.1182/bloodadvances.2018025817

Venardos, N., Gergen, A. K., Jarrett, M., Weyant, M. J., Reece, T. B., Meng, X., et al. (2022). Warfarin Induces Calcification of the Aortic Valve through Extracellular Signal-Regulated Kinase 1/2 and β-catenin Signaling. *Ann. Thorac. Surg.* 133 (9), 824–835. doi:10.1016/j.athoracsur.2021.03.099

Walker, G. A., Masters, K. S., Shah, D. N., Anseth, K. S., and Leinwand, L. A. (2004). Valvular Myofibroblast Activation by Transforming Growth Factor-Beta: Implications for Pathological Extracellular Matrix Remodeling in Heart Valve Disease. *Circ. Res.* 95 (3), 253–260. doi:10.1161/01.RES.0000136520.07995.aa

Wallby, L., Steffensen, T., Jonasson, L., and Broqvist, M. (2013). Inflammatory Characteristics of Stenotic Aortic Valves: A Comparison between Rheumatic and Nonrheumatic Aortic Stenosis. *Cardiol. Res. Pract.* 2013, 895215. doi:10.1155/2013/895215

Wang, C., Xia, Y., Qu, L., Liu, Y., Liu, X., and Xu, K. (2021). Cardamonin Inhibits Osteogenic Differentiation of Human Valve Interstitial Cells and Ameliorates Aortic Valve Calcification via Interfering in the NF-Kb/nlrp3 Inflammasome Pathway. *Food Funct.* 12 (23), 11808–11818. doi:10.1039/d1fo00813g

Weber, M., Arnold, R., Rau, M., Brandt, R., Berkovitsch, A., Mitrovic, V., et al. (2004). Relation of N-Terminal Pro-B-type Natriuretic Peptide to Severity of Valvular Aortic Stenosis. *Am. J. Cardiol.* 94 (6), 740–745. doi:10.1016/j.amjcard.2004.05.055

Weisell, J., Ohukainen, P., Näpänkangas, J., Ohlmeier, S., Bergmann, U., Peltonen, T., et al. (2019). Heat Shock Protein 90 Is Downregulated in Calcific Aortic Valve Disease. *BMC Cardiovasc Disord.* 19 (1), 306. doi:10.1186/s12872-019-01294-2

Weiss, R. M., Chu, Y., Brooks, R. M., Lund, D. D., Cheng, J., Zimmerman, K. A., et al. (2018). Discovery of an Experimental Model of Unicuspid Aortic Valve. *J. Am. Heart Assoc.* 7 (13). doi:10.1161/JAHA.117.006908

Weiss, R. M., Ohashi, M., Miller, J. D., Young, S. G., and Heistad, D. D. (2006). Calcific Aortic Valve Stenosis in Old Hypercholesterolemic Mice. *Circulation* 114 (19), 2065–2069. doi:10.1161/CIRCULATIONAHA.106.634139

Wilschefski, S. C., and Baxter, M. R. (2019). Inductively Coupled Plasma Mass Spectrometry: Introduction to Analytical Aspects. *Clin. Biochem. Rev.* 40 (3), 115–133. doi:10.33176/AACB-19-00024

Wipff, P. J., and Hinz, B. (2008). Integrins and the Activation of Latent Transforming Growth Factor Beta1 - an Intimate Relationship. *Eur. J. Cell Biol.* 87 (8-9), 601–615. doi:10.1016/j.ejcb.2008.01.012

Wyss, K., Yip, C. Y., Mirzaei, Z., Jin, X., Chen, J. H., and Simmons, C. A. (2012). The Elastic Properties of Valve Interstitial Cells Undergoing Pathological Differentiation. *J. Biomech.* 45 (5), 882–887. doi:10.1016/j.jbiomech.2011.11.030

Xing, Y., He, Z., Warnock, J. N., Hilbert, S. L., and Yoganathan, A. P. (2004). Effects of Constant Static Pressure on the Biological Properties of Porcine Aortic Valve Leaflets. *Ann. Biomed. Eng.* 32 (4), 555–562. doi:10.1023/b:abme.0000019175.12013.8f

Yip, C. Y., Chen, J. H., Zhao, R., and Simmons, C. A. (2009). Calcification by Valve Interstitial Cells Is Regulated by the Stiffness of the Extracellular Matrix. *Arterioscler. Thromb. Vasc. Biol.* 29 (6), 936–942. doi:10.1161/ATVBAHA.108.182394

Yousry, M., Rickenlund, A., Petrini, J., Gustavsson, T., Prahl, U., Liska, J., et al. (2012). Real-time Imaging Required for Optimal Echocardiographic Assessment of Aortic Valve Calcification. *Clin. Physiol. Funct. Imaging* 32 (6), 470–475. doi:10.1111/j.1475-097X.2012.01153.x

Yousry, M., Rickenlund, A., Petrini, J., Jenner, J., Liska, J., Eriksson, P., et al. (2015). Aortic Valve Type and Calcification as Assessed by Transthoracic and Transoesophageal Echocardiography. *Clin. Physiol. Funct. Imaging* 35 (4), 306–313. doi:10.1111/cpf.12166

Yperman, J., De Visscher, G., Holvoet, P., and Flameng, W. (2004). Molecular and Functional Characterization of Ovine Cardiac Valve-Derived Interstitial Cells in Primary Isolates and Cultures. *Tissue Eng.* 10 (9-10), 1368–1375. doi:10.1089/ten.2004.10.1368

Yu, B., Khan, K., Hamid, Q., Mardini, A., Siddique, A., Aguilar-Gonzalez, L. P., et al. (2018). Pathological Significance of Lipoprotein(a) in Aortic Valve Stenosis. *Atherosclerosis* 272, 168–174. doi:10.1016/j.atherosclerosis.2018.03.025

Zabirnyk, A., Perez, M. D. M., Blasco, M., Stensløkken, K. O., Ferrer, M. D., Salcedo, C., et al. (2020). A Novel *Ex Vivo* Model of Aortic Valve Calcification. A Preliminary Report. *Front. Pharmacol.* 11, 568764. doi:10.3389/fphar.2020.568764

Zhang, X. W., Zhang, B. Y., Wang, S. W., Gong, D. J., Han, L., Xu, Z. Y., et al. (2014). Twist-related Protein 1 Negatively Regulated Osteoblastic Transdifferentiation of Human Aortic Valve Interstitial Cells by Directly Inhibiting Runt-Related Transcription Factor 2. *J. Thorac. Cardiovasc Surg.* 148 (4), 1700–e1. doi:10.1016/j.jtcvs.2014.02.084

Zhao, M., Li, P., Xu, H., Pan, Q., Zeng, R., Ma, X., et al. (2018). Dexamethasone-Activated MSCs Release MVs for Stimulating Osteogenic Response. *Stem Cells Int.* 2018, 7231739. doi:10.1155/2018/7231739

Conflict of Interest: Author MP was employed by Sanifit Therapeutics.

The remaining authors declare that the research was conducted in the absence of any commercial or financial relationships that could be construed as a potential conflict of interest.

Publisher's Note: All claims expressed in this article are solely those of the authors and do not necessarily represent those of their affiliated organizations, or those of the publisher, the editors and the reviewers. Any product that may be evaluated in this article, or claim that may be made by its manufacturer, is not guaranteed or endorsed by the publisher.

frontiers | Frontiers in Pharmacology

REVIEW
published: 03 June 2022
doi: 10.3389/fphar.2022.909801

Mechanisms and Drug Therapies of Bioprosthetic Heart Valve Calcification

Shuyu Wen†, Ying Zhou†, Wai Yen Yim, Shijie Wang, Li Xu, Jiawei Shi, Weihua Qiao and Nianguo Dong**

Department of Cardiovascular Surgery, Union Hospital, Tongji Medical College, Huazhong University of Science and Technology, Wuhan, China

Valve replacement is the main therapy for valvular heart disease, in which a diseased valve is replaced by mechanical heart valve (MHV) or bioprosthetic heart valve (BHV). Since the 2000s, BHV surpassed MHV as the leading option of prosthetic valve substitute because of its excellent hemocompatible and hemodynamic properties. However, BHV is apt to structural valve degeneration (SVD), resulting in limited durability. Calcification is the most frequent presentation and the core pathophysiological process of SVD. Understanding the basic mechanisms of BHV calcification is an essential prerequisite to address the limited-durability issues. In this narrative review, we provide a comprehensive summary about the mechanisms of BHV calcification on 1) composition and site of calcifications; 2) material-associated mechanisms; 3) host-associated mechanisms, including immune response and foreign body reaction, oxidative stress, metabolic disorder, and thrombosis. Strategies that target these mechanisms may be explored for novel drug therapy to prevent or delay BHV calcification.

Keywords: bioprosthetic heart valve, ectopic calcification, structural valve degeneration, mechanisms, drug therapy

OPEN ACCESS

Edited by:
Jing Xie,
Sichuan University, China

Reviewed by:
Chunli Wang,
Chongqing University, China
Taisiya Bezhaeva,
Leiden University Medical Center, Netherlands

****Correspondence:***
Weihua Qiao
weihua_qiao@hust.edu.cn
Nianguo Dong
dongnianguo@hotmail.com

†These authors have contributed equally to this work and share first authorship

Specialty section:
This article was submitted to Experimental Pharmacology and Drug Discovery, a section of the journal Frontiers in Pharmacology

Received: *31 March 2022*
Accepted: *26 April 2022*
Published: *03 June 2022*

Citation:
Wen S, Zhou Y, Yim WY, Wang S, Xu L, Shi J, Qiao W and Dong N (2022) Mechanisms and Drug Therapies of Bioprosthetic Heart Valve Calcification. Front. Pharmacol. 13:909801. doi: 10.3389/fphar.2022.909801

1 INTRODUCTION

Valvular heart disease (VHD) inflicts a heavy burden on global health care, with an incidence rate of 13.3% for people over 75 (Roger et al., 2011; Virani et al., 2021). Given the aging of population worldwide, the prevalence of VHD is expected to rise exponentially and will double before 2050 (D'arcy et al., 2016; Dziadzko et al., 2018). Currently, surgery replacement of the dysfunctional native valves with artificial valves is the standard therapy for VHD, and artificial valves generally fall into one of the two categories: mechanical heart valve (MHV) or bioprosthetic heart valve (BHV) (Vahanian et al., 2021). The annual demand for interventions is expected to hit 850,000 by 2050, owing to the increasing prevalence of VHD (Yacoub and Takkenberg, 2005). In the past 2 decades, the application of BHV has surpassed MHV. Rapid advances in the field of transcatheter aortic valve replacement (TAVR) also contributed to the extending scope and appreciation for BHV (Wen et al., 2020).

In contrast to MHV, BHV has significant advantages by eliminating the need for anticoagulation therapy while possessing exquisite hemodynamic properties similar to those of native valves. However, its durability was hampered by inevitable structural valve degeneration (SVD). In brief, SVD is defined as a permanent intrinsic change of the valve resulting in calcification, leaflet tear, pannus deposition of a valve, which eventually manifested as stenosis or regurgitation prompting high-risk reintervention (Capodanno et al., 2017; Dvir et al., 2018).

Thus, SVD is becoming a major issue for surgeons and researchers. Calcification is the most prevalent pathological form of SVD (Koziarz et al., 2020) and is believed to be the final pathway for valve dysfunction, leading to progressive cusp stiffness and obstruction as well as leaflet fragility (Cartlidge et al., 2019). Therefore, we review current knowledge of the pathogenesis for BHV calcification.

BHV calcification has been once considered a passive degenerative process, but now is seen as a complex mechanism actively regulated by several factors (Kostyunin A. E. et al., 2020). Recent studies provided evidence that multiple processes were involved in BHV calcification, including glutaraldehyde (GLUT) pretreatment, material composition, mechanical stress, and immune response. In this review, we sought to clarify pathophysiological features and mechanisms of BHV calcification as well as potential drug strategies to prevent or delay BHV calcification.

2 TYPES OF BHV

Since the 1960s, techniques and technologies of surgical aortic valve replacement as well as the implanted aortic valves themselves have been flourishing. Despite the superior long-term durability, patients fitted with MHV face the burden of lifelong anticoagulant treatment.

In the recent 2 decades, with the advent of TAVR and the improvement of BHV, there has been a substantial shift toward the use of BHVs compared to MHVs. Studies have demonstrated that the overall usage of BHV in isolated aortic valve procedures was up to 87% (Beckmann et al., 2016). Generally, BHV can be classified according to materials that derived from pulmonary autografts, homografts, and xenografts. Xenografts are the main materials of commercial BHV, so the discussion we present below focuses on xenografts BHV. Conventionally, porcine aortic valve leaflets or pericardial bovine patches used for BHV are preserved by GLUT fixation and other anti-mineralization treatments, partly preventing immunogenicity and improving durability. Of note, prior studies have shown that pericardial bovine valves have significantly better hemodynamic results with lower gradient pressure and larger orifice areas than porcine valves (Ruzicka et al., 2009; Yap et al., 2013). In order to serve the needs of various innovative technologies and pathoanatomical diversity of the aortic roots, the design of BHV can be subdivided into stented or stentless surgical valve and balloon-expandable or self-expanding transcatheter valve. Stented valve is composed of polymeric material or scallop-shaped external sewing ring located outside of the stent frame, while stentless valve have neither a stent frame nor a base ring that supports valve leaflets providing greater effective orifice areas and lower transprosthetic gradients (Paradis et al., 2015; Dangas et al., 2016).

3 DURABILITY AND FAILURE OF BHV

Despite the many advantages of BHV over MHV, particularly without the need for lifelong anticoagulative treatment, BHV is still not devoid of shortcoming. Numerous cohort studies indicate the existing commercial BHV are not fully addressing long-term needs as a prosthetic valve substitute due to inevitable SVD. A retrospective study (Forcillo et al., 2013) reported the freedom rate from reoperation after implanted Carpentier-Edwards valve due to prosthesis dysfunction averaged 98 % ± 0.2%, 96% ± 1%, and 67% ± 4% at 5, 10, and 20 years, respectively. Tirone et al. (David et al., 2010) evaluated 1,134 patients underwent aortic valve replacement surgery with Hancock II bioprosthesis, showing survival rate and freedom rate from SVD at 20 years were 19.2% ± 2% and 63.4% ± 4.2%, respectively. The mean duration of SVD after implantation of Mitroflow bioprosthesis was only 3.8 ± 1.4 years (Senage et al., 2014). Therefore, Long-term outcomes of surgical BHV remain suboptimal, irrespective of their brands and special anti-calcification pretreatment.

Since TAVR has only been widely generalized after 2007, studies for durability of transcatheter valves are almost circumscribed to the first 5 years of follow-up. Five-year rate of BHV dysfunction undergoing TAVR was 1.4% (Barbanti et al., 2015). Noteworthy, SVD usually begins 8 years after implantation, with an increasing rate of SVD after 10 years (Dvir et al., 2018). Generally, transcatheter valves are assumed to have even worse durability compared with surgical valves due to several factors. Transcatheter valves are thinner than surgical valve to permit transcatheter delivery. Moreover, transcatheter valves were under higher mechanical stresses and strains because of non-circular, asymmetric stent deployment. Transcatheter valves is vulnerable to traumatic injury during implantation, while surgical valves remain well conserved without any contact during operation. In this context, the SVD rate of transcatheter valves was substantially underestimated.

Limited durability severely impedes broadening the scope of BHV usage. Great care should be taken to decide whether to choose BHV before surgery, especially for patients with extremely high risks for SVD. Multiple factors are associated with early SVD onset, including young age of patients, end-stage renal disease, diabetes mellitus, hyperparathyroidism, smoking, and prosthesis-patient mismatch (Kostyunin A. E. et al., 2020; Ochi et al., 2020), which suggest that BHV failure is a continuous variable process, rather than a binary categorical parameter. Given the similarities of risk factors of BHV failure, atherosclerosis, and calcific aortic valve disease, they may share the same molecular mechanisms, in which calcification is the core signature and important target for intervention. Understanding the biomolecular mechanisms related to BHV calcification is the essential first step to explore potential therapeutic targets to inhibit or at least slow the progression of SVD and open novel avenues for improving the longevity of BHV to fulfill clinical requirements.

4 GENERAL FEATURES OF BHV CALCIFICATION

BHV calcification is one form of ectopic calcification, referring to the aberrant deposition of calcium phosphate complexes in soft tissues (**Figures 1A,B**). Based on the pathogenic mechanisms, ectopic calcification can be classified as dystrophic, metastatic,

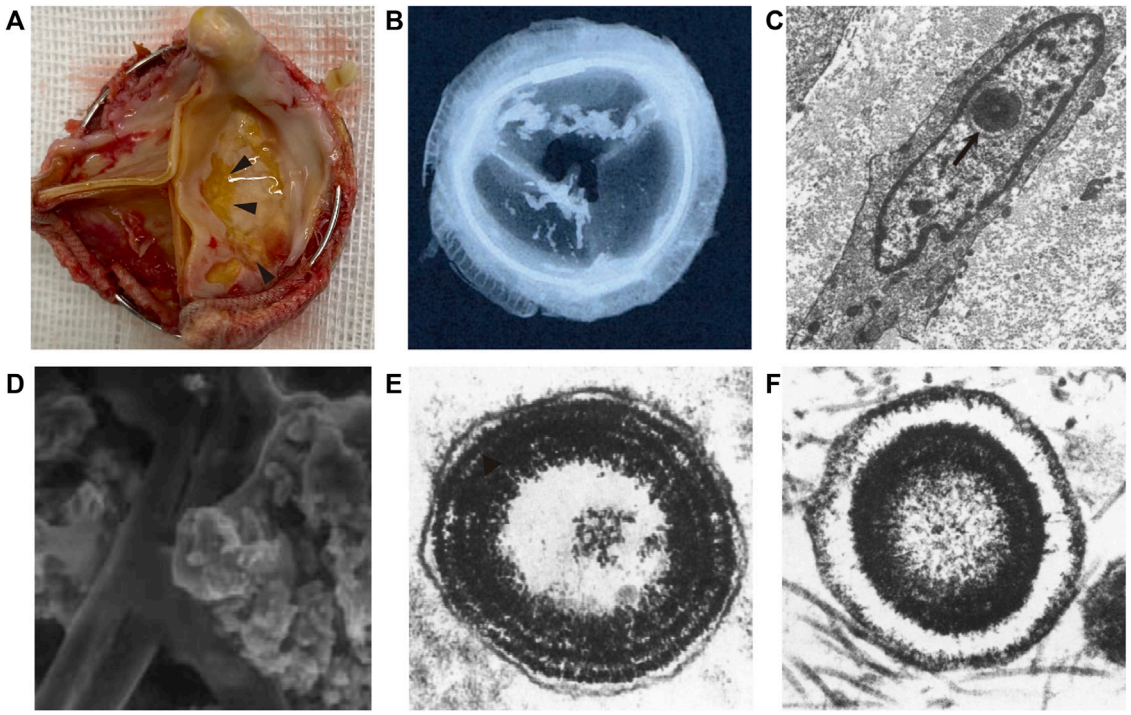

FIGURE 1 | Schematic of bioprosthetic heart valve calcification. **(A)** Gross view of bioprosthetic heart valve calcification (arrowhead). **(B)** Low-energy radiography of bioprosthetic heart valve calcification (Delogne et al., 2007). **(C)** Ultrastructure of calcium deposits in the cell nuclei (arrow) (Schoen et al., 1994). **(D)** Scanned electron microscopy view of calcific loci depositing on collagen and elastin (Delogne et al., 2007). **(E,F)** calcospherulae arranged in concentric rings with and without a central core (Valente et al., 1985).

idiopathic, iatrogenic, or tumoral (Chander and Gordon, 2012; Li et al., 2014; Boraldi et al., 2021). In fact, to date, the pathogenesis of BHV calcification remains unclear. However, the determinants of all kinds of ectopic calcification cannot be separated from the original level of calcium, the presence of scaffolding for mineral deposition, and abnormal regulations during calcification. This chapter will draw a comprehensive picture of BHV calcification as possible from 1) the composition of the calcific foci in BHV; 2) micro and macro-level perceptions for BHV calcification sites. Compositions and sites of calcific foci are not only the final manifestation but could reflect mechanisms of BHV calcification.

4.1 The Composition of Calcifications

Calcium phosphate (CaP) is the common name of the calcific deposits family, and different type of CaP is formed under different physiological and pathophysiological situations (Eliaz and Metoki, 2017). Although several studies have confirmed the mineral salt of calcific BHV is a mixture of CaP, the major components of BHV calcifications from different studies were inconsistent and conflicting. Delogne et al. (2007). showed spectral features very similar to a crystalline hydroxyapatite (HAP) spectrum, and refuted the findings of Mikroulis et al. (2002), who reported the presence of dicalcium phosphate dihydrate (DCPD), octacalcium phosphate (OCP), and β-tricalcium phosphate (β-TCP). However, Tomazic et al. (1994) characterized calcific deposits from 10 failed BHV that had been implanted in patients for 2–13 years and suggested BHV calcifications were composed of either an apatitic and/or OCP-like material, but also eliminated HAP as a significant fraction in BHV calcifications due to measured refraction index. CaP mixture complexity and significant individual differences contribute to different results. Despite these differences, all of these studies collectively highlight that the Ca/P molar ratio of BHV calcific deposits ranges from 1.34 to 1.67, considerably lower than 1.70 found in mature atherosclerotic plaque, natural valve calcification, and mature skeletal (Tomazic et al., 1994; Mikroulis et al., 2002; Delogne et al., 2007). Collectively, it is worth raising the possibility of the presence of precursor phases associated during the early stages of calcification with substantial incorporation of sodium, magnesium, silicon, and carbonate. Regardless, different condition contributes to a different type of CaP deposited. Thus, further studies in the component of BHV calcification may help make the BHV calcification pathology progression clearer.

4.2 The Location of CaP

Some ultrastructures of cell and extracellular matrix (ECM) provide scaffolding or abundant feedstock for calcium deposits that are prone to calcification. Despite differences in the infrastructure of the porcine aortic valve and bovine pericardium, the site features of calcification of these materials were virtually similar (Schoen et al., 1986). Initial calcification deposits were localized predominantly to cell remnants (Valente et al., 1985; Schoen et al., 1986; Schoen et al., 1994).

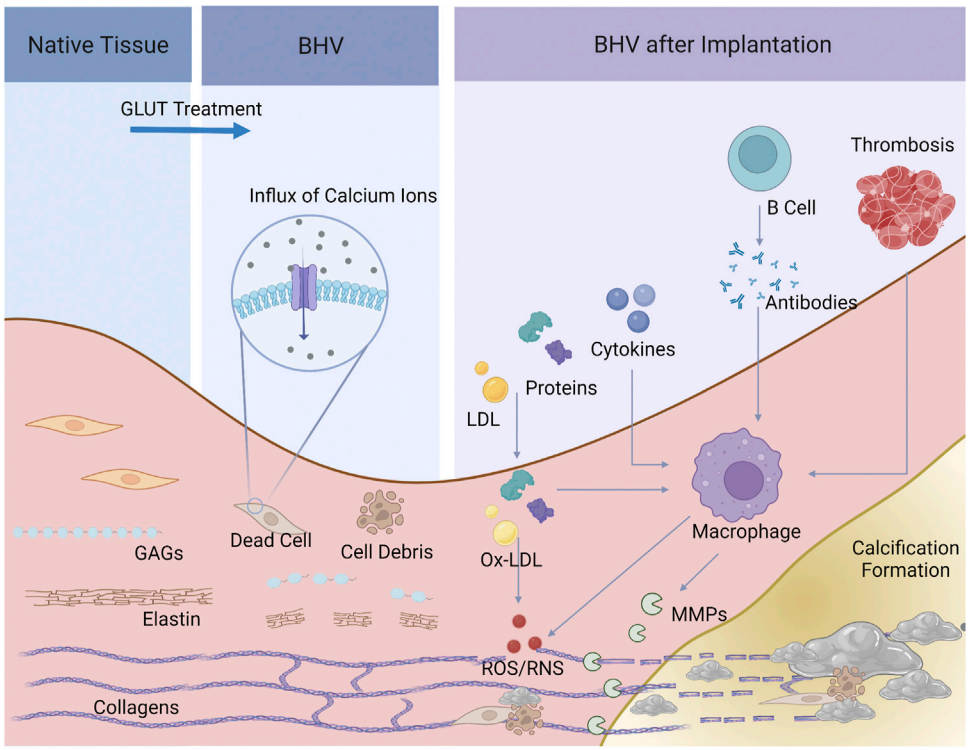

FIGURE 2 | Schematic of the process of BHV calcification. Dead cells and cell debris, and elastin and GAGs degradation, and collagen crosslinks were present after GLUT treatment, providing calcium ions and the specific space structure for calcification. Serum protein and lipid infiltrated, cytokines, xenoantibodies secreted by B cells and thrombosis would activate macrophages and induce inflammatory response. Macrophages further secret MMPs and product ROS/RNS, leading to BHV calcification.

Microscopically, the earliest deposits were noted in the nuclei, but it also appears to be at residual organelles or associated with the plasma membrane in the cytoplasm (Schoen et al., 1994). In addition, calcific deposits are also involved in the fibrosa, and later deposits expanded the spongiosa. Namely, cellular debris, collagen, and elastin can serve as foci for calcification (**Figures 1C,D**). The concrete mechanisms for this progression are described below. When considering BHV as a whole, cuspal commissures and basal attachment sites are more susceptible to calcification (Schoen et al., 1994; Schoen and Levy, 1999). Different implanted positions could be expected to have different degrees of BHV calcification, as calcification developed more commonly in inflow valves (ventricular valve) than the outflow valve (aortic valve) (Liao et al., 2008), which may be ascribed to different mechanical stress.

5 PATHOPHYSIOLOGICAL MECHANISM OF BHV CALCIFICATION

By analogy with the pathology of native valve calcification, the mechanism of BHV calcification should not be entirely attributed to a passive process of calcium deposits but is probably complex and multifactorial, and a comprehensive understanding remains elusive. In this review, we categorized BHV calcification mechanism into two major categories: material-associated mechanism and host-associated mechanism. The former involves the specific nature of valve materials and physicochemical properties that lead to the high susceptibility of calcification. On the other hand, the host-associated mechanism is implicated in several processes after BHV implantation, such as protein adsorption, oxidative stress, activation of immune systems, and local inflammatory response (**Figure 2**).

5.1 Material-Associated Mechanism

5.1.1 GLUT and Cell Debris

GLUT efficiently crosslinks collagen and mask xenoantigens, showing substantial advantages like no other crosslinkers. However, the mechanism of BHV calcification induced by GLUT has been corroborated (Kim et al., 1999; Schoen and Levy, 1999). Among these, calcification of implanted BHV is mainly due to cytotoxic effects treated by GLUT. Under normal physiological circumstances, the intracellular calcium level is up to a thousand-fold lower than the extracellular one (Kiełbik et al., 2020), tightly maintained by the mitochondria through the calcium pump. *In-vitro* studies revealed that GLUT treatment causes cell death and inactivation of calcium pump, triggering an immediate influx of calcium ions from extracellular spaces and a rise of intracellular phosphate ions in a dose-dependent manner

(Kim et al., 1999). However, due to very poor vascularization in implanted BHV tissue, cell debris cannot be promptly scavenged by macrophages. In this scenario, cell-membrane-derived acidic phospholipids form the so-called "calcium-phospholipid-phosphate complexes" (Boskey and Posner, 1976; Schoen and Levy, 1992), so that calcium appears to deposit in the cell debris. Another major mineral nucleation site is involved in cell-derived matrix vesicles, the production of cell byproducts, including multiply undefined forms, like "matrix vesicles", "apoptotic bodies", "exosomes" et al. (Schraer and Gay, 1977). These initial calcific foci consist of concentrically arranged, multi-laminated vesicular bodies that were named spherulites or calcospherulae (**Figures 1E,F**) (Valente et al., 1985; Lee, 1993), which have been reported to have robust facilitatory effects on mineral deposition. Moreover, free aldehyde groups and impairing charges balances after GLUT treatment may hence promote calcification as well, and aldehyde-free treatment was an effective method to enhance the anti-calcification properties (Chen et al., 1994; Rodriguez-Gabella et al., 2017; Meuris et al., 2018; Badria et al., 2020).

5.1.2 Extracellular Matrix Damage

ECM, mainly composed of fibrillar collagens, elastin, and glycosaminoglycans (GAGs), is the largest source of free calcium ions during the process of BHV calcification. Of concern, mineralization of ECM is a secondary process that occurs after collagen and elastin fibers were embedded by dead cells or vesicles induced calcium deposition (Kim, 2002). GLUT-fixed tissues are not entirely resistant to enzymatic attack and are not metabolically inert. Degradation and breakdown of ECM provide spatial facilitation for calcification. GAGs provide hydration and lubrication in the native valves and are important for the stable assembly of the ECM. In particular, GAGs interact specifically with type I collagen fibrils, bridging and stabilizing adjacent collagen fibrils (MacGrogan et al., 2014). Nevertheless, GAGs cannot be crosslinked by GLUT, and are gradually lost during the preparation, storage, and implantation of BHV (Leong et al., 2013). Degradation of GAGs disrupts collagen integrity, resulting in exposing hole zones, a 3-dimensional structure favoring nucleation of CaP crystals. In parallel, GLUT doesn't react with elastin. And when undergoing proteolysis, elastin possesses a special structure that smooths the path of calcium deposition (Bailey et al., 2003; Simionescu et al., 2003; Wang et al., 2015). Multiple studies suggested that stabilizing GAGs and elastin help reduce BHV calcification (Ohri et al., 2004; Raghavan et al., 2007; Leong et al., 2013; Lei et al., 2019). Except for degradation, fibers ruptured and damaged by mechanical stress are also presented with calcium-binding sites (Whelan et al., 2021).

In short, the residual cell debris and cell-derived matrix vesicles are the primary loci of calcification in BHV, while the ECM provides massive calcium ions and a specific space structure for mineralization during the degradation.

5.2 Host-Associated Mechanism

5.2.1 Immune/Inflammatory Response

Young patient age has been considered as an exact risk factor for early SVD of BHV (Dvir et al., 2018; Pibarot et al., 2020). The predicted 15-year risk of needing reoperation because of SVD is 50% for patients at age of 20, but patients >65 years old may show greater freedom from SVD (Chan et al., 2006; Siddiqui et al., 2009; Otto et al., 2021a). This phenomenon is widely believed to be attributable to immune response because young adults mount a more vigorous immune response than elderly people. In fact, mounting evidence has accumulated over the past decade that strongly points toward a crucial involvement of immune response in the calcification and degradation of BHV (Hopkins, 2006; Siddiqui et al., 2009; Manji et al., 2015b; Costa, 2020). Significantly increased immune cellular infiltration, including T cells, macrophages, B cells, neutrophils, and plasma cells, was observed in the implanted calcific BHV tissue, with an elevated cytokine concentration accompanied (Manji et al., 2015a; Bozso et al., 2021). Senage and his colleagues (Senage et al., 2022) carried out a large cohort study demonstrating graft-special antibodies significantly increase and deposit on calcific BHV tissue 1 month after BHV implantation. Animal studies also showed T cells and macrophages infiltration and antibody rise in GLUT fixed valve tissues (Manji et al., 2006). The above studies indicate that inflammatory reaction and immune response may play vital roles in BHV calcification processes.

BHV implantation necessarily induces foreign body reactions. Foreign body reaction is an immune-mediated reaction to implanted materials where a cascade of inflammatory events results in granuloma and fibrous encapsulation (Veiseh and Vegas, 2019). Different from other biomaterials, the implanted BHV does not form a visible fibrous capsule under high shear forces and complex haemodynamic profile, but allows non-specific protein adsorption (Shen et al., 2001; Sakaue et al., 2018) and inflammatory cells infiltrating (Kostyunin A. et al., 2020). Host plasma proteins adsorption leads to a series of subsequent effects including complement system and platelet activation, coagulation cascade, and cell adherence (Zhu et al., 2019). Moreover, Antonio et al. (Frasca et al., 2020) have found that human serum albumin and glycation infiltration lead to BHV tissue matrix disruption and change the biomechanical properties of valve leaflets. In detail, glycation end products not only alter collagen fiber interactions, potentially causing leaflet stiffening, but result in modulation of cell phenotypes and instigation of inflammation via glycation product-mediated receptor signaling (Frasca et al., 2020).

Subsequently, monocyte/macrophages are recruited by the layer of protein adsorbed onto the valve surface. Through the electron microscopy visualization of calcified BHV, Alexander et al. (Kostyunin A. et al., 2020) have elaborately illustrated a multi-step process that monocyte infiltration followed by a macrophage-driven ECM disintegration. Monocytes/macrophages roll and then adhere to the surface of BHV, tearing the ECM proteins by invadopodia. Moreover, (neo) vascularization facilitates the migration of macrophages and other immune cells and alters microenvironmental pH as well as bring available mineral ions (Kitagawa et al., 2015; Kostyunin A. et al., 2020; Katsi et al., 2021). Infiltrated macrophages concentrate the cytoplasmic granules at the leading edge of the cells and release proteolytic enzymes, such as matrix metalloproteinases (MMP) (Simionescu et al., 1996;

Simionescu et al., 2003), and plasminogen (Sakaue et al., 2018), leading to degradation and delamination of the ECM (Kostyunin A. et al., 2020). MMP-2 and MMP-9 were markedly elevated in the calcified BHV tissues, compared to the noncalcified BHV. MMPs could degrade partially GLUT-fixed collagen and particularly large amounts of elastin. Furthermore, MMPs play a vital role in the promotion of inflammatory, fibrotic, and osteogenic genes overexpression (Matilla et al., 2020). In addition, plasminogen was strongly stained in CD68-positive macrophages among calcified BHV (Sakaue et al., 2018). To our knowledge, plasminogen, acting as a potent proinflammatory mediator, contributes to the induction of cytokines and intracellular signaling events and stimulates the activation of macrophages (Shen et al., 2012). Under these circumstances, the strong MMP-dependent proteolysis and the fibrinolytic system can cleave most ECM proteins (Kostyunin A. E. et al., 2020).

Besides, macrophages also secret calcium-binding proteins, such as osteopontin and osteonectin, which are adapted for engendering BHV calcification. Osteonectin, also known as BM-40 or SPARC (secreted protein acidic and rich in cysteine) (Wang et al., 2006), has a considerable high affinity to calcium (Busch et al., 2000). Osteonectin also modulates cell function by interacting with cell-surface receptors, metalloproteinases, growth factors, and other bioeffector molecules, involved in tissue remodeling, repair, development, and cell turnover (Bradshaw and Sage, 2001; Zhu et al., 2020). Given to macrophage-derived matrix vesicles contribute to microcalcification in atherosclerotic plaques (New et al., 2013), macrophages may also secrete extracellular vesicles capable of inducing BHV mineralization.

Xenoantigens are the primary cause of provoking adaptive immune reactions after BHV implantation. Although GLUT fixation and other pretreatments minimize the immunological determinants of bioprosthetic leaflet tissue to avoid xenograft rejection, the hurdle still exists because the immunogenicity of such tissue is not sufficiently abolished, especially carbohydrate antigens. It is well-established that the alpha-gal epitope is the dominant mediator in discordant xenoimplants (Naso et al., 2013; Kim et al., 2015; Li, 2019). In this regard, Gal-knockout BHV represented a novel and potentially useful strategy for reducing BHV calcification (Lila et al., 2010; Park et al., 2010; McGregor et al., 2013). The additional two immunogenic carbohydrate antigens that have been identified are N-glycolylneuramic acid (Neu5Gc) antigen (Lee et al., 2016; Reuven et al., 2016) and the Sid blood group antigen (Sda) (Li, 2019). Apart from carbohydrate antigens, Katherine et al. (Gates et al., 2019) have identified 19 specific protein antigens from GLUT fixed bovine pericardial heart valves that stimulate the graft-specific humoral immune response in patients. Intriguingly, they found calcium-binding proteins were the most highly over-represented biological function of antigens, but such antibody-binding effect of those proteins on BHV calcification is yet to be elucidated.

In the humoral response triggered by unmasked xenoantigens, pre-existing antibodies play a vital role in the opsonization of inflammatory cells to recruitment and proliferation, phagocytosis, efferocytosis, etc, thereby distinctly facilitating the overall immune response. Inflammatory cells, such as neutrophils and macrophages, adhesion onto BHV tissue surface and subsequently infiltrate into the leaflets, releasing stored MMPs (Ground et al., 2021). Similarly, cellular immunity participates in BHV calcification. Histological studies of BHV removed from patients showed leukocytes destroying collagen fibers, with crystalline material present on their surfaces, suggesting it may have been acting as a nidus for calcification (Stein et al., 1988). Regardless, humoral or cellular immunity would decidedly undermine the integrity of valve, leading to exposure to calcification site or increasement in calcification composition.

5.2.2 Oxidative Stress

It is well known that reactive oxygen and nitrogen species (ROS/RNS) have a potentially severe impact on both host and implanted biomaterials. ROS/RNS are continuously generated as normal by-products of cell metabolism and act as signaling molecules at lower concentrations controlling cell proliferation and differentiation in many cell types (Manolagas, 2010). But the excessive productions of ROS/RNS participate in numerous pathogenesis of diseases including cancer, inflammatory disorders, and metabolic diseases, leading to DNA, proteins, and carbohydrates damage, denoted as oxidative distress (Sies and Jones, 2020), Christian et al. (2014) have analyzed fifteen clinical failed BHV using mass spectrometry and found that levels of ortho-tyrosine, meta-tyrosine, and dityrosine conspicuously increase among failed BHV. Furthermore, 3-Chlorotyrosine, an oxidized amino acid formed by myeloperoxidase-catalyzed chlorinating oxidants, was correlated with BHV calcification (Lee et al., 2017). GLUT treated bovine pericardium modified with the antioxidant, 3-(4-hydroxy-3,5-di-tert-butylphenyl) propyl amine (DBP), showed significant reducing degree of calcification after implanted in the subdermal area of a rat model (Christian et al., 2015). And after exposed to H_2O_2 and $FeSO_4$ to mimick the action of oxidative distress, GLUT treated bovine pericardium was detected with loss of GLUT crosslinking and morphology changes (Christian et al., 2015). Collectively, oxidative stress, causes collagen breakdown and a uniform susceptibility to collagenase for valve tissue, particularly via hydroxyl radical and tyrosyl radical mediated pathways, bring about BHV calcification.

5.2.3 Metabolic Disorders

Several studies have indicated that BHV calcification is an atherosclerotic-like process. Namely, several factors involved in the pathogenesis of atherosclerosis and calcific aortic valve disease were also implicated in BHV calcification, especially lipid-driven factors (Wang et al., 2021a). Clinical researchers have stated that after BHV implanted, plasma levels of total-cholesterol, low-density lipoprotein-cholesterol (LDL), apolipoprotein B (ApoB), oxidized low-density lipoprotein (ox-LDL) were notably higher among patients with SVD than those without SVD (Mahjoub et al., 2013; Nsaibia et al., 2016; Nsaibia et al., 2018), and ApoB/ApoA-I ratio (Mahjoub et al., 2013) and OxLDL/HDL ratio (Nsaibia et al., 2016) could be considered as strong independent predictors of BHV failure.

Taken together these findings all emphasize the pivotal role of lipid-mediated mechanism for BHV failure and calcification. Immunohistochemistry staining of failed BHV showed that ox-LDL was present in the fibrosa layer of BHV and surrounded by CD68-positive macrophages (Shetty et al., 2009). The crux of the lipid-mediated BHV degrading and calcification lies in the *in situ* formation of ox-LDL and subsequent activation of macrophages. After BHV implantation, high levels of circulating LDL deposit in the valve tissue where LDL is oxidized to ox-LDL. Ox-LDL is being phagocytosed by macrophages resulting in polarization and foam cell formation, and further retained by GAGs that infiltrated macrophages generate (Plakkal Ayyappan et al., 2016).

Despite lacking an in-depth understanding, some studies attempt to explain the lipid-mediated inflammatory mechanisms involved in BHV calcification. Shetty and colleagues deemed ox-LDL were bound and internalized by macrophages through CD36 (Shetty et al., 2009), a scavenger receptor with the highest affinity for ox-LDL (Miller et al., 2011). Activated lipid-laden macrophages form pseudopods, as well as produce cytokines and MMP9, finally resulting in weakening and calcification of the leaflet matrix. Additionally, elevated activity of lipoprotein-associated phospholipase A2 (Lp-PLA2) both in plasma and failed BHV tissues give support to the hypothesis that Lp-PLA2 takes part in BHV calcification (Mahmut et al., 2014; Mahmut et al., 2016). The primary source of Lp-PLA2 might be tissue macrophages instead of circulating leucocytes (Ferguson et al., 2012). Ox-LDL can upregulate Lp-PLA2 expression in monocytes/macrophages through the PI3K and p38 MAPK pathway (Wang et al., 2010). Lp-PLA2 rapidly cleaves oxidized phosphatidylcholine molecules produced during the oxidation of LDL, generating the soluble proinflammatory and lyso-phosphatidylcholine (Wilensky and Macphee, 2009), while the latter is a strong candidate for osteogenic stimuli (Vickers et al., 2010). Another function of ox-LDL is to induce the expression of PCSK9 in macrophages and stimulate Toll-like receptors (TLRs) (Nsaibia et al., 2018), promoting an osteogenic inflammatory response by activating the NF-κB pathway (Tang et al., 2012; Wang et al., 2021b). Collectively, ox-LDL is a substantial contributor to BHV calcification.

In addition to lipid disorder, metabolic syndrome (MS), also known as syndrome X, insulin resistance, etc, is an aggregate of clinical conditions characterized by central and abdominal obesity, systemic hypertension, and insulin resistance (McCracken et al., 2018). Previous research suggested MS is a strong independent predictor of bioprosthetic valve degeneration (Briand et al., 2006). And patients with type 2 diabetes mellitus undergoing bioprosthetic valve implantation are more susceptible to BHV calcification (Lorusso et al., 2012). Currently, the metabolic mechanisms responsible for BHV calcification are poorly defined, but oxidative stress secondary to diabetes mellitus is hypothetically involved in BHV calcification (Cote et al., 2010).

5.2.4 Platelets and Subclinical Thrombosis

Bioprosthetic valve thrombosis is a rare but life-threatening complication that causes prosthetic valve obstruction (Brown et al., 2012). However, subclinical leaflet thrombosis occurred frequently, as it was detected in 12% of patients after BHV implanted (Chakravarty et al., 2017). Recently, literature illustrates that subclinical leaflet thrombosis is associated with BHV calcification. Cartlidge et al. (2019) observed a close spatial interaction of calcification with leaflet thrombosis and suggested thrombosis may be a potential upstream trigger for calcification.

Von Willebrand Factor (vWF) is the primary mediator of thrombosis, interacting with platelets. vWF is deactivated and cleaved by thrombospondin type-1 motif family and then maintained at a low concentration in the blood under high wall shear stress conditions in patients with aortic stenosis (Van Belle et al., 2019). Once the shear stress level was corrected after surgery, the concentration of vWF increased instantaneously (Sedaghat et al., 2017). The acute release of vWF promotes thrombus formation *in vivo*. Physiologically, the interaction of plasma VWF with platelets is induced by subendothelial collagen. In fact, the confluent endothelial layer is entirely lost in commercial BHV, so collagen type I, which is the main ECM component, is directly exposed to activate vWF. The formation of subclinical leaflet thrombosis induces inflammatory responses, valve fibrosis, and calcification. Moreover, a steep increase in calcium levels was shown on platelets when they were in contact with type 1 Collagen, possibly by activating calcium channels via phospholipase C and inositol 1,4,5 trisphosphate (Asselin et al., 1997; Roberts et al., 2004). The analysis above may help explain the relationship between thrombosis and calcification.

6 POTENTIAL DRUG THERAPY

Although BHV has been the mainstay of prosthetic valve substitutes for valve replacement surgery, mechanisms and pathogenetic factors of BHV calcification still being far from a clear elucidation of their nature, impeding the development of drug intervention to prevent or slow the process of BHV calcification.

No clinical drug targeting BHV calcification is currently available, however, statin treatment, both rosuvastatin, and atorvastatin could significantly diminish BHV calcification (Lorusso et al., 2010; Lee et al., 2019). In a rat subdermal implantation model, Sak Lee et al. (Lee et al., 2019) suggested that rosuvastatin attenuated BHV calcification associated though interleukin-6 and bone morphogenetic protein two downturns. Similarly, atorvastatin changes the global extent of inflammatory infiltrates but the proportions of the single inflammatory subsets, contributing to reduction of BHV calcification, either in terms of microcalcification or global calcium content (Lorusso et al., 2010). Some researchers showed that statin treatment is associated with significantly less BHV calcification and improved long-term outcomes (Antonini-Canterin et al., 2003; Sasaki et al., 2021). Yet, in one observational study by Kulik and colleagues, early lipid-lowering therapy did not lower BHV calcification (Kulik et al., 2010). Overall, statin treatment may be an effective therapeutic means after BHV implantation but requires more high-level evidence to support.

According to the linkages between immune response and BHV calcification, immunosuppressive therapy represented a potential candidate to delay BHV calcification and failure,

especially for young patients. A study reported that the calcific degree of BHV in patients who had been given steroid treatment for aortitis was decreased (Eishi et al., 1996). Rabbit anti-thymocyte globulin (ATG) is a polyclonal IgG preparation used for induction treatment of immunosuppression used in malignancies, graft-versus-host disease, and autoimmune diseases, to decrease early rejection (Mohty, 2007). ATG treatment may induce long-lasting anti-Neu5Gc IgG responses with immune memory (Couvrat-Desvergnes et al., 2015; Amon et al., 2017). These researches reveal a potential therapeutic strategy for preventing BHV calcification, and ATG treatment immediately following surgery deserves more molecular mechanism research and clinically relevant trial in the future. However, due to the many side effects of immunosuppressive therapy, it should be carefully considered.

Currently, Oral anticoagulation for the first 3 months after surgical implantation of BHV is recommended according to the European Society of Cardiology/the European Association for Cardio-Thoracic Surgery and American College of Cardiology/American Heart Association Guidelines (Otto et al., 2021b; Vahanian et al., 2021). Since subclinical leaflet thrombosis may be a cause of BHV calcification, another possible treatment option could be considered is prolonged, even life-long use of anticoagulant drugs. But in such a way, the uppermost advantage of BHV over MHV would be weakened. So how long it is justified for anticoagulant treatment after BHV implantation merits further discussion.

Given the well-recognized association between end-stage renal disease, diabetes mellitus, hyperparathyroidism and BHV calcification, aggressive treatment should be applied. Notably, sevelamer hydrochloride, a phosphate binder used to treat hyperphosphatemia in patients with chronic kidney disease, has been showing the ability to decrease BHV calcification (Meng et al., 2021).

7 CONCLUSION AND OUTLOOK

In the past few decades, BHV possess significant advantages by alleviating the need for anticoagulation treatment and their exquisite hemodynamic properties after constant updating and optimization. However, the limited durability mainly due to SVD remains a challenging barrier to widen the scope of usage. Calcification is the most frequent presentation and the core pathophysiological process of SVD. Uncovering the basic mechanisms of BHV calcification is an essential prerequisite to address issues that currently exist.

Mechanisms of BHV calcification are described in detail in the current review (**Figure 3**). In summary, residual cell debris after GLUT treatment and degeneration of ECM components are absolute necessities for BHV calcification. We also highlight the value of inflammatory reaction and immune response, oxidative stress, formation of ox-LDL, and subclinical leaflet thrombosis in the pathogenesis of BHV calcification. As alluded to above, just a few studies focusing on the pharmacological strategies of BHV calcification have been conducted, either animal or clinical studies. Currently, the potential therapies include lipid-lowering therapy, immunosuppressive therapy and aggressive treatment for comorbidities.

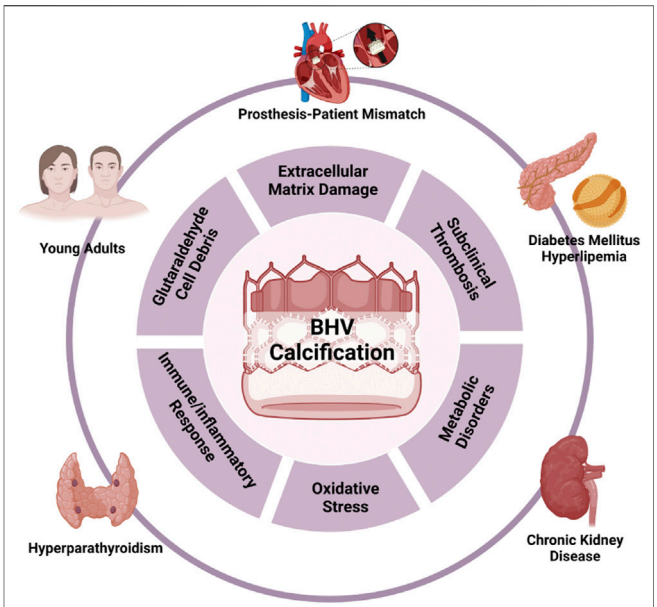

FIGURE 3 | Risk factors and mechanisms of BHV calcification.

Basic research and explorations to obtain a better understanding of BHV calcification are still in their infancy. There are still a number of unknowns which require further exploration and discussion. First of all, the mechanisms leading to increased immune cells infiltration, and how this effect correlates with BHV calcification are unclear. As such, this should be a focus of subsequent research. Secondly, current known main cell types of pathological process in calcific aortic valve disease have been described in detail (Xu et al., 2020), but whether other cells than immune cells involved in BHV calcification still remains a certain. To shed more light on the mechanisms of BHV calcification, further studies will be dedicated to the unraveling of cell-type atlas and intercellular interactions. Thirdly, Screening for more effective drugs to prevent or delay BHV calcification warrants further research. In conclusion, the increasing demand for BHV implantation mandates enhanced the investment in BHV calcification research and the transition from bench to bedside.

AUTHOR CONTRIBUTIONS

ND and WQ proposed the concept of the review. SW collected and analyzed documentation, and drafted the manuscript. YZ revised the manuscript. WY and SW modified the manuscript. LX drew the figures. All authors contributed to discussions and gave final approval of the submitted manuscript.

FUNDING

This work was supported by the National Natural Science Foundation of China (81900351 and 81930052).

REFERENCES

Amon, R., Ben-Arye, S. L., Engler, L., Yu, H., Lim, N., Berre, L. L., et al. (2017). Glycan Microarray Reveal Induced IgGs Repertoire Shift against a Dietary Carbohydrate in Response to Rabbit Anti-human Thymocyte Therapy. *Oncotarget* 8, 112236–112244. doi:10.18632/oncotarget.23096

Antonini-Canterin, F., Zuppiroli, A., Popescu, B. A., Granata, G., Cervesato, E., Piazza, R., et al. (2003). Effect of Statins on the Progression of Bioprosthetic Aortic Valve Degeneration. *Am. J. Cardiol.* 92, 1479–1482. doi:10.1016/j.amjcard.2003.08.066

Asselin, J., Gibbins, J. M., Achison, M., Lee, Y. H., Morton, L. F., Farndale, R. W., et al. (1997). A Collagen-like Peptide Stimulates Tyrosine Phosphorylation of Syk and Phospholipase C Gamma2 in Platelets Independent of the Integrin Alpha2beta1. *Blood* 89, 1235–1242. doi:10.1182/blood.v89.4.1235

Badria, A. F., Koutsoukos, P. G., and Mavrilas, D. (2020). Decellularized Tissue-Engineered Heart Valves Calcification: what Do Animal and Clinical Studies Tell Us? *J. Mater Sci. Mater Med.* 31, 132. doi:10.1007/s10856-020-06462-x

Bailey, M. T., Pillarisetti, S., Xiao, H., and Vyavahare, N. R. (2003). Role of Elastin in Pathologic Calcification of Xenograft Heart Valves. *J. Biomed. Mater Res. A* 66, 93–102. doi:10.1002/jbm.a.10543

Barbanti, M., Petronio, A. S., Ettori, F., Latib, A., Bedogni, F., De Marco, F., et al. (2015). 5-Year Outcomes after Transcatheter Aortic Valve Implantation with CoreValve Prosthesis. *JACC Cardiovasc Interv.* 8, 1084–1091. doi:10.1016/j.jcin.2015.03.024

Beckmann, A., Funkat, A. K., Lewandowski, J., Frie, M., Ernst, M., Hekmat, K., et al. (2016). German Heart Surgery Report 2015: The Annual Updated Registry of the German Society for Thoracic and Cardiovascular Surgery. *Thorac. Cardiovasc Surg.* 64, 462–474. doi:10.1055/s-0036-1592124

Boraldi, F., Lofaro, F. D., and Quaglino, D. (2021). Apoptosis in the Extraosseous Calcification Process. *Cells* 10, 131. doi:10.3390/cells10010131

Boskey, A. L., and Posner, A. S. (1976). Extraction of a Calcium-Phospholipid-Phosphate Complex from Bone. *Calcif. Tissue Res.* 19, 273–283. doi:10.1007/BF02564010

Bozso, S. J., Kang, J. J. H., Basu, R., Adam, B., Dyck, J. R. B., Oudit, G. Y., et al. (2021). Structural Valve Deterioration Is Linked to Increased Immune Infiltrate and Chemokine Expression. *J. Cardiovasc Transl. Res.* 14, 503–512. doi:10.1007/s12265-020-10080-x

Bradshaw, A. D., and Sage, E. H. (2001). SPARC, a Matricellular Protein that Functions in Cellular Differentiation and Tissue Response to Injury. *J. Clin. Invest.* 107, 1049–1054. doi:10.1172/JCI12939

Briand, M., Pibarot, P., Després, J. P., Voisine, P., Dumesnil, J. G., Dagenais, F., et al. (2006). Metabolic Syndrome Is Associated with Faster Degeneration of Bioprosthetic Valves. *Circulation* 114, I512–I517. doi:10.1161/CIRCULATIONAHA.105.000422

Brown, M. L., Park, S. J., Sundt, T. M., and Schaff, H. V. (2012). Early Thrombosis Risk in Patients with Biologic Valves in the Aortic Position. *J. Thorac. Cardiovasc Surg.* 144, 108–111. doi:10.1016/j.jtcvs.2011.05.032

Busch, E., Hohenester, E., Timpl, R., Paulsson, M., and Maurer, P. (2000). Calcium Affinity, Cooperativity, and Domain Interactions of Extracellular EF-Hands Present in BM-40. *J. Biol. Chem.* 275, 25508–25515. doi:10.1074/jbc.M001770200

Capodanno, D., Petronio, A. S., Prendergast, B., Eltchaninoff, H., Vahanian, A., Modine, T., et al. (2017). Standardized Definitions of Structural Deterioration and Valve Failure in Assessing Long-Term Durability of Transcatheter and Surgical Aortic Bioprosthetic Valves: a Consensus Statement from the European Association of Percutaneous Cardiovascular Interventions (EAPCI) Endorsed by the European Society of Cardiology (ESC) and the European Association for Cardio-Thoracic Surgery (EACTS). *Eur. Heart J.* 38, 3382–3390. doi:10.1093/eurheartj/ehx303

Cartlidge, T. R. G., Doris, M. K., Sellers, S. L., Pawade, T. A., White, A. C., Pessotto, R., et al. (2019). Detection and Prediction of Bioprosthetic Aortic Valve Degeneration. *J. Am. Coll. Cardiol.* 73, 1107–1119. doi:10.1016/j.jacc.2018.12.056

Chakravarty, T., Søndergaard, L., Friedman, J., De Backer, O., Berman, D., Kofoed, K. F., et al. (2017). Subclinical Leaflet Thrombosis in Surgical and Transcatheter Bioprosthetic Aortic Valves: an Observational Study. *Lancet* 389, 2383–2392. doi:10.1016/S0140-6736(17)30757-2

Chan, V., Jamieson, W. R., Germann, E., Chan, F., Miyagishima, R. T., Burr, L. H., et al. (2006). Performance of Bioprostheses and Mechanical Prostheses Assessed by Composites of Valve-Related Complications to 15 Years after Aortic Valve Replacement. *J. Thorac. Cardiovasc Surg.* 131, 1267–1273. doi:10.1016/j.jtcvs.2005.11.052

Chander, S., and Gordon, P. (2012). Soft Tissue and Subcutaneous Calcification in Connective Tissue Diseases. *Curr. Opin. Rheumatol.* 24, 158–164. doi:10.1097/BOR.0b013e32834ff5cd

Chen, W., Schoen, F. J., and Levy, R. J. (1994). Mechanism of Efficacy of 2-amino Oleic Acid for Inhibition of Calcification of Glutaraldehyde-Pretreated Porcine Bioprosthetic Heart Valves. *Circulation* 90, 323–329. doi:10.1161/01.cir.90.1.323

Christian, A. J., Alferiev, I. S., Connolly, J. M., Ischiropoulos, H., and Levy, R. J. (2015). The Effects of the Covalent Attachment of 3-(4-Hydroxy-3,5-Di-Tert-Butylphenyl) Propyl Amine to Glutaraldehyde Pretreated Bovine Pericardium on Structural Degeneration, Oxidative Modification, and Calcification of Rat Subdermal Implants. *J. Biomed. Mater Res. A* 103, 2441–2448. doi:10.1002/jbm.a.35380

Christian, A. J., Lin, H., Alferiev, I. S., Connolly, J. M., Ferrari, G., Hazen, S. L., et al. (2014). The Susceptibility of Bioprosthetic Heart Valve Leaflets to Oxidation. *Biomaterials* 35, 2097–2102. doi:10.1016/j.biomaterials.2013.11.045

Costa, C. (Edtior) (2020). Xenotransplantation: Methods and Protocols, 2nd Edition. Totowa, NJ: Humana Press Inc.

Côté, N., Pibarot, P., Pépin, A., Fournier, D., Audet, A., Arsenault, B., et al. (2010). Oxidized Low-Density Lipoprotein, Angiotensin II and Increased Waist Cirumference Are Associated with Valve Inflammation in Prehypertensive Patients with Aortic Stenosis. *Int. J. Cardiol.* 145, 444–449. doi:10.1016/j.ijcard.2009.05.054

Couvrat-Desvergnes, G., Salama, A., Le Berre, L., Evanno, G., Viklicky, O., Hruba, P., et al. (2015). Rabbit Antithymocyte Globulin-Induced Serum Sickness Disease and Human Kidney Graft Survival. *J. Clin. Invest.* 125, 4655–4665. doi:10.1172/JCI82267

D'arcy, J. L., Coffey, S., Loudon, M. A., Kennedy, A., Pearson-Stuttard, J., Birks, J., et al. (2016). Large-scale Community Echocardiographic Screening Reveals a Major Burden of Undiagnosed Valvular Heart Disease in Older People: the OxVALVE Population Cohort Study. *Eur. Heart J.* 37, 3515–3522. doi:10.1093/eurheartj/ehw229

Dangas, G. D., Weitz, J. I., Giustino, G., Makkar, R., and Mehran, R. (2016). Prosthetic Heart Valve Thrombosis. *J. Am. Coll. Cardiol.* 68, 2670–2689. doi:10.1016/j.jacc.2016.09.958

David, T. E., Armstrong, S., and Maganti, M. (2010). Hancock II Bioprosthesis for Aortic Valve Replacement: the Gold Standard of Bioprosthetic Valves Durability? *Ann. Thorac. Surg.* 90, 775–781. doi:10.1016/j.athoracsur.2010.05.034

Delogne, C., Lawford, P. V., Habesch, S. M., and Carolan, V. A. (2007). Characterization of the Calcification of Cardiac Valve Bioprostheses by Environmental Scanning Electron Microscopy and Vibrational Spectroscopy. *J. Microsc.* 228, 62–77. doi:10.1111/j.1365-2818.2007.01824.x

Dvir, D., Bourguignon, T., Otto, C. M., Hahn, R. T., Rosenhek, R., Webb, J. G., et al. (2018). Standardized Definition of Structural Valve Degeneration for Surgical and Transcatheter Bioprosthetic Aortic Valves. *Circulation* 137, 388–399. doi:10.1161/CIRCULATIONAHA.117.030729

Dziadzko, V., Clavel, M. A., Dziadzko, M., Medina-Inojosa, J. R., Michelena, H., Maalouf, J., et al. (2018). Outcome and Undertreatment of Mitral Regurgitation: a Community Cohort Study. *Lancet* 391, 960–969. doi:10.1016/S0140-6736(18)30473-2

Eishi, K., Ishibashi-Ueda, H., Nakano, K., Kosakai, Y., Sasako, Y., Kobayashi, J., et al. (1996). Calcific Degeneration of Bioprosthetic Aortic Valves in Patients Receiving Steroid Therapy. *J. Heart Valve Dis.* 5, 668–672.

Eliaz, N., and Metoki, N. (2017). Calcium Phosphate Bioceramics: A Review of Their History, Structure, Properties, Coating Technologies and Biomedical Applications. *Mater. (Basel)* 10, 334. doi:10.3390/ma10040334

Ferguson, J. F., Hinkle, C. C., Mehta, N. N., Bagheri, R., Derohannessian, S. L., Shah, R., et al. (2012). Translational Studies of Lipoprotein-Associated Phospholipase A_2 in Inflammation and Atherosclerosis. *J. Am. Coll. Cardiol.* 59, 764–772. doi:10.1016/j.jacc.2011.11.019

Forcillo, J., Pellerin, M., Perrault, L. P., Cartier, R., Bouchard, D., Demers, P., et al. (2013). Carpentier-Edwards Pericardial Valve in the Aortic Position: 25-years

Experience. *Ann. Thorac. Surg.* 96, 486–493. doi:10.1016/j.athoracsur.2013.03.032

Frasca, A., Xue, Y., Kossar, A. P., Keeney, S., Rock, C., Zakharchenko, A., et al. (2020). Glycation and Serum Albumin Infiltration Contribute to the Structural Degeneration of Bioprosthetic Heart Valves. *JACC Basic Transl. Sci.* 5, 755–766. doi:10.1016/j.jacbts.2020.06.008

Gates, K. V., Xing, Q., and Griffiths, L. G. (2019). Immunoproteomic Identification of Noncarbohydrate Antigens Eliciting Graft-specific Adaptive Immune Responses in Patients with Bovine Pericardial Bioprosthetic Heart Valves. *Proteomics Clin. Appl.* 13, e1800129. doi:10.1002/prca.201800129

Ground, M., Waqanivavalagi, S., Walker, R., Milsom, P., and Cornish, J. (2021). Models of Immunogenicity in Preclinical Assessment of Tissue Engineered Heart Valves. *Acta Biomater.* 133, 102–113. doi:10.1016/j.actbio.2021.05.049

Hopkins, R. A. (2006). Bioprosthetic Valves and Laudable Inflammation. *Circulation* 114, 261–264. doi:10.1161/CIRCULATIONAHA.106.639005

Katsi, V., Magkas, N., Antonopoulos, A., Trantalis, G., Toutouzas, K., and Tousoulis, D. (2021). Aortic Valve: Anatomy and Structure and the Role of Vasculature in the Degenerative Process. *Acta Cardiol.* 76, 335–348. doi:10.1080/00015385.2020.1746053

Kiełbik, A., Szlasa, W., Michel, O., Szewczyk, A., Tarek, M., Saczko, J., et al. (2020). *In Vitro* Study of Calcium Microsecond Electroporation of Prostate Adenocarcinoma Cells. *Molecules* 25. doi:10.3390/molecules25225406

Kim, K. M. (2002). Cells, rather Than Extracellular Matrix, Nucleate Apatite in Glutaraldehyde-Treated Vascular Tissue. *J. Biomed. Mater Res.* 59, 639–645. doi:10.1002/jbm.10038

Kim, K. M., Herrera, G. A., and Battarbee, H. D. (1999). Role of Glutaraldehyde in Calcification of Porcine Aortic Valve Fibroblasts. *Am. J. Pathol.* 154, 843–852. doi:10.1016/S0002-9440(10)65331-X

Kim, M. S., Jeong, S., Lim, H. G., and Kim, Y. J. (2015). Differences in Xenoreactive Immune Response and Patterns of Calcification of Porcine and Bovine Tissues in α-Gal Knock-Out and Wild-type Mouse Implantation Models. *Eur. J. Cardiothorac. Surg.* 48, 392–399. doi:10.1093/ejcts/ezu501

Kitagawa, T., Yamamoto, H., Sentani, K., Takahashi, S., Tsushima, H., Senoo, A., et al. (2015). The Relationship between Inflammation and Neoangiogenesis of Epicardial Adipose Tissue and Coronary Atherosclerosis Based on Computed Tomography Analysis. *Atherosclerosis* 243, 293–299. doi:10.1016/j.atherosclerosis.2015.09.013

Kostyunin, A., Mukhamadiyarov, R., Glushkova, T., Bogdanov, L., Shishkova, D., Osyaev, N., et al. (2020). Ultrastructural Pathology of Atherosclerosis, Calcific Aortic Valve Disease, and Bioprosthetic Heart Valve Degeneration: Commonalities and Differences. *Int. J. Mol. Sci.* 21, 7434. doi:10.3390/ijms21207434

Kostyunin, A. E., Yuzhalin, A. E., Rezvova, M. A., Ovcharenko, E. A., Glushkova, T. V., and Kutikhin, A. G. (2020). Degeneration of Bioprosthetic Heart Valves: Update 2020. *J. Am. Heart Assoc.* 9, e018506. doi:10.1161/JAHA.120.018506

Koziarz, A., Makhdoum, A., Butany, J., Ouzounian, M., and Chung, J. (2020). Modes of Bioprosthetic Valve Failure: a Narrative Review. *Curr. Opin. Cardiol.* 35, 123–132. doi:10.1097/HCO.0000000000000711

Kulik, A., Masters, R. G., Bédard, P., Hendry, P. J., Lam, B. K., Rubens, F. D., et al. (2010). Postoperative Lipid-Lowering Therapy and Bioprosthesis Structural Valve Deterioration: Justification for a Randomised Trial? *Eur. J. Cardiothorac. Surg.* 37, 139–144. doi:10.1016/j.ejcts.2009.06.051

Lee, S., Kim, D. H., Youn, Y. N., Joo, H. C., Yoo, K. J., and Lee, S. H. (2019). Rosuvastatin Attenuates Bioprosthetic Heart Valve Calcification. *J. Thorac. Cardiovasc Surg.* 158, 731–e1. doi:10.1016/j.jtcvs.2018.12.042

Lee, S., Levy, R. J., Christian, A. J., Hazen, S. L., Frick, N. E., Lai, E. K., et al. (2017). Calcification and Oxidative Modifications Are Associated with Progressive Bioprosthetic Heart Valve Dysfunction. *J. Am. Heart Assoc.* 6, e005648. doi:10.1161/JAHA.117.005648

Lee, W., Long, C., Ramsoondar, J., Ayares, D., Cooper, D. K., Manji, R. A., et al. (2016). Human Antibody Recognition of Xenogeneic Antigens (NeuGc and Gal) on Porcine Heart Valves: Could Genetically Modified Pig Heart Valves Reduce Structural Valve Deterioration? *Xenotransplantation* 23, 370–380. doi:10.1111/xen.12254

Lee, Y. S. (1993). Morphogenesis of Calcification in Porcine Bioprosthesis: Insight from High Resolution Electron Microscopic Investigation at Molecular and Atomic Resolution. *J. Electron Microsc. (Tokyo)* 42, 156–165.

Lei, Y., Ning, Q., Xia, Y., and Wang, Y. (2019). Enzyme-oxidative-polymerization Method for Improving Glycosaminoglycans Stability and Reducing Calcification in Bioprosthetic Heart Valves. *Biomed. Mater* 14, 025012. doi:10.1088/1748-605X/aafd7c

Leong, J., Munnelly, A., Liberio, B., Cochrane, L., and Vyavahare, N. (2013). Neomycin and Carbodiimide Crosslinking as an Alternative to Glutaraldehyde for Enhanced Durability of Bioprosthetic Heart Valves. *J. Biomater. Appl.* 27, 948–960. doi:10.1177/0885328211430542

Li, K. Y. C. (2019). Bioprosthetic Heart Valves: Upgrading a 50-Year Old Technology. *Front. Cardiovasc Med.* 6, 47. doi:10.3389/fcvm.2019.00047

Li, Q., Jiang, Q., and Uitto, J. (2014). Ectopic Mineralization Disorders of the Extracellular Matrix of Connective Tissue: Molecular Genetics and Pathomechanisms of Aberrant Calcification. *Matrix Biol.* 33, 23–28. doi:10.1016/j.matbio.2013.06.003

Liao, K. K., Li, X., John, R., Amatya, D. M., Joyce, L. D., Park, S. J., et al. (2008). Mechanical Stress: an Independent Determinant of Early Bioprosthetic Calcification in Humans. *Ann. Thorac. Surg.* 86, 491–495. doi:10.1016/j.athoracsur.2008.03.061

Lila, N., Mcgregor, C. G., Carpentier, S., Rancic, J., Byrne, G. W., and Carpentier, A. (2010). Gal Knockout Pig Pericardium: New Source of Material for Heart Valve Bioprostheses. *J. Heart Lung Transpl.* 29, 538–543. doi:10.1016/j.healun.2009.10.007

Lorusso, R., Corradi, D., Maestri, R., Bosio, S., Curulli, A., Beghi, C., et al. (2010). Atorvastatin Attenuates Post-implant Tissue Degeneration of Cardiac Prosthetic Valve Bovine Pericardial Tissue in a Subcutaneous Animal Model. *Int. J. Cardiol.* 141, 68–74. doi:10.1016/j.ijcard.2008.11.174

Lorusso, R., Gelsomino, S., Lucà, F., De Cicco, G., Billè, G., Carella, R., et al. (2012). Type 2 Diabetes Mellitus Is Associated with Faster Degeneration of Bioprosthetic Valve: Results from a Propensity Score-Matched Italian Multicenter Study. *Circulation* 125, 604–614. doi:10.1161/CIRCULATIONAHA.111.025064

MacGrogan, D., Luxán, G., Driessen-Mol, A., Bouten, C., Baaijens, F., and De La Pompa, J. L. (2014). How to Make a Heart Valve: from Embryonic Development to Bioengineering of Living Valve Substitutes. *Cold Spring Harb. Perspect. Med.* 4, a013912. doi:10.1101/cshperspect.a013912

Mahjoub, H., Mathieu, P., Sénéchal, M., Larose, E., Dumesnil, J., Després, J. P., et al. (2013). ApoB/ApoA-I Ratio Is Associated with Increased Risk of Bioprosthetic Valve Degeneration. *J. Am. Coll. Cardiol.* 61, 752–761. doi:10.1016/j.jacc.2012.11.033

Mahmut, A., Mahjoub, H., Boulanger, M. C., Dahou, A., Bouchareb, R., Capoulade, R., et al. (2016). Circulating Lp-PLA2 Is Associated with High Valvuloarterial Impedance and Low Arterial Compliance in Patients with Aortic Valve Bioprostheses. *Clin. Chim. Acta* 455, 20–25. doi:10.1016/j.cca.2016.01.014

Mahmut, A., Mahjoub, H., Boulanger, M. C., Fournier, D., Després, J. P., Pibarot, P., et al. (2014). Lp-PLA2 Is Associated with Structural Valve Degeneration of Bioprostheses. *Eur. J. Clin. Invest.* 44, 136–145. doi:10.1111/eci.12199

Manji, R. A., Hara, H., and Cooper, D. K. (2015a). Characterization of the Cellular Infiltrate in Bioprosthetic Heart Valves Explanted from Patients with Structural Valve Deterioration. *Xenotransplantation* 22, 406–407. doi:10.1111/xen.12187

Manji, R. A., Lee, W., and Cooper, D. K. C. (2015b). Xenograft Bioprosthetic Heart Valves: Past, Present and Future. *Int. J. Surg.* 23, 280–284. doi:10.1016/j.ijsu.2015.07.009

Manji, R. A., Zhu, L. F., Nijjar, N. K., Rayner, D. C., Korbutt, G. S., Churchill, T. A., et al. (2006). Glutaraldehyde-fixed Bioprosthetic Heart Valve Conduits Calcify and Fail from Xenograft Rejection. *Circulation* 114, 318–327. doi:10.1161/CIRCULATIONAHA.105.549311

Manolagas, S. C. (2010). From Estrogen-Centric to Aging and Oxidative Stress: a Revised Perspective of the Pathogenesis of Osteoporosis. *Endocr. Rev.* 31, 266–300. doi:10.1210/er.2009-0024

Matilla, L., Roncal, C., Ibarrola, J., Arrieta, V., García-Peña, A., Fernández-Celis, A., et al. (2020). A Role for MMP-10 (Matrix Metalloproteinase-10) in Calcific Aortic Valve Stenosis. *Arterioscler. Thromb. Vasc. Biol.* 40, 1370–1382. doi:10.1161/ATVBAHA.120.314143

McCracken, E., Monaghan, M., and Sreenivasan, S. (2018). Pathophysiology of the Metabolic Syndrome. *Clin. Dermatol* 36, 14–20. doi:10.1016/j.clindermatol.2017.09.004

McGregor, C. G., Kogelberg, H., Vlasin, M., and Byrne, G. W. (2013). Gal-knockout Bioprostheses Exhibit Less Immune Stimulation Compared to Standard Biological Heart Valves. *J. Heart Valve Dis.* 22, 383–390.

Meng, Z., Li, Z., Zhang, E., Zhang, L., Liu, Q., and Wu, Y. (2021). Sevelamer Attenuates Bioprosthetic Heart Valve Calcification. *Front. Cardiovasc Med.* 8, 740038. doi:10.3389/fcvm.2021.740038

Meuris, B., De Praetere, H., Strasly, M., Trabucco, P., Lai, J. C., Verbrugghe, P., et al. (2018). A Novel Tissue Treatment to Reduce Mineralization of Bovine Pericardial Heart Valves. *J. Thorac. Cardiovasc Surg.* 156, 197–206. doi:10.1016/j.jtcvs.2018.01.099

Mikroulis, D., Mavrilas, D., Kapolos, J., Koutsoukos, P. G., and Lolas, C. (2002). Physicochemical and Microscopical Study of Calcific Deposits from Natural and Bioprosthetic Heart Valves. Comparison and Implications for Mineralization Mechanism. *J. Mater Sci. Mater Med.* 13, 885–889. doi:10.1023/a:1016556514203

Miller, Y. I., Choi, S. H., Wiesner, P., Fang, L., Harkewicz, R., Hartvigsen, K., et al. (2011). Oxidation-specific Epitopes Are Danger-Associated Molecular Patterns Recognized by Pattern Recognition Receptors of Innate Immunity. *Circ. Res.* 108, 235–248. doi:10.1161/CIRCRESAHA.110.223875

Mohty, M. (2007). Mechanisms of Action of Antithymocyte Globulin: T-Cell Depletion and beyond. *Leukemia* 21, 1387–1394. doi:10.1038/sj.leu.2404683

Naso, F., Gandaglia, A., Bottio, T., Tarzia, V., Nottle, M. B., D'apice, A. J., et al. (2013). First Quantification of Alpha-Gal Epitope in Current Glutaraldehyde-Fixed Heart Valve Bioprostheses. *Xenotransplantation* 20, 252–261. doi:10.1111/xen.12044

New, S. E., Goettsch, C., Aikawa, M., Marchini, J. F., Shibasaki, M., Yabusaki, K., et al. (2013). Macrophage-Derived Matrix Vesicles: An Alternative Novel Mechanism for Microcalcification in Atherosclerotic Plaques. *Circ. Res.* 113, 72–77. doi:10.1161/CIRCRESAHA.113.301036

Nsaibia, M. J., Boulanger, M. C., Bouchareb, R., Mkannez, G., Dahou, A., Salaun, E., et al. (2018). Soluble CD14 Is Associated with the Structural Failure of Bioprostheses. *Clin. Chim. Acta* 485, 173–177. doi:10.1016/j.cca.2018.06.045

Nsaibia, M. J., Mahmut, A., Mahjoub, H., Dahou, A., Bouchareb, R., Boulanger, M. C., et al. (2016). Association between Plasma Lipoprotein Levels and Bioprosthetic Valve Structural Degeneration. *Heart* 102, 1915–1921. doi:10.1136/heartjnl-2016-309541

Ochi, A., Cheng, K., Zhao, B., Hardikar, A. A., and Negishi, K. (2020). Patient Risk Factors for Bioprosthetic Aortic Valve Degeneration: A Systematic Review and Meta-Analysis. *Heart Lung Circ.* 29, 668–678. doi:10.1016/j.hlc.2019.09.013

Ohri, R., Hahn, S. K., Hoffman, A. S., Stayton, P. S., and Giachelli, C. M. (2004). Hyaluronic Acid Grafting Mitigates Calcification of Glutaraldehyde-Fixed Bovine Pericardium. *J. Biomed. Mater Res. A* 70, 328–334. doi:10.1002/jbm.a.30088

Otto, C. M., Nishimura, R. A., Bonow, R. O., Carabello, B. A., Erwin, J. P., 3rd, Gentile, F., et al. (2021a). 2020 ACC/AHA Guideline for the Management of Patients with Valvular Heart Disease: A Report of the American College of Cardiology/American Heart Association Joint Committee on Clinical Practice Guidelines. *Circulation* 143, e72–e227. doi:10.1161/CIR.0000000000000923

Otto, C. M., Nishimura, R. A., Bonow, R. O., Carabello, B. A., Erwin, J. P., 3rd, Gentile, F., et al. (2021b). 2020 ACC/AHA Guideline for the Management of Patients with Valvular Heart Disease: Executive Summary: A Report of the American College of Cardiology/American Heart Association Joint Committee on Clinical Practice Guidelines. *Circulation* 143, e35–e71. doi:10.1161/CIR.0000000000000932

Paradis, J. M., Del Trigo, M., Puri, R., and Rodés-Cabau, J. (2015). Transcatheter Valve-In-Valve and Valve-In-Ring for Treating Aortic and Mitral Surgical Prosthetic Dysfunction. *J. Am. Coll. Cardiol.* 66, 2019–2037. doi:10.1016/j.jacc.2015.09.015

Park, C. S., Park, S.-S., Choi, S. Y., Yoon, S. H., Kim, W.-H., and Kim, Y. J. (2010). Anti Alpha-Gal Immune Response Following Porcine Bioprosthesis Implantation in Children. *J. Heart Valve Dis.* 19, 124–130.

Pibarot, P., Ternacle, J., Jaber, W. A., Salaun, E., Dahou, A., Asch, F. M., et al. (2020). Structural Deterioration of Transcatheter versus Surgical Aortic Valve Bioprostheses in the PARTNER-2 Trial. *J. Am. Coll. Cardiol.* 76, 1830–1843. doi:10.1016/j.jacc.2020.08.049

Plakkal Ayyappan, J., Paul, A., and Goo, Y. H. (2016). Lipid Droplet-Associated Proteins in Atherosclerosis (Review). *Mol. Med. Rep.* 13, 4527–4534. doi:10.3892/mmr.2016.5099

Raghavan, D., Simionescu, D. T., and Vyavahare, N. R. (2007). Neomycin Prevents Enzyme-Mediated Glycosaminoglycan Degradation in Bioprosthetic Heart Valves. *Biomaterials* 28, 2861–2868. doi:10.1016/j.biomaterials.2007.02.017

Reuven, E. M., Leviatan Ben-Arye, S., Marshanski, T., Breimer, M. E., Yu, H., Fellah-Hebia, I., et al. (2016). Characterization of Immunogenic Neu5Gc in Bioprosthetic Heart Valves. *Xenotransplantation* 23, 381–392. doi:10.1111/xen.12260

Roberts, D. E., Mcnicol, A., and Bose, R. (2004). Mechanism of Collagen Activation in Human Platelets. *J. Biol. Chem.* 279, 19421–19430. doi:10.1074/jbc.M308864200

Rodriguez-Gabella, T., Voisine, P., Puri, R., Pibarot, P., and Rodés-Cabau, J. (2017). Aortic Bioprosthetic Valve Durability: Incidence, Mechanisms, Predictors, and Management of Surgical and Transcatheter Valve Degeneration. *J. Am. Coll. Cardiol.* 70, 1013–1028. doi:10.1016/j.jacc.2017.07.715

Roger, V. L., Go, A. S., Lloyd-Jones, D. M., Adams, R. J., Berry, J. D., Brown, T. M., et al. (2011). Heart Disease and Stroke Statistics-2011 Update: a Report from the American Heart Association. *Circulation* 123, e18–e209. doi:10.1161/CIR.0b013e3182009701

Ruzicka, D. J., Hettich, I., Hutter, A., Bleiziffer, S., Badiu, C. C., Bauernschmitt, R., et al. (2009). The Complete Supraannular Concept: *In Vivo* Hemodynamics of Bovine and Porcine Aortic Bioprostheses. *Circulation* 120, S139–S145. doi:10.1161/CIRCULATIONAHA.109.844332

Sakaue, T., Nakaoka, H., Shikata, F., Aono, J., Kurata, M., Uetani, T., et al. (2018). Biochemical and Histological Evidence of Deteriorated Bioprosthetic Valve Leaflets: the Accumulation of Fibrinogen and Plasminogen. *Biol. Open* 7, bio034009. doi:10.1242/bio.034009

Sasaki, K., Watanabe, Y., Kozuma, K., Kataoka, A., Hioki, H., Nagura, F., et al. (2021). Comparison of Long-Term Mortality in Patients Who Underwent Transcatheter Aortic Valve Replacement with or without Anti-atherosclerotic Therapy. *Heart Vessels* 36, 1892–1902. doi:10.1007/s00380-021-01873-4

Schoen, F. J., Hirsch, D., Bianco, R. W., and Levy, R. J. (1994). Onset and Progression of Calcification in Porcine Aortic Bioprosthetic Valves Implanted as Orthotopic Mitral Valve Replacements in Juvenile Sheep. *J. Thorac. Cardiovasc Surg.* 108, 880–887. doi:10.1016/s0022-5223(94)70186-5

Schoen, F. J., and Levy, R. J. (1992). Bioprosthetic Heart Valve Calcification: Membrane-Mediated Events and Alkaline Phosphatase. *Bone Min.* 17, 129–133. doi:10.1016/0169-6009(92)90723-q

Schoen, F. J., and Levy, R. J. (1999). Founder's Award, 25th Annual Meeting of the Society for Biomaterials, Perspectives. Providence, RI, April 28-May 2, 1999. Tissue Heart Valves: Current Challenges and Future Research Perspectives. *J. Biomed. Mater Res.* 47, 439–465. doi:10.1002/(sici)1097-4636(19991215)47:4<439::aid-jbm1>3.0.co;2-o

Schoen, F. J., Tsao, J. W., and Levy, R. J. (1986). Calcification of Bovine Pericardium Used in Cardiac Valve Bioprostheses. Implications for the Mechanisms of Bioprosthetic Tissue Mineralization. *Am. J. Pathol.* 123, 134–145.

Schraer, H., and Gay, C. V. (1977). Matrix Vesicles in Newly Synthesizing Bone Observed after Ultracryotomy and Ultramicroincineration. *Calcif. Tissue Res.* 23, 185–188. doi:10.1007/BF02012785

Sedaghat, A., Kulka, H., Sinning, J. M., Falkenberg, N., Driesen, J., Preisler, B., et al. (2017). Transcatheter aortic valve implantation leads to a restoration of von Willebrand factor (VWF) abnormalities in patients with severe aortic stenosis - Incidence and relevance of clinical and subclinical VWF dysfunction in patients undergoing transfemoral TAVI. *Thromb. Res.* 151, 23–28. doi:10.1016/j.thromres.2016.12.027

Sénage, T., Le Tourneau, T., Foucher, Y., Pattier, S., Cueff, C., Michel, M., et al. (2014). Early Structural Valve Deterioration of Mitroflow Aortic Bioprosthesis: Mode, Incidence, and Impact on Outcome in a Large Cohort of Patients. *Circulation* 130, 2012–2020. doi:10.1161/CIRCULATIONAHA.114.010400

Senage, T., Paul, A., Le Tourneau, T., Fellah-Hebia, I., Vadori, M., Bashir, S., et al. (2022). The Role of Antibody Responses against Glycans in Bioprosthetic Heart Valve Calcification and Deterioration. *Nat. Med.* 28, 283–294. doi:10.1038/s41591-022-01682-w

Shen, M., Carpentier, S. M., Berrebi, A. J., Chen, L., Martinet, B., and Carpentier, A. (2001). Protein Adsorption of Calcified and Noncalcified Valvular Bioprostheses after Human Implantation. *Ann. Thorac. Surg.* 71, S406–S407. doi:10.1016/s0003-4975(01)02501-2

Shen, Y., Guo, Y., Mikus, P., Sulniute, R., Wilczynska, M., Ny, T., et al. (2012). Plasminogen Is a Key Proinflammatory Regulator that Accelerates the Healing

of Acute and Diabetic Wounds. *Blood* 119, 5879–5887. doi:10.1182/blood-2012-01-407825

Shetty, R., Pibarot, P., Audet, A., Janvier, R., Dagenais, F., Perron, J., et al. (2009). Lipid-mediated Inflammation and Degeneration of Bioprosthetic Heart Valves. *Eur. J. Clin. Invest.* 39, 471–480. doi:10.1111/j.1365-2362.2009.02132.x

Siddiqui, R. F., Abraham, J. R., and Butany, J. (2009). Bioprosthetic Heart Valves: Modes of Failure. *Histopathology* 55, 135–144. doi:10.1111/j.1365-2559.2008.03190.x

Sies, H., and Jones, D. P. (2020). Reactive Oxygen Species (ROS) as Pleiotropic Physiological Signalling Agents. *Nat. Rev. Mol. Cell Biol.* 21, 363–383. doi:10.1038/s41580-020-0230-3

Simionescu, A., Simionescu, D. T., and Deac, R. F. (1996). Matrix Metalloproteinases in the Pathology of Natural and Bioprosthetic Cardiac Valves. *Cardiovasc Pathol.* 5, 323–332. doi:10.1016/s1054-8807(96)00043-9

Simionescu, D. T., Lovekamp, J. J., and Vyavahare, N. R. (2003). Extracellular Matrix Degrading Enzymes Are Active in Porcine Stentless Aortic Bioprosthetic Heart Valves. *J. Biomed. Mater Res. A* 66, 755–763. doi:10.1002/jbm.a.10066

Stein, P. D., Wang, C. H., Riddle, J. M., and Magilligan, D. J., Jr. (1988). Leukocytes, Platelets, and Surface Microstructure of Spontaneously Degenerated Porcine Bioprosthetic Valves. *J. Card. Surg.* 3, 253–261. doi:10.1111/j.1540-8191.1988.tb00246.x

Tang, Z., Jiang, L., Peng, J., Ren, Z., Wei, D., Wu, C., et al. (2012). PCSK9 siRNA Suppresses the Inflammatory Response Induced by oxLDL through Inhibition of NF-Kb Activation in THP-1-Derived Macrophages. *Int. J. Mol. Med.* 30, 931–938. doi:10.3892/ijmm.2012.1072

Tomazic, B. B., Brown, W. E., and Schoen, F. J. (1994). Physicochemical Properties of Calcific Deposits Isolated from Porcine Bioprosthetic Heart Valves Removed from Patients Following 2-13 Years Function. *J. Biomed. Mater Res.* 28, 35–47. doi:10.1002/jbm.820280106

Vahanian, A., Beyersdorf, F., Praz, F., Milojevic, M., Baldus, S., Bauersachs, J., et al. (2021). 2021 ESC/EACTS Guidelines for the Management of Valvular Heart Disease. *Eur. J. Cardiothorac. Surg.* 60, 727–800. doi:10.1093/ejcts/ezab389

Valente, M., Bortolotti, U., and Thiene, G. (1985). Ultrastructural Substrates of Dystrophic Calcification in Porcine Bioprosthetic Valve Failure. *Am. J. Pathol.* 119, 12–21.

Van Belle, E., Vincent, F., Rauch, A., Casari, C., Jeanpierre, E., Loobuyck, V., et al. (2019). von Willebrand Factor and Management of Heart Valve Disease: JACC Review Topic of the Week. *J. Am. Coll. Cardiol.* 73, 1078–1088. doi:10.1016/j.jacc.2018.12.045

Veiseh, O., and Vegas, A. J. (2019). Domesticating the Foreign Body Response: Recent Advances and Applications. *Adv. Drug Deliv. Rev.* 144, 148–161. doi:10.1016/j.addr.2019.08.010

Vickers, K. C., Castro-Chavez, F., and Morrisett, J. D. (2010). Lysophosphatidylcholine Induces Osteogenic Gene Expression and Phenotype in Vascular Smooth Muscle Cells. *Atherosclerosis* 211, 122–129. doi:10.1016/j.atherosclerosis.2010.04.005

Virani, S. S., Alonso, A., Aparicio, H. J., Benjamin, E. J., Bittencourt, M. S., Callaway, C. W., et al. (2021). Heart Disease and Stroke Statistics-2021 Update: A Report from the American Heart Association. *Circulation* 143, e254–e743. doi:10.1161/CIR.0000000000000950

Wang, C., Huang, Y., Liu, X., Li, L., Xu, H., Dong, N., et al. (2021a). Andrographolide Ameliorates Aortic Valve Calcification by Regulation of Lipid Biosynthesis and Glycerolipid Metabolism Targeting MGLL Expression *In Vitro* and *In Vivo*. *Cell Calcium* 100, 102495. doi:10.1016/j.ceca.2021.102495

Wang, C., Xia, Y., Qu, L., Liu, Y., Liu, X., and Xu, K. (2021b). Cardamonin Inhibits Osteogenic Differentiation of Human Valve Interstitial Cells and Ameliorates Aortic Valve Calcification via Interfering in the NF-Kb/nlrp3 Inflammasome Pathway. *Food Funct.* 12, 11808–11818. doi:10.1039/d1fo00813g

Wang, H., Workman, G., Chen, S., Barker, T. H., Ratner, B. D., Sage, E. H., et al. (2006). Secreted Protein Acidic and Rich in Cysteine (SPARC/osteonectin/BM-40) Binds to Fibrinogen Fragments D and E, but Not to Native Fibrinogen. *Matrix Biol.* 25, 20–26. doi:10.1016/j.matbio.2005.09.004

Wang, W. Y., Li, J., Yang, D., Xu, W., Zha, R. P., and Wang, Y. P. (2010). OxLDL Stimulates Lipoprotein-Associated Phospholipase A2 Expression in THP-1 Monocytes via PI3K and P38 MAPK Pathways. *Cardiovasc Res.* 85, 845–852. doi:10.1093/cvr/cvp367

Wang, X., Zhai, W., Wu, C., Ma, B., Zhang, J., Zhang, H., et al. (2015). Procyanidins-crosslinked Aortic Elastin Scaffolds with Distinctive Anti-calcification and Biological Properties. *Acta Biomater.* 16, 81–93. doi:10.1016/j.actbio.2015.01.028

Wen, S., Qiao, W., Zhang, Y., and Dong, N. (2020). Development and Trend in the Field of Valvular Heart Disease in China: an Analysis Based on the National Natural Science Foundation of China. *Ann. Transl. Med.* 8, 449. doi:10.21037/atm.2020.03.165

Whelan, A., Williams, E., Fitzpatrick, E., Murphy, B. P., Gunning, P. S., O'reilly, D., et al. (2021). Collagen Fibre-Mediated Mechanical Damage Increases Calcification of Bovine Pericardium for Use in Bioprosthetic Heart Valves. *Acta Biomater.* 128, 384–392. doi:10.1016/j.actbio.2021.04.046

Wilensky, R. L., and Macphee, C. H. (2009). Lipoprotein-associated Phospholipase A(2) and Atherosclerosis. *Curr. Opin. Lipidol.* 20, 415–420. doi:10.1097/MOL.0b013e3283307c16

Xu, K., Xie, S., Huang, Y., Zhou, T., Liu, M., Zhu, P., et al. (2020). Cell-Type Transcriptome Atlas of Human Aortic Valves Reveal Cell Heterogeneity and Endothelial to Mesenchymal Transition Involved in Calcific Aortic Valve Disease. *Arterioscler. Thromb. Vasc. Biol.* 40, 2910–2921. doi:10.1161/ATVBAHA.120.314789

Yacoub, M. H., and Takkenberg, J. J. (2005). Will Heart Valve Tissue Engineering Change the World? *Nat. Clin. Pract. Cardiovasc Med.* 2, 60–61. doi:10.1038/ncpcardio0112

Yap, K. H., Murphy, R., Devbhandari, M., and Venkateswaran, R. (2013). Aortic Valve Replacement: Is Porcine or Bovine Valve Better? *Interact. Cardiovasc Thorac. Surg.* 16, 361–373. doi:10.1093/icvts/ivs447

Zhu, F. J., Tong, Y. L., Sheng, Z. Y., and Yao, Y. M. (2019). Role of Dendritic Cells in the Host Response to Biomaterials and Their Signaling Pathways. *Acta Biomater.* 94, 132–144. doi:10.1016/j.actbio.2019.05.038

Zhu, Y. S., Gu, Y., Jiang, C., and Chen, L. (2020). Osteonectin Regulates the Extracellular Matrix Mineralization of Osteoblasts through P38 Signaling Pathway. *J. Cell Physiol.* 235, 2220–2231. doi:10.1002/jcp.29131

Conflict of Interest: The authors declare that the research was conducted in the absence of any commercial or financial relationships that could be construed as a potential conflict of interest.

Publisher's Note: All claims expressed in this article are solely those of the authors and do not necessarily represent those of their affiliated organizations, or those of the publisher, the editors and the reviewers. Any product that may be evaluated in this article, or claim that may be made by its manufacturer, is not guaranteed or endorsed by the publisher.

frontiers | Frontiers in Pharmacology

ORIGINAL RESEARCH
published: 14 July 2022
doi: 10.3389/fphar.2022.935804

P2X7 Purinoceptor Affects Ectopic Calcification of Dystrophic Muscles

Robin M. H. Rumney[1], *Justyna Róg*[2], *Natalia Chira*[1], *Alexander P. Kao*[3], *Rasha Al-Khalidi*[1†] *and Dariusz C. Górecki*[1,4*]

[1]School of Pharmacy and Biomedical Sciences, University of Portsmouth, Portsmouth, United Kingdom, [2]Department of Biochemistry, Laboratory of Cellular Metabolism, Nencki Institute of Experimental Biology, Polish Academy of Sciences, Warsaw, Poland, [3]Zeiss Global Centre, School of Mechanical and Design Engineering, University of Portsmouth, Portsmouth, United Kingdom, [4]Military Institute of Hygiene and Epidemiology, Warsaw, Poland

Ectopic calcification (EC) of myofibers is a pathological feature of muscle damage in Duchenne muscular dystrophy (DMD). Mineralisation of muscle tissue occurs concomitantly with macrophage infiltration, suggesting a link between ectopic mineral deposition and inflammation. One potential link is the P2X7 purinoceptor, a key trigger of inflammation, which is expressed on macrophages but also up-regulated in dystrophic muscle cells. To investigate the role of P2X7 in dystrophic calcification, we utilised the *Dmd*$^{mdx\text{-}\beta geo}$ dystrophin-null mouse model of DMD crossed with a global P2X7 knockout (*P2rx7*$^{-/-}$) or with our novel P2X7 knockin-knockout mouse (*P2x7*^{KiKo}), which expresses P2X7 in macrophages but not muscle cells. Total loss of P2X7 increased EC, indicating that P2X7 overexpression is a protective mechanism against dystrophic mineralisation. Given that muscle-specific P2X7 ablation did not affect dystrophic EC, this underlined the role of P2X7 receptor expression on the inflammatory cells. Serum phosphate reflected dystrophic calcification, with the highest serum phosphate levels found in genotypes with the most ectopic mineral. To further investigate the underlying mechanisms, we measured phosphate release from cells *in vitro*, and found that dystrophic myoblasts released less phosphate than non-dystrophic cells. Treatment with P2X7 antagonists increased phosphate release from both dystrophic and control myoblasts indicating that muscle cells are a potential source of secreted phosphate while macrophages protect against ectopic mineralisation. Treatment of cells with high phosphate media engendered mineral deposition, which was decreased in the presence of the P2X7 agonist BzATP, particularly in cultures of dystrophic cells, further supporting a protective role for P2X7 against ectopic mineralisation in dystrophic muscle.

Keywords: P2X7 purinoceptor protects against ectopic calcification of dystrophic muscles duchenne muscular dystrophy, ectopic calcification, knockout, knockin, macrophage, P2X7

OPEN ACCESS

Edited by:
Kang Xu,
Hubei University of Chinese Medicine, China

Reviewed by:
Jing Xie,
Sichuan University, China
Sandrine Herbelet,
Ghent University Hospital, Belgium

***Correspondence:**
Dariusz C. Górecki
darek.gorecki@port.ac.uk

†Present Address:
Rasha Al-Khalidi,
Department of Biotechnology, College of Science, University of Baghdad, Baghdad, Iraq

Specialty section:
This article was submitted to Experimental Pharmacology and Drug Discovery, a section of the journal Frontiers in Pharmacology

Received: *04 May 2022*
Accepted: *13 June 2022*
Published: *14 July 2022*

Citation:
Rumney RMH, Róg J, Chira N, Kao AP, Al-Khalidi R and Górecki DC (2022) P2X7 Purinoceptor Affects Ectopic Calcification of Dystrophic Muscles. Front. Pharmacol. 13:935804. doi: 10.3389/fphar.2022.935804

1 INTRODUCTION

Duchenne Muscular Dystrophy (DMD) is a devastating X-linked inherited disease, leading to severe disability and death in young men. Death is caused by the progressive degeneration of striated muscles aggravated by sterile inflammation (Sinadinos and Al-Khalidi, 2015). However, the pleiotropic effects of the mutant gene also include neuropsychiatric (Snow, Anderson, and Jakobson 2013) and bone structure abnormalities (Rufo et al., 2011), both irrespective of functional muscle impairment. These data indicate a much greater complexity of DMD

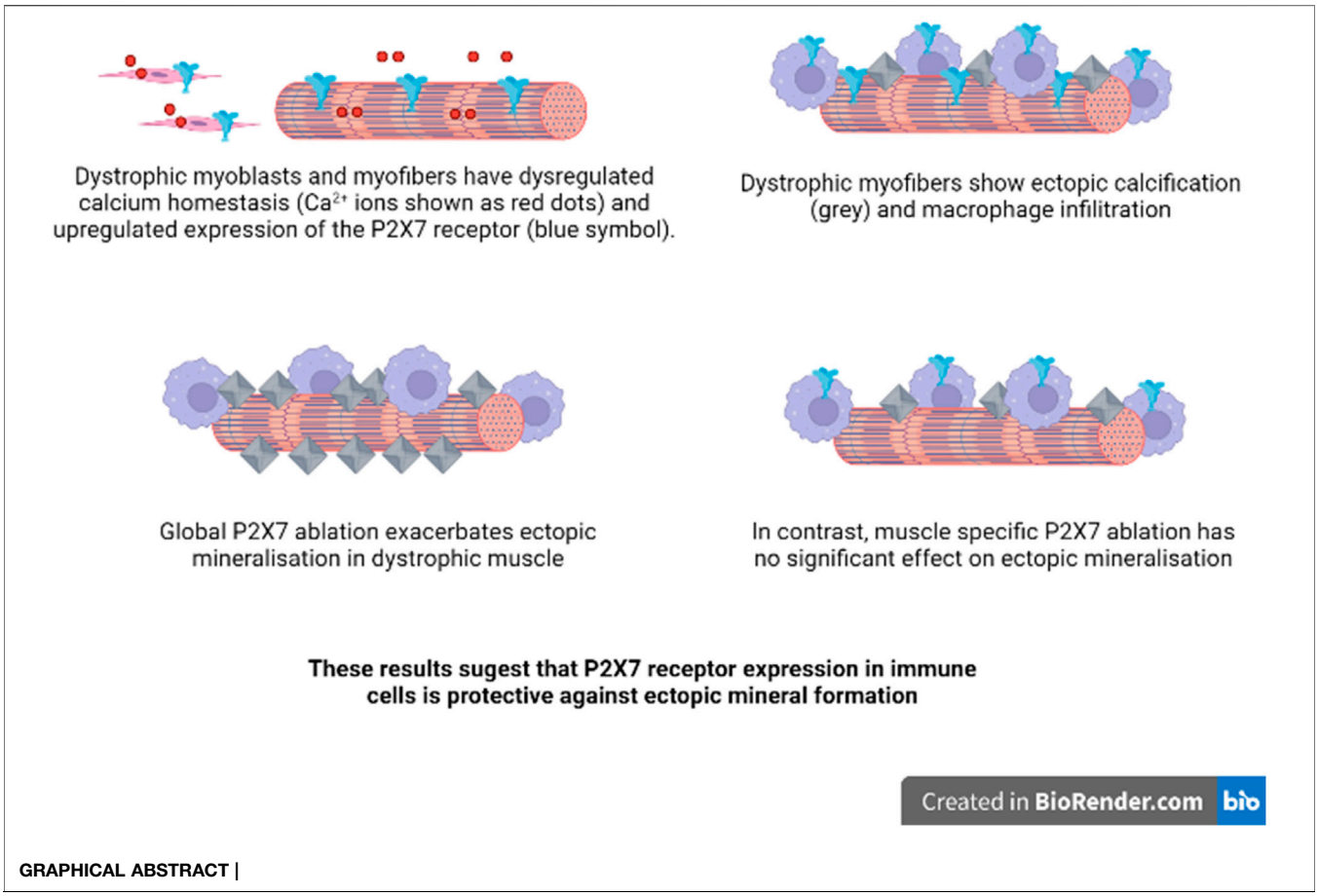

GRAPHICAL ABSTRACT |

pathology than the loss of structural integrity of muscle fibre sarcolemma. Indeed, while abnormalities of calcium homeostasis are widespread in DMD, its mechanisms, albeit not completely understood, have cell-specific components and can present in tissues structurally and functionally very dissimilar to muscle (Zabłocka, Górecki, and Zabłocki 2021).

Abnormally elevated resting cytosolic Ca^{2+} concentration is the common feature found across diverse cells affected by Duchenne muscular dystrophy (DMD) (Zabłocka, Górecki, and Zabłocki 2021). Recent studies revealed DMD pathology, including this calcium dys-homeostasis, to be active prior to diagnosis, with functional (van Dommelen et al., 2020) and molecular (Pescatori et al., 2007) abnormalities presenting in babies. In fact, studies in DMD foetuses and embryos from various animal disease models (Toop and Emery 1974; Emery 1977; Vassilopoulos and Emery 1977; Nguyen et al., 2002; Bassett et al., 2003; Merrick et al., 2009) revealed that this disease starts already in prenatal development, even before muscle specialisation (Mournetas et al., 2021). These developmental abnormalities are then recapitulated in myogenic cells in adult dystrophic muscle during their regeneration (Gosselin et al., 2021). However, once fully differentiated, myofibres appear to cope without dystrophin, as its ablation in mature skeletal muscle did not trigger their degeneration (Seno et al., 2008; Rader et al., 2016).

Furthermore, severe sterile inflammation is important in both the initiation (Pescatori et al., 2007; Y. W.; Chen et al., 2005; Haslett et al., 2002) and progression of the dystrophic phenotype (Lozanoska-Ochser et al., 2018; Peterson and Guttridge 2009). While an acute inflammatory response helps regeneration of damaged muscle (Tidball and Armando Villalta, 2010), chronic inflammation existing in DMD is detrimental (Tidball, Welc, and Wehling-Henricks 2018). Foci of inflammation generally precede irreversible muscle loss and fibrosis and are often associated with ectopic calcification (EC).

We observed recently that increased ectopic myofibre calcification is associated with altered macrophage infiltration patterns, particularly a close association of macrophages with calcified fibres (Young et al., 2020). Given that treatments reducing immune cell infiltrations significantly reduced the dystrophic pathology (Spencer et al., 2001; Farini et al., 2007; Evans et al., 2009; Boursereau et al., 2018; Sagheddu et al., 2018) and specifically that the more targeted reduction of inflammation *via* genetic ablation (Sinadinos and Al-Khalidi. 2015) or pharmacological inhibition (Al-Khalidi et al., 2018) of the P2X7 purinoceptor, the key inducer of the inflammatory response, produced a widespread functional attenuation of DMD symptoms (Górecki 2019), we investigated the role of this member of the P2X ATP gated ion channel family (Illes et al., 2021) in EC.

The association of P2X7 with inflammation and immunity is of critical importance (Adinolfi et al., 2018). P2X7 is involved in a

range of responses: cytokine release, lymphocyte proliferation, intracellular pathogen killing, stimulation of gut mucosal immunity and even pain perception (reviewed in Di Virgilio et al., 2017; Young and Górecki 2018). P2X7 is expressed by virtually all cells of innate and adaptive immunity. Not surprisingly, P2X7 activation has been linked to a number of human diseases with an inflammatory component. Given that its overexpression was also found in dystrophic muscle cells (Yeung et al., 2006) and lymphocytes (Ferrari et al., 1994), we analysed the impact of both global and cell-specific ablation of the P2X7 purinoceptor on EC in dystrophic mice.

To facilitate this process, in this project we have used the dual purpose P2X7 knockin/knockout ($P2X7^{KiKo}$) mouse. These mice were developed by us as a tool to better understand tissue-specific expression and function of this receptor, its subunit assembly, signalling pathways, molecular interactions, and functional regulation. While P2X7 receptor is an appealing therapeutic target, these vital data are still needed and mouse models are a very important tool in purinergic receptor studies (Rumney and Górecki 2020). To be able to explore the role of P2X7 in the variety of inflammatory and immune cells as well as in muscle, we generated mice expressing tandem-tagged receptors and with key exons flanked by *loxP* sites to allow identification of the native P2X7R composition and the full repertoire of its interacting partners by utilising the "genetic-proteomic" approach (Bienvenu et al., 2010) and also enabling tissue-specific ablation of this receptor by crossing this mouse with tissue-specific and/or conditional *Cre* recombinase expressing strains, leading to the excision of the *loxP*-flanked P2X7 region.

Using this approach allowed us to identify the tissue specific role of P2X7 receptor in EC of dystrophic mouse muscle. Understanding this alteration may lead to the development of new therapies for this debilitating disease but also for other pathologies where EC presents a real problem (Proudfoot 2019; Daniela, Federica, and Lofaro 2020).

2 MATERIALS AND METHODS

2.1 Animals

Male C57BL/6-DmdGt (ROSAbgeo)1Mpd/J ($Dmd^{mdx\text{-}\beta geo}$) and C57BL/6 eight week old mice were used in accordance with institutional Ethical Review Board and the Home Office (United Kingdom) Approvals. All mice were maintained under pathogen-free conditions and in a controlled environment (12-h light/dark cycle, 19–23°C ambient temperature, 45–65% humidity). For environmental enrichment, tubes, toys and nesting materials were routinely placed in cages. $Dmd^{mdx\text{-}\beta geo}$ mice were generated in C57BL/6 by insertion of the ROSAβgeo promoter-less gene trap construct downstream from the dystrophin DP71 promoter, resulting in the reading-frame disruption and loss of all dystrophin isoforms (Wertz and Martin Füchtbauer 1998) and $P2rX7^{-/-}$ knockout mice (Jackson lab s/n: 005576) were described before (Solle et al., 2001). The genotypes of all experimental animals were confirmed by PCR, as described before (Sinadinos and Al-Khalidi. 2015) (Specific primer sequences are summarised in **Supplementary Table S1**). Animals were killed by CO_2 inhalation, tissues were dissected and used immediately for protein extraction, frozen in Liquid N_2 or fixed with 10% buffered formalin for subsequent analyses. Blood samples were left to clot for 30 min prior to centrifugation at 2000g for 10 min to isolate serum.

2.2 RNA Extraction, cDNA Synthesis and qPCR Analysis

2.2.1 RNA extraction and cDNA synthesis

Total RNA was extracted from tibialis anterior muscles using the RNEasy Plus Universal Mini kit (Qiagen 73404) according to kit manufacturer's instructions. RNA quality and concentration were measured using a NanoDrop 1000 Spectrophotometer (Thermo Scientific). RNA integrity was assessed using electrophoresis of 100 ng of total RNA in a 1% agarose gel (Sigma A4718) in TAE buffer or using an automated capillary electrophoresis system (2100 Bioanalyzer Instrument G2939BA, Agilent) using a kit assay (Agilent RNA 6000 Nano Kit 5067-1511, Agilent). Total RNA samples were converted to cDNA using SuperScript VILO cDNA Synthesis Kit (Invitrogen 11754050) as per manufacturer instructions.

2.2.2 Real Time Quantitative PCR

SYBR Green real-time qPCR reactions were ran as previously described (Sinadinos and Al-Khalidi. 2015). Based on our previous normalization of quantitative RT-PCR data using a set of 12 candidate reference genes (Primer Design) to ensure accurate quantification (Vandesompele et al., 2002), *Gapdh* was found amongst the most stably expressed genes (Sinadinos and Al-Khalidi, 2015). Therefore, it was used as reference to establish individual gene expression values ($2^{-\Delta\Delta CT}$). Amplifications were performed in duplicates using 25 ng of cDNA per reaction with Precision Plus Mastermix (Primer Design PPLUS-LR), forward and reverse primers (**Supplementary Table S1**) (Eurofins) and DEPC treated water (Fisher Bioreagents BP561) as per manufacturer instructions, on 96 well plates using an Applied Biosystem ViiA7 Real Time PCR instrument.

2.3 Cell Culture and Assays

2.3.1 Isolation of Peritoneal Macrophages

Mice were killed by CO_2 exposure, abdomens sterilised with 70% ethanol and 6 ml DMEM was injected into the peritoneal cavity. The peritoneum was then gently massaged and fluid aspirated. Collected peritoneal cells were centrifuged at 300 g for 8 min at 4°C. Supernatant was discarded and pelleted cells were re-suspended in 5 ml DMEM high glucose (HG) with 20% (v/v) FBS, 2 mM L- Glutamine, 100U/ml Penicillin and 100U/ml Streptomycin (Fisher Scientific, United Kingdom). Cell suspension was plated in polystyrene petri dish and incubated at 37°C in a humidified environment of 5% CO_2 overnight. Non-adherent cells were then thoroughly rinsed after 2 h.

2.3.2 Isolation of Bone-Marrow Derived Macrophages

Femora and tibiae were dissected and cleaned mechanically using paper tissue to remove the surrounding muscle tissue. Bones were placed in cold PBS in a petri dish and transferred to a sterile hood. After soaking for 30 s in 70% ethanol and two washes in sterile PBS,

the contents of bone marrow cavities were flushed out with cold PBS using a syringe and a needle. Eluates were passed through a 70 μm cell strainer into falcon tubes and centrifuged at 300 g for 8 min at 4°C. Supernatant was discarded and each cell pellet was re-suspended in 3 ml ACK lysis buffer (Life technologies Ltd.) and incubated for 5–10 min at room temperature (RT) for red blood cell elimination. 3ml PBS was added to stop the reaction and cells were centrifuged at 300 g for 6 min. Supernatant was discarded and each pellet re-suspended in 10 ml DMEM F12 with 10% (v/v) FBS, 2 mM L- Glutamine, 100U/ml Penicillin, 100 μg/ml Streptomycin and 20 ng/ml Macrophage-colony stimulating factor (M-CSF) (Sigma Aldrich Ltd.). Suspensions were plated in 10 mm polystyrene petri dishes or 6-well tissue culture plates (Fisher Scientific Ltd.) and incubated at 37°C in a humidified environment of 5% CO_2. After 3 days in culture, 3 ml of fresh media was added to each petri dish or well. On day 7, non-adherent cells were removed, and adherent cells were considered macrophages.

2.3.3 Cell Lines

The SC5 (mdx) and IMO (WT) cell lines were derived from the leg muscle of the H2Kb-tsA58 line (Morgan et al., 1994). Cells were cultured in DMEM HG supplemented with 20% FBS, 4 mM L-glutamine, 100 unit/ml penicillin, 100 μg/ml streptomycin and 20 unit/ml murine γ-interferon (Invitrogen) at 33°C, 5% CO_2 humidified atmosphere (Yeung et al., 2006).

RAW 264.7 cells were maintained in DMEM HG with 10% FBS, 2 mM L-glutamine, 100 unit/mL penicillin and 100 μg/ml streptomycin at 37°C and 5% CO_2.

Cells were passaged and counted using a C-CHIP haemocytometer with trypan blue. All cells were plated at 20,000 per well in 96 well plates (Sarstedt) and incubated for 24 h to allow cell attachment prior to treatment.

Cells were treated for 48 h at 37°C using a basal media consisting of KnockOut DMEM, supplemented with 1% Knockout Serum Replacement (KSR), 0.5% v/v Donor Horse Serum (DHS, Sera Labs), 2 mM L-glutamine, 100 unit/mL penicillin and 100 μg/ml streptomycin. High phosphate media additionally contained 5 mM inorganic phosphate, 10 nM dexamethasone and 50 m g/ml ascorbic acid (Gartland et al., 2012). Additional treatments included were 20 μM AZT (Zidovudine), 1 μM brilliant blue G (BBG) and 350 μM BzATP.

Phosphate was quantified from serial dilutions of serum and cell conditioned media using the malachite green assay following manufacturer's instructions on the SpectraMax i3x multi-mode microplate reader (Molecular Devices, Wokingham, United Kingdom). Phosphate measurements from conditioned media were normalised to total protein from cell lysates measured with the Bicinchoninic Acid (BCA) assay (Sigma).

Cell viability experiments were quantified using the Presto Blue assay using a POLARstar Optima plate reader (BMG labtech, Ortenberg, Germany) and SpectraMax i3x.

For Alizarin Red staining, plates were fixed with ice cold 70% ethanol for 20 min and air dried for 24 h. Plates were stained with 100μl/well of 40 mM Alizarin Red S (pH 4.2) for 20 min on an orbital shaker. Excess stain was removed and plates left to air dry. Dried plates were scanned in on an EPSON flatbed scanner at 1200dpi, prior to extraction with cetylpyridinium chloride and quantification of optical density at 560 nm (Stanford et al., 1995) on a SpectraMax i3x.

2.3.4 Intracellular Ca^{2+} Measurements

Peritoneal macrophages were cultured on glass coverslips in 3.5 cm diameter dishes at 70–80% confluency in culture medium described above. After 24 h, cells were loaded with Fura-2 AM (Molecular Probes, Oregon) in culture medium for 20 min at 37°C in a 95% O_2, 5% CO_2 atmosphere. After two brief washes in the assay buffer (5 mM KCl, 1 mM $MgCl_2$, 0.5 mM Na_2HPO_4, 25 mM HEPES, 130 mM NaCl, 1 mM pyruvate, 25 mM D-glucose, 2 mM $CaCl_2$ pH 7.4) the coverslips were mounted in a cuvette and cells were treated with 300 μM of the P2X7 agonist BzATP. The calcium influx was measured in fluorescence spectrophotometer (F-7000 Hitachi). Fluorescence was recorded at 510 nm with excitation at 340/380 nm. Delta ratio of both signals was then calculated. Each experiment was repeated three times.

2.3.5 Immunoblotting

Cells were scraped off in a minimal volume of extraction buffer composed of 1x LysisM extraction buffer (Cat. #04719956001, Roche), 1 protease inhibitor cocktail tablet, 1 phosphatase inhibitor cocktail tablets (both Roche) per 10 ml of buffer. Samples were homogenised by passing through a 25-gauge needle 20 times, centrifuged and protein concentrations of extracts determined using the bicinchoninic acid kit (Sigma-Aldrich Ltd.). 5–50 μg of protein were mixed with Laemmli sample buffer (Bio-Rad Laboratories Ltd.) supplemented with 5% (v/v) β-mercaptoethanol, heated at 95°C for 5 min and chilled on ice before being separated by electrophoresis in polyacrylamide gels. Samples were electrotransferred onto methanol-activated polyvinylidene fluoride membranes (Amersham System, GE Healthcare Life Sciences Ltd.). Membranes were incubated on a horizontal shaker for 1 h at RT in a blocking solution containing Tris-buffered saline with 0.1% Tween (ThermoFisher Scientific) and 5% w/v non-fat dried cow milk powder. Membranes were subsequently incubated with primary antibodies (P2X7 and P2X7-TAG, diluted 1:1000) in the same blocking solution overnight at 4°C. Membranes were washed 3 × 10 min in TBS-Tween, and incubated with appropriate HRP-conjugated secondary antibodies in the blocking solution for 1 h. Finally, membranes were washed 3 × 10 min and incubated with LuminataTM Forte chemiluminescence development reagent (Merck, Burlington, MA, United States) and subsequently imaged using a ChemiDoc MP system (Bio-Rad, Hertfordshire, United Kingdom).

2.3.6 Immunocytofluorescence

Cells were cultured on coverslips (50–60%) in growth medium. After rinsing twice with cold PBS (w/o calcium and magnesium) the peritoneal macrophages were fixed in a 4% w/v paraformaldehyde solution (PFA) in PBS for 15 min on ice. Then cells were permeabilized using PBS with 0.1% Triton X-100 for 5 min and blocked in a 5% v/v normal goat serum (NGS, S-1000, Vector Laboratories IVD) in PBS for 1 h at RT and incubated overnight at 4°C with primary antibodies (anti-P2X7; 177003, Synaptic Systems, anti-TAG, PA1-984B, Invitrogen and marker of macrophages anti-F4/80; ab6640, Abcam 1:100 dilution) in

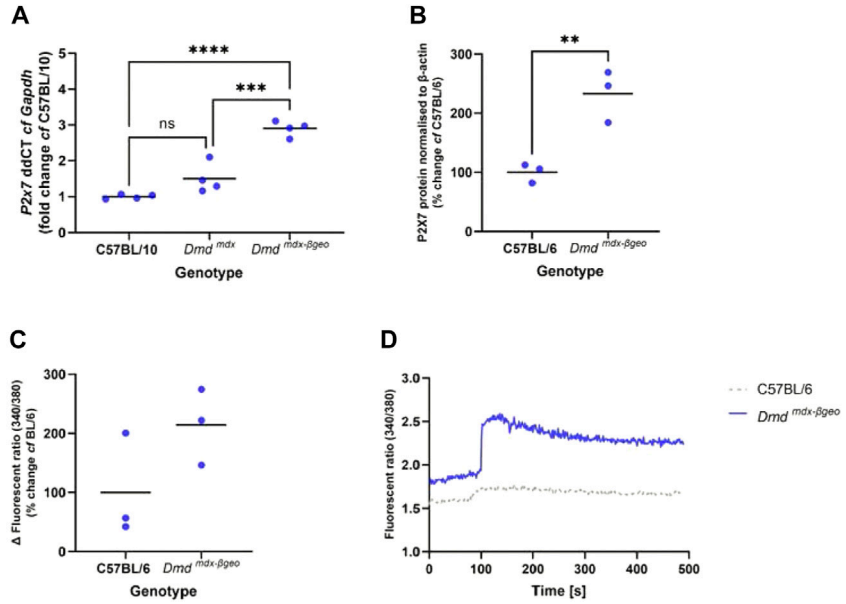

FIGURE 1 | P2X7 receptor expression and function in *Dmd* $^{mdx\text{-}\beta Geo}$ tissues. **(A)** qPCR analysis of *P2x7* gene expression in tibialis anterior muscle from *Dmd* $^{mdx\text{-}\beta Geo}$ mice compared to *Dmd* ^{mdx} (*** = $p < 0.001$) and wild type (**** = $p < 0.0001$), ANOVA with Tukey's post tests. **(B).** Western blot analysis of P2X7 protein expression in mouse BMM showing twice as much P2X7 in *Dmd* $^{mdx\text{-}\beta Geo}$ mice compared to C57BL/6 controls (** = p <0.01, unpaired t-test). **(C).** P2X7 activation was measured with the calcium influx assay, showing increased P2X7 activity in *Dmd* $^{mdx\text{-}\beta Geo}$ peritoneal macrophages. **(D).** Representative traces showing clear differences in P2X7 activation in C57BL/6 and *Dmd* $^{mdx\text{-}\beta geo}$ macrophages.

blocking buffer. The secondary antibody (diluted 1:1000 in 5% NGS in PBS, Alexa Fluor 488 goat anti-Rabbit, Thermo Fisher Scientific and Alexa Fluor 555 goat anti-Rat, respectively) was added for 1 h RT in dark. Then cells were rinsed 3 times for 10 min each wash with agitation between each step. After staining, cells on coverslips were mounted onto microscope slides sealed in Glycergel Mounting Medium with DAPI (H-1200 VectaShield®, Vector Laboratories) prior to imaging. Images were obtained using a confocal microscope (Zeiss Spinning Disk Confocal Microscope) and image analysis was performed by using ImageJ software.

2.4 X-Ray Micro-computed Tomography and Analysis

Animals were harvested at 8 weeks of age. The left quadriceps muscle was fixed in 10% formalin for 48 h, then to transferred to 70% ethanol prior to scanning. Quadriceps were placed within a 2-ml tube (Eppendorf, Stevenage, United Kingdom) and supported by a polyurethane foam saturated in 70% ethanol. Muscles were imaged using a Zeiss Xradia 520 Versa X-ray microscope (Zeiss) operating at an energy of 50 kV, a power of 4 W, and a tube current of 80 μA with a Zeiss LE1 filter was positioned directly after the X-ray source. The sample distance to the x-ray source was 200mm, and the sample distance to detector was 225mm, A total of 1601 X-ray projection images were collected over 360° at equal intervals with an exposure time for each projection of 3 s. The projections were reconstructed using the manufacturer's integrated software, which uses a filtered back projection reconstruction algorithm. TXRM files were imported into FiJi with the plugin to read XRM files and export Z-stack images (Schindelin et al., 2012; Metscher 2020). Mineralised areas within exported z-stack images (pixel size ranging from 32.25 to 34.45 μM depending upon sample) were quantified using the threshold function in ImageJ and used to calculate the volume.

2.5 Statistical Analysis

Statistical analyses were carried out with GraphPad Prism 9 and IBM SPSS Statistics 27. In GraphPad Prism, unpaired t-tests were used to compare two normally distributed data sets. Mann-Whitney tests were used for the comparison of two non-normally distributed data sets. Where there were three non-normally distributed data sets, a Kruskal-Wallis test was carried out with Tukey's or Dunn's multiple comparison tests. Where specific sets of columns required comparison, a Holm-Šídák test was used. Outliers were identified with ROUT tests. All figures containing data were made with GraphPad Prism 9. Where data was pooled from multiple replicate experiments, a Univariate analysis was carried out with Tukey's and Dunnett's post-tests using IBM SPSS Statistics 27.

3 RESULTS

3.1 Elevated P2X7 Expression and Function in the Dystrophic *Dmd* $^{mdx\text{-}\beta Geo}$ Mouse Cells and Tissues

We have previously demonstrated that the *Dmd* $^{mdx\text{-}\beta geo}$ dystrophin-null mouse muscle presents with significantly

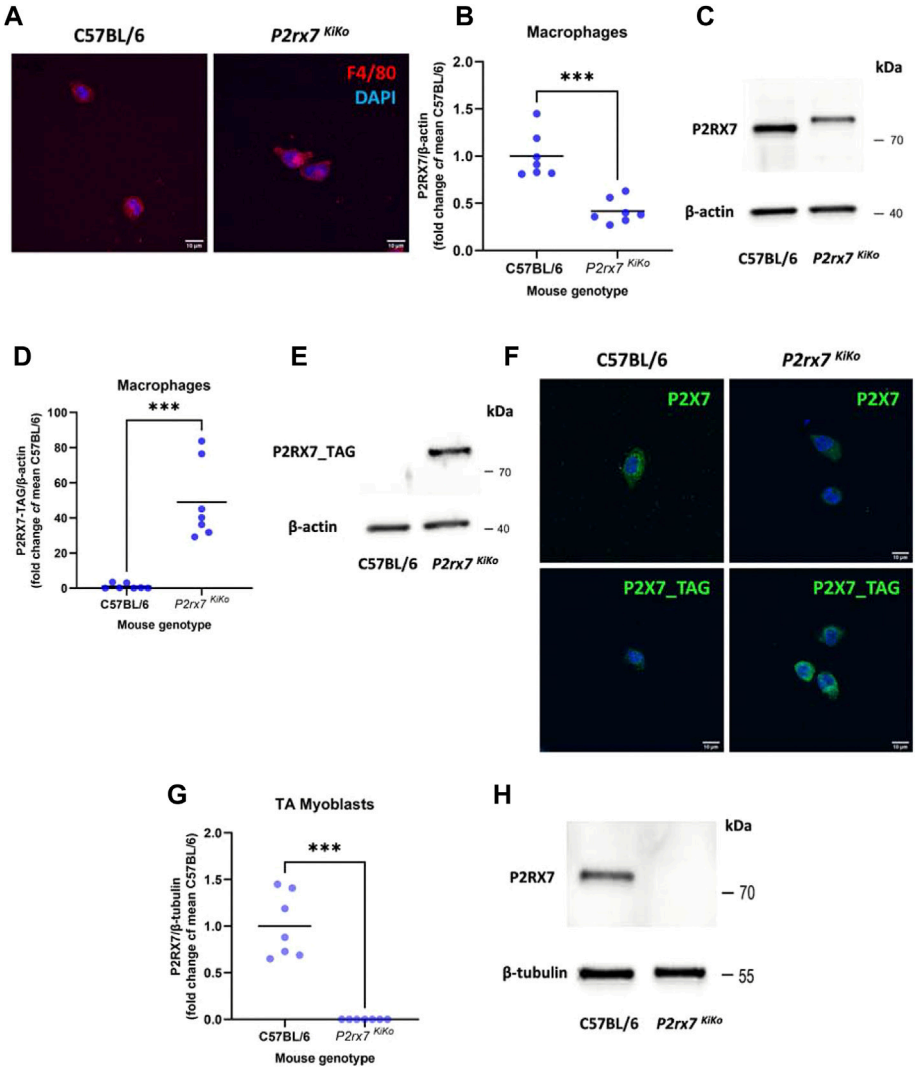

FIGURE 2 | Characterisation of the *P2rx7* ^{KiKo} mouse tissues. **(A).** Immunofluorescent (IF) labelling of isolated macrophages from C57BL/6 and *P2x7* ^{KiKo} mice, using the marker F4/80 to confirm the presence of macrophages. **(B,C).** Western blot analysis of P2X7 protein expression in macrophages showing partial decrease of P2X7 tagged protein levels in *P2x7* ^{KiKo} mice compared to C57BL/6 controls (*** = p <0.01, unpaired t-test). **(D,E).** Western blot analysis of P2X7-TAG protein expression in macrophages demonstrating presence of P2X7-TAG in *P2x7* ^{KiKo} mice and its absence in C57BL/6 controls (*** = p <0.01, unpaired t-test). **(F).** IF labelling showing expression of P2X7 and P2X7-TAG in macrophages from C57BL/6 and *P2x7* ^{KiKo} mice, respectively. **(G,H).** Western blot analysis of P2X7 protein expression in myoblasts isolated from the Tibialis Anterior (TA) showing an absence of P2X7 expression in *P2x7* ^{KiKo} cells, in contrast to C57BL/6 controls (*** = p <0.01, unpaired t-test).

increased ectopic myofibre calcification and altered macrophage infiltration patterns, particularly the close association of macrophages with calcified fibres (Young et al., 2020). Otherwise, the ectopic calcification had the same temporal pattern of presentation and resolution in *Dmd*$^{mdx\text{-}\beta geo}$ as in the *Dmd*^{mdx} mice, the most widely used animal model of DMD (Massopust et al., 2020). Therefore, we used the *Dmd*$^{mdx\text{-}\beta geo}$ mouse to investigate whether the P2X7 receptor, being the key mediator of the inflammatory response, could be linked to ectopic mineral formation. Firstly, we compared *P2x7* mRNA expression in *Dmd*$^{mdx\text{-}\beta geo}$ and control mouse *Tibialis anterior* muscle and found that receptor expression in *Dmd*$^{mdx\text{-}\beta geo}$ muscle is significantly elevated compared to WT muscle (**Figure 1A**, p <0.001 *cf* *Dmd*^{mdx}, p <0.0001 *cf* C57BL/10, ANOVA with Tukey's post tests). As this receptor expression in dystrophic muscle may result from its overexpression in muscle cells or from infiltrating inflammatory cells, we compared P2X7 expression and function between bone marrow derived macrophages (BMM) isolated from wild-type C57BL/6 and *Dmd*$^{mdx\text{-}\beta geo}$ mice. Using this approach, we compared naïve dystrophic and WT macrophages that were not exposed to any inflammatory signals present in the dystrophic mouse due to the chronic muscle inflammation. Such signals could

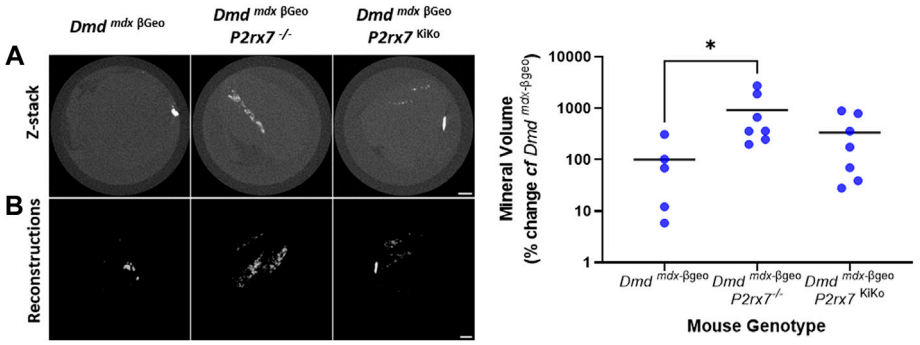

FIGURE 3 | Ectopic mineralisation in *Dmd* $^{mdx\text{-}\beta Geo}$, *Dmd* $^{mdx\text{-}\beta Geo}$ *P2rx7* $^{-/-}$ and *Dmd* $^{mdx\text{-}\beta Geo}$ *P2rx7* ^{KiKo} quadriceps. Isolated quadriceps muscles were scanned *ex vivo* by XCT and analysed in FIJI. **(A)** Z-stack images and 3D reconstructions from representative *Dmd*$^{mdx\text{-}\beta Geo}$, *Dmd*$^{mdx\text{-}\beta Geo}$ *P2rx7*$^{-/-}$ and *Dmd*$^{mdx\text{-}\beta Geo}$ *P2rx7*^{KiKo} quadriceps muscles. **(B)**. Quantification of mineralised volume within whole quadriceps muscles revealed increased mineralised volume in *Dmd*$^{mdx\text{-}\beta Geo}$ *P2rx7*$^{-/-}$ compared to *Dmd*$^{mdx\text{-}\beta Geo}$ but not *Dmd*$^{mdx\text{-}\beta Geo}$ *P2rx7*^{KiKo} mice (* = p <0.05, Kruskal-Wallis test with Dunn's multiple comparison test).

confound the expression data because of the priming effect in these cells on their subsequent reactivity (Netea et al., 2016). P2X7 protein levels quantified by Western blotting were 130% higher in *Dmd*$^{mdx\text{-}\beta geo}$ cells compared to C57BL/6 controls (**Figure 1B**, p < 0.01, unpaired t-test; **Supplementary Figure S1**). The functional P2X7 response evaluated using the intracellular calcium measurements assay showed that calcium influx after BzATP treatment was 114% higher in *Dmd*$^{mdx\text{-}\beta geo}$ macrophages than in C57BL/6 controls (**Figures 1C,D**, p = 0.1425, unpaired t-test).

3.2 Generation of the Novel *P2rx7*^{KiKo} Mouse Model

Targeting DNA constructs encoding tandem-tagged receptors and additionally flanked by *loxP* sites was used to generate the knock-in mouse strain. This part of the project was commissioned to the commercial developer (Ingenious Targeting Laboratory, United States). The N-termini of the P2X7a and P2X7k variants, that are uniquely expressed in mice (Xu et al., 2012) were tagged with AU1 and IRS tags, respectively to allow future identification of the native P2X7 receptor composition (subunit organization) and the full repertoire of its interacting partners (signalling and scaffolding proteins) by utilising the "genetic-proteomic" approach (Bienvenu et al., 2010). Furthermore, this P2X7^{KiKo} can be crossed with tissue-specific and/or conditional *Cre* recombinase expressing strains, leading to the excision of the *loxP*-flanked P2X7 coding region and generation of a cell/tissue specific and/or conditional P2X7 knockout (**Supplementary Figure S2**).

3.3 P2X7 Expression and Function in *P2rx7*^{KiKo} Mouse Tissues

The immunodetection, molecular and functional characterisation of the resulting tagged receptor subunits in *P2rx7*^{KiKo} mouse tissues revealed that in peritoneal macrophages the endogenous tagged P2X7 protein characterised by its slightly higher molecular weight (**Figure 2C**) was expressed at a slightly lower levels than the wild-type receptor but was fully functional and the responses elicited by the stimulation of the tagged P2X7 were unaffected (**Figures 2A–F**). In contrast, expression of the tagged P2X7 in myoblasts isolated from TA muscle was ablated, even in the absence of any *Cre* recombinase (**Figures 2G,H**). This unexpected outcome allowed us to use the *P2rx7*^{KiKo} as a muscle-specific P2X7 knockout.

3.4 Tissue-specific P2X7 Expression Affects Ectopic Muscle Calcification

To investigated the role of P2X7 in ectopic calcification, *Dmd*$^{mdx\text{-}\beta geo}$ mice were crossed with either global *P2rx7* knockout or *P2rx7* ^{KiKo} mice, treated as a muscle-specific knockout that retains functional P2X7 in macrophages. Quadriceps muscles isolated from 8-week-old mice were scanned by X-ray microscopy and reconstructed muscle images (**Figures 3A,B**) were quantified in ImageJ. There was significantly more mineral volume in quadriceps muscles from *Dmd*$^{mdx\text{-}\beta geo}$ *P2rx7*$^{-/-}$ double negative mice compared to *Dmd*$^{mdx\text{-}\beta geo}$ mice (**Figure 3C**, 926% *cf Dmd*$^{mdx\text{-}\beta geo}$, p < 0.05, Kruskal-Wallis test, with Dunn's multiple comparison). These calcifications were distributed throughout the muscle and did not form localised agglomerations observable in *Dmd*$^{mdx\text{-}\beta geo}$ (see animations of the 3D reconstructions from representative quadriceps included in the supplementary data). In contrast, there was no significant difference in mineralised volume between *Dmd*$^{mdx\text{-}\beta geo}$ and *Dmd*$^{mdx\text{-}\beta geo}$ *P2rx7* ^{KiKo} quadriceps, which lack P2X7 in muscle cells (**Figure 3C**, 337% *cf Dmd*$^{mdx\text{-}\beta geo}$, adjusted p value = 0.5981). These data indicate that P2X7 may have a protective effect against ectopic mineral formation in dystrophic muscle. Given that global loss of this receptor increased mineralisation but this effect was absent when P2X7 was ablated in muscle cells only, it is the loss of P2X7 in the immune cells, most likely macrophages, that is responsible for this increased calcification. Conversely, it is the expression of P2X7 in macrophages and not its overexpression in the

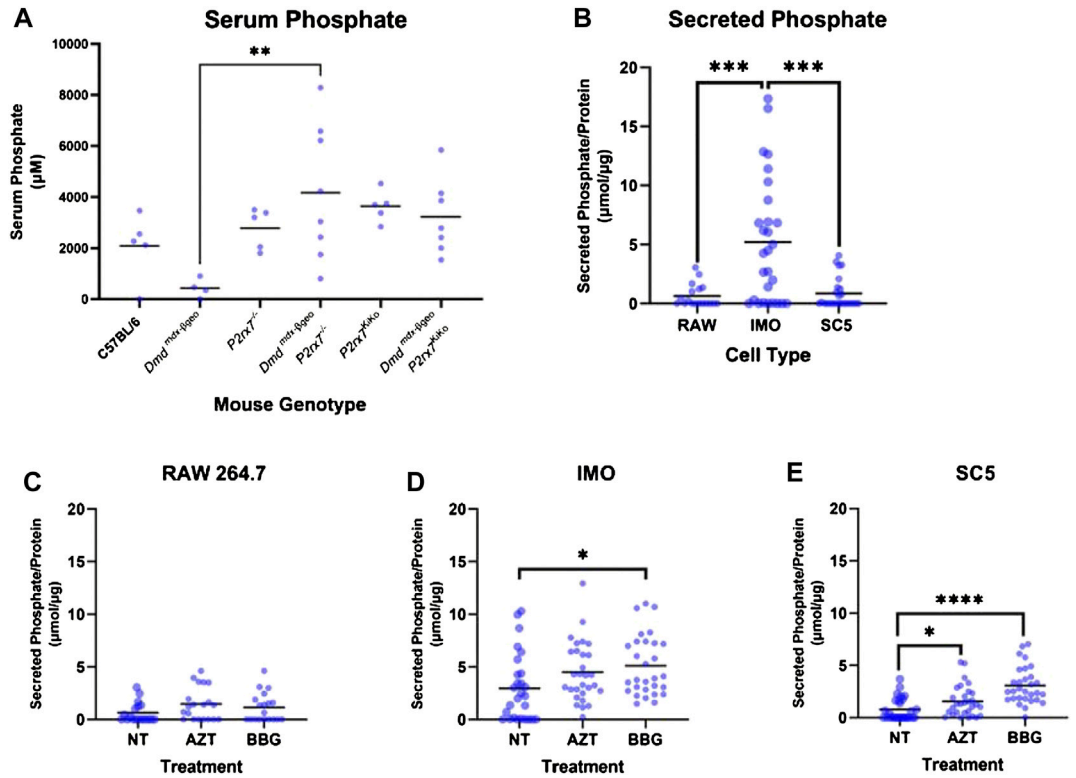

FIGURE 4 | Phosphate in serum and cell conditioned media. Phosphate was measured from mouse serum and cell conditioned media using the malachite green assay. **(A)** Serum phosphate was higher in *Dmd* $^{mdx\text{-}\beta Geo}$ *P2rx7* $^{-/-}$ compared to *Dmd* $^{mdx\text{-}\beta Geo}$ but not *Dmd* $^{mdx\text{-}\beta Geo}$ *P2rx7*^{KiKo} mice (** = p <0.01, Ordinary one-way ANOVA with Holm-Šídák's multiple comparison test). **(B)** Phosphate levels were higher in cell conditioned media (CM) from IMO cells than from either RAW cells or SC5 cells (p <0.001, Univariate analysis in SPSS with Tukey's post-tests). **(C)** Phosphate secretion by RAW cells was unaltered by treatment with the P2x7 inhibitors AZT and Coomassie brilliant blue G (BBG). **(D)** Phosphate secretion by IMO cells was increased in the presence of BBG (* = p <0.05, Univariate analysis in SPSS with Tukey's post-tests). **(E)** Phosphate secretion by SC5 cells was increased in the presence of AZT (* = p <0.05) and BBG (**** = p <0.0001, Univariate analysis in SPSS with Tukey's post-tests).

dystrophic muscle cells that protects against ectopic calcification.

3.5 Phosphate Secretion is Affected by Dystrophy and Regulated by P2X7

To further investigate the underlying mechanism of ectopic mineralisation, phosphate was quantified in serum samples from 8-week-old C57BL/6, *Dmd*$^{mdx\text{-}\beta geo}$, *P2rx7*$^{-/-}$, *Dmd*$^{mdx\text{-}\beta geo}$ *P2rx7*$^{-/-}$, *P2rx7* ^{KiKo}, and *Dmd*$^{mdx\text{-}\beta geo}$ *P2rx7* ^{KiKo} mice. Serum phosphate values were significantly increased in *Dmd*$^{mdx\text{-}\beta geo}$ *P2rx7*$^{-/-}$ compared to *Dmd*$^{mdx\text{-}\beta geo}$ mice (**Figure 4A**, p < 0.01, Ordinary one-way ANOVA with Holm-Šídák's multiple comparisons test).

To better understand the cellular origins of these changes in serum phosphate across mouse genotypes, phosphate secretion was measured by analysing cell-conditioned media from RAW 264.7 monocytes, IMO non-dystrophic and SC5 dystrophic myoblast cell lines (**Figure 4B**, mean values of 0.64 μmol/μg, 5.2 μmol/μg and 0.85 μmol/μg normalised to total protein from cell lysates, respectively). This analysis demonstrated that control IMO myoblasts secreted more phosphate than dystrophic SC5 cells (p < 0.001, univariate analysis with Tukey post-tests). The RAW 264.7 monocytes secreted phosphate at levels comparable to SC5 cells.

As loss of P2X7 *in vivo* was associated with significantly altered serum phosphate, cells *in vitro* were treated with the P2X7 antagonist BBG and also with AZT, identified by us as an effective P2X7 blocker with good potential for repurposing for therapeutic applications (Al-Khalidi et al., 2018). Secreted phosphate levels were normalised to total protein contents in cell lysates. Phosphate secretion from RAW 264.7 cells was unaltered by P2X7 antagonists (**Figure 4C**). In contrast, phosphate secretion from IMO and SC5 cells was increased by treatment with BBG and AZT (**Figures 4D,E**, p < 0.0001 and p < 0.01 respectively, univariate analysis with Dunn's post-tests). Interestingly, the phosphate secretion from IMO control myoblasts, which was higher than from SC5, was only mildly augmented by BBG (**Figure 4D**).

These data demonstrate that myoblasts are a source of secreted phosphate, and that phosphate secretion from these cells is

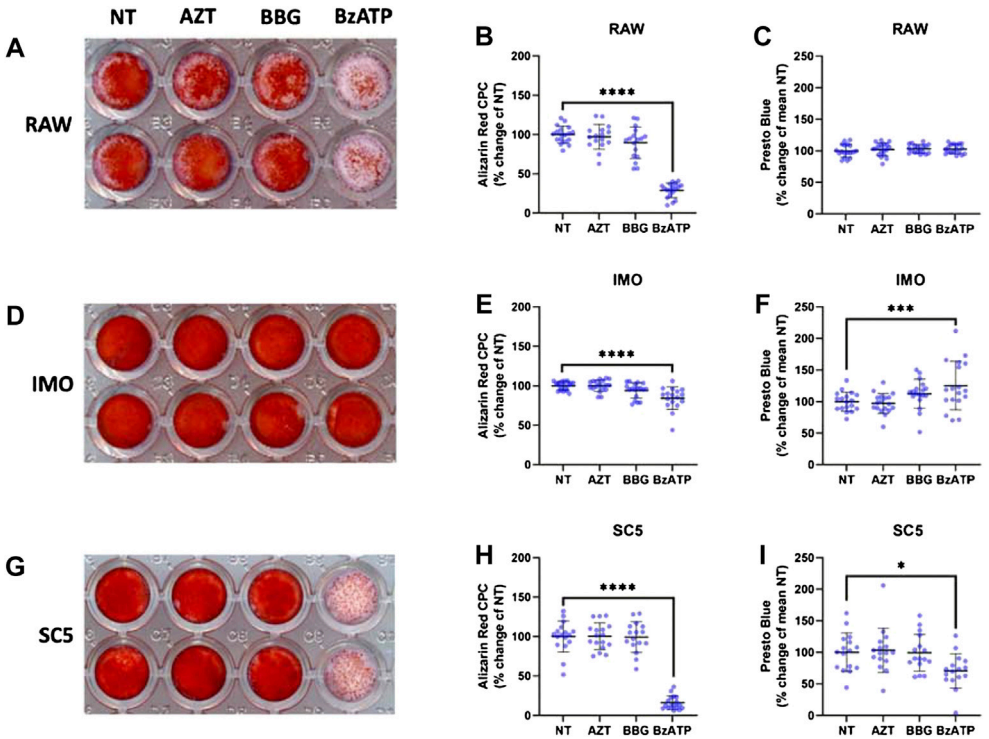

FIGURE 5 | Role of P2X7 in mineralisation of RAW 264.7, IMO and SC5 cells. Cultures of RAW 264.7, IMO and SC5 cells were treated with high phosphate (HP) media, in combination with the P2X7 inhibitors AZT and BBG and the agonist BzATP for 48 h. Cell viability was measured with the Presto Blue assay and mineralisation visualised with Alizarin Red staining that was quantified with the CPC method. **(A,B)** Mineralisation of RAW 264.7 cells in HP media was decreased by the P2X7 agonist BzATP (**** = $p < 0.0001$, univariate analysis with Dunnett's post-tests in SPSS). **(C)** Viability of RAW 264.7 cells remained unaltered across treatment groups. **(D,E)** Mineralisation of IMO cells in HP media is decreased by the P2X7 agonist BzATP (**** = $p < 0.0001$, univariate analysis with Dunnett's post-tests in SPSS). **(F)** Viability of IMO cells was increased by the P2X7 agonist BzATP (*** = $p < 0.0001$, univariate analysis with Dunnett's post-tests in SPSS). **(G,H).** Mineralisation of SC5 cells in HP media was decreased by the P2X7 agonist BzATP (**** = $p < 0.0001$, univariate analysis with Dunnett's post-tests in SPSS). **(I).** Viability of SC5 cells was decreased by the P2X7 agonist BzATP (*** = $p < 0.0001$, univariate analysis with Dunnett's post-tests in SPSS).

affected by the loss of dystrophin expression. Moreover, phosphate secretion from dystrophic myoblasts is regulated by P2X7. Its increase in response to P2X7 blockade demonstrates that P2X7 overexpression on dystrophic cells (Yeung et al., 2006) may constitute a protective mechanism.

3.6 Induced Mineralisation of RAW 264.7, IMO and SC5 Cells is Regulated by P2X7

As macrophages are localised to regions of ectopic mineralisation *in vivo* but our data show that muscle cells act as a source of secreted phosphate *in vitro*, in the next step we investigated whether the addition of phosphate to RAW 264.7 monocyte cells in culture could engender mineralisation *in vitro* in a P2X7-dependent manner. Alizarin red (AR) staining quantified using the CPC method, revealed that RAW 264.7 cells in high phosphate media can accumulate calcified mineral deposits. In these cultures, treatment with the P2X7 agonist BzATP decreased these deposits by 71% (**Figures 5A,B**, $p < 0.0001$ univariate analysis with Dunn's post-tests). Similar to phosphate secretion, mineralisation in RAW 264.7 cells was unaltered by P2X7 antagonists (**Figures 5A,B**). To ensure that changes in mineralisation were not connected to loss of cells or cell viability, which may occur with P2X7 activation, cells were assayed using Presto Blue prior to fixation for AR staining. There were no changes to RAW 264.7 cell viability in response to any of the treatments used (**Figure 5C**).

To examine the role of dystrophin in mineralisation of myoblasts, IMO control myoblasts were treated in the same manner and stained with AR (**Figure 5D**). CPC quantification revealed a 16% decrease in mineralisation with BzATP treatment (**Figure 5E**, $p < 0.0001$, Univariate analysis with Dunn's post-tests), while cell viability quantified with Presto Blue showed an increase of ~ 25% (**Figure 5F**, $p < 0.0001$, Univariate analysis with Dunn's post-tests). Similar to the effects on phosphate secretion, P2X7 blockers did not evoke significant effect on mineralisation in IMO cells.

In SC5 dystrophic myoblast cells treated and analysed for AR, there was an 84% decrease in mineral accumulation in response to BzATP (**Figure 5G**, $p < 0.0001$, Univariate analysis with Dunn's post-tests). However, in stark contrast to IMO, SC5 cell viability decreased by 30% in response to BzATP treatment (**Figure 5H**, $p < 0.0001$).

These data show that mineral deposits can form in cultures of both monocytes and myoblasts in high phosphate conditions, typical of the dystrophic environment. Mineralisation in these cells is

prevented by P2X7 activation. Loss of dystrophic myoblasts upon BzATP treatment is consistent with the overexpression and overactivation of P2X7 purinoceptor on dystrophic muscle cells (Young et al., 2012, 2015; Sinadinos and Al-Khalidi. 2015).

In conclusion, accumulation of mineral in the high phosphate environment can occur in both macrophages and muscle cells but myoblasts are the main source of phosphate release. Importantly, P2X7 purinoceptor overexpression regulates this process in dystrophic cells but it is the expression of this receptor in macrophages that protects against the ectopic mineralisation in dystrophic muscle *in vivo*.

4 DISCUSSION

The main aim of this study was to investigate the role of the P2X7 receptor in ectopic mineralisation using the *Dmd*$^{mdx\text{-}\beta geo}$ mouse model of muscular dystrophy which exhibits chronic inflammation associated with ectopic mineralisation of muscle fibres (Young et al., 2020). Prior to our investigation we had anticipated that activation of P2X7 could exacerbate ectopic mineralisation by driving additional inflammation. To our surprise, we found that P2X7 expression is actually protective against ectopic mineralisation, and from *in vivo* data using our novel *P2X7* ^{KiKo} mouse crossed with the *Dmd*$^{mdx\text{-}\beta geo}$ model we determined that P2X7 on macrophages is protective.

To further investigate this phenomenon, we quantified secreted phosphate from serum and conditioned media and found that the overall pattern of serum phosphate across *Dmd*$^{mdx\text{-}\beta geo}$ genotypes was consistent with ectopic mineralisation in the order of *Dmd*$^{mdx\text{-}\beta geo}$ < *Dmd*$^{mdx\text{-}\beta geo}$ *P2rx7* ^{KiKo} < *Dmd*$^{mdx\text{-}\beta geo}$ *P2rx7* $^{-/-}$. Although serum phosphate has previously been reported to be higher in *Dmd*^{mdx} mice than BL10 wild type controls (Kikkawa et al., 2009), we instead found a trend towards decreased serum phosphate from *Dmd*$^{mdx\text{-}\beta geo}$ mice compared to C57BL/6 controls. RAW 264.7 cells secreted less phosphate than control IMO myoblast cells, suggesting that in non-dystrophic muscle the main source of secreted phosphate could be the myoblast, rather than circulatory monocytes or macrophages. The decrease in serum phosphate observed in *Dmd*$^{mdx\text{-}\beta geo}$ mice was supported by a significant decrease in phosphate secretion from dystrophic SC5 myoblasts compared to non-dystrophic IMO myoblasts. Our data are consistent with previous studies on the *Dmd*^{mdx} mouse insofar that we find that loss of dystrophin function leads to dysregulated phosphate secretion. The dissimilarities in data from previous studies on *Dmd*^{mdx} mice and in the present study on *Dmd*$^{mdx\text{-}\beta geo}$ mice might be attributable to the difference in dystrophin isoforms expressed in these two dystrophic models. In the *Dmd*^{mdx} mouse there is a point mutation (Sicinski et al., 1989) preventing transcription of the full-length dystrophin isoforms, but not affecting expression of the shorter isoforms. In contrast, insertion in *Dmd*$^{mdx\text{-}\beta geo}$ mice prevents expression of all dystrophin isoforms (Wertz and Martin Füchtbauer 1998). This previous body of research, together with the data presented in the current study, show that dystrophin influences phosphate secretion, and suggests that different dystrophin isoforms could have specific roles in phosphate metabolism.

We have previously found that mineralised volumes in the *Dmd*^{mdx} mouse exhibit electron backscatter profiles consistent with tricalcium phosphate (hydroxyapatite) (Young et al., 2020). In this study, we found that when cells were grown under high phosphate conditions (to better mirror the dystrophic microenvironment), calcified mineral deposits were formed within cultures. Such calcification was preventable by P2X7 activation. The source of the phosphate could be myoblasts as our data suggest, while the calcium component could be found as a results of calcium dys-homeostasis, that is found across dystrophic cells (Róg et al., 2019; Zabłocka, Górecki, and Zabłocki 2021) and is a common feature of multiple forms of ectopic mineralisation (Proudfoot 2019).

Although our *in vivo* data demonstrated that P2X7 function on macrophages was protective against increased serum phosphate and ectopic mineralisation, we found little phosphate secretion from RAW 264.7 cells *in vitro*, even in the presence of the P2X7 antagonists AZT and BBG. As myoblasts secrete the bulk of phosphate and RAW 264.7 cells do not, then this is yet more evidence that macrophages may not cause the ectopic mineralisation. Macrophages have been implicated in extracellular matrix remodelling (Valentin et al., 2009; Wang et al., 2020) and more recently it has been suggested that they may even secret matrix vesicles that contribute towards ectopic mineralisation (Chen et al., 2016). In one recent study, phosphate was demonstrated to drive macrophages towards the M2 like phenotype, with increased secretion of pyrophosphate, a known inhibitor of mineralisation (Villa-Bellosta, Hamczyk, and André 2017). This is consistent with our data suggesting that macrophages may be protective against mineralisation in *Dmd*$^{mdx\text{-}\beta geo}$ mice.

Global loss of P2X7 increased serum phosphate and ectopic mineral in *Dmd*$^{mdx\text{-}\beta geo}$ mice; concordant with these *in vivo* findings, inhibition of P2X7 in IMO and SC5 cells *in vitro* increased phosphate secretion and activation of P2X7 in SC5 and RAW 264.7 cells in high phosphate media almost totally prevented mineral deposition. This helps to explain why retention of P2X7 in macrophages in the *Dmd*$^{mdx\text{-}\beta geo}$ *P2rx7* ^{KiKo} model was associated with less ectopic mineralisation than that which occurred in *Dmd*$^{mdx\text{-}\beta geo}$ *P2rx7* $^{-/-}$ mice, as P2X7 activation in RAW 264.7 cells is associated with decreased mineral deposition. These data suggest that in *Dmd*$^{mdx\text{-}\beta geo}$ mice overall dysregulation of calcium homeostasis, coupled with phosphate secretion by myoblasts may be responsible for the initial ectopic mineralisation around both myoblasts and macrophages, but overall the role of macrophages is to protect against such ectopic mineralisation.

DATA AVAILABILITY STATEMENT

The original contributions presented in the study are included in the article/**Supplementary Material**, further inquiries can be directed to the corresponding author.

ETHICS STATEMENT

The animal study was reviewed and approved by Ethical Review Board University of Portsmouth and the Home Office (United Kingdom) project licence.

AUTHOR CONTRIBUTIONS

RR and DCG designed the study, RR conducted the experiments with help from JR, NC, APK and RA. RR and DCG wrote the manuscript with help from all co-authors.

FUNDING

The Defence and Security Accelerator (DSTLX1000142627 for IFA010 - P2RX7: the front-line therapeutic target in soft tissue trauma), the NCN grant no. 2018/29/B/NZ4/02440 and the Polish Ministry of National Defence project "Kościuszko" no: 523/2017/DA.

SUPPLEMENTARY MATERIAL

The Supplementary Material for this article can be found online at: https://www.frontiersin.org/articles/10.3389/fphar.2022.935804/full#supplementary-material

REFERENCES

Adinolfi, E., Giuliani, A. L., De Marchi, E., Pegoraro, A., Orioli, E., and Di Virgilio, F. (2018). The P2X7 Receptor: A Main Player in Inflammation. *Biochem. Pharmacol.* 151 (May), 234–244. doi:10.1016/J.BCP.2017.12.021

Al-Khalidi, R., Panicucci, C., Cox, P., Chira, N., Róg, J., Young, C. N. J., et al. (2018). Zidovudine Ameliorates Pathology in the Mouse Model of Duchenne Muscular Dystrophy via P2RX7 Purinoceptor Antagonism. *acta neuropathol. Commun.* 6. doi:10.1186/s40478-018-0530-4

Bassett, D. I., Bryson-Richardson, R. J., Daggett, D. F., Gautier, P., Keenan, D. G., and Currie, P. D. (2003). Dystrophin Is Required for the Formation of Stable Muscle Attachments in the Zebrafish Embryo. *Development* 130 (23), 5851–5860. doi:10.1242/DEV.00799

Bienvenu, F., Jirawatnotai, S., Elias, J. E., Meyer, C. A., Mizeracka, K., Marson, A., et al. (20102010). Transcriptional Role of Cyclin D1 in Development Revealed by a Genetic-Proteomic Screen. *Nature* 463 (7279), 374–378. doi:10.1038/nature08684

Boursereau, R., Abou-Samra, M., Lecompte, S., Noel, L., and Brichard, S. M. (2018). Downregulation of the NLRP3 Inflammasome by Adiponectin Rescues Duchenne Muscular Dystrophy. *BMC Biol.* 16 (1), 33–17. doi:10.1186/S12915-018-0501-Z/FIGURES/10

Chen, Q., Bei, J. J., Liu, C., Feng, S. B., Zhao, W. B., Zhou, Z., et al. (2016). HMGB1 Induces Secretion of Matrix Vesicles by Macrophages to Enhance Ectopic Mineralization. *PLoS ONE* 11 (5), e0156686. doi:10.1371/JOURNAL.PONE.0156686

Chen, Y. W., Nagaraju, K., Bakay, M., McIntyre, O., Rawat, R., Shi, R., et al. (2005). Early Onset of Inflammation and Later Involvement of TGFbeta in Duchenne Muscular Dystrophy. *Neurology* 65 (6), 826–834. doi:10.1212/01.WNL.0000173836.09176.C4

Daniela, Q., Federica, B., and Lofaro, F. D. (2020). The Biology of Vascular Calcification. *Int. Rev. Cell. Mol. Biol.* 354 (January), 261–353. doi:10.1016/BS.IRCMB.2020.02.007

Di Virgilio, F., Dal Ben, D., Sarti, A. C., Giuliani, A. L., and Falzoni, S. (2017). The P2X7 Receptor in Infection and Inflammation. *Immunity* 47, 15–31. doi:10.1016/j.immuni.2017.06.020

Emery, A. E. (19771977). Muscle Histology and Creatine Kinase Levels in the Foetus in Duchenne Muscular Dystrophy. *Nature* 266 (5601), 472–473. doi:10.1038/266472a0

Evans, N. P., Misyak, S. A., Robertson, J. L., Bassaganya-Riera, J., and Grange, R. W. (2009). Immune-Mediated Mechanisms Potentially Regulate the Disease Time-Course of Duchenne Muscular Dystrophy and Provide Targets for Therapeutic Intervention. *PM&R* 1 (8), 755–768. doi:10.1016/J.PMRJ.2009.04.010

Farini, A., Meregalli, M., Belicchi, M., Battistelli, M., Parolini, D., D'Antona, G., et al. (2007). T and B Lymphocyte Depletion Has a Marked Effect on the Fibrosis of Dystrophic Skeletal Muscles in the Scid/Mdx Mouse. *J. Pathol.* 213 (2), 229–238. doi:10.1002/PATH.2213

Ferrari, D., Munerati, M., Melchiorri, L., Hanau, S., Di Virgilio, F., and Baricordi, O. R. (1994). Responses to Extracellular ATP of Lymphoblastoid Cell Lines from Duchenne Muscular Dystrophy Patients. *Am. J. Physiol.* 267. C886. doi:10.1152/AJPCELL.1994.267.4.C886

Gartland, A., Rumney, R. M., Dillon, J. P., and Gallagher, J. A. (2012). Isolation and Culture of Human Osteoblasts. *Methods Mol. Biol.* 806, 337–355. doi:10.1007/978-1-61779-367-7_22

Ghahramani Seno, M. M., Graham, I. R., Athanasopoulos, T., Trollet, C., Pohlschmidt, M., Crompton, M. R., et al. (2008). RNAi-Mediated Knockdown of Dystrophin Expression in Adult Mice Does Not Lead to Overt Muscular Dystrophy Pathology. *Hum. Mol. Genet.* 17 (17), 2622–2632. doi:10.1093/HMG/DDN162

Górecki, D. C. (2019). P2X7 Purinoceptor as a Therapeutic Target in Muscular Dystrophies. *Curr. Opin. Pharmacol.* 47 (August), 40–45. doi:10.1016/J.COPH.2019.02.003

Gosselin, Maxime R. F., Mournetas, Virginie, Borczyk, Malgorzata, Bozycki, Lukasz, Korostynski, Michal, Robson, Samuel C., et al. (2021). *Loss of Full-Length Dystrophin Expression Results in Major Cell-Autonomous Abnormalities in Proliferating Myoblasts*. BioRxiv. doi:10.1101/2021.08.24.457331

Haslett, J. N., Sanoudou, D., Kho, A. T., Bennett, R. R., Greenberg, S. A., Kohane, I. S., et al. (2002). Gene Expression Comparison of Biopsies from Duchenne Muscular Dystrophy (DMD) and Normal Skeletal Muscle. *Proc. Natl. Acad. Sci. U. S. A.* 99 (23), 15000–15005. doi:10.1073/pnas.192571199

Illes, P., Müller, C. E., Jacobson, K. A., Grutter, T., Nicke, A., Fountain, S. J., et al. (2021). Update of P2X Receptor Properties and Their Pharmacology: IUPHAR Review 30. *Br. J. Pharmacol.* 178 (3), 489–514. doi:10.1111/BPH.15299

Kikkawa, N., Ohno, T., Nagata, Y., Shiozuka, M., Kogure, T., and Matsuda, R. (2009). Ectopic Calcification Is Caused by Elevated Levels of Serum Inorganic Phosphate in Mdx Mice. *Cell. Struct. Funct.* 34, 77–88. doi:10.1247/csf.08039

Lozanoska-Ochser, B., Benedetti, A., Rizzo, G., Marrocco, V., Di Maggio, R., Fiore, P., et al. (2018). Targeting Early PKCθ-dependent T-Cell Infiltration of Dystrophic Muscle Reduces Disease Severity in a Mouse Model of Muscular Dystrophy. *J. Pathol.* 244 (3), 323–333. doi:10.1002/PATH.5016

Massopust, R. T., Lee, Y. i., Pritchard, A. L., Nguyen, V.-K. M., McCreedy, D. A., Thompson, W. J., et al. (2020). Lifetime Analysis of Mdx Skeletal Muscle Reveals a Progressive Pathology that Leads to Myofiber Loss. *Sci. Rep.* 10 (1). doi:10.1038/S41598-020-74192-9

Merrick, D., Stadler, L. K., Larner, D., and Smith, J. (2009). Muscular Dystrophy Begins Early in Embryonic Development Deriving from Stem Cell Loss and Disrupted Skeletal Muscle Formation. *Dis. Model. Mech.* 2 (7–8), 374–388. doi:10.1242/DMM.001008

Metscher, B. (2020). MicroCT Methods Forum: FiJi Plugin to Read XRM Files. Available at: https://microtomography.blogspot.com/2020/06/fiji-plugin-to-read-xrm-files.html.

Morgan, J. E., Beauchamp, J. R., Pagel, C. N., Peckham, M., Ataliotis, P., Jat, P. S., et al. (1994). Myogenic Cell Lines Derived from Transgenic Mice Carrying a Thermolabile T Antigen: A Model System for the Derivation of Tissue-specific and Mutation-specific Cell Lines. *Dev. Biol.* 162 (2), 486–498. doi:10.1006/DBIO.1994.1103

Mournetas, V., Massouridès, E., Dupont, J. B., Kornobis, E., Polvèche, H., Jarrige, M., et al. (2021). Myogenesis Modelled by Human Pluripotent Stem Cells: a Multi-Omic Study of Duchenne Myopathy Early Onset. *J. Cachexia Sarcopenia Muscle* 12 (1), 209–232. doi:10.1002/JCSM.12665

Netea, M. G., Joosten, L. A., Latz, E., Mills, K. H., Natoli, G., Stunnenberg, H. G., et al. (2016). Trained Immunity: A Program of Innate Immune Memory in

Health and Disease. *Science* 352 (6284), aaf1098. doi:10.1126/SCIENCE.AAF1098

Nguyen, F., Cherel, Y., Guigand, L., Goubault-Leroux, I., and Wyers, M. (2002). Muscle Lesions Associated with Dystrophin Deficiency in Neonatal Golden Retriever Puppies. *J. Comp. Pathol.* 126 (2–3), 100–108. doi:10.1053/JCPA.2001.0526

Pescatori, M., Broccolini, A., Minetti, C., Bertini, E., Bruno, C., D'amico, A., et al. (2007). Gene Expression Profiling in the Early Phases of DMD: A Constant Molecular Signature Characterizes DMD Muscle from Early Postnatal Life throughout Disease Progression. *FASEB J.* 21 (4), 1210–1226. doi:10.1096/FJ.06-7285COM

Peterson, Jennifer M., and Guttridge, Denis C. (2009). Skeletal Muscle Diseases, Inflammation, and NF-Kb Signaling: Insights and Opportunities for Therapeutic Intervention. *Int. Rev. Immunol.* 27 (5), 375–387. doi:10.1080/08830180802302389

Proudfoot, D. (2019). Calcium Signaling and Tissue Calcification. *Cold Spring Harb. Perspect. Biol.* 11 (10), a035303. doi:10.1101/CSHPERSPECT.A035303

Rader, E. P., Turk, R., Willer, T., Beltrán, D., Inamori, K., Peterson, T. A., et al. (2016). Role of Dystroglycan in Limiting Contraction-Induced Injury to the Sarcomeric Cytoskeleton of Mature Skeletal Muscle. *Proc. Natl. Acad. Sci. U. S. A.* 113 (39), 10992–10997. doi:10.1073/PNAS.1605265113/SUPPL_FILE/PNAS.201605265SI

Róg, J., Oksiejuk, A., Gosselin, M. R. F., Brutkowski, W., Dymkowska, D., Nowak, N., et al. (2019). Dystrophic Mdx Mouse Myoblasts Exhibit Elevated ATP/UTP-Evoked Metabotropic Purinergic Responses and Alterations in Calcium Signalling. *Biochim. Biophys. Acta Mol. Basis Dis.* 1865 (6), 1138–1151. doi:10.1016/J.BBADIS.2019.01.002

Rufo, A., Del Fattore, A., Capulli, M., Carvello, F., De Pasquale, L., Ferrari, S., et al. (2011). Mechanisms Inducing Low Bone Density in Duchenne Muscular Dystrophy in Mice and Humans. *J. Bone Min. Res.* 26 (8), 1891–1903. doi:10.1002/JBMR.410

Rumney, R. M. H., and Górecki, D. C. (2020). Knockout and Knock-In Mouse Models to Study Purinergic Signaling. *Methods Mol. Biol.* 2041, 17–43. doi:10.1007/978-1-4939-9717-6_2

Sagheddu, R., Chiappalupi, S., Salvadori, L., Riuzzi, F., Donato, R., and Sorci, G. (2018). Targeting RAGE as a Potential Therapeutic Approach to Duchenne Muscular Dystrophy. *Hum. Mol. Genet.* 27 (21), 3734–3746. doi:10.1093/HMG/DDY288

Schindelin, J., Arganda-Carreras, I., Frise, E., Kaynig, V., Longair, M., Pietzsch, T., et al. (2012). Fiji: an Open-Source Platform for Biological-Image Analysis. *Nat. Methods* 9 (7), 676–682. doi:10.1038/NMETH.2019

Sicinski, P., Geng, Y., Ryder-Cook, A. S., Barnard, E. A., Darlison, M. G., and Barnard, P. J. (1989). The Molecular Basis of Muscular Dystrophy in the Mdx Mouse: A Point Mutation. *Science* 244 (4912), 1578–1580. doi:10.1126/SCIENCE.2662404

Sinadinos, A., Young, C. N. J., Al-Khalidi, R., Teti, A., Kalinski, P., Mohamad, S., et al. (2015). P2RX7 Purinoceptor: A Therapeutic Target for Ameliorating the Symptoms of Duchenne Muscular Dystrophy. *PLoS Med.* 12 (10), e1001888. doi:10.1371/journal.pmed.1001888

Snow, W. M., Anderson, J. E., and Jakobson, L. S. (2013). Neuropsychological and Neurobehavioral Functioning in Duchenne Muscular Dystrophy: A Review. *Neurosci. Biobehav Rev.* 37 (5), 743–752. doi:10.1016/J.NEUBIOREV.2013.03.016

Solle, M., Labasi, J., Perregaux, D. G., Stam, E., Petrushova, N., Koller, B. H., et al. (2001). Altered Cytokine Production in Mice Lacking P2X(7) Receptors. *J. Biol. Chem.* 276 (1), 125–132. doi:10.1074/JBC.M006781200

Spencer, M. J., Montecino-Rodriguez, E., Dorshkind, K., and Tidball, J. G. (2001). Helper (CD4(+)) and Cytotoxic (CD8(+)) T Cells Promote the Pathology of Dystrophin-Deficient Muscle. *Clin. Immunol.* 98 (2), 235–243. doi:10.1006/CLIM.2000.4966

Stanford, C. M., Jacobson, P. A., Eanes, E. D., Lembke, L. A., and Midura, R. J. (1995). Rapidly Forming Apatitic Mineral in an Osteoblastic Cell Line (UMR 106-01 BSP). *J. Biol. Chem.* 270, 9420–9428. doi:10.1074/jbc.270.16.9420

Tidball, J. G., and Villalta, S. A. (2010). Regulatory Interactions between Muscle and the Immune System during Muscle Regeneration. *Am. J. Physiol. Regul. Integr. Comp. Physiol.* 298 (5), R1173–R1187. doi:10.1152/AJPREGU.00735.2009

Tidball, J. G., Welc, S. S., and Wehling-Henricks, M. (2018). Immunobiology of Inherited Muscular Dystrophies. *Compr. Physiol.* 8 (4), 1313–1356. doi:10.1002/CPHY.C170052

Toop, J., and Emery, A. E. (1974). Muscle Histology in Fetuses at Risk for Duchenne Muscular Dystrophy. *Clin. Genet.* 5 (3), 230–233. doi:10.1111/J.1399-0004.1974.TB01687.X

Valentin, J. E., Stewart-Akers, A. M., Gilbert, T. W., and Badylak, S. F. (2009). Macrophage Participation in the Degradation and Remodeling of Extracellular Matrix Scaffolds. *Tissue Eng. Part A* 15 (7), 1687–1694. doi:10.1089/TEN.TEA.2008.041910.1089/ten.tea.2008.0419

van Dommelen, P., van Dijk, O., de Wilde, J. A., and Verkerk, P. H. (2020). Early Developmental Milestones in Duchenne Muscular Dystrophy. *Dev. Med. Child. Neurol.* 62 (10), 1198–1204. doi:10.1111/DMCN.14623

Vandesompele, J., De Preter, K., Pattyn, F., Poppe, B., Van Roy, N., De Paepe, A., et al. (2002). Accurate Normalization of Real-Time Quantitative RT-PCR Data by Geometric Averaging of Multiple Internal Control Genes. *Genome Biol.* 3 (7), RESEARCH0034–12. doi:10.1186/GB-2002-3-7-RESEARCH0034/COMMENTS

Vassilopoulos, D., and Emery, A. E. (1977). Muscle Nuclear Changes in Fetuses at Risk for Duchenne Muscular Dystrophy. *J. Med. Genet.* 14 (1), 13–15. doi:10.1136/JMG.14.1.13

Villa-Bellosta, R., Hamczyk, M. R., and Andrés, V. (2017). Novel Phosphate-Activated Macrophages Prevent Ectopic Calcification by Increasing Extracellular ATP and Pyrophosphate. *PLoS ONE* 12, e0174998. doi:10.1371/journal.pone.0174998

Wang, Y., Chaffee, T. S., Larue, R. S., Huggins, D. N., Witschen, P. M., Ibrahim, A. M., et al. (2020). Tissue-Resident Macrophages Promote Extracellular Matrix Homeostasis in the Mammary Gland Stroma of Nulliparous Mice. *ELife* 9 (June), 1–27. doi:10.7554/ELIFE.57438

Wertz, Karin, and Martin Füchtbauer, Ernst (1998). Dmd(Mdx-Bgeo): A New Allele for the Mouse Dystrophin Gene. *Dev. Dyn.* 212, 229. doi:10.1002/(sici)1097-0177(199806)212:2<229::aid-aja7>3.0.co;2-j

Xu, X. J., Boumechache, M., Robinson, L. E., Marschall, V., Gorecki, D. C., Masin, M., et al. (2012). Splice Variants of the P2X7 Receptor Reveal Differential Agonist Dependence and Functional Coupling with Pannexin-1. *J. Cell. Sci.* 125 (16), 3776–3789. doi:10.1242/JCS.099374

Yeung, D., Zablocki, K., Lien, C. F., Jiang, T., Arkle, S., Brutkowski, W., et al. (2006). Increased Susceptibility to ATP via Alteration of P2X Receptor Function in Dystrophic Mdx Mouse Muscle Cells. *FASEB J.* 20 (6), 610–620. doi:10.1096/FJ.05-4022COM

Young, C. N., Brutkowski, W., Lien, C. F., Arkle, S., Lochmüller, H., Zabłocki, K., et al. (2012). P2X7 Purinoceptor Alterations in Dystrophic Mdx Mouse Muscles: Relationship to Pathology and Potential Target for Treatment. *J. Cell. Mol. Med.* 16 (5), 1026–1037. doi:10.1111/J.1582-4934.2011.01397.X

Young, C. N. J., Gosselin, M. R. F., Rumney, R., Oksiejuk, A., Chira, N., Bozycki, L., et al. (2020). Total Absence of Dystrophin Expression Exacerbates Ectopic Myofiber Calcification and Fibrosis and Alters Macrophage Infiltration Patterns. *Am. J. Pathol.* 190 (1), 190–205. doi:10.1016/J.AJPATH.2019.09.021

Young, C. N. J., and Górecki, D. C. (2018). P2RX7 Purinoceptor as a Therapeutic Target-The Second Coming? *Front. Chem.* 6, 248. doi:10.3389/fchem.2018.00248

Young, C. N., Sinadinos, A., Lefebvre, A., Chan, P., Arkle, S., Vaudry, D., et al. (2015). A Novel Mechanism of Autophagic Cell Death in Dystrophic Muscle Regulated by P2RX7 Receptor Large-Pore Formation and HSP90. *Autophagy* 11, 113–130. doi:10.4161/15548627.2014.994402

Zabłocka, B., Górecki, D. C., and Zabłocki, K. (2021). Disrupted Calcium Homeostasis in Duchenne Muscular Dystrophy: A Common Mechanism behind Diverse Consequences. *Int. J. Mol. Sci.* 22 (20). doi:10.3390/IJMS222011040

Conflict of Interest: The authors declare that the research was conducted in the absence of any commercial or financial relationships that could be construed as a potential conflict of interest.

Publisher's Note: All claims expressed in this article are solely those of the authors and do not necessarily represent those of their affiliated organizations, or those of the publisher, the editors and the reviewers. Any product that may be evaluated in this article, or claim that may be made by its manufacturer, is not guaranteed or endorsed by the publisher.

frontiers | Frontiers in Pharmacology

TYPE Original Research
PUBLISHED 08 August 2022
DOI 10.3389/fphar.2022.932092

OPEN ACCESS

EDITED BY
Anna Malashicheva,
Institute of Cytology, Russia

REVIEWED BY
Wanqian Liu,
Chongqing University, China
Muhammad Farrukh Nisar,
Cholistan University of Veterinary and Animal Sciences, Pakistan

*CORRESPONDENCE
Jianhua Xie,
tjmedxjh@163.com
Zhipeng Zeng,
512527720@qq.com
Tingwen Zhou,
zhoutingwen@hust.edu.cn

†These authors have contributed equally to this work and share first authorship

SPECIALTY SECTION
This article was submitted to Experimental Pharmacology and Drug Discovery, a section of the journal Frontiers in Pharmacology

RECEIVED 29 April 2022
ACCEPTED 11 July 2022
PUBLISHED 08 August 2022

CITATION
Zhang S, Fan L, Wang Y, Xu J, Shen Q, Xie J, Zeng Z and Zhou T (2022), Dihydromyricetin ameliorates osteogenic differentiation of human aortic valve interstitial cells by targeting c-KIT/interleukin-6 signaling pathway. *Front. Pharmacol.* 13:932092. doi: 10.3389/fphar.2022.932092

Dihydromyricetin ameliorates osteogenic differentiation of human aortic valve interstitial cells by targeting c-KIT/interleukin-6 signaling pathway

Shaoshao Zhang[1,2†], Leilei Fan[3†], Yongjun Wang[1], Jianjun Xu[4], Qiang Shen[1], Jianhua Xie[2*], Zhipeng Zeng[5*] and Tingwen Zhou[1*]

[1]Department of Cardiovascular Surgery, Union Hospital, Tongji Medical College, Huazhong University of Science and Technology, Wuhan, China, [2]Department of Cardiology, Union Hospital, Tongji Medical College, Huazhong University of Science and Technology, Wuhan, China, [3]Department of Gastrointestinal Surgery, Central Hospital of Enshi Tujia and Miao Autonomous Prefecture, Enshi, China, [4]Department of Hepatobiliary Surgery, Union Hospital, Tongji Medical College, Huazhong University of Science and Technology, Wuhan, China, [5]Department of Rheumatology and Immunology, Tongji Hospital, Tongji Medical College, Huazhong University of Science and Technology, Wuhan, China

Aims: Calcific aortic valve disease (CAVD) is a chronic cardiovascular disease with high morbidity that lacks effective pharmacotherapeutics. As a natural flavonoid extracted from Ampelopsis grossedentata, dihydromyricetin (DHM) has been shown to be effective in protecting against atherosclerosis; yet, the therapeutic role of DHM in CAVD remains poorly understood. Herein, we aimed to clarify the therapeutic implications of DHM in CAVD and the underlying molecular mechanisms in human valvular interstitial cells (hVICs).

Methods and Results: The protein levels of two known osteogenesis-specific genes (alkaline phosphatase, ALP; runt-related transcription factor 2, Runx2) and calcified nodule formation in hVICs were detected by Western blot and Alizarin Red staining, respectively. The results showed that DHM markedly ameliorated osteogenic induction medium (OM)–induced osteogenic differentiation of hVICs, as evidenced by downregulation of ALP and Runx2 expression and decreased calcium deposition. The SwissTargetPrediction database was used to identify the potential AVC-associated direct protein target of DHM. Protein–protein interaction (PPI) analysis revealed that c-KIT, a tyrosine-protein kinase, can act as a credible protein target of DHM, as evidenced by molecular docking. Mechanistically, DHM-mediated inhibition of c-KIT phosphorylation drove interleukin-6 (IL-6) downregulation in CAVD, thereby ameliorating OM-induced osteogenic differentiation of hVICs and aortic valve calcification progression.

Conclusion: DHM ameliorates osteogenic differentiation of hVICs by blocking the phosphorylation of c-KIT, thus reducing IL-6 expression in CAVD. DHM could be a viable therapeutic supplement to impede CAVD.

KEYWORDS

dihydromyricetin, interleukin-6, c-kit, human valvular interstitial cells, calcific aortic valve disease dihydromyricetin ameliorates aortic valve calcification

Introduction

Calcific aortic valve disease (CAVD) is an irreversible disease associated with severe aortic valve stenosis and is a major contributor to mortality in cardiac patients (Kraler et al., 2022). Despite mounting evidence proving a crucial role for lipoprotein (a) and low-density lipoprotein cholesterol in the progression of CAVD (Mundal et al., 2019; Chen et al., 2020; Kaltoft et al., 2022), lipid-lowering has failed to blunt CAVD progression (Chan et al., 2010; Teo et al., 2011). Thus, transaortic and surgical valvular replacement remains the most effective treatments for CAVD, and there is an urgent need to explore novel disease-modifying pharmacotherapies for nonsurgical CAVD treatment. Human aortic valve interstitial cells (hVICs) play a pivotal role in mediating aortic valve calcification (AVC) by switching from quiescent hVICs to an osteoblast-like phenotype (Peeters et al., 2018; Issa et al., 2019). This phenotypic switch is identified as a prominent hallmark and driving factor of accelerated AVC (Wang et al., 2020; Wang Y et al., 2021). Thus, a deeper understanding of the pathophysiology of phenotypic transformation in hVICs is critical for providing novel therapeutic options for CAVD.

Increasing evidence shows that traditional Chinese herbal medicines have protective and curative pharmacological effects on cardiovascular diseases (Zhao et al., 2020; Zhang et al., 2021a; Zhang et al., 2021b; Zhu et al., 2021). Ampelopsis grossedentata (also known as vine tea) is a traditional Chinese edible herb widely consumed not only as a healthy tea but also as a medicinal herb that possesses numerous pharmacological activities. Dihydromyricetin (DHM), the most bioactive constituent of ampelopsis grossedentata, has increasingly drawn attention as an effective drug for the treatment of cardiovascular diseases, including vascular calcification (Feng et al., 2021), myocardial hypertrophy (Chen et al., 2018), doxorubicin-induced cardiotoxicity (Sun et al., 2020), and cardiac ischemia/reperfusion injury (Wei et al., 2019). Specifically, Yang et al. reported that DHM could ameliorate the progression of atherosclerosis in low-density lipoprotein receptor-deficient ($LDLr^{-/-}$) mice by countering hyperlipidemia and aortic inflammation (Liu et al., 2017). A more recent study also demonstrated that DHM ameliorates atherosclerotic lesion formation by increasing endothelial nitric oxide production in apolipoprotein E-deficient mice (Yang et al., 2020). Importantly, numerous experimental and clinical studies suggest that CAVD and atherosclerosis share similar pathological features (Hutcheson et al., 2014; Cho et al., 2018). Thus, these findings suggest that DHM might also have a pharmacological effect on CAVD.

C-KIT (also known as CD117) is an oncogene belonging to the family of receptor kinases that is expressed in various cell types and tissues (Mukhopadhyay et al., 2011). Upon activation *via* its ligand, stem cell factor (SCF), c-KIT can activate several signaling pathways and thereby play a regulatory role in cardiovascular diseases, including vascular diseases (Kim et al., 2014; Hernandez et al., 2019), cardioprotection (Ebeid et al., 2020), and cardiac stem cell migration (Kuang et al., 2008). Moreover, given its biological properties, c-KIT has been widely recognized as a biomarker to identify presumptive cardiac stem cells that respond to myocardial injury (Gude et al., 2018) and hypertrophic cardiomyopathy (Sonnenschein et al., 2021). Furthermore, c-KIT-positive progenitor cells have been observed in pathological human cardiac valves (Veinot et al., 2006; Gendron et al., 2021). Nevertheless, the regulatory role of c-KIT in CAVD progression has not been experimentally investigated.

In the present study, the molecular docking results showed that DHM successfully formed hydrogen bonds with c-KIT with a docking binding energy of −10.3 kcal/mol. Moreover, the osteogenic induction medium (OM) significantly enhances the phosphorylation of c-KIT, thereby promoting osteogenic differentiation of hVICs, while DHM can markedly ameliorate the osteogenic differentiation of hVICs by inhibiting the phosphorylation of c-KIT. Importantly, the present data also indicated that IL-6 is a downstream target of c-KIT, contributing to DHM-mediated inhibition of the osteogenic differentiation of hVICs. Hence, DHM may represent a novel pharmacological supplement for preventing CAVD progression.

Materials and methods

Cell culture and treatment

Primary hVICs were isolated from human aortic valves as we previously described (Zhou et al., 2020; Wang Y et al., 2021). First, to remove valvular endothelial cells, noncalcified aortic valve leaflets were digested in 1 mg/ml type I collagenase (Sigma–Aldrich, Saint Louis, MO) for 30 min. Subsequently, the tissues were further digested in 2 mg/ml type I collagenase at 37°C in 5% CO_2 for 8 h. Then, isolated hVICs were cultured in Dulbecco′s modified Eagle′s medium (DMEM, Gibco, Invitrogen Corporation, United States) containing 10% fetal bovine serum, 100 μg/ml streptomycin, and 100 U/ml penicillin with 5% CO_2 at 37°C. Osteogenic induction medium (DMEM supplemented with 0.1% fetal bovine serum, 5 mmol/L β-glycerophosphate, 50 ng/ml ascorbic acid, 50 ng/ml BMP-2, and 100 nmol/L dexamethasone) was used to establish the osteogenic

differentiation model of hVICs as previously described (Wang et al., 2020; Zhou et al., 2021). The treatment groups included the control (10% DMEM-treated group), OM (OM-treated group), and OM plus DHM (Selleck, Cat. No. S2399; 20 μM) (OM + DHM-treated group). ISCK03 (Selleck, Cat. No. S2070; at 5 μM final concentration in OM) was used to specifically inhibit c-KIT activity. Stem cell factor (Sigma–Aldrich, Catalog# H8416; at 50 ng/ml final concentration in OM) was used to induce phosphorylation of c-KIT. IL-6 (Sigma–Aldrich, Catalog# I1395; at 50 ng/ml final concentration in OM) was used to explore the underlying mechanism of the DHM-mediated inhibitory effect on the osteogenic differentiation of hVICs. The treatment groups included the OM group, IL-6+OM group, and IL-6+OM + DHM group. The medium was changed every 3 days.

Cell viability analysis

To evaluate cell viability, a CCK-8 (K1018, APEXBIO) assay was carried out according to the manufacturer's instructions as previously described (Zhou et al., 2020). First, primary hVICs were seeded in 48-well plates and incubated for 12 h in DMEM supplemented with 10% fetal bovine serum (FBS). Subsequently, the cells were further cultured in low-serum medium (2% FBS) for 24 h and then treated with different concentrations of DHM for 72 h to determine the half-maximal inhibitory concentration (IC_{50}) values of DHM in hVICs. Furthermore, after treatment with 20 μM DHM for 6 days, cell viability was also measured. In brief, cells were washed with phosphate-buffered saline (PBS) and subsequently incubated with serum-free medium that contained 10% CCK-8 reagents for 2 h. Finally, light absorption at 450 nm was measured using an enzyme labeling instrument.

Quantitative real-time polymerase chain reaction analysis

qRT–PCR analysis was performed as previously described (Xu et al., 2019; Wang Y et al., 2021). In brief, after treatment with the indicated medium, total RNA was isolated using TRIzol reagent (Invitrogen). The PrimeScript RT Reagent Kit (TaKaRa Bio, Otsu, Shiga, Japan) was used to synthesize cDNA according to the manufacturer's instructions. Subsequently, qRT–PCR was conducted by a Step One Real-Time PCR System (Applied Biosystems, Foster City, CA, United States) using SYBR Green PCR reagent (TaKaRa). The data were normalized relative to glyceraldehyde-6-phosphate dehydrogenase (GAPDH) and expressed as a relative ratio using the $-2^{\Delta\Delta Ct}$ method. The following primer sequences were used in the present study: ALP (forward: 5′-CGCTGTGTCAACTCCACCT-3′; reverse: 5′-CCAGAAGGTTCTGTTAACTTG-3′); RUNX2 (forward: 5′-GCGTCAACACCATCATTCTG-3′; reverse:5′-CAGACCAGCAGCACTCCATC-3′); IL-6 (forward: 5′-TGG CTGCAGGACATGACAACT-3′; reverse:5′-ATCTGAGGTGCCCATGCTACA-3′); GAPDH (forward:5′-CCTCAAGAT CATCAGCAAT-3′; reverse: 5′-CCATCCACA GTCTTCTGGGT-3′).

Western blotting assay

Western blotting assays were conducted as previously described (Wang Y et al., 2021; Zhou et al., 2021). In brief, after treatment with the indicated medium, total proteins were extracted from the hVICs using radioimmunoprecipitation assay (RIPA) buffer. The concentration of the protein lysate was calculated with the bicinchoninic acid (BCA) protein assay kit (Beyotime, Shanghai, China). Subsequently, equal protein extracts (30 μg/well) from each group were separated by 4–20% sodium dodecyl sulfate–polyacrylamide gel electrophoresis (SDS–PAGE) and then transferred to polyvinylidene fluoride (PVDF) membranes (Millipore, Billerica, MA, United States) in the presence of methanol. Next, the membranes were blocked with 5% nonfat milk in TBST and incubated with primary antibodies against ALP (1:1,000, 11187-1-AP, Proteintech), RUNX2 (1:1,000, #12556, Cell Signaling Technology), GAPDH (1:1,000, 60004-1-Ig, Proteintech), and phospho-c-Kit (Tyr703, 1:1,000, #3073, Cell Signaling Technology). Phospho-c-Kit (Tyr823, 1:1,000, #77522, Cell Signaling Technology), Phospho-c-Kit (Tyr721, 1:1,000, 44-494G, Invitrogen), Phospho-c-Kit (Tyr568, 1:1,000, #48347, Cell Signaling Technology), Phospho-c-Kit (Tyr719, 1:1,000, #3391, Cell Signaling Technology), c-KIT (1:1,000, 34-8800, Invitrogen), and IL-6 (1:1,000, P620, Invitrogen) at 4 °C. Finally, the membranes were specifically incubated with the HRP-conjugated secondary antibody for 2 h at room temperature and detected by chemiluminescence using a Western blot imaging system (Clinx Science Instruments, Shanghai, China). GAPDH acted as an internal reference, and all data were analyzed by ImageJ 1.55 software (National Institutes of Health).

Alizarin red staining

The Alizarin Red staining method was used to visualize calcified nodule formation in hVICs as previously described (Xu et al., 2018; Wang et al., 2020). First, after the indicated treatments, hVICs from each group were rinsed in 1×PBS three times and fixed in 4% paraformaldehyde (PFA) for 15 min at room temperature. After that, the cells were washed and exposed to 2% Alizarin Red stain (Sigma–Aldrich) for 15 min according to the manufacturer's instructions. Subsequently, after washing three times with deionized water to remove excess Alizarin Red dye, images were visualized using an Olympus BX51 microscope.

The red staining (arbitrary units shown) indicated calcified nodule formation. The quantification of Alizarin Red staining was performed as we described previously (Wang Y et al., 2021). After obtaining high-resolution images, Adobe Photoshop CC was used to edit the image contrast and brightness. Then, ImageJ 1.55 (National Institutes of Health) software was used to determine the positive stained area (arbitrary units shown) of Alizarin Red per magnified field, and the data were averaged for three independent biological replicates.

Molecular target analysis

The potential protein targets of DHM were obtained from the SwissTargetPrediction database (http://www.swisstargetprediction.ch). The aortic valve calcification differentially expressed genes (AVCDEGs) were collected based on our previously uploaded RNA-seq data in the NCBI SRA database at PRJNA643215 and PRJNA552159. After data extraction, a comprehensive bioinformatic analysis of the top 10 candidate targets and 216 AVCDEGs was performed by protein–protein interaction (PPI) analysis according to STRING (https://www.string-db.org/) with Cytoscape software (Wang C et al., 2021). The potential AVC-associated molecular target of DHM was selected, and c-KIT with the highest degree at a confidence value of 0.4 was chosen as a potential DHM molecular target for further analysis.

Molecular docking

Molecular docking was performed as previously described (Ye et al., 2019). The compound name, molecular weight, and three-dimensional (3D) structure of DHM were obtained from the PUBCHEM database. The 3D structure of c-KIT was obtained from the Protein Data Bank (PDB, ID: 1 pkg) database. Subsequently, AutoDock Vina software (http://vina.scripps.edu/) was used to prepare the ligands and proteins required for molecular docking. Finally, the docking results were analyzed by Discovery Studio software 2019 (DS 2019). The combination capability of DHM and c-KIT was evaluated by the affinity (kcal/mol) value.

Immunofluorescence staining

Immunofluorescence staining was applied for the detection of ALP, RUNX2, phospho-c-Kit (Tyr703), phospho-c-Kit (Tyr721), and IL-6 in hVICs as previously described (Dai et al., 2019; Zhou et al., 2021). Briefly, following the indicated treatments, hVICs were rinsed in 1× PBS and then fixed in 4% PFA for 20 min. Subsequently, the fixed cells were permeabilized with 0.1% Triton X-100 in PBS for another 20 min and incubated with the following primary antibodies at 4°C overnight: ALP (1:200, 11187-1-AP, Proteintech), RUNX2 (1:200, #12556, Cell Signaling Technology), phospho-c-Kit (Tyr703, 1:200, 710762, Invitrogen), phospho-c-Kit (Tyr721, 1:200, 44-494G, Invitrogen), and IL-6 (1:200, P620, Invitrogen). Finally, followed by incubation with fluorescently conjugated secondary antibody (Abcam, Cambridge, MA, United States) and counterstaining with 4′,6-diamidino-2-phenylindole (DAPI) (Sigma–Aldrich), the cells were then visualized by a confocal laser scanning microscope FV3000 (Olympus, GmbH, Hamburg, Germany).

Statistical analysis

All values are presented as the mean ± standard deviation (SD) and were analyzed using GraphPad Prism 8 software (GraphPad Software, Inc., CA, United States). For continuous data with a normal distribution and equal variances, Student's *t* test was applied between two groups and one-way analysis of variance (one-way ANOVA) followed by Bonferroni multiple comparison *post hoc test* was performed for multiple comparisons (≥3 groups). All semiquantitative measurements were performed by ImageJ 1.55 (National Institutes of Health) software. $p < 0.05$ was considered statistically significant.

Results

DHM inhibits osteogenic differentiation of hVICs *in vitro*

Figure 1A shows the chemical formula and 3D molecular structure of DHM (molecular weight, 320.25 Da) obtained from the PubChem database. In the present study, the IC_{50} values of DHM-treated hVICs were approximately 20–30 μM (Figure 1B). Thus, a final DHM concentration of 20 μM was used for further experiments. Furthermore, the CCK-8 assay indicated that the viability of hIVCs did not differ from that of the control group after treatment with DHM for 5 days (Figure 1C). As the osteoblast-like phenotypic conversion of hVIC is a critical step in CAVD pathogenesis (Wang Y et al., 2021; Zhou et al., 2021), we investigated whether DHM orchestrated osteogenic differentiation of hVIC. To stimulate osteogenic differentiation, hVICs were exposed to OM for 14 days as previously described (Wang Y et al., 2021). Then, we explored the effects of DHM in hVICs and found that DHM treatment significantly negated the OM-induced increase in both the mRNA (Figure 1D) and protein (Figures 1E–G) levels of two known osteogenesis-specific genes (ALP and Runx2). Finally, DHM treatment significantly reduced the OM-induced increase in calcified nodule formation in hVICs (Figure 1H). These results suggest that DHM exhibits highly inhibitory effects on the osteogenic differentiation of hVICs.

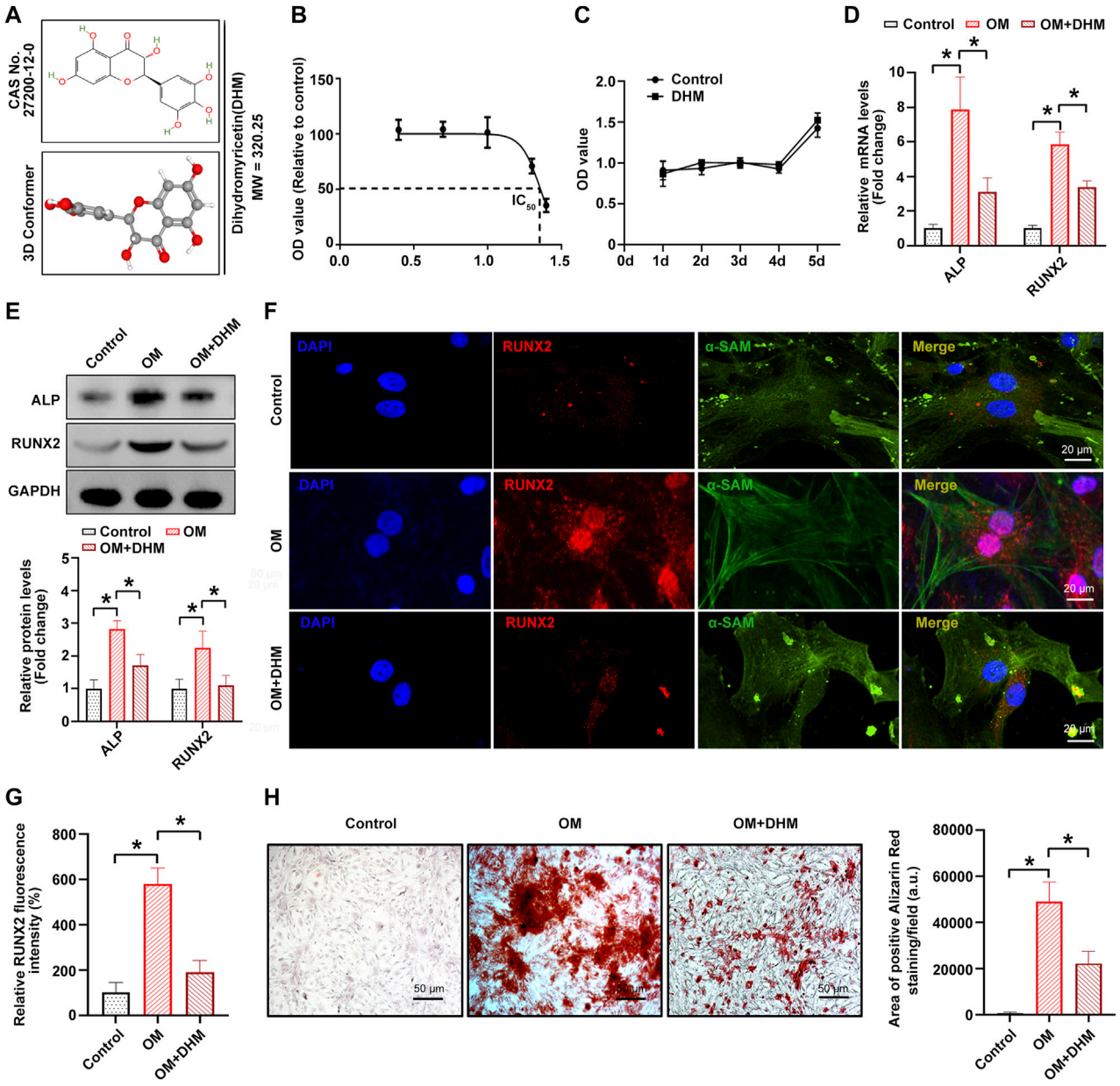

FIGURE 1
Dihydromyricetin (DHM) inhibits osteogenic differentiation of human valvular interstitial cells (hVICs). **(A)** Molecular structure of DHM. **(B)** Half-maximal inhibitory concentration (IC_{50}) of DHM on hVICs; concentrations were transferred to Log**(C)**. **(C)** Cell Counting Kit-8 (CCK-8) assay was conducted to detect the cell proliferation rate of hVICs with the indicated treatment for 5 days. The mRNA **(D)** and protein **(E)** levels of osteogenesis-specific genes (alkaline phosphatase, ALP, and runt-related transcription factor 2, RUNX2) in hVICs stimulated with osteogenic induction medium (OM) and then treated with or without DHM. One-way ANOVA followed by Bonferroni *post hoc test*. Immunofluorescence staining **(F)** and semiquantification **(G)** of RUNX2 in hVICs stimulated with OM and then treated with or without DHM. One-way ANOVA followed by Bonferroni *post hoc test*. **(H)** Alizarin red staining of mineralization nodules in hVICs stimulated with OM and then treated with or without DHM. One-way ANOVA followed by a Bonferroni *post hoc test*. $N = 3$ per group. Values are the mean ± SD. $^*p < 0.05$ indicates a significant difference.

DHM targets c-KIT and inhibits its phosphorylation induced by OM in hVICs

We next used the online tool SwissTargetPrediction to further investigate the precise mechanism by which osteogenic differentiation of hVICs is regulated by DHM. Figure 2A shows the flowchart of the identification of AVC-associated target genes regulated by DHM. First, 100 potential target proteins of DHM were identified by SwissTargetPrediction. Then, a comprehensive bioinformatic analysis of the top 10 candidate targets and

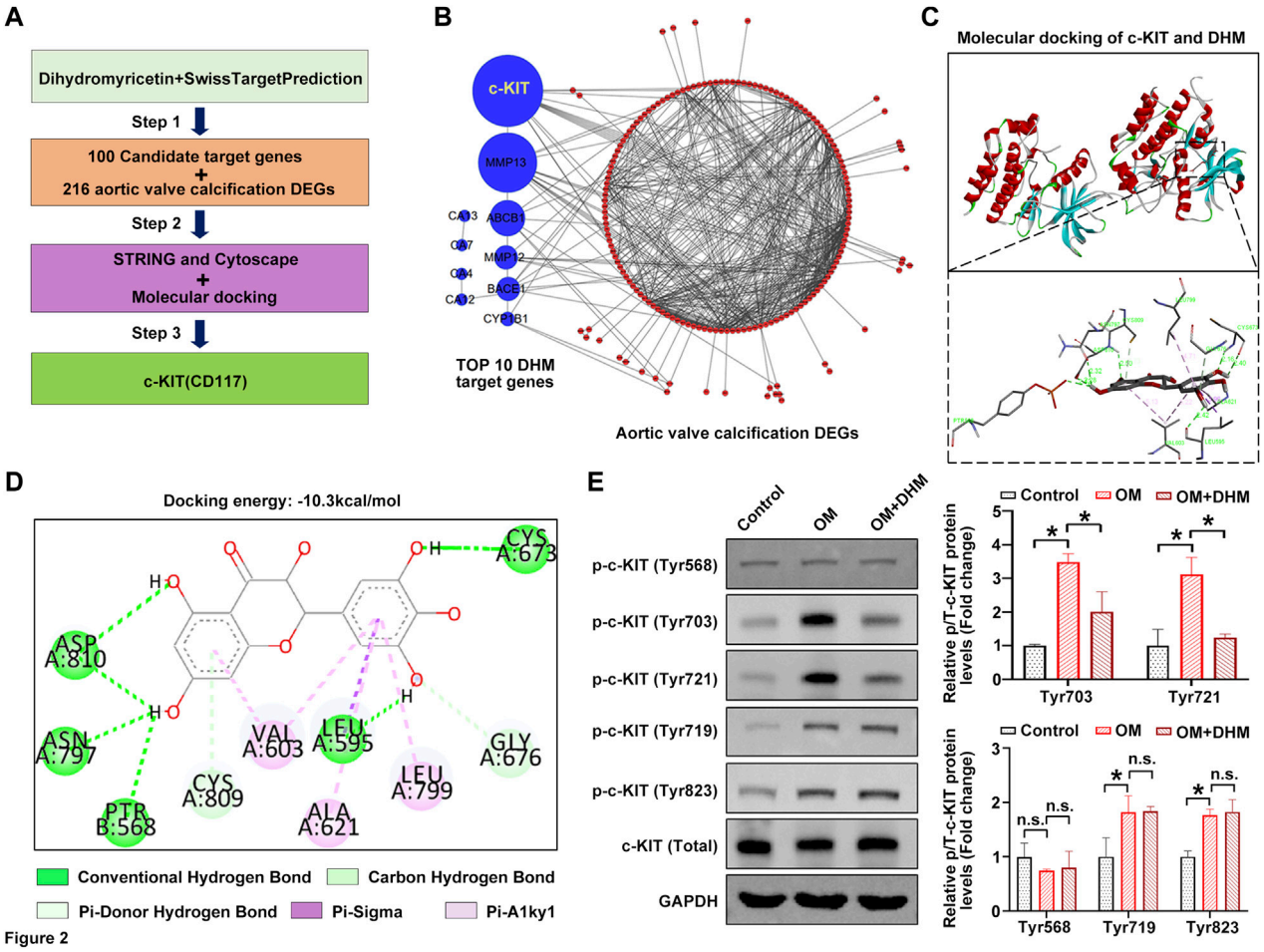

Figure 2

FIGURE 2
Dihydromyricetin (DHM) targets c-KIT involved in the regulation of aortic valve calcification (AVC). **(A)** Flowchart of the identification of AVC-associated target genes regulated by DHM. **(B)** Protein–protein interaction (PPI) network of the top 10 candidate targets of DHM and 216 AVC differentially expressed genes (DEGs). **(C)** Molecular docking of DHM and c-KIT. **(D)** Two-dimensional (2D) diagram of the binding position between DHM and c-KIT. **(E)** Western blotting was used to detect the phosphorylation levels of c-KIT in human valvular interstitial cells (hVICs) stimulated with osteogenic induction medium (OM) and then treated with or without DHM. One-way ANOVA followed by Bonferroni *post hoc test*. $N = 3$ per group. Values are the mean ± SD. $^*p < 0.05$ indicates a significant difference. The n. s. indicates no significant difference.

216 AVC differentially expressed genes (AVCDEGs) was performed to identify target proteins underlying the effect of DHM on CAVD. The AVCDEGs were obtained from our previous upload to the NCBI SRA database at PRJNA643215 and PRJNA552159 (Xu et al., 2020). Subsequently, the protein–protein interaction (PPI) network of the top 10 candidate targets and AVCDEGs was generated by the STRING database (https://www.string-db.org/) with Cytoscape software, which found c-KIT with the highest degree at a confidence value of 0.4 (Figure 2B). To identify the possible modes and sites of c-KIT responsible for DHM binding, we performed molecular docking using AutoDock Vina software. The 3D docking mode and interaction details show that DHM successfully formed hydrogen bonds with c-KIT, with a docking binding energy of −10.3 kcal/mol (Figure 2C). As shown in Figure 2D, for the c-KIT-DHM complex, ASP810, ASN797, PTR568, LEU595, CYS673, CYS809, GLY676, VAL603, ALA621, and LEU799 formed some interactions with different moieties of DHM, which made the binding of c-KIT and DHM stable. Upon phosphorylation by its cytokine ligand, SCF, c-KIT can activate several signaling pathways (Kim et al., 2014). Thus, we explored whether its phosphorylation was altered following DHM treatment in hVICs. The results revealed that DHM significantly negated the OM-induced increase in the levels of phosphorylated c-Kit at sites Tyr703 and Tyr721 in hVICs (Figure 2E). These data suggest that DHM significantly reduced the OM-induced phosphorylation of c-KIT in hVICs.

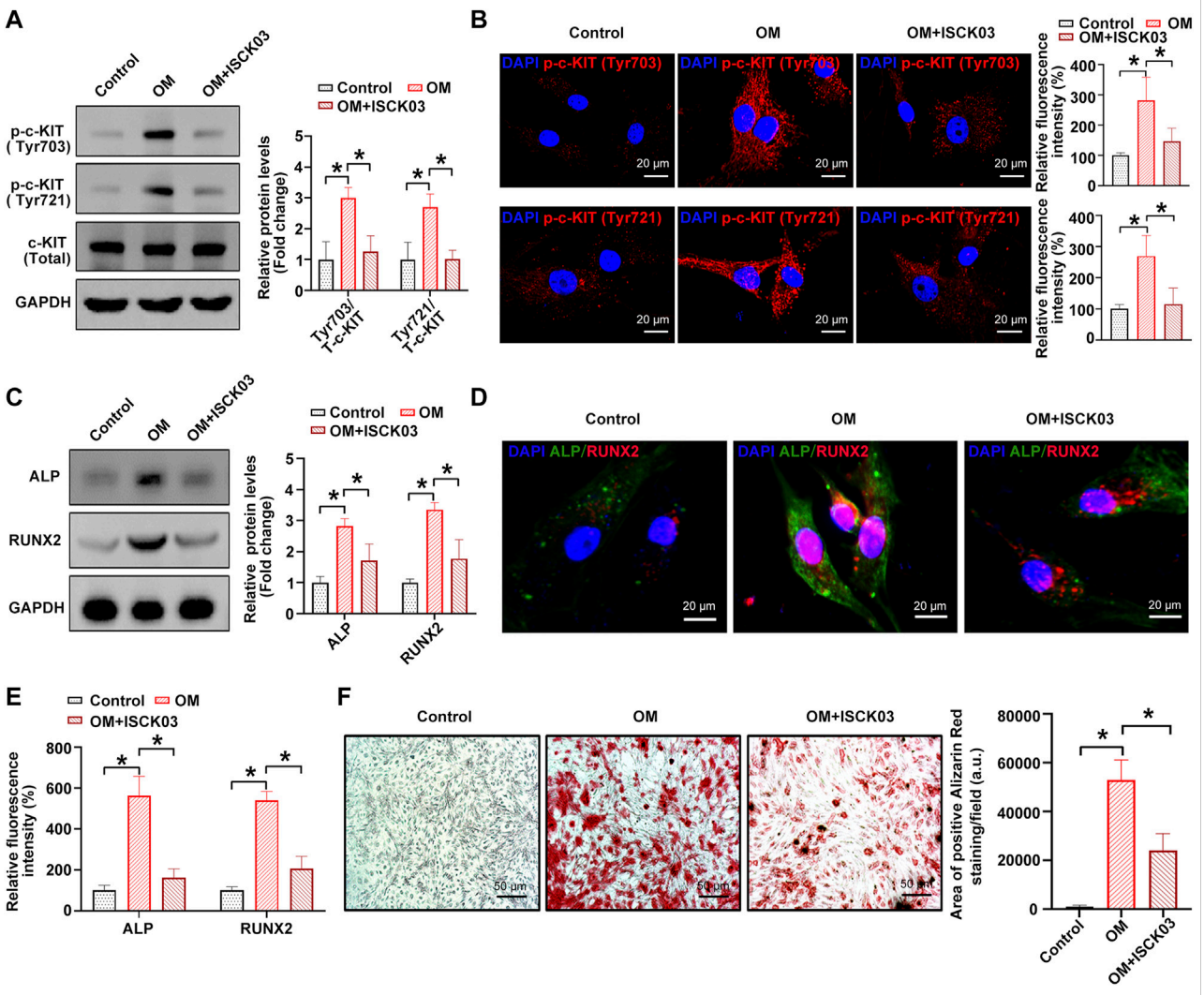

FIGURE 3
c-KIT inhibition prevents the osteogenic differentiation of human valvular interstitial cells (hVICs). Western blotting **(A)** and immunofluorescent staining **(B)** were used to confirm the inhibitory effect of ISCK03 (specific inhibitor of c-KIT) on c-KIT activity. One-way ANOVA followed by a Bonferroni *post hoc test*. Western blotting **(C)** and immunofluorescent staining **(D)** were used to detect the protein levels of osteogenesis-specific genes (alkaline phosphatase, ALP, and runt-related transcription factor 2, RUNX2) in human valvular interstitial cells (hVICs) stimulated with osteogenic induction medium (OM) and then treated with or without ISCK03. **(E)** Semiquantification of the fluorescence intensity of RUNX2 and ALP. One-way ANOVA followed by Bonferroni *post hoc test*. **(F)** Alizarin red staining of mineralization nodules in hVICs stimulated with OM and then treated with or without ISCK03. One-way ANOVA followed by Bonferroni *post hoc test*. $N = 3$ per group. Values are the mean ± SD. $^*p < 0.05$ indicates a significant difference.

C-KIT phosphorylation inhibition alleviates the osteogenic differentiation of hVICs

Next, [4-t-butylphenyl]-N-(4-imidazol-1-yl phenyl) sulfonamide (also known as ISCK03), a selective c-KIT kinase activity inhibitor, was used to inhibit the phosphorylation of c-KIT in hVICs, thereby confirming whether c-KIT plays a role in AVC. The results showed that OM-induced phosphorylation of c-Kit at sites Tyr703 and Tyr721 was successfully decreased by ISCK03, as evidenced by Western blotting (Figure 3A) and immunofluorescence (Figure 3B), respectively. Next, hVICs were exposed to OM for 14 days to stimulate osteogenic differentiation and then treated with ISCK03 (5 μM). The results indicated that ISCK03 significantly negated the OM-induced increase in the protein levels of two known osteogenesis-specific genes (ALP and Runx2), as evidenced by Western blotting (Figure 3C) and immunofluorescence (Figures 3D,E). Importantly, ISCK03 treatment significantly alleviated the OM-induced increase in calcified nodule formation in hVICs

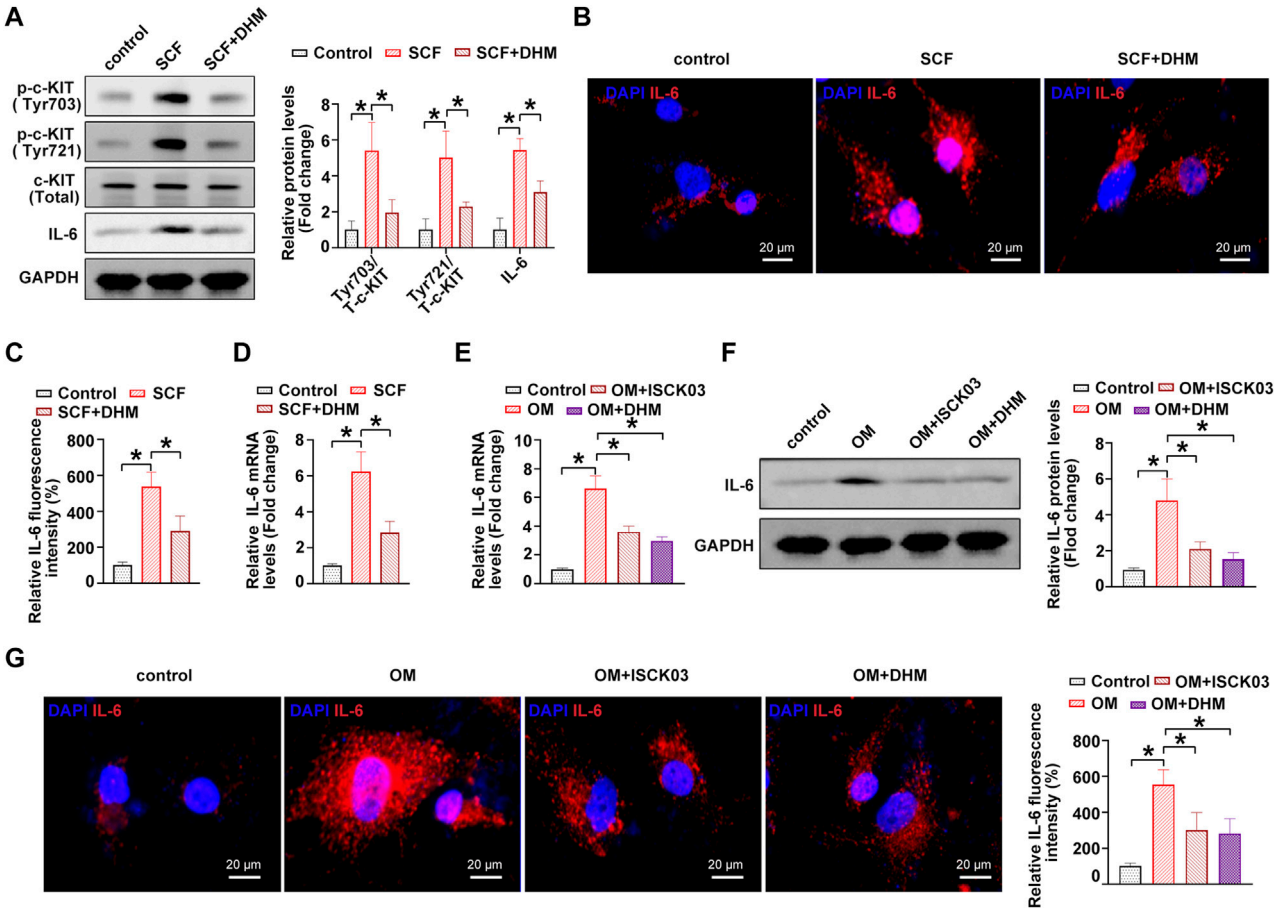

FIGURE 4
Dihydromyricetin (DHM) represses interleukin-6 (IL-6) through c-KIT inhibition in human valvular interstitial cells (hVICs). **(A)** IL-6 and phosphorylated c-Kit (sites of Tyr703 and Tyr721) protein levels in hVICs stimulated with stem cell factor (SCF, 100 ng/ml), the c-kit ligand, or cotreated with DHM. One-way ANOVA followed by Bonferroni *post hoc test*. **(B)** Immunofluorescent staining was used to detect the protein levels of IL-6 in hVICs following different conditioned culturing conditions. **(C)** Semiquantification of the fluorescence intensity of IL-6. One-way ANOVA followed by Bonferroni post hoc test. One-way ANOVA followed by Bonferroni *post hoc test*. **(D)** mRNA level of IL-6 in hVICs stimulated with SCF and then treated with or without DHM. One-way ANOVA followed by Bonferroni *post hoc test*. **(E)** IL-6 mRNA levels in hVICs stimulated with osteogenic induction medium (OM), or cotreated with ISCK03 or DHM. One-way ANOVA followed by Bonferroni *post hoc test*. **(F)** IL-6 protein levels in hVICs stimulated with OM or cotreated with ISCK03 or DHM. One-way ANOVA followed by Bonferroni *post hoc test*. **(G)** Immunofluorescent staining was used to detect the protein level of IL-6 in hVICs following different conditioned culturing conditions. One-way ANOVA followed by Bonferroni *post hoc test*. $N = 3$ per group. Values are the mean ± SD. $^*p < 0.05$ indicates a significant difference.

(Figure 3F). These results suggest that inhibition of c-KIT phosphorylation exhibits highly inhibitory effects on osteogenic differentiation of hVICs.

DHM represses interleukin-6 through c-KIT inhibition in hVICs

A previous study showed that c-KIT is an important regulator of interleukin-6 (IL-6) secretion (Krishnamoorthy et al., 2008). The overactivation of c-KIT stimulates the secretion of IL-6, thereby inducing inflammation (Das Roy et al., 2013). In addition, IL-6 was experimentally shown to be a strong inducer of the mineralization of valve interstitial cells (El Husseini et al., 2013; El Husseini et al., 2014). Thus, we hypothesized that IL-6 might be the downstream target of c-KIT in the phenotypic switching of hVICs and thereby affect OM-induced AVC *in vitro*. To address this issue, we further explored the role of IL-6 in the DHM-mediated inhibitory effects on the osteogenic differentiation of hVICs. Western blot (Figure 4A), immunofluorescence (Figures 4B,C) and qRT–PCR (Figure 4D) results showed that IL-6 levels were significantly increased upon treatment with the c-kit ligand, SCF, while DHM treatment partially abolished the SCF-induced upregulation of IL-6, as expected. Moreover, IL-6 mRNA (Figure 4E) and protein (Figures 4F,G) levels were

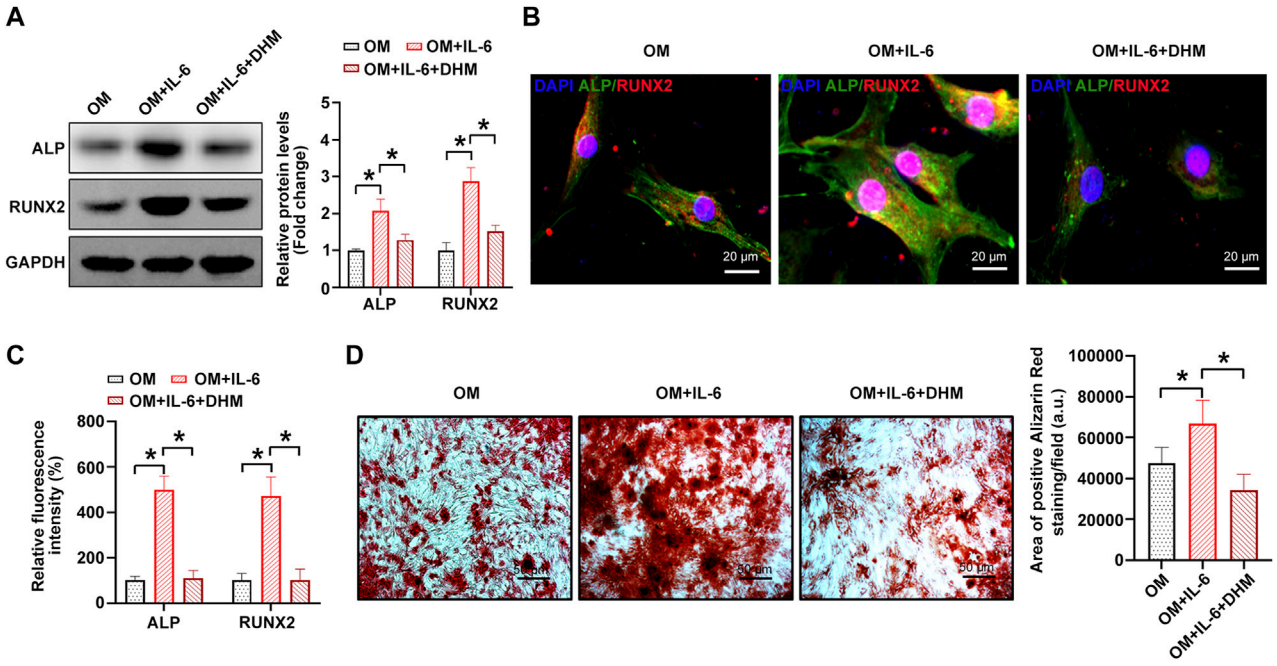

FIGURE 5
Dihydromyricetin (DHM) rescues the osteogenic differentiation phenotypes induced by interleukin-6 (IL-6) in human valvular interstitial cells (hVICs). Western blotting**(A)** and immunofluorescent staining **(B)** were used to detect the protein levels of osteogenesis-specific genes (alkaline phosphatase, ALP, and runt-related transcription Factor 2, RUNX2) in hVICs stimulated with osteogenic induction medium (OM) and then cotreated with IL-6 or IL-6+DHM. One-way ANOVA followed by Bonferroni *post hoc test*. **(C)** Semiquantification of the fluorescence intensity of ALP and RUNX2. One-way ANOVA followed by Bonferroni *post hoc test*. **(D)** Alizarin red staining of mineralization nodules in hVICs stimulated with OM and then cotreated with IL-6 or IL-6+DHM. One-way ANOVA followed by Bonferroni *post hoc test*. $N = 3$ per group. Values are the mean ± SD. $^*p < 0.05$ indicates a significant difference.

significantly increased upon OM stimulation, and inhibition of c-KIT with ISCK03 markedly reduced this effect in hVICs. Importantly, we also found that DHM was able to effectively reverse the OM-induced increases in IL-6 mRNA (Figure 4E) and protein levels (Figures 4F,G). These results suggest that DHM functions as a novel inhibitor of c-KIT, thereby decreasing IL-6 protein expression in hVICs.

DHM inhibits the osteogenic differentiation of hVICs *via* IL-6 downregulation

Next, we performed a rescue experiment to confirm whether IL-6 downregulation contributes to the inhibitory effect of DHM on the osteogenic differentiation of hVICs. The results indicate that the procalcific effects of IL-6 were partially reversed by DHM, as evidenced by decreased osteogenesis-specific gene (ALP and RUNX2) expression (Figures 5A–C) and reduced calcium deposition in hVICs (Figure 5D). Collectively, these data suggest that DHM inhibits the osteogenic differentiation of hVICs by downregulating IL-6.

Discussion

The key pathogenesis of CAVD involves inflammation, lipoprotein deposition, and osteogenic differentiation of hVICs (Aikawa and Libby, 2017). Currently, although a few risk factors have been identified, there are still no approved pharmacotherapies in the clinic for the treatment and prevention of CAVD (Tsimikas, 2019). Hence, there is growing interest in exploring effective pharmacotherapeutic interventions for CAVD. Our current study showed that DHM administration functions as an effective medical therapy for negating the osteogenic differentiation of hVICs. We provide the first evidence that DHM exerts inhibitory effects on IL-6 expression by interacting with c-KIT and thereby blocking OM-induced c-KIT phosphorylation. Notably, c-KIT inhibition markedly reduced AVC progression *in vitro*. Importantly, we also identified IL-6 as a substantial downstream target of DHM for ameliorating the osteogenic differentiation of hVICs. These findings pinpoint a previously unidentified regulatory DHM/c-KIT/IL-6 axis contributing to CAVD, suggesting that DHM might be an effective chemical drug for the treatment of CAVD.

Mounting evidence suggests that DHM exhibits cardiovascular protective properties in cardiovascular diseases,

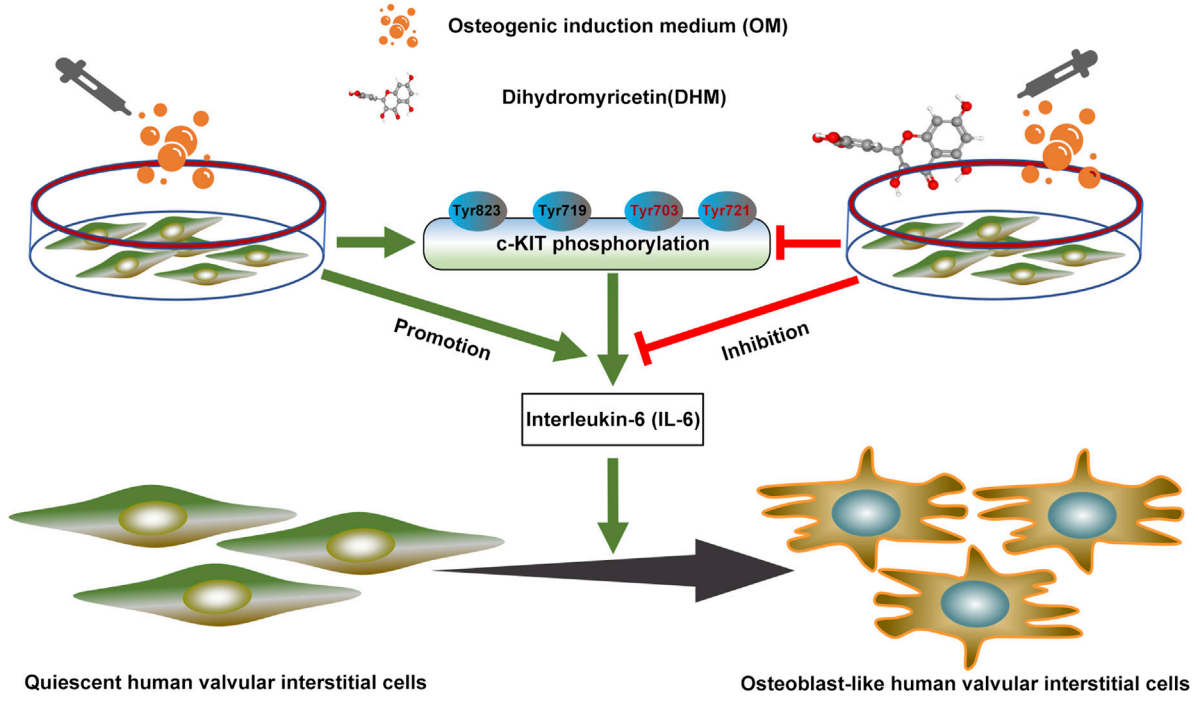

FIGURE 6
Dihydromyricetin (DHM) downregulated interleukin-6 (IL-6) expression by antagonizing phosphorylation of c-KIT, thereby preventing osteogenic differentiation of human valvular interstitial cells.

such as vascular calcification (Feng et al., 2021), endothelial protection (Chen et al., 2021), and pulmonary arterial hypertension (Li Q et al., 2017). In atherosclerosis, which shares similar pathological features with CAVD (Kostyunin et al., 2020), DHM has been shown to increase endothelial nitric oxide production in apolipoprotein E-deficient mice ($ApoE^{-/-}$) (Yang et al., 2020) and protect human umbilical vein endothelial cells from oxidative damage (Zhang et al., 2019). Whether DHM exhibits a protective role against CAVD progression in humans requires further study. Our present study demonstrated that DHM prevents the osteogenic differentiation of hVICs *via* a c-KIT/IL-6-dependent pathway at noncytotoxic concentrations of 20 μM, as evidenced by decreased protein levels of two osteogenesis-specific genes (ALP and Runx2) and calcified nodule formation, which is consistent with several previous findings involving the protective role of DHM in atherosclerosis and vascular calcification (Liu et al., 2017; Yang et al., 2020; Feng et al., 2021). In addition, a recent study indicated that DHM significantly suppressed foam cell formation by regulating cholesterol efflux in macrophages (Zeng et al., 2018), thereby protecting $ApoE^{-/-}$ mice from atherosclerosis. Importantly, Matsumoto et al. (2010) reported that endothelial integrity of the aortic valves serves as a crucial cellular mechanism of CAVD progression, and our previous study also revealed that macrophage polarization could regulate AVC progression (Li G et al., 2017). Thus, further investigation is needed to elucidate whether DHM could ameliorate AVC by regulating the pathological processes attributed to endothelial cells and macrophages in the valve district. Importantly, DHM supplementation was shown to exert a strong beneficial effect on improving the glycemic control of type 2 diabetes mellitus (T2DM) patients (Ran et al., 2019), and a previous randomized controlled trial confirmed the therapeutic effects of DHM supplementation in patients with nonalcoholic fatty liver disease (Chen et al., 2015). Thus, DHM supplementation may provide an effective and safe pharmacological strategy for patients suffering from CAVD. However, as we stated, prior to clinical use, randomized clinical trials are still needed to sufficiently validate the safety and therapeutic potential of DHM in CAVD treatment.

Increasing evidence suggests that inflammatory infiltration and subsequent endothelial damage are hallmarks of early lesions in CAVD (Bartoli-Leonard et al., 2021; Lu et al., 2022; Zhang et al., 2022). Inflammatory factors are secreted by several resident cells of the valve layer or inflammatory cells, which in turn can facilitate the process of CAVD. Notably, it was reported that not only valve endothelial cells (Mahler et al., 2013) but also valve interstitial cells (El Husseini et al., 2014) could produce IL-6, which is a strong promoter of CAVD.

Several *in vitro* studies have shown that DHM prevents atherosclerosis by reducing IL-6 production (Li Q et al., 2017; Liu et al., 2017). In addition, it has previously been shown that activation of c-KIT could significantly promote IL-6 expression (Das Roy et al., 2013). However, the interactive relationship of DHM, c-KIT, and IL-6 in CAVD remains uncharacterized. Here, we demonstrated for the first time that DHM interacted with c-KIT and thereby ameliorated the osteogenic differentiation of hVICs by inhibiting IL-6 expression. In fact, c-KIT activation could also promote the expression of some other inflammatory factors, such as TNF-α and IL-10 (41). Thus, whether additional inflammatory factors could be downstream targets of the DHM/c-KIT pathway requires further investigation. Interestingly, in a previous study, Song et al. (2016) demonstrated that c-KIT is atheroprotective in hyperlipidemic mice by antagonizing kruppel-like Factor 4, which was supported by some of the authors' latest studies (Song et al., 2019; Zigmond et al., 2021). However, our present study indicates that the DHM-mediated increase in c-KIT phosphorylation exerts procalcific effects through IL-6 upregulation. We argue that the stage of the disease was an important confounding factor, resulting in this difference.

Only *in vitro* experiments were conducted in the present study to explore the role of DHM and c-KIT in the progression of osteogenic differentiation of hVICs. Thus, whether DHM and c-KIT regulate CAVD progression *in vivo* still requires further investigation using preclinical animal models. Specifically, further *in vivo* studies using c-KIT gene-deficient mice or a murine model harboring a cell-type-specific deletion of c-KIT in valve interstitial cells may provide more compelling evidence. Furthermore, to the best of our knowledge, the pathological mechanisms of bicuspid CAVD are different from those of tricuspid CAVD (Kostina et al., 2018). The results of the present study were only based on hVICs isolated from tricuspid aortic valves (TAVs) rather than bicuspid aortic valves (BAVs) and may only be applied to tricuspid CAVD. Thus, whether DHM also plays a protective role in bicuspid CAVD warrants further investigation.

Conclusion

In this study, we confirmed that DHM significantly ameliorates the osteogenic differentiation of hVICs. Mechanistically, DHM repressed c-KIT phosphorylation, thereby resulting in IL-6 downregulation in hVICs. These findings pinpoint a previously unidentified DHM/c-KIT/IL-6 axis contributing to the inhibition of osteogenic differentiation of hVICs (Figure 6). Thus, DHM treatment may represent a potent pharmacological remedy to prevent CAVD progression.

Data availability statement

The datasets presented in this study can be found in online repositories. The names of the repository/repositories and accession number(s) can be found in the article/supplementary material.

Ethics statement

The studies involving human participants were reviewed and approved by the Tongji Medical College Institutional Review Board at Huazhong University of Science and Technology. The patients/participants provided their written informed consent to participate in this study.

Author contributions

SZ and LF initiated the project with guidance from TZ, ZZ, and JX. SZ and LF performed *in vitro* cell studies and data analysis. YW, JX, and QS prepared the figures. LF and JX wrote the manuscript. TZ and ZZ provided critical revision of the manuscript and supervised the project.

Funding

This work was supported by the National Natural Science Foundation of China (No. 82000422).

Conflict of interest

The authors declare that the research was conducted in the absence of any commercial or financial relationships that could be construed as a potential conflict of interest.

Publisher's note

References

Aikawa, E., and Libby, P. (2017). A rock and a hard place: Chiseling away at the multiple mechanisms of aortic stenosis. *Circulation* 135 (20), 1951–1955. doi:10.1161/CIRCULATIONAHA.117.027776

Bartoli-Leonard, F., Zimmer, J., and Aikawa, E. (2021). Innate and adaptive immunity: The understudied driving force of heart valve disease. *Cardiovasc. Res.* 117 (13), 2506–2524. doi:10.1093/cvr/cvab273

Chan, K. L., Teo, K., Dumesnil, J. G., Ni, A., and Tam, J. (2010). Effect of lipid lowering with rosuvastatin on progression of aortic stenosis: Results of the aortic stenosis progression observation: Measuring effects of rosuvastatin (ASTRONOMER) trial. *Circulation* 121 (2), 306–314. doi:10.1161/CIRCULATIONAHA.109.900027

Chen, H. Y., Cairns, B. J., Small, A. M., Burr, H. A., Ambikkumar, A., Martinsson, A., et al. (2020). Association of FADS1/2 locus variants and polyunsaturated fatty acids with aortic stenosis. *JAMA Cardiol.* 5 (6), 694–702. doi:10.1001/jamacardio.2020.0246

Chen, S., Lv, K., Sharda, A., Deng, J., Zeng, W., Zhang, C., et al. (2021). Anti-thrombotic effects mediated by dihydromyricetin involve both platelet inhibition and endothelial protection. *Pharmacol. Res.* 167, 105540. doi:10.1016/j.phrs.2021.105540

Chen, S., Zhao, X., Wan, J., Ran, L., Qin, Y., Wang, X., et al. (2015). Dihydromyricetin improves glucose and lipid metabolism and exerts anti-inflammatory effects in nonalcoholic fatty liver disease: A randomized controlled trial. *Pharmacol. Res.* 99, 74–81. doi:10.1016/j.phrs.2015.05.009

Chen, Y., Luo, H. Q., Sun, L. L., Xu, M. T., Yu, J., Liu, L. L., et al. (2018). Dihydromyricetin attenuates myocardial hypertrophy induced by transverse aortic constriction via oxidative stress inhibition and SIRT3 pathway enhancement. *Int. J. Mol. Sci.* 19 (9), E2592. doi:10.3390/ijms19092592

Cho, K. I., Sakuma, I., Sohn, I. S., Jo, S. H., and Koh, K. K. (2018). Inflammatory and metabolic mechanisms underlying the calcific aortic valve disease. *Atherosclerosis* 277, 60–65. doi:10.1016/j.atherosclerosis.2018.08.029

Dai, Y., Song, J., Li, W., Yang, T., Yue, X., Lin, X., et al. (2019). RhoE fine-tunes inflammatory response in myocardial infarction. *Circulation* 139 (9), 1185–1198. doi:10.1161/CIRCULATIONAHA.118.033700

Das Roy, L., Curry, J. M., Sahraei, M., Besmer, D. M., Kidiyoor, A., Gruber, H. E., et al. (2013). Arthritis augments breast cancer metastasis: Role of mast cells and SCF/c-Kit signaling. *Breast Cancer Res.* 15 (2), R32. doi:10.1186/bcr3412

Ebeid, D. E., Firouzi, F., Esquer, C. Y., Navarrete, J. M., Wang, B. J., Gude, N. A., et al. (2020). PIM1 promotes survival of cardiomyocytes by upregulating c-kit protein expression. *Cells* 9 (9), E2001. doi:10.3390/cells9092001

El Husseini, D., Boulanger, M-C., Fournier, D., Pibarot, P., Bosse, Y., and Mathieu, P. (2013). *Il-6 in aortic stenosis: Amplification loop between inflammation and calcification*. United States: Am Heart Assoc.

El Husseini, D., Boulanger, M. C., Mahmut, A., Bouchareb, R., Laflamme, M. H., Fournier, D., et al. (2014). P2Y2 receptor represses IL-6 expression by valve interstitial cells through akt: Implication for calcific aortic valve disease. *J. Mol. Cell. Cardiol.* 72, 146–156. doi:10.1016/j.yjmcc.2014.02.014

Feng, L., Que, D., Li, Z., Zhong, X., Yan, J., Wei, J., et al. (2021). Dihydromyricetin ameliorates vascular calcification in chronic kidney disease by targeting AKT signaling. *Clin. Sci.* 135 (21), 2483–2502. doi:10.1042/CS20210259

Gendron, N., Rosa, M., Blandinieres, A., Sottejeau, Y., Rossi, E., Van Belle, E., et al. (2021). Human aortic valve interstitial cells display proangiogenic properties during calcific aortic valve disease. *Arterioscler. Thromb. Vasc. Biol.* 41 (1), 415–429. doi:10.1161/ATVBAHA.120.314287

Gude, N. A., Firouzi, F., Broughton, K. M., Ilves, K., Nguyen, K. P., Payne, C. R., et al. (2018). Cardiac c-kit biology revealed by inducible transgenesis. *Circ. Res.* 123 (1), 57–72. doi:10.1161/CIRCRESAHA.117.311828

Hernandez, D. R., Rojas, M. G., Martinez, L., Rodriguez, B. L., Zigmond, Z. M., Vazquez-Padron, R. I., et al. (2019). c-Kit deficiency impairs nitric oxide signaling in smooth muscle cells. *Biochem. Biophys. Res. Commun.* 518 (2), 227–232. doi:10.1016/j.bbrc.2019.08.037

Hutcheson, J. D., Aikawa, E., and Merryman, W. D. (2014). Potential drug targets for calcific aortic valve disease. *Nat. Rev. Cardiol.* 11 (4), 218–231. doi:10.1038/nrcardio.2014.1

Issa, H., Hénaut, L., Abdallah, J. B., Boudot, C., Lenglet, G., Avondo, C., et al. (2019). Activation of the calcium-sensing receptor in human valvular interstitial cells promotes calcification. *J. Mol. Cell. Cardiol.* 129, 2–12. doi:10.1016/j.yjmcc.2019.01.021

Kaltoft, M., Langsted, A., Afzal, S., Kamstrup, P. R., and Nordestgaard, B. G. (2022). Lipoprotein(a) and body mass compound the risk of calcific aortic valve disease. *J. Am. Coll. Cardiol.* 79 (6), 545–558. doi:10.1016/j.jacc.2021.11.043

Kim, J. Y., Choi, J. S., Song, S. H., Im, J. E., Kim, J. M., Kim, K., et al. (2014). Stem cell factor is a potent endothelial permeability factor. *Arterioscler. Thromb. Vasc. Biol.* 34 (7), 1459–1467. doi:10.1161/ATVBAHA.114.303575

Kostina, A., Shishkova, A., Ignatieva, E., Irtyuga, O., Bogdanova, M., Levchuk, K., et al. (2018). Different Notch signaling in cells from calcified bicuspid and tricuspid aortic valves. *J. Mol. Cell. Cardiol.* 114, 211–219. doi:10.1016/j.yjmcc.2017.11.009

Kostyunin, A., Mukhamadiyarov, R., Glushkova, T., Bogdanov, L., Shishkova, D., Osyaev, N., et al. (2020). Ultrastructural pathology of atherosclerosis, calcific aortic valve disease, and bioprosthetic heart valve degeneration: Commonalities and differences. *Int. J. Mol. Sci.* 21 (20), E7434. doi:10.3390/ijms21207434

Kraler, S., Blaser, M. C., Aikawa, E., Camici, G. G., and Lüscher, T. F. (2022). Calcific aortic valve disease: From molecular and cellular mechanisms to medical therapy. *Eur. Heart J.* 43 (7), 683–697. doi:10.1093/eurheartj/ehab757

Krishnamoorthy, N., Oriss, T. B., Paglia, M., Fei, M., Yarlagadda, M., Vanhaesebroeck, B., et al. (2008). Activation of c-Kit in dendritic cells regulates T helper cell differentiation and allergic asthma. *Nat. Med.* 14 (5), 565–573. doi:10.1038/nm1766

Kuang, D., Zhao, X., Xiao, G., Ni, J., Feng, Y., Wu, R., et al. (2008). Stem cell factor/c-kit signaling mediated cardiac stem cell migration via activation of p38 MAPK. *Basic Res. Cardiol.* 103 (3), 265–273. doi:10.1007/s00395-007-0690-z

Li, G., Qiao, W., Zhang, W., Li, F., Shi, J., Dong, N., et al. (2017). The shift of macrophages toward M1 phenotype promotes aortic valvular calcification. *J. Thorac. Cardiovasc. Surg.* 153 (6), 1318–1327. doi:10.1016/j.jtcvs.2017.01.052

Li, Q., Wang, J., Zhu, X., Zeng, Z., Wu, X., Xu, Y., et al. (2017). Dihydromyricetin prevents monocrotaline-induced pulmonary arterial hypertension in rats. *Biomed. Pharmacother. = Biomedecine Pharmacother.* 96, 825–833. doi:10.1016/j.biopha.2017.10.007

Liu, T. T., Zeng, Y., Tang, K., Chen, X., Zhang, W., Xu, X. L., et al. (2017). Dihydromyricetin ameliorates atherosclerosis in LDL receptor deficient mice. *Atherosclerosis* 262, 39–50. doi:10.1016/j.atherosclerosis.2017.05.003

Lu, J., Xie, S., Deng, Y., Xie, X., and Liu, Y. (2022). Blocking the NLRP3 inflammasome reduces osteogenic calcification and M1 macrophage polarization in a mouse model of calcified aortic valve stenosis. *Atherosclerosis* 347, 28–38. doi:10.1016/j.atherosclerosis.2022.03.005

Mahler, G. J., Farrar, E. J., and Butcher, J. T. (2013). Inflammatory cytokines promote mesenchymal transformation in embryonic and adult valve endothelial cells. *Arterioscler. Thromb. Vasc. Biol.* 33 (1), 121–130. doi:10.1161/ATVBAHA.112.300504

Matsumoto, Y., Adams, V., Jacob, S., Mangner, N., Schuler, G., Linke, A., et al. (2010). Regular exercise training prevents aortic valve disease in low-density lipoprotein-receptor-deficient mice. *Circulation* 121 (6), 759–767. doi:10.1161/CIRCULATIONAHA.109.892224

Mukhopadhyay, A., Do, D. V., Ong, C. T., Khoo, Y. T., Masilamani, J., Chan, S. Y., et al. (2011). The role of stem cell factor and c-KIT in keloid pathogenesis: Do tyrosine kinase inhibitors have a potential therapeutic role? *Br. J. Dermatol.* 164 (2), 372–386. doi:10.1111/j.1365-2133.2010.10035.x

Mundal, L. J., Hovland, A., Igland, J., Veierød, M. B., Holven, K. B., Bogsrud, M. P., et al. (2019). Association of low-density lipoprotein cholesterol with risk of aortic valve stenosis in familial hypercholesterolemia. *JAMA Cardiol.* 4 (11), 1156–1159. doi:10.1001/jamacardio.2019.3903

Peeters, F., Meex, S. J. R., Dweck, M. R., Aikawa, E., Crijns, H., Schurgers, L. J., et al. (2018). Calcific aortic valve stenosis: Hard disease in the heart: A biomolecular approach towards diagnosis and treatment. *Eur. Heart J.* 39 (28), 2618–2624. doi:10.1093/eurheartj/ehx653

Ran, L., Wang, X., Lang, H., Xu, J., Wang, J., Liu, H., et al. (2019). Ampelopsis grossedentata supplementation effectively ameliorates the glycemic control in patients with type 2 diabetes mellitus. *Eur. J. Clin. Nutr.* 73 (5), 776–782. doi:10.1038/s41430-018-0282-z

Song, L., Selman, G., Santos, N., Martinez, L., Lassance-Soares, R. M., Webster, K., et al. (2016). Ckit expression in vascular smooth muscle cells protects mice against excessive atherosclerosis. *Circulation* 134, A14889. doi:10.1161/circ.134.suppl_1.14889

Song, L., Zigmond, Z. M., Martinez, L., Lassance-Soares, R. M., Macias, A. E., Velazquez, O. C., et al. (2019). c-Kit suppresses atherosclerosis in hyperlipidemic mice. *Am. J. Physiol. Heart Circ. Physiol.* 317 (4), H867–H876. doi:10.1152/ajpheart.00062.2019

Sonnenschein, K., Fiedler, J., de Gonzalo-Calvo, D., Xiao, K., Pfanne, A., Just, A., et al. (2021). Blood-based protein profiling identifies serum protein c-KIT as a novel biomarker for hypertrophic cardiomyopathy. *Sci. Rep.* 11 (1), 1755. doi:10.1038/s41598-020-80868-z

Sun, Z., Lu, W., Lin, N., Lin, H., Zhang, J., Ni, T., et al. (2020). Dihydromyricetin alleviates doxorubicin-induced cardiotoxicity by inhibiting NLRP3 inflammasome through activation of SIRT1. *Biochem. Pharmacol.* 175, 113888. doi:10.1016/j.bcp.2020.113888

Teo, K. K., Corsi, D. J., Tam, J. W., Dumesnil, J. G., and Chan, K. L. (2011). Lipid lowering on progression of mild to moderate aortic stenosis: meta-analysis of the randomized placebo-controlled clinical trials on 2344 patients. *Can. J. Cardiol.* 27 (6), 800–808. doi:10.1016/j.cjca.2011.03.012

Tsimikas, S. (2019). Potential causality and emerging medical therapies for lipoprotein(a) and its associated oxidized phospholipids in calcific aortic valve stenosis. *Circ. Res.* 124 (3), 405–415. doi:10.1161/CIRCRESAHA.118.313864

Veinot, J. P., Prichett-Pejic, W., Song, J., Waghray, G., Parks, W., Mesana, T. G., et al. (2006). CD117-positive cells and mast cells in adult human cardiac valves--observations and implications for the creation of bioengineered grafts. *Cardiovasc. Pathol.* 15 (1), 36–40. doi:10.1016/j.carpath.2005.08.005

Wang, C., Huang, Y., Liu, X., Li, L., Xu, H., Dong, N., et al. (2021). Andrographolide ameliorates aortic valve calcification by regulation of lipid biosynthesis and glycerolipid metabolism targeting MGLL expression *in vitro* and *in vivo*. *Cell calcium* 100, 102495. doi:10.1016/j.ceca.2021.102495

Wang, Y., Han, D., Zhou, T., Chen, C., Cao, H., Zhang, J. Z., et al. (2021). DUSP26 induces aortic valve calcification by antagonizing MDM2-mediated ubiquitination of DPP4 in human valvular interstitial cells. *Eur. Heart J.* 42 (30), 2935–2951. doi:10.1093/eurheartj/ehab316

Wang, Y., Han, D., Zhou, T., Zhang, J., Liu, C., Cao, F., et al. (2020). Melatonin ameliorates aortic valve calcification via the regulation of circular RNA CircRIC3/miR-204-5p/DPP4 signaling in valvular interstitial cells. *J. Pineal Res.* 69 (2), e12666. doi:10.1111/jpi.12666

Wei, L., Sun, X., Qi, X., Zhang, Y., Li, Y., Xu, Y., et al. (2019). Dihydromyricetin ameliorates cardiac ischemia/reperfusion injury through Sirt3 activation. *Biomed. Res. Int.* 2019, 6803943. doi:10.1155/2019/6803943

Xu, K., Huang, Y., Zhou, T., Wang, C., Chi, Q., Shi, J., et al. (2019). Nobiletin exhibits potent inhibition on tumor necrosis factor alpha-induced calcification of human aortic valve interstitial cells via targeting ABCG2 and AKR1B1. *Phytother. Res.* 33 (6), 1717–1725. doi:10.1002/ptr.6360

Xu, K., Xie, S., Huang, Y., Zhou, T., Liu, M., Zhu, P., et al. (2020). Cell-type transcriptome atlas of human aortic valves reveal cell heterogeneity and endothelial to mesenchymal transition involved in calcific aortic valve disease. *Arterioscler. Thromb. Vasc. Biol.* 40 (12), 2910–2921. doi:10.1161/ATVBAHA.120.314789

Xu, K., Zhou, T., Huang, Y., Chi, Q., Shi, J., Zhu, P., et al. (2018). Anthraquinone emodin inhibits tumor necrosis factor Alpha-induced calcification of human aortic valve interstitial cells via the NF-κB pathway. *Front. Pharmacol.* 9, 1328. doi:10.3389/fphar.2018.01328

Yang, D., Yang, Z., Chen, L., Kuang, D., Zou, Y., Li, J., et al. (2020). Dihydromyricetin increases endothelial nitric oxide production and inhibits atherosclerosis through microRNA-21 in apolipoprotein E-deficient mice. *J. Cell. Mol. Med.* 24 (10), 5911–5925. doi:10.1111/jcmm.15278

Ye, X., Pang, Z., and Zhu, N. (2019). Dihydromyricetin attenuates hypertrophic scar formation by targeting activin receptor-like kinase 5. *Eur. J. Pharmacol.* 852, 58–67. doi:10.1016/j.ejphar.2019.02.039

Zeng, Y., Peng, Y., Tang, K., Wang, Y. Q., Zhao, Z. Y., Wei, X. Y., et al. (2018). Dihydromyricetin ameliorates foam cell formation via LXRα-ABCA1/ABCG1-dependent cholesterol efflux in macrophages. *Biomed. Pharmacother. = Biomedecine Pharmacother.* 101, 543–552. doi:10.1016/j.biopha.2018.02.124

Zhang, J. Y., Chen, Q. Q., Li, J., Zhang, L., and Qi, L. W. (2021). Neuraminidase 1 and its inhibitors from Chinese herbal medicines: An emerging role for cardiovascular diseases. *Am. J. Chin. Med.* 49 (4), 843–862. doi:10.1142/S0192415X21500403

Zhang, P., The, E., Luo, Z., Zhai, Y., Yao, Q., Ao, L., et al. (2022). Pro-inflammatory mediators released by activated monocytes promote aortic valve fibrocalcific activity. *Mol. Med.* 28 (1), 5. doi:10.1186/s10020-022-00433-4

Zhang, Q., Liu, J., Duan, H., Li, R., Peng, W., Wu, C., et al. (2021). Activation of Nrf2/HO-1 signaling: An important molecular mechanism of herbal medicine in the treatment of atherosclerosis via the protection of vascular endothelial cells from oxidative stress. *J. Adv. Res.* 34, 43–63. doi:10.1016/j.jare.2021.06.023

Zhang, X., Wang, L., Peng, L., Tian, X., Qiu, X., Cao, H., et al. (2019). Dihydromyricetin protects HUVECs of oxidative damage induced by sodium nitroprusside through activating PI3K/Akt/FoxO3a signalling pathway. *J. Cell. Mol. Med.* 23 (7), 4829–4838. doi:10.1111/jcmm.14406

Zhao, C., Li, S., Zhang, J., Huang, Y., Zhang, L., Zhao, F., et al. (2020). Current state and future perspective of cardiovascular medicines derived from natural products. *Pharmacol. Ther.* 216, 107698. doi:10.1016/j.pharmthera.2020.107698

Zhou, T., Han, D., Liu, J., Shi, J., Zhu, P., Wang, Y., et al. (2021). Factors influencing osteogenic differentiation of human aortic valve interstitial cells. *J. Thorac. Cardiovasc. Surg.* 161 (2), e163–e185. doi:10.1016/j.jtcvs.2019.10.039

Zhou, T., Wang, Y., Liu, M., Huang, Y., Shi, J., Dong, N., et al. (2020). Curcumin inhibits calcification of human aortic valve interstitial cells by interfering NF-κB, AKT, and ERK pathways. *Phytother. Res.* 34 (8), 2074–2081. doi:10.1002/ptr.6674

Zhu, Y. C., Liang, B., and Gu, N. (2021). Cellular and molecular mechanism of traditional Chinese medicine on ventricular remodeling. *Front. Cardiovasc. Med.* 8, 753095. doi:10.3389/fcvm.2021.753095

Zigmond, Z. M., Song, L., Martinez, L., Lassance-Soares, R. M., Velazquez, O. C., Vazquez-Padron, R. I., et al. (2021). c-Kit expression in smooth muscle cells reduces atherosclerosis burden in hyperlipidemic mice. *Atherosclerosis* 324, 133–140. doi:10.1016/j.atherosclerosis.2021.03.004

frontiers | Frontiers in Pharmacology

TYPE Original Research
PUBLISHED 31 August 2022
DOI 10.3389/fphar.2022.909784

OPEN ACCESS

EDITED BY
Anna Malashicheva,
Institute of Cytology, Russia

REVIEWED BY
Guangqi Qin,
Lund University, Sweden
Shi Lei,
First Affiliated Hospital of Zhengzhou University, China

*CORRESPONDENCE
Xiaoyong Pu,
pxyurol@163.com
Jiumin Liu,
15927243779@163.com

†These authors have contributed equally to this work

SPECIALTY SECTION
This article was submitted to Experimental Pharmacology and Drug Discovery, a section of the journal Frontiers in Pharmacology

RECEIVED 31 March 2022
ACCEPTED 29 July 2022
PUBLISHED 31 August 2022

CITATION
Feng C, Wang Z, Liu C, Liu S, Wang Y, Zeng Y, Wang Q, Peng T, Pu X and Liu J (2022), Integrated bioinformatical analysis, machine learning and in vitro experiment-identified m6A subtype, and predictive drug target signatures for diagnosing renal fibrosis. *Front. Pharmacol.* 13:909784. doi: 10.3389/fphar.2022.909784

Integrated bioinformatical analysis, machine learning and *in vitro* experiment-identified m6A subtype, and predictive drug target signatures for diagnosing renal fibrosis

Chunxiang Feng[1†], Zhixian Wang[2,3†], Chang Liu[4], Shiliang Liu[5], Yuxi Wang[6], Yuanyuan Zeng[7], Qianqian Wang[1], Tianming Peng[1], Xiaoyong Pu[1*] and Jiumin Liu[1*]

[1]Department of Urology, Guangdong Provincial People's Hospital, Guangdong Academy of Medical Sciences, Guangdong Guangzhou, Wuhan, China, [2]Department of Urology, Wuhan Hospital of Traditional Chinese and Western Medicine, Tongji Medical College, Huazhong University of Science and Technology, Wuhan, China, [3]Department of Urology, Wuhan No. 1 Hospital, Wuhan, China, [4]Department of Geriatrics, Tongji Hospital, Tongji Medical College, Huazhong University of Science and Technology, Wuhan, China, [5]Department of Urology, Tongji Hospital, Tongji Medical College, Huazhong University of Science and Technology, Wuhan, China, [6]Department of Nephrology, Tongji Hospital, Tongji Medical College, Huazhong University of Science and Technology, Wuhan, China, [7]School of Life Science and Engineering, Southwest Jiaotong University, Chengdu, China

Renal biopsy is the gold standard for defining renal fibrosis which causes calcium deposits in the kidneys. Persistent calcium deposition leads to kidney inflammation, cell necrosis, and is related to serious kidney diseases. However, it is invasive and involves the risk of complications such as bleeding, especially in patients with end-stage renal diseases. Therefore, it is necessary to identify specific diagnostic biomarkers for renal fibrosis. This study aimed to develop a predictive drug target signature to diagnose renal fibrosis based on m6A subtypes. We then performed an unsupervised consensus clustering analysis to identify three different m6A subtypes of renal fibrosis based on the expressions of 21 m6A regulators. We evaluated the immune infiltration characteristics and expression of canonical immune checkpoints and immune-related genes with distinct m6A modification patterns. Subsequently, we performed the WGCNA analysis using the expression data of 1,611 drug targets to identify 474 genes associated with the m6A modification. 92 overlapping drug targets between WGCNA and DEGs (renal fibrosis vs. normal samples) were defined as key drug targets. A five target gene predictive model was developed through the combination of LASSO regression and stepwise logistic regression (LASSO-SLR) to diagnose renal fibrosis. We further performed drug sensitivity analysis and extracellular matrix analysis on model genes. The ROC curve showed that the risk score (AUC = 0.863) performed well in diagnosing renal fibrosis in the training dataset. In addition, the external validation dataset further confirmed the outstanding predictive performance of the risk score (AUC = 0.755). These results indicate that the risk model has an excellent predictive performance for diagnosing the

disease. Furthermore, our results show that this 5-target gene model is significantly associated with many drugs and extracellular matrix activities. Finally, the expression levels of both predictive signature genes EGR1 and PLA2G4A were validated in renal fibrosis and adjacent normal tissues by using qRT-PCR and Western blot method.

KEYWORDS

logistic regression, prective model, drug sensitivity, renal fibrosis, immune microenvironment

Introduction

Renal fibrosis is a process of wound-healing failure in renal tissues after chronic injury, calcium deposits, and inflammation. It is a common pathway and pathological marker of almost all types of chronic kidney diseases (CKD) (Farup et al., 2021) (Xie et al., 2021). The main pathological feature of renal fibrosis is nephrogenesis. Fibroblasts are massively activated and proliferated. The extracellular matrix (ECM) deposited in the renal interstitium is excessively synthesized and secreted, resulting in structural damage, renal function impairment, and, ultimately end-stage renal disease (Yan et al., 2021). Renal biopsy is the gold standard for defining renal fibrosis. However, it is invasive and involves the risk of complications such as bleeding, especially in patients with end-stage renal diseases. Therefore, it is necessary to search for more accessible and specific biomarkers of renal fibrosis (Jia et al., 2020).

Despite the significant progress made by modern medicine, non-invasive diagnostic techniques (Nielsen et al., 2020) and effective treatment measures for renal fibrosis are still limited (Zhang et al., 2021a). Currently, there is no specific treatment (Deng et al., 2020). In recent years, many efforts have been devoted to finding novel biomarkers and therapeutics of renal fibrosis, focusing on the properties of unknown mediators and pathways involved in developing renal fibrosis (Prakoura et al., 2019). Machine learning (ML) is an emerging field with enormous resources being applied to medical problems that fuse computer science and statistics together (Handelman et al., 2018). So far, it has shown good performance in a wide range of tasks in biomedicines (Cilluffo et al., 2021). Machine learning techniques have been widely applied to identify disease biomarkers for diagnosis, prognosis, and risk assessment (Dockès et al., 2021; Field et al., 2021).

Combined with machine learning, Cao et al. (2016) found that the urinary TREM-1/TREM-2 ratio can be a potential biomarker for diagnosing renal fibrosis in CKD patients (Guerquin et al., 2013). Hypoxia promotes the development of renal fibrosis. Armutcu ADAMTS protease may provide some important signals for the early diagnosis and treatment of renal fibrosis. Elevated plasma CDH11, SMOC2, and PEDF and urinary CDH11 and PEDF levels were associated with interstitial fibrosis and significantly correlated with increased severity of tubular atrophy. In both the cohorts, elevated plasma and urinary SMOC2 and urinary CDH11 levels were independently associated with progression to end-stage renal diseases (Ma et al., 2021a). These biomarkers provided new ideas for treating renal fibrosis. EVR may delay impaired autophagic flux and block the activation of the NF-kB pathway (Wang et al., 2019), and rAAV9 acts as a carrier of miR-29b anti-fibrotic factors (Xu et al., 2020). Twist1/galectin-3 signaling pathway regulates macrophage plasticity (M2 phenotype) and promotes renal fibrosis (Liu et al., 2021). However, the underlying mechanisms of renal fibrosis have not been fully elucidated, and current treatments can only delay disease progression. Therefore, exploring novel potential drug targets are of great significance for the treatment of renal fibrosis (Sun et al., 2022).

Massive gene expression profiling databases provide opportunities to discover novel prognostic and predictive biomarkers using sophisticated deep learning algorithms. These datasets also allow extensive external validation (Sun et al., 2022). We first searched three datasets from the GEO database, removed the batch correspondence through the SVA algorithm, and merged them into the training dataset. We then performed a panel of 21 putative m6A regulators (7 writers, 12 readers and 2 erasers) to identify distinct patterns of m6A methylation modification. We then performed an unsupervised consensus clustering analysis of 175 renal fibrosis samples based on the expressions of 21 m6A regulators. To further clarify the role of m6A modification patterns in the immune microenvironment, we used the ESTIMATE algorithm to evaluate immune infiltration characteristics in different m6A patterns. We next analyzed the expression of canonical immune checkpoints and immune-related genes with distinct m6A modification patterns. We then performed the WGCNA analysis using the expression data of 1,611 drug targets obtained from the GeneCards database to identify 474 genes associated with m6A modification. 92 overlapping drug targets between WGCNA and DEGs (renal fibrosis vs. normal samples) were defined as key drug targets. A prediction model for renal fibrosis composed of five drug targets was developed using LASSO regression and stepwise logistic regression (LASSO-LR). The ROC curve shows that the risk model has an excellent predictive performance. Finally, we performed drug sensitivity and gene and extracellular matrix analysis. Five genes

were significantly associated with drug sensitivity and extracellular matrix activity.

Materials and methods

RNA-sequencing data and data preprocessing

The expression profile dataset was searched from the NCBI GEO database (http://www.ncbi.nlm.nih.gov/geo/) with "Renal fibrosis, *Homo sapiens*" as keywords, and a total of three sets of expression data. The analysis of the m6A modulators was performed after batch effects were removed by the SVA algorithm.

Identification of m6A-modified subtypes

An unsupervised consensus clustering analysis was performed on 175 renal fibrosis samples based on the expressions of 21 m6A regulators. The principal component analysis (PCA) showed that the three subtypes could clearly distinguish the samples. We performed the GSVA analysis using the R package. The GSVA algorithm calculated the m6A score between the three subtypes. Significant differences in the m6A score were found among the three subtypes.

Immune infiltration characterization

We obtained microenvironment scores through the ESTIMATE package to quantify the immune microenvironment (TME) levels across different m6A patterns. We further employed the CIBERSORT method to compare the infiltration levels of 22 immune cells among the three m6A subtypes. Finally, we performed a GSVA enrichment analysis of the enrichment scores for the immune gene set using the R package. The results showed significant differences in the enrichment of 17 immune gene sets among the three m6A subtypes. Adjusted $p < 0.05$ was considered statistically significant.

Detection of m6A modification-related drug target modules based on WGCNA

WCGNA clustered drug targets with similar expression patterns to construct a scale-free gene co-expression network and analyzed the correlation between modules and specific phenotypes (m6A modified subtypes). According to the correlation between modules and target genes and the correlation between modules, important target gene modules are screened. It has significant advantages in analyzing gene association patterns as a comprehensive biological algorithm. Two of its highlights are clustering modules with genes with similar expression patterns and the correlation analysis between modules and m6A-modified subtypes. This study performed a hierarchical cluster analysis on the expression profiles to exclude outliers. Subsequently, the Pearson correlation coefficient of any two genes was calculated, and a correlation matrix was established. The topological overlap matrix was transformed into a topological overlap matrix using the topological overlap matrix similarity function. Co-expressed genes were assigned into modules by a dynamic minimal tree-cutting algorithm. The module genes with the highest correlation were obtained for subsequent analysis.

Differential identification and functional enrichment analysis

DAVID is an online bioinformatics tool designed to predict many gene functions. Therefore, we used DAVID to observe the gene enrichment of the pathways ($p < 0.05$). We used the clusterProfiler R package to perform a functional annotation of the key genes.

Least absolute contraction and selection operator analysis

Drug targets associated with renal fibrosis were integrated in least absolute contraction and selection operator (LASSO) regression to identify prognostic biomarkers. We use the "timeeroc" package to plot the receiver operator characteristic (ROC) curves of the datasets separately. Then, we calculated and compared the area under the curve (AUC) of the ROC curves to test the performance of the classifier.

qRT-PCR

Total RNA was extracted by the TRIzol reagent. Then, qRT-PCR was performed with One Plus Step (Thermo Fisher, United States) and SYBR Premix (Takara, Japan) following the manufacturer's instructions. The primer sequences of the relevant genes are listed in Supplementary Table S1. A unilateral ureteral obstruction (UUO) kidney disease model was established for harvesting fibrotic kidneys. C57Bl/6J mice (SLAC Laboratory Animal Company) were given left ureteral ligation to establish a UUO model as previously described (Guerquin et al., 2013).

Western blotting

To detect the EGR1 and PLA2G4A protein expression levels, the protein was extracted by a radio-immunoprecipitation assay protein lysis buffer (Beyotime Institute of Biotechnology) and

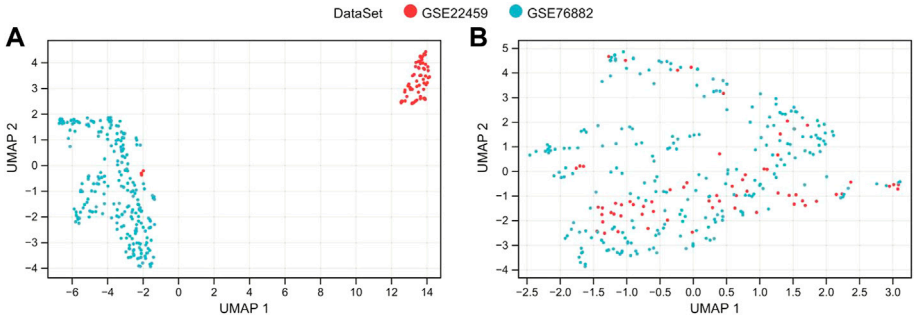

FIGURE 1
De-batch analysis. **(A,B)** are the sample step-by-step diagrams before and after de-batching, respectively.

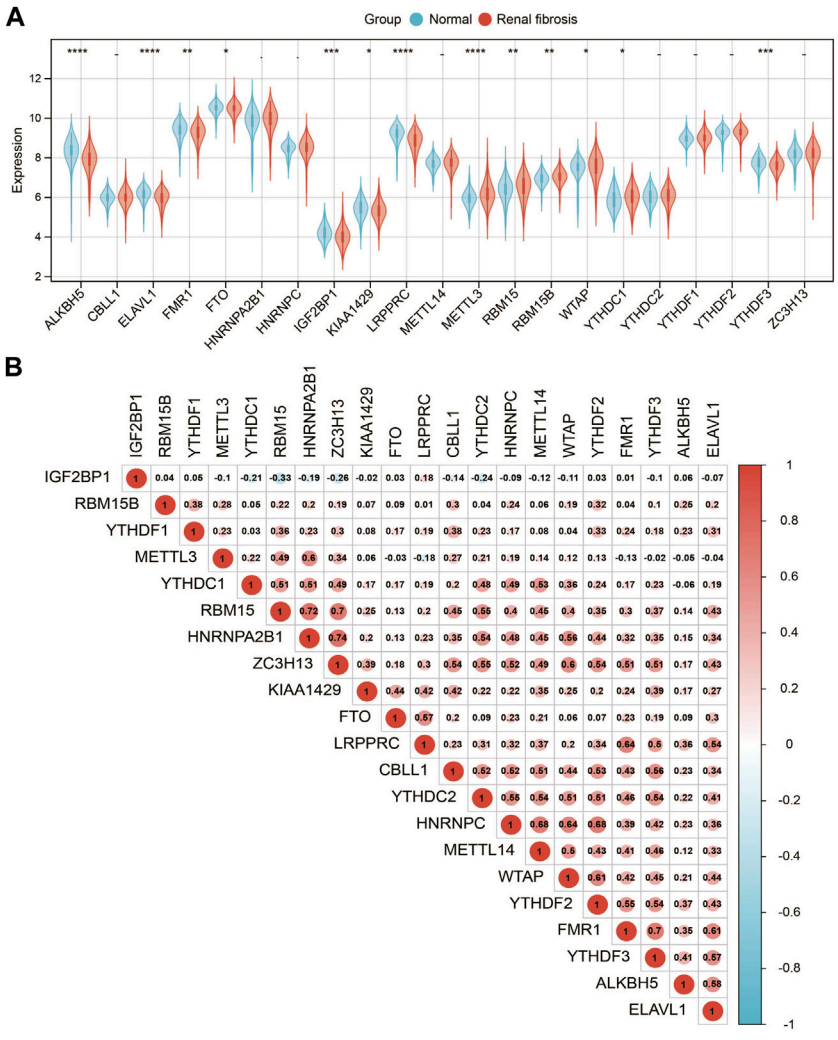

FIGURE 2
Expression landscape of m6A RNA methylation regulators in renal fibrosis. **(A)** Boxplot of the transcriptome expressions of 21 m6A regulators between healthy and renal fibrosis samples. **(B)** Heatmap of expression level correlations of 21 m6A regulators. * means *p* less than 0.05; ** means *p* less than 0.01, *** means *p* less than 0.001.

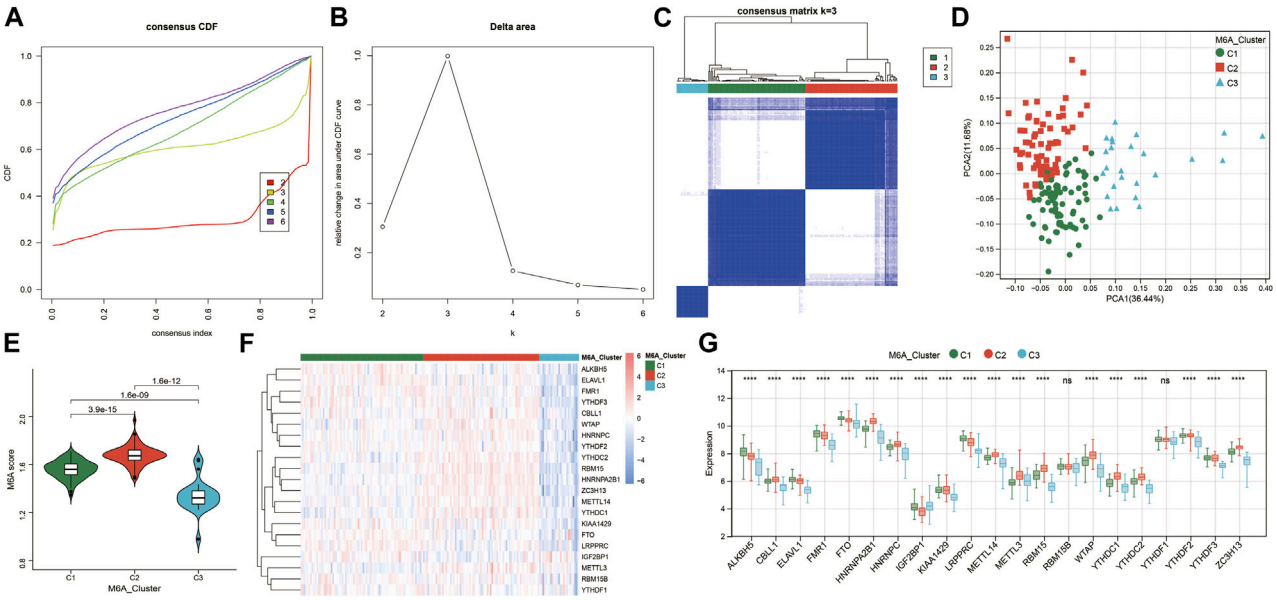

FIGURE 3
Identification of m6A-modified subtypes. **(A)** Consensus cluster cumulative distribution function (CDF) for k = 2–6. **(B)** Relative change in the area under the CDF curve at k = 2–6. **(C)** Consensus clustering matrix for optimal k = 3. **(D)** Principal component analysis (PCA) of the three m6A subtypes in renal fibrosis. **(E)** Violin plot of m6A score differences among the three m6A subtypes. **(F)** Heatmap of the m6A regulator expression among the three m6A subtypes. Red represents high expression and blue represents low expression. **(G)** The expression statuses of 21 m6A regulators in the three m6A subtypes. * means p less than 0.05; ** means p less than 0.01, *** means p less than 0.001.

FOCUS Global Fractionation kit (G-Biosciences). The proteins were separated by SDS-PAGE and transferred onto polyvinyl difluoride membranes. The membranes were incubated in 5 % non-fat milk for blocking, followed by incubation with primary antibodies EGR1 and PLA2G4A (1:1,000, Abclonal Technology) at 4°C overnight. Finally, the membranes were washed and incubated in a blocking buffer with horseradish peroxidase-conjugated secondary antibodies for 2 h before detection.

Results

Data collection and de-batch processing

Expression profile datasets were searched from the NCBI GEO database (http://www.ncbi.nlm.nih.gov/geo/; March 2022) with "Renal fibrosis, *Homo sapiens*" as keywords. A total of three sets of the expression data were obtained:

A. GSE22459: 65 samples; 25 normal and 40 renal fibrosis samples were included. Sequencing platform: GPL570.
B. GSE76882: Contains 234 samples; 99 normal and 135 renal fibrosis samples. Sequencing platform: GPL13158.
C. GSE57731: Contains 73 samples; 45 normal and 28 renal fibrosis samples. Sequencing platform: GPL17244 for the subsequent validation analysis.

Then, the SVA algorithm removed the two sets of the gene expression profile data of A and B and merged them into a training dataset containing 124 normal and 175 renal fibrosis samples. The sample relationship distribution before and after batch effect removal is shown in Figures 1A, B.

Expression landscape of m6A regulators

We analyzed a panel of 21 putative m6A regulators (7 writers, 12 readers, and 2 erasers) to identify distinct patterns of m6A methylation modification. As shown in Figures 2A 13 m6A regulators were significantly different between renal fibrosis and normal samples (p < 0.05). To explore the association between different m6A modulators, we describe the correlation pattern between three m6A modulators (Figure 2B).

Identification of m6A modification subtypes in renal fibrosis

To investigate the m6A modification patterns in renal fibrosis, we performed an unsupervised consensus clustering analysis of 175 renal fibrosis samples based on the expressions of 21 m6A regulators (Figures 3A–C). By setting the K value in the range of 2–6 and choosing the optimal K = 3, three different

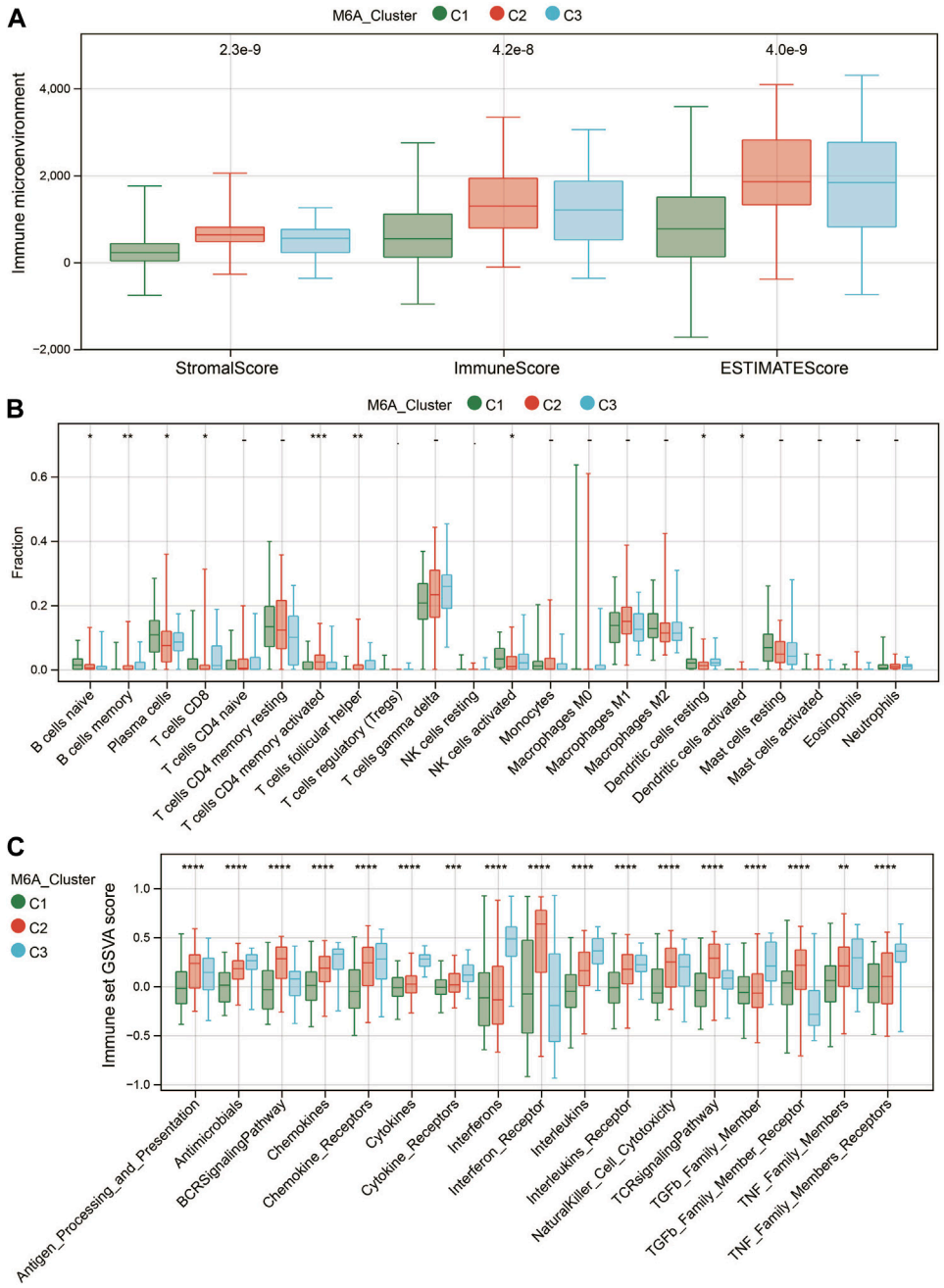

FIGURE 4
Characteristics of the immune microenvironment in different m6A modification patterns. **(A)** Differences in TME scores among the three m6A-modified subtypes. **(B)** Differences in the abundance of 22 immune cells among the three m6A modification patterns. **(C)** Differences in the activity of 17 immune response gene sets under the three m6A modification patterns. * means *p* less than 0.05; ** means *p* less than 0.01, *** means *p* less than 0.001.

m6A modified subtypes of renal fibrosis were identified, among which, C1, C2, and C3 contained 77, 73, and 25 samples, respectively. The principal component analysis (PCA) showed that the three subtypes could clearly distinguish the samples (Figure 3D). We calculated m6A scores by using the GSVA algorithm and found that m6A scores were significantly different among the three subtypes (Figure 3E). There are diverse m6A modification patterns. In addition, we also found 19 m6A

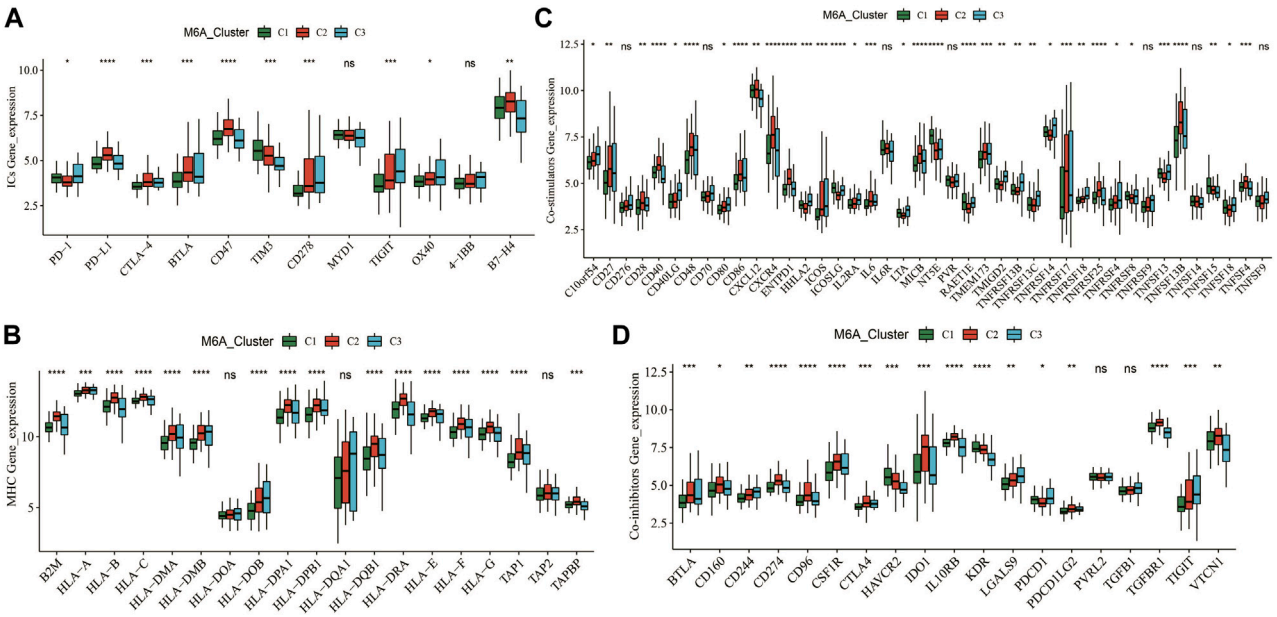

FIGURE 5
Expression patterns of typical immune-related genes. **(A–D)** Differential expression of immune checkpoint, MHC, co-suppression and co-stimulatory genes among different m6A clusters. * means *p* less than 0.05; ** means *p* less than 0.01, *** means *p* less than 0.001.

regulators whose expressions were significantly different among the three subtypes (Figures 3F,G). Notably, except for IGF2BP1, the remaining m6A regulators generated a unique m6A low transcription profile in C3.

Characteristics of immune infiltration in different m6A patterns

Recent studies have shown that the m6A modification of RNA plays a crucial role in forming immune responses and the immune environment. Then, we utilized the ESTIMATE algorithm to measure the immune microenvironment (TME) level. C2 exhibited higher immune and stromal scores (Figure 4A). We further compared the infiltration levels of 22 immune cells among the three m6A subtypes using the CIBERSORT method (Figure 4B). Nine significantly differentially expressed immune cells (DICs) were found ($p < 0.05$). To better illustrate the immune gene set activity changes among m6A modified subtypes, we calculated the enrichment scores for 17 immune gene sets from the ImmPort database using GSVA. The results showed significant differences in the enrichment of the 17 immune gene sets among the three m6A subtypes (Figure 4C). These results demonstrated that m6A methylation modification had an essential regulatory role in shaping different immune microenvironments in renal fibrosis.

Immune checkpoints, MHC, co-suppression, and co-stimulatory molecular signatures in different m6A patterns

We further analyzed the expression of canonical immune checkpoints and immune-related genes with different m6A modification patterns. The expressions of PD-1, PD-L1, CTLA-4, BTLA, CD47, TIM3, CD278, TIGIT, OX40, and B7-H4 were significantly different among the three subtypes (Figure 5A). In addition, the expressions of multiple MHC, co-stimulatory, and co-repressor-related genes were significantly different across m6A (Figures 5B–D). This means that the m6A modification patterns may benefit more from immunotherapy responses.

WGCNA analysis revealed m6A modification-related drug targets

The m6A modification subtype was used as the clinical feature to implement the WGCNA analysis. The expression data of 1,611 drug targets that were obtained from the GeneCards database (relevance score >7) were used. We set the network construction parameter and calculated the scale-free distribution topology matrix. As shown in Figure 6A, we selected

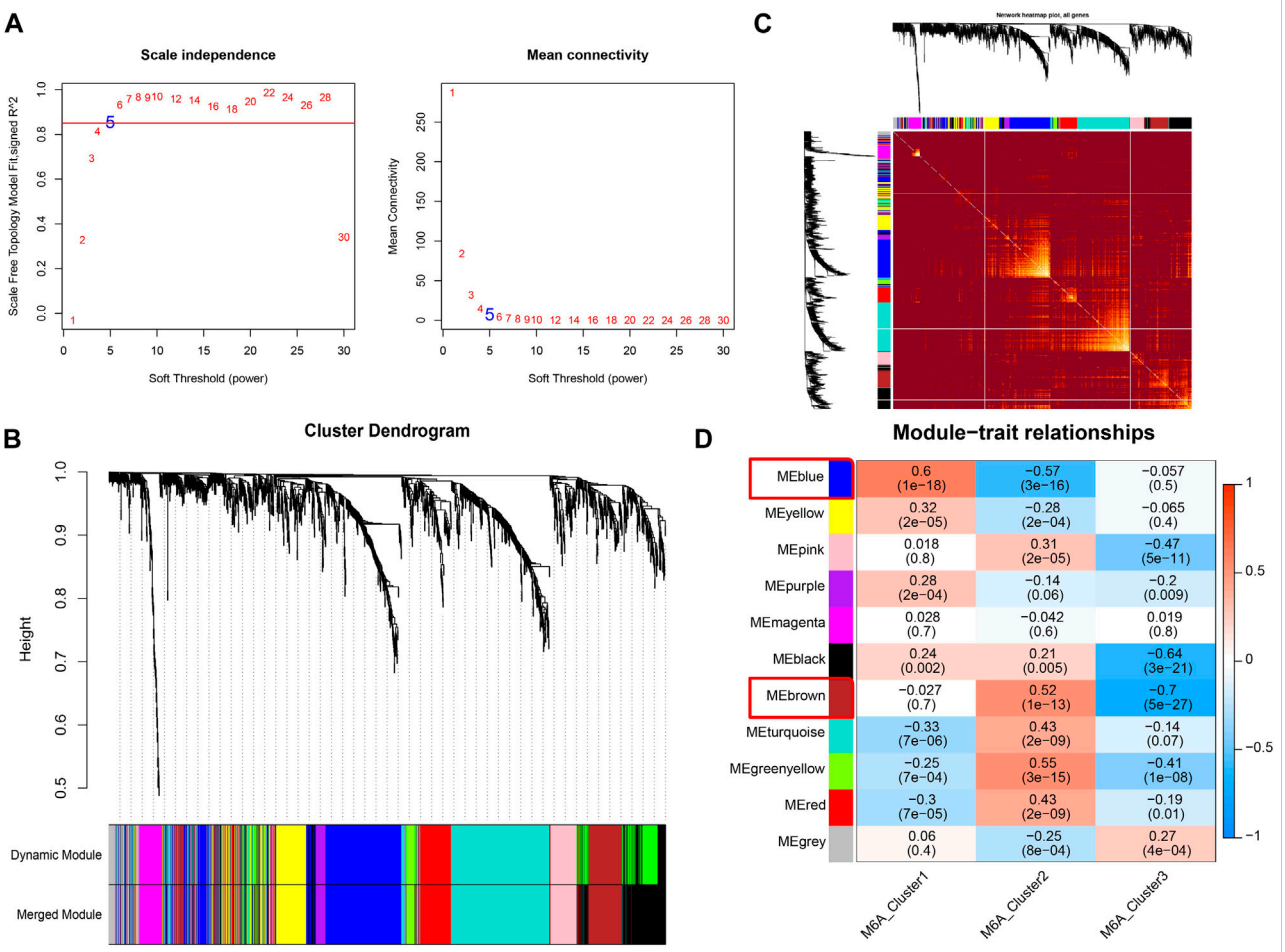

FIGURE 6
Co-expression identifies drug targets associated with m6A modification. **(A)** Left image: Adjacency matrix weight parameter power selection graph. The horizontal axis represents the weight parameter power, and the vertical axis represents the square of the correlation coefficient between log (k) and log [p(k)] in the corresponding network. The higher the squared value of the correlation coefficient, the closer the network is to the distribution without network scale. The red line represents the standard line where the squared value of the correlation coefficient reaches 0.85. Right image: Schematic diagram of the average connection degree of genes under different adjacency matrix weight parameters, power parameter. The red line represents the value of the average connection degree of network nodes under the value of the power parameter of the adjacency matrix weight parameter in the left image. **(B)** Module division tree diagram. Each color represents a different module. **(C)** Heatmap of the Topological Overlap Metric (TOM) matrix. Light yellow represents lower TOM, and darker red represents higher TOM. **(D)** Heatmap of the correlations of individual modules with m6A-modified subtypes.

the power five when the squared value of the correlation coefficient reached 0.85 for the first time (red line). The 1,611 drug targets were divided into 11 modules based on dynamic pruning (Figure 6B) and topological overlap measurement (TOM) clustering (Figure 6C). Subsequently, the associations between each module and clinical features were calculated (Figure 6D). We selected the blue and brown modules with the highest degree of correlation with m6A modified subtypes. Therefore, the 474 genes in blue and brown modules served as m6A modification-related drug targets for the subsequent analysis.

Differential gene identification and functional enrichment analysis

To understand the association between drug targets and renal fibrosis, we performed a differential gene analysis on renal fibrosis and normal samples based on the expression of 1,611 drug targets (FDR<0.05). 289 drug targets with altered expressions were identified (|log2FC|>0.5; Figure 7A). 92 overlapping drug targets between WGCNA and DEGs were defined as key drug targets (Figure 7B). To characterize the roles and underlying mechanisms of key genes, we performed

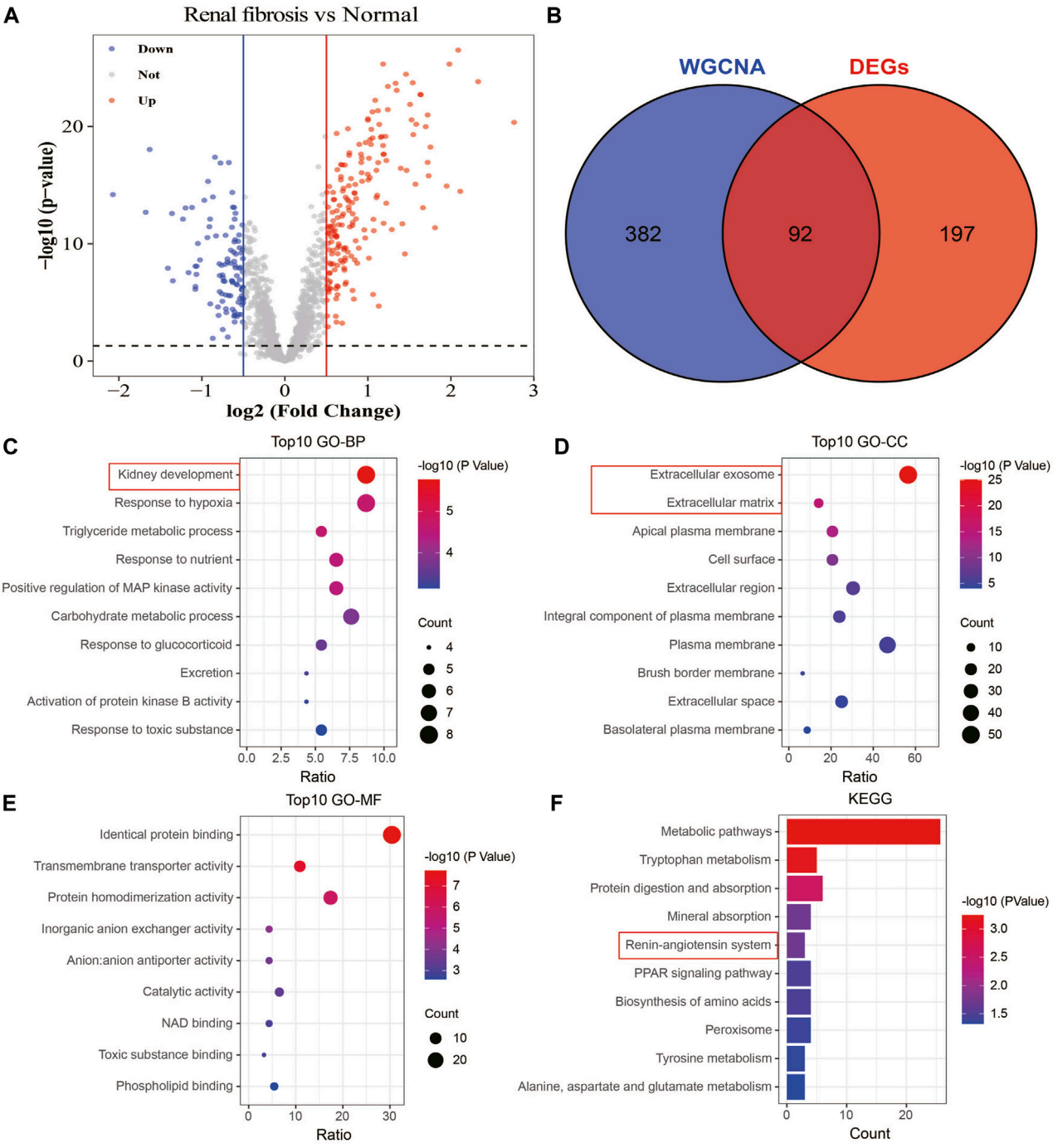

FIGURE 7
Identification and enrichment analysis of key drug targets. **(A)** Volcano plot showing information on changes in the expressions of drug targets between healthy and renal fibrosis samples. **(B)** Venn plot of the intersection of WGCNA and differential analysis. **(C)** Biological processes of the key drug targets. **(D)** Cellular components involved in the key drug targets. **(E)** Molecular functions of the key drug targets. **(F)** Signaling pathways involved in the key drug targets.

Gene Ontology (GO) and KEGG analyses. The analyses showed that key genes were mainly related to kidney development, extracellular exosome, extracellular matrix, and the angiotensin system (Figures 7C–F). These findings suggest that key drug targets may be involved in the development and progression of renal fibrosis.

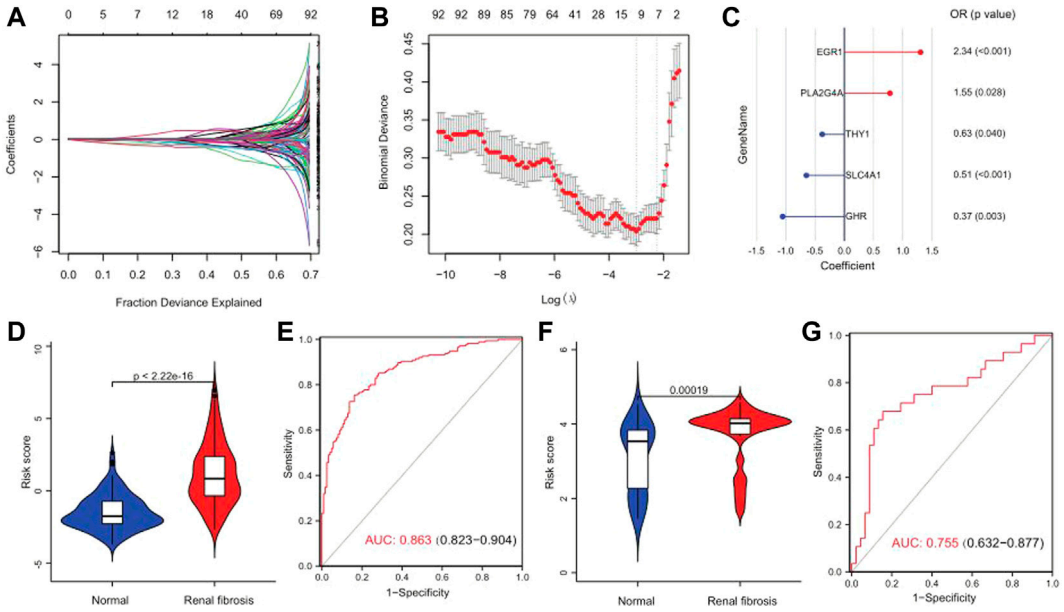

FIGURE 8
Risk scores can differentiate healthy and renal fibrosis samples. **(A)** Distribution of the LASSO coefficients for 92 drug targets. **(B)** 10-fold cross-validation with adjusted parameter selection in LASSO regression. Partial likelihood deviations are plotted against log (λ), where λ is the tuning parameter. **(C)** A gene signature with five drug targets was developed by stepwise logistic regression, and risk scores were calculated. **(D)** Violin plot of the risk score distribution between normal samples and renal fibrosis in the training set. **(E)** Predicted ROC curve for the risk scores in the training set. **(F)** Distribution of the differences in risk scores between normal samples and renal fibrosis in the GSE57731 validation set. **(G)** Predicted ROC curve of the GSE57731 validation central risk score.

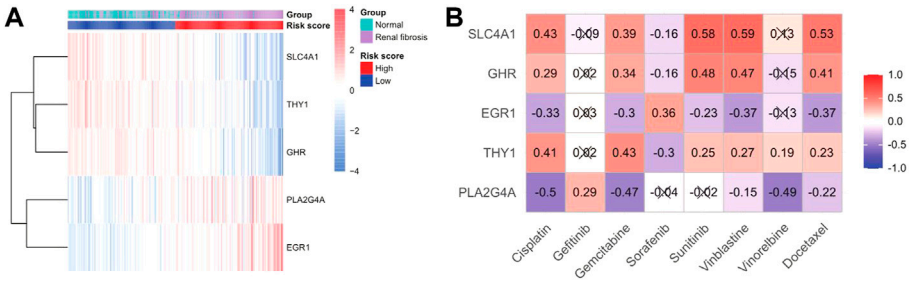

FIGURE 9
Sensitivity analysis of gene and drug therapy. **(A)** Heatmap of the expression of model genes in disease and risk groups. **(B)** Heatmap of model gene–drug associations.

Construction and validation of a risk model

A series of bioinformatics algorithms were used to further study the contribution of the key drug targets to the pathogenesis of renal fibrosis. First, we performed feature selection and dimensionality reduction on 92 drug targets related to renal fibrosis by using LASSO regression and found 11 important drug targets (Figures 8A,B). Subsequently, we developed a predictive model composed of five drug targets using stepwise logistic regression to diagnose renal fibrosis (Figure 8C). Finally, we calculated the risk score for each sample with the five drug target expression values and regression coefficients. The risk score is calculated as follows: RiskScore = 10 + (0.4402 × PLA2G4A) + (−0.4683 × THY1) + (0.8501 × EGR1) + (-0.9986 × EGR1) + (−0.6811 × SLC4A1). The risk score could differentiate between healthy and renal fibrosis samples well, with renal

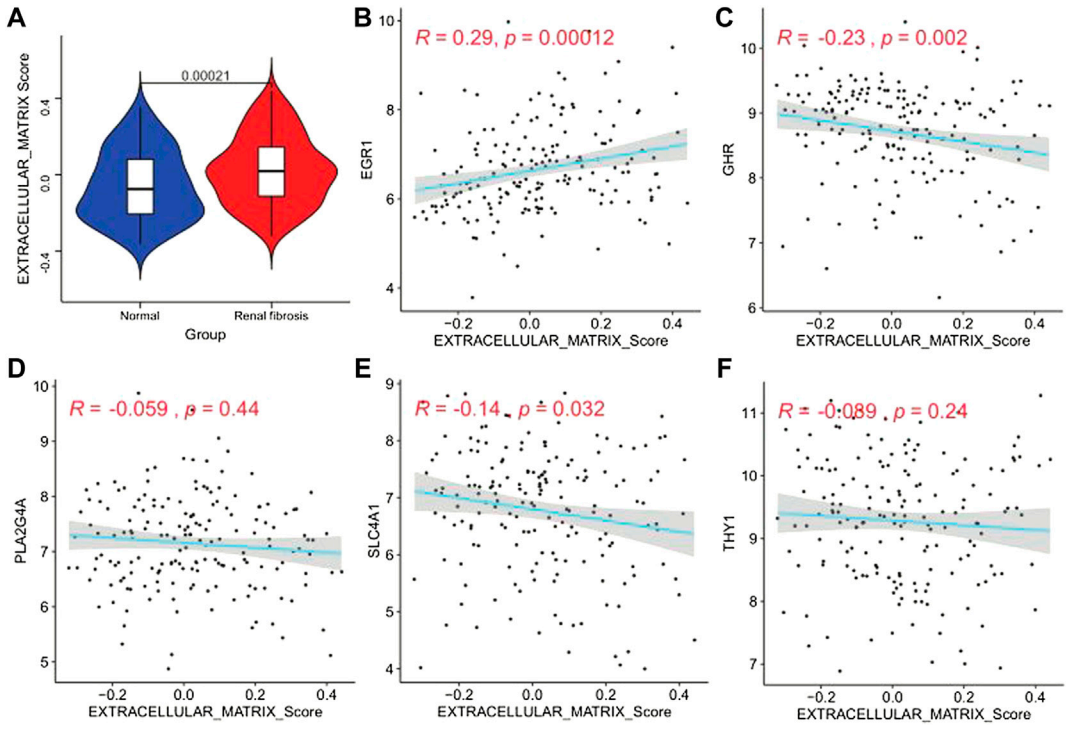

FIGURE 10
Extracellular matrix activity profile. **(A)** Differential distribution of extracellular matrix activity in normal and renal fibrotic tissues, **(B–F)** scatter of the correlations between five genes (EGR1, GHR, PLA2G4A, SLC4A1, and THY1) and extracellular matrix activity in renal fibrotic tissues.

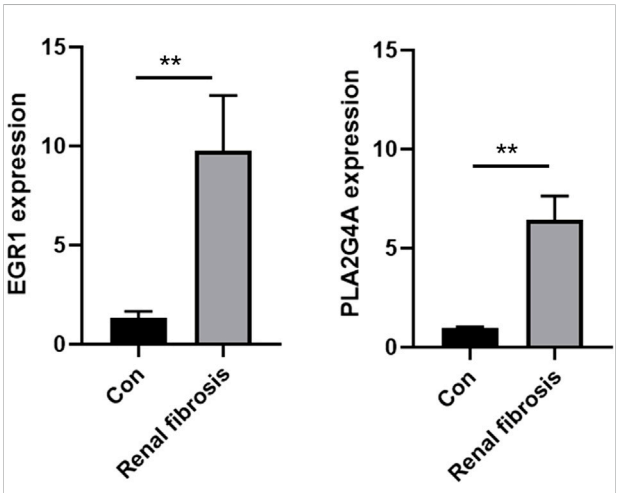

FIGURE 11
EGR1 and PLA2G4A mRNA expressions were analyzed by using the qRT-PCR assay in renal fibrosis and adjacent normal tissues.

fibrosis having a much higher risk score than the healthy samples (Figure 8D). The ROC curve showed that the risk score (AUC = 0.863) performed well in predicting renal fibrosis (Figure 8E). In addition, the external validation set GSE57731 also further confirmed the predictive performance of the risk score (AUC = 0.755) (Figures 8F,G). Therefore, these results indicate that the risk model has excellent predictive performance.

Drug sensitivity analysis

We drew a heat map of the model genes to further explore the role of model genes in the development of renal fibrosis and the correlation between drug treatments (Figure 9A). We found that SLC4A1, THY1, and GHR were significantly under-expressed in renal fibrosis, and PLA2G4A and EGR1 were significantly over-expressed compared with the normal group. Subsequently, the sensitivity of each renal fibrosis patient to drug treatment was estimated based on the Genomics of Cancer Drug Sensitivity (GDSC) database. IC50 quantification was performed by the pRRophetic package in R. We compared the IC50 levels of five model genes with eight drugs (Figure 9B) and found that the IC50 levels of cisplatin, gemcitabine, vinblastine, and docetaxel significantly correlated with the expressions of the five model genes.

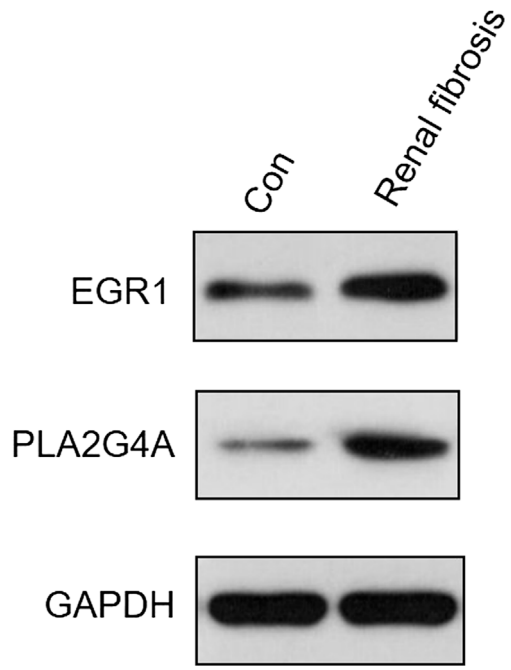

FIGURE 12
EGR1 and PLA2G4A protein expressions were analyzed by Western blot in renal fibrosis and adjacent normal tissues.

Analysis of genes and extracellular matrix

Studies have found that renal fibrosis is significantly correlated with the extracellular matrix. Therefore, we used the GSVA enrichment analysis to evaluate the activation state of the extracellular matrix. The extracellular matrix enrichment in renal fibrosis scores was significantly higher than that of normal tissues (p = 0.00021; Figure 10A). We performed a correlation analysis to further explore the ECM activity status regulated by the five model genes (Figures 10B–F). We found that EGR1 was significantly positively correlated with ECM activity (r = 0.29, p = 0.00012). GHR (r = −0.23, p = 0.002) and SLC4A1 (r = −0.14, p = 0.032) were significantly negatively correlated with the extracellular matrix activity. PLA2G4A and THY1 did not correlate with the extracellular matrix activity.

Validating the expression levels of EGR1 and PLA2G4A *via* qRT-PCR and Western blot

The expression levels of both EGR1 and PLA2G4A were detected in renal fibrosis and adjacent normal tissues by qRT-PCR and Western blot method. Our results revealed that, compared with normal tissues, the EGR1 and PLA2G4A genes have higher expressions in tissues of renal fibrosis (p < 0.05) (Figure 11). It was consistent with the PCR results that EGR1 and PLA2G4A have the higher protein expression in the tissues of renal fibrosis as validated by the Western blot analysis (Figure 12).

Discussion

Our study analyzed three datasets of gene expression profiles in whole blood, with batch effects removed by the SVA algorithm for subsequent analysis. First, an unsupervised consensus clustering analysis was performed based on the expressions of m6A regulators. The ESTIMATE algorithm evaluated the immune infiltration characteristics in different m6A patterns. Finally, the expression analysis of typical immune checkpoints and immune-related genes was performed. We developed a 5-gene predictive target gene signature based on the WGCNA of drug targets, differential gene analysis, logistic regression analysis, etc. Finally, we performed drug sensitivity and gene and extracellular matrix analysis. Five genes were significantly associated with drug sensitivity and extracellular matrix activity.

m6A is the most prevalent mRNA post-transcriptional methylation in eukaryotic cells (Cao et al., 2016). Especially in mammals, m6A-dependent mRNA modification is a critical process. It regulates multiple biological processes such as self-renewal and differentiation, DNA damage response, tissue development, RNA–protein interactions, and primary microRNA processing by regulating RNA splicing, stability, translocation, and translation into proteins (Cao et al., 2016). Growing literature studies have reported the critical role of m6A methylation in epigenetic regulation and how this modification affects the pathogenesis of various diseases, including renal injury. It has been reported that m6A is involved in the epithelial–mesenchymal transition of cancer cells and is regulated by methyltransferases, demethylases, and m6A-binding proteins (Ma et al., 2021a). Recent evidence suggests that m6A methylation is associated with acute kidney injury (Wang et al., 2019; Xu et al., 2020).

It is known that in the study of key cancer genes, using the gene signature as the input for feature selection may be a better modeling algorithm than genome-wide gene expression profiles when using expression regression models of the lasso strategy (Liu et al., 2021). Traditional genome-wide analysis has been used for an early diagnosis and prognostic model of renal fibrosis (Sun et al., 2022). The reported biomarkers also indicated that renal fibrosis was closely related to immunity, which is consistent with our conclusion. But the correlation with the extracellular matrix is not mentioned in the study. However, we studied the modification pattern based on m6A and found that different m6A modified subtypes have different immune infiltrations. In addition, the key drug targets we found are closely related to the

extracellular matrix, indicating the feasibility of our m6A-based gene signature may be more convincing and feasible.

This study revealed that the progression of renal fibrosis is closely related to the m6A methylation pattern. m6A methylation is an abundant endoepigenetic modification that has recently received much attention. Recent studies have shown that m6A modification is essential in regulating immune responses. We divided renal fibrosis patients into three subtypes with different prognoses and different immune statuses based on 21 m6A modulators. Renal fibrosis, a pathological change driven by inflammatory responses and calcium desposits, is a feature of renal transplant failure (Hu et al., 2022). However, it is difficult to characterize the immune status of a specific patient due to the immune heterogeneity in renal fibers. While immune function is broadly regulated by m6A methylation (Li et al., 2021), the three m6A subtypes have enhanced the understanding of the molecular characteristics and subpopulation-specific immune status of renal fibers. These results help predict the clinical treatment outcome of renal fibrosis and search for drug targets. Our follow-up study found significant differences in the expression of immune checkpoints and immune-related genes in different m6A patterns. This means that m6A modification patterns may benefit more from immunotherapy responses. Subsequent analysis of key drug targets based on m6A modified subtypes revealed that key genes were associated with the extracellular matrix, consistent with previous studies on the progression of renal fibrosis (Bülow and Boor, 2019).

EGR1 (Early Growth Response 1) has long been dysregulated in many cancers and is known to regulate tumor progression, making it an attractive target for cancer therapy (Saha et al., 2021). EGR1-activated LINC01503 epigenetically silences the DUSP5/CDKN1A expression, mediating cell cycle progression and tumorigenesis (Su et al., 2019; Ma et al., 2021b). Another example is the loss of Nm23-H1 in invasive breast cancer caused by the downregulation of CTCF and EGR1 (Wong et al., 2021). EGR1 may interact with DNMT3L, inhibit the miR-195-AKT3 axis, and regulate gastric cancer cell apoptosis (Yang et al., 2019). There is a strong correlation between the EGR1 expression and HIV reactivation, with the active transcription in response to the peak expression of EGR1 (Wong et al., 2022). Curcumin sensitizes prolactinoma cells to bromocriptine by activating ERK/EGR1 and inhibiting the AKT/GSK-3β signaling pathway *in vitro* and *in vivo* (Tang et al., 2021). The high expression of EGR1 promotes the proliferation of mast cells, plasma cells, and macrophages, which promote the expansion of the abdominal aorta and affect the immune process (Guo et al., 2022).

The GHR signaling pathways play important roles in growth, metabolism, cell cycle control, immunity, homeostatic processes, and chemoresistance. Dysregulation of GHR signaling is associated with various diseases and chronic diseases, such as acromegaly, cancer, aging, metabolic diseases, fibrosis, inflammation, and autoimmunity (Strous et al., 2020). Wang et al. (2020) showed that GHR gene polymorphisms are associated with esophageal cancer in the general population, and GHR signaling can be applied to cancers and other therapeutic strategies (Gao et al., 2020). The extracellular domain of GHR can be cleaved during shedding, reducing the number of cell-surface signaling receptors, which modulate the sensitivity of cells to GH (Frank, 2001). In muscle tissue, GHR disruption has been reported to enhance insulin sensitivity and prolong lifespan (List et al., 2020).

Phospholipase A2-iva (PLA2G4A) is the most abundant subtype of cytosolic phospholipase A2 (cPLA2) and is an important enzyme in tumorigenesis (Zhang et al., 2018). The eicosanoid signaling pathway based on arachidonic acid (AA) is involved in the development of human cancer. The cytoplasmic phospholipase A2-α (cPLA2α) encoded by the PLA2G4A gene acts as an upstream regulator of the eicosanoid signaling pathway by providing intracellular AA (Bazhan and Khaniani, 2018). Studies have shown that the PLA2G4A gene can be used as a biomarker in various diseases such as gastric cancer (Bazhan and Khaniani, 2018), acute myeloid leukemia (Hassan et al., 2021; Lai et al., 2021), cholangiocarcinoma (Sun et al., 2019), and colorectal cancer (Zhan et al., 2021a). PLA2G4A activates the colorectal cancer microenvironment to produce pro-cytokines IL-17A and adenosine, thereby establishing an effective immunosuppressive microenvironment and promoting immune evasion and tumor metastasis (Zhan et al., 2021b). Trametinib inhibits the cell viability and signaling of organoids to a greater extent by inhibiting the expression of PLA2G4A (Klotsman et al., 2007).

SLC4A1 is a member of the solute carrier family 4 (Zhang et al., 2021b). Studies have shown that this gene is associated with distal renal tubular acidosis (Elhayek et al., 2013; Deejai et al., 2019). The epithelial transporter SLC4A1 is involved in immune response-related biological processes and is characterized by its upregulation in kidney transplantation (Hruba et al., 2019). It is involved in regulatory pathways, including immune response, granulocyte activation, and T cell activation (Han et al., 2021). The SLC4A1-related pathway analysis revealed increased gene enrichment in extracellular matrix–receptor interactions and axon guidance pathways (Saraf et al., 2018). Thymocyte differentiation antigen-1 (THY1) has been reported to affect lung fibroblast proliferation and fibrotic signaling (Chen et al., 2019). In addition, a high expression of Thy1 was associated with poorer recurrence-free survival in breast cancer patients. Thy1 methylation may track the transfer of bipotent progenitors to differentiated cells. Thy1 is a good candidate biomarker for basal-like breast cancer. Thy1 expression was downregulated in xenografts due to promoter methylation. Thy1-knockdown responded to targeted therapy with increased EGFR and Notch1 expressions. THY1 is doxorubicin-resistant in tumors of offsprings exposed to high-fat diets (Montales et al., 2016). Skeletal muscle from patients with type 2 diabetes exhibits degenerative remodeling of the extracellular matrix, which is associated with a selective increase in a subset of fibrolipogenic progenitors marked by the expression of THY1 (Farup et al., 2021). Since DNA

methylation is often altered in early cancer development, candidate methylation markers may be used as biomarkers for basal-like breast cancer (Montanari et al., 2019).

Conclusion

Renal fibrosis is a process of wound-healing failure in renal tissue after chronic injury, calcium deposits, and inflammation. In the study, we used an integrated bioinformatics approach, machine learning, regression algorithms, and *in vitro* experiments to study m6A modifications and drug targets in renal fibrosis. We identified three different m6A subtypes of renal fibrosis through an unsupervised consensus clustering analysis and evaluated immune infiltration characteristics and the expression of immune checkpoints and immune-related genes among distinct m6A subtypes. Overlapping drug targets between WGCNA and DEGs were defined as key drug targets. We used LASSO-SLR to develop a 5 drug target-based prediction model to diagnose renal fibrosis. The 5-gene model had a good predictive effect and was significantly associated with many drugs and extracellular matrix activities. The expression levels of both predictive signature genes EGR1 and PLA2G4A were validated in renal fibrosis and adjacent normal tissues by using the qRT-PCR and Western blot methods.

Data availability statement

The original contributions presented in the study are included in the article/Supplementary Material; further inquiries can be directed to the corresponding authors.

Author contributions

Writing—original draft preparation, CL, SL, and YW; writing—review and editing, SW and XS; data processing, YZ, QW, and TP; supervision, XP and JL; All authors have read and agreed to the published version of the manuscript.

Funding

This research was supported by NSFC Incubation Project of Guangdong Provincial People's Hospital (KY0120220029) and Medical Science and Technology Research Foundation of Guangdong Province (2021112601417154).

Conflict of interest

The authors declare that the research was conducted in the absence of any commercial or financial relationships that could be construed as a potential conflict of interest.

Publisher's note

Supplementary material

The Supplementary Material for this article can be found online at: https://www.frontiersin.org/articles/10.3389/fphar.2022.909784/full#supplementary-material

SUPPLEMENTARY FIGURE S1
Correlation box plot of M6A_Cluster and Disease_state.

SUPPLEMENTARY TABLE S1
Primers used in PCR.

References

Bazhan, D., and Khaniani, M. S. (2018). Supplementation with omega fatty acids increases the mRNA expression level of PLA2G4A in patients with gastric cancer. *J. Gastrointest. Oncol.* 6, 1176–1183. doi:10.21037/jgo.2018.08.12

Bülow, R. D., and Boor, P. (2019). Extracellular matrix in kidney fibrosis: More than just a scaffold. *J. Histochem. Cytochem.* 9, 643–661. doi:10.1369/0022155419849388

Cao, G., Li, H. B., Yin, Z., and Flavell, R. A. (2016). Recent advances in dynamic m6A RNA modification. *Open Biol.* 4, 160003. doi:10.1098/rsob.160003

Chen, L., Tang, R., Ruan, J., Zhu, X., and Yang, Y. (2019). Up-regulation of THY1 attenuates interstitial pulmonary fibrosis and promotes lung fibroblast apoptosis during acute interstitial pneumonia by blockade of the WNT signaling pathway. *Cell. CYCLE* 6-7, 670–681. doi:10.1080/15384101.2019.1578144

Cilluffo, G., Fasola, S., Ferrante, G., Malizia, V., Montalbano, L., and La Grutta, S. (2021). Machine learning: An overview and applications in pharmacogenetics. *Genes.* 10, 1511. doi:10.3390/genes12101511

Deejai, N., Wisanuyotin, S., Nettuwakul, C., Khositseth, S., Sawasdee, N., Saetai, K., et al. (2019). Molecular diagnosis of solute carrier family 4 member 1 (SLC4A1) mutation–related autosomal recessive distal renal tubular acidosis. *Lab. Med.* 1, 78–86. doi:10.1093/labmed/lmy051

Deng, B., Yang, W., Wang, D., Cheng, L., Bu, L., Rao, J., et al. (2020). Peptide DR8 suppresses epithelial-to-mesenchymal transition via the TGF-β/MAPK signaling pathway in renal fibrosis. *LIFE Sci.* 261, 118465. doi:10.1016/j.lfs.2020.118465

Dockès, J., Varoquaux, G., and Poline, J. (2021). Preventing dataset shift from breaking machine-learning biomarkers. *GigaScience* 9, giab055. doi:10.1093/gigascience/giab055

Elhayek, D., Perez, D. N. G., Chouchane, S., Hamami, S., Mlika, A., Troudi, M., et al. (2013). Molecular diagnosis of distal renal tubular acidosis in Tunisian patients: Proposed algorithm for northern africa populations for the ATP6V1B1, ATP6V0A4 and SCL4A1 genes. *BMC Med. Genet.* 14, 119. doi:10.1186/1471-2350-14-119

Farup, J., Just, J., de Paoli, F., Lin, L., Jensen, J. B., Billeskov, T., et al. (2021). Human skeletal muscle CD90(+) fibro-adipogenic progenitors are associated with muscle degeneration in type 2 diabetic patients. *Cell. Metab.* 11, 2201–2214.e11. doi:10.1016/j.cmet.2021.10.001

Field, M., Hardcastle, N., Jameson, M., Aherne, N., and Holloway, L. (2021). Machine learning applications in radiation oncology. *Phys. Imaging Radiat. Oncol.* 19, 13–24. doi:10.1016/j.phro.2021.05.007

Frank, S. J. (2001). Growth hormone signalling and its regulation: Preventing too much of a good thing. *Growth Horm. IGF Res.* 4, 201–212. doi:10.1054/ghir.2001.0237

Gao, S., Ni, Q., Wu, X., and Cao, T. (2020). GHR knockdown enhances the sensitivity of HCC cells to sorafenib. *Aging (Albany NY)* 18, 18127–18136. doi:10.18632/aging.103625

Guerquin, M., Charvet, B., Nourissat, G., Havis, E., Ronsin, O., Bonnin, M., et al. (2013). Transcription factor EGR1 directs tendon differentiation and promotes tendon repair. *J. Clin. Invest.* 8, 3564–3576. doi:10.1172/JCI67521

Guo, C., Liu, Z., Yu, Y., Zhou, Z., Ma, K., Zhang, L., et al. (2022). EGR1 and KLF4 as diagnostic markers for abdominal aortic aneurysm and associated with immune infiltration. *Front. Cardiovasc. Med.* 9, 781207. doi:10.3389/fcvm.2022.781207

Han, Z., Feng, W., Hu, R., Ge, Q., Ma, W., Zhang, W., et al. (2021). RNA-seq profiling reveals PBMC RNA as a potential biomarker for hepatocellular carcinoma. *Sci. Rep.* 1, 17797. doi:10.1038/s41598-021-96952-x

Handelman, G. S., Kok, H. K., Chandra, R. V., Razavi, A. H., Lee, M. J., and Asadi, H. (2018). eDoctor: machine learning and the future of medicine. *J. Intern. Med.* 6, 603–619. doi:10.1111/joim.12822

Hassan, J. J., Lieske, A., Dörpmund, N., Klatt, D., Hoffmann, D., Kleppa, M., et al. (2021). A multiplex CRISPR-screen identifies PLA2G4A as prognostic marker and druggable target for HOXA9 and MEIS1 dependent AML. *Int. J. Mol. Sci.* 17, 9411. doi:10.3390/ijms22179411

Hruba, P., Krejcik, Z., Stranecky, V., Maluskova, J., Slatinska, J., Gueler, F., et al. (2019). Molecular patterns discriminate accommodation and subclinical antibody-mediated rejection in kidney transplantation. *TRANSPLANTATION* 5, 909–917. doi:10.1097/TP.0000000000002604

Hu, Z., Liu, Y., Zhu, Y., Cui, H., and Pan, J. (2022). Identification of key biomarkers and immune infiltration in renal interstitial fibrosis. *Ann. Transl. Med.* 4, 190. doi:10.21037/atm-22-366

Jia, H., Ma, T., and Hao, C. (2020). Identification of candidate lncRNA biomarkers for renal fibrosis: A systematic review. *LIFE Sci.* 262, 118566. doi:10.1016/j.lfs.2020.118566

Klotsman, M., York, T. P., Pillai, S. G., Vargas-Irwin, C., Sharma, S. S., van den Oord, E. J., et al. (2007). Pharmacogenetics of the 5-lipoxygenase biosynthetic pathway and variable clinical response to montelukast. *Pharmacogenet. Genomics* 3, 189–196. doi:10.1097/FPC.0b013e3280120043

Lai, Y., OuYang, G., Sheng, L., Zhang, Y., Lai, B., and Zhou, M. (2021). Novel prognostic genes and subclasses of acute myeloid leukemia revealed by survival analysis of gene expression data. *BMC Med. Genomics* 1, 39. doi:10.1186/s12920-021-00888-0

Li, Y., Qi, D., Zhu, B., and Ye, X. (2021). Analysis of m6A RNA methylation-related genes in liver hepatocellular carcinoma and their correlation with survival. *Int. J. Mol. Sci.* 3, 1474. doi:10.3390/ijms22031474

List, E. O., Duran-Ortiz, S., and Kopchick, J. J. (2020). Effects of tissue-specific GH receptor knockouts in mice. *Mol. Cell. Endocrinol.* 515, 110919. doi:10.1016/j.mce.2020.110919

Liu, B., Jin, Y., Xu, D., Wang, Y., and Li, C. (2021). A data calibration method for micro air quality detectors based on a LASSO regression and NARX neural network combined model. *Sci. Rep.* 1, 21173. doi:10.1038/s41598-021-00804-7

Ma, X., Long, C., Wang, F., Lou, B., Yuan, M., Duan, F., et al. (2021). METTL3 attenuates proliferative vitreoretinopathy and epithelial-mesenchymal transition of retinal pigment epithelial cells via wnt/β-catenin pathway. *J. Cell. Mol. Med.* 9, 4220–4234. doi:10.1111/jcmm.16476

Ma, Z., Gao, X., Shuai, Y., Wu, X., Yan, Y., Xing, X., et al. (2021). EGR1-mediated linc01503 promotes cell cycle progression and tumorigenesis in gastric cancer. *Cell. Prolif.* 1, e12922. doi:10.1111/cpr.12922

Montales, M. T., Melnyk, S. B., Liu, S. J., Simmen, F. A., Liu, Y. L., and Simmen, R. C. (2016). Metabolic history impacts mammary tumor epithelial hierarchy and early drug response in mice. *Endocr. Relat. Cancer* 9, 677–690. doi:10.1530/ERC-16-0136

Montanari, M., Carbone, M. R., Coppola, L., Giuliano, M., Arpino, G., Lauria, R., et al. (2019). Epigenetic silencing ofTHY1 tracks the acquisition of the notch1–EGFR signaling in a xenograft model of CD44+/CD24low/CD90+ myoepithelial cells. *Mol. Cancer Res.* 2, 628–641. doi:10.1158/1541-7786.MCR-17-0324

Nielsen, P. M., Mariager, C. Ø., Mølmer, M., Sparding, N., Genovese, F., Karsdal, M. A., et al. (2020). Hyperpolarized [1-13 C] alanine production: A novel imaging biomarker of renal fibrosis. *Magn. Reson. Med.* 4, 2063–2073. doi:10.1002/mrm.28326

Prakoura, N., Hadchouel, J., and Chatziantoniou, C. (2019). Novel targets for therapy of renal fibrosis. *J. Histochem. Cytochem.* 9, 701–715. doi:10.1369/0022155419849386

Saha, S. K., Islam, S., Saha, T., Nishat, A., Biswas, P. K., Gil, M., et al. (2021). Prognostic role of EGR1 in breast cancer: A systematic review. *BMB Rep.* 10, 497–504. doi:10.5483/bmbrep.2021.54.10.087

Saraf, S. L., Sysol, J. R., Susma, A., Setty, S., Zhang, X., Gudehithlu, K. P., et al. (2018). Progressive glomerular and tubular damage in sickle cell trait and sickle cell anemia mouse models. *Transl. Res.* 197, 1–11. doi:10.1016/j.trsl.2018.01.007

Strous, G. J., Almeida, A., Putters, J., Schantl, J., Sedek, M., Slotman, J. A., et al. (2020). Growth hormone receptor regulation in cancer and chronic diseases. *Front. Endocrinol.* 11, 597573. doi:10.3389/fendo.2020.597573

Su, T., Liu, P., Ti, X., Wu, S., Xue, X., Wang, Z., et al. (2019). HIF1α, EGR1 and SP1 co-regulate the erythropoietin receptor expression under hypoxia: An essential role in the growth of non-small cell lung cancer cells. *Cell. Commun. Signal.* 1, 152. doi:10.1186/s12964-019-0458-8

Sun, R., Liu, Z., Qiu, B., Chen, T., Li, Z., Zhang, X., et al. (2019). Annexin10 promotes extrahepatic cholangiocarcinoma metastasis by facilitating EMT via PLA2G4A/PGE2/STAT3 pathway. *EBioMedicine* 47, 142–155. doi:10.1016/j.ebiom.2019.08.062

Sun, Y., Qiu, Z., Wen, F., Yin, J., and Zhou, H. (2022). Revealing potential diagnostic gene biomarkers associated with immune infiltration in patients with renal fibrosis based on machine learning analysis. *J. Immunol. Res.* 20, 3027200. doi:10.1155/2022/3027200

Tang, C., Zhu, J., Yuan, F., Yang, J., Cai, X., and Ma, C. (2021). Curcumin sensitizes prolactinoma cells to bromocriptine by activating the ERK/EGR1 and inhibiting the AKT/GSK-3β signaling pathway *in vitro* and *in vivo*. *Mol. Neurobiol.* 12, 6170–6185. doi:10.1007/s12035-021-02541-4

Wang, J., Ishfaq, M., Xu, L., Xia, C., Chen, C., and Li, J. (2019). METTL3/m(6)A/miRNA-873-5p attenuated oxidative stress and apoptosis in colistin-induced kidney injury by modulating keap1/nrf2 pathway. *Front. Pharmacol.* 10, 517. doi:10.3389/fphar.2019.00517

Wang, R., Si, L., Zhu, D., Shen, G., Long, Q., and Zhao, Y. (2020). Genetic variants inGHR andPLCE1 genes are associated with susceptibility to esophageal cancer. *Mol. Genet. Genomic Med.* 10, e1474. doi:10.1002/mgg3.1474

Wong, K. M., Song, J., and Wong, Y. H. (2021). CTCF and EGR1 suppress breast cancer cell migration through transcriptional control of Nm23-H1. *Sci. Rep.* 1, 491. doi:10.1038/s41598-020-79869-9

Wong, L. M., Li, D., Tang, Y., Mendez-Lagares, G., Thompson, G. R., Hartigan-O'Connor, D. J., et al. (2022). Human immunodeficiency virus-1 latency reversal via the induction of early growth response protein 1 to bypass protein kinase C agonist-associated immune activation. *Front. Microbiol.* 13, 836831. doi:10.3389/fmicb.2022.836831

Xie, H., Miao, N., Xu, D., Zhou, Z., Ni, J., Yin, F., et al. (2021). FoxM1 promotes Wnt/β-catenin pathway activation and renal fibrosis via transcriptionally regulating multi-Wnts expressions. *J. Cell. Mol. Med.* 4, 1958–1971. doi:10.1111/jcmm.15948

Xu, Y., Yuan, X. D., Wu, J. J., Chen, R. Y., Xia, L., Zhang, M., et al. (2020). The N6-methyladenosine mRNA methylase METTL14 promotes renal ischemic

reperfusion injury via suppressing YAP1. *J. Cell. Biochem.* 1, 524–533. doi:10.1002/jcb.29258

Yan, H., Xu, J., Xu, Z., Yang, B., Luo, P., and He, Q. (2021). Defining therapeutic targets for renal fibrosis: Exploiting the biology of pathogenesis. *Biomed. Pharmacother.* 143, 112115. doi:10.1016/j.biopha.2021.112115

Yang, Y., Wu, F., Zhang, J., Sun, R., Li, F., Li, Y., et al. (2019). EGR1 interacts with DNMT3L to inhibit the transcription of miR-195 and plays an anti-apoptotic role in the development of gastric cancer. *J. Cell. Mol. Med.* 11, 7372–7381. doi:10.1111/jcmm.14597

Zhan, Y., Zheng, L., Liu, J., Hu, D., Wang, J., Liu, K., et al. (2021). PLA2G4A promotes right-sided colorectal cancer progression by inducing CD39+ γ δ Treg polarization. *Res. ARTICLE* 6, e148028. doi:10.1172/jci.insight.148028

Zhan, Y., Zheng, L., Liu, J., Hu, D., Wang, J., Liu, K., et al. (2021). PLA2G4A promotes right-sided colorectal cancer progression by inducing CD39+γδ Treg polarization. *JCI Insight* 16, 148028. doi:10.1172/jci.insight.148028

Zhang, R., Chen, Z., Song, Q., Wang, S., Liu, Z., Zhao, X., et al. (2021). Identification of seven exonic variants in theSLC4A1 , ATP6V1B1 , andATP6V0A4 genes that alter RNA splicing by minigene assay. *Hum. Mutat.* 9, 1153–1164. doi:10.1002/humu.24246

Zhang, W., Wang, X., Zhang, L., Geng, D., Wang, Y., Sun, D., et al. (2018). Inhibition of PLA2G4A reduces the expression of lung cancer-related cytokines. *DNA Cell. Biol.* 12, 1076–1081. doi:10.1089/dna.2018.4286

Zhang, X., Chen, Q., Zhang, L., Zheng, H., Lin, C., Yang, Q., et al. (2021). Tubule-specific protein nanocages potentiate targeted renal fibrosis therapy. *J. Nanobiotechnology* 1, 156. doi:10.1186/s12951-021-00900-w

frontiers | Frontiers in Pharmacology

TYPE Brief Research Report
PUBLISHED 04 January 2023
DOI 10.3389/fphar.2022.909668

OPEN ACCESS

EDITED BY
Jing Xie,
Sichuan University, China

REVIEWED BY
Hanwei Cui,
Shenzhen Samii Medical Center, China
Muhammad Farrukh Nisar,
Cholistan University of Veterinary and Animal Sciences, Pakistan

*CORRESPONDENCE
Ting Sun,
yc17622@umac.mo
Hua-Ping Liang,
13638356728@163.com

SPECIALTY SECTION
This article was submitted to Experimental Pharmacology and Drug Discovery, a section of the journal Frontiers in Pharmacology

RECEIVED 01 April 2022
ACCEPTED 02 December 2022
PUBLISHED 04 January 2023

CITATION
Chi Q, Wang D, Sun T and Liang H-P (2023), Integrated bioinformatical and *in vitro* study on drug targets for liver cirrhosis based on unsupervised consensus clustering and immune cell infiltration.
Front. Pharmacol. 13:909668.
doi: 10.3389/fphar.2022.909668

Integrated bioinformatical and *in vitro* study on drug targets for liver cirrhosis based on unsupervised consensus clustering and immune cell infiltration

Qingjia Chi[1,2], Di Wang[3], Ting Sun[4]* and Hua-Ping Liang[2]*

[1]Department of Engineering Structure and Mechanics, School of Science, Wuhan University of Technology, Wuhan, China, [2]State Key Laboratory of Trauma, Burns and Combined Injury, Department of Wound Infection and Drug, Research Institute of Surgery, Daping Hospital, Army Medical University, Chongqing, China, [3]School of Life Science and Engineering, Southwest Jiaotong University, Chengdu, Sichuan, China, [4]Surgical Laboratory, General Hospital of Ningxia Medical University,, Yinchuan, Ningxia, China

Liver cirrhosis is one of the most common cause of death in the world. The progress of liver cirrhosis involves health, liver cirrhosis and liver cancer, leading to great challenges in the diagnosis of the disease. Drug targets, which could be obtained conveniently, can help clinicians improve prognosis and treatment. Liver cirrhosis is associated with serum calcium levels. And studies reported Tanshinone IIA plays a therapeutic role in liver injury through activating calcium-dependent apoptosis. In this study, we explored the diagnostic key targets of Tanshinone IIA in liver cirrhosis through exploration of comprehensive dataset including health, liver cirrhosis and liver cancer patients. The unsupervised consensus clustering algorithm identified 3 novel subtypes in which differentially expressed genes (DEGs) between both subtypes were found by pairwise comparison. Then, 4 key drug targets of Tanshinone IIA were determined through the intersection of these DEGs. The diagnostic performance of target genes was assessed and further verified in the external dataset. We found that the 4 key drug targets could be used as effective diagnostic biomarkers. Then the immune scores in the high and low expression groups of target genes were estimated to identify significantly expressed immune cells. In addition, the immune infiltration of high and low target gene expression groups in several immune cells were significantly different. The findings suggest that 4 key drug targets may be a simple and useful diagnostic tool for predicting patients with cirrhosis. We further studied the carcinogenesis role of AKR1C3 and TPX2 *in vitro*. Both mRNA and protein expression in hepatoma carcinoma cells was detected using qRT-PCR and Western blot. And the knockdown of AKR1C3 and TPX2 significantly suppressed cell proliferation, migration and invasion.

KEYWORDS

liver cirrhosis, gene expression, prognostic value, immune microenvironment, unsupervised clustering

Introduction

Liver cirrhosis is a worrisome medical condition worldwide (Duah and Nkrumah, 2019). It is a sequelae of chronic liver diseases and is characterized by replacing liver tissue with fibrosis, scar tissue, and regenerative nodules (Wong, 2016). Cirrhosis can remain compensated for many years before a decompensation event occurs. Decompensated cirrhosis is an end-stage liver disease characterized by developing complications, including jaundice, variceal bleeding, ascites, and encephalopathy, and significantly reduced survival (EAF Of liver, 2018; Gines et al., 2021).

Common causes of liver cirrhosis are infection with hepatitis virus and alcohol-related liver disease. Liver cirrhosis is the 11th most common cause of death in the world. About 2 million people die from liver cirrhosis each year. In China, patients with cirrhosis account for 20% of the total patients with liver chronic. About 50% of the world's liver cancer death and 15% of liver cirrhosis occur in China (Tan et al., 2022). In China, more than 80% of patients developed HCC (Tsai et al., 2020) in the context of liver cirrhosis. There is no effective treatment for liver cirrhosis. Treatment is mainly concentrated on the cause and symptoms, which can only relieve the disease. It is difficult to predict the development and prognosis of liver cirrhosis. The uncertainty of the disease is likely to cause the deterioration of the medical behavior of the patient and the interruption of the disease treatment (Wu et al., 2022).

The 1-year mortality rate of compensated liver cirrhosis is 1%–3.4%, but the mortality rate after compensatory decompensation increases to 20%–57% (D'Amico et al., 2006). The high mortality of late liver cirrhosis highlights the necessity of prognostic improvement. Therefore, identifying diagnostic biomarkers and exploring reliable drug targets can guide clinical treatment. Liver cirrhosis is associated with serum calcium levels (Bandi et al., 1997; Kim et al., 2021). Platelet calcium ion depth was significantly lower in cirrhotic patients than in normal controls. Tanshinone IIA induces an increase in intracellular calcium and lead to increased mobilization (Yang et al., 2005; Fan et al., 2011). And studies reported Tanshinone IIA plays a therapeutic role in liver injury through activating calcium-dependent apoptosis (Dai et al., 2012). The drug targets can be obtained through simple, non-invasive, and repeated ways. Thus, key targets of Tanshinone IIA provided solutions for diagnosing liver cirrhosis and therapy intervention.

We previously used machine learning algorithms to examine the role of immune infiltration in various diseases (Xu et al., 2022; Zhao et al., 2022). In this paper, we have determined the clinical and prognosis of patients with cirrhosis and discussed their potential applications in the future. We generated three groups with significant differences through the unsupervised consensus cluster algorithm. The volcanic plot selected Differentially expressed genes (DEG) in these three groups. Then we used the Venn plot to determine the four key drug targets of Tanshinone IIA. Use the violin diagram to evaluate the diagnostic value of the target gene. The scores of 22 immune cells in targets are high-expression and low-expression, and they have identified significantly different cells through. We further studied the carcinogenesis role of several key targets *in vitro*.

Materials and methods

Microarray data

Microarray data were downloaded from the Gene Expression Omnibus (GEO) (2022.4.1) database GSE54238 based on platform GPL16955 (26 HCC samples, 228 cirrhotic samples, and 10 adjacent non-cancerous samples) and GSE63898 (228 HCC samples and 168 cirrhotic samples) based on platform GPL13667. The data obtained by the GEO data access policy is publicly available and open access.

Unsupervised clustering

We download the "ConsensusClusterPlus" R package to perform unsupervised consensus clustering. The algorithm is based on the computational method, namely consensus clustering. It allowed cases to be divided or compressed into multiple distinct clusters based on provided flags or signatures clusters. Furthermore, landmark gene sets summarize and represent specific well-defined biological states or processes and show consistent expression. Based on Molecular Signature Database.

Functional enrichment analysis

DAVID was used to perform functional and pathway enrichment analyses to assess the biological significance (Dennis et al., 2003; Xie et al., 2011). We used GOplot and ggalluvial respectively and R package for analysis.

Differentially expressed gene (DEG) analysis

The R package "limma" was used to compare each other between Cluster 1, Cluster 2 and Cluster 3. And DEGs related to drug targets were identified (|log 2-fold change (FC)| > 1.0 and FDR < .05).

Independent prognostic value of target genes

A violin plot was drawn to demonstrate the differential expression of target genes (HCC vs cirrhosis). We calculated the area under the AUC of the target gene.

Relationship between target genes and immune cell infiltration

The CIBERSORT and ESTIMATE algorithms were performed. The ESTIMATE algorithm was used to determine the immune scores of all samples. The differences in immune cell infiltration between high and low target genes were analyzed based on the CIBERSORT algorithm.

TIMER database analysis

TIMER is a comprehensive database that applies a deconvolution approach to assess immune infiltration (Li et al., 2016). We analyzed the correlation of the expression of four drug targets with immune infiltrate abundance in liver tissue.

Cell lines and cultured medium

Human hepatocellular carcinoma cell line SNU423 was purchased from ATCC. The cells were cultured in RPMI 1640 supplemented with 10% FBS. Cell line was tested mycoplasma free using colorimetric mycoplasma detection assay with HEK-Blue-2 cells as described before.

qRT-PCR and Western blot

Total RNAs were extracted by using RNeasy Kit from Qiagen following the manufacturer's protocol. RNA concentration was measured by Nano Drop 2000. First strand of cDNA was synthesized by using PrimeScript RT Reagent Kit from TAKARA. qPCR was performed by using SYBR Green master mix purchased from Bio-rad company. Primers for beta-ACTIN (Forward: CACCATTGGCAATGAGCGGTTC, Reverse: AGGTCTTTGCGGATGTCCACGT), Primers for AKR1C3 (forward: TCCGACCAGCCTTGGAAAAC, reverse: TCTGTTGGTGAAAGTTCCTCAC). Primers for TPX2 (Forward: 5′-ATATGTGCCCCTTGCACAGC-3′, reverse: 5′-ACAGGAGTCTGTGGGTCTCT-3′).

Total cellular protein were extracted with RIPA lysis buffer. Protein concerntration was diluted to 1 mg/ml with distilled water and lysis buffer, then heated in 95°C metal bath for 7 min. Electrophoresis was performed loading as 20 μg/well and proteins were transferred onto PVDF membranes using bio-rad semi-dry transfer machine. Membrane was blocked by 5% milk in PBST for 1 h at room temperature and them incubated with primary antibody for overnight. After washing out primary antibody, membrane was incubated with secondary antibody for 1 h and goes for imaging. A primary antibody against β-actin (1:3,000) was purchased from Santa Cruz Biotechnology. Antibody against AKR1C3 was purchased from Invitrogen (ARC0857). Antibody against TPX2 was purchased from Cell Signaling Technology.

Cell proliferation, migration and invasion

Cells were seeded in 6-well plates and transfected with siRNAs, respectively. siRNAs targeted AKR1C3 or TPX2 were ordered from BGI Genomic. Sequences of siRNAs are listed below. AKR1C3 siRNA1: 5′-UUUACACACUGGUGUUUGGAA-3′, siRNA2: 5′- AUCAUUUAGCUUUACACACUG-3′; TPX2 siRNA1:5′- UUCUUUCUGUUCCAAAUCCUU-3′, TPX2 siRNA2: 5′-UUUUUACAUGAUGCUUUUCUU-3′.

For cell proliferation, cells were seeded as 1×10^5 per well in 6 well plates. After 72 h, cells were harvested and counted with cell counting chamber. For migration assay, cells were detached from tissue culture plate by using 0.25% Trypsin-EDTA solution and resuspended in serum free culture medium seeded as 5×10^5 per well in a 6-well plate before scratching. 24 h later, cells were scratched with a 20 μl tip and washed twice with PBS and cultured in serum-free medium. Images were captured immediately after scratching, and then at 24 h. Nine measurements were performed for each group. Migration distances were measured by ImageJ software.

Cell invasion assay was performed using 8 μm Matrigel invasion chambers (Corning Company). Cells were detached after being transfected with siRNAs for 48 h. Then 2.5×10^4 cells were seeded on top of the insert with serum-free medium. Lower chambers were filled with growth medium with 10% FBS. After 22 h, media containing remaining cells that did not migrate from the top of the membrane was carefully removed. Cells were fixed by putting the insert in formalin for 15 min, air-drying for 10 min at room temperature, and staining with 1% crystal violet solution

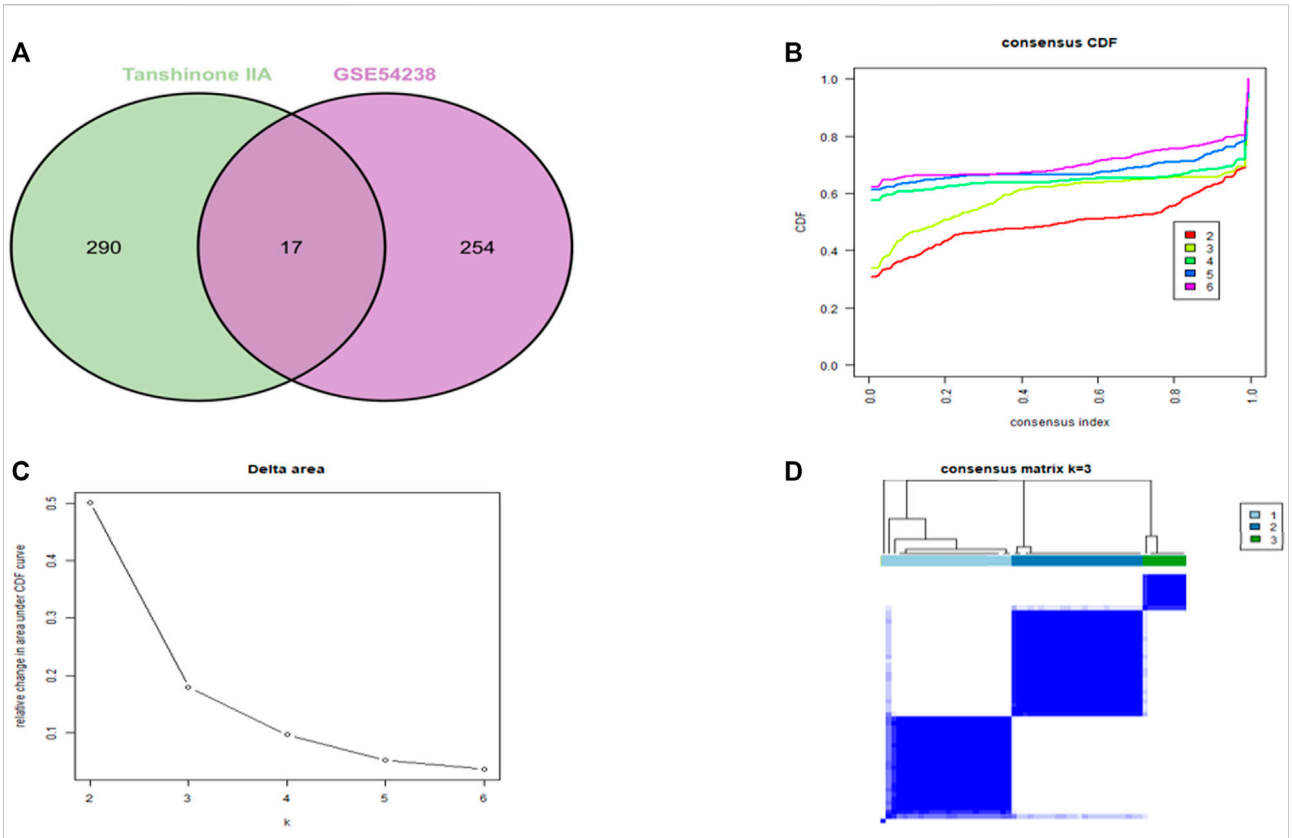

FIGURE 1
Selection of target genes. **(A)** Venn diagram for screening drug target genes. **(B)** CDF plot showing consensus distribution of target genes for each cluster (K). **(C)** Delta area plot, reflecting the relative change in the area under the CDF curve. **(D)** Consensus matrix heatmap depicting consensus values on a white to blue scale for each cluster.

for 10 min. The fixed inserts were then washed with distilled water. Three replicate experiments were performed. Trans-wells were imaged by microscope after staining with crystal violet. Five views were counted for each group.

Statistical methods

Statistical data obtained from GEO were statistically analyzed by R (3.6.1) software (https://www.r-project.org/). The t-test was used between the two independent samples in the research, and $p < .05$ was considered statistically significant.

Results

Unsupervised consensus clustering identified three novel subgroups

We utilized intersections between drug targets of Tanshinone IIA and GSE54238 to select overlapping genes (Figure 1A). The CDF plot shows the consistency distribution for each cluster (Figure 1B). The elta area plot shows the relative change in the area under the CDF curve (Figure 1C). The largest change in area occurs between k = 2 and k = 4, where the relative increase in the area becomes significantly smaller. The mean cluster of the three clusters consensus scores were comparable (Figure 1D). Therefore, three novel subgroups that best represent data patterns in patients were identified using consensus clustering analysis.

Functional pathway enrichment analysis

We performed GO analysis on the intersected drug targets to reveal changes in biological process (BP), molecular function (MF) and cellular components (CC). The daunorubicin metabolism, doxorubicin metabolism, progesterone metabolism, prostaglandin metabolism, and the positive regulation of protein kinase B signaling were significantly enriched BP (Figure 2A). The drug target's

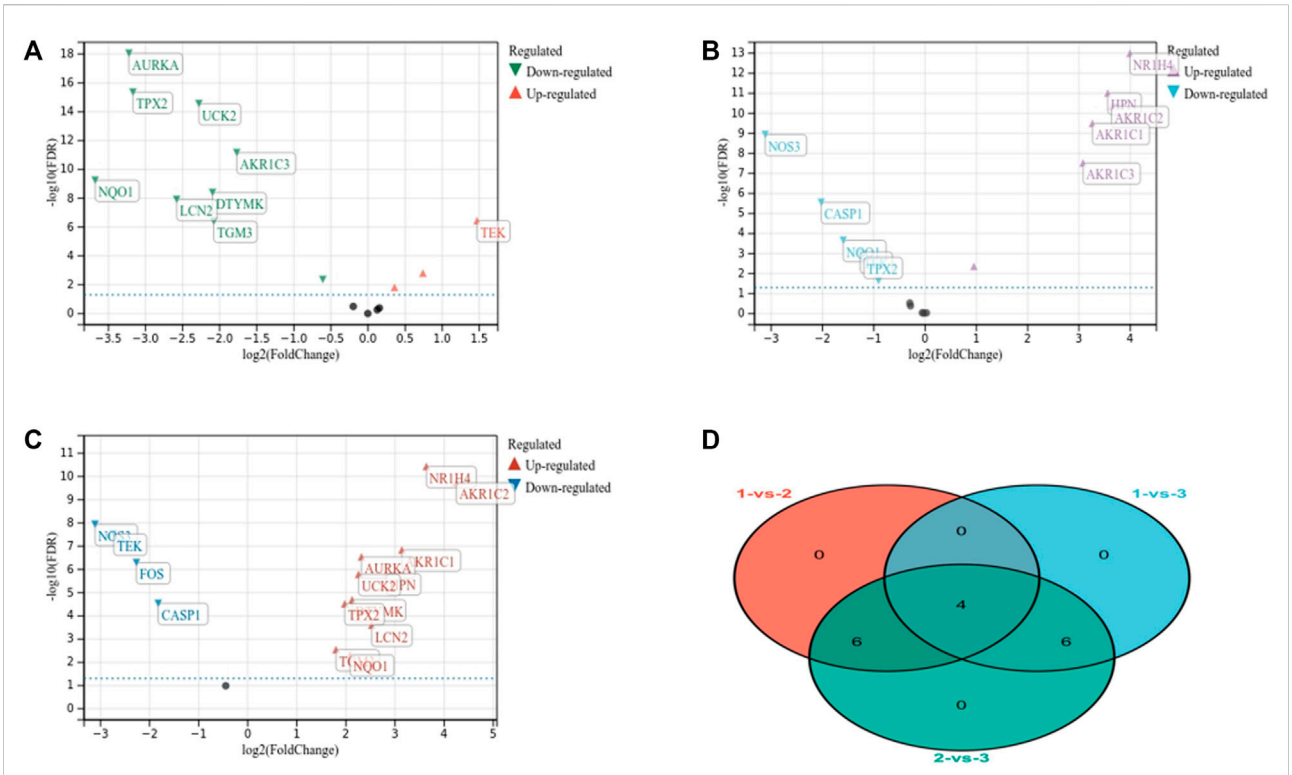

FIGURE 2
GO and KEGG enrichment analysis. **(A)** Biological process. **(B)** Cellular components. **(C)** Molecular function. **(D)** KEGG pathway.

main CC was in the cytosol, axon terminals and cytoplasm (Figure 2B). These targets were mainly involved in MF including bile acid-binding, ketosteroid monooxygenase activity, steroid dehydrogenase activity, androsterone dehydrogenase activity, carboxylic acid-binding and the same protein binding (Figure 2C). Meanwhile, the drug targets were significantly enriched in the KEGG pathway, including steroid hormone biosynthesis, fluid shear stress, atherosclerosis-pyrimidine metabolism, ubiquinone, and other terpenoid quinone biosynthesis (Figure 2D).

Identification of differentially expressed genes between clusters

There were 10 DEGs, including 9 downregulated and 1 upregulated gene (clusters 1 and 2) (Figure 3A). A total of 10 DEGs were found between clusters 1 and 3, including 4 downregulated and 6 upregulated genes between (clusters 2 vs. 3) (Figure 3B). And 16 DEGs, including 4 downregulated and 12 upregulated genes were determined (cluster 1 vs. 2) (Figure 3C). These DEGs were overlapped to determine 4 genes as key diagnostic target genes for subsequent analysis (Figure 3D).

Key target genes demonstrated significant differential expression between cirrhosis and other group

A violin plot shows that the expression of AKR1C3, NQO1, TEK and TPX2 was significantly associated with different disease states (normal, cirrhosis or liver cancer) ($p < .05$) (Figures 4A–D) (GSE54238). The above results suggest that target genes can be used as independent prognostic factors or combined with existing clinical indicators.

Evaluation and validation of the diagnostic performances of the target genes on cirrhosis

The AUCs for AKR1C3, NQO1, TEK, and TPX2 were .62, .78, .66, and .74 in the TCGA dataset (Supplementary Figure S1A). These genes also demonstrated good diagnostic performance in the validation dataset GSE63898. The AUCs of expression of AKR1C3, NQO1, TEK, and TPX2 between cirrhosis and HCC were .9, .74, .77, and .89(Supplementary Figure S1B), proving that the four target genes have predictive

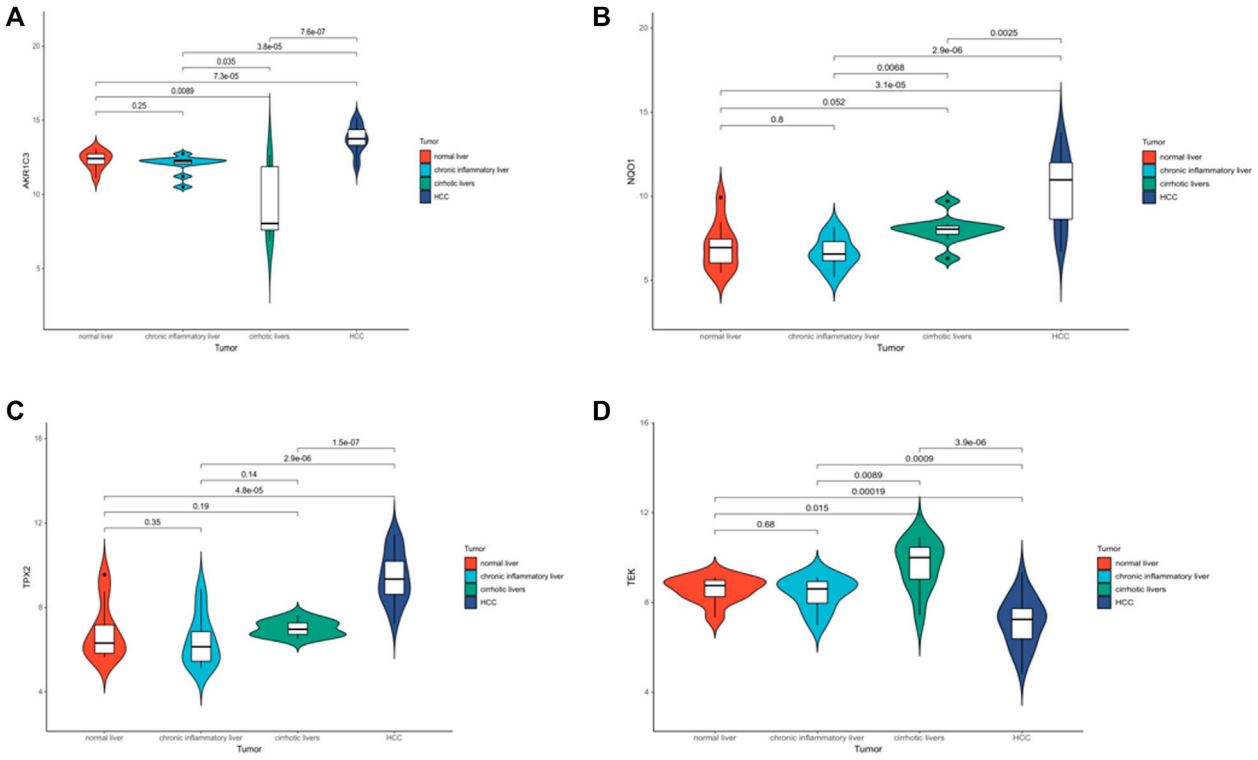

FIGURE 3
Identification of differentially expressed genes. **(A)** Identification of highly correlated genes between clusters 1 and 2. **(B)** Identification of highly correlated genes between clusters 1 and 3. **(C)** Identification of highly correlated genes between clusters 2 and 3. **(D)** Gene intersection between clusters was screened for overlapping genes.

value. The violin plot with GSE63898 were also consistent with the GSE54238 analysis (Supplementary Figures S1C, D).

The relationship between target genes and immune infiltration

We tried to determine whether the expression of target genes is related to tumor immune infiltration. We used CIBERSORT to infer the abundance of 22 immune cells. AKR1C3 expression was significantly different among CD4 helper T cells, CD4 memory resting T cells, regulatory T cells (Tregs), and resting NK cells (Supplementary Figure S2A). The expression of NQO1 varied among CD4 memory resting T cells, regulatory T cells (Tregs), resting NK cells, etc. (Supplementary Figure S2B). TEK expression was significantly inconsistent in immune cells such as $CD8^+$ T cells and $CD4^+$ memory resting T cells (Supplementary Figure S2C). TPX2 differs among cells such as CD4 helper T cells, $CD4^+$ memory resting T cells, and regulatory T cells (Tregs) (Supplementary Figure S2D). The target genes obtained by the intersection of the above immune cells were significantly correlated with $CD4^+$ memory resting T cells ($p < .05$).

Therefore, we investigated whether drug targets were associated with immune infiltration in HCC from the TIMER database. AKR1C3 expression was significantly correlated with tumor purity (p = 4.71e-01) (Supplementary Figure S3A). NQO1 expression was significantly correlated with tumor purity (p = 2.25e-03) (Supplementary Figure S3B). TEK expression was significantly correlated with tumor purity (p = 4.29e-16) (Supplementary Figure S3C). TPX2 expression was significantly correlated with tumor purity (p = 1.23e-03) (Supplementary Figure S3D).

Knockdown of AKR1C3 and TPX2 suppressed tumor magliance of HCC cells

Considering the important role of AKR1C and TPX2 in carcinogenesis. We knocked down the 2 genes with 2 specific siRNAs of each gene in SNU423 cells, respectively. qRT-PCR and western blot was performed to evaluate the efficiency of siRNAs (Supplementary Figures S4A, S5B). Knockdown of AKR1C3 and TPX2 significantly suppressed cell proliferation (Supplementary Figure S4C). Woundhealing assay revealed that knockdown of

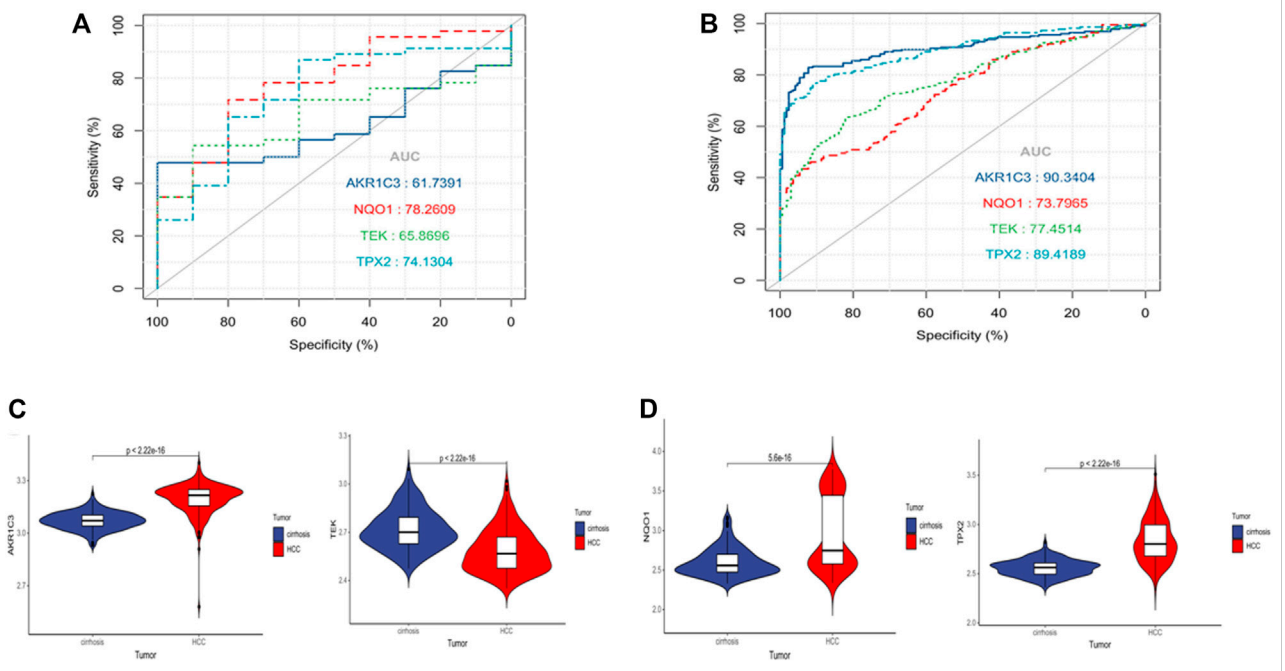

FIGURE 4
Analysis of the prognostic value of target genes. **(A–D)** Violin plots showing the relative expression of AKR1C3, NQO1, TEK and TPX2 in normal, cirrhotic and HCC.

AKR1C3 suppressed cell migration significantly (Supplementary Figure S5A), and knockdown of TPX2 also slightly suppressed cell migration (Supplementary Figure S5B). Trans-well assay was performed to evaluate invasive ability of HCC cells. As shown in Supplementary Figures S5C, D, knockdown of either AKR1C3 or TPX2 suppressed invasive ability of SNU423 cell significantly.

Discussion

The liver is the major organ that metabolizes three major nutrients: protein, fat, and carbohydrate (Moriwaki et al., 2004; Charlton, 2006). The gut-liver axis is essential in liver fibrosis and cirrhosis (Bajaj, 2019). It is a complex and regulated process that balances substrate production and degradation (Qin et al., 2014). Identifying diagnostic therapeutic biomarkers may help clinicians improve treatment strategies (Acharya and Bajaj, 2019). Therefore, it is necessary to evaluate the key drug targets in liver cirrhosis.

We use the bioinformatical analysis to verify that AKR1C3, NQO1, TEK, and TPX2 have good diagnostic performance in patients with cirrhosis. These genes may serve as key biomarkers for diagnosing patients with cirrhosis. We further explored the impact of AKR1C3 or TPX2 on the development of liver cancer *in vitro*. We found that knockouts of AKR1C3 or TPX2 can significantly inhibit the invasion of liver cancer cells. AKR1C isotic enzyme 2 and 3 may work in male-related liver diseases such as cirrhosis (White et al., 2014). Studies have proved that STAT3 and NF-κB inhibitors have caused liver star apoptosis and accelerated live fibrosis recovery (Sommerhalder et al., 2021). NF-κB and STAT3 activate the proliferation and metastasis of hepatoma carcinoma cells (He and Karin, 2011). Knockout of TPX2 in the hepatoma carcinoma cell system can reduce cell growth and induce apoptosis by blocking G2/m. Activating PI3K/AKT signaling pathway can promote the production of internal blood vessels, aggravating the process of liver cirrhosis (Wang et al., 2019). TPX2 can promote the development of HCC by activating the PI3K/AKT pathway (Zeng et al., 2020; Huang et al., 2019). The expression of NQO1 is related to HCC's internal liver recurrence and poor prognosis (Shimokawa et al., 2020). TEK delays tumor growth, slows down metastasis, and enhances the response to accompanying cytotoxic therapy (Goel et al., 2013). Verifying our research results can provide new ideas for the progress of cirrhosis.

Furthermore, immune infiltration analysis shows a correlation between target genes and several immune cells (Tian et al., 2022). We revealed that 4 target genes are significantly related to $CD4^+$ memory static T cells. $CD4^+$ memory static T cells secrete iconic cytokines IL-4, IL-10, and IFN-G, and stimulate other immune cells such as NK cells, to media the progress of liver fibrosis (Liu et al., 2022). The $CD4^+$

T cells and CD4/CD8 ratio in liver cirrhosis is reduced. $CD4^+$ T cells, including $CD4^+$ effects T cells and $CD4^+$ memory T cells increase (Bárcena et al., 2019). The change in the target gene reflects the liver fibrosis immune microenvironment changes. Therefore, we investigated whether the drug target is related to the immunohistos in HCC. The expression of the 4 target genes is significantly related to the purity of the tumor. Compared with normal liver cells, $CD4^+$ memory static T cells in HCC increased significantly (Viveiros et al., 2019). Emerging cancer cells can be identified and killed by many immune cells in tumor treatment, such as $CD8^+$ and $CD4^+$ memory static T cells (Mukaida and Nakamoto, 2018). For instance, $CD4^+$ memory static T cells inhibit the development of liver cancer and media for tumor retreat (Ma et al., 2016). The increase in cytotoxic $CD4^+$ T cells is related to disease-free survival and total survival (Fu et al., 2013). Our results are consistent with these reports and verify the correlation between immune cells and target genes.

The development of cirrhosis is an essential clinical marker in patients with chronic liver disease. It predicts an increased risk of morbidity and a decreased probability of survival. Therefore, a comprehensive understanding of the prognostic character model of liver cirrhosis is critical to improve clinical outcomes. In addition, further studies on the interactions between drug targets and immune cells can elucidate the pathogenesis of liver cirrhosis and provide new opportunities for immunotherapy.

Conclusion

We explored the diagnostic key targets of Tanshinone IIA in liver cirrhosis through exploaration of comprehensive dataset including health, liver cirrhosis and liver cancer patients. The diagnostic performance of target genes was assessed and further verified in the external dataset. We found that the 4 key drug targets could be used as effective diagnostic biomarkers. And the knockouts of AKR1C3 or TPX2 can significantly inhibit the invasion of liver cancer cells.

Data availability statement

The datasets presented in this study can be found in online repositories. The names of the repository/repositories and accession number(s) can be found in the article/ Supplementary Material.

Author contributions

QC prepared the manuscript and implemented the data analysis. DW was responsible for figure preparation and data processing. TS completed in vitro experiments. H-PL proposed the idea and supervised the whole project. All authors contributed to the paper and approved the submitted version.

Funding

This work was supported by the Fund of Biosecurity Specialized Project of PLA (No. 19SWAQ18).

Conflict of interest

The authors declare that the research was conducted in the absence of any commercial or financial relationships that could be construed as a potential conflict of interest.

Publisher's note

All claims expressed in this article are solely those of the authors and do not necessarily represent those of their affiliated organizations, or those of the publisher, the editors and the reviewers. Any product that may be evaluated in this article, or claim that may be made by its manufacturer, is not guaranteed or endorsed by the publisher.

Supplementary material

The Supplementary Material for this article can be found online at: https://www.frontiersin.org/articles/10.3389/fphar.2022.909668/full#supplementary-material

SUPPLEMENTARY FIGURE S1
Evaluation and validation of target genes for diagnosis of cirrhosis. **(A)** ROC analysis of key target genes in GSE54238. **(B)** ROC curve of the key target genes in GSE63898. **(C)** Differential expression of key target genes in cirrhosis and HCC group in GSE63898.

SUPPLEMENTARY FIGURE S2
Immune infiltration relationship between target genes and 22 immune cell subsets. **(A)** Differences in immune cell distribution between high and low AKR1C3 expression groups and low. **(B)** Differences in immune cell distribution between high and low NQO1 expression groups and low. **(C)** Differences in immune cell distribution between high and low TEK expression groups and low. **(D)** Differences in immune cell distribution between high and low TPX2 expression groups and low.

SUPPLEMENTARY FIGURE S3
Correlation of target gene expression with TME. **(A)** AKR1C3 expression was significantly correlated with tumor purity. **(B)** NQO1 expression was significantly correlated with tumor purity. **(C)** TEK expression significantly correlated with tumor purity. **(D)** TPX2 expression significantly correlated with tumor purity.

SUPPLEMENTARY FIGURE S4
mRNA and protein expression of AKR1C3 and TPX2 **(A)** qRT-PCR of AKR1C3 and TPX2 in SNU423 cells after transfecting with specific siRNAs. **(B)** Western blot of AKR1C3 and TPX2 after knockdown of the specific gene. **(C)** Cell numbers of the cells on 72 h post-transfection with siRNA.

SUPPLEMENTARY FIGURE S5
Knockdown of AKR1C3 and TPX2 suppressed tomor magliance of HCC cells. **(A)** Left panel: wound healing assay of cells after transfecting with AKR1C3 siRNAs. Right panel: statistical anaylsis results of migration diatance percentage, 5 measurements was calculated for each group. **(B)** Left panel: wound healing assay of cells after transfecting with TPX2 siRNAs. Right panel: statistical anaylsis results of migration distance percentage, scale bar: 400 μm. **(C)** Trans-well assay of cells after knockdown of AKR1C3 or TPC2. **(D)** Statistical analysis of invasive cells, data was shown as percentage. Five views was calculated for each group. Each experiment has been repeated for at least 3 times. *, $p < .05$; **, $p < .01$.

References

Acharya, C., and Bajaj, J. S. (2019). Altered microbiome in patients with cirrhosis and complications. *Clin. Gastroenterol. Hepatol.* 17, 307–321. doi:10.1016/j.cgh.2018.08.008

Bajaj, J. S. (2019). Altered microbiota in cirrhosis and its relationship to the development of infection. *Clin. Liver Dis.* 14, 107–111. doi:10.1002/cld.827

Bandi, J. C., Poch, E., García-Pagán, J. C., Luca, A., Jiménez, W., Escorsell, A., et al. (1997). Platelet cytosolic calcium concentration in patients with liver cirrhosis. Relationship with hepatic and systemic hemodynamics. *J. Hepatol.* 27, 824–829. doi:10.1016/s0168-8278(97)80319-4

Bárcena, C., Aran, G., Perea, L., Sanjurjo, L., Téllez, É., Oncins, A., et al. (2019). CD5L is a pleiotropic player in liver fibrosis controlling damage, fibrosis and immune cell content. *EBIOMEDICINE* 43, 513–524. doi:10.1016/j.ebiom.2019.04.052

Charlton, M. (2006). Branched-chain amino acid enriched supplements as therapy for liver disease. *J. Nutr.* 136, 295S–298S. doi:10.1093/jn/136.1.295S

D'Amico, G., Garcia-Tsao, G., and Pagliaro, L. (2006). Natural history and prognostic indicators of survival in cirrhosis: A systematic review of 118 studies. *J. Hepatol.* 44, 217–231. doi:10.1016/j.jhep.2005.10.013

Dai, Z., Qin, J., Huang, J., Luo, Y., Xu, Q., and Zhao, H. (2012). Tanshinone IIA activates calcium-dependent apoptosis signaling pathway in human hepatoma cells. *J. Nat. Med.* 66, 192–201. doi:10.1007/s11418-011-0576-0

Dennis, G. J., Sherman, B. T., Hosack, D. A., Yang, J., Gao, W., Lane, H. C., et al. (2003). David: Database for annotation, visualization, and integrated Discovery. *Genome Biol.* 4, P3. doi:10.1186/gb-2003-4-5-p3

Duah, A., and Nkrumah, K. N. (2019). Prevalence and predictors for spontaneous bacterial peritonitis in cirrhotic patients with ascites admitted at medical block in Korle-Bu Teaching Hospital, Ghana. *Pan Afr. Med. J.* 33, 35. doi:10.11604/pamj.2019.33.35.18029

EAF Of liver (2018). EASL Clinical Practice Guidelines for the management of patients with decompensated cirrhosis. *J. Hepatol.* 69, 406–460. doi:10.1016/j.jhep.2018.03.024

Fan, G., Zhu, Y., Guo, H., Wang, X., Wang, H., and Gao, X. (2011). Direct vasorelaxation by a novel phytoestrogen tanshinone IIA is mediated by nongenomic action of estrogen receptor through endothelial nitric oxide synthase activation and calcium mobilization. *J. Cardiovasc. Pharmacol.* 57, 340–347. doi:10.1097/FJC.0b013e31820a0da1

Fu, J., Zhang, Z., Zhou, L., Qi, Z., Xing, S., Lv, J., et al. (2013). Impairment of CD4+ cytotoxic T cells predicts poor survival and high recurrence rates in patients with hepatocellular carcinoma. *HEPATOLOGY* 58, 139–149. doi:10.1002/hep.26054

Gines, P., Krag, A., Abraldes, J. G., Sola, E., Fabrellas, N., and Kamath, P. S. (2021). Liver cirrhosis. *LANCET* 398, 1359–1376. doi:10.1016/S0140-6736(21)01374-X

Goel, S., Gupta, N., Walcott, B. P., Snuderl, M., Kesler, C. T., Kirkpatrick, N. D., et al. (2013). Effects of vascular-endothelial protein tyrosine phosphatase inhibition on breast cancer vasculature and metastatic progression. *J. Natl. Cancer Inst.* 105, 1188–1201. doi:10.1093/jnci/djt164

He, G., and Karin, M. (2011). NF-κB and STAT3 - key players in liver inflammation and cancer. *Cell Res.* 21, 159–168. doi:10.1038/cr.2010.183

Huang, D., Jian, J., Li, S., Zhang, Y., and Liu, L. (2019). TPX2 silencing exerts anti-tumor effects on hepatocellular carcinoma by regulating the PI3K/AKT signaling pathway. *Int. J. Mol. Med.* 44, 2113–2122. doi:10.3892/ijmm.2019.4371

Kim, S. H., Kim, J. Y., Park, S. Y., Jeong, W. T., Kim, J. M., Bae, S. H., et al. (2021). Activation of the EGFR-PI3K-CaM pathway by PRL-1-overexpressing placenta-derived mesenchymal stem cells ameliorates liver cirrhosis via ER stress-dependent calcium. *Stem Cell Res. Ther.* 12, 551. doi:10.1186/s13287-021-02616-y

Li, B., Severson, E., Pignon, J. C., Zhao, H., Li, T., Novak, J., et al. (2016). Comprehensive analyses of tumor immunity: Implications for cancer immunotherapy. *Genome Biol.* 17, 174. doi:10.1186/s13059-016-1028-7

Liu, Y., Dong, Y., Wu, X., Wang, X., and Niu, J. (2022). Identification of immune microenvironment changes and the expression of immune-related genes in liver cirrhosis. *Front. Immunol.* 13, 918445. doi:10.3389/fimmu.2022.918445

Ma, C., Kesarwala, A. H., Eggert, T., Medina-Echeverz, J., Kleiner, D. E., Jin, P., et al. (2016). NAFLD causes selective CD4(+) T lymphocyte loss and promotes hepatocarcinogenesis. *NATURE* 531, 253–257. doi:10.1038/nature16969

Moriwaki, H., Miwa, Y., Tajika, M., Kato, M., Fukushima, H., and Shiraki, M. (2004). Branched-chain amino acids as a protein- and energy-source in liver cirrhosis. *Biochem. Biophys. Res. Commun.* 313, 405–409. doi:10.1016/j.bbrc.2003.07.016

Mukaida, N., and Nakamoto, Y. (2018). Emergence of immunotherapy as a novel way to treat hepatocellular carcinoma. *World J. Gastroenterol.* 24, 1839–1858. doi:10.3748/wjg.v24.i17.1839

Qin, N., Yang, F., Li, A., Prifti, E., Chen, Y., Shao, L., et al. (2014). Alterations of the human gut microbiome in liver cirrhosis. *NATURE* 513, 59–64. doi:10.1038/nature13568

Shimokawa, M., Yoshizumi, T., Itoh, S., Iseda, N., Sakata, K., Yugawa, K., et al. (2020). Modulation of Nqo1 activity intercepts anoikis resistance and reduces metastatic potential of hepatocellular carcinoma. *Cancer Sci.* 111, 1228–1240. doi:10.1111/cas.14320

Sommerhalder, C., Cummins, C. B., Wang, X., Ramdas, D., Lopez, O. N., Gu, Y., et al. (2021). HJC0416 attenuates fibrogenesis in activated hepatic stellate cells via STAT3 and NF-κB pathways. *J. Surg. Res.* 261, 334–342. doi:10.1016/j.jss.2020.12.045

Tan, J., Tang, X., He, Y., Xu, X., Qiu, D., Chen, J., et al. (2022). In-patient expenditure between 2012 and 2020 concerning patients with liver cirrhosis in chongqing: A hospital-based multicenter retrospective study. *Front. Public Health* 10, 780704. doi:10.3389/fpubh.2022.780704

Tian, F., Hu, H., Wang, D. I., Ding, H., Chi, Q., Liang, H., et al. (2022). *Immune-related DNA methylation signature associated with APLN expression predicts prognostic of hepatocellular carcinoma*. United States: Tech Science Press.

Tsai, F., Yang, P., Chen, C., Li, J., Li, T., Chiou, J., et al. (2020). Decreased overall mortality rate with Chinese herbal medicine usage in patients with decompensated liver cirrhosis in Taiwan. *BMC Complement. Med. Ther.* 20, 221. doi:10.1186/s12906-020-03010-6

Viveiros, P., Riaz, A., Lewandowski, R. J., and Mahalingam, D. (2019). Current state of liver-directed therapies and combinatory approaches with systemic therapy in hepatocellular carcinoma (HCC). *Cancers (Basel)* 11, 1085. doi:10.3390/cancers11081085

Wang, L., Feng, Y., Xie, X., Wu, H., Su, X. N., Qi, J., et al. (2019). Neuropilin-1 aggravates liver cirrhosis by promoting angiogenesis via VEGFR2-dependent PI3K/Akt pathway in hepatic sinusoidal endothelial cells. *EBIOMEDICINE* 43, 525–536. doi:10.1016/j.ebiom.2019.04.050

White, D. L., Liu, Y., Garcia, J., El-Serag, H. B., Jiao, L., Tsavachidis, S., et al. (2014). Sex hormone pathway gene polymorphisms are associated with risk of advanced hepatitis C-related liver disease in males. *Int. J. Mol. Epidemiol. Genet.* 5, 164–176.

Wong, F. (2016). Acute kidney injury in liver cirrhosis: New definition and application. *Clin. Mol. Hepatol.* 22, 415–422. doi:10.3350/cmh.2016.0056

Wu, L., Ning, B., Yang, J., Chen, Y., Zhang, C., and Yan, Y. (2022). Diagnosis of liver cirrhosis and liver fibrosis by artificial intelligence algorithm-based multislice spiral computed tomography. *Comput. Math. Methods Med.* 2022, 1217003–1217008. doi:10.1155/2022/1217003

Xie, C., Mao, X., Huang, J., Ding, Y., Wu, J., Dong, S., et al. (2011). Kobas 2.0: A web server for annotation and identification of enriched pathways and diseases. *Nucleic Acids Res.* 39, W316–W322. doi:10.1093/nar/gkr483

Xu, R., Wu, Q., Gong, Y., Wu, Y., Chi, Q., and Sun, D. A. (2022). A novel prognostic target-gene signature and nomogram based on an integrated bioinformatics analysis in hepatocellular carcinoma. *Biocell* 46 (5), 1261–1288. doi:10.32604/biocell.2022.018427

Yang, L., Jeng, C., Kung, H., Chang, C., Wang, A., Chau, G., et al. (2005). Tanshinone IIA isolated from Salvia miltiorrhiza elicits the cell death of human endothelial cells. *J. Biomed. Sci.* 12, 347–361. doi:10.1007/s11373-005-0973-z

Zeng, X., Zhang, L., Liao, W., Ao, L., Lin, Z., Kang, W., et al. (2020). Screening and identification of potential biomarkers in hepatitis B virus-related hepatocellular carcinoma by bioinformatics analysis. *Front. Genet.* 11, 555537. doi:10.3389/fgene.2020.555537

Zhao, H., Guo, J., Chi, Q., and Fang, M. (2022). Molecularmechanisms of Tanshinone IIA in hepatocellular carcinoma therapy via WGCNA-based network pharmacology analysis. *Biocell* 46 (5), 1245–1259. doi:10.32604/biocell.2022.018117

Frontiers in Pharmacology

Explores the interactions between chemicals and living beings

The most cited journal in its field, which advances access to pharmacological discoveries to prevent and treat human disease.

Discover the latest Research Topics

See more →

Frontiers

Avenue du Tribunal-Fédéral 34
1005 Lausanne, Switzerland
frontiersin.org

Contact us

+41 (0)21 510 17 00
frontiersin.org/about/contact